UNIVERSITAT POLITÈCNICA DE VALÈNCIA

DOCTORADO EN INGENIERÍA Y PRODUCCIÓN INDUSTRIAL

TESIS DOCTORAL

Desarrollo y optimización de nuevas formulaciones de biopolímeros con principios activos para aplicaciones en el sector envase-embalaje

Autor:

Sandra Paola Rojas Lema

Dirigida por:

Dr. Rafael Balart Gimeno

Dr. Daniel García García

Fecha de presentación:

Diciembre de 2022

UNIVERSITAT POLITÈCNICA DE VALÈNCIA

DOCTORADO EN INGENIERÍA Y PRODUCCIÓN INDUSTRIAL

TESIS DOCTORAL

Desarrollo y optimización de nuevas formulaciones de biopolímeros con principios activos para aplicaciones en el sector envase-embalaje

SANDRA PAOLA ROJAS LEMA

El Dr. Rafael Antonio Balart Gimeno, Catedrático de Universidad del Departamento de Ingeniería Mecánica y de Materiales de la Universitat Politècnica de València y el Dr. Daniel García García, Profesor Contratado Doctor del Departamento de Ingeniería Mecánica y de Materiales de la Universitat Politècnica de València en calidad de directores de la Tesis Doctoral (modalidad Doctorado Internacional) presentada por Dña. Sandra Paola Rojas Lema, con el título "**Desarrollo y optimización de nuevas formulaciones de biopolímeros con principios activos para aplicaciones en el sector envase-embalaje".**

CERTIFICAN

Que la presente memoria, "**Desarrollo y optimización de nuevas formulaciones de biopolímeros con principios activos para aplicaciones en el sector envase-embalaje",** para aspirar al grado de Doctor por la Universitat Politècnica de València reúne las condiciones adecuadas para constituir la tesis doctoral de Dña. Sandra Paola Rojas Lema (modalidad Doctorado Internacional).

Asimismo, certifican que la citada tesis doctoral se ha realizado en el Instituto de Tecnología de Materiales de la Universitat Politècnica de València y en el Departamento de Ingeniería Química y Metalurgia de la Universidad Aalto (Finlandia).

Y para que conste a los efectos oportunos, firman la presente en Alcoy a 21 de octubre de 2022.

Fdo. Dr. Rafael Antonio Balart Gimeno Fdo. Dr. Daniel García García

A mis padres.

"Sin fe, nada es posible. Con ella, nada es imposible".

Mary McLeod Bethune

AGRADECIMIENTOS

En primer lugar, deseo agradecer a mis directores de tesis, el Catedrático Rafael Balart Gimeno y el Profesor Contratado Doctor Daniel García García, por todo su apoyo, consejos y guía durante estos tres años. A Rafa por confiar en mí y haberme abierto las puertas del Instituto de Tecnología de Materiales (ITM), ya que sin tu gestión y organización, esto no habría sido posible. Mis más sinceros agradecimientos. A Dani, por estar siempre presto a ayudar en todo momento, gracias a tu gestión también tuve la oportunidad de hacer mi estancia en el extranjero, por lo cual, te quedo enormemente agradecida.

A la Generalitat Valenciana por el apoyo financiero a través de la beca Santiago Grisolía (GRISOLIAP/2019/132).

Al Instituto de Tecnología de Materiales (ITM) de la Universitat Politècnica de València, lugar donde se llevó a cabo la presente tesis doctoral.

A los catedráticos Juan López Martínez, Lourdes Sánchez Nácher y David García Sanoguera, por toda su apertura, buen ánimo y colaboración a lo largo de esta etapa.

A los profesores Octavio Fenollar, Sergio Torres Giner, Néstor Montañés, María Dolores Samper, Teodomiro Boronat y Vicent Fombuena, por toda su ayuda y orientación a lo largo de este proceso.

A los técnicos de laboratorio Javi y Matías por toda su ayuda, paciencia y prontitud para la resolución de las dificultades técnicas a lo largo de este tiempo.

Un especial agradecimiento al Dr. Jon Trifol, quién no solo fue mi supervisor durante la estancia en la Universidad Aalto (Finlandia), sino que también fue quien tramitó y consiguió el financiamiento para dicha estancia. Jon muchas gracias por tu guía y apoyo en todo momento, tu buena actitud y ánimo siempre hizo más ameno el trabajo. ¡Muchas gracias!

A mis amigos y compañeros de oficina Cris y Diego gracias por todos los momentos compartidos, sus ánimos y consejos. Cris gracias por haber estado siempre que te he necesitado, tanto en asuntos de índole académico como en aquellos más personales, eres una gran amiga. Diego a ti mis gracias infinitas... por haber sido un

apoyo desde el primer día que llegué, por tu paciencia al enseñarme tantas cosas y tu ayuda desinteresada. Gracias por tu tiempo amigo.

A mis compañeros de laboratorio Pelayo, Luis, Harrison, Jaume, Ramón, Juan y Antonio. Gracias por toda su ayuda en los momentos que la he requerido, por su apertura y buena predisposición siempre.

A mi familia en Alcoy, Erick, Cris, Migue, Verito y los peques (Miguelito y Martín). Su amistad y cariño hicieron todo este tiempo valioso y memorable.

Y no puedo dejar de agradecer a las personas más importantes de mi vida, ¡mi familia! Mis padres, hermanos, cuñado y mis queridas sobrinas. Pienso que no existen palabras que puedan expresar todo el agradecimiento y cariño hacia ustedes, son y serán siempre mi mayor apoyo y también motivación para salir adelante. La culminación de esta etapa de mi vida no habría sido posible sin todo el ánimo y apoyo que me dieron cuando decidí emprender una nueva aventura en el extranjero. Solo decirles que pese a la distancia su amor siempre se ha sentido cerca.

A Germán, gracias por todos los momentos compartidos, por tu apoyo incondicional y sobre todo por tu compresión durante esta etapa.

A Cris F., mi amiga, mi hermana, gracias por ser mi familia aquí y por estar pendiente de mí en todo momento. Gracias por esas charlas y consejos que me animan y de las que siempre aprendo algo.

A Monita y André, mis grandes amigos, gracias por haber permanecido a mi lado en cada paso, por estar siempre y en todo lugar.

A mis tías que han estado pendientes de mi durante todo este tiempo. Gracias por sus bendiciones, llamadas, saludos. Su apoyo siempre lo he valorado.

RESUMEN

"Desarrollo y optimización de nuevas formulaciones de biopolímeros con principios activos para aplicaciones en el sector envase-embalaje"

Esta tesis doctoral tuvo como objetivo principal el estudio, desarrollo y caracterización de nuevos materiales poliméricos mediante el uso de diferentes matrices poliméricas de origen natural y biodegradables, así como también de aditivos naturales y residuos agroindustriales, todo ello con la finalidad de obtener biopolímeros útiles en el sector envase y embalaje.

Una de las matrices seleccionadas para su uso fue el bio-poli(etileno) de alta densidad (bio-HDPE). El bio-HDPE es un material que se puede obtener a partir de fuentes naturales renovables. Sin embargo, no es susceptible de biodegradación, es por ello que se planteó la adición de cargas y aditivos naturales a la matriz polimérica, con la finalidad de obtener nuevos materiales en los que el uso de estas cargas permita una disminución de la cantidad de matriz polimérica necesaria, además de la posibilidad de proporcionarle al polímero nuevas características y propiedades gracias a los principios activos (fenoles, flavonoides, etc.) que poseen en su estructura. Las cargas utilizadas fueron por un lado harina de piel de caqui (PPF) y, por otro, lignina Kraft (KL). Teniendo en consideración la baja compatibilidad que existe entre la matriz polimérica y las cargas naturales debido básicamente a su inherente hidrofobicidad e hidrofilicidad, respectivamente, se propuso el uso de diferentes técnicas de compatibilización. Se observó como el uso de un poli(etileno) injertado con anhídrido maleico (PE-*g*-MA) y el tratamiento de silanización realizado a las cargas de (PPF) permitió una mejora en las propiedades mecánicas en comparación con las muestras con cargas sin compatibilizar, indicando por tanto una mejora en la interacción de las fases. Por su parte, el tratamiento con cloruro de palmitoil a las cargas de (PPF), si bien no mejoró las propiedades mecánicas permitió un incremento en la hidrofobicidad de los materiales compuestos obtenidos. Por otro lado, la utilización de peróxido de dicumilo (DCP) para la generación de una extrusión reactiva entre la matriz de bio-HDPE y la KL dio lugar una mejora en las propiedades mecánicas, lo que indica que la interacción entre las fases se incrementó. Adicionalmente, teniendo en consideración que las cargas de origen natural tienen

diferentes principios activos en su estructura, algunos de ellos con capacidad antioxidante, se analizó su efecto en las propiedades térmicas de las muestras con (PPF) y se evidenció que repercuten en la estabilidad a la oxidación, debido a un retraso en la degradación térmica (OIT) del material analizado en condiciones isotérmicas, este mismo efecto se observó al agregar directamente principios activos fenólicos, como el ácido gálico y quercetina a la matriz de bio-HDPE.

El estudio continuó con la utilización de poli(ésteres) como el poli(ácido láctico) (PLA) y poli(butilén succinato) (PBS). En el caso del PLA se buscó mejorar la fragilidad propia del material mediante la adición de un oligómero de ácido láctico (OLA) como agente plastificante y se obtuvo que a mayor cantidad de plastificante la ductilidad del PLA incrementaba. Adicionalmente, con el fin de enfocar el material al uso en el sector de envase y embalaje, se buscó mejorar sus propiedades barrera mediante la incorporación de nanomateriales, concretamente nanotubos de haloisita (HNTs), lográndose una importante disminución en la permeabilidad al vapor de agua (WVP) y al limoneno (LP) en aquellas muestras de PLA/OLA/HNTs con un contenido de 3 phr de HNTs.

En el caso del PBS, si bien es un material biodegradable, su obtención aún depende de fuentes petroquímicas total o parcialmente, además que su producción implica un alto costo, por tanto, es importante la búsqueda de alternativas que permitan combinarlo con recursos naturales, para lograr un material menos costoso y más respetuoso con el medio ambiente. Es por ello que se consideró el uso de harina de cáscara de pistacho (SPF) como carga natural. Del mismo modo como se indicó anteriormente se vio la necesidad de añadir el poli(butilén succinato) injertado con anhídrido maleico (PBS-*g*-MAH) como agente compatibilizante para mejorar la interacción entre las fases, lo cual tuvo un efecto positivo, ya que se observó que la carga actuaba como refuerzo para la matriz, mejorando las propiedades mecánicas de las muestras. Su efecto también se pudo ver en la estabilidad térmica, donde se observó un incremento en la temperatura de inicio de degradación con los valores más bajos de carga estudiados. Sin embargo, el uso de SPF incrementó la capacidad de las muestras para absorber agua debido básicamente a la característica hidrofílica de las cargas.

Una última fase de la tesis consistió en el aprovechamiento de los residuos agroindustriales, mediante la extracción de algunos de sus biopolímeros, entre ellos

proteínas, lignina y nanocristales de celulosa (CNC), los cuales luego fueron combinados, con la finalidad de obtener películas para su posible uso en el sector envase y embalaje. La lignina y los CNC fueron obtenidos a partir de las piñas de pino y utilizados como materiales de refuerzo para la matriz de proteína procedente del haba. La incorporación de dichos compuestos en la película de proteína dio lugar a un incremento en las propiedades mecánicas en términos de módulo de Young y resistencia a la tracción, además tuvo repercusión en las propiedades barrera, reduciendo la permeabilidad al vapor de agua y al oxígeno. En las muestras con CNC se observó un incremento en la hidrofobicidad de las películas obtenidas, relacionado también con la disminución en el contenido de humedad y la solubilidad reportados.

Por tanto, de manera general se puede decir que con el trabajo desarrollado se pudieron obtener materiales biopoliméricos con características prometedoras para su aplicación en el sector envase y embalaje, planteando con ello opciones al uso de materiales poliméricos derivados del petróleo.

RESUM

“Desenvolupament i optimització de noves formulacions de biopolímers amb principis actius per a aplicacions en el sector envase-embalatge”

Aquesta tesi doctoral va tindre com a objectiu principal l'estudi, desenvolupament i caracterització de nous materials polimèrics mitjançant l'ús de diferents matrius polimèriques d'origen natural i biodegradables, així com també d'additius naturals i residus agroindustrials, tot això amb la finalitat d'obtindre biopolímers útils en el sector envase i embalatge.

Una de les matrius seleccionades per al seu ús va ser el bio-poli(etilé) d'alta densitat (bio-HDPE). El bio-HDPE és un material que es pot obtindre a partir de fonts naturals renovables. No obstant això, no és susceptible de biodegradació, és per això que es va plantejar l'addició de càrregues i additius naturals a la matriu polimèrica, , a més de la possibilitat de proporcionar-li al polímer noves característiques i propietats gràcies als principis actius (fenols, flavonoides, etc.) que posseeixen en la seua estructura. Les càrregues utilitzades van ser d'una banda farina de pell de caqui (PPF) i, per un altre, lignina Kraft (KL). Tenint en consideració la baixa compatibilitat que existeix entre la matriu polimèrica i les càrregues naturals degut bàsicament a la seua inherent hidrofobicitat i hidrofilicitat, respectivament, es va proposar l'ús de diferents tècniques de compatibilització. Es va observar com l'ús d'un polietilé empeltat amb anhídrid maleic (PE-*g*-DT.) i el tractament de silanització realitzat a les càrregues de (PPF) va permetre una millora en les propietats mecàniques en comparació amb les mostres amb càrregues sense compatibilitzar, indicant per tant una millora en la interacció de les fases. Per part seua, el tractament amb clorur de palmitoil a les càrregues de (PPF), si bé no va millorar les propietats mecàniques va permetre un increment en la hidrofobicitat dels materials compostos obtinguts. D'altra banda, la utilització de peròxid de dicumil (DCP) per a la generació d'una extrusió reactiva entre la matriu de bio-HDPE i la KL va donar lloc una millora en les propietats mecàniques, la qual cosa indica que la interacció entre les fases es va incrementar. Addicionalment, tenint en consideració que les càrregues d'origen natural tenen diferents principis actius en la seua estructura, alguns d'ells amb capacitat antioxidant, es va analitzar el seu efecte en les propietats tèrmiques de les

mostres amb (PPF) i es va evidenciar que repercuteixen en l'estabilitat a l'oxidació, a causa d'un retard en la degradació tèrmica (OIT) del material analitzat en condicions isotèrmiques, aquest mateix efecte es va observar al agregar directament principis actius fenòlics, com l'àcid gàl·lic i quercetina a la matriu de bio-HDPE.

L'estudi va continuar amb la utilització de polièsters com el poli(àcid làctic) (PLA) i poli(butilén succinat) (PBS). En el cas del PLA es va buscar millorar la fragilitat pròpia del material mitjançant l'addició d'un oligòmer d'àcid làctic (ONA) com a agent plastificant i es va obtindre que a major quantitat de plastificant la ductilitat del PLA incrementava. Addicionalment, amb la fi que enfocar el material a l'ús en el sector d'envàs i embalatge, es va buscar millorar les seues propietats barrera mitjançant la incorporació de nanomaterials, concretament nanotubs d'haloisita (HNTs), aconseguint-se una important disminució en la permeabilitat al vapor d'aigua (WVP) i al limonè (LP) en aquelles mostres de PLA/ONA/HNTs amb un contingut de 3 phr de HNTs.

En el cas del PBS, si bé és un material biodegradable, la seua obtenció encara depén de fonts petroquímiques totalment o parcialment, a més que la seua producció implica un alt cost, per tant, és important la cerca d'alternatives que permeten combinar-lo amb recursos naturals, per a aconseguir un material menys costós i més respectuós amb el medi ambient. És per això que es va considerar l'ús de farina de corfa de pistatxo (SPF) com a càrrega natural. De la mateixa manera com es va indicar anteriorment es va veure la necessitat d'afegir el poli(butilén succinat) empeltat amb anhídrid maleic (PBS-*g*-MAH) com a agent compatibilitzant per a millorar la interacció entre les fases, la qual cosa va tindre un efecte positiu, ja que es va observar que la càrrega actuava com a reforç per a la matriu, millorant les propietats mecàniques de les mostres. El seu efecte també es va poder veure en l'estabilitat tèrmica, on es va observar un increment en la temperatura d'inici de degradació amb els valors més baixos de càrrega estudiats. No obstant això, l'ús de SPF va incrementar la capacitat de les mostres per a absorbir aigua degut bàsicament a la característica hidrofílica de les càrregues.

Una última fase de la tesi va consistir en l'aprofitament dels residus agroindustrials, mitjançant l'extracció d'alguns dels seus biopolímers, entre ells proteïnes, lignina i nanocristals de cel·lulosa (CNC), els quals després van ser combinats, amb la finalitat d'obtindre pel·lícules per al seu possible ús en el sector envase i embalatge. La lignina i els CNC van ser obtinguts a partir de les pinyes de pi i utilitzats

com a materials de reforç per a la matriu de proteïna procedent de la fava. La incorporació d'aquests compostos en la pel·lícula de proteïna va donar lloc a un increment en les propietats mecàniques en termes de mòdul de Young i resistència a la tracció, a més va tindre repercussió en les propietats barrera, reduint la permeabilitat al vapor d'aigua i a l'oxigen. En les mostres amb CNC es va observar un increment en la hidrofobicitat de les pel·lícules obtingudes, relacionat també amb la disminució en el contingut d'humitat i la solubilitat reportats.

Per tant, de manera general es pot dir que amb el treball desenvolupat es van poder obtindre materials biopolimerics amb característiques prometedores per a la seua aplicació en el sector envase i embalatge, plantejant amb això opcions a l'ús de materials polimèrics derivats del petroli.

ABSTRACT

"Development and optimization of new biopolymer formulations with active principles for applications in the packaging sector"

The main objective of this doctoral thesis was the study, development, and characterization of new polymeric materials using different polymeric matrices of natural origin and biodegradables, as well as natural additives and agro-industrial wastes, all with the aim of obtaining biopolymers useful in the packaging sector.

One of the matrices selected for use was high-density bio-poly(ethylene) (bio-HDPE). Bio-HDPE is a material that can be obtained from natural renewable sources. However, it is not susceptible to biodegradation, which is why the addition of fillers and natural additives to the polymeric matrix was proposed. All of this with the purpose of obtaining new materials in which the use of these fillers allows a decrease in the amount of polymeric matrix required. In addition to the possibility of providing the polymer with new characteristics and properties thanks to the active principles (phenols, flavonoids, etc.) contained in its structure. The fillers used were persimmon peel flour (PPF) and Kraft lignin (KL). Considering the low compatibility between the polymeric matrix and the natural fillers, basically due to their inherent hydrophobicity and hydrophilicity, respectively, the use of different compatibilization techniques was proposed. It was observed how the use of polyethylene grafted with maleic anhydride (PE-*g*-MA) and the silanization treatment performed to (PPF) fillers improved the mechanical properties compared to the samples with non-compatibilized fillers, thus indicating an improvement in the interaction of the phases. For its part, the treatment with palmitoyl chloride to the (PPF) fillers, although it did not improve the mechanical properties, allowed an increase in the hydrophobicity of the composite materials obtained. On the other hand, the use of dicumyl peroxide (DCP) for generating a reactive extrusion between the bio-HDPE matrix and KL resulted in an improvement in the mechanical properties, indicating that the interaction between the phases was increased. In addition, taking into consideration that the fillers of natural origin have different active principles in their structure, some of them with antioxidant capacity, their effect on the thermal properties of the samples with (PPF) was analyzed, and it was evidenced that they affect the oxidation stability, due to a delay in the thermal degradation (OIT)

of the analyzed material under isothermal conditions, this same effect was observed with the direct addition of phenolic active principles such as gallic acid and quercetin to the bio-HDPE matrix.

The study continued with the use of polyesters such as poly(lactic acid) (PLA) and poly(butylene succinate) (PBS). In the case of PLA, the aim was to improve the fragility of the material by adding a lactic acid oligomer (OLA) as a plasticizing agent. It was found that the greater the amount of plasticizer, the higher the ductility of PLA. Additionally, in order to focus the material for use in the packaging sector, it was sought to improve its barrier properties by incorporating nanomaterials, specifically halloysite nanotubes (HNTs), achieving a significant decrease in water vapor permeability (WVP) and limonene permeability (LP) in those PLA/OLA/HNTs samples with a content of 3 phr of HNTs.

In the case of PBS, although it is a biodegradable material, its obtention still depends totally or partially on petrochemical sources, and its production implies a high cost; therefore, it is crucial to look for alternatives that allow combining it with natural resources, in order to achieve a less expensive and more environmentally friendly material. For this reason, pistachio shell flour (SPF) was considered as a natural filler. Similarly, as indicated above, it was necessary to add poly(butylene succinate) grafted with maleic anhydride (PBS-*g*-MAH) as a compatibilizing agent to improve the interaction between the phases. This had a positive effect since it was observed that the filler acted as a reinforcement for the matrix, improving the mechanical properties of the samples. Its effect could also be seen in the thermal stability, where an increase in the onset temperature of degradation was observed at the lowest filler values studied. However, the use of SPF increased the ability of the samples to absorb water, basically due to the hydrophilic character of the fillers.

A final phase of the thesis consisted of using natural resources and agro-industrial wastes by extracting some of their biopolymers, including proteins, lignin, and cellulose nanocrystals (CNC), which were then combined in order to obtain films for possible use in the packaging sector. Lignin and CNCs were obtained from pine cones and used as reinforcing materials for the protein matrix obtained from faba beans. Incorporating these compounds in the protein film resulted increased mechanical properties in terms of Young's modulus and tensile strength, and also impacted on the

barrier properties, reducing the permeability to water vapor and oxygen. In the CNC samples, an increase in the film's hydrophobicity was observed, which is also related to the decrease in moisture content and solubility reported.

Therefore, in general, it is possible to say that with the work developed, it was possible to obtain biopolymeric materials with promising characteristics for their application in the packaging sector, thus offering options for the use of petroleum-derived polymeric materials.

TABLA DE CONTENIDOS

LISTADO DE ARTÍCULOS

La presente tesis doctoral consta de un compendio de los siguientes artículos.

I. On the use of phenolic compounds present in citrus fruits and grapes as natural antioxidants for thermo-compressed bio-based high-density polyethylene films.

II. Manufacturing and characterization of high-density polyethylene composites with active fillers from persimmon peel flour with improved antioxidant activity and hydrophobicity.

III. Improved performance of environmentally friendly blends of biobased polyethylene and kraft lignin compatibilized by reactive extrusion with dicumyl peroxide.

IV. Tailoring the properties of thermo-compressed polylactide films for food packaging applications by individual and combined additions of lactic acid oligomer and halloysite nanotubes.

V. Peroxide-induced synthesis of maleic anhydride-grafted poly(butylene succinate) and its compatibilizing effect on poly(butylene succinate)/pistachio shell flour composites.

VI. Faba bean protein films reinforced with cellulose nanocrystals as edible food packaging material.

VII. The effect of pine cone lignin on mechanical, thermal and barrier properties of faba bean protein films for packaging applications.

A continuación, se indica el estudio previo llevado a cabo como parte de la presente tesis doctoral.

I. Microencapsulation of copper(II) sulfate in ionically cross-linked chitosan by spray drying for the development of irreversible moisture indicators in paper packaging.

ECUACIONES

$\text{Moisture content} = \left[\frac{W_i - W_f}{W_i}\right] \times 100\ (\%)$	W_i = peso inicial de la muestra. W_f = peso final de la muestra.
$\Delta E_{ab}^{*} = \sqrt{(\Delta L^{*})^2 + (\Delta a^{*})^2 + (\Delta b^{*})^2}$	ΔL^{*} = Diferencia de luminosidad entre dos muestras. Δa^{*} = Diferencia en las coordenadas de a^{*}. Δb^{*} = Diferencia en las coordenadas de b^{*}. ΔE_{ab}^{*} = Diferencia total de color.
$X_C = \left[\frac{\Delta H_m - \Delta H_{CC}}{\Delta H_m^0 \times w}\right] \times 100\ (\%)$	X_C = Grado de cristalinidad. ΔH_m = Entalpía de fusión. ΔH_{CC} = Entalpía de cristalización en frío. ΔH_m^0 = Entalpía de fusión para un polímero 100% cristalino. w = Fracción de peso del polímero.
$\text{DPPH Inhibition} = \left[\frac{A_c - (A_s - A_b)}{A_c}\right] \times 100\ (\%)$	A_c = Valor de la absorbancia de DPPH sin la muestra. A_s = Valor de la absorbancia de DPPH con la muestra. A_b = Valor de absorbancia de la muestra en metanol sin DPPH.
$\text{Water absorption} = \left[\frac{W_t - W_0}{W_0}\right] \times 100\ (\%)$	W_t = Peso seco de la muestra en un tiempo determinado. W_0 = Peso seco inicial de la muestra.
$G_d(\%) = \left[\frac{N \times (V_1 - V_0) \times 98.06}{1000 \times W \times 2}\right] \times 100$	N = Concentración de KOH en [M]. V_0 = Volumen de KOH para el blanco. V_1 = Volumen de KOH para la titración de PBS-*g*-MAH. W = Peso de la muestra. G_d = Grado de injerto.

$\text{Weight loss} = \left[\frac{W_0 - W_{te}}{W_0}\right] \times 100\ (\%)$	W_0 = Peso seco inicial de la muestra. W_{te} = Peso de la muestra luego de un tiempo de enterramiento.
$\text{Solubility} = \left[\frac{W_i - W_f}{W_i}\right] \times 100\ (\%)$	W_i = Peso inicial de la muestra. W_f = Peso de la muestra luego del secado.
$\text{Transparency} = \left[\frac{\text{Log}T_{600}}{x}\right]$	T_{600} = Transmitancia a 600 nm de cada muestra. x = Espesor de la muestra.
$\text{WVTR} = \left[\frac{\Delta m}{t \times A}\right]$	Δm = Incremento de peso del recipiente que contiene la muestra. t = Tiempo al que se toma cada medición. A = Área expuesta de la muestra. WVTR = Tasa de transmisión de vapor de agua.
$\text{WVP} = \left[\frac{\text{WVTR}}{S \times (RH_1 - RH_2)}\right] \times e$	S = Presión de saturación del vapor de agua. RH_1= Humedad reltiva dentro del desecador. RH_2= Humedad reltiva dentro del recipiente. e = Espesor medio de la muestra. WVTR = Tasa de transmisión de vapor de agua. WVP = Permeabilidad al vapor de agua.

ABREVIATURAS Y TÉRMINOS

ΔH_{CC}	entalpía de cristalización en frío
ΔH_m	entalpía de fusión
A	área expuesta de la muestra
a*	coordenada de color de rojo a verde
AA	ácido adípico
A_b	valor de absorbancia de la muestra en metanol sin DPPH
A_c	valor de la absorbancia de DPPH sin la muestra
AL	lignina alcalina
As	valor de la absorbancia de DPPH con la muestra
ASA	anhídrido alquenil succínico
ATA	3-amino-1,2,4-triazole
b*	coordenada de color de amarillo a azul
BDO	1,4-butanodiol
BHT	hidroxitolueno butilado
bio-HDPE	bio-poli(etileno) de alta densidad
bio-LDPE	bio-poli(etileno) de baja densidad
bio-LLDPE	bio-poli(etileno) lineal de baja densidad
bio-PA	bio-poli(amida)
bio-PC	bio-poli(carbonato)
bioPE	bio-poli(etileno)
bio-PET	bio-poli(etilén tereftalato)
bio-PP	bio-poli(propileno)
bio-PU	bio-poli(uretano)
CA	ácido cafeico
CNCs	nanocristales de celulosa
CNTs	nanotubos de carbono
CNWs	nanodiscos de celulosa
Đ	dispersidad
DCP	peróxido de dicumilo

DD	desacetilación
DMTA	análisis térmico mecánico dinámico
DPPH	2,2-difenil-1-picrilhidrazilo
DSC	calorimetría diferencial de barrido
DTG	primera derivada del porcentaje de masa con respecto a la temperatura
e	espesor medio de la muestra
E'	módulo de almacenamiento
E_f	módulo de flexión
EG	etilenglicol
EMT	tomografía de microscopía electrónica
EPDM	etileno-propileno-dieno
E, E_T	módulo de elasticidad o módulo de Young
EVA	etileno acetato de vinilo
EVA-c	copolímero de etileno-acetato de vinilo
EVOH	poli(etileno-*co*-alcohol vinílico)
ε_B	elongación a la rotura
FBP	proteína de haba
FDA	administración de alimentos y medicamentos
FDCA	ácido 2,5 furandicarboxílico
FESEM	microscopía electrónica de barrido de emisión de campo
FTIR	espectroscopia infrarroja por transformada de Fourier
G_d	grado de injerto
GA	ácido gálico
GLYMO	(3-gliciloxipropil)trimetoxisilano
GMA	metacrilato de glicidilo
GNPs	nanoplacas de grafeno
HDPE	poli(etileno) de alta densidad
HNTs	nanotubos de haloisita
KL	lignina kraft
L	coordenada de luminosidad

L/D	relación longitud/diámetro
LA	ácido láctico
LDPE	poli(etileno) de baja densidad
LLDPE	poli(etileno) lineal de baja densidad
LNP	nanopartículas de lignina
LP	permeabilidad al limoneno
N	concentración de KOH en [M].
MA, MAH	anhídrido maleico
MAF	fracción amorfa móvil
MFI	índice de fluidez
MLO	aceite de linaza maleinizado
MMT	montmorillonita
M_n	número de pesos moleculares medios
M_W	peso molecular
NAR	naringina
NBR	caucho de acrilonitrilo-butadieno
NFRP	plásticos reforzados con fibra natural
OIT	tiempo de inducción de la oxidación
OLA	oligómero de ácido láctico
OMMT	montmorillonita modificada orgánicamente
OOT	temperatura de inicio de la oxidación
OPF	harina de cáscara de naranja
OTR	tasa de transmisión de oxígeno
PA	poli(amida)
PA 1010	poli(amida) 1010
PA 410	poli(amida) 410
PA 510	poli(amida) 510
PA 610	poli(amida) 610
PBA	poli(butilén adipato)
PBAT	poli(butilén adipato-*co*-tereftalato)

PBS	poli(butilén succinato)
PBSA	poli(butilén succinato-*co*-adipato)
PBS-*g*-MAH	poli(butilén succinato) injertado con anhídrido maleico
PBST	poli(butilén succinato-*co*-tereftalato)
PBT	poli(butilén terftalato)
PC	poli(carbonato)
PCL	poli(ε-caprolactona)
PDLA	poli(D-ácido láctico)
PDLLA	poli(DL-ácido láctico)
PE	poli(etileno)
PEEK	poli(éter-éter-cetona)
PEF	poli(etilén furanoato)
PE-*g*-GMA	poli(etileno) injertado con metacrilato de glicidilo
PE-*g*-MA	poli(etileno) injertado con anhídrido maleico
PEK	poli(eter cetona)
ΔE_{ab}*	diferencia total de color
PEO	poli(óxido de etileno)
PES	poli(etilén succinato)
PET	poli(etilén tereftalato)
PPF	harina de piel de caqui
PGA	poli(ácido glicólico)
PHAs	poli(hidroxialcanoatos)
PHB	poli(3-hidroxibutirato)
ΔH_m^0	entalpía de fusión para un polímero 100% cristalino
PHBV	poli(3-hidroxibutirato-*co*-3-hidroxivalerato)
phr	partes por cada cien de resina
PL	lignina de piña de pino
PLA	poli(ácido láctico)
PLLA	poli(L-ácido láctico)
PNCs	polímeros nanocompuestos
POE	elastómeros de poliolefina

POE-MA	poli(etileno octano) injertado con anhídrido maleico
POM	poli(oximetileno)
PP	poli(propileno)
PS	poli(estireno)
PSF	harina de cáscara de pistacho
PTMC	poli(trimetilén carbonato)
PTT	poli(trimetilén tereftalato)
PU	poli(uretano)
PVA	poli(vinil alcohol)
PVC	poli(cloruro de vinilo)
QUER	quercetina
RAF	fracción amorfa rígida
REX	extusión reactiva
RH	humedad relativa
ROP	polimerización por apertura de anillo
S	presión de saturación del vapor de agua
SA	ácido succínico
SBF	suero fetal bovino
SEBS-*g*-MA	estireno-etileno/butileno-estireno injertado con anhídrido maleico
SEM	microscopía electrónica de barrido
SKL	lignina kraft de madera blanda
STPP	tripolifosfato de sodio
T_0	temperatura cuando se pierde el 1 % de masa inicial
$T_{5\%}$	temperatura cuando se pierde el 5 % de masa inicial
tan (δ)	factor de amortiguación dinámico
T_c	temperatura de cristalización
T_d	temperatura de desnaturalización
T_{deg}, T_{max}	temperatura de degradación máxima
TEM	microscopía electrónica de transmisión
T_g	temperatura de transición vítrea

TGA	análisis termogravimétrico
T_m	temperatura de fusión
TMSPM	3-(trimetoxisilil) metacrilato de propilo
T_{onset}	temperatura de inicio de degradación
TPA	ácido tereftálico
TPS	almidón termoplástico
UV-Vis	espectroscopía ultravioleta-visible
V_0	volumen de KOH para el blanco
V_1	volumen de KOH para la titración de PBS-*g*-MAH
w	fracción de peso del polímero
W_0	peso seco inicial de la muestra
WF	harina de madera
W_f	peso final de la muestra
W_i	peso inicial de la muestra
WPC	compuestos de madera y plástico
WS	solubilidad al agua
W_t	peso seco de la muestra en un tiempo determinado
W_{te}	peso de la muestra luego de un tiempo de enterramiento
wt%, wt.%	porcentaje en peso
WVP	permeabilidad al vapor de agua
WVTR	tasa de transmisión de vapor de agua
X	peso de la muestra
x	espesor del film
X_c	grado de cristalinidad
Δ_m	incremento de peso del recipiente que contiene la muestra
ε	deformación
θ	ángulo de contacto
σ	tensión
σ_T, TS	resistencia a la tracción
σ_y	resistencia a la tracción en el límite elástico
σ_{max}	resistencia a la tracción máxima

%w/v	porcentaje peso a volumen
%w/w	porcentaje peso a peso

LISTADO DE FIGURAS

LISTADO DE TABLAS

I. INTRODUCCIÓN

I.1. Materiales poliméricos y su uso en el sector de envase-embalaje

En la actualidad los materiales poliméricos conocidos generalmente como plásticos son considerados materiales de gran valor y uso diario en la sociedad, por lo que su fabricación ha aumentado con el paso de los años, debido al desarrollo de la tecnología, así como por el incremento de la población a nivel mundial. El auge de estos materiales se dio con más fuerza a partir del año 1839 con el descubrimiento de la vulcanización del caucho y del poli(estireno). Posteriormente, en 1907 se desarrolló el primer polímero sintético conocido como bakelita, mientras que el primer polímero moderno fue el poli(cloruro de vinilo) (PVC) en 1920. Por otro lado, la producción en masa de los materiales poliméricos se dio a partir del año 1940, lo que coincide con el periodo en el que se llevó a cabo la Segunda Guerra Mundial. Una vez concluido este periodo, el uso de los plásticos continuó en aumento claro que esta vez enfocado más en el consumo de la sociedad civil [1, 2], en ámbitos como la industria tecnológica con el desarrollo de nuevos dispositivos y equipos, así como también en lo referente al cuidado de la salud, con la fabricación de equipos, herramientas, dispositivos médicos, teniendo gran acogida también en el sector automovilístico para el desarrollo de piezas y partes de los vehículos. Pero, sobre todo, su consumo masivo se encuentra en productos de uso diario como botellas, bolsas, cajas, zapatos, etc. [3].

Si bien la mayor parte de los materiales poliméricos proviene de fuentes petroquímicas su uso se ha expandido básicamente debido a sus características, entre ellas la facilidad de moldeo durante su producción, la fabricación en masa que permite disminuir los costos por volumen generado, la susceptibilidad a modificaciones en su estructura, bajo peso, buena durabilidad, además de buenas propiedades mecánicas y térmicas. Todo ello ha contribuido a que se genere un abanico de nuevas aplicaciones, lo cual los convierte en materiales competitivos en el mercado. Otras de las propiedades que caracterizan a los polímeros son su buena flexibilidad, luminosidad, estabilidad, impermeabilidad, propiedades barrera, etc. [3, 4], lo que hace que estos sean materiales atractivos para su uso en el sector envase y embalaje, así como también en otro tipo de ámbitos, entre ellos el agrícola, médico, automovilístico, e impresión 3D, etc.

Según los datos proporcionados por Plastics Europe [5], se evidencia claramente el incremento en la producción de plástico a nivel mundial, se tiene que para el año 2002

el volumen de producción fue de 200 millones de toneladas de material plástico y para el año 2020 alcanzó un valor de 367 millones de toneladas, lo que representa un incremento de cerca del 84%. Si se enfoca la producción a nivel europeo se tiene que esta constituyó cerca del 15% de la producción de plástico a nivel mundial en el año 2020, lo que evidencia el alto grado de demanda y consumo de materiales plásticos, esto indiscutiblemente conlleva a la generación de cantidades considerables de desechos.

España por su parte se encuentra dentro de los seis países con mayor demanda de plásticos en Europa que representa cerca del 70% de la demanda del mercado. Siendo los sectores de envase y embalaje, construcción y automóvil aquellos con mayor uso en el mercado con un 40,5%, 20,4% y 8,8%, respectivamente [5]. Si bien estos materiales son de uso indispensable y diario en los diferentes sectores hay que considerar que muchos de ellos se quedan en el medio ambiente sin poder ser nuevamente procesados o utilizados, este es el caso sobre todo de productos fabricados para el sector envase y embalaje que son de un solo uso. Según datos aportados por Plastics Europe [5], en el año 2020 en Europa hubo una recolección de plástico de 29 millones de toneladas, de las cuales solo cerca del 35% fue reciclado, el 42% fue utilizado como fuente de energía y alrededor del 23% se llevó a vertederos. Pero la preocupación no termina ahí, ya que los plásticos al ser materiales ligeros pueden ser transportados fácilmente, ya sea por el viento u otras condiciones ambientales y por ello no contaminan únicamente la tierra sino que inclusive pueden llegar a ríos y posteriormente a océanos, con lo cual la vida marina también se ve fuertemente afectada [6]. Estos datos nos indican evidentemente que aún queda trabajo por hacer en lo referente al tratamiento de los desechos plásticos.

Por lo tanto, si bien los plásticos han permitido el desarrollo de nuevos productos y han facilitado la vida de las personas también han traído consigo contaminación y daño al medio ambiente, sobre todo los desechos plásticos procedentes de envases y embalajes, ya que es el sector más grande del mercado con cerca de un 48% del total del volumen de materiales poliméricos producidos y, por tanto, como se indicó anteriormente es el grupo que más desperdicio genera, básicamente porque provienen de productos de un solo uso y con una vida útil muy corta. Entre los principales y más populares polímeros utilizados se encuentran el poli(etileno) (PE), poli(propileno) (PP), poli(etilén tereftalato) (PET), poli(cloruro de vinilo) (PVC) y poli(estireno) (PS) [7].

La preocupación mundial llega sobre todo por los polímeros sintéticos que tienen su origen a partir del petróleo, ya que este es un recurso no renovable y que se agotará en los próximos años. Además, su producción hoy en día genera gran cantidad de gases de efecto invernadero, lo cual está destruyendo cada vez más la capa de ozono. Adicionalmente, estos materiales en su mayoría no son biodegradables, es decir, que tras su uso serán desechos que no se pueden eliminar, lo cual genera gran cantidad de basura que contamina atmósfera, suelos, ríos, etc.

Esta problemática ha promovido la concienciación social, lo cual ha permitido abrir puertas para la búsqueda de nuevas opciones que minimicen esta contaminación y sean más respetuosas con el medio ambiente. Una de ellas ha sido la modificación de normativas ya existentes, por ejemplo, en España en el año en curso 2022, se ha actualizado la Ley 7/2022 que trata sobre residuos y suelos contaminados y en la cual se considera el ciclo de vida de los materiales, con lo que da énfasis a la economía circular, así como a un uso más consciente y eficiente de los recursos, buscando fomentar la reutilización y reciclaje de materiales. Esta es la primera vez que en la ley se hace una importante referencia al uso de plásticos, con lo cual se busca sin duda prevenir y reducir el impacto ocasionado por la gran cantidad de envases y sus residuos generados. Esta normativa, por su parte, plantea objetivos y plazos a ser alcanzados en los próximos años. Con esto se evidencia la preocupación latente sobre esta problemática, sin embargo, se debe considerar que los cambios no serán inmediatos, sino que llevará tiempo hasta que se pueda ver los resultados de su aplicación. Otra alternativa que se ha venido investigando y desarrollando con el paso de los años para reemplazar los plásticos sintéticos provenientes de la industria petroquímica es la de la obtención de materiales más respetuosos con el medio ambiente. Dentro de ellos están los biopolímeros, conocidos también como bioplásticos, estos materiales constituyen una opción prometedora, ya que pueden provenir de fuentes naturales renovables (biobasados), ser susceptibles a degradación (biodegradables) o presentar inclusive ambas características [8, 9]. Los materiales biobasados se producen a partir de la biomasa pero no necesariamente son biodegradables. Por otro lado, los materiales biodegradables pueden obtenerse a partir de fuentes renovables o no renovables como el petróleo pero son susceptibles a descomposición por la acción de microorganismos como bacterias, hongos, entre otros, en condiciones controladas y en cierto periodo de tiempo, desintegrando el polímero en pequeños fragmentos producidos por la ruptura de los

enlaces de la cadena polimérica, con lo que se genera agua, dióxido de carbono y nuevo compost, entre los principales productos [10, 11]. Por lo que, en este caso se puede indicar que su capacidad de biodegradación depende básicamente de la estructura química que tenga el material y no de su origen. Sin embargo, pese a la cada vez mayor producción de materiales biopoliméricos en el mercado estos aún representan menos del 1% de la producción total de plásticos, la cual se estimó en 367 millones de toneladas para el año 2020 [12]. Por lo tanto, aún queda un camino largo por recorrer en el desarrollo de nuevos materiales.

I.1.1. Polímeros de alto rendimiento medioambiental

Considerando los dos enfoques indicados anteriormente que comprenden origen de los materiales poliméricos, así como su capacidad de biodegradación al final del ciclo de vida, estos se pueden clasificar como se indica en la **Figura I.1**.

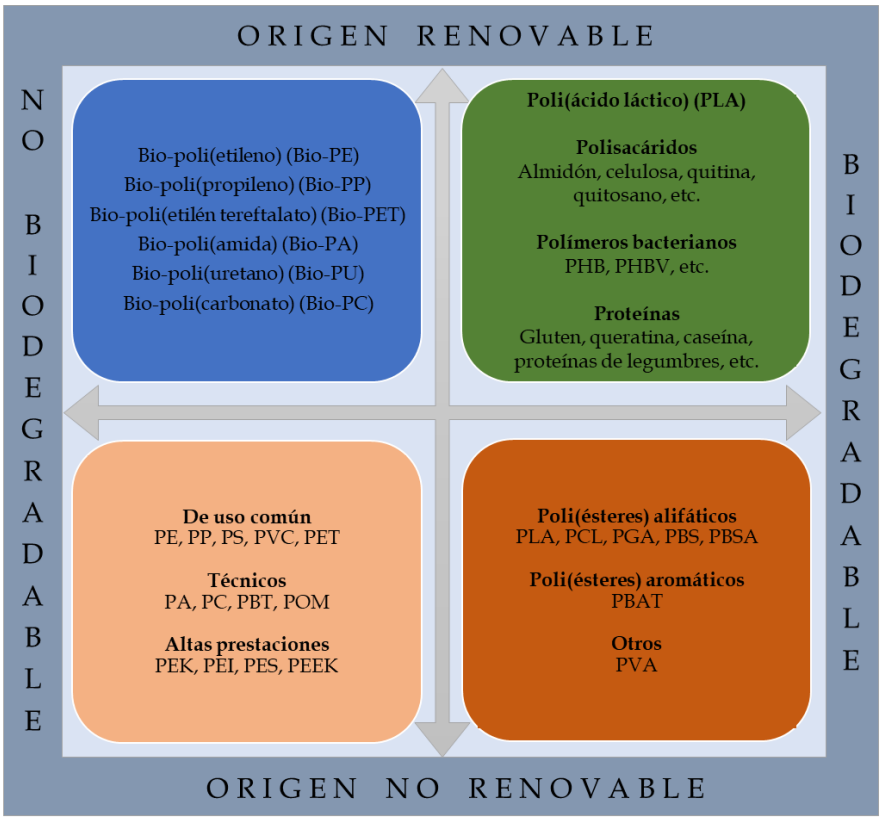

Figura I.1. Clasificación de los materiales poliméricos en función de su origen (renovable - no renovable) y su potencial biodegradación (biodegradable – no biodegradable) al final del ciclo de vida.

Mediante esta clasificación se puede distinguir cuatro grupos. Uno de ellos considera los polímeros de origen no renovable (petróleo) y que además no son biodegradables. Entre estos, se encuentran la gran mayoría de plásticos de uso diario y técnicos. Luego se tienen los tres grupos siguientes que corresponden a los biopolímeros, los cuales presentan características más respetuosas con el medio ambiente. El grupo de los biopolímeros está constituido por tres grandes subgrupos con alta eficiencia medioambiental en origen, en final de ciclo de vida, o en ambos. El primero de ellos abarca los polímeros de origen petroquímico, pero con capacidad de biodegradarse. El segundo grupo incluye los polímeros provenientes de origen renovable pero que no son susceptibles a biodegradación. Finalmente, el tercer grupo considera los materiales de origen renovable y con capacidad de biodegradarse, siendo por tanto este uno de los grupos más prometedores para su desarrollo y uso.

I.1.2. Polímero de origen no renovable y biodegradables

En esta categoría se encuentran materiales que provienen de recursos petroquímicos, pero que tienen la capacidad de desintegrarse (en condiciones de compost). Esto, sin duda, es un gran avance en el desarrollo de nuevos materiales, ya que, si bien su origen sigue siendo de una fuente no renovable como el petróleo, estos aún pueden ser aprovechados. Este grupo está constituido por poli(ésteres) con estructuras alifáticas como son la poli(ε-caprolactona) (PCL), el poli(ácido glicólico) (PGA), el poli(butilén adipato) (PBA), el poli(butilén succinato) (PBS), así como también sus copoli(ésteres) como el poli(butilén succinato-*co*-adipato) (PBSA). Por otro lado, en este grupo también se pueden encontrar copoli(ésteres) que tienen en su estructura grupos alifáticos y aromáticos. Entre ellos se encuentra el poli(butilén adipato-*co*-tereftalato) (PBAT) y el poli(butilén succinato-*co*-tereftalato) (PBST).

Dentro de este grupo se encuentran algunos polímeros que hoy en día tienen su aplicación en el ámbito médico, debido a su buena biocompatibilidad y la degradación antes mencionada. Entre ellos destaca la poli(ε-caprolactona) (PCL), el poli(ácido glicólico) (PGA), cuyas estructuras químicas se pueden observar en la **Figura I.2**. La PCL es un polímero semicristalino e hidrofóbico, cuya cristalinidad puede disminuir con el incremento del peso molecular. Tiene una temperatura de transición vítrea (T_g) de alrededor de -60 ^{o}C [13]. Por su parte el PGA se considera un polímero cristalino con

valores de cristalinidad entre 45% y 55%, con una temperatura de fusión alta (T_m) entre 220 y 225 ºC y una temperatura de transición vítrea (T_g) entre 35 y 40 ºC. Estos dos biopolímeros se usan principalmente para aplicaciones médicas, ya que además de su buena biocompatibilidad se absorben rápidamente por el organismo, por lo que se pueden usar para liberación controlada de medicamentos, en ingeniería de tejidos, huesos y para la fabricación de placas de fijación, clavos, tornillos, entre otras aplicaciones. Por otro lado, se pueden utilizar también en el sector de envase y embalaje debido a que presentan buenas propiedades barrera empleándose en aplicaciones como bolsas, películas y botellas [14, 15]. Sin embargo, la limitación que presentan estos dos materiales son su alto costo de fabricación además de la complejidad de su procesado [13].

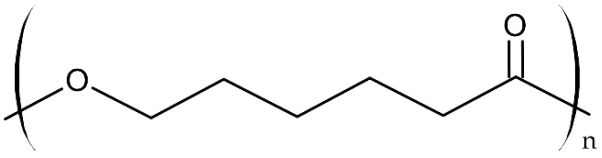

Poli(ε-caprolactona) (PCL)

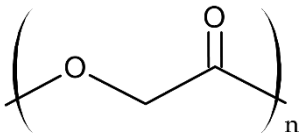

Poli(ácido glicólico) (PGA)

Figura I.2. Representación de la estructura química de poli(ésteres) alifáticos poli(ε-caprolactona) (PCL) y poli(ácido glicólico) (PGA).

Continuando con los poli(ésteres) alifáticos otro de los más empleados hoy en día es el poli(butilén succinato) (PBS). Este polímero se obtiene a partir de la reacción de policondensación del ácido succínico y 1,4-butanodiol. El ácido succínico, a su vez, se puede obtener de dos maneras: a partir de recursos no renovables (combustibles fósiles), que es el procedimiento más común y ampliamente utilizado, o a partir de recursos renovables como residuos agroforestales a los que se les somete a fermentación microbiana [16]. El PBS es un polímero semicristalino y cuenta con buenas propiedades mecánicas comparables con polímeros ampliamente utilizados como el poli(propileno). Además, que presenta una buena estabilidad térmica. Todo esto, junto con sus bajos costos de producción, lo hacen un material con buenas perspectivas en la industria [17-19]. Una de las aplicaciones en las que ya se está empleando el PBS es en el sector de

envase y embalaje, ya que al ser susceptible de biodegradación (desintegración en compost) en periodos cortos de tiempo, representa un material deseable para productos de un solo uso [17]. Por otro lado, el PBS tiene la ventaja de que mediante copolimerización con otros ácidos carboxílicos o dioles puede variar su estructura y, con ello, sus propiedades. Este es el caso del poli(butilén succinato-*co*-adipato) (PBSA), el cual se obtiene mediante copolimerización de 1,4-butanodiol con una mezcla de ácido succínico y ácido adípico, dando lugar a un material con una mayor capacidad de biodegradación [20, 21]. En la **Figura I.3**, se muestra la representación de cada uno de ellos.

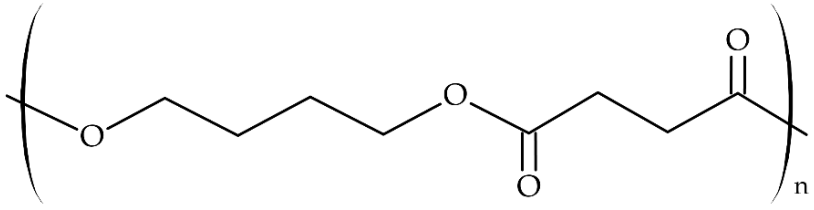

Poli(butilén succinato) (PBS)

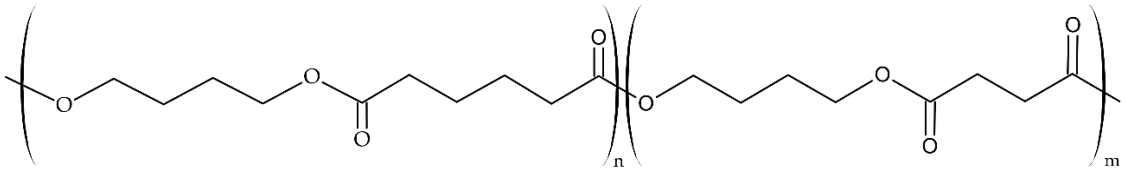

Poli(butilén succinato-*co*-adipato) (PBSA)

Figura I.3. Representación de la estructura química del poli(butilén succinato) (PBS) y poli(butilén succinato-*co*-adipato) (PBSA).

Otro polímero biodegradable con interesantes características es el copoli(éster) alifático-aromático conocido como poli(butilén adipato-*co*-tereftalato) (PBAT), cuya estructura se observa en la **Figura I.4**. Este se obtiene mediante policondensación entre 1,4-butanodiol (BDO), ácido adípico (AA) y ácido tereftálico (TPA). Este material ha ido sumando buenas expectativas debido a que su estructura cuenta con unidades alifáticas y aromáticas que le aportan buenas propiedades mecánicas como alta elongación a la rotura y flexibilidad, además de buena procesabilidad [22, 23]. Para su aplicación en el sector envase y embalaje (bolsas de basura, contenedores de comida, entre otros), comúnmente se encuentra como *blend* con PLA. De esta manera no se ve comprometida la biodegradabilidad del material resultante; además permite mejorar algunas propiedades del PLA como su fragilidad [24]. El PBAT también se utiliza en otros ámbitos como la higiene personal y biomedicina [25].

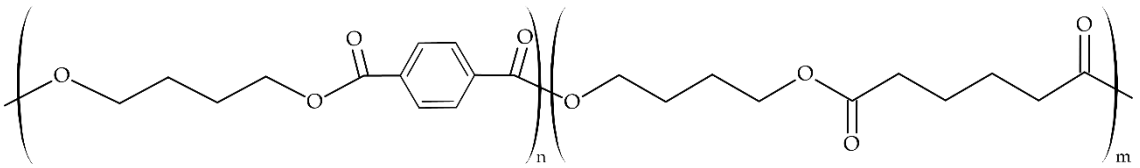

Poli(butilén adipato-*co*-tereftalato) (PBAT)

Figura I.4. Representación de la estructura química del poli(butilén adipato-*co*-tereftalato).

Los materiales antes mencionados constituyen, por tanto, una opción interesante para su aplicación en diferentes ámbitos como medicina o envase y embalaje, ya que no solo aportan buenas propiedades, sino que permiten reducir la contaminación generada por los residuos de los materiales poliméricos sintéticos al final de su ciclo de vida. Si bien estos polímeros se obtienen de fuentes no renovables, su impacto sobre el medio ambiente se ve disminuido por el hecho de ser materiales biodegradables.

I.1.3. Polímeros de origen renovable no biodegradable

En este grupo se encuentran aquellos polímeros susceptibles de obtenerse de manera parcial o total a partir de recursos renovables. Estos polímeros son químicamente idénticos a sus equivalente petroquímicos y, al igual que estos, no son susceptibles de biodegradación [26]. Una de las ventajas que presentan estos biopolímeros es el hecho de que presentan un menor impacto medio ambiental al compararlos con sus homólogos petroquímicos, ya que provienen de fuentes renovables, reduciendo así la huella de carbono. En este grupo se incluyen biopolímeros como el poli(etileno) (bio-PE), poli(amidas) (bio-PA), poli(etilén tereftalato) (bio-PET), poli(propileno) (bio-PP), poli(cloruro de vinilo) (bio-PVC), poli(uretano) (bio-PU), entre otros.

Uno de los biopolímeros más utilizados en este grupo es el conocido como el bio-poli(etileno) (bio-PE), el cual es producido a partir del etileno que se obtiene del etanol, el cual a su vez se obtiene de la fermentación de caña de azúcar, almidón de maíz y almidón de trigo. Según datos del 2021, los materiales bioplásticos estuvieron constituidos por un 64,2% de materiales biodegradables y un 35,8% de materiales biobasados y no biodegradables, de este último grupo el bio-PE fue el biopolímero que presentó una mayor producción con un total de 9,5% [12]. Por lo que, constituye una alternativa natural prometedora al poli(etileno) obtenido a parir de recursos fósiles. Su

aplicación se centra principalmente en envases rígidos y flexibles para el sector alimenticio, de bebidas, detergentes, entre otros, además de su uso para contenedores y bolsas plásticas.

El poli(propileno) (PP) es tras el poli(etileno), uno de los materiales poliméricos más utilizados. Su uso se debe a su buena resistencia y rigidez, además del buen comportamiento térmico gracias a los grupos metilo en su estructura [26]. Por ello, el interés en la obtención de bio-poli(propileno) (bio-PP) a partir de biomasa es muy relevante, ya que en principio sus propiedades serían similares al PP convencional sintético. Sin embargo, existe una limitación en su producción que surge por la escasa disponibilidad de obtener sus precursores (n-butanol o isopropanol) a partir de la biomasa.

Por otro lado, entre los materiales obtenidos de fuentes parcialmente renovables, se encuentra el bio-poli(etilén tereftalato) (bio-PET). Este se obtiene a partir de dos precursores. El primero es el etilenglicol (EG), que se obtiene del etanol extraído de la caña de azúcar y almidón. El segundo es el ácido tereftálico (TPA), que es de origen petroquímico [26]. Un aspecto importante a considerar es que el bio-PET se equipara en propiedades al PET convencional, el cual presenta buenas propiedades mecánicas. Por tanto, el ámbito de aplicación del bio-PET se encuentra también en productos textiles, envasado de alimentos, botellas, etc. [27]. Por otro lado, ya se ha desarrollado una opción completamente biobasada que se equipara químicamente y en propiedades al PET convencional, conocido como poli(etilén furanoato) (PEF), que es un poli(éster) aromático. En su obtención se sustituye el ácido tereftálico purificado (TPA) de origen petroquímico, por el ácido 2,5 furandicarboxílico (FDCA) de origen renovable. Al combinarse el FDCA con el etilenglicol (EG), también de origen renovable dan como resultado un polímero 100% biobasado [28]. Con ello, no solo se aprovechan los recursos renovables, sino que además se logra reducir la huella de carbono en el ambiente. Por su parte, este material presenta incluso mejores propiedades barrera y térmicas que el PET, lo que permite que sea un material versátil y pueda emplearse en diferentes ámbitos, entre ellos el envasado de alimentos [29].

Otro grupo interesante es el correspondiente a poli(amidas) que provienen de materias primas renovables (bio-PA). Estos biopolímeros pueden obtenerse de fuentes renovables de manera parcial (PA 610, PA 410) o total (PA 1010, PA 510). En la

actualidad, para la producción comercial de bio-poli(amidas) se utiliza el aceite de ricino, procedente principalmente de Asia y África, como fuente renovable. Las aplicaciones más relevantes de algunas bio-poli(amidas) se encuentran en el sector automoción, textil, electrónico o de construcción, además para la fabricación de envases. Adicionalmente, se han realizado estudios con el fin de obtener bio-PA a partir de azúcares. Sin embargo, debido a su alto costo de producción, no se ha logrado desarrollar en gran medida [30, 31] .

Por último, destacar el uso creciente del bio-poli(uretano) (bio-PU) que se obtiene al igual que el PU convencional mediante reacciones de polimerización entre polioles y poli-isocianato sintéticos. La diferencia radica en que el poliuretano parcialmente biobasado se obtiene utilizando polioles, obtenidos en gran medida, a partir de aceites vegetales que se extraen de semillas de plantas como ricino, algodón, palma, soja, entre otros, mientras que el isocianato en la mayoría de los casos continúa siendo obtenido de recursos fósiles [32-34]. La ventaja que presenta este material polimérico es la gran disponibilidad de aceites vegetales en la naturaleza, lo que permite tener diferentes tipos de polioles para su fabricación, con lo cual dependiendo de las características que se le quiera aportar al bio-PU, se puede seleccionar el tipo de bio-poliol a emplear [35]. A continuación, en la **Figura I.5**, se presentan las estructuras químicas de algunos de los biopolímeros mencionados anteriormente.

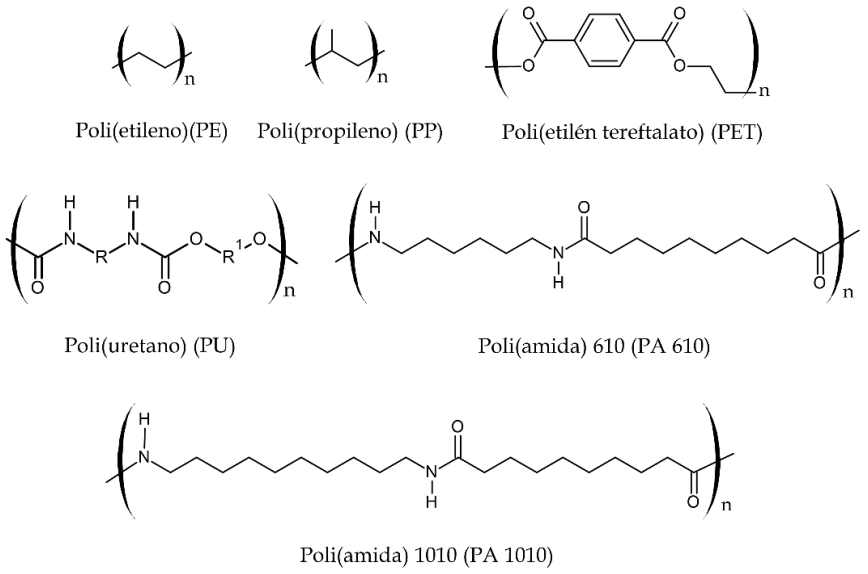

Figura I.5. Representación esquemática de las estructuras químicas de algunos biopolímeros de origen renovable no biodegradables.

I.1.4. Polímeros de origen renovable y biodegradables

Este grupo de polímeros es uno de los más prometedores, ya que se trata de polímeros obtenidos a partir de recursos naturales renovables y que a su vez pueden biodegradarse bajo condiciones contraladas de compost. Con ello se trabaja en dos frentes para la reducción del impacto medioambiental generado por los plásticos convencionales. Sin embargo, estos biopolímeros presentan algunas limitaciones en cuanto a propiedades y costos, por lo que hoy en día la investigación de estos va más allá de su obtención y, por lo tanto, se busca además su modificación y la mejora de sus propiedades. Todo esto con el fin de convertirlos en materiales con mejores prestaciones, además de un alto rendimiento medioambiental. Este tipo de polímeros han tenido gran auge y acogida sobre todo en el sector de envase y embalaje, ya que es el responsable del mayor impacto medioambiental por la gran cantidad de productos de un solo uso empleados en este sector.

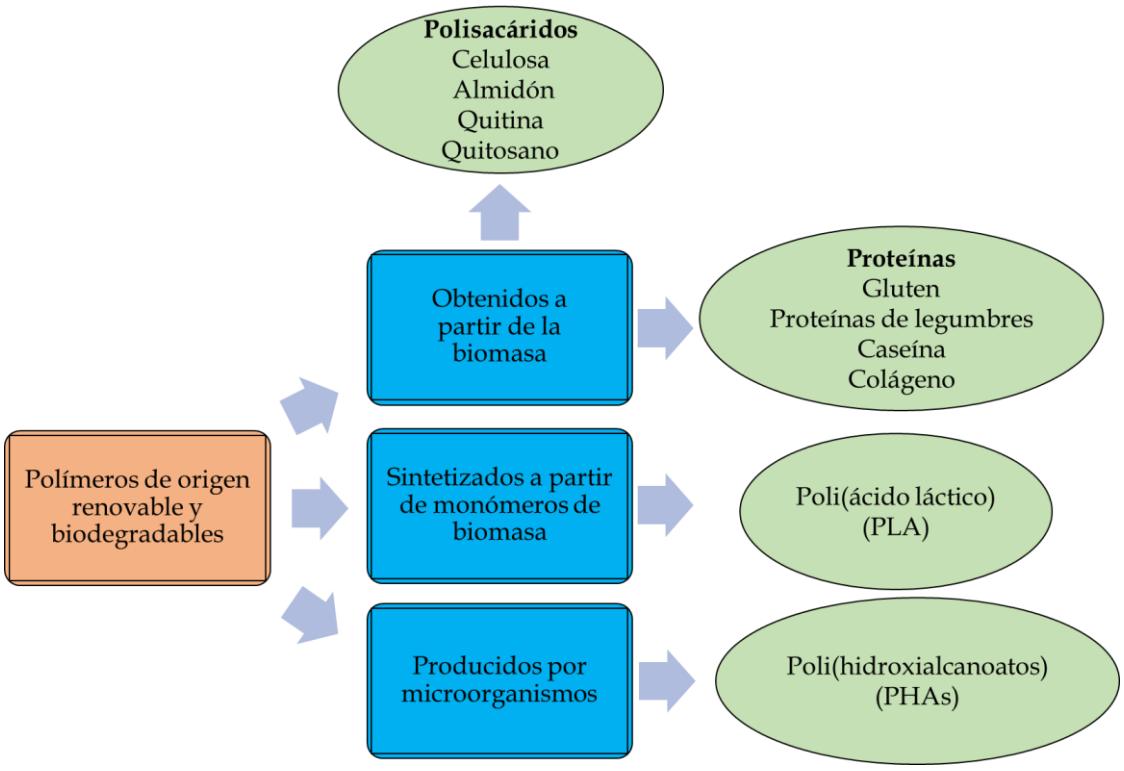

Figura I.6. Representación de la clasificación de los biopolímeros según su origen.

Según se puede observar en la **Figura I.6** se distinguen tres grandes subgrupos. El primero de ellos incluye a los polímeros que se obtienen de la biomasa como son las proteínas de origen vegetal (legumbres, trigo, gluten, entre otros) y origen animal

(gelatina, suero, caseína y queratina), así como los polisacáridos obtenidos a partir de plantas (celulosa, almidón) y los obtenidos a partir de animales (quitina, quitosano) por nombrar a los principales [36]. El segundo está constituido por aquellos polímeros que se obtienen mediante síntesis convencional a partir de monómeros obtenidos de la biomasa como es el caso del poli(ácido láctico) (PLA) derivado de la láctida (LA) obtenida por la fermentación de compuestos ricos en almidón. Finalmente, el tercer grupo está formado por polímeros que se obtienen a partir de microorganismos, entre los más conocidos están los poli(hidroxialcanoatos) (PHA) cuyo principal exponente es el poli(3-hidroxibutirato) (P3HB).

I.1.4.1. Polímeros obtenidos a partir de la biomasa

En este grupo se incluyen las proteínas y polisacáridos tanto de origen vegetal como animal. A continuación, se detallan los más representativos de cada grupo.

- Polímeros obtenidos a partir de proteínas.

Del grupo correspondiente a las proteínas vegetales, las obtenidas de legumbres constituyen el segundo subgrupo más importante y, dentro de este, el mayor representante es la proteína de soja. Ello se debe a su gran abundancia en la naturaleza, biodegradabilidad, bajo costo, entre otros [37, 38]. Este tipo de proteína se usa en gran medida para la obtención de películas y revestimientos, básicamente porque permite que estos sean flexibles, comestibles y compatibles con la comida. Además, ofrecen buenas propiedades barrera frente a gases comparadas con los lípidos o los polisacáridos. Por otro lado, no presentan buenas propiedades mecánicas o de barrera al vapor de agua, debido a su hidrofilicidad inherente. Sin embargo, para solventar estas desventajas se han desarrollados métodos de modificación, ya sea de manera superficial o en masa [38, 39].

Entre las proteínas de origen animal, la gelatina es uno de los mayores representantes. Esta proteína es soluble en agua y se obtiene a partir del colágeno. Una de sus ventajas es la posibilidad que tiene de formar geles transparentes, algo que, según su aplicación, puede ser muy requerido. La gelatina es muy similar al colágeno natural, por lo que abre su abanico de posibilidades a ser utilizado en nuevos ámbitos como la ingeniería de tejidos en el sector biomédico [40]. Por otro lado, se usa comúnmente en aplicaciones farmacéuticas y alimentarias donde ha logrado una gran visibilidad por su

posibilidad de formar películas. Entre las características más importantes se encuentran su bajo costo, biodegradabilidad, compostabilidad, entre otros [41].

- Polímeros derivados de polisacáridos.

Los polisacáridos, por su parte, constituyen la materia prima renovable más abundante [42]. Se caracterizan porque son biocompatibles, biodegradables y no presentan toxicidad. Esta última propiedad los convierte en candidatos con gran potencial para ser utilizados en ámbitos médicos y de envasado de alimentos como recubrimiento comestible, películas, envases inteligentes, entre otros. Algunas de las desventajas que presentan los polisacáridos son su baja resistencia al agua y pobres propiedades barrera frente al vapor de agua. Como en otros casos, la posibilidad de mejorar estas propiedades es viable mediante la modificación química. Además, se pueden mezclar con otros biopolímeros que permitan reforzar sus propiedades [43].

Dentro de los polisacáridos de origen vegetal destaca la celulosa, que es el polímero natural más abundante a nivel mundial. Se encuentra en plantas, bacterias, algas y algunos animales marinos como los tunicados [44]. Sin embargo, se obtiene principalmente a partir de la madera y el algodón, mientras que la pulpa de celulosa se puede obtener de subproductos agrícolas como el bagazo, tallos y pajas de cultivos [40]. La celulosa está formada por unidades de β-D-anhidroglucopiranosa unidas por enlaces glucosídicos β(1 → 4), como se muestra en la **Figura I.7**. Su uso ha crecido en gran medida debido a su disponibilidad y bajo costo, además de sus buenas propiedades mecánicas [45].

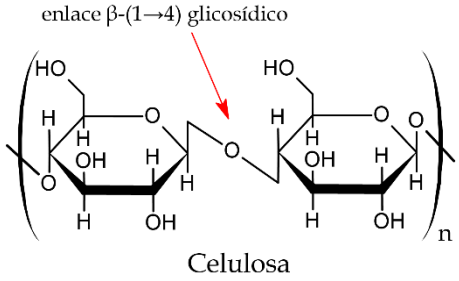

Figura I.7. Representación química de la celulosa.

En lo referente a polisacáridos de origen animal destaca la quitina y el quitosano, los cuales, además de presentar las características indicadas anteriormente, poseen una buena biocompatibilidad, no son tóxicas, y ofrecen una excelente adsorción [40]. La

quitina es considerada como el segundo polisacárido natural más abundante después de la celulosa. Se puede encontrar en el exoesqueleto de animales invertebrados como insectos y crustáceos. Además, también se localiza en diatomeas, algas, hongos y levaduras [46, 47]. Este polisacárido consiste en una cadena lineal de unidades de N-acetil-D-glucosamina que se encuentran unidas mediante enlaces glucosídicos β(1 → 4) La quitina tiene una estructura similar a la celulosa. No obstante, es un polímero altamente insoluble y con baja reactividad química [48, 49]. El quitosano por su parte es un biopolímero semicristalino obtenido a partir de la quitina mediante un proceso de desacetilación alcalina, aunque también se puede encontrar en algunos hongos. El quitosano es considerado como un material con gran potencial para distintos usos, debido básicamente a la versatilidad que presenta en propiedades biológicas, físicas y químicas [50, 51]. El campo de aplicación de estos dos biopolímeros engloba áreas como el tratamiento de agua, cosméticos, textiles, entre otros [47, 52]. En los últimos años se han explorado sus posibilidades en el campo de la biomedicina [53]. La estructura de estos biopolímeros se muestra en la **Figura I.8**.

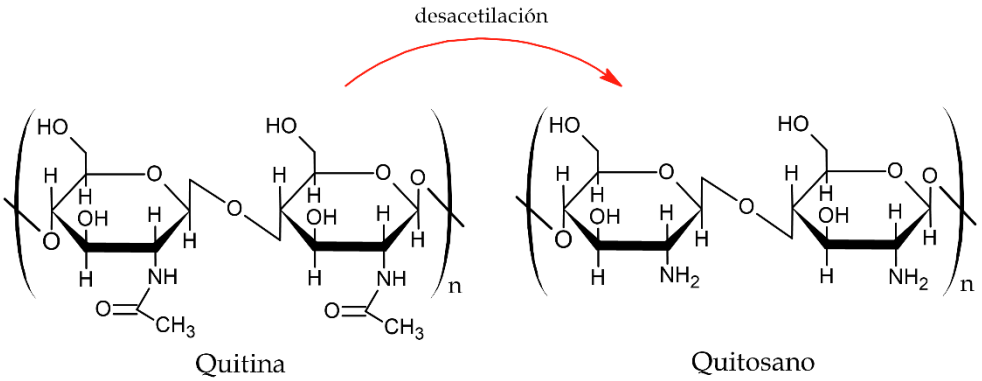

Figura I.8. Representación de la estructura química de la quitina y quitosano.

I.1.4.2. Polímeros sintetizados a partir de monómeros obtenidos de la biomasa

Otra característica interesante de la biomasa, es que no solo permite la obtención directa de biopolímeros de manera natural, sino que permite la síntesis de otros polímeros como el caso del poli(ácido láctico) (PLA) indicado en la **Figura I.9**, que es uno de los biopolímeros comerciales de mayor consumo en la actualidad.

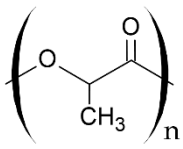

Poli(ácido láctico) (PLA)

Figura I.9. Representación esquemática del monómero del poli(ácido láctico) (PLA).

El PLA es un material termoplástico biobasado y biodegradable, de gran rigidez y transparencia similares al poli(estireno) (PS) o el poli(etilén tereftalato) (PET). Ello lo ha convertido con el paso de los años en uno de los materiales más explorados debido a sus características y costo competitivo en el mercado. La manera más común de obtenerlo es mediante polimerización por condensación directa a partir de ácido láctico, derivado de la fermentación de azúcares de carbohidratos provenientes de la caña de azúcar, maíz, patata, etc. [54]. Dentro de las características más importantes del PLA se encuentran las buenas propiedades mecánicas, térmicas, procesabilidad, además de la durabilidad y transparencia al compararse con otros polímeros biodegradables. Esta última característica lo convierte en un material idóneo para su uso en productos de envasado y embalaje que tienen un ciclo de vida corto [55]. Actualmente, ya se usa en productos como contenedores, recipientes para bebidas y ensaladas, botellas, películas flexibles para recubrimiento y blísteres, entre otros [56]. Los productos de PLA cuentan con la ventaja de que al final de su ciclo de vida se pueden biodegradar bajos condiciones de compost [54]. Por lo tanto, el desarrollo de materiales con PLA constituye una opción viable, debido a las buenas características que se logran con su fabricación, además que se aprovecha los recursos naturales renovables.

I.1.4.3. Polímeros bacterianos

En este grupo se encuentran los materiales que se producen a partir de microorganismos. Entre ellos destacan los poli(hidroxialcanoatos) (PHAs) como los más representativos debido, básicamente, a que son polímeros biodegradables que provienen de recursos renovables [57]. Los poli(hidroxialcanoatos) (PHA) son poli(ésteres) biológicos que son producidos por una amplia variedad de bacterias Gram-negativas y Gram-positivas (más de 300 identificadas hasta ahora que proceden, principalmente, de la familia *Halobactericeae*) como material de almacenamiento intracelular de carbono y energía [58, 59]. Los PHAs varían en su estructura y propiedades (flexibilidad, cristalinidad, temperatura de fusión, entre otras) de acuerdo al tipo de microorganismo

que los produce, la fuente de carbón sobre la cual las células crecen, así como la manera en que el carbón es metabolizado en las células. Además, también influye el número de átomos de carbono en las unidades monoméricas individuales y la estructura física de esos monómeros durante su incorporación en las cadenas poliméricas mediante enzimas bacterianas [57, 60].

Los PHAs incluyen un amplio grupo de polímeros y copolímeros [61]. Entre los más comerciales destaca el poli(3-hidroxibutirato) (PHB), cuyas características térmicas y mecánicas son similares al poli(propileno) (PP). El PHB es un homopolímero con una cristalinidad elevada, rigidez y fragilidad. Además, presenta alta inestabilidad a temperaturas cercanas a su punto de fusión (175 – 185 °C) [62]. Su peso molecular, al igual que el de otros tipos de PHAs, depende básicamente, de la fuente de la cual se produce, las condiciones de crecimiento y el método de extracción [59]. Otro PHA comercial es el poli(3-hidroxibutirato-*co*-3-hidroxivalerato) (PHBV) que ha reemplazado en algunas aplicaciones al PHB debido a que presenta una temperatura de fusión mayor, lo que le permite tener una ventana de procesado más amplia. Por otro lado, presenta mejores propiedades físicas, destacando una mayor flexibilidad y baja cristalinidad [63].

Estos biopolímeros se consideran como una opción viable en diferentes campos como sustitutos de los polímeros petroquímicos, elastómeros e incluso algunos polímeros de uso masivo como el poli(etileno) o el poli(propileno) [64]. Los PHA presentan una alta biodegradabilidad en diferentes ambientes. Además, cuentan con una importante biocompatibilidad, lo que permite su uso en aplicaciones médicas en ámbitos como liberación controlada de fármacos, implantes, etc. [59, 62]. Por otro lado, los PHAs pueden emplearse como películas flexibles de diferente espesor, dentro de las cuales se encuentran membranas semipermeables, filamentos, adhesivos y materiales para envasado (contenedores, botellas, y cajas) [60].

I.2. Tecnología del bio-poli(etileno) (bio-PE)

I.2.1. Obtención y estructura del bio-PE

Como se ha comentado anteriormente, en la actualidad se busca alternativas más amigables con el medio ambiente para la producción de monómeros que den paso a la obtención de polímeros. Uno de ellos es el monómero de etileno a partir del cual se

pueden obtener entre otros, poli(etileno) de origen bio. El bioetileno a su vez se fabrica a partir del bioetanol, obtenido por fermentación a partir de biomasa. En función del origen se puede producir etanol de primera generación y etanol de segunda generación. El etanol de primera generación se obtiene, básicamente, de materia prima rica en azúcares como el jugo de la caña de azúcar y almidón obtenido a partir del maíz, aunque también se puede obtener a partir de remolacha, mandioca, patata, trigo y cebada. El etanol de segunda generación se obtiene a partir de materiales lignocelulósicos o residuos de otros procesos como el bagazo, hoja de caña de azúcar, paja de trigo, residuos de madera, etc. Sin embargo, esta tecnología aún se encuentra en desarrollo y no cuenta con producción a gran escala. El proceso de obtención de etanol a partir del maíz requiere de la extracción del almidón del grano de maíz mediante trituración (seca o húmeda), seguida de hidrólisis de la glucosa y fermentación de la misma para obtener etanol. Por otro lado, la producción de etanol a partir de la caña de azúcar es un proceso más simple, ya que la sacarosa se puede obtener directamente de la trituración de la caña de azúcar, y pasa directamente a fermentación para obtener el etanol [65].

Aunque se pueda pensar que la producción de bio-PE es muy reciente, en realidad tuvo sus inicios en los años 1980s por la compañía Braskem, con la producción de bio-PE y bio-PVC a partir de bioetanol. Sin embargo, debido a las limitaciones tecnológicas y económicas no se pudo dar continuidad a su producción [66]. No fue sino hasta el 2010 cuando Braskem dio comienzo a la producción a gran escala de bio-PE [67]. Hoy en día, esta compañía con sede en São Paulo, Brasil, es considerada una de las primeras y más importantes en el desarrollo de poliolefinas biobasadas. Su alta tasa de producción ha sido posible gracias a que Brasil es el primer productor de caña de azúcar en el mundo, además de ser considerado como el segundo mayor productor de bioetanol obtenido a partir de la fermentación de la caña de azúcar. Esto a su vez dio paso a la obtención de etileno, a partir del cual se pueden obtener diferentes materiales biobasados, siendo, sin duda, uno de los mayores productos comerciales el poli(etileno) biobasado (bio-PE) también conocido como "*green PE*" [68, 69]. Sin embargo, como se ha mencionado anteriormente si bien es posible obtener bioetanol de otras fuentes, la caña de azúcar sigue ofreciendo ventajas debido a su gran disponibilidad y bajo costo, puesto que se cosecha anualmente durante al menos 4 años con una alta productividad, sin necesidad de replantar durante este ciclo [70].

El proceso para la obtención de bio-PE a partir de caña de azúcar inicia con la trituración de la misma para obtener su jugo, dando como subproducto el bagazo. A continuación, el jugo se somete a un proceso de fermentación anaeróbica para obtener el etanol también denominado bioetanol, puesto que proviene de fuentes naturales renovables. Seguidamente, el bioetanol se destila para eliminar el agua, lo que produce una solución azeotrópica de etanol hidratado al 95,5% en volumen y vinaza como subproducto. El etileno se produce por una reacción de deshidratación de etanol a temperaturas que pueden variar entre 300 °C y 600 °C, en condiciones de catálisis heterogénea. Posteriormente, se realiza la polimerización del monómero de etileno cuyo proceso es similar al que se lleva a cabo cuando se emplea etileno derivado de petróleo [67, 71]. En la **Figura I.10** se presenta un esquema del proceso de producción del bio-PE.

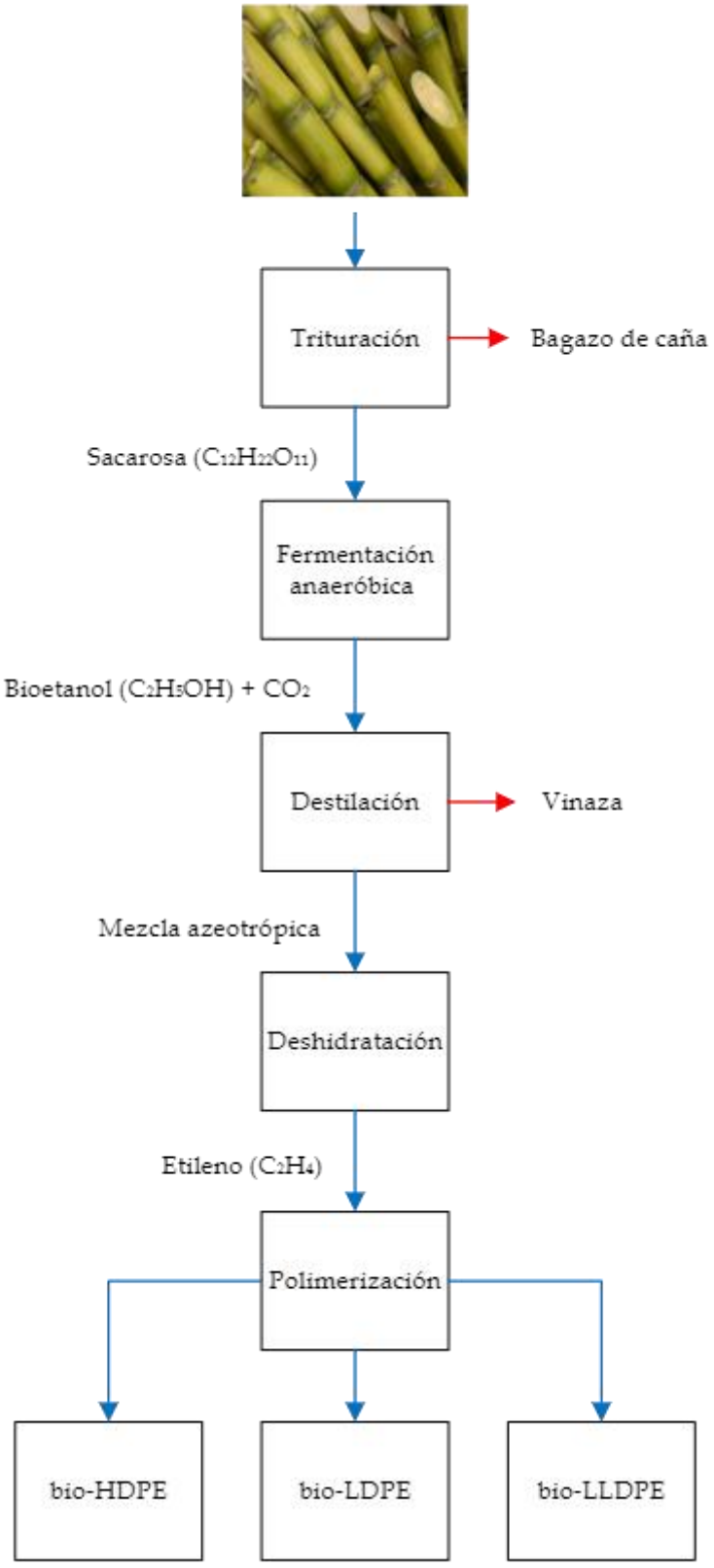

Figura I.10. Esquema general de la producción de bio-PE a partir de caña de azúcar.

Mediante el proceso indicado anteriormente es posible la obtención de diferentes tipos de bio-PE, entre ellos el bio-poli(etileno) de alta densidad (bio-HDPE), bio-poli(etileno) lineal de baja densidad (bio-LLDPE) y bio-poli(etileno) de baja densidad (bio-LDPE). El bio-HDPE, representa la mayor parte del bio-PE fabricado. Este cuenta con propiedades interesantes como alta resistencia a la temperatura, rigidez, buenas propiedades barrera, mientras que por otro lado puede ser frágil. El bio-LLDPE cuenta con buenas propiedades ópticas, buena tenacidad, sellabilidad y relativamente bajas propiedades barrera. Finalmente, el bio-LDPE presenta facilidad de procesado y buenas propiedades ópticas; sin embargo, no ofrece alta dureza [72]. La **Figura I.11** muestra de forma esquemática la estructura de las cadenas características de los diferentes tipos de bio-PE.

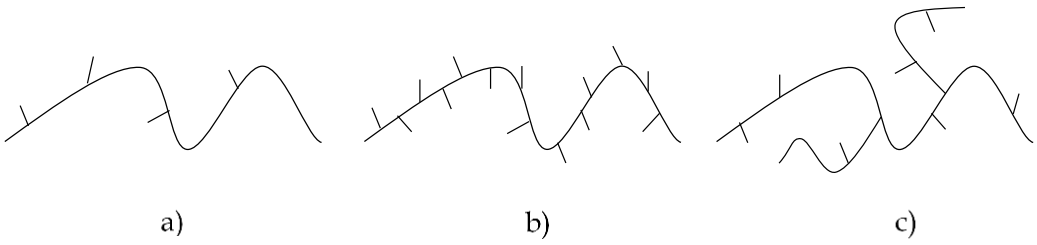

Figura I.11. Representación de la estructura de las cadenas poliméricas de a) bio-HDPE, b) bio-LLDPE y c) bio-LDPE.

Finalmente, se puede resaltar el uso de caña de azúcar como materia prima, pues contribuye a la transición hacia una economía circular, ya que esta planta tiene la capacidad de absorber CO_2 atmosférico. Posteriormente los productos fabricados con estos polímeros se degradarán o serán incinerados al final de su ciclo de vida, liberando a la atmósfera el CO_2. Sin embargo, este CO_2 a su vez, será nuevamente absorbido por las plantas, lo que permite que se cierre el ciclo, por lo que, su balance de emisión de CO_2 es prácticamente nulo. Por lo tanto, se contribuye positivamente con la reducción de los niveles de emisiones de gases de efecto invernadero [73].

I.2.2. Características del bio-poli(etileno) (bio-PE)

En lo que respecta a la industria del plástico, el poli(etileno) representa más del 30% de los plásticos comerciales a nivel mundial, siendo el poli(etileno) de alta densidad (HDPE) uno de los más usados y, por tanto, producidos en todo el mundo después del poli(cloruro de vinilo) (PVC) y del poli(propileno) (PP) [74]. Aunque, por otro lado, el

poli(etileno) de baja densidad (LDPE) también es bastante usado, sobre todo en el sector envase y embalaje debido a su buena flexibilidad. En este contexto, el desarrollo de materiales biobasados que cuenten con propiedades similares a los obtenidos mediante la industria petroquímica y que contribuyan con la reducción de la contaminación, resulta necesario. El bio-PE presenta las mismas propiedades físicas y mecánicas que el PE sintético obtenido a partir de combustibles fósiles. Entre ellas destaca sin duda la durabilidad, baja absorción de agua, buena resistencia mecánica, y alta ductilidad. Adicionalmente, presenta alta resistencia eléctrica y buenas propiedades térmicas [66, 73, 75, 76]. Es importante señalar que el procesado del bio-PE es también idéntico al del PE sintético. Por lo tanto, con el empleo de bio-PE no se requieren ajustes o nuevos equipamientos para su transformación [77, 78].

- **Propiedades térmicas**

En la **Tabla I.1** se muestra una comparativa de densidades y propiedades térmicas como son temperatura de transición vítrea (T_g), temperatura de fusión (T_m) y porcentaje de cristalinidad de los diferentes grados de PE. Dichas propiedades son de gran utilidad a la hora de trabajar con estos polímeros pues indican el rango de trabajo para su procesado y óptimo desempeño.

Tabla I.1. Comparativa de densidades y propiedades térmicas de: HDPE, LDPE Y LLDPE.

Material	Densidad (g cm^{-3})	T_g (ºC)	T_m (ºC)	Cristalinidad (%)
HDPE	0,94 – 0,97	-120 a -110	125 - 135	62 - 80
LDPE	0,91 – 0,93	-133 a -103	105 - 118	45 – 56
LLDPE	0,91 – 0,94	-120 a -80	120 - 126	45 - 62

Fuente: Menard and Menard [79] y deGroot *et al.* [80]

- **Propiedades mecánicas**

En lo referente a propiedades mecánicas, en la **Tabla I.2** se muestra la comparativa entre HDPE y bio-HDPE. Como se puede apreciar varios de los valores correspondientes al bio-HDPE se encuentran dentro del rango considerado para muestras de HDPE, lo que evidencia su similitud y posibilidad de reemplazo en los diferentes ámbitos. Las propiedades consideradas son el módulo de elasticidad (E), resistencia a la tracción (σ_M), elongación a la rotura (ε_B) y módulo de flexión (E_f).

Tabla I.2. Comparativa de propiedades mecánicas entre HDPE y bio-HDPE.

Material	E (MPa)	σ_M (MPa)	ε_B (%)	E_f (MPa)
HDPE	400 - 1500	14,5 – 38	2 –150	1200
Bio-HDPE	750 - 870	~23,8	> 500	~1078

Fuente: Balart *et al.* [81], Ku *et al.* [82], Braskem [69], Kuciel *et al.* [83].

- **Permeabilidad**

El poli(etileno), en general, presenta buena procesabilidad, además de excelentes propiedades barrera al vapor de agua, lo cual es muy requerido para los productos alimenticios sensibles a la humedad. Sin embargo, este material no es apropiado para productos alimenticios sentibles a la oxidación, debido a las bajas propiedades barrera frente al oxígeno. En la **Tabla I.3** se indican los rangos de valores de permeabilidad a gases y tasa de transmisión de vapor de agua (WVTR) que presentan el HDPE y LDPE en comparación con el poli(etilén tereftalato) (PET) que se utiliza comúnmente en aplicaciones para envase y embalaje. Como se observa, tanto el HDPE como el LDPE presentan muy buena resistencia frente al vapor de agua mientras que su tasa de permeabilidad a otros gases es bastante más elevada.

Tabla I.3. Comparativa de permeabilidad a gases y tasa de transmisión de vapor de agua de PET, HDPE y LDPE utilizados en el envasado de alimentos.

Polímero	Permeabilidad a gases a 23 ºC (nmol m^{-1} s^{-1} GPa^{-1})			WVTR (nmol día m^{-1} s^{-1})
	O_2	N_2	CO_2	
PET	10 - 18	2 – 4	30 - 50	0,4 – 0,7
HDPE	300	-	1200	0,1
LDPE	500 – 700	200 – 400	2000 - 4000	0,2 – 0,4

WVTR se mide a 90% de humedad relativa y a 38 ºC. Fuente: Kim *et al.* [84].

- **Tipos de reciclado**

Por otro lado, pese a las buenas propiedades que presenta el bio-PE y su facilidad de uso en diferentes ámbitos, al igual que el PE sintético presenta muy poca o nula biodegradabilidad [77], lo cual constituye una desventaja desde el punto de vista medioambiental. No obstante, el bio-PE al ser 100% reciclable, de alguna manera mitiga su posible impacto en el medio ambiente [69]. El reciclado del bio-PE es el mismo que se realiza para el PE sintético. Por tanto, se tienen los siguientes tipos de reciclado: el

reciclado primario, que hace referencia a residuos limpios, sin contaminar y de un solo tipo. Este es considerado el reciclado más común, ya que tiene bajo costo y es simple de realizar; solo se debe considerar la adecuada recogida y limpieza del material. También es posible llevar a cabo el reciclado secundario, mediante el cual se convierte los residuos en productos con requisitos de rendimiento menos exigentes que el de los materiales originales. Finalmente, se tiene el reciclado terciario. Este incluye el reciclado químico, que como su nombre lo indica, utiliza procesos químicos para convertir residuo en moléculas de bajo peso molecular (intermedios químicos), que pueden ser líquidos, gases, e incluso sólidos o ceras que posteriormente pueden ser utilizados como materias primas, ya sea como combustibles, productos químicos o para la fabricación de polímeros para nuevos plásticos [85, 86]. Un ejemplo de reciclado químico es el que se realiza mediante pirólisis (termólisis), en el cual los residuos plásticos se someten a altas temperaturas en presencia de un catalizador. Sin embargo, el reciclado químico no es tan ampliamente utilizado a nivel industrial, ya que requiere mucho control de los métodos que se usan y, además, es necesaria una gran cantidad de energía [85].

Pese a que el reciclaje constituye una opción viable para el tratamiento de residuos de PE, también se debe considerar que puede tener ciertas limitaciones. Por un lado, el costo de procesado. Además, la clasificación del material de acuerdo a su color o aditivos puede presentar dificultad, entre otros [87]. Por ello, otra opción con la que se cuenta además del reciclado, es la mezcla del polímero con algún otro material biodegradable que actúe como carga o relleno. De esta manera se obtienen biocompuestos, permitiendo disminuir el volumen de residuos plásticos, ya que este podría degradarse de manera parcial. Además, con esto se puede disminuir la cantidad de matriz de bio-PE necesaria para la fabricación de materiales [88].

I.2.3. Aplicaciones del bio-PE

En la actualidad la compañía Braskem así como Dow-Crystalsev ofrecen diferentes grados de bio-PE según la aplicación deseada. Como se ha indicado anteriormente, el bio-PE posee características similares al PE de origen sintético, por lo que se puede utilizar en las mismas aplicaciones. Además, debido a su versatilidad, permite la fabricación de materiales flexibles y semiflexibles entre los que destacan los productos de aseo personal, envasado y embalaje, artículos de un solo uso, debido

básicamente, a su facilidad de procesado, excelente resistencia química, alta durabilidad y baja densidad [89, 90]. Adicionalmente, su empleo se ha expandido a diferentes campos como son el cosmético, fabricación de partes de automóviles, en el sector de juguetes, así como para contenedores, tuberías, cables eléctricos, entre otros [70, 71]. Hoy en día, existen empresas que utilizan el bio-PE para la fabricación de sus productos. Destaca Danone Actimel que produce botellas para su uso en bebidas lácteas. Otra empresa que ha incursionado en este ámbito es Amcor Flexibles, que ha apostado por la producción de envases cada vez más respetuosos con el medio ambiente, entre ellos botellas para jugos de frutas. Por su parte Tetra Pak usa, actualmente, bio-PE para la producción de tapas y otras recipientes de bebidas [91].

Hoy en día con el fin de obtener cada vez materiales más respetuosos con el medio ambiente se ha visto la posibilidad de combinar bio-PE con materiales biodegradables como fibras naturales, harinas, entre otros, que actúan como refuerzos o rellenos. Estos, además de proporcionar mayor degradabilidad al material, aportan propiedades como baja densidad, lo cual contribuye a la reducción de peso del producto [92]. Estos biocompuestos han encontrado gran aplicación en la industria del automóvil, en donde el peso de las piezas utilizadas es un factor determinante. Actualmente, se persigue la posibilidad de reemplazar las fibras sintéticas por fibras naturales, claro que estas también pueden presentar ciertas limitaciones, sobre todo en la temperatura de procesado, además de incompatibilidad de las fibras (hidrofílicas) con las matrices poliméricas (hidrofóbicas) [93].

Finalmente, se puede indicar que a la par de las aplicaciones ya consolidadas de bio-PE en el mercado, se continúan desarrollando otras alternativas que se consideren viables para el uso de este biopolímero. Torres-Giner *et al.* [94], consideran la adición de zeolitas del tipo chabasita a una matriz de bio-HDPE. Las piezas obtenidas mediante extrusión y posterior inyección, ofrecieron propiedades mejoradas respecto al bio-HDPE virgen en cuanto a rigidez y dureza, además de buena protección antimicrobiana. Estos resultados, por tanto, indican su posible uso en aplicaciones como envases rígidos, cubiertos, muebles de cocina y, en general, superficies en las que se requiera evitar la proliferación de microorganismos. Por otro lado, Mazur *et al.* [75], han estudiado la adición de fibras naturales de basalto en una matriz de bio-HDPE. Los compuestos obtenidos presentaron una mejora en propiedades mecánicas del material resultante, con posibles aplicaciones en el sector del automóvil, deporte, calzado, entre otros.

I.3. Tecnología de poli(ésteres)

La familia de poli(ésteres) comprende todos los polímeros con grupos funcionales éster en su estructura, la cual se muestra en la **Figura I.12.** Los grupos éster se pueden combinar de muchas maneras, dando como resultado un grupo amplio de polímeros que se pueden utilizar en diferentes ámbitos debido a la variedad de sus características. Los poli(ésteres) fueron de los primeros polímeros obtenidos por vía sintética, y han tenido un gran auge en el sector industrial a lo largo de los años.

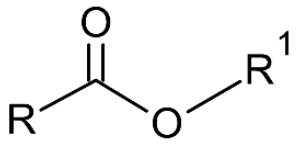

Figura I.12. Representación esquemática de la estructura del grupo éster.

Los poli(ésteres) se clasifican en dos grupos según el tipo de cadena: alifáticos y aromáticos. Los alifáticos más utilizados hoy en día son PLA, PCL, PBS, mientras que en los aromáticos destaca el PET. Los poli(ésteres) alifáticos han ganado gran relevancia dentro de esta familia, debido a que muchos de ellos presentan buenas características de biocompatibilidad, biodegradabilidad. Además, algunos se pueden obtener a partir de materias primas renovables y otros pueden ser, incluso, reciclados [95].

La síntesis de los poli(ésteres) alifáticos se da mediante polimerización por condensación en la que se da la reacción de un diol como el 1,2-etanodiol, 1,3-propanodiol o el 1,4-butanodiol con un ácido dicarboxílico como el ácido adípico, sebácico o succínico o mediante la condensación de un hidroxiácido. Las dos reacciones producen la eliminación de equivalentes estequiométricos de agua [96, 97]. Pese a que el proceso de polimerización por condensación promueve una importante ruta para poli(ésteres), la técnica más utilizada en poli(ésteres) como el PLA y PGA, es la polimerización por apertura de anillo de lactida o glicolida, respectivamente, ya que esta permite controlar de mejor manera el índice de polidispersión, propiedades físicas y, además, permite la obtención de polímeros con pesos moleculares más elevados [95].

Por su parte, los poli(ésteres) alifáticos, como el PLA, son más susceptibles a la biodegradación, ya que cuentan en su estructura con enlaces éster hidrolíticamente lábiles, y poseen segmentos de metilo cortos entre los enlaces éster. La degradación se

lleva a cabo mediante la acción de agua que rompe los enlaces éster de la cadena. Otra manera de biodegradación es mediante la acción enzimática, y también mediante la combinación de estos dos. La propiedad de biodegradabilidad de algunos poli(ésteres) ha permitido que sean considerados para aplicaciones donde no solo se busquen sus prestaciones, sino que además puedan contribuir a la protección del medio ambiente, por ejemplo, en el sector del envase y embalaje, en materiales de uso desechable y para películas de uso agrícola [98].

Los poli(ésteres) aromáticos, por su parte, son más difíciles de degradar, ya que minimizan la inestabilidad hidrolítica del grupo éster en la cadena del polímero, a través de la estructura con anillos aromáticos [98]. Este es el caso de poli(ésteres) aromáticos puros como el poli(etilén tereftalato) (PET) o el poli(butilén tereftalato) (PBT), que son prácticamente insensibles a cualquier tipo de degradación hidrolítica. Además, no son susceptibles al ataque microbiano o enzimático. Por ello, con el fin de incrementar su susceptibilidad hidrolítica se han combinado con algunos componentes alifáticos en su estructura, obteniéndose por tanto copoli(ésteres) alifáticos-aromáticos que permiten una mayor degradación del material [99]. Por otro lado, con el fin de darles un nuevo uso a los poli(ésteres) aromáticos, se ha propuesto el reciclado, sometiendo al residuo de PET a condiciones químicas extremas, como por ejemplo con el uso de ácido sulfúrico a 150 °C [99]. De esta manera, si bien no se elimina por completo la contaminación que producen estos materiales, se puede minimizar su efecto.

Una limitación que presentan los poli(ésteres) alifáticos es su alto costo al compararlos con otros materiales como el poli(etileno). Sin embargo, en la actualidad ya se han desarrollado materiales mezclados con rellenos/cargas que, de alguna manera, permitan mantener propiedades, pero abaratan notablemente los costos. Entre los rellenos más comunes se encuentran los derivados de recursos naturales como el almidón, gluten, trigo, entre otros. Por otro lado, estas mezclas de materiales están sujetas a una baja compatibilidad, lo que genera una importante pérdida de ciertas propiedades, entre ellas las mecánicas [98]. Por ello, esta mezcla debe incluir agentes compatibilizantes que permitan la mejora de estas interacciones, y no comprometan propiedades físicas ni mecánicas. En la **Tabla I.4** se presenta una comparativa de propiedades entre los poli(ésteres) aromáticos y alifáticos más representativos y usados comercialmente.

Tabla I.4. Comparativa de propiedades térmicas y mecánicas de algunos poli(ésteres) aromáticos y alifáticos.

Propiedad	Aromático	Alifático	Alifático	Alifático-aromático
	PET	**PLA**	**PBS**	**PBAT**
Densidad (g cm^{-3})	1,35–1,40	1,24-1,26	1,26	1,26-1,27
Módulo de Young (MPa)	2800-3170	2200-3145	470-540	96-120
Resistencia a la tracción (MPa)	57-86	43-70	28-35	≥25
Alargamiento a la rotura (%)	15-20	20-30	560-710	350-550
Temperatura de fusión (ºC)	225-255	130-230	115-120	60-120
Temperatura de transición vítrea (ºC)	70-80	57-62	-32 a -16	-45 a -32

Fuente: Carbonell-Verdu *et al.* [100], Shibata *et al.* [101], Arruda *et al.* [102].

Otra manera de clasificar a los poli(ésteres) es considerando su origen, lo que lleva a definir dos grupos, aquellos provenientes de recursos fósiles y los que se pueden obtener a partir de fuentes naturales renovables, a continuación, se amplía más esta información.

I.3.1.1. Poli(ésteres) de origen petroquímico

Desde hace muchos años los materiales obtenidos a partir del petróleo han tenido gran acogida y demanda, principalmente debido a sus buenas propiedades que permiten su uso en diferentes aplicaciones. Algunos de los poli(ésteres) como el poli(etilén tereftalato) (PET) o el poli(butilén tereftalato) (PBT) han sido los que más auge han tenido pues su producción y uso lleva alrededor de 50 años [103]. En los últimos años se ha desarrollado la tecnología de otro polímero, de menos consumo, pero que presenta buenas propiedades de tenacidad, como es el poli(trimetilén tereftalato) (PTT).

Los poli(ésteres) aromáticos obtenidos a partir del petróleo presentan propiedades como estabilidad química, y no se degradan. Entre los más representativos se encuentra el PET. Su aplicación ha tenido gran auge en ámbitos como la industria de bebidas carbonatadas con la producción de botellas para su uso. También se utiliza como fibra, y en el ámbito médico como material para prótesis [98]. Sin embargo, pese a que el PET tiene una gran demanda, sigue siendo un material que genera mucho residuo que no se puede eliminar. Por otro lado, los poli(ésteres) alifáticos son más susceptibles a la biodegradación, ya que sus grupos éster pueden ser hidrolizados, lo cual facilita la

desintegración en condiciones de compost, donde la humedad debe ser controlada. Uno de estos poli(ésteres) que está teniendo gran aceptación es el poli(butilén succinato) (PBS), que en la actualidad, se usa en ámbitos como la agricultura, ingeniería civil y el sector envase y embalaje.

I.3.1.2. Poli(ésteres) de origen renovable

En lo que respecta a los poli(ésteres) obtenidos a partir de recursos renovables, estos constituyen una alternativa viable al uso de polímeros obtenidos a partir de petróleo. Dentro de este grupo destaca el PLA, que es un poli(éster) alifático que se puede obtener en su totalidad a partir de fuentes naturales renovables y, además, es biodegradable. Su uso se ha visto incrementado debido, básicamente, a su buena connotación medioambiental, ya que es reciclable y compostable. Sin embargo, sus propiedades se ven limitadas debido a la degradación térmica e hidrolítica que puede sufrir durante su procesado. La presencia de humedad durante el procesado puede ocasionar hidrólisis de sus cadenas poliméricas, lo cual produce una reducción del peso molecular del polímero [104]. Es por ello que muchas veces se utiliza en ámbitos donde no se requiere un alto rendimiento, como es el caso de bolsas de plástico, embalaje para alimentos, envases desechables, contenedores de bebidas, entre otros [37, 61, 105].

I.3.2. Tecnología del poli(butilén succinato) (PBS)

I.3.2.1. Obtención y estructura del poli(butilén succinato)

La producción del poli(butilén succinato) (PBS), se lleva a cabo mediante policondensación de dos monómeros, el ácido succínico y el 1,4-butanodiol. Estos monómeros se obtienen generalmente, a partir de recursos no renovables (petróleo). En la actualidad existen ya algunas empresas que obtienen ácido succínico biobasado de manera comercial [106]. Una de ellas es Showa Highpolymer, que produce PBS comercialmente conocido con el nombre de "Bionolle", siendo este uno de los grandes precursores para el desarrollo de productos poliméricos biodegradables. Su producción inicia a partir de 1989, debido sobre todo a la preocupación medioambiental por la gran cantidad de residuos plásticos generados, aunque no fue hasta 1993 cuando la empresa comenzó la producción a gran escala. En términos generales, Bionolle es un poli(éster) alifático que se puede encontrar en dos grados: el poli(butilén succinato) (PBS) y el

poli(butilén succinato-*co*-adipato) (PBSA) [106]. Bionolle presenta una gran variedad de pesos moleculares y aditivos que permiten su uso en diferentes sectores.

La síntesis de PBS se puede separar en dos pasos como se muestra en la **Figura I.13.** El primero es posible llevarlo a cabo de dos maneras: a) esterificación del ácido succínico (SA) y 1,4-butanodiol (BDO) o b) la transesterificación de succinato de dimetilo y 1,4-butanodiol (BDO) para obtener oligómeros, siendo la esterificación (a) la más comúnmente utilizada. El segundo paso es la policondensación de los oligómeros para eliminar BDO y formar PBS de peso molecular alto. Para evitar la oxidación, es necesario utilizar atmósfera de nitrógeno a lo largo de todo el proceso [21, 107]. Para la síntesis se utilizan diferentes catalizadores como el isopropóxido de titanio (IV), isobutóxido de titanio (IV) o el n-butóxido de titanio (IV) [108].

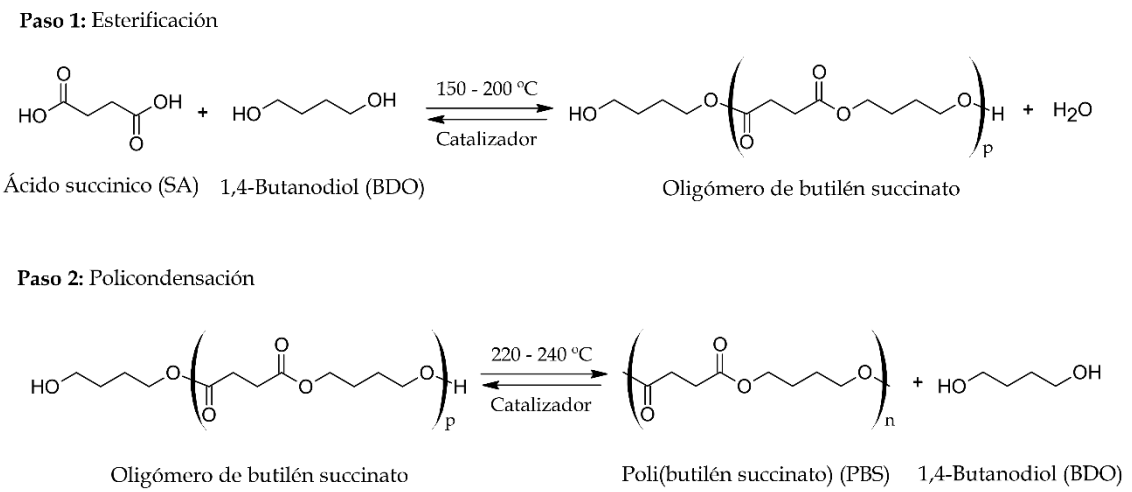

Figura I.13. Representación esquemática de la síntesis de poli(butilén succinato) (PBS).

Otra manera de obtener PBS es mediante polimerización por condensación seguido de extensión de cadena, con el fin de incrementar el peso molecular del PBS. La diferencia con el método de condensación es que este proceso añade un paso más para agregar una extensión de cadena con dos grupos funcionales que pueden reaccionar con los grupos terminales -OH o -COOH del PBS, cuyo objetivo es que se unan dos cadenas de PBS. La desventaja que presenta este método es que, al agregar los extensores, se puede afectar la biodegradabilidad del PBS. En consecuencia, el PBS obtenido por este método no se puede utilizar en aplicaciones alimenticias, ni médicas [107].

Como se ha indicado anteriormente, el PBS se obtiene a partir de monómeros derivados de petróleo. Sin embargo, en la actualidad es posible sintetizarlo a partir de

monómeros obtenidos de fuentes naturales renovables. Showa Highpolymer, empresa que ha incursionado desde el inicio en su producción, ha desarrollado un PBS a partir de recursos renovables (glucosa, almidón, etc.), en la **Figura I.14** se puede observar cómo es posible la obtención tanto de ácido succínico como butanodiol a partir de estos recursos. La desventaja que presenta este proceso es que requiere largos tiempos de fermentación, grandes cantidades de agua y el tratamiento de las aguas residuales del proceso. Además, la separación y purificación del producto final es algo más complicada. Finalmente, la obtención de poli(ésteres) alifáticos de alto peso molecular todavía presenta dificultades debido a su baja estabilidad térmica [107, 108].

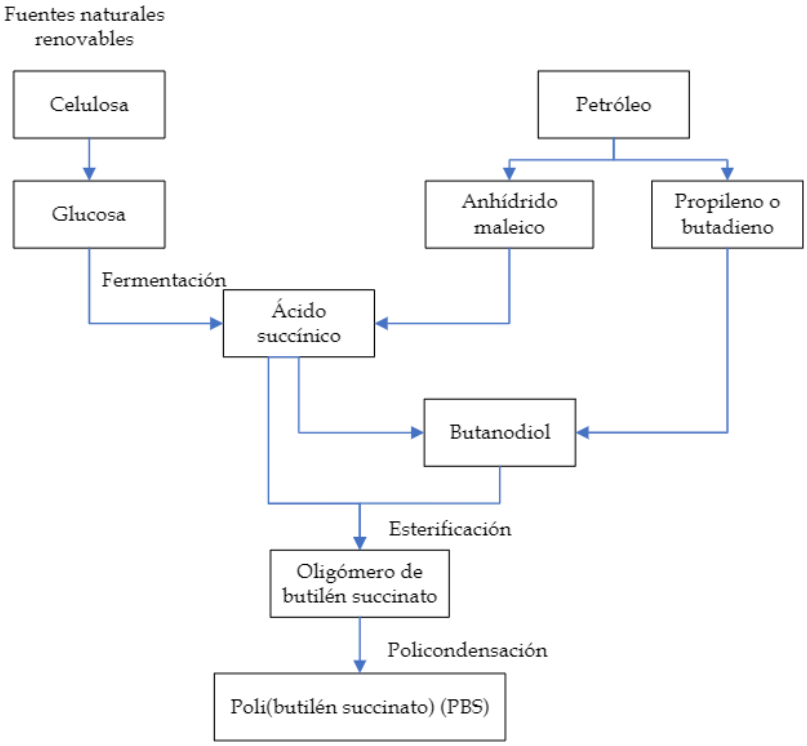

Figura I.14. Representación esquemática del proceso de obtención de monómeros para la síntesis de PBS.

I.3.2.2. Características del poli(butilén succinato) (PBS)

El PBS es un poli(éster) semicristalino con un punto de fusión alrededor de 115 ºC, lo cual es importante para aplicaciones en las que se requieran altos rangos de temperatura. En lo que respecta a la resistencia a la tracción de muestras no orientadas, alcanza valores entre 30 y 35 MPa, lo cual es comparable con el poli(propileno). El PBS es flexible y presenta un módulo de Young en el rango de 300 – 500 MPa, cuyos valores ya dependen del grado de cristalinidad (X_c) que tenga el polímero. Si el material presenta

una X_c alta, su resistencia a la tracción es elevada, mientras que la elongación a la rotura será baja [21].

El PBS con peso molecular menor a 100.000 (M_w) puede ser extruido e inyectado. Sin embargo, el material es frágil, la elongación a la rotura puede ser de solo 10%. Por otro lado, el PBS con pesos moleculares mayores a 180.000 (M_w) resulta ser un material más dúctil, y puede ser procesado incluso mediante soplado; además la elongación a la rotura puede alcanzar alrededor del 270%. Con esto, se incide en la importancia de obtener polímeros con alto peso molecular, por lo que se han desarrollado algunos métodos para ello. El primero de estos es la extensión de cadena mediante el uso de PBS con hexametilen diisocianato o bisoxazolina, biscaprolactamato de adipoílo o biscaprolactamato de tereftaloílo, que acopla dos cadenas de PBS para mejorar el peso molecular del producto final. La segunda manera es obedeciendo estrictamente la estequiometría 1:1 del ácido dibásico y el glicol y, en tercer lugar, eliminar el subproducto de peso molecular bajo de la esterificación de la mezcla para desplazar el equilibrio hacia el lado de un poli(éster) de peso molecular elevado [21].

- **Propiedades mecánicas**

En la **Tabla I.5** se muestra una comparativa de propiedades mecánicas del PBS (Bionolle) #1000 y PBSA (Bionolle) #3000 con algunos polímeros utilizados para productos de uso común como son el poli(etileno) de alta densidad (HDPE), poli(etileno) de baja densidad (LDPE) y poli(propileno) (PP).

Tabla I.5. Comparativa de propiedades mecánicas de poli(ésteres) alifáticos con polímeros de uso común.

Propiedades	Unidad	PBS (Bionolle) #1000	PBSA (Bionolle) #3000	HDPE	LDPE	PP
Resistencia a la tracción	MPa	34	19	25-28	10-18	33
Módulo de Young	MPa	470-540	320-340	400-1500	330-370	545
Alargamiento a la rotura	%	560	807	>590	>300	>200
Resistencia al impacto	kJ m^{-1}	300	>400	30-71	>400	20
Densidad	g cm^{-3}	1,26	1,23	0,94-0,97	0,91-0,93	0,90

Fuente: Xu and Guo [21], Shebani *et al.* [109], Shubhra *et al.* [110].

Es importante mencionar que mediante copolimerización con otros ácidos dicarboxílicos o dioles, se pueden ajustar las propiedades del PBS, lo cual permite que su empleo en diferentes aplicaciones. El proceso de copolimerización produce ciertas modificaciones en su comportamiento, como una disminución en el punto de fusión, el grado de cristalinidad y resistencia a la tracción. Sin embargo, otras propiedades se pueden ver beneficiadas con esta unión, como por ejemplo la elongación a la rotura, que experimenta un incremento, al igual que la resistencia al impacto. Para garantizar que los copolímeros de PBS tengan su punto de fusión entorno los 100 ºC el contenido de unidades de comonómero debe ser inferior al 15% [21].

- **Propiedades térmicas**

En lo referente a propiedades térmicas, el PBS tiene un punto de fusión entre 112 – 116 ºC, el cual depende del peso molecular y la historia térmica del material. La cristalización en frío aparece en las muestras de PBS cristalizadas a bajas temperaturas, entre 60 y 90 ºC. Además, el PBS muestra degradación térmica a partir de 200 ºC. Por su parte, las propiedades térmicas de los copolímeros de PBS dependen de la composición, ya que tanto el grado de cristalinidad como la temperatura de fusión disminuyen con el incremento del contenido de monómero. En lo que respecta a la temperatura de transición vítrea (T_g), esta puede cambiar su valor según el monómero agregado y su

estructura química [107]. En la **Tabla I.6** se resumen algunas de las propiedades térmicas del PBS y algunos polímeros de uso común.

Tabla I.6. Comparación de las principales propiedades térmicas del PBS con polímeros de uso común.

Propiedades	Unidad	PBS (Bionolle) #1000	PBSA (Bionolle) #3000	HDPE	LDPE	PP
Temperatura de transición vítrea (T_g)	^oC	-32	-45	-120	-120	-5
Temperatura de fusión (T_m)	^oC	114	96	125 - 135	110	163
Grado de cristalinidad (X_c)	%	35-45	20-35	69	49	56

Fuente: Xu and Guo [21].

- **Biodegradación**

Una de las mayores ventajas que ofrece el PBS es su bajo impacto medioambiental, ya que se puede degradar mediante la acción de enzimas y microorganismos, ya sea en agua y dióxido de carbono si el ambiente es aeróbico, o en dióxido de carbono y metano si el ambiente es anaeróbico. Entre los factores que pueden afectar la velocidad de degradación del polímero están su composición, el peso molecular y su distribución, así como también el grado de cristalinidad, el ambiente en que se lleve a cabo la biodegradación y en qué tipo de medio se realice. La biodegradabilidad de los copolímeros de PBS depende de la composición del copolímero. Diversos estudios demuestran que la mayor parte de biodegradabilidad sucede cuando el contenido de monómero se encuentra entre 30 y 50 mol%, lo cual puede estar relacionado con el bajo grado de cristalinidad que presentaría dicho material. La biodegradación del PBS puede darse mediante degradación enzimática o degradación hidrolítica en diferentes ambientes como agua, tierra enterrada, lodos activados y compost, siendo este último el más utilizado [107, 111].

La degradación enzimática se lleva a cabo por la acción de enzimas (excretadas por los microorganismos), que se encargan de atacar el polímero de manera superficial, fragmentando las cadenas poliméricas en oligómeros o monómeros de bajo peso molecular. De esta manera, es más fácil que los microorganismos puedan asimilarlos

como fuentes de carbono para, posteriormente, metabolizarlos y convertirlos en agua o dióxido de carbono. Por su parte la degradación hidrolítica se encarga de fragmentar las cadenas poliméricas por la acción del agua. En el caso de poli(ésteres) alifáticos como el PBS estos cuentan con grupos éster altamente hidrolizables con la acción del agua. Por tanto, este método es uno de los más utilizados para descomponer al PBS. El procedimiento de degradación tiene el mismo principio que el que se indicó para enzimas, solo que en este caso es el agua la que se encarga de fragmentar las cadenas poliméricas en oligómeros o monómeros de menor peso molecular que, posteriormente, serán incorporados a los microorganismos que los transforman en agua y dióxido de carbono. Generalmente, este procedimiento se lleva a cabo en condiciones de compost. Las condiciones de procesado, así como la composición del compost se especifican en la norma UNE-EN-ISO-20200. Es importante tener en cuenta que la degradación se puede ver afectada por el tipo de microorganismos (bacterias Gram-positivas y Gram-negativas, mohos, entre otros), nutrientes, temperatura y humedad [106]. La **Figura I.15** muestra una representación del proceso de degradación en PBS (Bionolle).

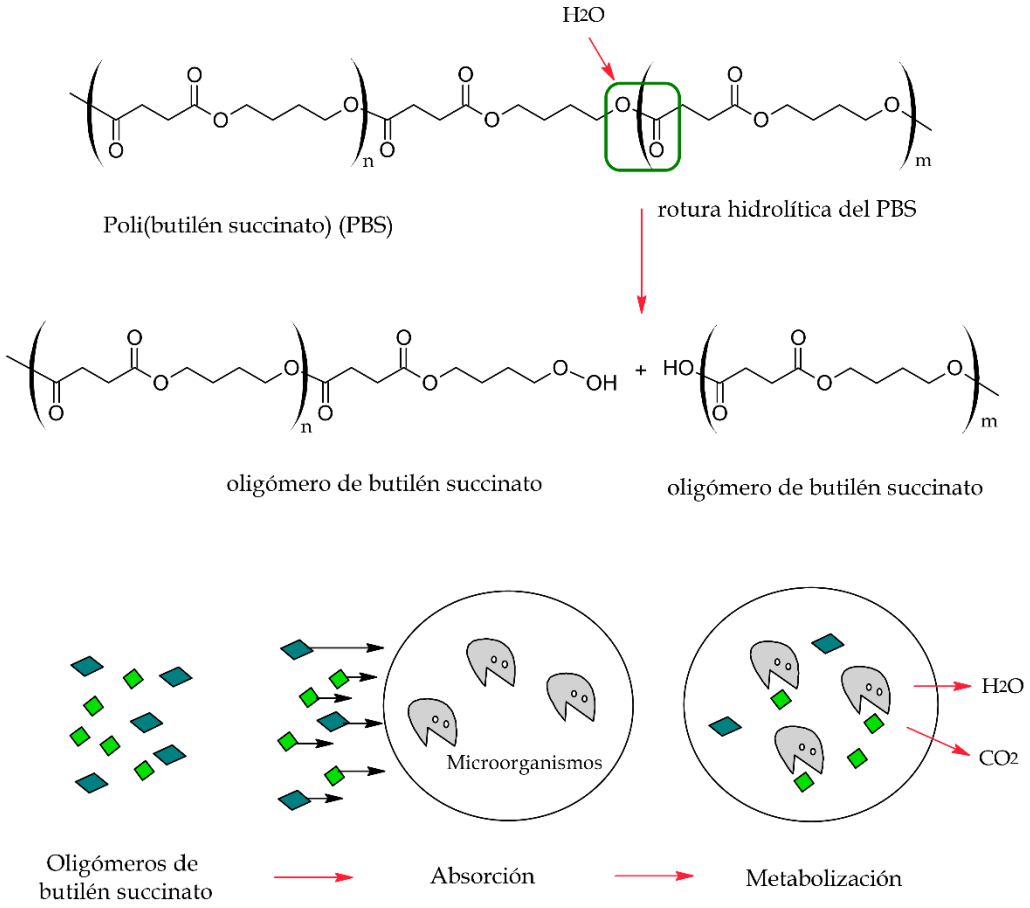

Figura I.15. Representación esquemática del mecanismo de biodegradación hidrolítica del PBS.

El PBS y sus copolímeros pueden degradarse en diferentes ambientes. Esta degradación dependerá tanto de las propiedades propias del poli(éster), como de las condiciones medioambientales (microorganismos, temperatura, humedad, etc.). En la **Tabla I.7** se muestra cómo se desarrolla el proceso de biodegradación del PBS y PBSA en diferentes ambientes. Como se observa el PBSA presenta mayor rapidez en prácticamente todos los ambientes considerados.

Tabla I.7. Comparativa entre poli(ésteres) (Bionolle) y la rapidez de biodegradación en diferentes ambientes.

Pruebas de biodegradabilidad	Poli(butilén succinato) (PBS)	Poli(butilén succinato-*co*-adipato) (PBSA)
En compost caliente	Normal	Rápido
En tierra húmeda	Normal	Rápido
En el mar	Lento	Rápido
En agua con lodos activados	Lento	Lento

Fuente: Xu and Guo [107].

I.3.2.3. Aplicaciones del poli(butilén succinato) (PBS)

El PBS y sus copolímeros encuentran aplicaciones en productos como bolsas plásticas, películas envasado, películas para su uso en la agricultura, así como en productos desechables. En grado comercial Bionolle cuenta con una amplia gama de aplicaciones, entre ellas películas, hojas, filamentos, no tejidos, laminados, productos de inyección por moldeo, que se pueden usar en ámbitos como la agricultura, ingeniería civil, así como en campos donde la recuperación o reciclaje no sea posible [106, 107].

Vytejčková *et al.* [112], proponen el uso de PBS y PBSA a partir de fuentes renovables con el fin de obtener películas para recubrir carne de aves. Su trabajo demuestra que, si bien existían diferencias con respecto a las propiedades físicas, químicas y mecánicas de películas de ácido poliláctico/poli(etileno) (PLA/PE), estas diferencias no fueron significativas y no afectaron los alimentos analizados. Por otra parte, Bhatia *et al.* [113], desarrollaron una mezcla de PLA con PBS en diferentes proporciones, con ello se consiguió un buen equilibrio de las propiedades de cada uno de los biopolímeros, fundamentalmente con resistencia al impacto mejorada.

Otra aplicación interesante del PBS es en el campo de los compuestos ecológicos también conocidos como "*green composites*", que se pueden definir como aquellos compuestos que obtienen a partir de una matriz polimérica en combinación con fibras naturales (sisal, cáñamo, coco, bagazo, etc.) o harinas de origen natural (trigo, maíz, madera, cascarilla de arroz, etc.). Con ello se consigue abaratar costos, ya que el PBS tiene un costo elevado comparado con los plásticos de uso común. Por otro lado, también permite la modificación o refuerzo de la matriz polimérica con la posibilidad de que el compuesto obtenido se pueda emplear en otros campos, como películas para envasado, para agricultura, bolsas de compost, productos desechables, etc. [114]. Merece la pena destacar algunas investigaciones que han considerado la adición de harinas de cáscara de almendra [115], de trigo [116], de maíz [117] en la matriz de PBS. La dificultad que presentan estos materiales es la falta de compatibilidad, por lo que también se requiere el uso de compatibilizantes para mejorar su interacción y, con ello, sus propiedades.

I.3.3. Tecnología del poli(ácido láctico) (PLA)

I.3.3.1. Obtención y estructura del poli(ácido láctico) (PLA)

El PLA es un poli(éster) termoplástico alifático lineal que se obtiene a partir del monómero de ácido láctico. El ácido láctico puede obtenerse mediante síntesis química de derivados de petróleo, o mediante fermentación de carbohidratos obtenidos de fuentes naturales renovables como el almidón de maíz, caña de azúcar, almidón de patata, remolacha, entre otros [118, 119]. El ácido láctico, debido a su quiralidad cuenta con dos configuraciones: los estereoisómeros de D(-)-ácido láctico y L(+)-ácido láctico [120], que se muestran en la **Figura I.16**.

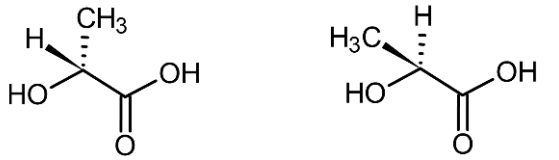

D(-)-Ácido Láctico L(+)-Ácido Láctico

Figura I.16. Estructura química de los estereoisómeros del ácido láctico.

Industrialmente, son diversos los métodos para obtener PLA mediante polimerización del ácido láctico: a) polimerización por condensación directa, b)

policondensación directa en una solución azeotrópica (considerando que un azeótropo es una mezcla de 2 o más líquidos químicos en proporción tal que su composición no puede cambiarse únicamente por destilación) y, finalmente c) polimerización por apertura de anillo de lactida conocida también como ROP *(ring opening polymerization)* [121]. El primer método se basa en la esterificación de monómeros mediante el uso de disolventes mientras que el agua se elimina con a un vacío progresivo y altas temperaturas. Sin embargo, con este método resultan poli(ésteres) con bajos pesos moleculares y bajas propiedades mecánicas. El PLA obtenido por este método es frágil y requiere el empleo de extensores de cadena que ayuden a incrementar el peso molecular del polímero. No obstante, esto también incrementa costos de producción [122]. El segundo método sí permite la obtención de PLA con mayor peso molecular, ya que la solución azeotrópica contribuye a la disminución de la presión de destilación, y facilita la separación del PLA del solvente mediante el uso de tamices moleculares. Finalmente, con el tercer método se logra eliminar el agua condensada en condiciones suaves y sin uso de disolventes, con lo cual se produce un dímero cíclico intermedio conocido como lactida. Este monómero se puede purificar fácilmente por destilación al vacío realizada por calentamiento, nuevamente sin necesidad de solvente. Posteriormente, mediante la polimerización por apertura de anillo de la lactida purificada se logra obtener PLA con mayor peso molecular y con mayor pureza (M_w > 100.000) [122, 123]. La síntesis de PLA inicia a partir de recursos naturales vegetales ricos en carbohidratos, como la patata o el almidón de maíz. En la **Figura I.17** se muestra cada una de las posibles opciones para la obtención de PLA.

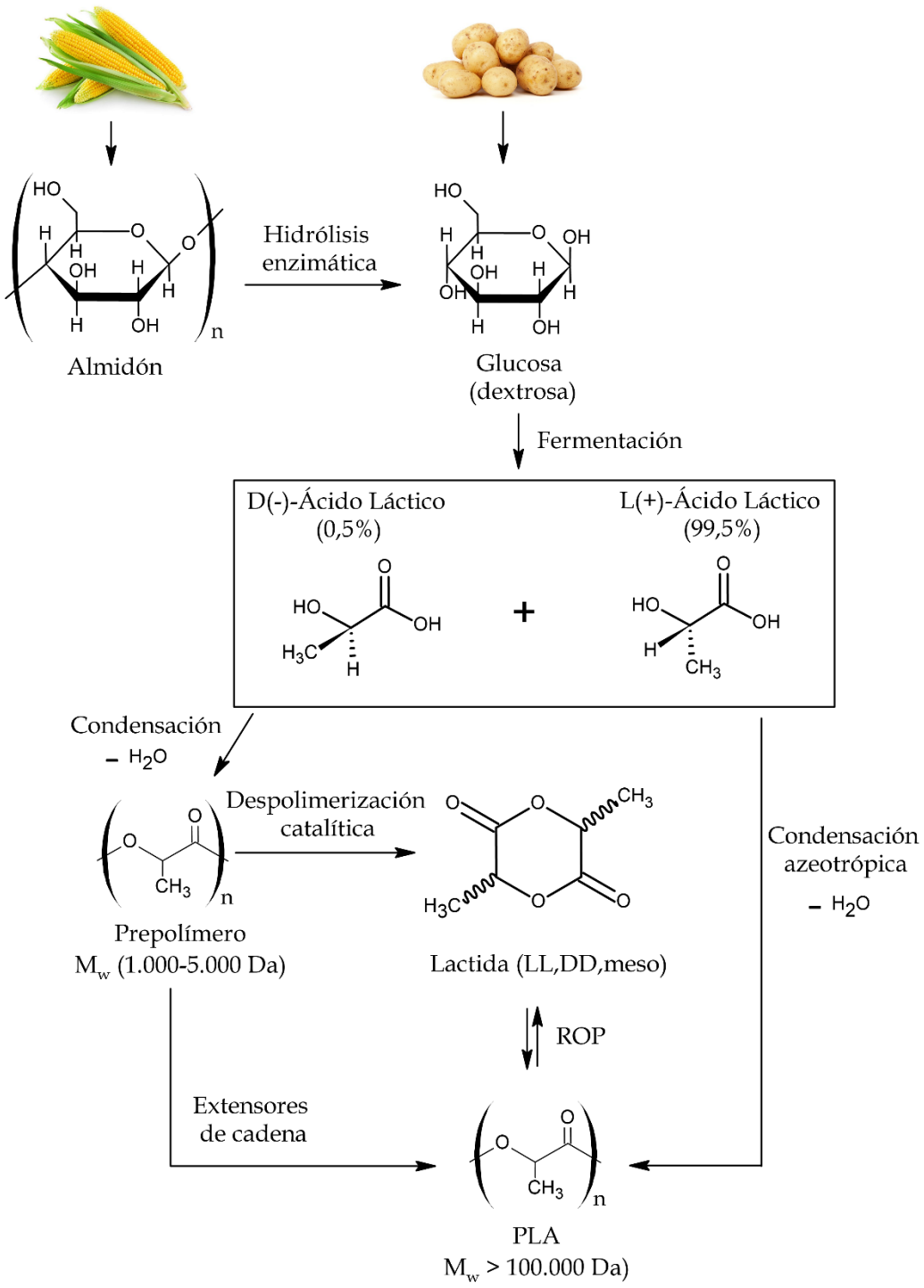

Figura I.17. Rutas posibles para la obtención de PLA.

El PLA puede presentarse de tres formas isoméricas distintas que dependen del monómero utilizado en la síntesis, el poli(L-ácido láctico) (PLLA), poli(D-ácido láctico) (PDLA) y poli(DL-ácido láctico) (PDLLA). Actualmente el PLLA es el que más se ha estudiado debido a que la producción comercial del ácido láctico se ha centrado en el L-

ácido láctico [124]. Este, al igual que el PDLA, es ópticamente activo y cristalizable, mientras que el PDLLA no se considera ópticamente activo ni cristalizable [125].

I.3.3.2. Características del poli(ácido láctico) (PLA)

La propiedades físicas, térmicas y mecánicas del PLA y sus copolímeros dependen fuertemente de su peso molecular (distribución) y de su composición. En estado sólido el PLA puede ser semicristalino o amorfo dependiendo de la composición y la historia térmica. Se obtiene un PLA semicristalino si contiene más de 93% del isómero L-ácido láctico, mientras que si el PLA contiene entre 50-93% del isómero L-ácido láctico se considera una estructura amorfa. Además, la mayor parte de PLA está constituido de copolímeros de L-ácido láctico y D,L-ácido láctico [56]. Por lo tanto, se puede decir que es posible la obtención de diferentes PLA con variedad de propiedades según la composición, su proceso de obtención y control del mismo.

- **Propiedades térmicas**

Para el PLA amorfo, la temperatura de transición vítrea (T_g) (~58 ^oC) determina la temperatura de uso superior, ya que este parámetro indica el paso del material desde su estado vítreo y frágil a uno más dúctil debido a la movilidad de las cadenas con la temperatura cuando sobrepasa la T_g. El PLA semicristalino presenta una temperatura de transición vítrea (T_g), correspondiente a su fase amorfa y una temperatura de fusión (T_m), asociada a la fase cristalina. El rango de T_m varía entre 130 ^oC a 230 ^oC, en función del peso molecular, distribución y composición del PLA. El conocimiento de estos parámetros condiciona su uso en las diferentes aplicaciones [124, 126]. El PLLA, que es el isómero de PLA más importante y utilizado, consiste en un polímero semicristalino con una temperatura de transición vítrea (T_g) de ~60 ^oC y una temperatura de fusión (T_m) alrededor de 180 ^oC [127].

- **Propiedades mecánicas**

En cuanto a su comportamiento mecánico, se puede afirmar que el grado de cristalinidad influye en gran medida en sus propiedades. Así pues, el PLA semicristalino tiene una resistencia a la tracción y módulo de Young superior a otros poli(ésteres) y, por consiguiente, su elongación a la rotura es baja, lo cual limita sus aplicaciones. El PLA amorfo, por su parte, puede presentar un comportamiento más dúctil [127]. Sin

embargo, en términos generales el PLA resulta un material rígido, frágil, con poca resistencia al impacto y baja ductilidad, aunque, por otro lado, también es susceptible de modificación. En la **Tabla I.8** se muestra una comparativa de propiedades mecánicas del PLA con polímeros de uso común como el poli(estireno) (PS), poli(etilén tereftalato) (PET) y poli(propileno) (PP). [4]

Tabla I.8. Comparativa de propiedades mecánicas de PLA con polímeros de uso común.

Propiedades	PLA	PS	PET	PP
Densidad (g cm^{-3})	1,24	1,05	1,39	0,9
Resistencia a la tracción (MPa)	53	45	57	31
Elongación a la rotura (%)	6	5	70	200
Resistencia al impacto (J m^{-1}) (con entalla)	12,8	21	59	53

Fuente: Jem *et al.* [128].

- ## Propiedades barrera

En relación con las propiedades barrera del PLA se puede concluir que estas dependen del grado de cristalinidad. Cuanto más amorfo es el material tendrá mayor permeabilidad, ya que al estar más desordenadas las cadenas, el volumen libre es mayor y ello permite el paso de gases o vapores a través de su estructura. Además, al ser un material hidrófobo no absorberá gran cantidad de agua, lo cual contribuye positivamente a que el material no se deteriore [129]. De manera general se puede decir que el PLA tiene propiedades barrera, relativamente pobres en cuanto a permeabilidad a gases como el CO_2 y el O_2. En relación con la permeabilidad al vapor de agua, es similar a la de otros termoplásticos como el poli(etilén tereftalato) (PET) [4, 55].

- ## Biodegradación

El PLA puede biodegradarse o desintegrarse en condiciones de compost. Este proceso sucede en dos etapas; la primera es la degradación hidrolítica y la segunda una degradación enzimática. El proceso inicia cuando el PLA absorbe la humedad provocando la hidrólisis de los enlaces éster. Esto genera una ruptura paulatina de los enlaces éster del polímero, y con ello se produce la reducción del peso molecular del polímero, llegando a formar oligómeros y ácido láctico que pueden ser asimilados por microorganismos como hongos y bacterias. Es importante señalar que el primer paso

hidrolítico puede ocurrir de manera superficial o, inclusive, internamente en el material con la difusión del agua, que está ligada a la composición química, estequiometría, peso molecular, morfología, orientación de la cadena y el propio medio de biodegradación. El segundo paso, ligado a los microorganismos solo ocurre en la superficie. Considerando que estos microorganismos solo pueden metabolizar cadenas de peso molecular con un rango máximo entre 10.000 y 20.000 g mol^{-1} para luego convertirlas en dióxido de carbono (CO_2), metano (CH_4) y agua (H_2O) dependiendo de las condiciones en que se lleve a cabo [127, 130, 131].

En términos generales el PLA puede ser procesado como cualquier otro polímero termoplástico, mediante los procesos de extrusión, inyección, soplado, termoconformado para formar películas, etc. Sin embargo, se debe considerar que el PLA cuenta con una inherente fragilidad y potencial degradación durante el procesado térmico debido a la sensibilidad a la degradación hidrolítica. Además, el PLA se puede recubrir mediante diferentes métodos como coextrusión multicapa, deposición de plasma, incorporación de nanoarcillas, entre otros, que permitan mejorar sus propiedades barrera [127, 132].

Destacar que, al no ser un polímero tóxico, se puede utilizar en otros campos como la biomedicina y sector alimentación. Aunque hay que considerar que su hidrofobicidad y carencia de grupos funcionales, de alguna manera limita su aplicación médica. Sin embargo, gracias a la modificación superficial es posible la obtención de materiales basados en PLA con biocompatibilidad mejorada [127].

I.3.3.3. Aplicaciones del poli(ácido láctico) (PLA)

El PLA se encuentra en diferentes presentaciones, para realizar fibras, formar películas rígidas, se puede extruir para formar hojas de embalaje termoformado, y se puede inyectar en moldes. En el ámbito textil se emplea en la fabricación de cortinas, toallas y prendas de vestir. En lo que respecta a no tejidos, se utiliza en la fabricación de toallas húmedas, rellenos de almohada, etc. En relación con piezas de inyección, se ha logrado obtener tazas, recipientes, juguetes, etc. En el caso de películas flexibles, estas se emplean en bolsas para la compra, y en campo de la agricultura. Sin embargo, debido a su fragilidad intrínseca el PLA suele mezclarse con otros polímeros para mejorar su flexibilidad y compostabilidad. Con ello, es posible mejorar propiedades como

resistencia al impacto y estabilidad térmica, que amplían sus aplicaciones en el campo de la ingeniería [128].

Por otro lado, el PLA es uno de los polímeros aprobados por la administración de alimentos y medicamentos (FDA) para su uso en aplicaciones biomédicas como implantes dentales, tornillos óseos, injertos vasculares, para administración de fármacos, etc. Otro ámbito en el que el PLA tiene la aprobación de la FDA, es para su uso en aplicaciones en las que tenga contacto directo con alimentos, lo que ha potenciado su empleo en materiales de envasado y embalaje para comida fresca. El PLA cuenta con propiedades como excelente resistencia a grasas y aceites, buena respirabilidad y permeabilidad al vapor de agua para vegetales, frutas y demás alimentos, adicionalmente cuenta con buena adhesión en superficies, así como buena transparencia y capacidad de impresión (similar al PET). Teniendo en cuenta que, pese a que se puede obtener PLA de diferente peso molecular, solo el PLA de alto peso molecular es el que se usa en la industria del envase y embalaje [128, 133, 134].

En la actualidad existen dos grandes empresas que producen PLA a escala industrial. Estas son NatureWorks LLC y Corbion, (las dos utilizan el proceso de polimerización por apertura de anillo de lactida para su producción). A partir de 2003, fue cuando el PLA con el nombre comercial Ingeo™, alcanza su mayor auge y producción de la mano de la empresa NatureWorks LLC, con cerca de 150.000 toneladas $año^{-1}$ [132]. Su importancia e interés en el campo del envasado de alimentos se da, básicamente, debido a sus excelentes propiedades como transparencia, su relativamente buena resistencia al agua. Por su parte, la permeabilidad al agua del PLA es mucho menor que en polímeros derivados de proteínas y polisacáridos, pero aun así sigue siendo más alta comparada con las poliolefinas y PET [133]. Por otro lado, la resistencia térmica es menor que la del PET, ya que el PLA tiene una T_g alrededor de 58 ^oC mientras que en el PET es cercana a 70 ^oC. Adicionalmente, cuenta con una alta rigidez. Para incrementar su flexibilidad es frecuente el uso de mezclas con otros polímeros y el empleo de plastificantes, entre otros. Sin embargo, se debe considerar que esto también puede conllevar a la disminución de propiedades barrera al oxígeno, agua o inclusive comprometer la transparencia [133].

Las aplicaciones del PLA abarcan diferentes campos. En el sector doméstico se emplea en productos de uso común, a continuación (**Tabla I.9**). Como se puede observar,

gran parte de las aplicaciones se centran en el sector envase y embalaje, aunque también se puede mencionar algunas en el sector de automoción.

Tabla I.9. Aplicaciones comerciales del PLA.

Aplicaciones	Empresas
Envases para champú.	Shiseido-Urara
Vasos y tapas para bebidas.	Fabri-kal / Coca Cola
Cubiertos para comida.	StalkMarket
Envase para ensalada.	Walmart
Envases de frituras (SunChip).	Frito-Lay
Bandejas de comida.	Sealed Air
Repuestos de coche.	Toyota
Alfombras / suelo laminado.	Saint Maclou / LG Hausys

Fuente: Sin [135].

Por otro lado, debido a sus propiedades, el PLA ha encontrado su espacio en el ámbito de la biomedicina, en especial en lo que respecta a la ingeniería de tejido. Zhang *et al.* [136], han desarrollado una mezcla de PLLA/nanodiamante funcionalizado con octadecilamina (ND-ODA). Los resultados muestran que las propiedades mecánicas del PLLA incrementaron (módulo de Young y dureza) con la adición de (ND-ODA), dando como resultado un nanocompuesto con propiedades similares a las de un hueso humano. Además, se comprobó la no toxicidad del material desarrollado. Otra aplicación posible para el PLA es en el tratamiento de heridas mediante el uso de suturas, cicatrización de heridas por extracción dental, prevención de adherencias postoperatorias, entre otras. En este contexto Qin *et al.* [137], han obtenido una mezcla de PLA con poli(trimetilén carbonato) (PTMC) mediante el método *cast film*. Los resultados demuestran que las películas obtenidas son más flexibles que el PLA puro, mientas que la resistencia a la tracción, el módulo de Young y la T_g son inferiores a las del PLA. La disminución de la T_g a medida que se incrementa el contenido PTMC, indica la buena compatibilidad entre los dos componentes. Los ensayos de citotoxicidad confirmaron que las mezclas no eran citotóxicas.

I.4. Biopolímeros derivados de estructura proteicas vegetales

Una opción viable y respetuosa con el medio ambiente implica la obtención de materiales biobasados, es decir obtenidos a partir de recursos naturales renovables, de los que se pueden extraer diferentes componentes como polisacáridos, proteínas, ligninas, lípidos, etc. [138, 139]. Las proteínas constituyen un grupo importante para el desarrollo de materiales biobasados, sobre todo películas poliméricas que tienen su mayor aplicación en el sector envase y embalaje de productos. Ello se debe principalmente a su bajo costo, abundancia en la naturaleza y su capacidad de biodegradación. Además, en algunos casos pueden llegar a presentar biocompatibilidad [140]. Las proteínas se pueden obtener de materias primas vegetales como soja, gluten de trigo, zeína, frijoles, entre otros.

De manera general, se puede definir a las proteínas como polímeros naturales que están formadas por hasta 20 grupos diferentes de aminoácidos, unidos mediante enlaces peptídicos que se producen a través de una reacción de condensación mediada por enzimas [141, 142]. Los aminoácidos, como su nombre lo indica, tienen dos grupos funcionales, el grupo amino (-NH_2) y el grupo carboxilo (-COOH). Estos grupos se unen a un solo carbono (alifático), por lo que los aminoácidos en las proteínas son todos α-aminoácidos [143]. Es importante señalar que el número de aminoácidos en la cadena polipeptídica y su posición a lo largo de ella, determinan las propiedades físicas y químicas de la proteína [144]. En la **Figura I.18** se puede evidenciar la formación de un enlace peptídico entre aminoácidos.

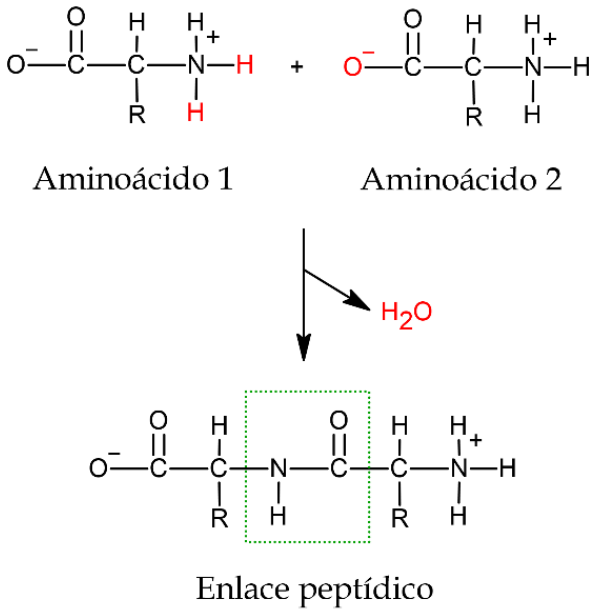

Figura I.18. Representación esquemática de la reacción de formación del enlace peptídico entre aminoácidos.

Las proteínas se pueden clasificar según a su forma y solubilidad en tres grupos de proteínas: fibrosas, globulares o membranas. Las fibrosas son las más simples con estructuras lineales regulares. Las proteínas globulares tienden a ser esféricas y son muy solubles en medios acuosos. Por su parte, las proteínas de membrana se encuentran en asociación con varios sistemas de membrana de las células y son bastante insolubles en medios acuosos [142].

Otra manera de clasificar las proteínas es según su estructura: primaria, secundaria, terciaria y cuaternaria. La estructura primaria indica una secuencia lineal en la que los aminoácidos están unidos por enlaces peptídicos. La estructura secundaria se relaciona con la estructura periódica en polipéptidos y proteína, siendo la helicoidal la estructura secundaria más común. La estructura terciaria se refiere al arreglo tridimensional de la cadena polipeptídica doblada con segmentos de estructura secundaria alineados en una forma compacta tridimensional. Finalmente, la estructura cuaternaria se refiere al arreglo espacial de la proteína que contiene una gran cantidad de cadenas polipeptídicas. Esta se conoce como estructura oligomérica con muchas subunidades. Es importante tener en cuenta que las estructuras terciarias y cuaternarias, así como las interacciones hidrofóbicas y enlaces hidrógeno, cambian cuando las proteínas se combinan, ya sea con agentes modificadores o plastificantes [145]. En la

Figura I.19 se pueden observar los diferentes niveles de la estructura interna de una proteína.

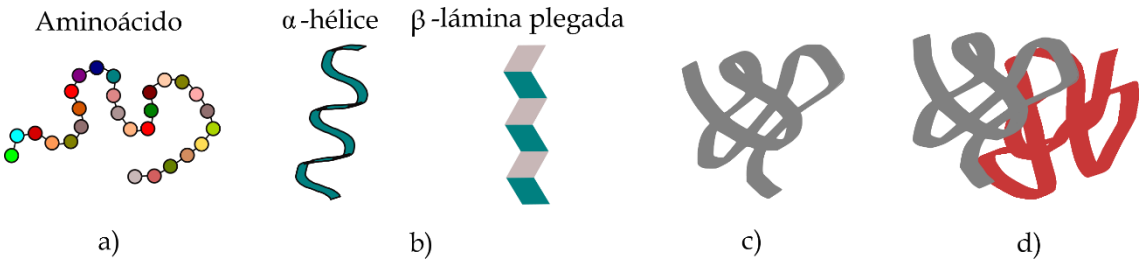

Figura I.19. Clasificación de proteínas según su estructura: a) primaria, b) secundaria (α-hélice y β-lámina plegada), c) terciaria, y d) cuaternaria.

En la **Tabla I.10** se presenta un resumen de los aminoácidos que se encuentran presentes en proteínas que se usan para el desarrollo de películas termoplásticas. Como se observa, existe una variación en la cantidad de aminoácidos entre las diferentes proteínas, lo que da como resultado propiedades variadas en el tipo y secuencia de aminoácidos se debe a las propias propiedades de la planta, así como a las condiciones de crecimiento que han tenido cada una de ellas.

Tabla I.10. Aminoácidos (g/100 g de proteína) disponibles en proteínas provenientes de cultivos cereales.

Aminoácidos	Trigo			Maíz	Soja	Cebada	Maní
	Gliadina	Gluten	Glutenina				
Ácido glutámico	30,2	28,7	27,4	24,2	19,0	27,3	22,8
Leucina	7,8	7,2	7,1	17,7	8,1	3,7	6,6
Prolina	17,1	14,1	12,4	8,9	5,1	3,7	2,8
Alanina	3,0	3,5	4,1	8,4	4,2	3,7	2,8
Fenilalanina	5,1	4,4	4,0	6,0	5,2	5,2	6,0
Serina	4,3	5,7	8,0	6,3	5,2	4,5	3,9
Tirosina	2,6	2,8	3,1	4,3	3,8	2,9	4,5
Histidina	1,7	1,7	1,7	0,9	2,6	2,3	2,2
Arginina	2,9	3,2	3,1	2,4	7,5	5,1	11
Lisina	0,6	1,4	2,0	0,5	6,2	3,6	2,5
Glicina	2,2	3,9	5,6	1,3	4,1	3,4	4,2
Ácido aspártico	1,7	4,2	2,5	4,2	11,5	5,8	12,6
Valina	4,0	2,9	4,3	3,4	5,0	4,9	4,8
Cisteína	1,8	1,7	1,5	1,0	1,3	1,3	0,2
Isoleucina	3,4	3,0	4,4	3,8	4,8	3,6	4,0

Fuente: Reddy and Yang [146].

I.4.1. Obtención y estructura de biopolímeros derivados de estructuras proteicas vegetales.

Entre las plantas, las legumbres son las que contienen la mayor cantidad de proteínas. Entre ellas, a su vez, destacan los guisantes, garbanzos, frijoles y lentejas que contienen alrededor de 170-300 g kg^{-1} de proteína. Por otro lado, además de proteínas, las legumbres contienen almidón, hemicelulosa, celulosa, entre otros. Por ello, con el fin de poder analizar las propiedades y aplicaciones posibles de las proteínas se deben aislar de los otros componentes. Esta separación/extracción se puede realizar bajo condiciones húmedas o secas, dando lugar a las proteínas aisladas y concentrados de proteínas, respectivamente [147]. El método húmedo comprende algunas fases que se describen a

continuación. En la primera, las legumbres se procesan mediante solubilización alcalina o neutra, seguida por una fase en la que se separa la proteína mediante precipitación isoeléctrica o ultrafiltración. Es importante señalar que, con este método, es posible alcanzar una extracción de proteína con alta pureza ~90%, a diferencia del método seco que permite una pureza no superior al 60%. No obstante, hay que tener en cuenta que la pureza no solo va a depender del procedimiento de separación de la proteína sino, del tipo de legumbre utilizado [147].

El proceso de extracción en húmedo que se indica en la **Figura I.20** es el que más se utiliza en las industrias. Este implica la extracción de proteína en solución alcalina, ácida, salada y alcohol dependiendo del tipo de proteína que se utilice y su grado de solubilidad. Sin embargo, el proceso de extracción alcalino y precipitación ácida es uno de los más utilizados para obtener proteína aislada. El proceso inicia con la trituración de la legumbre; luego se somete a un proceso donde se separa el aceite (en el caso de que lo contenga); posteriormente, el material se lleva a una solución acuosa a un pH entre 8 y 11 (dependiendo del tipo de materia prima), y a temperatura, con el fin de solubilizar la proteína. Posteriormente, mediante centrifugación, se separa el material insoluble como almidón y fibras y, la solución sobrenadante se lleva a pH ácido hasta alcanzar el punto isoeléctrico de la proteína, con lo cual se logra la precipitación final de la misma. Finalmente, se realiza una centrifugación en donde el precipitado (proteína) se separa de la solución que contiene básicamente azúcares con pesos moleculares bajos y fibras solubles [148, 149].

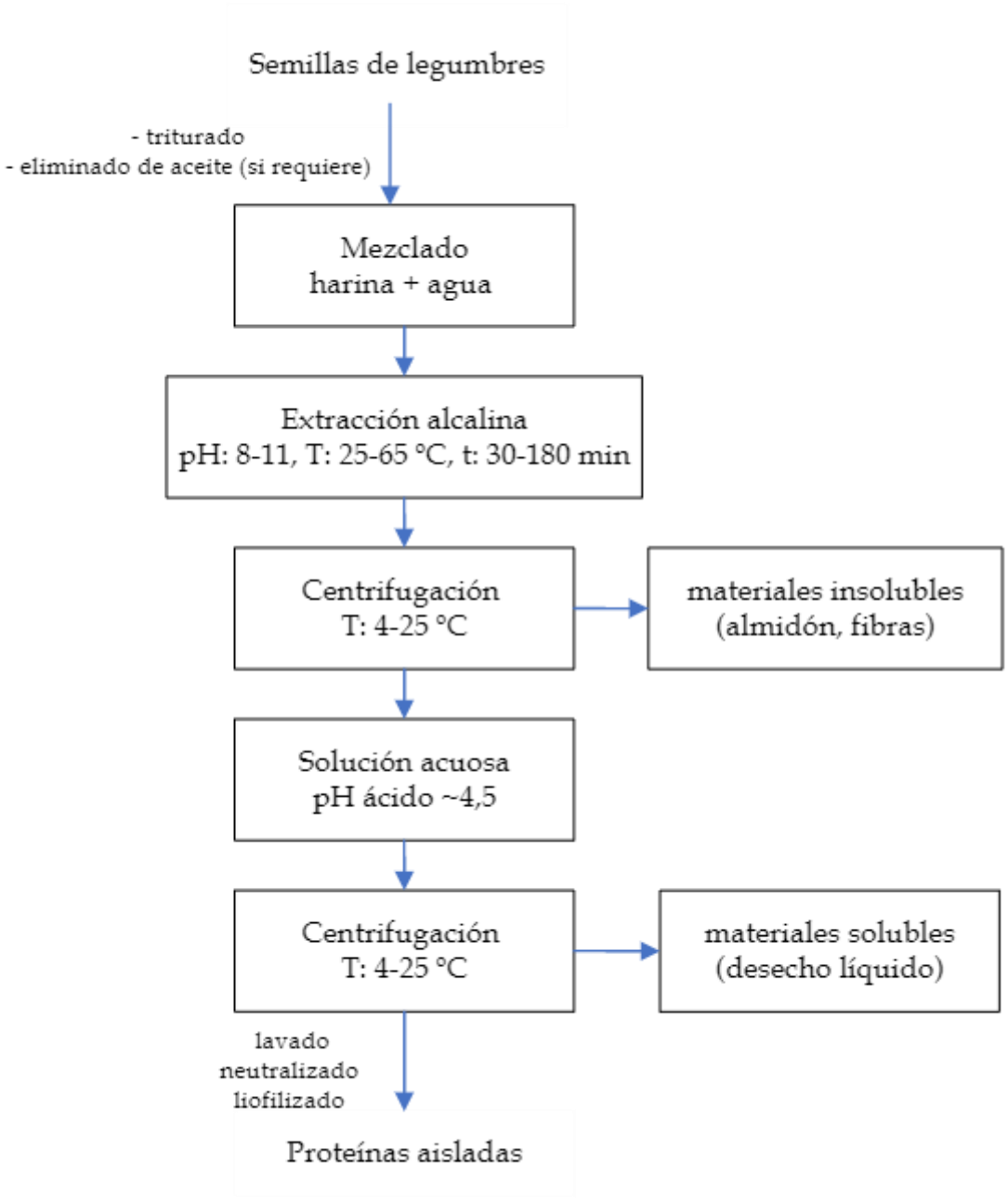

Figura I.20. Diagrama de flujo para obtener proteínas aisladas (método húmedo). Fuente: Klupšaitė and Juodeikienė [148].

Por otro lado, el método seco consiste básicamente en triturar las legumbres en un molino. Si la legumbre posee aceite, se añade un paso previo de extracción del mismo. Una vez triturado el material y convertido en harina se somete a una corriente de aire en espiral, donde las proteínas (denominadas fracción ligera o fina) se separan del almidón (denominado fracción pesada o gruesa) por su diferente tamaño, forma y densidad. El proceso puede terminar ahí, o repetirse varias veces hasta alcanzar concentrados de

proteína con mayor pureza [149]. En la **Figura I.21**, se pueden observar los pasos requeridos para la extracción de proteínas a partir de legumbres por el método seco.

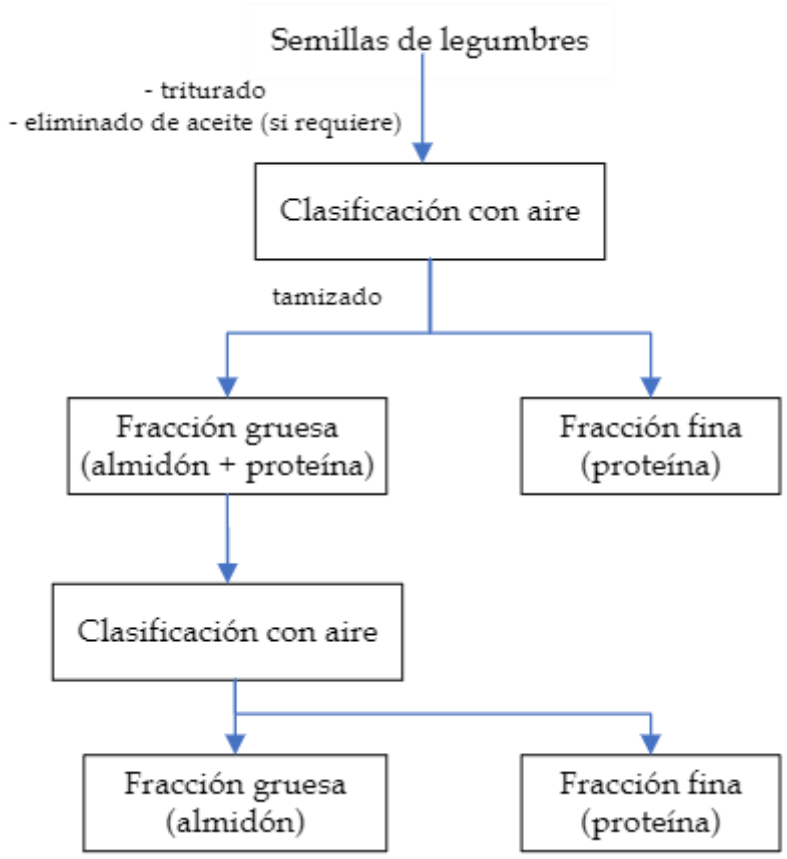

Figura I.21. Diagrama de flujo para obtener proteínas (método seco). Fuente: Amin *et al.* [149].

Una vez extraídas las proteínas se las puede utilizar para la obtención de películas. Este proceso se puede llevar a cabo de dos maneras: mediante un procedimiento húmedo (que utiliza solventes), y mediante un proceso seco. El proceso en húmedo que se conoce como "*solution casting*" o solución fundida, lo que hace básicamente es dispersar o solubilizar la proteína en un solvente. Por su parte, el proceso en seco incluye presión y calor o moldeo por compresión, así como técnicas de fusión y extrusión para la obtención de películas [150].

Como se ha indicado anteriormente, existen diferentes presentaciones de las proteínas. Una de ellas en forma de películas, su obtención se hace típicamente mediante el empleo de solventes o cast film, o se realiza mediante hidrólisis de las proteínas con soluciones alcalinas, con lo cual se logra desdoblar la estructura de la proteína. Sin embargo, existe cierta limitación al utilizar el método en húmedo (cast film), ya que solo

ciertas proteínas provenientes de plantas (gliadina y zeína) son solubles en solventes comunes. El resto, como es el caso de proteínas de soja, gluten de trigo, entre otros, no se disuelven en solventes comunes, y es necesario utilizar soluciones alcalinas en caliente. Por otro lado, la hidrólisis que sucede durante la disolución alcalina da lugar a proteínas como bajos pesos moleculares, lo que provoca que las películas resultantes tengan propiedades mecánicas pobres [146]. De manera general, el procedimiento de disolución alcalina en caliente, es uno de los más utilizados y comprende, básicamente, la disolución de la proteína en agua, donde se agrega normalmente algún tipo de plastificante, se ajusta el pH con alguna solución básica, posteriormente se homogeniza con agitación y calor a una temperatura de ~80 °C con el fin de desnaturalizar la proteína. A continuación, la solución se coloca en placas Petri que someten a secado para evaporar el agua, y así obtener las películas [150], como se muestra en la **Figura I.22**.

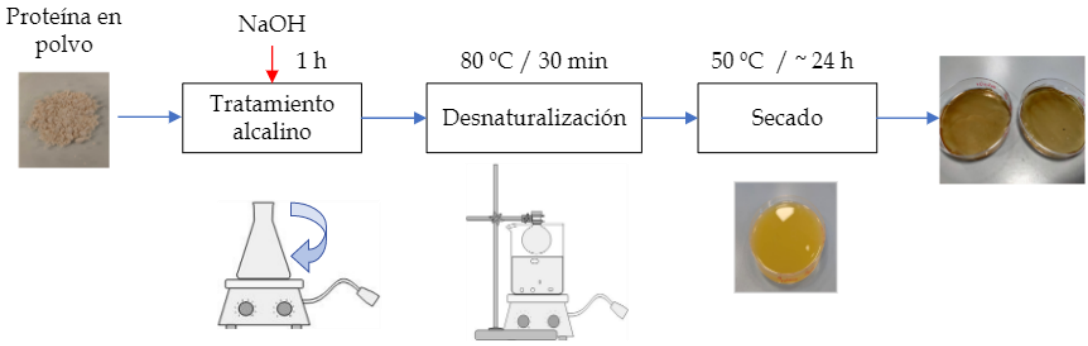

Figura I.22. Procedimiento de obtención de películas mediante el método húmedo (usando disolución alcalina).

Por su parte, el método seco permite obtener, además de películas, filamentos o hilos mediante procesos térmicos o termo mecánicos, en condiciones de baja humedad para el material. Esta consiste en someter a la proteína a la acción de calor generalmente mediante un proceso de extrusión, con el fin de superar la temperatura de transición vítrea del material, pasando de un estado vítreo estable a un estado gomoso inestable. Sin embargo, debido al amplio rango de interacciones moleculares que tienen las proteínas, la movilidad molecular es baja, dando lugar a valores de T_g elevados o incluso en algunos casos, mayores a la temperatura de descomposición. El reblandecimiento de proteínas requiere, por tanto, desnaturalización, lo que implica el desdoblamiento desde un estado nativo estructurado a un estado (parcialmente) no estructurado con poca o ninguna estructura residual fija. Por otro lado, debido a la analogía con el comportamiento de los polímeros semicristalinos, la temperatura de desnaturalización

(T_d), a menudo se denomina temperatura de fusión. Sin embargo, esto no implica necesariamente que las proteínas se desarrollen por completo en una estructura semicristalina como pasaría normalmente con la fusión en los polímeros. Esto se debe a que, en su entorno natural, una proteína se pliega en estructuras secundarias, terciarias y cuaternarias estabilizadas mediante interacciones hidrofóbicas, enlaces de hidrógeno e interacciones electrostáticas entre grupos funcionales de aminoácidos. Por tanto, la temperatura de desnaturalización de las proteínas depende de la secuencia de aminoácidos, el tipo de aditivos químicos usados, y el método de procesado empleado. Por lo tanto, generalmente para que se pueda procesar la proteína mediante este método, es necesario realizar una modificación física y/o química de las proteínas, o realizar tratamientos térmicos y/o mezclas con plastificantes [147, 151].

I.4.2. Características de derivados de estructura proteicas vegetales

Las proteínas son polímeros naturales con características complejas, ya que su funcionamiento y propiedades depende directa o indirectamente de diferentes factores como su estructura, pH, humedad relativa, aditivos, entre otros. A continuación, se indican las propiedades a destacar y considerar en la fabricación de películas de proteínas mediante el método "*solution casting*".

- **Permeabilidad**

Las proteínas, al ser polímeros hidrofílicos, contienen grupos polares con enlaces hidrógeno que pueden permitir la absorción del agua del medio ambiente, ya sea del aire o, incluso, del alimento que contienen cuando se emplean en envases. Por ello, la presencia de agua en el biopolímero puede afectar la penetración de gases y vapores. De manera general, se puede decir que la permeabilidad de gases y vapores en proteínas incrementa con la mayor absorción de agua, ya que esta actúa como plastificante e incrementa el volumen libre del biopolímero [152], excepto en proteínas como zeína y gluten, que son insolubles en agua, por lo que se puede deducir que la permeabilidad de la película está ligada a su estructura, así como al origen de las mismas [153]. Por otro lado, pese a que se pueda creer que las propiedades barrera en las películas de proteínas son bajas, en lo que respecta a la barrera a ciertos gases resultan ser mejores comparadas con las películas basadas en lípidos o polisacáridos [154]. Adicionalmente, entre las

principales propiedades con las que cuentan los películas a base de proteínas se tienen la de sus buenas propiedades barrera a aromas, aceites y oxígeno [146].

- **Propiedades mecánicas**

En relación con las propiedades mecánicas, las películas a base de proteínas presentan mejores propiedades que las películas a base de polisacáridos y de lípidos. Esto se debe a que las proteínas cuentan con una estructura basada en 20 monómeros diferentes de aminoácidos, los cuales aportan un amplio rango de propiedades funcionales, en especial un alto potencial de unión intermolecular, lo que permite que puedan formar diferentes enlaces. Sin embargo, sus propiedades mecánicas y de barrera siguen siendo pobres comparadas con polímeros de uso común como poliolefinas. Por ello, se han buscado alternativas que permitan solventar estos inconvenientes, siendo una de ellas el uso de agentes de entrecruzamiento que permitan mejorar la interacción de las cadenas y, con ello, la mejora de propiedades mecánicas. Algunos agentes de entrecruzamiento son el formaldehido, glutaraldehído, ácido ferúlico, entre otros. Con su incorporación se logra incrementar la resistencia mecánica y reducir la permeabilidad a los gases y al vapor de agua [154]. Otra posibilidad es la adición de agentes plastificantes que permitan reducir la fragilidad inherente de las películas fabricadas con proteína. Los plastificantes, además de mejorar la flexibilidad y la resistencia al impacto, pueden prevenir la fractura durante la manipulación, transporte o almacenamiento posterior, ya que un fallo en alguna de estas etapas puede suponer una disminución o total eliminación de las propiedades barrera de las películas [155, 156]. Adicionalmente se pueden mencionar otros métodos como el tratamiento enzimático para la mejora de la resistencia mecánica. Otro tratamiento consiste en la adición de lípidos en sistemas de multicapa o dispersado en la solución de proteínas con el fin de mejorar flexibilidad y aportar protección contra la humedad [157].

- **Desnaturalización de proteínas**

La desnaturalización se produce cuando hay una pérdida del orden estructural de las macromoléculas que conforman la proteína, es decir, cuando hay una pérdida de las propiedades más características como la actividad enzimática y solubilidad [143]. En principio, las proteínas tienen que mantener su conformación natural para tener un normal funcionamiento, por lo que cualquier factor que cambie la conformación de las proteínas es una fuente potencial de desnaturalización [143]. La desnaturalización puede

ocurrir debido a incrementos de temperatura, cambios de pH, acción de solventes orgánicos, tratamientos alcalinos o ácidos, entre otros. No obstante, el calentamiento es el factor más común que ocasiona la desnaturalización de proteínas, ya que incrementa la movilidad molecular, lo que a su vez produce la ruptura de enlaces intermoleculares e intramoleculares de la estructura. También debe tenerse en cuenta que la desnaturalización puede ser reversible o irreversible; todo depende de cómo se haya llevado a cabo el proceso [143].

- **Comportamiento térmico**

En lo que respecta al comportamiento térmico de las proteínas, este depende en gran medida, de la composición que tenga, es decir, el tipo de aminoácidos que las conforman, además de la temperatura, pH, presión, aditivos utilizados, contenido de sal, entre otros [146, 157]. Enfocándose en uno de los métodos para la obtención de películas de proteínas que es el de fusión, se puede indicar que la acción de la temperatura es un factor importante cuando se produce la desnaturalización, y también debe tenerse en cuenta cuando se produce el secado de la película, ya que la forma de las proteínas puede cambiar a medida que se evapora el agua [157]. La desnaturalización de las proteínas se produce entre 70 ºC y 100 ºC, y a esta temperatura se logra la formación de estructuras más fuertes en la solución de proteínas. Cuanto más desnaturalizada se encuentra la proteína es más fácil que las cadenas del polímero puedan interactuar entre sí, especialmente a través de enlaces disulfuro, por lo que se debe tener en cuenta que la buena o mala formación de estos enlaces es lo que determinará las características de las películas. En resumen, al incrementarse la temperatura se incrementan las interacciones hidrofílicas, disminuyen las interacciones por enlaces de hidrógeno y las interacciones electrostáticas. Todo ello facilita la formación de enlaces con plastificantes y demás componentes añadidos a la disolución de proteína. Teniendo en cuenta que la temperatura determina un papel importante, un calor excesivo en la disolución de proteína o una evaporación excesivamente rápida durante el secado de las películas puede producir un deterioro en sus propiedades [157].

- **Solubilidad**

La solubilidad es otro factor importante que puede afectar las propiedades de las películas de proteínas. Esta se define como una manifestación de equilibrio entre las interacciones proteína-solvente y proteína-proteína. En este contexto, aminoácidos

polares y cargados eléctricamente promueven las interacciones proteína-agua, lo que implica un incremento en la solubilidad. Por ello, si las proteínas contienen más grupos polares y con carga eléctrica, con forma globular y con pesos moleculares relativamente pequeños, tendrán mejor solubilidad [143]. Por otro lado, las proteínas altamente hidrofóbicas, las proteínas con estructura aleatoria, o los polímeros de proteínas altamente agregados, generalmente son insolubles o inestables en disolución [143]. El pH también desempeña un papel importante en la fabricación de películas de proteínas en medios acuosos, donde la solubilidad de las proteínas incrementa conforme su valor de pH se desplaza del punto isoeléctrico [157].

I.4.2.1. Aplicaciones de películas a base de proteínas

Las proteínas procedentes de legumbres han logrado gran atención con el paso de los años para la fabricación de materiales biobasados, así como también para su uso en el sector alimenticio, básicamente debido a su gran disponibilidad, buena sostenibilidad, alto valor nutricional, además de su baja acción alérgica [158]. En este sentido surge el estudio y desarrollo de películas a base de proteínas para su uso en diferentes ámbitos como en el sector de envase y embalaje en forma de películas y como recubrimientos comestibles. Este último está teniendo cada vez más atención debido a las características propias de la proteína que los convierten en materiales con protección frente a gases, aromas y lípidos. Además de su habilidad para transportar aditivos alimentarios (antioxidantes, sabores, agentes antimicrobianos). Las películas cuentan con su inherente biodegradabilidad al final de su vida útil, lo que las convierte en materiales con potencial para sustituir a plásticos sintéticos tradicionales para envases y embalajes [159].

Las películas y recubrimientos comestibles buscan preservar la calidad de los alimentos durante períodos de tiempos cada vez más prolongados, y protegerlos de la descomposición física, química y biológica a lo largo de su vida útil [160]. La principal diferencia entre películas y recubrimientos comestibles radica en cómo se aplican al producto alimenticio. La película comestible es, básicamente, una lámina delgada sólida que sirve para recubrir el alimento. Un recubrimiento comestible se deposita sobre el alimento en un estado de agregado líquido. Esta deposición se puede realizar mediante métodos como inmersión, rociado, entre otros, lo que permite que se pueda comer de manera conjunta con el alimento recubierto [160, 161].

Las películas comestibles se han utilizado tradicionalmente como materiales para envasado de alimentos, con el fin de protegerlos de las influencias ambientales no deseadas. Sin embargo, hoy en día se apuesta por su uso como envases activos para alimentos; es decir, que son capaces de proporcionar características deseadas. Hoy en día existen varias aplicaciones comerciales de películas y recubrimientos de proteína en el sector alimentación. Cabe indicar que se utilizan sobre todo proteínas de origen animal como colágeno, gelatina, suero, entre otros, para el envasado de productos cárnicos. La principal utilidad que tienen las películas comestibles en este sector, es la de proteger y mantener frescos los diferentes productos como carne, mariscos, frutas, verduras, granos, así como también para mezclas de alimentos que se pueden enlatar, congelar o guardar en alguna otra forma de almacenamiento [160]. Un ejemplo importante es el uso de películas de colágeno como tripas para embutidos, lo cual ha tenido gran éxito dentro de la industria cárnica [161].

Por otro lado, en las últimas décadas se están desarrollando cada vez más materiales basados en películas de proteína de origen vegetal en las que se considera el uso de la soja y otras leguminosas. Hopkins *et al.* [162], desarrollan una comparativa del uso de diferentes proteínas obtenidas de distintas fuentes (haba, guisante, lupino, lenteja y soja) y el uso de glicerol como plastificante, obteniendo una notable mejora de propiedades físico-químicas, entre ellas resistencia, elongación y propiedades barrera contra la humedad. Bamdad *et al.* [163], utilizan como materia prima lenteja para la elaboración de películas comestibles. Estas películas presentaron buenas propiedades mecánicas, de permeabilidad al agua, además de buena solubilidad. Por otra parte, Pagno *et al.* [164], consideran para la fabricación de películas con materia prima de harina de quinoa y aceites esenciales de orégano y tomillo. Los materiales desarrollados mejoran la capacidad antimicrobiana contra *Escherichia coli* y *Staphylococcus aureus*, además de una ligera mejora en las propiedades mecánicas y de barrera. En el trabajo desarrollado por Yildiz *et al.* [165], se estudian las películas formadas por proteínas de haba, empleando mezclas con quitosano, curcumina y ácido cítrico como agente de entrecruzamiento. Los resultados demuestran un incremento en la hidrofobicidad, además de una mejora en las propiedades barrera de las películas, con lo cual es posible su uso como material de envase activo para alimentos.

I.5. Aditivos naturales en formulaciones de polímeros

Según lo indicado en los diferentes apartados, se ha podido constatar que los polímeros descritos anteriormente presentan ciertas limitaciones, ya sea en sus propiedades mecánicas por excesiva fragilidad como es el caso del PLA, o la falta de buenas propiedades barrera al vapor de agua en el caso de las películas de proteínas. Con el fin de mejorar estas limitaciones e inclusive otorgarles otras características adicionales, se plantea la incorporación de aditivos mediante diferentes procedimientos.

I.5.1. Incorporación de principios activos y componentes de origen renovable.

Actualmente, con la fuerte sensibilización de la sociedad en relación con el medio ambiente surgen nuevas líneas de investigación que contemplan la valorización de diversos residuos agroindustriales, para su aplicación en el desarrollo de nuevos materiales. La industria de alimentos es una de las que genera gran cantidad de residuos orgánicos, debido al gran consumo y producción global. Entre otros destacan las pieles de frutas, residuos de cáscaras o semillas, etc. Por otro lado, en este ámbito también se pueden considerar residuos naturales procedentes de plantas como sus frutos, ramas, tallos, entre otros.

Considerando que estos residuos naturales contienen en su estructura diferentes principios activos como compuestos fenólicos, flavonoides, carbohidratos, además de componentes interesantes como proteínas, lignina, celulosa, etc., se ha planteado su uso y aprovechamiento para la obtención de nuevos materiales en forma de películas y con ello ampliar el rango de aplicaciones en ámbitos como el envase y embalaje. Estos principios activos permiten que se pueda proteger la calidad de los alimentos, además de incrementar su tiempo de vida útil, mediante la adecuada barrera a gases, protección UV, capacidad antioxidante, estabilidad térmica, etc. [166]. Kurek *et al.* [167], demostraron la transferencia de las propiedades antioxidantes propias del residuo de orujo de mora a las películas formadas por quitosano, dando lugar a los denominados envases antioxidantes activos. La importancia de que estos envases detengan o eviten las reacciones oxidativas radica en el hecho de que permite mantener la calidad de los productos envasados y evitar, por tanto, la decoloración o el deterioro de los productos.

Por otro lado, Corrales *et al.* [168], aprovecharon la propiedad antimicrobiana presente en los extractos de semillas de uva para la obtención de películas con matriz de almidón de guisante. Se pudo constatar un efecto inhibidor en el crecimiento de microorganismos. Adicionalmente, las películas también presentaron propiedades antioxidantes debido a su importante contenido de fenoles y flavonoides. Por su parte, Espinoza Acosta *et al.* [169], estudiaron la obtención de películas poliméricas con mezcla de lignina a partir de paja de trigo y almidón obtenido a partir de granos de trigo. Los resultados indicaron que, en lo referente a propiedades mecánicas, tanto el módulo de Young como la resistencia a la tracción experimentaron un ligero decremento que, por otro lado, permitió un incremento en la elongación a la rotura. Adicionalmente se constató que las películas presentaron una alta resistencia a la degradación térmica por la adición de la lignina, la cual, además proporcionó actividad antioxidante a las películas.

Otra interesante alternativa es el uso de estos residuos agroindustriales en forma de relleno/carga también conocidos como biocargas, cuya finalidad es la fabricación de materiales compuestos, utilizando para ello matrices biopoliméricas. El uso de estas cargas o rellenos se ha incrementado debido a que no solo permiten la posibilidad de modificar y mejorar propiedades de las matrices biopoliméricas, sino que mediante su uso también se puede reducir costos. Entre las principales características que pueden aportar estas biocargas se encuentran su alta tenacidad, baja densidad, bajo costo, buenas propiedades de resistencia, biodegradabilidad, etc. [170], lo que los hace materiales competitivos contra los refuerzos convencionales que se han utilizado a lo largo de la historia como la fibra de vidrio [171], fibra de carbono [172, 173], etc. Algunos estudios muestran que el uso de desechos agrícolas para la obtención de materiales compuestos, ha permitido una mejora de propiedades mecánicas, térmicas, barrera al agua y oxígeno, estabilidad dimensional, así como resistencia al desgaste, entre otros. De hecho, muchas de estas cargas ya se utilizan y comercializan en sectores como la automoción, donde se han aprovechado principalmente por sus buenas propiedades y bajo peso, una característica indispensable para este tipo de industria [174].

Sin embargo, una de las principales limitaciones que presentan las matrices biopoliméricas reforzadas es la baja interacción entre las fases del material compuesto. Esto se debe, básicamente, a la naturaleza de las fases, ya que las cargas, al provenir de fuentes naturales son intrínsicamente hidrofílicas, mientras que las matrices poliméricas

son generalmente hidrofóbicas, dando como resultado una baja interacción que repercute negativamente en las propiedades del material. Liminana *et al.* [115] demostraron estos fenómenos en compuestos con matriz de PBS y cargas de harina de cáscara de almendra, lo que ocasionó un empobrecimiento en las propiedades. La elongación a la rotura experimentó una disminución de alrededor del 97%, que también se evidencia con el incremento del módulo de Young, haciéndose por tanto un material más rígido. Con el fin de minimizar esta aparente desventaja de los biocompuestos se plantean diferentes métodos que permiten mejorar la compatibilización de las fases, teniéndose entre ellos tratamientos químicos que incluyen mercerización [175], acetilación [176], silanización [177], uso de agentes de acoplamiento maleados [178], etc. Todos estos tratamientos pretenden mejorar la adhesión entre la superficie de la biocarga y la matriz polimérica, así como también su dispersión a lo largo de la matriz. Con ello, se produce una mejora en propiedades mecánicas como la resistencia al impacto, resistencia a la tracción del material compuesto o mejora en propiedades térmicas, etc.

I.5.1.1. Silanización

La silanización ha sido una técnica ampliamente utilizada debido a los buenos resultados obtenidos. Se trata de un tratamiento que utiliza silano con diversas funcionalidades. En general, los silanos presentan doble funcionalidad, que hace posible que su componente hidrofílico se una a la superficie de la biocarga disminuyendo, de esta manera, el número de grupos hidroxilos presente en esa superficie, mientras que su segunda funcionalidad (grupo funcional orgánico) reaccionará con la matriz polimérica [179]. Este procedimiento se lleva a cabo en presencia de agua, para lo cual el grupo alcoxi hidrolizable lleva a la formación de grupos silanol (SiOH). Los silanoles por su parte reaccionan luego con grupos hidroxilos disponibles en la biocarga, formando así enlaces covalentes estables con la pared celular. Con este tratamiento lo que se busca es que la biocarga aumente su hidrofobicidad y, con ello, mejorar su dispersión e interacción con la matriz biopolimérica [177, 180]. En la **Figura I.23** se puede observar el esquema del proceso de silanización realizada sobre una biocarga.

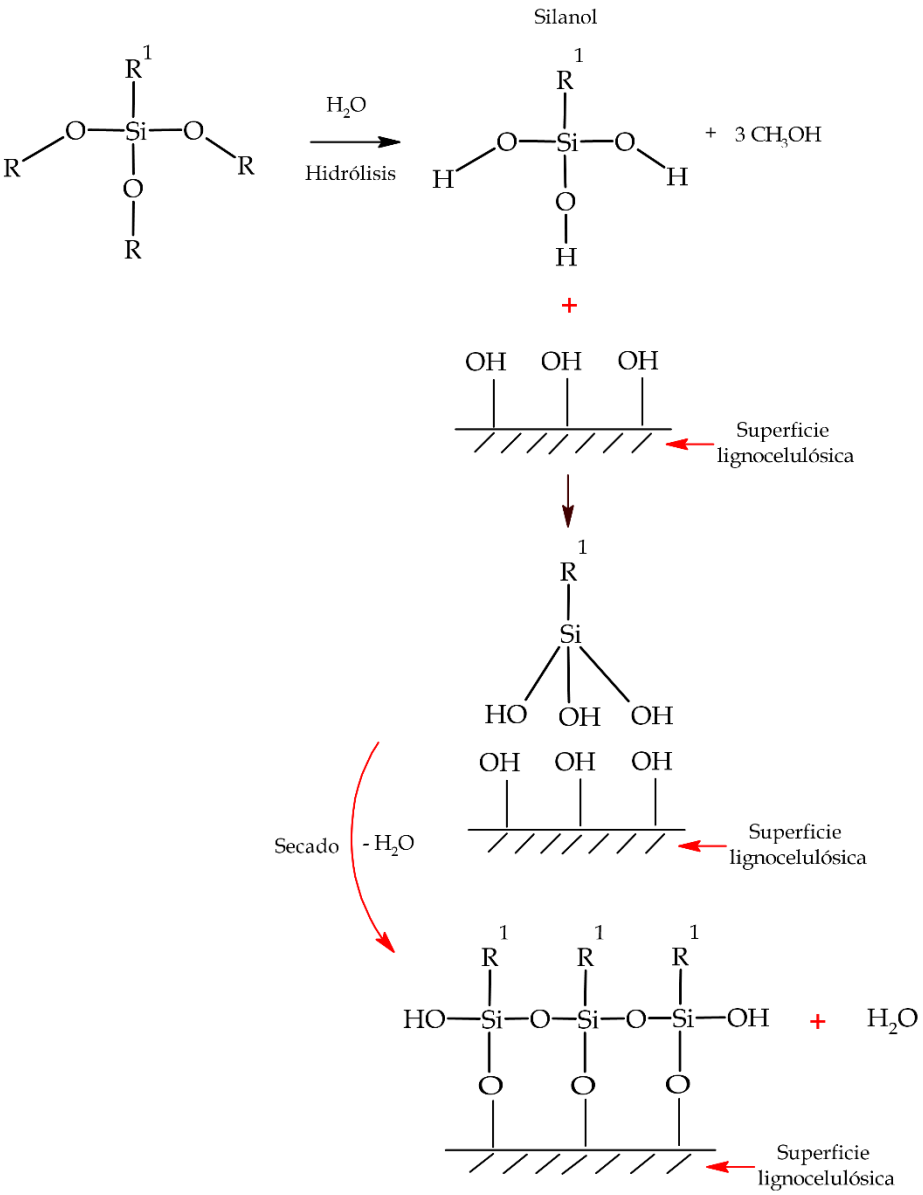

Figura I.23. Esquema de procedimiento para la silanización de biocargas.

La utilización de este tipo de tratamiento se puede evidenciar en el trabajo de Lule and Kim [181], donde se analiza la interacción entre una matriz de PLA y una carga de cáscaras de café tratada con silanos. Se constata una mejora en la interacción de la entre cara que repercute en un incremento en la cristalinidad, así como un incremento en la resistencia a la tracción y módulo en un 25% y un 20%, respectivamente. Laaziz *et al.* [182], por su parte, plantean la obtención de un biocompuesto a partir de una matriz de PLA con un refuerzo cáscaras de nuez de argan tratadas con silano. Los resultados indicaron que se produjo un incremento en la resistencia a la tracción debido a la buena adhesión y distribución de la biocarga en la matriz. Sin embargo, no se logró una mejora

en la estabilidad térmica (temperatura de inicio de degradación), mientras que se obtuvo un incremento en el ángulo de contacto, así como en la resistencia al agua, lo que indica claramente un incremento en la hidrofobicidad del biocompuesto obtenido. Por su parte, Miedzińska *et al.* [183] analizaron la adición de semillas de ciruela tratadas (1, 2 y 5% en peso) mediante silanización en una matriz biobasada de poliuretano. Se concluyó que con 5% de esta biocarga se logró una mejora en propiedades de flexión, además de estabilidad termo mecánica y térmica. Por otro lado, se evidenció un incremento del ángulo de contacto y una reducción en la absorción de agua del material biocompuesto.

I.5.1.2. Copolímeros modificados con anhídrido maleico como agente compatibilizante

Los copolímeros modificados mediante injerto de radicales libres de anhídrido maleico (MA) se añaden a compuestos formados por la matriz polimérica y la biocarga, con la finalidad de mejorar su interacción [184]. Sabiendo que la estructura del copolímero está formada por (X-*g*-MA), donde X puede ser cualquier polímero que se requiera utilizar, se tiene por un lado que los grupos reactivos del anhídrido maleico reaccionan con los grupos hidroxilo de la superficie de la biocarga formando así enlaces químicos. Por otro lado, se da la interacción física entre la fase polimérica y (X) donde X generalmente corresponde al mismo tipo de polímero con el que se desea interactuar y que, por tanto, tendrá una polaridad similar [185, 186]. De esta manera, se puede lograr una mejora en la adhesión en la entre cara y la adecuada dispersión de las biocargas, lo cual repercute, sobre todo, en las propiedades mecánicas de los biocompuestos [186]. En el trabajo llevado a cabo por Liu *et al.* [186] se constata que al utilizar PE-*g*-MA como compatibilizante se mejora la interacción entre la matriz de poli(etileno) y la biocarga (almidón). Esta adición tuvo un impacto positivo en la transferencia de tensiones, lo que permitió una mejora en la resistencia a la tracción y elongación a la rotura, siendo esta mejora más evidente con mayor cantidad de biocarga, aunque el valor óptimo determinado donde la resistencia a la tracción se logró estabilizar fue con un contenido de 10% en peso de PE-*g*-MA respecto a la biocarga. En otro trabajo realizado por Quiroz-Castillo *et al.* [187], se estudió la adición de PE-*g*-MA (5, 10, 15, y 20% en peso) como compatibilizante, y glicerol como plastificante, en compuestos formados por poli(etileno) y quitosano con 5% en peso como biocarga. Los resultados demostraron que la adición del compatibilizante permitió una ligera mejora en la estabilidad térmica de las películas, lo cual puede indicar a su vez una buena miscibilidad entre las dos fases

del biocompuesto. En lo que respecta a las propiedades mecánicas, se observó que la resistencia a la tracción se redujo alrededor de un 20%. Por su parte, el módulo de Young no mostró variación; sin embargo, se pudo constatar que con un 5% en peso de PE-*g*-MA se logró una mejora en la ductilidad de cerca del 60% al compararlo con el material biocompuesto no compatibilizado.

I.5.1.3. Peróxido de dicumilo como agente compatibilizante

El peróxido de dicumilo (DCP), es un peróxido iniciador de radicales libres, que se usa sobre todo como iniciador de polimerización, aunque también se lo usa como un agente vulcanizante de caucho natural, e incluso como agente de entrecruzamiento, por ejemplo para poli(etileno) o para el copolímero de etileno acetato de vinilo (EVA), etc. [188, 189]. Su adición a los polímeros se hace mediante una mezcla física a temperaturas elevadas, lo cual permite que se descomponga y se generen los radicales cumiloxi, que son capaces de extraer átomos de hidrógeno de cualquier grupo CH presentes en las cadenas poliméricas. Con ello, se generan radicales poliméricos. Por su parte, estos radicales libres formados se pueden combinar con otras cadenas poliméricas y así formar enlaces C-C, dando lugar a un fenómeno de compatibilización reactiva. En la **Figura I.24**, se observa el mecanismo de reacción donde: a) indica la rotura homolítica del peróxido de dicumilo en sus radicales cumiloxi, b) indica la abstracción de hidrógeno de la cadena polimérica (P) y c) muestra la combinación de radicales libres de cadenas poliméricas.

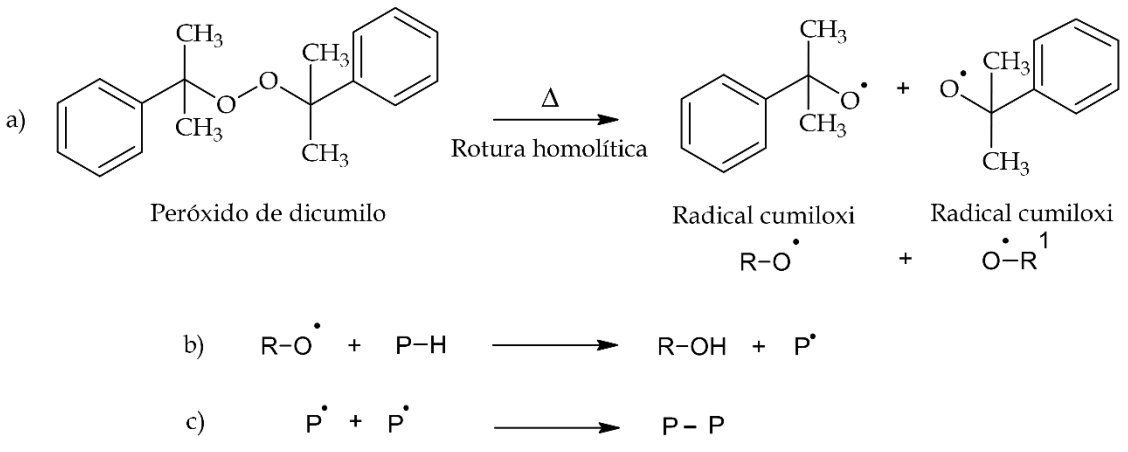

Figura I.24. Esquema de la descomposición del peróxido de dicumilo (DCP) y su reacción con cadenas poliméricas.

Es importante señalar que este tipo de compatibilización puede afectar a las propiedades mecánicas del polímero o compuesto resultante. Dicho efecto se evidencia

en el trabajo de Dong *et al.* [190], centrado en la mejora de la interacción entre mezclas de PHB y PDLLA, con la adición de una cantidad baja de DCP (0.5% en peso). Los resultados mostraron un incremento en la resistencia a la tracción, además de una importante mejora en la absorción de energía. En otro trabajo realizado por Ma *et al.* [191] los resultados indicaron que con la adición de 0.5% en peso de DCP, se logró un incremento en la elongación a la rotura, así como una mejora en la absorción de impacto, en mezclas de PHBV-PBS y PHB-PBS.

En resumen, el uso biocargas presenta una gran ventaja medioambiental, ya que además de aprovechar los desechos naturales que normalmente terminan en vertederos, se contribuye con la disminución del uso de fuentes de energía o de materiales no renovables. Además, permite la reducción de emisiones contaminantes, y promueve una mayor biodegradabilidad del material al final de su vida útil [170].

I.5.2. Incorporación de nanocargas

En la actualidad se ha incrementado el auge de la obtención y uso de nanomateriales (nanotubos, nanopartículas y nanocapas) [192], para su adición en diferentes matrices (arcillas, metales y polímeros) [193]. Cuando los nanomateriales se añaden a las matrices poliméricas adquieren el nombre de nanocargas, nanorefuerzos o nanorellenos. Para que un material sea considerado como nano, al menos una de sus dimensiones espaciales debe encontrarse en la escala nanométrica, en un rango entre 1 y 100 nm [194]. Existen algunas maneras de clasificar los nanomateriales, pero una de las más utilizadas es la que se indica en la Norma ISO/TS 80004-2:2017 [195], según la cual los nanomateriales se dividen de acuerdo a sus dimensiones en: nanomateriales unidimensionales (1D) que son aquellos con una dimensión dentro de la escala nanométrica, es decir (<100 nm), los nanomateriales bidimensionales (2D) que presentan dos dimensiones dentro de la escala nanométrica y por último los nanomateriales tridimensionales (3D) que presentan sus tres dimensiones dentro de la escala nanométrica [196]. En la **Tabla I.11** se muestra esta clasificación con los diferentes tipos en cada grupo, mientras que en la **Figura I.25** se puede observar una representación gráfica de dicha clasificación.

Tabla I.11. Clasificación de nanomateriales según su dimensión.

Dimensión	Tipo
(1D) Unidimensional	Nanoplaca, nanopelículas, nanocapas.
(2D) Bidimensional	Nanovarillas, nanocables, nanofibras, nanotubos.
(3D) Tridimensional	Nanopartículas, racimo (*"clusters"*).

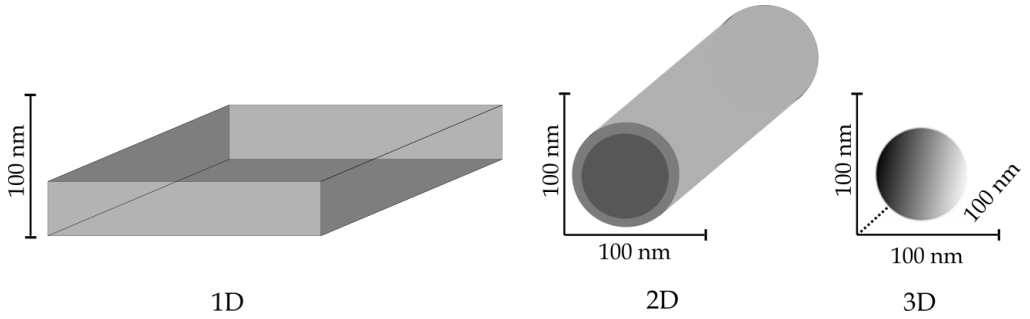

Figura I.25. Clasificación de nanomateriales según las dimensiones que presentan en el rango nanométrico.

Los polímeros nanocompuestos (PNCs) son estructuras sólidas multifase, en las cuales, al menos una de las fases tiene por lo menos una dimensión en la escala nanométrica (100 nm). Además, tienen una alta relación superficie/volumen, lo que marca la diferencia con otros materiales compuestos [197]. Constituyen, por tanto, materiales de gran importancia por las posibilidades científicas e industriales que presentan. Ello se debe a las mejoras que se logran al combinar con otros materiales. Los polímeros nanocompuestos (NPCs) están conformados por dos o más materiales, de los cuales uno es la matriz polimérica, y otro la fase dispersa (nanomaterial) [198]. Dichos nanomateriales se añaden a las matrices poliméricas en cantidades bajas, entre 1% y 10% en peso [192]. Esta adición produce un importante efecto en las propiedades y morfología de los polímeros nanocompuestos, debido a que estas nanocargas presentan una gran superficie específica y alta energía superficial. Ello produce una interacción entre los componentes, lo que puede alterar la química del polímero; es decir, pueden afectar la movilidad de sus cadenas, el grado de entrecruzamiento, etc. [199]. Esto permite la obtención de nuevos materiales con propiedades mejoradas en lo que respecta a propiedades mecánicas, térmicas, ópticas, eléctricas, magnéticas, mayor barrera contra gases y humedad, etc. [200]. Otra ventaja que se puede atribuir al uso de nanomateriales, es que, además de modificar las propiedades de los polímeros, pueden contribuir con la

reducción del costo y peso de los nanocompuestos obtenidos. Para escoger los nanomateriales que se utilizarán es importante tener en cuenta los siguientes factores: tamaño y morfología de los nanomateriales, carga eléctrica de la superficie y permeabilidad, grado de biocompatibilidad, biodegradabilidad, citotóxidad, etc. [194]. Entre los tipos de nanomateriales que más se utilizan se pueden mencionar las nanoarcillas, nanotubos de carbono, nanocristales de celulosa y nanotubos de haloisita [198].

Sin embargo, la baja compatibilidad de los nanomateriales con los polímeros, además de la predisposición de formar aglomerados entre sí debido a las fuerzas intermoleculares fuertes que presentan las partículas, dificultan su buena dispersión en la matriz. Ello constituye una importante limitación a la hora de obtener un buen material reforzado. De hecho, en algunos casos incluso pueden empeorar las propiedades del nanocompuesto [193, 201]. Por tanto, al escoger las nanocargas o nanomateriales, además de lo indicado anteriormente, es necesario tener en cuenta la estructura química de las matrices, ya que todo esto contribuye con la dispersión uniforme de los nanomateriales. Con ello se logra una mayor área superficial entre los constituyentes del nanocompuesto y se consigue la mejora de propiedades [198]. Otra manera de abordar esta limitación es mediante la adición de surfactantes orgánicos y compatibilizantes [193]. También se dispone de tratamientos superficiales que buscan debilitar las fuerzas intermoleculares entre las partículas, con lo cual se disminuye su aglomeración [201]. A continuación, se detallan dos nanocargas que son de gran interés hoy en día para la mejora en las propiedades de los materiales poliméricos.

- **Haloisita**

Los nanotubos de haloisita (HNTs) son un tipo de arcilla de aluminosilicato [198] que presentan una estructura similar a la caolinita, aunque esta última tiene una estructura de placas apiladas, mientras que los HNTs cuentan con una estructura micro y nanotubular hueca y con altas relaciones de aspecto. Adicionalmente, los HNTs se distinguen por la presencia de agua entre sus capas [202]. Su fórmula molecular es $Al_2Si_2O_5(OH)_4 \cdot nH_2O$, donde n equivale a 2 o 0 que representan los HNTs hidratados y deshidratados, respectivamente. Se considera un material respetuoso con el medio ambiente puesto que su extracción no supone ningún daño al ecosistema. Se extrae de

depósitos naturales situados, principalmente, en países como China, Brasil, Francia, etc. Normalmente es de color blanco, pero a veces puede adquirir tonalidad rojiza [203].

Los HNTs presentan condiciones diferentes de cristalización, por lo que pueden presentarse como partículas en diferentes morfologías: tubulares, esferoidales y como placas. Sin embargo, la estructura más común y ampliamente conocida es la tubular. Los HNTs de forma tubular presentan una longitud en el rango de las micras, mientras que su diámetro se encuentra en el rango de los nanómetros. El diámetro interno puede presentar valores entre (1 – 30) nm, el diámetro externo entre (30 – 50) nm, mientras que la longitud tiene valores entre (0.1 – 2) µm. Por otro lado, los HNTs se clasifican de acuerdo a su estado de hidratación en dos grupos; HNTs hidratados con estructura cristalina que mantiene una distancia basal de 10 Å entre capas, y HNTs deshidratados con estructura cristalina que presenta una distancia basal de 7 Å [204]. Un nanotubo de haloisita, como se observa en la **Figura I.26**, consta de una estructura en capas y está formada por dos, una correspondiente a una estructura octaédrica con grupos aluminol (Al-OH) en su superficie interna, y otra tetraédrica con grupos siloxanos (Si–O-Si) en su superficie externa, con cargas positiva y negativa, respectivamente, y que además se encuentran en una relación estequiométrica 1:1 [202].

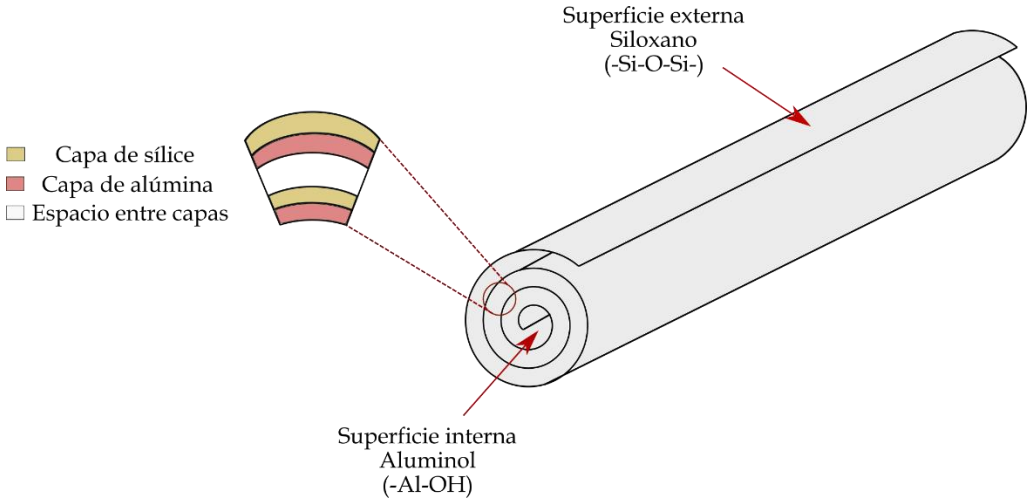

Figura I.26. Representación de la estructura tubular de los nanotubos de haloisita.

La gran relación de aspecto que tienen los HNTs permiten reforzar las matrices poliméricas, ya que optimizan la transferencia de carga desde la matriz polimérica hacia los nanotubos. Presentan, además, una densidad baja, lo que los hace convenientes para su uso cuando se busca obtener compuestos ligeros. Adicionalmente, estos nanotubos se

encuentran disponibles en la naturaleza, tienen buena biocompatibilidad, y alta resistencia mecánica, lo cual da lugar a buenas propiedades mecánicas, térmicas y biológicas. Además, tienen bajo costo lo que sin duda los hace competitivos en el mercado. Esto se ve reflejado en su uso cada vez mayor como alternativa a los nanotubos de carbono (CNT) de paredes múltiples con los que tienen una estructura similar y que normalmente son más costosos. Otra ventaja que ofrecen las HNTs es que no se requieren grandes cantidades para proporcionar mejoras. Se ha reportado que con contenidos de alrededor del 5% de HNTs, se logran mejoras en propiedades mecánicas de los polímeros en lo que respecta a módulo, resistencia al impacto y rigidez [202]. Dichas mejoras se pueden evidenciar en trabajos como el de Prashantha *et al.* [205] que combina el nanomaterial con poli(ácido láctico) (PLA), Jia *et al.* [206], por su parte, describe los resultados positivos obtenidos al combinar los HNTs con poli(etileno) lineal de baja densidad (LLDPE). Otra posibilidad que presentan los HNTs y que ha permitido su uso a nivel industrial, se debe a su forma tubular, que permite cargar ciertos tipos de sustancias para su posterior liberación controlada. Adicionalmente, la incorporación de HNTs a los polímeros produce, sin duda, una mejora considerable en la estabilidad térmica y la resistencia al fuego. Ello se debe a que proporcionan una barrera de aislamiento térmico en su superficie, lo cual impide que se desarrolle fuertemente la combustión del material [203]. Este comportamiento se ve reflejado en diferentes trabajos en los que se ha combinado los HNTs con matrices poliméricas como poli(propileno) (PP) [207], y poli(vinil alcohol) (PVA) [208].

Los HNTs, poseen relativa hidrofobicidad, básicamente debido a que tienen pocos grupos hidroxilo en su superficie externa, esto hace factible su dispersión en polímeros no polares; sin embargo, en algunos casos esto no es suficiente, ya que los nanotubos tienden a aglomerarse, por lo que con el fin de contrarrestar esta limitación se debe realizar algún tipo de tratamiento a los HNTs para mejorar su interacción interfacial y, con ello, su dispersión y adherencia a los materiales poliméricos [202]. Entre las posibilidades que se presentan destacan los tratamientos superficiales como la silanización, con lo que se beneficia por tanto su dispersión en las matrices poliméricas. Existen algunos trabajos en los que se ha considerado esta modificación y se ha constatado la mejora en propiedades mecánicas [209, 210].

- **Nanocristales de celulosa (CNC)**

Los nanocristales de celulosa (CNC) se obtienen a partir de celulosa, que es el biopolímero natural renovable más abundante en la tierra. La molécula de celulosa de cadena larga y alto peso molecular es un polisacárido lineal conformado por unidades de $_{B\text{-}D\text{-}}$anhidroglucopiranosa (que comprende unidades de anhídrido glucosa y glucopiranosa), unidos mediante enlaces glucosídicos β(1 → 4). La unidad de repetición de este polímero es un dímero de celulosa conocido como celobiosa [211, 212]. Cada monómero contiene en su estructura tres grupos hidroxilo, lo que hace posible que se formen enlaces con otras cadenas de celulosa. Esto a su vez, permite una mayor compactación de la estructura con lo que incrementa su cristalinidad y da lugar a la mejora en las propiedades [213].

La celulosa se encuentra en las fibras celulósicas conjuntamente con hemicelulosa y lignina, motivo por el cual se debe primero separar de estas dos, mediante el conocido "*top-down approach*", que consiste en un procedimiento por etapas. En una primera se realiza la separación de hemicelulosa y lignina [214], y a continuación se realiza un proceso para eliminar las secciones amorfas de las fibras. Este último paso se puede llevar a cabo mediante hidrólisis ácida o mediante un método enzimático. Sin embargo, el método más utilizado es el de hidrólisis ácida que consiste, básicamente, en degradar las partes no cristalinas (amorfas) de las fibras de celulosa, con lo cual se liberan las estructuras cristalinas presentes en ella. En este paso es posible la utilización de diferentes tipos de ácidos como el ácido fosfórico (H_3PO_4), nítrico (HNO_3), clorhídrico (HCl), sulfúrico (H_2SO_4) e incluso combinaciones entre ácido clorhídrico y ácidos orgánicos. No obstante, el tratamiento con ácido sulfúrico (H_2SO_4) es el que mejores resultados ha proporcionado, ya que los CNC obtenidos con este se pueden dispersar mejor en solventes, además que la suspensión que se forma es más estable [215, 216]. Siguiendo con el proceso, se procede con una etapa de centrifugación, diálisis y posterior liofilización, en el caso de que se requiera del material en estado sólido. En la **Figura I.27** se muestra el procedimiento de obtención de CNC utilizando hidrólisis ácida.

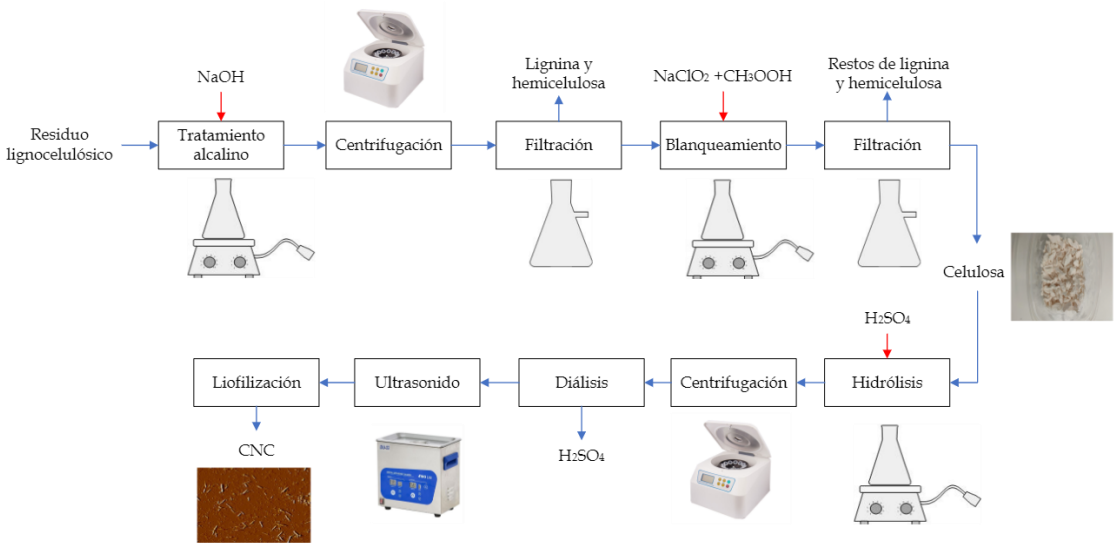

Figura I.27. Procedimiento para obtención a nanocristales de celulosa (CNC) mediante hidrólisis ácida.

Los CNC presentan forma de varillas con una alta relación de aspecto, aunque se debe considerar que sus dimensiones geométricas dependerán en gran medida del origen que tenga la celulosa, así como de las condiciones de procesado, en específico de la hidrólisis [215]. Entre los principales atributos de los CNC se encuentran su amplia disponibilidad, ligereza, pequeña dimensión y bajo costo, si se lo compara con otros nanomateriales. Además, cuenta con gran área superficial, y gran cantidad de grupos hidroxilo que permiten la formación de enlaces de hidrógeno, lo que mejora su interacción y les proporciona características como buena transparencia, pureza, cristalinidad, buena estabilidad térmica, y buenas propiedades mecánicas como rigidez y resistencia [211, 217]. Adicionalmente, esta disponibilidad de los grupos hidroxilo hace que los CNC tengan una superficie altamente reactiva, lo que los hace susceptibles a modificaciones y, por tanto, pueden ser funcionalizados.

Cuando los CNC se emplean como aditivo en matrices poliméricas se puede evidenciar el impacto en sus propiedades. La gran relación superficie/volumen de estos nanocristales produce una mayor área de contacto con la matriz polimérica, lo que proporciona a los CNC mayor interacción superficial con el polímero. Por ello, se requiere menor cantidad de CNC para que se produzca la mejora de propiedades. En cuanto a la relación de aspecto (L/D), que es otro parámetro bastante importante a la hora de reforzar la matriz polimérica, diversos estudios han reportado que relaciones de aspecto mayores a 30 pueden proporcionar mayor refuerzo, ya que permiten una mayor

interacción entre los CNC y la matriz. Esto contribuye positivamente a la transferencia de tensión o carga entre estas dos fases, y repercute en una mejora en las propiedades mecánicas y de barrera [214].

Uno de los ámbitos en las que se está prestando gran atención a los CNC, es para la fabricación de los materiales bionanocompuestos, donde los CNC actúan como cargas sobre matrices biopoliméricas. De esta manera, se aprovechan las buenas características indicadas de estos nanomateriales en matrices que son renovables, biodegradables y, en algunos casos, incluso biocompatibles. Los CNCs se han empleado ampliamente como aditivo funcional en películas para su uso en el sector envase y embalaje, con matrices de PLA [218, 219] y proteínas [220, 221].

La incorporación de CNCs en matrices poliméricas en forma de finas películas, contribuye a fragilizar los materiales. Por ello, se requiere, en muchas ocasiones, del empleo de plastificantes. Estos cumplen la función de reducir las fuerzas intermoleculares entre las cadenas poliméricas, e incrementar el espacio intermolecular entre ellas, con lo cual se hace más fácil su movimiento. Ello a su vez ocasiona una disminución en la temperatura de transición vítrea. Por tanto, puede mejorar las propiedades mecánicas, ya que la fragilidad disminuye e incrementa la flexibilidad del material. Por otro lado, el incremento de espacio entre las cadenas pueden perjudicar sus propiedades barrera, pues permitiría una mayor transferencia de gases y vapor de agua a través de las películas [156]. Para escoger un plastificante es necesario tener en consideración tanto la composición, como el tamaño, la forma y polaridad, así como su compatibilidad con el polímero, ya que esto puede afectar la interacción entre estos dos. Cuando el plastificante tiene tamaño molecular pequeño, alta polaridad y tiene más de un grupo polar por molécula, se puede incorporar más fácilmente a las cadenas poliméricas [150, 222]. Adicionalmente, para la selección del tipo de plastificante se considera su permanencia en el polímero, limitación de los fenómenos de migración, además de las propiedades físicas que se buscan lograr en las películas [223].

Entre los plastificantes más comunes utilizados para la producción de películas con proteínas están el agua, glicerol, oligosacáridos, polioles, lípidos, destacando entre ellos el glicerol y el sorbitol [139, 150, 222, 223]. El agua, por su parte, puede ser un plastificante eficaz, pero se evapora cuando la temperatura de procesado es superior a 100 °C y la película se vuelve quebradiza. Por tanto, lo que se requiere es un plastificante

menos volátil, como el glicerol, que tiene la capacidad de interactuar mediante enlaces de hidrógeno con la proteína en los sitios de amina, amida, carboxilo e hidroxilo, disminuyendo, con ello, las interacciones intermoleculares e intramoleculares entre las cadenas de proteínas. De esta manera se mejora su capacidad de movimiento y se obtienen películas flexibles [147, 224]. Se han desarrollado diferentes trabajos en los que se utiliza glicerol como plastificante de diferentes matrices proteicas obtenidas a partir de maní [225], trigo [226, 227], guisantes [228], soja [229, 230], etc.

REFERENCIAS

[1] R.U. Halden. *Plastics and health risks.* Annual review of public health, 2010, 31, p. 179-194.

[2] R. Geyer. *Production, use, and fate of synthetic polymers*, in *Plastic Waste and Recycling*. 2020, Elsevier, p. 13-32.

[3] H. Millet, P. Vangheluwe, C. Block, A. Sevenster, L. Garcia, and R. Antonopoulos. *The nature of plastics and their societal usage*, in *Plastics and the Environment*. 2019, The Royal Society of Chemistry, p. 1-20.

[4] K.J. Jem and B. Tan. *The development and challenges of poly (lactic acid) and poly (glycolic acid).* Advanced Industrial and Engineering Polymer Research, 2020, 3(2), p. 60-70.

[5] Plastics-Europe. *Plastics - the Facts 2021. Analysis of European plastics production, demand and waste data*. 2021, Plastics Europe: Brussels - Belgium, p. 1 - 34.

[6] R. Geyer. *A brief history of plastics*, in *Mare Plasticum-The Plastic Sea*. 2020, Springer, p. 31-47.

[7] P. Li, X. Wang, M. Su, X. Zou, L. Duan, and H. Zhang. *Characteristics of plastic pollution in the environment: a review.* Bulletin of environmental contamination and toxicology, 2021, 107(4), p. 577-584.

[8] European-bioplastics. *What are bioplastics?*. [Consulta 29 de marzo de 2022] ; Disponible en https://www.european-bioplastics.org/bioplastics/.

[9] Plastics-Industry-Association. *Bioplastics*. [Consulta: 07 de abril de 2022] Disponible en https://www.plasticsindustry.org/supply-chain/recycling-sustainability/bioplastics.

[10] M.S. Muthusamy and S. Pramasivam. *Bioplastics–an eco-friendly alternative to petrochemical plastics.* Current World Environment, 2019, 14(1), p. 49.

[11] M.F. Valero-Valdivieso, Y. Ortegón, and Y. Uscategui. *Biopolímeros: avances y perspectivas.* Dyna, 2013, 80(181), p. 171-180.

[12] European-Bioplastics. *Bioplastics market development update 2021*. 2021. [Consulta: 12 de abril de 2022]; Disponible en https://www.european-bioplastics.org/market/.

[13] R.M. Mohamed and K. Yusoh. *A review on the recent research of polycaprolactone (PCL).* Advanced Materials Research, 2016, 1134, p. 249-255.

[14] M. Thakur, I. Majid, S. Hussain, and V. Nanda. *Poly (ε-caprolactone): A potential polymer for biodegradable food packaging applications.* Packaging Technology and Science, 2021, 34(8), p. 449-461.

[15] K. Budak, O. Sogut, and U. Aydemir Sezer. *A review on synthesis and biomedical applications of polyglycolic acid.* Journal of Polymer Research, 2020, 27(8), p. 208.

[16] D.N. Putri, M. Sahlan, L. Montastruc, M. Meyer, S. Negny, and H. Hermansyah. *Progress of fermentation methods for bio-succinic acid production using agro-industrial waste by Actinobacillus succinogenes.* Energy Reports, 2020, 6, p. 234-239.

[17] S. Rafiqah, A. Khalina, A.S. Harmaen, I.A. Tawakkal, K. Zaman, M. Asim, M. Nurrazi, and C.H. Lee. *A review on properties and application of bio-based poly (butylene succinate).* Polymers, 2021, 13(9), p. 1436.

[18] X. Dai and Z. Qiu. *Synthesis and properties of novel biodegradable poly (butylene succinate-co-decamethylene succinate) copolyesters from renewable resources.* Polymer Degradation and Stability, 2016, 134, p. 305-310.

[19] J.H. Zhao, X.Q. Wang, J. Zeng, G. Yang, F.H. Shi, and Q. Yan. *Biodegradation of poly (butylene succinate) in compost.* Journal of Applied Polymer Science, 2005, 97(6), p. 2273-2278.

[20] S.S. Ray, J. Bandyopadhyay, and M. Bousmina. *Thermal and thermomechanical properties of poly [(butylene succinate)-co-adipate] nanocomposite.* Polymer Degradation and Stability, 2007, 92(5), p. 802-812.

[21] J. Xu and B.H. Guo. *Poly (butylene succinate) and its copolymers: Research, development and industrialization.* Biotechnology journal, 2010, 5(11), p. 1149-1163.

[22] J. Jian, Z. Xiangbin, and H. Xianbo. *An overview on synthesis, properties and applications of poly (butylene-adipate-co-terephthalate)–PBAT.* Advanced Industrial and Engineering Polymer Research, 2020, 3(1), p. 19-26.

[23] Y.-X. Weng, Y.-J. Jin, Q.-Y. Meng, L. Wang, M. Zhang, and Y.-Z. Wang. *Biodegradation behavior of poly (butylene adipate-co-terephthalate)(PBAT), poly (lactic acid)(PLA), and their blend under soil conditions.* Polymer Testing, 2013, 32(5), p. 918-926.

[24] L.-F. Wang, J.-W. Rhim, and S.-I. Hong. *Preparation of poly (lactide)/poly (butylene adipate-co-terephthalate) blend films using a solvent casting method and their food packaging application.* LWT-Food Science and Technology, 2016, 68, p. 454-461.

[25] F.V. Ferreira, L.S. Cividanes, R.F. Gouveia, and L.M. Lona. *An overview on properties and applications of poly (butylene adipate-co-terephthalate)–PBAT based composites.* Polymer Engineering & Science, 2019, 59(s2), p. E7-E15.

[26] C. Andreeßen and A. Steinbüchel. *Recent developments in non-biodegradable biopolymers: Precursors, production processes, and future perspectives.* Applied microbiology and biotechnology, 2019, 103(1), p. 143-157.

[27] D. Damayanti, D. Supriyadi, D. Amelia, D.R. Saputri, Y.L.L. Devi, W.A. Auriyani, and H.S. Wu. *Conversion of lignocellulose for bioethanol production, applied in bio-polyethylene terephthalate.* Polymers, 2021, 13(17), p. 2886.

[28] L. Jiang, A. Gonzalez-Diaz, J. Ling-Chin, A. Malik, A. Roskilly, and A. Smallbone. *PEF plastic synthesized from industrial carbon dioxide and biowaste.* Nature Sustainability, 2020, 3(9), p. 761-767.

[29] K. Loos, R. Zhang, I. Pereira, B. Agostinho, H. Hu, D. Maniar, N. Sbirrazzuoli, A.J. Silvestre, N. Guigo, and A.F. Sousa. *A perspective on PEF synthesis, properties, and end-life.* Frontiers in Chemistry, 2020, 8, p. 585.

[30] S. Kuciel, P. Koźniar, and A. Liber-Kneć. *Polyamides from renewable sources as matrices of short fiber reinforced biocomposites.* Polimery, 2012, 57(9), p. 627-634.

[31] B. Brehmer. *Polyamides from biomass derived monomers.* Bio-Based Plastics: Materials and Applications, 2013, p. 275-293.

[32] D.V. Palaskar, A. Boyer, E. Cloutet, C. Alfos, and H. Cramail. *Synthesis of biobased polyurethane from oleic and ricinoleic acids as the renewable resources via the AB-type self-condensation approach.* Biomacromolecules, 2010, 11(5), p. 1202-1211.

[33] A. Noreen, K.M. Zia, M. Zuber, S. Tabasum, and A.F. Zahoor. *Bio-based polyurethane: An efficient and environment friendly coating systems: A review.* Progress in Organic Coatings, 2016, 91, p. 25-32.

[34] J.-M. Raquez, M. Deléglise, M.-F. Lacrampe, and P. Krawczak. *Thermosetting (bio) materials derived from renewable resources: A critical review.* Progress in polymer science, 2010, 35(4), p. 487-509.

[35] M.A. Sawpan. *Polyurethanes from vegetable oils and applications: a review.* Journal of Polymer Research, 2018, 25(8), p. 184.

[36] S. Kumar and K. Thakur. *Bioplastics-classification, production and their potential food applications.* Journal of Hill Agriculture, 2017, 8(2), p. 118-129.

[37] M. Ahmad, N.P. Nirmal, M. Danish, J. Chuprom, and S. Jafarzedeh. *Characterisation of composite films fabricated from collagen/chitosan and collagen/soy protein isolate for food packaging applications.* Rsc Advances, 2016, 6(85), p. 82191-82204.

[38] F. Song, D.-L. Tang, X.-L. Wang, and Y.-Z. Wang. *Biodegradable soy protein isolate-based materials: a review.* Biomacromolecules, 2011, 12(10), p. 3369-3380.

[39] T. Garrido, J. Uranga, P. Guerrero, and K.d.l. Caba. *The potential of vegetal and animal proteins to develop more sustainable food packaging*, in *Polymers for Food Applications*. 2018, Springer, p. 25-59.

[40] M.M. Reddy, S. Vivekanandhan, M. Misra, S.K. Bhatia, and A.K. Mohanty. *Biobased plastics and bionanocomposites: Current status and future opportunities.* Progress in polymer science, 2013, 38(10-11), p. 1653-1689.

[41] S. Molinaro, M. Cruz-Romero, A. Sensidoni, M. Morris, C. Lagazio, and J.P. Kerry. *Combination of high-pressure treatment, mild heating and holding time effects as a means of improving the barrier properties of gelatin-based packaging films using response surface modeling.* Innovative Food Science & Emerging Technologies, 2015, 30, p. 15-23.

[42] A. Nešić, G. Cabrera-Barjas, S. Dimitrijević-Branković, S. Davidović, N. Radovanović, and C. Delattre. *Prospect of polysaccharide-based materials as advanced food packaging.* Molecules, 2019, 25(1), p. 135.

[43] P. Nechita and M. Roman. *Review on polysaccharides used in coatings for food packaging papers.* Coatings, 2020, 10(6), p. 566.

[44] M. Poletto and H. Ornaghi Jr. *Cellulose: Fundamental Aspects and Current Trends*. 2015: BoD–Books on Demand, p. 1-284.

[45] Y. Liu, S. Ahmed, D.E. Sameen, Y. Wang, R. Lu, J. Dai, S. Li, and W. Qin. *A review of cellulose and its derivatives in biopolymer-based for food packaging application.* Trends in Food Science & Technology, 2021, 112, p. 532-546.

[46] J. Synowiecki and N.A. Al-Khateeb. *Production, properties, and some new applications of chitin and its derivatives.* Critical Reviews in Food Science and Nutrition, 2003, 43(2), p. 145-171.

[47] P.K. Dutta, J. Dutta, and V. Tripathi. *Chitin and chitosan: Chemistry, properties and applications.* Journal of Scientific & Industrial Research, 2004, 63, p. 20-31.

[48] M.N.R. Kumar. *A review of chitin and chitosan applications.* Reactive and functional polymers, 2000, 46(1), p. 1-27.

[49] Z. Shen and M. Jacobs-Lorena. *Evolution of chitin-binding proteins in invertebrates.* Journal of molecular evolution, 1999, 48(3), p. 341-347.

[50] S. Islam, M. Bhuiyan, and M. Islam. *Chitin and chitosan: structure, properties and applications in biomedical engineering.* Journal of Polymers and the Environment, 2017, 25(3), p. 854-866.

[51] C. Peniche, W. Argüelles-Monal, and F. Goycoolea. *Chitin and chitosan: major sources, properties and applications*, in *Monomers, polymers and composites from renewable resources*. 2008, Elsevier, p. 517-542.

[52] M. Jaworska, K. Sakurai, P. Gaudon, and E. Guibal. *Influence of chitosan characteristics on polymer properties. I: Crystallographic properties.* Polymer International, 2003, 52(2), p. 198-205.

[53] J.-K.F. Suh and H.W. Matthew. *Application of chitosan-based polysaccharide biomaterials in cartilage tissue engineering: a review.* Biomaterials, 2000, 21(24), p. 2589-2598.

[54] W. Groot, J. Van Krieken, O. Sliekersl, and S. De Vos. *Production and purification of lactic acid and lactide*, in *Poly (Lactic Acid) Synthesis, Structures, Properties, Processing, Applications, and End of Life*. 2022, p. 3-18.

[55] M.R. Yates and C.Y. Barlow. *Life cycle assessments of biodegradable, commercial biopolymers – A critical review.* Resources, Conservation and Recycling, 2013, 78, p. 54-66.

[56] R. Auras, B. Harte, and S. Selke. *An overview of polylactides as packaging materials.* Macromolecular bioscience, 2004, 4(9), p. 835-864.

[57] J. Lu, R.C. Tappel, and C.T. Nomura. *Mini-review: biosynthesis of poly (hydroxyalkanoates).* Journal of Macromolecular Science®, Part C: Polymer Reviews, 2009, 49(3), p. 226-248.

[58] T. Tsuge. *Metabolic improvements and use of inexpensive carbon sources in microbial production of polyhydroxyalkanoates.* Journal of bioscience and bioengineering, 2002, 94(6), p. 579-584.

[59] Z.A. Raza, S. Riaz, and I.M. Banat. *Polyhydroxyalkanoates: Properties and chemical modification approaches for their functionalization.* Biotechnology Progress, 2018, 34(1), p. 29-41.

[60] T. Volova. *Polyhydroxyalkanoates-plastic materials of the 21st century: production, properties, applications*. 2004: Nova publishers.

[61] A. Tsui, Z.C. Wright, and C.W. Frank. *Biodegradable polyesters from renewable resources.* Annual review of chemical and biomolecular engineering, 2013, 4, p. 143-170.

[62] Y. Dai, Z. Yuan, K. Jack, and J. Keller. *Production of targeted poly (3-hydroxyalkanoates) copolymers by glycogen accumulating organisms using acetate as sole carbon source.* Journal of Biotechnology, 2007, 129(3), p. 489-497.

[63] F. Masood. *Polyhydroxyalkanoates in the food packaging industry*, in *Nanotechnology Applications in Food*. 2017, Elsevier, p. 153-177.

[64] M. Koller, H. Niebelschütz, and G. Braunegg. *Strategies for recovery and purification of poly [(R)-3-hydroxyalkanoates](PHA) biopolyesters from surrounding biomass.* Engineering in Life Sciences, 2013, 13(6), p. 549-562.

[65] A. Morschbacker, C.E. Siqueira Campos, L.C. Cassiano, L. Roza, F. Almada, and R.W. do Carmo. *Bio-polyethylene*, in *Handbook of Green Materials: 4 Biobased composite materials, their processing properties and industrial applications*. 2014, World Scientific, p. 89-104.

[66] R.P. Babu, K. O'connor, and R. Seeram. *Current progress on bio-based polymers and their future trends.* Progress in biomaterials, 2013, 2(1), p. 8.

[67] L. Shen, E. Worrell, and M. Patel. *Present and future development in plastics from biomass.* Biofuels, Bioproducts and Biorefining: Innovation for a sustainable economy, 2010, 4(1), p. 25-40.

[68] D. Garcia-Garcia, A. Carbonell-Verdu, A. Jordá-Vilaplana, R. Balart, and D. Garcia-Sanoguera. *Development and characterization of green composites from bio-based polyethylene and peanut shell.* Journal of Applied Polymer Science, 2016, 133(37), p. 43940.

[69] Braskem. *I'm green polyethylene*. 2014. [Consulta: 11 de mayo de 2022]; Disponible en https://bioplasticsnews.com/wp-content/uploads/2019/08/Im-Green-Brochure.pdf.

[70] C.M. Mendieta, M.E. Vallejos, F.E. Felissia, G. Chinga-Carrasco, and M.C. Area. *Bio-polyethylene from wood wastes.* Journal of Polymers and the Environment, 2020, 28(1), p. 1-16.

[71] V. Siracusa and I. Blanco. *Bio-polyethylene (Bio-PE), Bio-polypropylene (Bio-PP) and Bio-poly (ethylene terephthalate)(Bio-PET): Recent developments in bio-based polymers analogous to petroleum-derived ones for packaging and engineering applications.* Polymers, 2020, 12(8), p. 1641.

[72] R.M. Patel. *Types and basics of polyethylene.* Handbook of industrial polyethylene and technology, 2017, p. 105-138.

[73] Q. Tarrés and M. Ardanuy. *Evolution of interfacial shear strength and mean intrinsic single strength in biobased composites from bio-polyethylene and thermo-mechanical pulp-corn stover fibers.* Polymers, 2020, 12(6), p. 1308.

[74] T. Raj, K. Chandrasekhar, A.N. Kumar, and S.-H. Kim. *Lignocellulosic biomass as renewable feedstock for biodegradable and recyclable plastics production: A sustainable approach.* Renewable and Sustainable Energy Reviews, 2022, 158, p. 112130.

[75] K. Mazur, P. Jakubowska, P. Romańska, and S. Kuciel. *Green high density polyethylene (HDPE) reinforced with basalt fiber and agricultural fillers for technical applications.* Composites Part B: Engineering, 2020, 202, p. 108399.

[76] C. Dolza, E. Fages, E. Gonga, J. Gomez-Caturla, R. Balart, and L. Quiles-Carrillo. *Development and characterization of environmentally friendly wood plastic composites from biobased polyethylene and short natural fibers processed by injection moulding.* Polymers, 2021, 13(11), p. 1692.

[77] P. Bazan, D. Mierzwiński, R. Bogucki, and S. Kuciel. *Bio-based polyethylene composites with natural fiber: Mechanical, thermal, and ageing properties.* Materials, 2020, 13(11), p. 2595.

[78] F.M. Lamberti, L.A. Román-Ramírez, and J. Wood. *Recycling of bioplastics: routes and benefits.* Journal of Polymers and the Environment, 2020, 28(10), p. 2551-2571.

[79] K. Menard and N. Menard. *Thermal analysis of polyethylene.* Handbook of Industrial Polyethylene and Technology. MA Spalding and AM Chatterjee (Eds.). Scrivener Publishing, Beverly, Massachusetts, 2017, p. 217-238.

[80] A.W. deGroot, D. Gillespie, R. Cong, Z. Zhou, and R. Paradkar. *Molecular Structural Characterization of Polyethylene.* Handbook of Industrial Polyethylene and Technology: Definitive Guide to Manufacturing, Properties, Processing, Applications and Markets, 2017, p. 139-216.

[81] R. Balart, J. López, L. Sánchez, and A. Nadal. *Introducción a la ciencia e ingeniería de polímeros.* Alfagràfic SA: Alcoy, 2001.

[82] H. Ku, H. Wang, N. Pattarachaiyakoop, and M. Trada. *A review on the tensile properties of natural fiber reinforced polymer composites.* Composites Part B: Engineering, 2011, 42(4), p. 856-873.

[83] S. Kuciel, P. Jakubowska, and P. Kuźniar. *A study on the mechanical properties and the influence of water uptake and temperature on biocomposites based on polyethylene from renewable sources.* Composites Part B: Engineering, 2014, 64, p. 72-77.

[84] Y.T. Kim, B. Min, and K.W. Kim. *General characteristics of packaging materials for food system*, in *Innovations in Food Packaging*. 2014, Elsevier, p. 13-35.

[85] R. Hatti-Kaul, L.J. Nilsson, B. Zhang, N. Rehnberg, and S. Lundmark. *Designing biobased recyclable polymers for plastics.* Trends in biotechnology, 2020, 38(1), p. 50-67.

[86] S. Kumar, A.K. Panda, and R.K. Singh. *A review on tertiary recycling of high-density polyethylene to fuel.* Resources, Conservation and Recycling, 2011, 55(11), p. 893-910.

[87] M. Ratajska and S. Boryniec. *Biodegradation of some natural polymers in blends with polyolefines.* Polymers for Advanced Technologies, 1999, 10(10), p. 625-633.

[88] D. Nguyen, T. Vu, A.-C. Grillet, H.H. Thuc, and C.H. Thuc. *Effect of organoclay on morphology and properties of linear low density polyethylene and Vietnamese cassava starch biobased blend.* Carbohydrate polymers, 2016, 136, p. 163-170.

[89] C. Huang, J. He, R. Narron, Y. Wang, and Q. Yong. *Characterization of kraft lignin fractions obtained by sequential ultrafiltration and their potential application as a biobased component in blends with polyethylene.* ACS Sustainable Chemistry & Engineering, 2017, 5(12), p. 11770-11779.

[90] S. Lüftl and P. Visakh. *Polyethylene-based biocomposites and bionanocomposites*. 2016: John Wiley & Sons.

[91] S. Sid, R.S. Mor, A. Kishore, and V.S. Sharanagat. *Bio-sourced polymers as alternatives to conventional food packaging materials: A review.* Trends in Food Science & Technology, 2021, 115, p. 87-104.

[92] A. Guilhen, R. Gadioli, F.C. Fernandes, W.R. Waldman, and M. Aurelio De Paoli. *High-density green polyethylene biocomposite reinforced with cellulose fibers and using lignin as antioxidant.* Journal of Applied Polymer Science, 2017, 134(35), p. 45219.

[93] Q. Tarrés, J.K. Melbø, M. Delgado-Aguilar, F. Espinach, P. Mutjé, and G. Chinga-Carrasco. *Bio-polyethylene reinforced with thermomechanical pulp fibers: Mechanical and micromechanical characterization and its application in 3D-printing by fused deposition modelling.* Composites Part B: Engineering, 2018, 153, p. 70-77.

[94] S. Torres-Giner, A. Torres, M. Ferrándiz, V. Fombuena, and R. Balart. *Antimicrobial activity of metal cation-exchanged zeolites and their evaluation on injection-molded pieces of bio-based high-density polyethylene.* Journal of Food Safety, 2017, 37(4), p. e12348.

[95] J.N. Hoskins and S.M. Grayson. *Cyclic polyesters: synthetic approaches and potential applications.* Polymer Chemistry, 2011, 2(2), p. 289-299.

[96] C.K. Williams. *Synthesis of functionalized biodegradable polyesters.* Chemical Society Reviews, 2007, 36(10), p. 1573-1580.

[97] L. Avérous. *Biocomposites Based on Biodegradable Thermoplastic Polyester and Lignocellulose Fibers*, in *Cellulose Fibers: Bio-and Nano-Polymer Composites*. 2011, Springer, p. 453-478.

[98] U. Edlund and A.-C. Albertsson. *Polyesters based on diacid monomers.* Advanced drug delivery reviews, 2003, 55(4), p. 585-609.

[99] R.-J. Müller, I. Kleeberg, and W.-D. Deckwer. *Biodegradation of polyesters containing aromatic constituents.* Journal of Biotechnology, 2001, 86(2), p. 87-95.

[100] A. Carbonell-Verdu, J. Ferri, F. Dominici, T. Boronat, L. Sanchez-Nacher, R. Balart, and L. Torre. *Manufacturing and compatibilization of PLA/PBAT binary blends by cottonseed oil-based derivatives.* Express Polymer Letters, 2018, 12(9), p. 808-823.

[101] M. Shibata, Y. Inoue, and M. Miyoshi. *Mechanical properties, morphology, and crystallization behavior of blends of poly (L-lactide) with poly (butylene succinate-co-L-lactate) and poly (butylene succinate).* Polymer, 2006, 47(10), p. 3557-3564.

[102] L.C. Arruda, M. Magaton, R.E.S. Bretas, and M.M. Ueki. *Influence of chain extender on mechanical, thermal and morphological properties of blown films of PLA/PBAT blends.* Polymer Testing, 2015, 43, p. 27-37.

[103] K. Pang, R. Kotek, and A. Tonelli. *Review of conventional and novel polymerization processes for polyesters.* Progress in polymer science, 2006, 31(11), p. 1009-1037.

[104] F. Carrasco, P. Pagès, J. Gámez-Pérez, O. Santana, and M.L. Maspoch. *Processing of poly (lactic acid): Characterization of chemical structure, thermal stability and mechanical properties.* Polymer Degradation and Stability, 2010, 95(2), p. 116-125.

[105] E. Petinakis, L. Yu, G. Simon, and K. Dean. *Fiber Reinforced Polymers–The Technology Applied for Concrete Repair.* Chapter, 2013, 2, p. 41-54.

[106] Y. Ichikawa and T. Mizukoshi. *Bionolle (polybutylenesuccinate).* Synthetic Biodegradable Polymers, 2011, p. 285-313.

[107] J. Xu and B.-H. Guo. *Microbial succinic acid, its polymer poly (butylene succinate), and applications*, in *Plastics from Bacteria*. 2010, Springer, p. 347-388.

[108] N. Jacquel, F. Freyermouth, F. Fenouillot, A. Rousseau, J.P. Pascault, P. Fuertes, and R. Saint-Loup. *Synthesis and properties of poly (butylene succinate): Efficiency of different transesterification catalysts.* Journal of Polymer Science Part A: Polymer Chemistry, 2011, 49(24), p. 5301-5312.

[109] A. Shebani, A. Klash, R. Elhabishi, S. Abdsalam, H. Elbreki, and W. Elhrari. *The influence of LDPE content on the mechanical properties of HDPE/LDPE blends.* Research & Development in Material Science, 2018, 7(5), p. 791-797.

[110] Q.T. Shubhra, A.M. Alam, and M.A. Quaiyyum. *Mechanical properties of polypropylene composites: A review.* Journal of thermoplastic composite materials, 2013, 26(3), p. 362-391.

[111] G.-Q. Chen. *Introduction of Bacterial Plastics PHA, PLA, PBS, PE, PTT, and PPP*, in *Plastics from Bacteria*. 2010, Springer, p. 1-16.

[112] S. Vytejčková, L. Vápenka, J. Hradecký, J. Dobiáš, J. Hajšlová, C. Loriot, L. Vannini, and J. Poustka. *Testing of polybutylene succinate based films for poultry meat packaging.* Polymer Testing, 2017, 60, p. 357-364.

[113] A. Bhatia, R.K. Gupta, S.N. Bhattacharya, and H. Choi. *Compatibility of biodegradable poly (lactic acid)(PLA) and poly (butylene succinate)(PBS) blends for packaging application.* Korea-Australia rheology journal, 2007, 19(3), p. 125-131.

[114] M.J. Mochane, S.I. Magagula, J.S. Sefadi, and T.C. Mokhena. *A review on green composites based on natural fiber-reinforced polybutylene succinate (PBS).* Polymers, 2021, 13(8), p. 1200.

[115] P. Liminana, D. Garcia-Sanoguera, L. Quiles-Carrillo, R. Balart, and N. Montanes. *Optimization of maleinized linseed oil loading as a biobased compatibilizer in poly (butylene succinate) composites with almond shell flour.* Materials, 2019, 12(5), p. 685.

[116] M. Soccio, F. Dominici, S. Quattrosoldi, F. Luzi, A. Munari, L. Torre, N. Lotti, and D. Puglia. *PBS-based green copolymer as an efficient compatibilizer in thermoplastic inedible wheat flour/poly (butylene succinate) blends.* Biomacromolecules, 2020, 21(8), p. 3254-3269.

[117] F. Jbilou, C. Joly, S. Galland, L. Belard, V. Desjardin, R. Bayard, P. Dole, and P. Degraeve. *Biodegradation study of plasticised corn flour/poly (butylene succinate-co-butylene adipate) blends.* Polymer Testing, 2013, 32(8), p. 1565-1575.

[118] S. Inkinen, M. Hakkarainen, A.-C. Albertsson, and A. Södergård. *From lactic acid to poly (lactic acid)(PLA): characterization and analysis of PLA and its precursors.* Biomacromolecules, 2011, 12(3), p. 523-532.

[119] K. Hamad, M. Kaseem, H. Yang, F. Deri, and Y. Ko. *Properties and medical applications of polylactic acid: A review.* Express Polymer Letters, 2015, 9(5), p. 435-455.

[120] J. Ahmed and S.K. Varshney. *Polylactides – chemistry, properties and green packaging technology: a review.* International journal of food properties, 2011, 14(1), p. 37-58.

[121] M. Jamshidian, E.A. Tehrany, M. Imran, M. Jacquot, and S. Desobry. *Poly-Lactic Acid: production, applications, nanocomposites, and release studies.* Comprehensive reviews in food science and food safety, 2010, 9(5), p. 552-571.

[122] D. Garlotta. *A literature review of poly (lactic acid).* Journal of Polymers and the Environment, 2001, 9(2), p. 63-84.

[123] R. Mehta, V. Kumar, H. Bhunia, and S. Upadhyay. *Synthesis of poly (lactic acid): a review.* Journal of Macromolecular Science, Part C: Polymer Reviews, 2005, 45(4), p. 325-349.

[124] D.E. Henton, P. Gruber, J. Lunt, and J. Randall. *Polylactic acid technology.* Natural fibers, biopolymers, and biocomposites, 2005, 16, p. 527-577.

[125] H. Tsuji. *Poly (lactic acid).* Bio-Based Plastics: Materials and Applications, 2013, p. 171-239.

[126] L.-T. Lim, R. Auras, and M. Rubino. *Processing technologies for poly (lactic acid).* Progress in polymer science, 2008, 33(8), p. 820-852.

[127] X. Pang, X. Zhuang, Z. Tang, and X. Chen. *Polylactic acid (PLA): research, development and industrialization.* Biotechnology journal, 2010, 5(11), p. 1125-1136.

[128] K.J. Jem, J.F. Pol, and S.d. Vos. *Microbial lactic acid, its polymer poly (lactic acid), and their industrial applications*, in *Plastics from Bacteria*. 2010, Springer, p. 323-346.

[129] L. Avérous. *Polylactic acid: synthesis, properties and applications*, in *Monomers, polymers and composites from renewable resources*. 2008, Elsevier, p. 433-450.

[130] I. Armentano, N. Bitinis, E. Fortunati, S. Mattioli, N. Rescignano, R. Verdejo, M.A. López-Manchado, and J.M. Kenny. *Multifunctional nanostructured PLA materials for packaging and tissue engineering.* Progress in polymer science, 2013, 38(10-11), p. 1720-1747.

[131] M.L. Di Lorenzo and R. Androsch. *Synthesis, structure and properties of poly (lactic acid)*. Vol. 279, 2018: Springer.

[132] I. Gan and W. Chow. *Antimicrobial poly (lactic acid)/cellulose bionanocomposite for food packaging application: A review.* Food packaging and shelf life, 2018, 17, p. 150-161.

[133] J.-M. Lagarón. *Polylactic acid (PLA) nanocomposites for food packaging applications*, in *Multifunctional and Nanoreinforced Polymers for Food Packaging*. 2011, Elsevier, p. 485-497.

[134] C. Ingrao, M. Gigli, and V. Siracusa. *An attributional Life Cycle Assessment application experience to highlight environmental hotspots in the production of foamy polylactic acid trays for fresh-food packaging usage.* Journal of cleaner production, 2017, 150, p. 93-103.

[135] L.T. Sin. *Polylactic acid: PLA biopolymer technology and applications*. 2012: William Andrew.

[136] Q. Zhang, V.N. Mochalin, I. Neitzel, I.Y. Knoke, J. Han, C.A. Klug, J.G. Zhou, P.I. Lelkes, and Y. Gogotsi. *Fluorescent PLLA-nanodiamond composites for bone tissue engineering.* Biomaterials, 2011, 32(1), p. 87-94.

[137] Y. Qin, M. Yuan, L. Li, S. Guo, M. Yuan, W. Li, and J. Xue. *Use of polylactic acid/polytrimethylene carbonate blends membrane to prevent postoperative adhesions.* Journal of Biomedical Materials Research Part B: Applied Biomaterials, 2006, 79(2), p. 312-319.

[138] V. Sharma, M. Kaur, K.S. Sandhu, and S.K. Godara. *Effect of cross-linking on physico-chemical, thermal, pasting, in vitro digestibility and film forming properties of Faba bean (Vicia faba L.) starch.* International journal of biological macromolecules, 2020, 159, p. 243-249.

[139] V. Perez, M. Felix, A. Romero, and A. Guerrero. *Characterization of pea protein-based bioplastics processed by injection moulding.* Food and bioproducts processing, 2016, 97, p. 100-108.

[140] K.K. Sadasivuni, P. Saha, J. Adhikari, K. Deshmukh, M.B. Ahamed, and J.J. Cabibihan. *Recent advances in mechanical properties of biopolymer composites: A review.* Polymer Composites, 2020, 41(1), p. 32-59.

[141] C. Brigham. *Biopolymers: Biodegradable alternatives to traditional plastics*, in *Green Chemistry*. 2018, Elsevier, p. 753-770.

[142] L. Avérous and E. Pollet. *Biodegradable polymers*, in *Environmental Silicate Nano-Biocomposites*. 2012, Springer, p. 13-39.

[143] L. Zhang and M. Zeng. *Proteins as sources of materials*, in *Monomers, polymers and composites from renewable resources*. 2008, p. 479-493.

[144] S. Kumar, I.B. Basumatary, A. Mukherjee, and J. Dutta. *An overview of natural biopolymers in food packaging*, in *Biopolymer-Based Food Packaging: Innovations and Technology Applications*. 2022, John Wiley & Sons, Ltd.: Hoboken, NJ, USA, p. 1-28.

[145] A.K. Mohanty, M. Misra, and L.T. Drzal. *Natural fibers, biopolymers, and biocomposites*. 2005: CRC press.

[146] N. Reddy and Y. Yang. *Thermoplastic films from plant proteins.* Journal of Applied Polymer Science, 2013, 130(2), p. 729-738.

[147] L. Ricci, E. Umiltà, M.C. Righetti, T. Messina, C. Zurlini, A. Montanari, S. Bronco, and M. Bertoldo. *On the thermal behavior of protein isolated from different legumes investigated by DSC and TGA.* Journal of the Science of Food and Agriculture, 2018, 98(14), p. 5368-5377.

[148] D. Klupšaitė and G. Juodeikienė. *Legume: Composition, protein extraction and functional properties. A review.* Chemical Technology, 2015, 66(1), p. 5-12.

[149] A. Amin, I.L. Petersen, C. Malmberg, and V. Orlien. *Perspective on the Effect of Protein Extraction Method on the Antinutritional Factor (ANF) Content in Seeds.* ACS Food Science & Technology, 2022, 2(4), p. 604-612.

[150] P. Guerrero, A. Retegi, N. Gabilondo, and K. De la Caba. *Mechanical and thermal properties of soy protein films processed by casting and compression.* Journal of food engineering, 2010, 100(1), p. 145-151.

[151] D. Jagadeesh, K. Kanny, and K. Prashantha. *A review on research and development of green composites from plant protein-based polymers.* Polymer Composites, 2017, 38(8), p. 1504-1518.

[152] S.J. Kim and Z. Ustunol. *Solubility and moisture sorption isotherms of whey-protein-based edible films as influenced by lipid and plasticizer incorporation.* Journal of agricultural and food chemistry, 2001, 49(9), p. 4388-4391.

[153] D. Turan, G. Gunes, and A. Kilic. *Perspectives of bio-nanocomposites for food packaging applications*, in *Bionanocomposites for packaging applications*. 2018, p. 1-32.

[154] S. Ou, K. Kwok, and Y. Kang. *Changes in in vitro digestibility and available lysine of soy protein isolate after formation of film.* Journal of food engineering, 2004, 64(3), p. 301-305.

[155] P. Barreto, A. Pires, and V. Soldi. *Thermal degradation of edible films based on milk proteins and gelatin in inert atmosphere.* Polymer Degradation and Stability, 2003, 79(1), p. 147-152.

[156] M. Aydinli and M. Tutas. *Water sorption and water vapour permeability properties of polysaccharide (locust bean gum) based edible films.* LWT-Food Science and Technology, 2000, 33(1), p. 63-67.

[157] S. Pirsa and K. Aghbolagh Sharifi. *A review of the applications of bioproteins in the preparation of biodegradable films and polymers.* Journal of Chemistry Letters, 2020, 1(2), p. 47-58.

[158] J. Yang, G. Liu, H. Zeng, and L. Chen. *Effects of high pressure homogenization on faba bean protein aggregation in relation to solubility and interfacial properties.* Food hydrocolloids, 2018, 83, p. 275-286.

[159] S. Saremnezhad, M. Azizi, M. Barzegar, S. Abbasi, and E. Ahmadi. *Properties of a new edible film made of faba bean protein isolate.* Journal of Agricultural Science and Technology, 2011, 13(2), p. 181-192.

[160] M. Vukić, S. Grujić, and B. Odzaković. *Application of edible films and coatings in food production*, in *Advances in Applications of Industrial Biomaterials*. 2017, Springer, p. 121-138.

[161] H.-J. Kang, S.-J. Kim, Y.-S. You, M. Lacroix, and J. Han. *Inhibitory effect of soy protein coating formulations on walnut (Juglans regia L.) kernels against lipid oxidation.* LWT-Food Science and Technology, 2013, 51(1), p. 393-396.

[162] E.J. Hopkins, A.K. Stone, J. Wang, D.R. Korber, and M.T. Nickerson. *Effect of glycerol on the physicochemical properties of films based on legume protein concentrates: A comparative study.* Journal of texture studies, 2019, 50(6), p. 539-546.

[163] F. Bamdad, A.H. Goli, and M. Kadivar. *Preparation and characterization of proteinous film from lentil (Lens culinaris): Edible film from lentil (Lens culinaris).* Food Research International, 2006, 39(1), p. 106-111.

[164] C.H. Pagno, T.V. Klug, T.M.H. Costa, A. de Oliveira Rios, and S.H. Flôres. *Physical and antimicrobial properties of quinoa flour-based films incorporated with essential oil.* Journal of Applied Polymer Science, 2016, 133(16), p. 43311.

[165] E. Yildiz, E. Ilhan, L.N. Kahyaoglu, G. Sumnu, and M.H. Oztop. *The effects of crosslinking agents on faba bean flour–chitosan-curcumin films and their characterization.* Legume Science, 2022, 4(1), p. e121.

[166] J. Wyrwa and A. Barska. *Innovations in the food packaging market: Active packaging.* European Food Research and Technology, 2017, 243(10), p. 1681-1692.

[167] M. Kurek, I.E. Garofulić, M.T. Bakić, M. Ščetar, and V.D. Uzelac. *Development and evaluation of a novel antioxidant and pH indicator film based on chitosan and food waste sources of antioxidants.* Food hydrocolloids, 2018, 84, p. 238-246.

[168] M. Corrales, J.H. Han, and B. Tauscher. *Antimicrobial properties of grape seed extracts and their effectiveness after incorporation into pea starch films.* International Journal of Food Science & Technology, 2009, 44(2), p. 425-433.

[169] J.L. Espinoza Acosta, P.I. Torres Chávez, B. Ramírez-Wong, L.A. Bello-Pérez, A. Vega Ríos, E. Carvajal Millán, M. Plascencia Jatomea, and A.I. Ledesma Osuna. *Mechanical, thermal, and antioxidant properties of composite films prepared from durum wheat starch and lignin*. Starch-Stärke, 2015, 67(5-6), p. 502-511.

[170] A.S. Bashir and Y. Manusamy. *Recent developments in biocomposites reinforced with natural biofillers from food waste.* Polymer-Plastics Technology and Engineering, 2015, 54(1), p. 87-99.

[171] G. Wang, D. Zhang, G. Wan, B. Li, and G. Zhao. *Glass fiber reinforced PLA composite with enhanced mechanical properties, thermal behavior, and foaming ability.* Polymer, 2019, 181, p. 121803.

[172] N. Maqsood and M. Rimašauskas. *Characterization of carbon fiber reinforced PLA composites manufactured by fused deposition modeling.* Composites Part C: Open Access, 2021, 4, p. 100112.

[173] J.H. Lin, C.L. Huang, C.K. Chen, J.M. Liao, and C.W. Lou. *Manufacturing and mechanical property evaluations of PLA/carbon fiber/glass fiber composites*. in *Applied Mechanics and Materials*. 2015. Trans Tech Publ. p. 261-264.

[174] P. Choudhary, P. Suriyamoorthy, J. Moses, and C. Anandharamakrishnan. *Bio-composites from food wastes.* Composites for Environmental Engineering, 2019, p. 319-345.

[175] D. Verma and K.L. Goh. *Effect of mercerization/alkali surface treatment of natural fibres and their utilization in polymer composites: Mechanical and morphological studies.* Journal of Composites Science, 2021, 5(7), p. 175.

[176] H. Jeong, J. Park, S. Kim, J. Lee, and J.W. Cho. *Use of acetylated softwood kraft lignin as filler in synthetic polymers.* Fibers and Polymers, 2012, 13(10), p. 1310-1318.

[177] M. Masłowski, J. Miedzianowska, and K. Strzelec. *Silanized cereal straw as a novel, functional filler of natural rubber biocomposites.* Cellulose, 2019, 26(2), p. 1025-1040.

[178] G. Cantero, A. Arbelaiz, R. Llano-Ponte, and I. Mondragon. *Effects of fibre treatment on wettability and mechanical behaviour of flax/polypropylene composites.* Composites Science and Technology, 2003, 63(9), p. 1247-1254.

[179] B. Koohestani, A. Darban, P. Mokhtari, E. Yilmaz, and E. Darezereshki. *Comparison of different natural fiber treatments: a literature review.* International Journal of Environmental Science and Technology, 2019, 16(1), p. 629-642.

[180] X. Li, L.G. Tabil, and S. Panigrahi. *Chemical treatments of natural fiber for use in natural fiber-reinforced composites: a review.* Journal of Polymers and the Environment, 2007, 15(1), p. 25-33.

[181] Z. Lule and J. Kim. *Surface treatment of lignocellulose biofiller for fabrication of sustainable polylactic acid biocomposite with high crystallinity and improved burning antidripping performance.* Materials Today Chemistry, 2022, 23, p. 100741.

[182] S.A. Laaziz, M. Raji, E. Hilali, H. Essabir, D. Rodrigue, and R. Bouhfid. *Bio-composites based on polylactic acid and argan nut shell: Production and properties.* International journal of biological macromolecules, 2017, 104, p. 30-42.

[183] K. Miedzińska, S. Członka, A. Strąkowska, and K. Strzelec. *Biobased polyurethane composite foams reinforced with plum stones and silanized plum stones.* International Journal of Molecular Sciences, 2021, 22(9), p. 4757.

[184] W. Qiu, T. Endo, and T. Hirotsu. *A novel technique for preparing of maleic anhydride grafted polyolefins.* European Polymer Journal, 2005, 41(9), p. 1979-1984.

[185] H. Gao, Y. Xie, R. Ou, and Q. Wang. *Grafting effects of polypropylene/polyethylene blends with maleic anhydride on the properties of the resulting wood–plastic composites.* Composites Part A: Applied Science and Manufacturing, 2012, 43(1), p. 150-157.

[186] W. Liu, Y.J. Wang, and Z. Sun. *Effects of polyethylene-grafted maleic anhydride (PE-g-MA) on thermal properties, morphology, and tensile properties of low-density polyethylene (LDPE) and corn starch blends.* Journal of Applied Polymer Science, 2003, 88(13), p. 2904-2911.

[187] J. Quiroz-Castillo, D. Rodríguez-Félix, H. Grijalva-Monteverde, T. del Castillo-Castro, M. Plascencia-Jatomea, F. Rodríguez-Félix, and P. Herrera-Franco. *Preparation of extruded polyethylene/chitosan blends compatibilized with polyethylene-graft-maleic anhydride.* Carbohydrate polymers, 2014, 101, p. 1094-1100.

[188] L. Quiles-Carrillo, N. Montanes, A. Jorda-Vilaplana, R. Balart, and S. Torres-Giner. *A comparative study on the effect of different reactive compatibilizers on injection-molded pieces of bio-based high-density polyethylene/polylactide blends.* Journal of Applied Polymer Science, 2019, 136(16), p. 47396.

[189] K. Wu, H. Hou, and C. Shu. *Thermal phenomena studies for dicumyl peroxide at various concentrations by DSC.* Journal of Thermal Analysis and Calorimetry, 2006, 83(1), p. 41-44.

[190] W. Dong, P. Ma, S. Wang, M. Chen, X. Cai, and Y. Zhang. *Effect of partial crosslinking on morphology and properties of the poly (β-hydroxybutyrate)/poly (d, l-lactic acid) blends.* Polymer Degradation and Stability, 2013, 98(9), p. 1549-1555.

[191] P. Ma, D.G. Hristova-Bogaerds, P.J. Lemstra, Y. Zhang, and S. Wang. *Toughening of phbv/pbs and phb/pbs blends via in situ compatibilization using dicumyl peroxide as a free-radical grafting initiator.* Macromolecular Materials and Engineering, 2012, 297(5), p. 402-410.

[192] N. Saba, P. Md Tahir, and M. Jawaid. *A review on potentiality of nano filler/natural fiber filled polymer hybrid composites.* Polymers, 2014, 6(8), p. 2247-2273.

[193] S.H. Pezzin, S.C. Amico, L.A.F. Coelho, and M.J.d. Andrade. *Nanoreinforcements for nanocomposite materials*, in *Nanostructured Materials for Engineering Applications*. 2011, Springer, p. 119-131.

[194] S. Sundar, J. Kundu, and S.C. Kundu. *Biopolymeric nanoparticles.* Science and Technology of Advanced Materials, 2010, 11(1), p. 014104.

[195] ISO. *Nanotecnologías. Vocabulario. Parte 2: Nano-objetos (ISO/TS 80004-2:2015) (Ratificada por la Asociación Española de Normalización en agosto de 2017.)*. 2017.

[196] C. Buzea, I.I. Pacheco, and K. Robbie. *Nanomaterials and nanoparticles: sources and toxicity.* Biointerphases, 2007, 2(4), p. MR17-MR71.

[197] L.A. Kolahalam, I.K. Viswanath, B.S. Diwakar, B. Govindh, V. Reddy, and Y. Murthy. *Review on nanomaterials: Synthesis and applications.* Materials Today: Proceedings, 2019, 18, p. 2182-2190.

[198] A.D. de Oliveira and C.A.G. Beatrice. *Polymer nanocomposites with different types of nanofiller.* Nanocomposites-Recent Evolutions, 2018, p. 103-104.

[199] A.K. Haghi. *Update on nanofillers in nanocomposites: from introduction to application*. 2013: Smithers Rapra, p. 1-155.

[200] Q. Yang and K. Loos. *Janus nanoparticles inside polymeric materials: Interfacial arrangement toward functional hybrid materials.* Polymer Chemistry, 2017, 8(4), p. 641-654.

[201] R. Petrucci and L. Torre. *Filled polymer composites*, in *Modification of Polymer Properties*. 2017, Elsevier, p. 23-46.

[202] M. Liu, Z. Jia, D. Jia, and C. Zhou. *Recent advance in research on halloysite nanotubes-polymer nanocomposite.* Progress in polymer science, 2014, 39(8), p. 1498-1525.

[203] D. Rawtani and Y. Agrawal. *Multifarious applications of halloysite nanotubes: a review.* Reviews on Advanced Materials Science, 2012, 30(3), p. 282-295.

[204] M. Du, B. Guo, and D. Jia. *Newly emerging applications of halloysite nanotubes: a review.* Polymer International, 2010, 59(5), p. 574-582.

[205] K. Prashantha, B. Lecouvet, M. Sclavons, M.F. Lacrampe, and P. Krawczak. *Poly (lactic acid)/halloysite nanotubes nanocomposites: Structure, thermal, and mechanical properties as a function of halloysite treatment.* Journal of Applied Polymer Science, 2013, 128(3), p. 1895-1903.

[206] Z. Jia, Y. Luo, B. Guo, B. Yang, M. Du, and D. Jia. *Reinforcing and flame-retardant effects of halloysite nanotubes on LLDPE.* Polymer-Plastics Technology and Engineering, 2009, 48(6), p. 607-613.

[207] M. Du, B. Guo, and D. Jia. *Thermal stability and flame retardant effects of halloysite nanotubes on poly (propylene).* European Polymer Journal, 2006, 42(6), p. 1362-1369.

[208] S. KI, R. MP, and R. Stephen. *Thermal properties of poly (vinyl alcohol)(PVA)/halloysite nanotubes reinforced nanocomposites.* International Journal of Plastics Technology, 2015, 19(1), p. 124-136.

[209] M.W. Spencer, D. Hunter, B. Knesek, and D. Paul. *Morphology and properties of polypropylene nanocomposites based on a silanized organoclay.* Polymer, 2011, 52(23), p. 5369-5377.

[210] S. Deng, J. Zhang, and L. Ye. *Halloysite–epoxy nanocomposites with improved particle dispersion through ball mill homogenisation and chemical treatments.* Composites Science and Technology, 2009, 69(14), p. 2497-2505.

[211] S. Eyley and W. Thielemans. *Surface modification of cellulose nanocrystals.* Nanoscale, 2014, 6(14), p. 7764-7779.

[212] Y. Habibi, L.A. Lucia, and O.J. Rojas. *Cellulose nanocrystals: chemistry, self-assembly, and applications.* Chemical reviews, 2010, 110(6), p. 3479-3500.

[213] G. Siqueira, J. Bras, and A. Dufresne. *Cellulosic bionanocomposites: a review of preparation, properties and applications.* Polymers, 2010, 2(4), p. 728-765.

[214] H.-M. Ng, L.T. Sin, T.-T. Tee, S.-T. Bee, D. Hui, C.-Y. Low, and A. Rahmat. *Extraction of cellulose nanocrystals from plant sources for application as reinforcing agent in polymers.* Composites Part B: Engineering, 2015, 75, p. 176-200.

[215] M. Mariano, N. El Kissi, and A. Dufresne. *Cellulose nanocrystals and related nanocomposites: Review of some properties and challenges.* Journal of Polymer Science Part B: Polymer Physics, 2014, 52(12), p. 791-806.

[216] N. Grishkewich, N. Mohammed, J. Tang, and K.C. Tam. *Recent advances in the application of cellulose nanocrystals.* Current Opinion in Colloid & Interface Science, 2017, 29, p. 32-45.

[217] S. Xie, X. Zhang, M.P. Walcott, and H. Lin. *Applications of cellulose nanocrystals: a review.* Engineered Science, 2018, 2(16), p. 4-16.

[218] S. Salmieri, F. Islam, R.A. Khan, F.M. Hossain, H.M. Ibrahim, C. Miao, W.Y. Hamad, and M. Lacroix. *Antimicrobial nanocomposite films made of poly (lactic acid)–cellulose nanocrystals (PLA–CNC) in food applications—part B: effect of oregano essential oil release on the inactivation of Listeria monocytogenes in mixed vegetables.* Cellulose, 2014, 21(6), p. 4271-4285.

[219] E. Fortunati, F. Luzi, D. Puglia, R. Petrucci, J.M. Kenny, and L. Torre. *Processing of PLA nanocomposites with cellulose nanocrystals extracted from Posidonia oceanica waste: Innovative reuse of coastal plant.* Industrial Crops and Products, 2015, 67, p. 439-447.

[220] Y. Xiao, Y. Liu, S. Kang, and H. Xu. *Insight into the formation mechanism of soy protein isolate films improved by cellulose nanocrystals.* Food chemistry, 2021, 359, p. 129971.

[221] Z. Yu, L. Sun, W. Wang, W. Zeng, A. Mustapha, and M. Lin. *Soy protein-based films incorporated with cellulose nanocrystals and pine needle extract for active packaging.* Industrial Crops and Products, 2018, 112, p. 412-419.

[222] N. Cao, X. Yang, and Y. Fu. *Effects of various plasticizers on mechanical and water vapor barrier properties of gelatin films.* Food hydrocolloids, 2009, 23(3), p. 729-735.

[223] L.H. Cheng, A.A. Karim, and C.C. Seow. *Effects of water-glycerol and water-sorbitol interactions on the physical properties of konjac glucomannan films.* Journal of food science, 2006, 71(2), p. E62-E67.

[224] T. Garrido, I. Leceta, S. Cabezudo, P. Guerrero, and K. de la Caba. *Tailoring soy protein film properties by selecting casting or compression as processing methods.* European Polymer Journal, 2016, 85, p. 499-507.

[225] N. Reddy, Q. Jiang, and Y. Yang. *Preparation and properties of peanut protein films crosslinked with citric acid.* Industrial Crops and Products, 2012, 39, p. 26-30.

[226] L. Chen, N. Reddy, X. Wu, and Y. Yang. *Thermoplastic films from wheat proteins.* Industrial Crops and Products, 2012, 35(1), p. 70-76.

[227] Ó.L. Ramos, I. Reinas, S.I. Silva, J.C. Fernandes, M.A. Cerqueira, R.N. Pereira, A.A. Vicente, M.F. Poças, M.E. Pintado, and F.X. Malcata. *Effect of whey protein purity and glycerol content upon physical properties of edible films manufactured therefrom.* Food hydrocolloids, 2013, 30(1), p. 110-122.

[228] W.S. Choi and J.H. Han. *Physical and mechanical properties of pea-protein-based edible films.* Journal of food science, 2001, 66(2), p. 319-322.

[229] S. Kokoszka, F. Debeaufort, A. Hambleton, A. Lenart, and A. Voilley. *Protein and glycerol contents affect physico-chemical properties of soy protein isolate-based edible films.* Innovative Food Science & Emerging Technologies, 2010, 11(3), p. 503-510.

[230] S.Y. Cho and C. Rhee. *Sorption characteristics of soy protein films and their relation to mechanical properties.* LWT-Food Science and Technology, 2002, 35(2), p. 151-157.

II. ESTUDIO PREVIO

Previamente a la realización del trabajo de investigación de la tesis doctoral enfocado en el desarrollo de nuevas formulaciones de biopolímeros para el sector envase y embalaje, se llevó a cabo un estudio preliminar que se centró en la obtención de un material inteligente que permita reportar la existencia o no de humedad en el ambiente, cuya aplicación tiene gran potencial en el sector envase y embalaje, así como también en el ámbito textil.

Para ello, se llevó a cabo una microencapsulación de sulfato de cobre (II) en quitosano utilizando para ello tripolifosfato de sodio (STPP) como agente de reticulación y posteriormente empleando el método "*spry drying*" para obtener las micropartículas. Este procedimiento se realizó modificando algunos de los parámetros del equipo como temperaturas y flujos, con la finalidad de optimizar aquellos que permitan obtener un mejor rendimiento y control de humedad en el material microencapsulado. Dichas micropartículas posteriormente fueron colocadas sobre un sustrato de papel mediante dos vías, una primera utilizando STTP para potenciar el entrecruzamiento de las micropartículas y otra mediante el uso de un hidrogel de quitosano que actuó como soporte para las micropartículas sobre el papel. Siendo este último el que proporcionó mejores resultados, ya que permitió conservar mejor la calidad del sustrato. Posteriormente, estos sustratos de celulosa recubiertos con las micropartículas fueron reducidos y expuestos finalmente a diferentes condiciones de humedad, con el fin de determinar si eran capaces de reportar dichos cambios de humedad de manera visible mediante su cambio de color en las muestras. Los resultados indicaron que efectivamente se produjo un cambio de color en las muestras que pasaron de un color marrón a uno azul, y cuya intensidad dependió de la cantidad de humedad al que las muestras fueron expuestas.

Adaptado del artículo

II.1. Microencapsulation of copper(II) sulfate in ionically cross-linked chitosan by spray drying for the development of irreversible moisture indicators in paper packaging.

Sandra Rojas-Lema[1], Jorge Terol[2], Eduardo Fages[2], Rafael Balart[1], Luis Quiles-Carrillo[1], Cristina Prieto[3], and Sergio Torres-Giner[3].

[1] Technological Institute of Materials (ITM), Universitat Politècnica de València (UPV), Plaza Ferrándiz y Carbonell 1, 03801 Alcoy, Spain.

[2] Textile Industry Research Association (AITEX), Plaza Emilio Sala 1, 03801 Alcoy, Spain.

[3] Novel Materials and Nanotechnology Group, Institute of Agrochemistry and Food Technology (IATA), Spanish National Research Council (CSIC), Calle Catedrático Agustín Escardino Benlloch 7, 46980 Paterna, Spain.

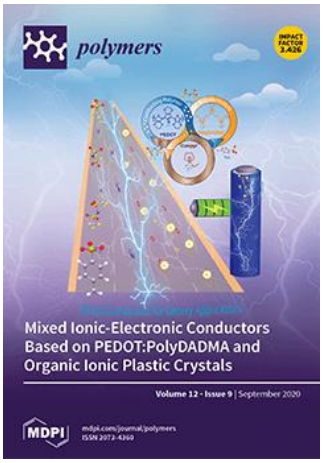

Polymers

2020, 12(9), p. 2039

polymers

MDPI

Article

Microencapsulation of Copper(II) Sulfate in Ionically Cross-Linked Chitosan by Spray Drying for the Development of Irreversible Moisture Indicators in Paper Packaging

Sandra Rojas-Lema [1], Jorge Terol [2], Eduardo Fages [2], Rafael Balart [1,*], Luis Quiles-Carrillo [1], Cristina Prieto [3] and Sergio Torres-Giner [3,*]

1 Technological Institute of Materials (ITM), Universitat Politècnica de València (UPV), Plaza Ferrándiz y Carbonell 1, 03801 Alcoy, Spain; sanrole@epsa.upv.es (S.R.-L.); luiquic1@epsa.upv.es (L.Q.-C.)
2 Textile Industry Research Association (AITEX), Plaza Emilio Sala 1, 03801 Alcoy, Spain; Jorgetd92@gmail.com (J.T.); efages@aitex.es (E.F.)
3 Novel Materials and Nanotechnology Group, Institute of Agrochemistry and Food Technology (IATA), Spanish National Research Council (CSIC), Calle Catedrático Agustín Escardino Benlloch 7, 46980 Paterna, Spain; cprieto@iata.csic.es
* Correspondence: rbalart@mcm.upv.es (R.B.); storresginer@iata.csic.es (S.T.-G.); Tel.: +34-963-900-022 (S.T.-G.)

Received: 13 August 2020; Accepted: 4 September 2020; Published: 8 September 2020

check for updates

Abstract: Copper(II) sulfate-loaded chitosan microparticles were herein prepared using ionic cross-linking with sodium tripolyphosphate (STPP) followed by spray drying. The microencapsulation process was optimal using an inlet temperature of 180 °C, a liquid flow-rate of 290 mL/h, an aspiration rate of 90%, and an atomizing gas flow-rate of 667 nL/h. Chitosan particles containing copper(II) sulfate of approximately 4 µm with a shrunken-type morphology were efficiently attained and, thereafter, fixated on a paper substrate either via cross-linking with STPP or using a chitosan hydrogel. The latter method led to the most promising system since it was performed at milder conditions and the original paper quality was preserved. The developed cellulose substrates were reduced and then exposed to different humidity conditions and characterized using colorimetric measurements in order to ascertain their potential as irreversible indicators for moisture detection. The results showed that the papers coated with the copper(II) sulfate-containing chitosan microparticles were successfully able to detect ambient moisture shown by the color changes of the coatings from dark brown to blue, which can be easily seen with the naked eye. Furthermore, the chitosan microparticles yielded no cytotoxicity in an in vitro cell culture experiment. Therefore, the cellulose substrates herein developed hold great promise in paper packaging as on-package colorimetric indicators for monitoring moisture in real time.

Keywords: copper; chitosan; cellulose; ionic cross-linking; spray drying; humidity sensors; intelligent packaging

1. Introduction

Intelligent packaging has been categorized both as a part of active packaging and, more recently, as a separate entity [1]. It can be defined as packaging types that can sense environmental changes and monitor the condition of packaged goods and/or the environment surrounding the goods. Therefore, it basically provides information about the state of the product to enhance convenience for manufacturing and distribution as well as to improve security and safety verification. Depending on the information provided, intelligent packaging is habitually classified into two main groups, namely,

Microencapsulation of copper(II) sulfate in ionically cross-linked chitosan by spray drying for the development of irreversible moisture indicators in paper packaging.

Abstract

Copper(II) sulfate-loaded chitosan microparticles were herein prepared using ionic cross-linking with sodium tripolyphosphate (STPP) followed by spray drying. The microencapsulation process was optimal using an inlet temperature of 180 ^{o}C, a liquid flow-rate of 290 mL h^{-1}, an aspiration rate of 90%, and an atomizing gas flow-rate of 667 nL h^{-1}. Chitosan particles containing copper(II) sulfate of approximately 4 μm with a shrunken-type morphology were efficiently attained and, thereafter, fixated on a paper substrate either via cross-linking with STPP or using a chitosan hydrogel. The latter method led to the most promising system since it was performed at milder conditions and the original paper quality was preserved. The developed cellulose substrates were reduced and then exposed to different humidity conditions and characterized using colorimetric measurements in order to ascertain their potential as irreversible indicators for moisture detection. The results showed that the papers coated with the copper(II) sulfate-containing chitosan microparticles were successfully able to detect ambient moisture shown by the color changes of the coatings from dark brown to blue, which can be easily seen with the naked eye. Furthermore, the chitosan microparticles yielded no cytotoxicity in an in vitro cell culture experiment. Therefore, the cellulose substrates herein developed hold great promise in paper packaging as on-package colorimetric indicators for monitoring moisture in real time.

Keywords: copper; chitosan; cellulose; ionic cross-linking; spray drying; humidity sensors; intelligent packaging.

INTRODUCTION

Intelligent packaging has been categorized both as a part of active packaging and, more recently, as a separate entity [1]. It can be defined as packaging types that can sense environmental changes and monitor the condition of packaged goods and/or the environment surrounding the goods. Therefore, it basically provides information about the state of the product to enhance convenience for manufacturing and distribution as well as to improve security and safety verification. Depending on the information provided, intelligent packaging is habitually classified into two main groups, namely, systems that act as data storage (e.g., smart labels) and those that perform as external indicators of different aspects of the product [2]. The latter group is quite broad and includes time–temperature indicators (TTIs) as well as indicators for freshness, ripeness, thawing, moisture, leakage, etc. For instance, tracking the condition of a package during its transportation through the whole supply chain can guarantee that the goods have not been exposed to the wrong conditions. In food technology, self-reading indicators can also help the consumer better judge food quality to avoid disposal of still-fresh food based merely on an estimated date [3].

In paper packaging applications, the use of sensors that perform as indicators in monitoring moisture becomes particularly relevant since cellulose is a highly hygroscopic material and its strength is considerably reduced when exposed to high relative humidity (RH) levels [4]. The moisture content, that is, the amount of water in paper, is not only determined by the RH level present but it also rather depends on the history of the RH changes in the packaging surroundings [5]. In this regard, there is currently a motivation in scientists to develop colorimetric detection methods because of their simplicity, rapidity, and especially their lack of need for expensive instruments [6]. At present, several efforts have been made to improve the sensing performance of cellulose paper-based materials by introducing organic molecules, loading metal particles or grafting polymer structures [7]. In recent times, there has been an increase in the use of copper as a material sensitive to humidity changes since it presents different colors depending on the oxidation state [8]. For instance, copper(II) sulfate, also known as copper sulphate, comprises a family of inorganic compounds with the chemical formula $CuSO_4(H_2O)_x$, where x ranges from 0 to 5. Pentahydrate (x = 5) is the most commonly encountered salt, which shows a bright blue color and is termed as “blue

vitriol" [9]. When copper(II) sulfate pentahydrate is heated at 100–150 °C, it is turned into its anhydrous form, which is a white solid, and develops high hygroscopic properties. Therefore, copper(II) sulfate shows a great deal of potential to be used as a colorimetric sensor for indicating the moisture conditions present inside industrial paper-based packaging, pointing out any penetration of moisture into the packaging and revealing the ambient conditions present during transportation.

Colorimetric sensors can be used in the form of vesicles, thin films, and membranes attached to the indicator support [10, 11]. Encapsulation of copper(II) sulfate in a biopolymer matrix can represent a feasible and sustainable alternative, which allows the crystal size to be reduced and thus increases the contact area with the environment [12]. Furthermore, it can serve as the adhesion material to the indicator substrate. Among the potential encapsulating matrices, chitosan has become one of the most widely used biopolymers in recent times. This natural copolymer is composed of β-(1,4)-glucosamine and β-(1,4)-acetylglucosamine, obtained from the deacetylation of chitin, and it is non-toxic, biocompatible, biodegradable, bioadhesive, and a natural polycationic agent [13].

In particular, chitosan has been described as a suitable biopolymer for the collection of metal ions since its amino and hydroxyl groups can act as chelation sites for metal ions [14]. For instance, adsorption of Cu^{2+} ion concentrations below 1 mg L^{-1} can be achieved after long exposure times (up to 3 days) [15, 16]. Furthermore, the chelation of copper ions with chitosan has received considerable attention [17] and results indicated that the activity of chitosan–metal complexes can depend on the property of metal ions, the molecular weight (M_W), and the degree of deacetylation (DD) of the biopolymer and environmental pH values [18].

Since chitosan is hydrophilic and easily swells in aqueous media, cross-linking is habitually required to avoid undesired burst release, improve the mechanical properties, and obtain better shape microparticles while avoiding agglomeration [19]. However, typical chitosan cross-linking with glutaraldehyde may induce undesirable toxic effects. For example, glutaraldehyde can cause irritation to mucosal membranes because of its toxicity [20]. To overcome the disadvantage of chemical cross-linkers, other cross-linkers (e.g., genipin) have been proposed, which offer 5,000-10,000 times less cytotoxicity than glutaraldehyde [21, 22], while ionic cross-linking interaction has also been explored. In the latter case, sodium tripolyphosphate (STPP) is a nontoxic polyanion that interacts

with chitosan in acidic medium via electrostatic forces to form ionically cross-linked networks [23]. Moreover, the unique polycationic structure of ionic cross-linkers allows an optimal use of chitosan for drug delivery [24, 25]. Indeed, STPP is classified as generally recognized as safe (GRAS) by the Food and Drug Administration (FDA) [25].

Chitosan microparticles can be prepared using different procedures depending on the kind of product to be encapsulated and the targeted application. Among them, ionic gelation, spray drying, electrospraying, emulsification-solvent evaporation, and coacervation have showed notable relevance [26, 27]. STPP-crosslinked chitosan micro or nanoparticles have been produced using either the emulsion or syringe method [28-30]. However, since these methods involve tedious processes and do not yield reproducible results, they could be unsuitable for large-scale production. In contrast, spray drying is nowadays widely used in the pharmaceutical and food industry for the preparation of microparticles since it is a one-stage continuous process, easy to scale up, and with a relatively low processing cost [31]. This process consists of spraying a solution inside a chamber at high temperature [32]. When the liquid is fed into the nozzle through a peristaltic pump, atomization occurs due to the force of the compressed air disrupting the liquid into small droplets. The solvent in the droplets is evaporated by hot air, and the dried particles are separated using a cyclone.

The aim of this work was to prepare microcapsules of chitosan containing copper(II) sulfate and carry out their preliminary assessment for the development of a colorimetric moisture indicator with application interest in intelligent paper packaging. To this end, copper(II) sulfate was first encapsulated in chitosan microparticles using ionic gelation with STPP followed by spray drying. The effect of the spray drying parameters on the production yield, moisture content of the microcapsules, and their morphology was analyzed. After that, the most optimal microcapsules were deposited on a cellulose substrate and fixed via two different methods, namely cross-linking by means of STPP or using a chitosan hydrogel. Finally, the potential of the indicator was evaluated by subjecting the sensor to different moisture conditions and quantifying the color change. In addition, cytotoxicity tests were performed on the microcapsules to confirm the non-toxicity of the resultant sensor for industrial applications.

MATERIALS AND METHODS

Materials

Chitosan, copper(II) sulfate, STPP, 2-hydroxypropyl-β-cyclodextrin, dimethyl sulfoxide (DMSO), and sodium borohydride ($NaBH_4$) were all purchased from Sigma Aldrich S.A. (Madrid, Spain). Acetic acid was obtained from VWR Chemicals (Llinars del Vallés, Spain). Dubelcco's modified Eagle's medium (DMEM) and InvitrogenTM Glutamax was purchased at Thermo Fisher Scientific (Waltham, MA, USA). Fetal bovine serum (SBF) of 10 wt% was delivered by Biochrom Ltd. (Holliston, Massachusetts, MA, USA). A colorimetric kit of cellular proliferation 3-(4,5-dimethylthiazole-2-yl)-2,5-diphenyltetrazolium bromide (MTT) assay was obtained from Hoffmann-La Roche (Basel, Switzerland). A cellulose non-woven mat with a surface density of 300 g m^{-2} provided by AITEX (Alcoy, Spain) was used as the paper substrate.

Preparation of the copper(II) sulfate-loaded chitosan particles

Chitosan was first dissolved in acetic acid 1% (vol/vol) at a concentration of 0.5 wt%. The solution was left under stirring for 24 h at room temperature to achieve total dissolution. After that, copper(II) sulfate was added at a rate of 2:1 (wt/wt) in relation to chitosan. The resultant solution was left under stirring for 10 min at room temperature. A STPP solution was prepared in deionized water at a concentration of 10 wt%. Chitosan colloids were spontaneously fabricated after dropwise addition of the aforementioned STPP solution to the chitosan solution at a chitosan-to-STPP ratio of 2:1 (wt/wt), under magnetic stirring for 30 min at room temperature. This chitosan-to-STPP ratio was selected based on previous studies based on saturation of amino groups in chitosan using STPP in acidic conditions, since it provided an opalescent solution, which is representative for the optimum cross-linking conditions [33, 34].

The chitosan particles were hardened and dried using a Mini Spray Dryer B-290 (Buchi Laboratoriums-Tecnik, Flawil, Switzerland). The adjustment of the operation parameters that ensured a stable and robust process was made experimentally. The operation parameters varied as follows: inlet air temperature in the range 160–220 ^{o}C, liquid flow-rate between 213 and 363 mL h^{-1} (15–25%), atomizing gas flow-rate between 439 and 667 nL h^{-1} (3–4 cm in the rotameter), and aspiration rate in the range 70–90%. The diameter of the nozzle used was 0.7 mm. The equipment operated in co-current flow

mode. In order to maintain homogeneity, the colloidal solution was kept under magnetic stirring during the spray drying process. The solid capsules were harvested from the apparatus collector and stored under vacuum at room temperature. Production yield was expressed as the ratio between the weight percentage of the final product versus the total amount of the materials sprayed. **Figure II.1.1** shows the spray-dryer unit with the operation parameters.

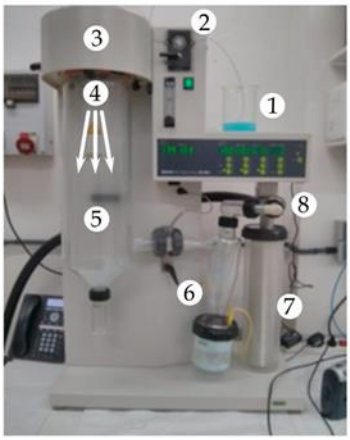

1 - Feed solution
2 - Peristaltic pump (liquid flow-rate 213-363 mL h^{-1})
3 - Heating the inlet air (160-220 °C)
4 - Nozzle (0.7 mm) and atomizing gas (439-667 nL h^{-1}) for drop formation by spraying
5 - Drying chamber
6 - Separation by cyclone and microparticle collector
7 - Outlet filter to collect the finest particles and to protect the user and the environment
8 - Aspiration of the drying gas (70-90%)

Figure II.1.1. Setup of the spray-dryer unit with indications of its components and working procedure.

Microscopy

The morphology of chitosan capsules was analyzed using focused ion beam scanning electron microscopy (FIB-SEM) in a Zeiss Neon 40 (Jena, Germany) with an electron beam acceleration of 2 kV. The samples were coated with a gold/palladium layer prior to FIB-SEM analysis. Particle diameters were determined using Image J Launcher v1.41 (National Institutes of Health, Bethesda, MD, USA), and the data presented were based on measurements from a minimum of 20 micrographs.

Moisture determination

The moisture content of the chitosan capsules was determined using gravimetric measurement performed in triplicate. To this end, 0.5 g of chitosan capsules were placed in a vacuum oven (JP Selecta, Barcelona, Spain) at 70 °C and −0.1 bar and their mass was recorded until a constant weight was reached. The moisture content was determined from the difference between the initial weight of the sample (W_i) and the final one (W_f) using **Equation II.1.1**:

$$\text{Moisture content} = \left[\frac{W_i - W_f}{W_i}\right] \times 100\ (\%) \qquad \textbf{Equation II.1.1}$$

Cytotoxicity tests

Cytotoxicity of the chitosan microcapsules was evaluated due to the presence of STPP in the formulations and also the use of copper(II) sulfate. The extractive method was used to analyze the samples according to the ISO 10993-5:2009 standard [35]. Different contents of copper(II) sulfate-loaded chitosan microcapsules in STTP were assayed as described in **Table II.1.1.** The ratios of STPP and chitosan microcapsules ranged between 5 and 20 mL of STPP per gram of chitosan using two different concentrations of chitosan in solution, that is, 0.5 and 1 wt%. L929 mouse fibroblasts were used as cell lines and cultured in 96-well plates using DMEM, glutamax, and SBF as culture medium. The extract of the cross-linked materials was placed over the cells. The contact time between the samples and cell lines was 24 h, and cell viability was quantified using MTT assay and spectrophotometry. The mitochondrial activity, which is directly proportional to the number of viable cells, was measured in a Multiskan Ascent microplate reader (MTX Lab Systems, Bradenton, FL, USA). A solution of DMSO at 5 wt% in DMEM and SBF was used as positive cytotoxic control. The analysis was performed in triplicate.

Table II.1.1. Set of liquid solutions prepared for the cytotoxicity tests according to the content of copper(II) sulfate-loaded chitosan microcapsules in sodium tripolyphosphate (STPP). All solutions were prepared with a total mass of 50 g.

Sample	Chitosan (g)	STTP (mL)	STTP/Chitosan Ratio (mL g^{-1})
1	0.25	1.25	5
2	0.25	2.50	10
3	0.25	3.75	15
4	0.25	5.00	20
5	0.50	2.50	5
6	0.50	5.00	10
7	0.50	7.50	15
8	0.50	10.00	20

Fixation of the copper(II) sulfate-loaded chitosan particles

Figure II.1.2 shows the methodology followed to incorporate the chitosan microcapsules containing copper(II) sulfate into the paper substrate in the form of coatings. This process was carried out using two methods: ionic cross-linking (**Figure II.1.2**a) and the formation of a chitosan hydrogel (**Figure II.1.2b**). For the first method, the chitosan particles were uniformly spread over the substrate, a solution of STPP at 25 wt% was sprayed, and the coated substrate was left in the oven at 60 ºC for 1 min. In the second method, 100 g of a chitosan solution at 1 wt% in acetic acid was stirred for 24 h at room temperature and the resultant solution was manually spread over the substrate. When the chitosan hydrogel started drying, the capsules were spread and left until drying was complete. Different drying times were assessed.

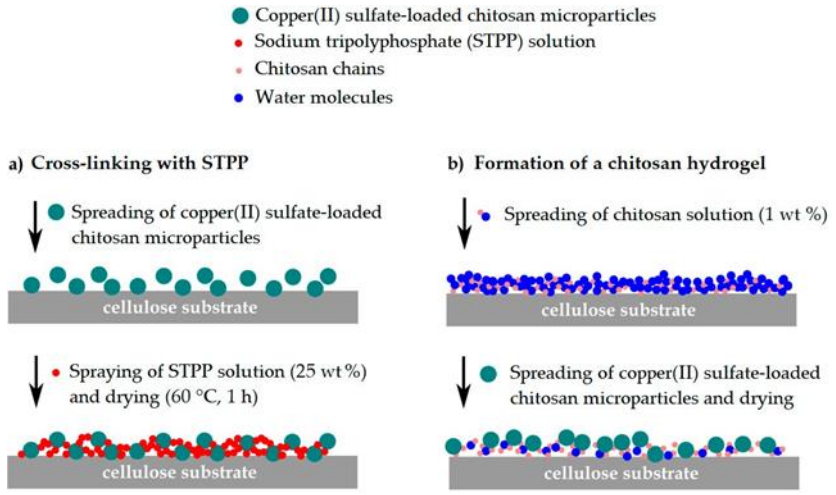

Figure II.1.2. Schematic procedure for the fixation of the copper(II) sulfate-loaded chitosan microparticles on the cellulose substrate by (a) ionic cross-linking with sodium tripolyphosphate (STPP) and (b) formation of a chitosan hydrogel.

Colorimetric measurements

A solution of $NaBH_4$ in water at 10 wt% was spread directly over the substrate containing the chitosan capsules until they reached a dark brown color. Thereafter, the substrates were placed at four different humidity conditions, that is, 0%, 15%, 60%, and 100% RH, which resemble dissimilar packaging conditions, for 24 h to study the color change. The colorimetric determination of the substrates was carried out in a benchtop spectrophotometer HunterLab ColorFlex EZ colorimeter from Hunter Associates Laboratory Inc. (Reston, VA, USA). The Commission Internationale de L'Eclairage (CIE) standard illuminant D65 was used to assess the CIE Lab color space coordinates L*a*b*

using an observer angle of 10º in which L* represents the luminance (black to white), a* indicates the change between green and red, and b* represents the change from blue to yellow. The colorimeter was calibrated with a white standard tile and a mirror device for black (no light reflection). An average of 20 measurements per sample were taken.

RESULTS AND DISCUSSION

Optimization of the spray drying process

Ionic cross-linking of chitosan was performed in order to develop water-resistant capsules after spray drying. This process consisted of the spontaneous reaction of cationic chitosan with the anionic STPP cross-linking agent according to the reaction scheme shown in **Figure II.1.3.** During this process, chitosan is first solubilized in acetic acid and the addition of the STPP solution results in a polyelectrolyte complex, stabilized by a cross-linked electrostatic interaction between the NH_3^+ groups of chitosan and the STPP-O−groups. After this, a three-dimensional entanglement is precipitated from an aqueous solution in the form of gel-like particles. The reaction was performed in diluted acid solution since the glucosamine groups are pH-sensitive (pKa ≈ 6), where the glucosamine units are converted into a soluble form of protonated amine ($R–NH_3^+$) [36].

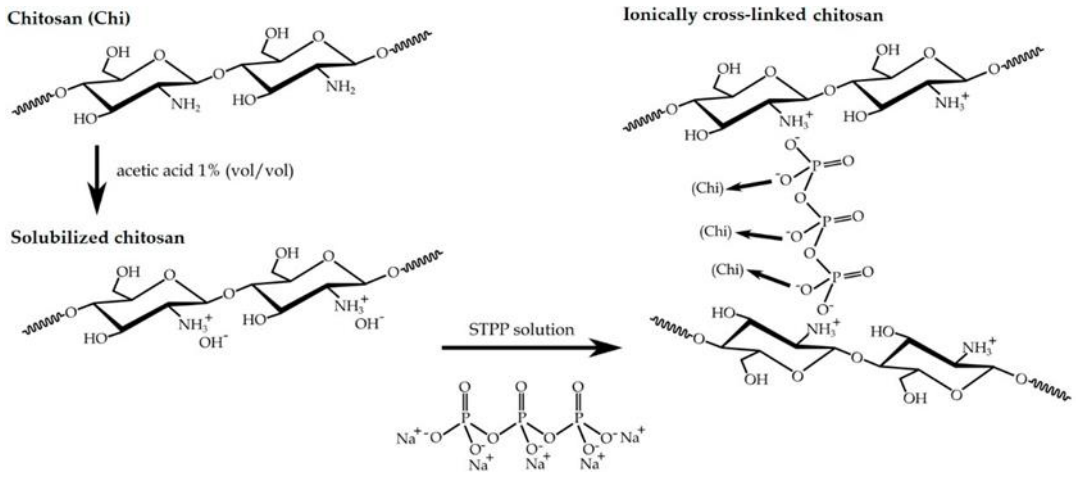

Figure II.1.3. Ionic cross-linking reaction of chitosan using sodium tripolyphosphate (STPP).

Spray drying was used to convert the copper(II) sulfate-containing chitosan-STPP colloidal solution into a dry powder with a relatively narrow particle size distribution. The physical properties of the resulting product, that is, the particle morphology and moisture content, were adjusted through the manipulation of the spray drying process variables. The main operating parameters include the inlet temperature,

liquid flow-rate, atomizing gas flow-rate, and aspiration rate. As shown in **Table II.1.2**, these parameters were varied in order to both maximize production yield and minimize moisture content in the resultant powder. Production yield may compromise the economic viability of the process, whereas moisture content of the powder could affect the stability of the indicator and also the morphology of the capsules.

Table II.1.2. Yield and moisture content for the different operating conditions evaluated.

Inlet Temperature	Atomizing Gas Flow-Rate (nL h^{-1})	Liquid Flow-Rate (mL h^{-1})	Aspiration Rate (%)	Yield (%)	Moisture (%)
160	538	290	80	42.73 ± 2.23	6.87 ± 0.32
		363		40.25 ± 3.67	7.99 ± 0.67
		290	90	30.30 ± 3.05	8.43 ± 1.03
		363		43.64 ± 4.14	5.50 ± 0.88
	667	290	80	46.52 ± 3.54	11.34 ± 0.98
		636		45.61 ± 4.70	7.33 ± 0.72
		290	90	46.82 ± 2.46	10.02 ± 0.54
		363		52.57 ± 2.20	6.17 ± 0.33
180	439	213	70	26.97 ± 2.01	11.30 ± 0.27
		290		23.09 ± 2.24	15.24 ± 1.12
		363		40.91 ± 1.87	10.95 ± 0.98
		213	80	40.00 ± 2.26	11.50 ± 1.36
		290		46.17 ± 3.03	10.49 ± 0.74
		363		26.29 ± 1.23	21.24 ± 0.54
		213	90	33.37 ± 1.41	10.40 ± 0.75
		290		36.57 ± 1.20	11.49 ± 1.00
		363		25.37 ± 1.96	13.45 ± 1.03
	538	213	70	52.80 ± 3.08	11.61 ± 0.98
		290		46.63 ± 2.79	9.15 ± 0.54
		363		44.11 ± 3.25	9.79 ± 0.76
		213	80	49.60 ± 2.68	9.19 ± 1.12
		290		48.00 ± 3.10	9.33 ± 0.97

		363		45.71 ± 2.41	8.15 ± 1.08
		213		69.26 ± 4.20	7.99 ± 0.44
		290	90	38.17 ± 2.98	6.81 ± 0.77
		363		39.31 ± 3.02	10.29 ± 0.36
		213		34.06 ± 1.87	11.09 ± 0.33
		290	70	49.83 ± 3.12	9.72 ± 0.78
		363		33.00 ± 2.98	12.46 ± 1.54
		213		67.20 ± 1.00	8.99 ± 0.89
	667	290	80	71.00 ± 3.32	8.89 ± 0.21
		363		62.63 ± 2.49	9.74 ± 1.20
		213		70.11 ± 3.88	14.91 ± 0.65
		290	90	66.97 ± 4.57	7.83 ± 1.01
		363		50.74 ± 3.23	8.67 ± 0.43
		213		41.21 ± 2.01	6.03 ± 0.26
		290	80	39.24 ± 3.22	6.81 ± 0.87
		363		40.25 ± 2.89	7.53 ± 0.22
200	667	213		34.39 ± 2.45	7.04 ± 1.04
		290	90	35.91 ± 1.89	4.86 ± 0.83
		363		34.09 ± 2.40	6.67 ± 1.36
		213		39.24 ± 3.20	5.27 ± 0.44
		290	80	33.64 ± 2.41	7.46 ± 0.80
		363		32.42 ± 1.09	6.54 ± 0.56
220	667	213		39.55 ± 2.08	5.83 ± 0.67
		290	90	44.24 ± 1.67	5.58 ± 0.71
		363		41.67 ± 3.32	5.50 ± 0.58

It can be observed that, at all the experimental conditions, spray drying showed a relatively low production yield of chitosan capsules due to the powder adhering to the cyclone walls. However, it was observed that the use of lower inlet temperatures, between 160 and 180 ^{o}C, significantly favored the production yield, with an increase of up to 51%. Moreover, higher air atomizing flow-rates produced an increase in the

production yield of approximately 15%. Furthermore, increasing the liquid flow-rate led to a decrease in the production yield. Finally, the higher the aspiration rate, the higher the production yield, being slightly higher for an aspiration rate of 80%.

Regarding the moisture content of the chitosan capsules, one can observe that higher temperatures favored water evaporation, and consequently, lower values were attained. A similar observation can be made by reducing the liquid flow-rate. By increasing the flow-rate, the drying capacity of the equipment is surpassed, obtaining higher moisture content in the particles. At higher aspiration rates, samples showed a higher moisture content as a consequence of the reduction in residence time inside the drying chamber. Finally, the moisture content decreased by increasing the atomizing gas flow-rate. It can be expected that by increasing the atomizing gas flow-rate, smaller droplets with a larger surface area are generated and, thus, they evaporate faster.

Therefore, the operating conditions that maximize production yield and a reduced moisture content were an inlet temperature of 180 ^{o}C, liquid flow-rate of 290 mL h^{-1}, aspiration rate of 90%, and atomizing gas flow-rate of 667 nL h^{-1}. These parameters are in agreement with those previously reported by other authors to encapsulate different types of compounds in chitosan using spray drying, including pharmaceutical compounds, enzymes or antioxidants, among others, where the inlet temperature varied between 120 and 180 ^{o}C and the liquid flow-rate between 120 and 420 mL h^{-1} [37]. Additionally, Helbling *et al.* [38] reported a maximum operation yield when encapsulating progesterone into STPP-cross-linked chitosan using spray drying, using an inlet temperature of 170 ^{o}C and a liquid flow-rate of 204 mL min^{-1}. Similarly, Learoyd *et al.* [39] selected an inlet temperature of 180 ^{o}C, a liquid flow-rate of 192 mL h^{-1}, an atomizing gas flow-rate of 600 L h^{-1}, and an aspiration rate of 85% for the encapsulation of beclometasone dipropionate in chitosan using spray drying, obtaining encapsulation efficiencies over 60%.

Morphological characterization of the chitosan microcapsules

Figure II.1.4 shows a SEM micrograph of the copper(II) sulfate-loaded chitosan particles obtained via spray drying at the aforementioned optimal operating conditions. Shrunken microparticles with a medium particle size of approximately 4 μm and a wide particle size distribution were obtained. The roughness of the surface of the

microparticles can be related to the rapid evaporation of the solvent and the formation of an external crust during the first stages of drying, which collapses when the solvent present in the inner parts of the droplet evaporates and leads to a partial shrinkage of the particle [26]. In addition, the use of STPP for chitosan cross-linking could also contribute to an increase in the surface roughness [37]. Similarly, Helbling *et al.* [38] observed that the addition of STPP favored the formation of shrunken microparticles with a mean size of 4 μm and a raisin morphology, when encapsulating progesterone into STPP-cross-linked chitosan using spray drying with an inlet temperature of 170 ^{o}C and a liquid flow-rate of 204 mL min^{-1}. In another study, Aranaz *et al.* [31] also obtained shrunken microparticles by encapsulating venlafaxine hydrochloride into STPP-cross-linked chitosan using spray drying with an inlet temperature of 160 ^{o}C. Furthermore, as demonstrated by Kašpar *et al.* [32], the raisin morphology could not be avoided by performing the cross-linking step combined with the spray drying process using a coaxial nozzle.

Figure II.1.5 shows a comparative scheme of the particles' morphologies obtained under different operating conditions. It was observed that increasing the liquid flow-rate exerted two effects on the morphology of the microparticles. On the one hand, it increased the particle size and yielded a wider particle size distribution. On the other, the number of indentations on the microparticle surface was reduced due to the slower evaporation rate. Regarding the atomizing gas flow-rate, increasing this parameter led to smaller chitosan particles since smaller droplets were generated in the nozzle. One can also notice that the increase in the aspiration rate did not show any significant morphological effect on the chitosan particles in the studied range.

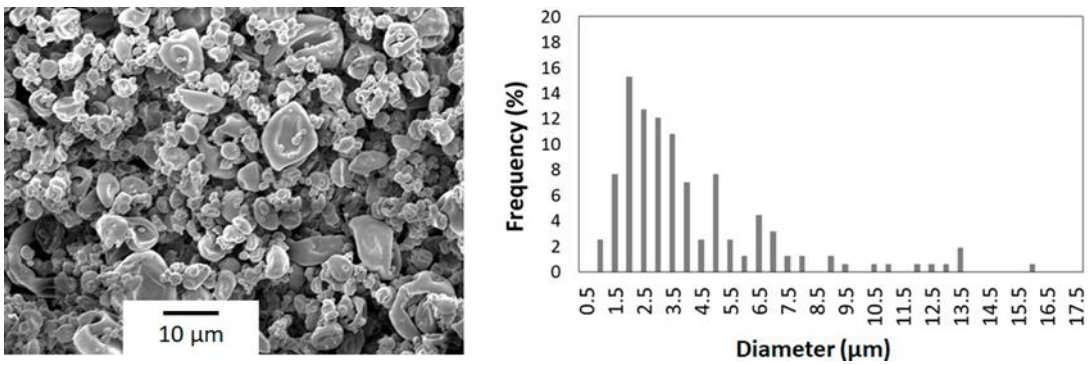

Figure II.1.4. Scanning electron microscopy (SEM) micrograph and diameter histogram of the copper(II) sulfate-loaded chitosan microparticles obtained for an inlet temperature of 180 ^{o}C, liquid flow-rate of 290 mL h^{-1}, aspiration rate of 90%, and atomizing gas flow-rate of 667 nL h^{-1}.

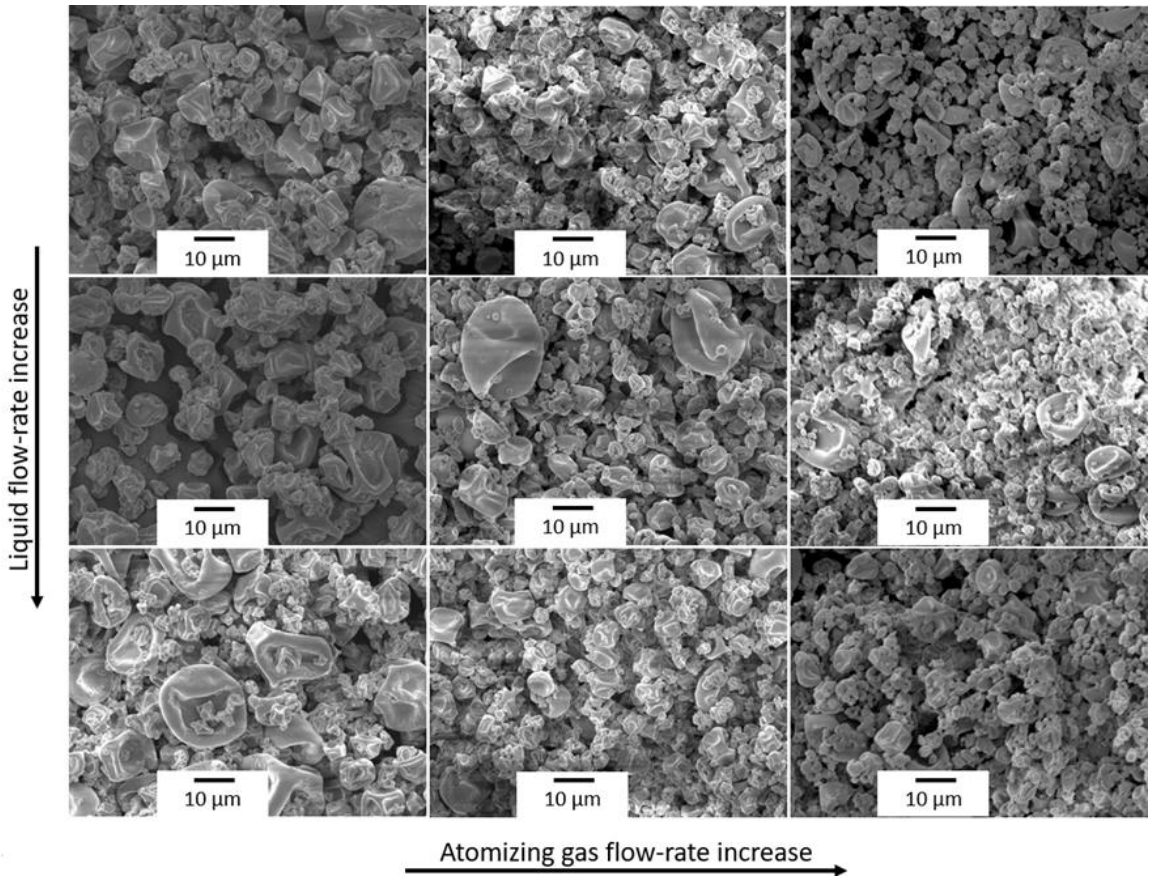

Figure II.1.5. Comparative scheme of the scanning electron microscopy (SEM) micrographs of the copper(II) sulfate-loaded chitosan microparticles obtained at 180 ^{o}C and a constant aspiration rate of 90%. The columns represent the atomizing gas flow-rates (439, 538, and 667 nL h^{-1}) and the rows represent liquid flow-rates (213, 290, and 363 mL h^{-1}). Scale markers of 10 µm.

However, as shown in **Figure II.1.6**, the increase in inlet temperature favored the formation of shrunken-type microparticles due to a faster evaporation rate. Similar observations were previously made by other authors [38, 40]. For instance, Wei *et al.* [40] recently observed that the particle size increased when increasing the liquid flow-rate, whereas the number of indentations increased by increasing the inlet temperature, during the encapsulation of theopylline in STPP-cross-linked chitosan using spray drying.

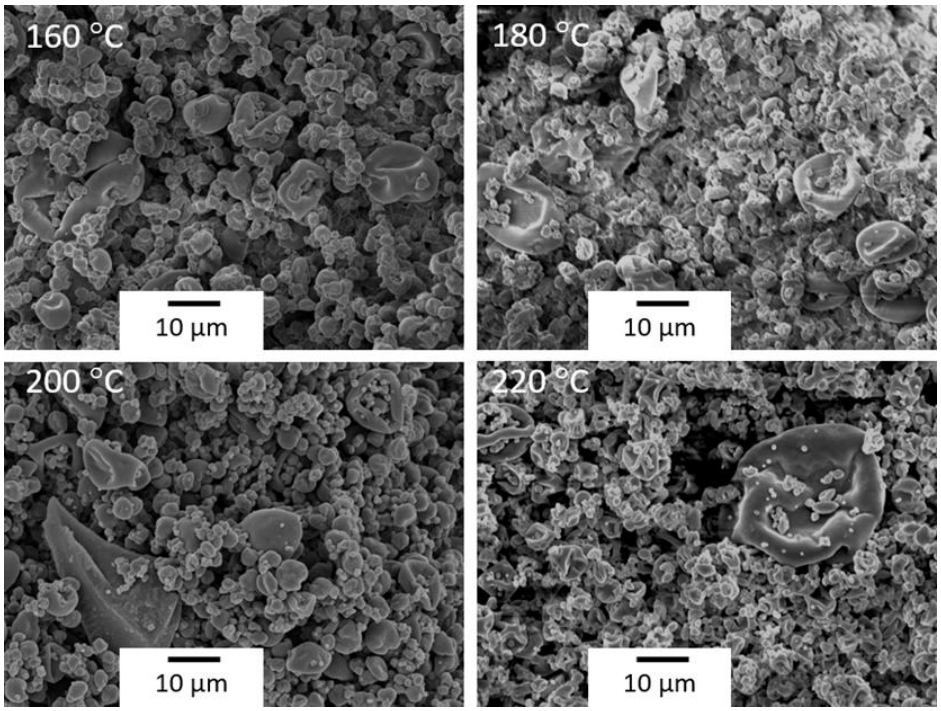

Figure II.1.6. Comparative scheme of the scanning electron microscopy (SEM) micrographs of the copper(II) sulfate-loaded chitosan microparticles obtained at different inlet temperatures for a constant aspiration rate of 90%, atomizing gas flow-rate of 667 nL h^{-1}, and liquid flow-rate of 290 mL h^{-1}. Scale markers of 10 µm.

Cytotoxicity of the chitosan microcapsules

Cytotoxicity of the copper(II) sulfate-containing chitosan microcapsules was evaluated in order to ascertain its potential in packaging and textile applications. **Figure II.1.7** shows the cell viability of the different solutions of copper(II) sulfate-loaded chitosan microparticles in STPP. The cytotoxicity tests carried out with the samples containing 0.5 wt% of chitosan microparticles, that is, samples from 1 to 4, indicated that none of the tested solutions showed cytotoxicity (see **Figure II.1.7**a). In these cases, cell viability was in the range of the control sample, that is, a solution medium without chitosan and STPP. In the case of the samples prepared with higher content of chitosan microcapsules, that is, 1 wt%, which were labelled as samples 5 to 8 and shown in **Figure II.1.7**b, the cell viability of the samples slightly decreased at the highest STTP/chitosan ratios, that is, 15 and 20 mL g^{-1}. Nevertheless, in all cases, the cell viability was greater than 70%. Similarly, in vitro culture of human fibroblasts performed by Liu and Gao [41] to assess the biocompatibility of chitosan nanoparticles ionically cross-linked by STPP showed that no difference in the cytoviability was found between the cells cultured in the medium containing chitosan nanoparticles and the fibroblasts cultured in the control

medium at all the culture times. In the study of Gritsch *et al.* [42], dealing with the antibacterial properties of copper(II)-chitosan complexes for potential uses in biomedicine, it was also indicated that it is possible to avoid cytotoxicity by fine tuning the amount of copper.

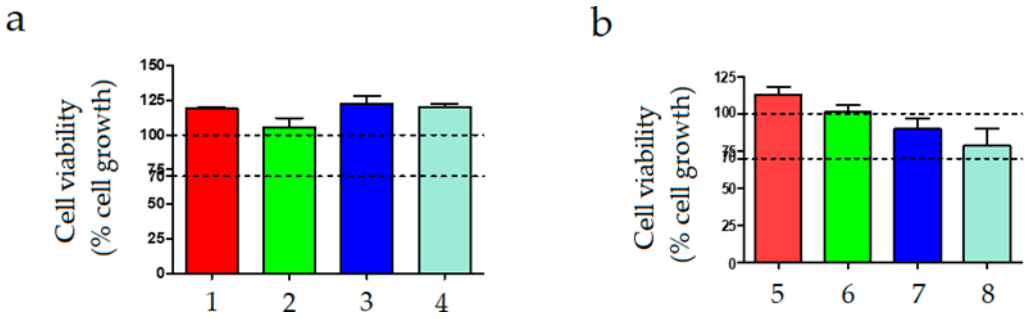

Figure II.1.7. Cell viability in terms of percentage (%) of cell growth with respect to the control of L929 cell lines in contact with solutions of copper(II) sulfate-loaded chitosan microcapsules in sodium tripolyphosphate (STPP) for 24 h of exposure at chitosan contents of: (a) 0.5 wt%; (b) 1 wt%.

Fixation of the chitosan microcapsules to the paper substrate

Figure II.1.8 presents the optical images of the copper(II) sulfate-containing chitosan microcapsules deposited on the cellulose substrates and fixated via cross-linking with STPP and by the use of a chitosan hydrogel. It was observed that the substrate fixated by means of the cross-linking method, shown in **Figure II.1.8**a, led to weak adhesion and the microcapsules easily detached. Furthermore, it can also be observed that the use of STPP visually contaminated the cellulose substrate during the fixation process and it lost its original physical–chemical properties, such as uniformity and smoothness. Alternatively, as it can be observed in **Figure II.1.8**b, the addition of the chitosan microcapsules using a hydrogel support successfully yielded a coating strongly adhered to the paper substrate. Furthermore, the visual appearance of the paper substrate remained unaltered. Nevertheless, drying time played a main role in assuring optimal adhesion and also avoiding the damage of the porous structure of paper. In particular, it was observed that the best fixation was achieved for a drying time of approximately 8 min when 100 g of chitosan microcapsules were deposited. Since the main force between cellulose fibers is a hydrogen bond, one can consider that the mild conditions applied herein were appropriate for preserving the original paper quality.

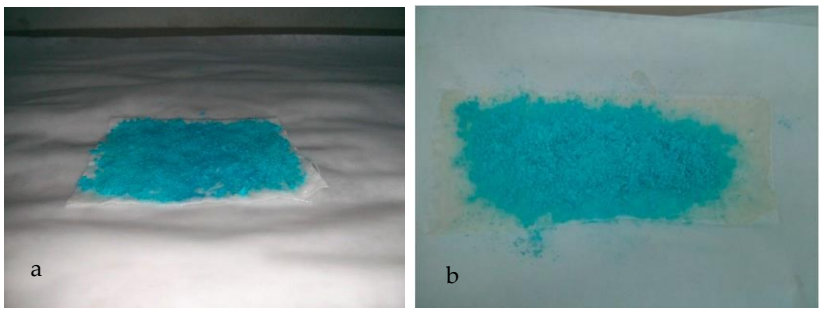

Figure II.1.8. Paper substrates with the different copper(II) sulfate-containing chitosan microcapsules fixated via (a) cross-linking with sodium tripolyphosphate (STPP) and (b) chitosan hydrogel support.

Evaluation of the paper substrates as moisture indicators

The colorimetric characterization of the samples was performed on the paper substrates in which the copper(II) sulfate-loaded chitosan microcapsules were fixed via the chitosan hydrogel support since it provided the best performance in terms of adhesion and paper quality. The substrates containing the chitosan microcapsules were thereafter reduced by wise dropping the aqueous $NaBH_4$ solution to yield copper metal, which is a reddish brown solid. As described by Glavee *et al.* [43], metallic copper plus hydrogen gas is formed in the redox reaction between copper ions with $NaBH_4$ following the reaction scheme shown in **Equation II.1.2**:

$$2\,Cu^{+2}{}_{(aq)} + 4\,BH_4^-{}_{(aq)} + 12\,H_2O \rightarrow 2\,Cu^0{}_{(s)} + 14\,H_{2\,(g)} + 4\,B(OH)_5 \quad \textbf{Equation II.1.2}$$

The process above led first to a yellow-to-brown material, followed by immediate gas evolution with the final formation of a dark brown solid that is characteristic of metallic copper, which was formed instead of the boride due to the positive redox potential of copper.

Table II.1.3 presents the color parameters of the substrates as a function of the %RH exposed for 24 h. Values of RH of 0%, 15%, 60%, and 100% were selected as being representative for dry, intermediate, and wet packaging conditions. One can observe that, at dry conditions, that is, 0% RH, the substrate presented color parameters typical of copper metal, having a* and b* values of 3.08 (red) and 9.55 (yellow), respectively. When the paper substrates were exposed to moisture, L increased slightly, while the a* and b* color coordinates shifted to lower and higher values, respectively. For instance, when the paper substrate was subjected to 60% RH, it showed a value of L of 60.01

(darker) and a* and b values of −18.76 (green) and 13.39 (yellow). Therefore, the blue hue of the paper substrates increased progressively with the %RH in the environment, confirming that the developed coating based on copper was highly sensitive to moisture at damp conditions.

Table II.1.3. Color parameters of the paper substrates stored at different relative humidity RH (%) for 24 h.

Test	RH (%)	L	a*	b*
1	0	54.33 ± 2.32	3.08 ± 0.49	9.55 ± 0.70
2	15	59.98 ± 1.89	−17.81 ± 1.03	9.63 ± 0.82
3	60	60.01 ± 2.04	−18.76 ± 1.16	13.39 ± 1.75
4	100	61.86 ± 2.04	−25.43 ± 2.07	27.65 ± 1.98

Figure II.1.9 shows the visual aspect of the paper substrates after reduction and prior to moisture exposure (**Figure II.1.9**a) and after being exposed at RH of 60% for 24 h (**Figure II.1.9**b), confirming their potential as colorimetric indicators for moisture detection since color changes can be easily seen with the naked eye. The color change of the paper substrates, before and after exposure to moisture, is related to the oxidation reaction between copper metal, oxygen, and water, which can be described using **Equation II.1.3** and **Equation II.1.4** [8]:

$$2\,Cu^{0}_{(s)} + O_{2\,(g)} + 2\,H_2O \rightarrow 2\,Cu^{+2}_{(aq)} + 4\,OH^{-}_{(aq)} \qquad \textbf{Equation II.1.3}$$

$$2\,Cu^{0}_{(s)} + 2\,H_2O \rightarrow 2\,Cu^{+2}_{(aq)} + H_{2\,(g)} + 2\,OH^{-}_{(aq)} \qquad \textbf{Equation II.1.4}$$

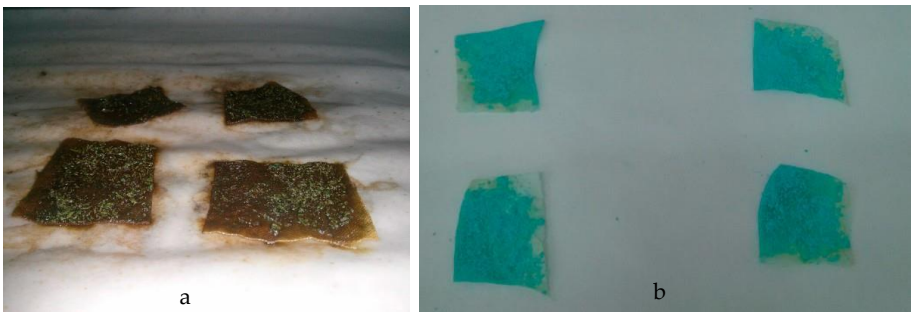

Figure II.1.9. Paper substrates with the different copper(II) sulfate-containing chitosan microcapsules: (a) reduced with sodium borohydride ($NaBH_4$); (b) oxidized at relative humidity (RH) of 60%.

In the hydrated substrates, water molecules act as ligands providing free electrons to Cu^{2+} ion (from oxygen atom of water), and the blue color is due to the d-d transition for the d9 configuration of Cu(II) [44]. Since the reduction process to attain copper metal has to be performed prior to incorporating the substrate into the packaging system, the resultant indicator becomes irreversible once the sensor is oxidized and the color change is produced in real time.

The amount of published work on moisture indicators for packaging applications is still limited. Some trials, however, have been performed to develop colorimetric humidity-indicating sensors based on copper. For instance, indicating agents of interest in humidity-adsorbing columns were recently prepared by Ulutan *et al.* [45] by drying silica hydrogels impregnated with a saturated copper sulfate solution at 100 ^{o}C. The prepared dried copper sulfate-containing gels containing light blue $CuSO_4 \cdot H_2O$ were transformed upon moisture adsorption at 25 ^{o}C into dark blue $CuSO_4 \cdot 3H_2O$, as clearly shown using visible spectroscopy.

CONCLUSIONS

Cellulose has the various advantages of low cost, good portability, excellent flexibility, and biocompatibility for several applications including paper packaging and textiles. However, paper quality is dependent on moisture conditions since cellulose fibers are highly hydrophilic. The present study aimed to microencapsulate copper(II) sulfate in ionically cross-linked chitosan using STPP and perform a preliminary assessment of the resultant microcapsules as on-package sensors for real-time moisture detection in the packaging environment. Spray drying was selected as the encapsulation process since it is a reproducible, rapid, and relatively easy to scale up. The encapsulation process was optimized in order to make it as efficient as possible and generated the capsules with the lowest moisture contents. The best conditions were attained for an inlet temperature of 180 ^{o}C, a liquid flow-rate of 290 mL h^{-1}, an aspiration rate of 90%, and an atomizing gas flow-rate of 667 nL h^{-1}. These conditions successfully yielded copper(II) sulfate-containing capsules of chitosan of approximately 4 μm with a shrunken-type morphology. Furthermore, it was observed that the copper(II) sulfate-loaded microcapsules, at different STPP-to-chitosan ratios, were not cytotoxic. Among the fixation methods, the formation of a chitosan hydrogel led to the most optimal support for the incorporation of the copper(II) sulfate-containing chitosan microcapsules

into the paper substrate since this was performed at milder conditions and the original paper quality was preserved. Finally, the resultant paper substrates coated with the copper(II) sulfate-containing microcapsules were evaluated at different moisture conditions, from 0% to 100% RH, yielding a color change from dark brown to blue. From the above, it can be considered that the here-developed paper substrates can find wide applicability in the packaging and textile fields as irreversible humidity indicators.

FUNDING

This research work was funded by the Spanish Ministry of Science and Innovation (MICI) project numbers RTI2018-097249-B-C21 and MAT2017-84909-C2-2-R.

ACKNOWLEDGMENTS

S. Rojas-Lema is a recipient of a Santiago Grisolia grant from Generalitat Valenciana (GVA) (GRISOLIAP/2019/132). S. Torres-Giner acknowledges MICI for his Juan de la Cierva–Incorporación contract (IJCI-2016-29675). L. Quiles-Carrillo. thanks GVA for his FPI grant (ACIF/2016/182) and the Spanish Ministry of Education, Culture, and Sports (MECD) for his FPU grant (FPU15/03812).

REFERENCES

[1] C.E. Realini and B. Marcos. *Active and intelligent packaging systems for a modern society.* Meat Science., 2014, 98(3), p. 404-419.

[2] E. Rodrigues and J. Han. *Intelligent Packaging*, in *Encyclopedia of Agricultural and Food Engineering*. 2003, Marcel Dekker: New York, NY, p. 528-535.

[3] S. Torres-Giner, L. Gil, L. Pascual-Ramírez, and J.A. Garde-Belza. *Packaging: Food waste reduction.* Encyclopedia of Polymer Applications; Mishra, M., Ed.; CRC Press: Boca Raton, FL, USA, 2018, 3, p. 1990-2009.

[4] T. Unander and H.-E. Nilsson. *Characterization of printed moisture sensors in packaging surveillance applications.* IEEE Sensors Journal, 2009, 9(8), p. 922-928.

[5] T. Uesaka. *Dimensional stability and environmental effects on paper properties*, in *Handbook of physical testing of paper*. 2001, CRC Press, p. 135-192.

[6] D. Xu, H. Chen, Q. Lin, Z. Li, T. Yang, and Z. Yuan. *Selective and sensitive colorimetric determination of cobalt ions using Ag–Au bimetallic nanoparticles.* RCS Advances, 2017, 7(27), p. 16295-16301.

[7] J. Fan, S. Zhang, F. Li, and J. Shi. *Cellulose-based sensors for metal ions detection.* Cellulose, 2020, 27(10), p. 5477-5507.

[8] F.C. De Godoi, R.B. Rabelo, F. da Cruz Vasconcellos, and M.M. Beppu. *Preparation of copper nanoparticles in chitosan membranes and their application as irreversible humidity indicators.* Chemical Engineering Transactions, 2011, 24, p. 217-222.

[9] M. Chandrawat, R. Yadav, and S.K. Sharma. *Investigation of blue vitriol (copper sulphate pentahydron) as an admixture on the properties of magnesia cement: An eco-friendly approach.* Rasayan Journal of Chemistry, 2008, 1, p. 914-919.

[10] P. Bamfield. *Chromic phenomena: technological applications of colour chemistry*. 2010, Cambridge, UK: Royal Society of Chemistry, 1-584.

[11] M. Bengisu and M. Ferrara. *Materials that change color: smart materials, intelligent design*. 2014, Springer International Publishing: Heidelberg, Germany, p. 1-139.

[12] B.B. Patel, J.K. Patel, S. Chakraborty, and D. Shukla. *Revealing facts behind spray dried solid dispersion technology used for solubility enhancement.* Saudi Pharmaceutical Journal, 2015, 23(4), p. 352-365.

[13] T.V. Nguyen, T.T.H. Nguyen, S.-L. Wang, T.P.K. Vo, and A.D. Nguyen. *Preparation of chitosan nanoparticles by TPP ionic gelation combined with spray drying, and the antibacterial activity of chitosan nanoparticles and a chitosan nanoparticle–amoxicillin complex.* Research on Chemical Intermediates, 2017, 43(6), p. 3527-3537.

[14] G. Steenkamp, K. Keizer, H. Neomagus, and H. Krieg. *Copper (II) removal from polluted water with alumina/chitosan composite membranes.* Journal of Membrane Science., 2002, 197(1-2), p. 147-156.

[15] J.R. Deans and B.G. Dixon. *Uptake of Pb2+ and Cu2+ by novel biopolymers.* Water Research, 1992, 26(4), p. 469-472.

[16] A. Findon, G. McKay, and H.S. Blair. *Transport studies for the sorption of copper ions by chitosan.* Journal of Environmental Science & Health Part A, 1993, 28(1), p. 173-185.

[17] F.S. Pereira, G.G. de Souza, P.G. Moraes, R.P. Barroso, S. Lanfredi, H.M. Gomes, A.J. Costa-Filho, and E.R.P. González. *Study of chitosans interaction with Cu (II) from the corresponding sulfate and chloride salts.* Cellulose, 2015, 22(4), p. 2391-2407.

[18] X. Wang, Y. Du, L. Fan, H. Liu, and Y. Hu. *Chitosan-metal complexes as antimicrobial agent: Synthesis, characterization and Structure-activity study.* Polymer Bulletin, 2005, 55(1), p. 105-113.

[19] L.B. Rodriguez, A. Avalos, N. Chiaia, and A. Nadarajah. *Effect of formulation and process parameters on chitosan microparticles prepared by an emulsion crosslinking technique.* AAPS PharmSciTech, 2017, 18(4), p. 1084-1094.

[20] L.Y. Lim, L.S. Wan, and P. Thai. *Chitosan microspheres prepared by emulsification and ionotropic gelation.* Drug Development and Industrial Pharmacy, 1997, 23(10), p. 981-985.

[21] M.P. Klein, C.R. Hackenhaar, A.S. Lorenzoni, R.C. Rodrigues, T.M. Costa, J.L. Ninow, and P.F. Hertz. *Chitosan crosslinked with genipin as support matrix for application in food process: Support characterization and β-d-galactosidase immobilization.* Carbohydrate Polymers, 2016, 137, p. 184-190.

[22] H.-W. Sung, R.-N. Huang, L.L. Huang, and C.-C. Tsai. *In vitro evaluation of cytotoxicity of a naturally occurring cross-linking reagent for biological tissue fixation.* Journal of Biomaterials Science, Polymer Edition, 1999, 10(1), p. 63-78.

[23] C. Aral and J. Akbuğa. *Alternative approach to the preparation of chitosan beads.* International Journal of Pharmaceutics., 1998, 168(1), p. 9-15.

[24] K.G.H. Desai and H.J. Park. *Preparation and characterization of drug-loaded chitosan–tripolyphosphate microspheres by spray drying.* Drug Development Research., 2005, 64(2), p. 114-128.

[25] U. Food and D. Administration. *Database of select committee on GRAS substances (SCOGS) Reviews*, in *US Food and Drug Administration*. 2006, Silver Spring, MD, USA.

[26] I. Panos, N. Acosta, and A. Heras. *New drug delivery systems based on chitosan.* Current Drug Discovery Technologies, 2008, 5(4), p. 333-341.

[27] S. Sreekumar, P. Lemke, B.M. Moerschbacher, S. Torres-Giner, and J.M. Lagaron. *Preparation and optimization of submicron chitosan capsules by water-based electrospraying for food and bioactive packaging applications.* Food Additives & Contaminants: Part A, 2017, 34(10), p. 1795-1806.

[28] J. Ko, H.J. Park, S.J. Hwang, J. Park, and J. Lee. *Preparation and characterization of chitosan microparticles intended for controlled drug delivery.* International Journal of Pharmaceutics, 2002, 249(1-2), p. 165-174.

[29] F.-L. Mi, H.-W. Sung, S.-S. Shyu, C.-C. Su, and C.-K. Peng. *Synthesis and characterization of biodegradable TPP/genipin co-crosslinked chitosan gel beads.* Polymer, 2003, 44(21), p. 6521-6530.

[30] X. Shu and K. Zhu. *A novel approach to prepare tripolyphosphate/chitosan complex beads for controlled release drug delivery.* International Journal of Pharmaceutics', 2000, 201(1), p. 51-58.

[31] I. Aranaz, I. Paños, C. Peniche, Á. Heras, and N. Acosta. *Chitosan spray-dried microparticles for controlled delivery of venlafaxine hydrochloride.* Molecules, 2017, 22(11), p. 1980.

[32] O. Kašpar, M. Jakubec, and F. Štěpánek. *Characterization of spray dried chitosan–TPP microparticles formed by two-and three-fluid nozzles.* Powder Technology, 2013, 240, p. 31-40.

[33] D.R. Bhumkar and V.B. Pokharkar. *Studies on effect of pH on cross-linking of chitosan with sodium tripolyphosphate: a technical note.* AAPS PharmSciTech, 2006, 7(2), p. E138-E143.

[34] T. Jóźwiak, U. Filipkowska, P. Szymczyk, J. Rodziewicz, and A. Mielcarek. *Effect of ionic and covalent crosslinking agents on properties of chitosan beads and sorption effectiveness of Reactive Black 5 dye.* Reactive and Functional Polymers, 2017, 114, p. 58-74.

[35] I.O.f. Standardization. *10993–5: 2009 Biological evaluation of medical devices – part 5: tests for in vitro cytotoxicity*, in *International Organization for Standardization*. 2009: Geneva, Switzerland, p. 1-34.

[36] F.G. de Carvalho, T.C. Magalhaes, N.M. Teixeira, B.L.C. Gondim, H.L. Carlo, R.L. Dos Santos, A.R. de Oliveira, and Â.M.L. Denadai. *Synthesis and characterization of TPP/chitosan nanoparticles: Colloidal mechanism of reaction and antifungal effect on C. albicans biofilm formation.* Materials Science and Engineering: C, 2019, 104, p. 109885.

[37] B.N. Estevinho, F. Rocha, L. Santos, and A. Alves. *Microencapsulation with chitosan by spray drying for industry applications–A review.* Trends in Food Science & Technology, 2013, 31(2), p. 138-155.

[38] I.M. Helbling, C.A. Busatto, S.A. Fioramonti, J.I. Pesoa, L. Santiago, D.A. Estenoz, and J.A. Luna. *Preparation of TPP-crosslinked chitosan microparticles by spray drying for the controlled delivery of progesterone intended for estrus synchronization in cattle.* Pharmaceutical Research, 2018, 35(3), p. 1-15.

[39] T.P. Learoyd, J.L. Burrows, E. French, and P.C. Seville. *Modified release of beclometasone dipropionate from chitosan-based spray-dried respirable powders.* Powder Technology, 2008, 187(3), p. 231-238.

[40] Y. Wei, Y.-H. Huang, K.-C. Cheng, and Y.-L. Song. *Investigations of the influences of processing conditions on the properties of spray dried chitosan-tripolyphosphate particles loaded with theophylline.* Scientific Reports, 2020, 10(1), p. 1-12.

[41] H. Liu and C. Gao. *Preparation and properties of ionically cross-linked chitosan nanoparticles.* Polymers for Advanced Technologies, 2009, 20(7), p. 613-619.

[42] L. Gritsch, C. Lovell, W.H. Goldmann, and A.R. Boccaccini. *Fabrication and characterization of copper (II)-chitosan complexes as antibiotic-free antibacterial biomaterial.* Carbohydrate Polymers, 2018, 179, p. 370-378.

[43] G.N. Glavee, K.J. Klabunde, C.M. Sorensen, and G.C. Hadjipanayis. *Borohydride reduction of nickel and copper ions in aqueous and nonaqueous media. Controllable*

chemistry leading to nanoscale metal and metal boride particles. Langmuir, 1994, 10(12), p. 4726-4730.

[44] C. Leygraf, T. Chang, G. Herting, and I.O. Wallinder. *The origin and evolution of copper patina colour.* Corrosion Science, 2019, 157, p. 337-346.

[45] S. Ulutan, A.P.T.z.m. Demir, and D. Balköse. *Use, preparation, and characterization of copper-containing silica gel.* Industrial & Engineering Chemistry Research, 2020, 59(21), p. 9939-9949.

III. OBJETIVOS

III.1. OBJETIVO GENERAL

El objetivo principal de esta tesis doctoral se centra en el estudio, desarrollo y caracterización de nuevos materiales poliméricos con bajo impacto medioambiental mediante la utilización de biopolímeros y residuos naturales agroindustriales con el fin de darles un nuevo uso, demás se aprovechar sus características y principios activos (fenoles, flavonoides, etc.) que pueden aportar a los materiales. Para ello se utilizarán diferentes matrices poliméricas de origen natural y/o biodegradables como el bio-poli(etileno) de alta densidad, el poli(ácido láctico) (PLA) y el poli(butilén succinato) (PBS), además del uso de componentes naturales y residuos agroindustriales para su revalorización, todo esto con el fin de obtener materiales para su posible aplicación en el sector envase y embalaje. Si bien el bio-poli(etileno) de alta densidad proviene de fuentes naturales renovables y permite por tanto disminuir de alguna manera la huella de carbono en el ambiente, sigue siendo un material no biodegradable, es por ello que con el propósito de disminuir el uso de esta matriz polimérica se planea combinarla con componentes naturales, los cuales además le puedan aportar nuevas características y con ello contribuir en la mejora de propiedades mecánicas, térmicas, antioxidantes, etc. Por otro lado, se plantea la modificación y mejora de propiedades mecánicas, térmicas, barrera, entre otras, de diferentes poli(ésteres) como el PLA y PBS mediante el uso de cargas naturales y aditivos como agentes plastificantes y agentes compatibilizantes. Finalmente, se busca aprovechar los componentes naturales (biopolímeros) presentes en diferentes residuos naturales agroindustriales (proteínas, lignina, nanocristales de celulosa) para la obtención de películas con potencial uso en el campo del envasado de alimentos.

III.2. OBJETIVOS PARCIALES

Con la finalidad de alcanzar el objetivo general se han planteado una serie de objetivos parciales. Estos objetivos se clasifican en tres bloques, considerando el tipo de matriz polimérica utilizada.

Materiales a partir de bio-poli(etileno) de alta densidad con propiedades mejoradas mediante la incorporación de compuestos y cargas naturales.

- Estudio de la adición de principios activos fenólicos (naringina, ácido gálico, ácido cafeico y quercetina) en una matriz de bio-poli(etileno) de alta densidad y su repercusión en las propiedades térmicas y antioxidantes de películas.
- Evaluación de diferentes métodos para mejorar la compatibilización entre una matriz de bio-poli(etileno) de alta densidad y harina de piel de caqui y su efecto en las propiedades mecánicas, térmicas y de humectabilidad.
- Estudio del efecto de la incorporación de diferentes cantidades de peróxido de dicumilo (DCP) en la compatibilidad y en las propiedades mecánicas, térmicas y de humectabilidad de materiales formados por una matriz de bio-poli(etileno) de alta densidad y lignina Kraft.

Materiales biopoliméricos a partir de matrices de poli(ésteres) combinados con aditivos, cargas y nanocargas naturales.

- Estudio del efecto de la incorporación de diferentes cantidades de un oligómero de ácido láctico (OLA) y nanotubos de haloisita (HNTs) en las propiedades mecánicas, térmicas y barrera de películas de poli(ácido láctico) (PLA).
- Evaluación del efecto compatibilizante del poli(butilén succinato) injertado con anhídrido maleico (PBS-*g*-MAH) en la obtención de materiales compuestos por poli(butilén succinato) (PBS) como matriz y harina de cáscara de pistacho (PSF) como carga.

Extracción de diferentes biopolímeros a partir de residuos agroindustriales para la obtención de películas.

- Estudio de la viabilidad del empleo de habas para la obtención de proteínas (FBP) y de piñas de pino para la obtención de nanocristales de celulosa (CNC).
- Estudio del efecto de la incorporación de diferentes contenidos de CNC en las propiedades mecánicas, térmicas y barrera de las películas de proteína.
- Estudio del efecto de la adición de diferentes contenidos de lignina obtenida a partir de piñas de pino (PL) en las propiedades mecánicas, térmicas y barrera de películas de proteínas de habas (FBP) para aplicaciones en el sector de envase y embalaje.

Los objetivos mencionados se presentan de forma esquemática en la siguiente **Figura III.1**.

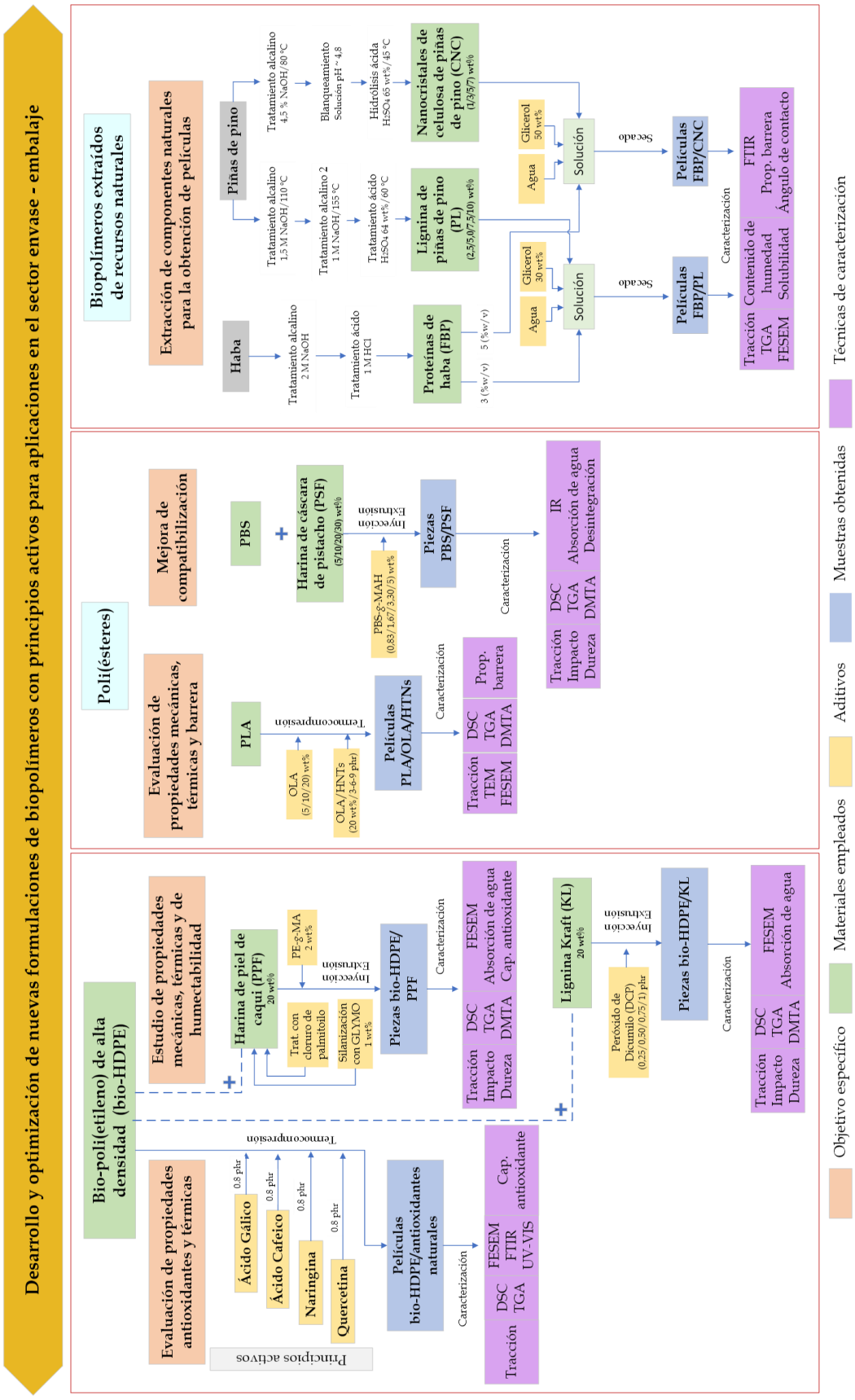

Figura III.1. Esquema de la planificación del trabajo de la tesis doctoral.

IV. RESULTS AND DISCUSSION

The following section covers the most relevant results obtained in the present doctoral thesis. They have been structured in three different blocks, with a total of seven chapters. The blocks have been organized according to the type of polymeric materials used as matrices.

Block 1. High-density bio-poly(ethylene) materials with improved properties by incorporating natural compounds and fillers.

This block includes the most relevant results obtained from the incorporation of natural additives and agro-industrial residues such as phenols, persimmon peel, and Kraft lignin to the high density bio-poly(ethylene) matrix and the use of different compatibilizers in order to improve the interaction between the materials.

Chapter IV.1.1

On the use of phenolic compounds present in citrus fruits and grapes as natural antioxidants for thermo-compressed bio-based high-density polyethylene films.

Chapter IV.1.2

Manufacturing and characterization of high-density polyethylene composites with active fillers from persimmon peel flour with improved antioxidant activity and hydrophobicity.

Chapter IV.1.3

Improved performance of environmentally friendly blends of biobased polyethylene and kraft lignin compatibilized by reactive extrusion with dicumyl peroxide.

Block 2. Biopolymeric materials from poly(ester) matrices combined with natural additives, fillers, and nanofillers.

This block contains the main results of the combination of poly(ester) matrices such as poly(lactic acid) (PLA) with nanomaterials and a plasticizer in order to improve the PLA toughness and to provide it barrier properties. In addition, it was used a matrix of poly(butylene succinate) (PBS) combined with an agro-industrial residue such as pistachio shell flour (PSF) and a compatibilizer to improve the interaction.

Chapter IV.2.1

Tailoring the properties of thermo-compressed polylactide films for food packaging applications by individual and combined additions of lactic acid oligomer and halloysite nanotubes.

Chapter IV.2.2

Peroxide-induced synthesis of maleic anhydride-grafted poly(butylene succinate) and its compatibilizing effect on poly(butylene succinate)/pistachio shell flour composites.

Block 3. Extraction of different biopolymers from agro-industrial residues and their combinations to obtain films.

This block includes the relevant results of the combination of different natural biopolymers (lignin, cellulose nanocrystals, and proteins) extracted from agro-industrial residues such as pine cone and faba beans and their possible use as films in the packaging sector.

Chapter IV.3.1

Faba bean protein films reinforced with cellulose nanocrystals as edible food packaging material.

Chapter IV.3.2

The effect of pine cone lignin on mechanical, thermal and barrier properties of faba bean protein films for packaging applications.

BLOCK 1

IV.1. High density bio-poly(ethylene) materials with improved properties through the incorporation of natural compounds and fillers.

Adaptado del artículo

IV.1.1. On the use of phenolic compounds present in citrus fruits and grapes as natural antioxidants for thermo-compressed bio-based high-density polyethylene films

Sandra Rojas-Lema[1,2], Sergio Torres-Giner[3], Luis Quiles-Carrillo[1], Jaume Gomez-Caturla[1], Daniel Garcia-Garcia[1], and Rafael Balart[1]

[1] Technological Institute of Materials (ITM), Universitat Politècnica de València (UPV), Plaza Ferrándiz y Carbonell 1, 03801 Alcoy, Spain.

[2] Escuela Politécnica Nacional, Quito 170517, Ecuador.

[3] Research Institute of Food Engineering for Development (IIAD), Universitat Politècnica de València (UPV), Camino de Vera s/n, 46022 Valencia, Spain.

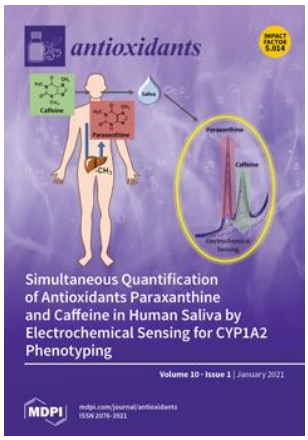

Antioxidants

2021, 10(1), p. 14.

antioxidants

MDPI

Article

On the Use of Phenolic Compounds Present in Citrus Fruits and Grapes as Natural Antioxidants for Thermo-Compressed Bio-Based High-Density Polyethylene Films

Sandra Rojas-Lema [1,2,*], Sergio Torres-Giner [3,*], Luis Quiles-Carrillo [1], Jaume Gomez-Caturla [1], Daniel Garcia-Garcia [1] and Rafael Balart [1]

[1] Technological Institute of Materials (ITM), Universitat Politècnica de València (UPV), Plaza Ferrándiz y Carbonell 1, 03801 Alcoy, Spain; luiquic1@epsa.upv.es (L.Q.-C.); jaugoca@epsa.upv.es (J.G.-C.); dagarga4@epsa.upv.es (D.G.-G.); rbalart@mcm.upv.es (R.B.)
[2] Escuela Politécnica Nacional, Quito 170517, Ecuador
[3] Research Institute of Food Engineering for Development (IIAD), Universitat Politècnica de València (UPV), Camino de Vera s/n, 46022 Valencia, Spain
* Correspondence: sanrole@epsa.upv.es (S.R.-L.); storresginer@upv.es (S.T.-G.)

Abstract: This study originally explores the use of naringin (NAR), gallic acid (GA), caffeic acid (CA), and quercetin (QUER) as natural antioxidants for bio-based high-density polyethylene (bio-HDPE). These phenolic compounds are present in various citrus fruits and grapes and can remain in their leaves, peels, pulp, and seeds as by-products or wastes after juice processing. Each natural additive was first melt-mixed at 0.8 parts per hundred resin (phr) of bio-HDPE by extrusion and the resultant pellets were shaped into films by thermo-compression. Although all the phenolic compounds colored the bio-HDPE films, their contact transparency was still preserved. The chemical analyses confirmed the successful inclusion of the phenolic compounds in bio-HDPE, though their interaction with the green polyolefin matrix was low. The mechanical performance of the bio-HDPE films was nearly unaffected by the natural compounds, presenting in all cases a ductile behavior. Interestingly, the phenolic compounds successfully increased the thermo-oxidative stability of bio-HDPE, yielding GA and QUER the highest performance. In particular, using these phenolic compounds, the onset oxidation temperature (OOT) value was improved by 43 and 41.5 °C, respectively. Similarly, the oxidation induction time (OIT) value, determined in isothermal conditions at 210 °C, increased from 4.5 min to approximately 109 and 138 min. Furthermore, the onset degradation temperature in air of bio-HDPE, measured for the 5% of mass loss ($T_{5\%}$), was improved by up to 21 °C after the addition of NAR. Moreover, the GA- and CA-containing bio-HDPE films showed a high antioxidant activity in alcoholic solution due to their favored release capacity, which opens up novel opportunities in active food packaging. The improved antioxidant performance of these phenolic compounds was ascribed to the multiple presence of hydroxyl groups and aromatic heterocyclic rings that provide these molecules with the features to permit the delocalization and the scavenging of free radicals. Therefore, the here-tested phenolic compounds, in particular QUER, can represent a sustainable and cost-effective alternative of synthetic antioxidants in polymer and biopolymer formulations, for which safety and environmental issues have been raised over time.

Keywords: green polyolefin; natural antioxidants; polyphenols; flavonoids; thermo-oxidative stability; active food packaging

check for updates

Citation: Rojas-Lema, S.; Torres-Giner, S.; Quiles-Carrillo, L.; Gomez-Caturla, J.; Garcia-Garcia, D.; Balart, R. On the Use of Phenolic Compounds Present in Citrus Fruits and Grapes as Natural Antioxidants for Thermo-Compressed Bio-Based High-Density Polyethylene Films. *Antioxidants* **2021**, *10*, 14. https://dx.doi.org/10.3390/antiox10010014

Received: 5 November 2020
Accepted: 21 December 2020
Published: 25 December 2020

Publisher's Note: MDPI stays neutral with regard to jurisdictional claims in published maps and institutional affiliations.

1. Introduction

The packaging industry is currently searching for sustainable novel materials that can provide food quality and safety but are also able to successfully reduce the fossil fuel dependence of polymers and contamination of single-use plastics [1]. In the food packaging market, biopolymers represent the most relevant option to replace current

On the use of phenolic compounds present in citrus fruits and grapes as natural antioxidants for thermo-compressed bio-based high-density polyethylene films.

Abstract

This study originally explores the use of naringin (NAR), gallic acid (GA), caffeic acid (CA), and quercetin (QUER) as natural antioxidants for bio-based high-density polyethylene (bio-HDPE). These phenolic compounds are present in various citrus fruits and grapes and can remain in their leaves, peels, pulp, and seeds as by-products or wastes after juice processing. Each natural additive was first melt-mixed at 0.8 parts per hundred resin (phr) of bio-HDPE by extrusion and the resultant pellets were shaped into films by thermo-compression. Although all the phenolic compounds colored the bio-HDPE films, their contact transparency was still preserved. The chemical analyses confirmed the successful inclusion of the phenolic compounds in bio-HDPE, though their interaction with the green polyolefin matrix was low. The mechanical performance of the bio-HDPE films was nearly unaffected by the natural compounds, presenting in all cases a ductile behavior. Interestingly, the phenolic compounds successfully increased the thermo-oxidative stability of bio-HDPE, yielding GA and QUER the highest performance. In particular, using these phenolic compounds, the onset oxidation temperature (OOT) value was improved by 43 and 41.5 ^{o}C, respectively. Similarly, the oxidation induction time (OIT) value, determined in isothermal conditions at 210 ^{o}C, increased from 4.5 min to approximately 109 and 138 min. Furthermore, the onset degradation temperature in air of bio-HDPE, measured for the 5% of mass loss ($T_{5\%}$), was improved by up to 21 ^{o}C after the addition of NAR. Moreover, the GA- and CA-containing bio-HDPE films showed a high antioxidant activity in alcoholic solution due to their favored release capacity, which opens up novel opportunities in active food packaging. The improved antioxidant performance of these phenolic compounds was ascribed to the multiple presence of hydroxyl groups and aromatic heterocyclic rings that provide these molecules with the features to permit the delocalization and the scavenging of free radicals. Therefore, the here-tested phenolic compounds, in particular QUER, can represent a sustainable and cost-effective alternative of synthetic antioxidants in polymer and biopolymer formulations, for which safety and environmental issues have been raised over time.

Keywords: green polyolefin; natural antioxidants; polyphenols; flavonoids; thermo-oxidative stability; active food packaging.

INTRODUCTION

The packaging industry is currently searching for sustainable novel materials that can provide food quality and safety but are also able to successfully reduce the fossil fuel dependence of polymers and contamination of single-use plastics [1]. In the food packaging market, biopolymers represent the most relevant option to replace current petrochemical polymers [2]. Among biopolymers, bio-based high-density polyethylene (bio-HDPE) is well positioned in the today's biopolymer industry. Bio-HDPE shows the sustainable benefit of being renewably produced at the industrial level by the addition polymerization of ethylene obtained by catalytic dehydration of bioethanol derived from sugar cane, from which it takes the name of "green" HDPE [3]. Moreover, bio-HDPE shows the same properties as its petrochemical counterpart, that is, high-density polyethylene (HDPE), which includes, for instance, high mechanical performance, water barrier, and chemical resistance [4, 5].

Bio-HDPE can be manufactured into food packaging articles and food contact disposables by conventional melt-processing technologies such as injection molding and extrusion. However, it also degrades easily in oxidizing atmospheres during melt processing [6]. In particular, it can undergo thermal degradation between 160 and 200 ^{o}C [7, 8]. Therefore, adequate stabilization by the addition of processing stabilizers, such as synthetic antioxidants, is essential to protect bio-HDPE during the manufacture of packaging articles and also hinders its degradation during use, which usually results in the gradual deterioration of its physical properties. The function of an antioxidant is to prevent the propagation steps of oxidation. Antioxidants can be divided into two main groups, depending on the method by which they prevent oxidation. Primary antioxidants (e.g., phenols, amines, or metal salts) act as radical scavengers and function by donating their reactive hydrogen to the peroxy free radical to avoid the propagation of subsequent free radicals. The antioxidant free radical is rendered stable by electron delocalization. Secondary antioxidants (e.g., organophosphites or thioesters) retard oxidation by preventing the proliferation of alkoxy and hydroxyl radicals by decomposing hydroperoxides to yield nonreactive products.

Nowadays, the plastic industry usually employs a synergistic combination of primary and secondary antioxidants to provide a higher stability to the polymer during melt processing but also to protect it from degradation during shelf life. Nevertheless,

despite the fact that these additives can provide good protection from oxidation at a relatively low cost, there are some uncertainties regarding the effect of their reaction products on human health [9] and also the hazard they can produce to the environment in the long term [10]. Therefore, the use of natural additives has been currently envisioned as a safe and environmentally friendly alternative to replace synthetic ones. Natural phenolic compounds and other renewable substances with antioxidant activity can be found in vegetables and fruits and are known to have a beneficial effect on human health. Examples of these natural compounds include α-tocopherol (vitamin E), curcumin, or dihydromyricetin (DMH), which have been reported to stabilize polyolefins [10]. In this regard, some studies have already reported that the incorporation of natural antioxidants, for instance flavonoids, can reduce or avoid the degradation of polypropylene (PP) [11] and low-density polyethylene (LDPE) [12, 13].

Natural antioxidants, in most cases, are found in vegetables and fruits, which contain lignin and polyphenols such as carotenes, flavonoids, or tannins [14, 15]. From a more sustainable approach, natural antioxidants can also be obtained from agro-food wastes to promote the so-called Circular Bioeconomy concept [16]. In this context, citrus fruits and grapes contain a considerable amount of different phenolic compounds in leaves, peels, pulp, and seeds. Citrus peel is the primary waste product from juice processing, which represents an important inexpensive source of polyphenols, such as flavonoids and phenolic acids [17]. For instance, orange peels contain about 13.5 g of flavonoids per kg of dry matter, in which naringin (NAR) or 4^{t},5,7-trihydroxyflavanone 7-rhamnoglucoside, is among the most important ones [18]. NAR is a phenolic compound whose chemical structure is based on two aromatic rings connected by a bridge consisting of three carbon atoms, forming an oxygenated heterocycle [19, 20]. Phenolic compounds are also present mainly in the skins and seeds of red grape berries. Gallic acid (GA) or 3,4,5-trihydroxybenzoic acid is another phenolic compound that is present in grapes and other fruits such as strawberries and bananas as well as in the leaves of several plants [21].

GA is a water soluble phenolic acid that has been widely explored for its antioxidant effects, but also as a homeopathic and antiinflammatory drug or, more recently, as an anticarcinogenic agent, among other uses, in the medical and pharmaceutical fields [22]. Caffeic acid (CA), or 3,4-dihydroxybenzeneacrylic acid, is considered as the predominant phenolic acid contributing to the hydroxycinnamic acid

content in coffee and various citric fruits. CA has a high antioxidant effect, performs as a cancer inhibitor, and shows some antimicrobial activity [23, 24]. Finally, quercetin (QUER), or 3,3^{t},4^{t},5,6-pentahydroxyflavone, is another relevant metabolite flavonoid found in some plants and foods, such as onions, grapes, berries cherries, broccoli, and citrus fruits [25, 26]. QUER shows both excellent antioxidant and anticancer activities [27].

This research study focuses, for the first time, on the use of the phenolic compounds NAR, GA, CA, and QUER present in citrus fruits and grapes as natural antioxidants for bio-HDPE films. To this end, the different natural compounds were melt-mixed with bio-HDPE at 0.8 parts per hundred resin (phr) and the resultant pellets were shaped into films by thermo-compression. In order to determine the best performing antioxidants and their potential applications in sustainable food packaging, the resultant thermo-compressed bio-HDPE films were characterized in terms of their optical properties and morphology, chemical characteristics, and mechanical and thermal properties as well as their antioxidant capacity.

EXPERIMENTAL

Materials

Bio-HDPE was provided by Braskem (São Paulo, Brazil) as SHA7260 and supplied in pellets form by FKuR Kunststoff GmbH (Willich, Germany). It has a density of 0.955 g cm^{-3} and its weight and number-average-molecular weights (M_W, M_n) are 192,099 g mol^{-1} and 10,475 g mol^{-1}, which results in a dispersity (Đ) value of 18.3 [28]. This grade has been developed for injection molding and it shows a melt flow index (MFI) of 20 g (10 min)$^{-1}$ (2.16 kg, 190 ^{o}C), while its minimum renewable content is 94% as determined by ASTM D6866.

Natural phenols were all supplied commercially, in powder form, by Sigma-Aldrich S.A. (Madrid, Spain). NAR, with CAS number 10236-47-2, and a product number N1376 is flavanone glycoside ≥ 90% purity and derived from citrus fruit, with a molecular weight (M_W) of 580.53 g mol^{-1}. GA, with product number G7384, and a CAS number of 149-91-7, has a purity over 97.5% and a M_W of 170.12 g mol^{-1}. CA, with a CAS number 331-39-5, and a product number C0625, has a purity of ≥98.0% and M_W of 180.16 g mol^{-1}. QUER, with a CAS number of 117-39-5, purity of ≥95% and a M_W of 302.24 g

mol^{-1}, was provided with the product number Q4951. The chemical structures of these phenolic compounds are gathered in **Figure IV.1.1.1**.

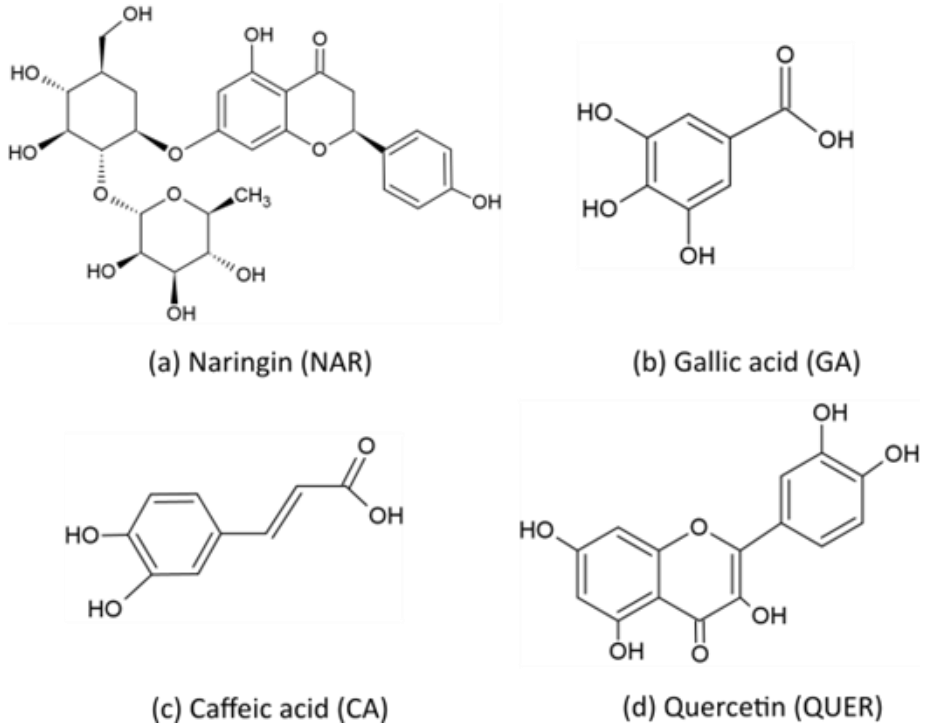

Figure IV.1.1.1. Chemical structure of (a) Naringin (NAR); (b) Gallic acid (GA); (c) Caffeic acid (CA); and (d) Quercetin (QUER).

Manufacturing of films

Bio-HDPE were manually premixed in a zipper bag with each natural antioxidant and then processed by melt compounding in a co-rotating twin-screw extruder (Construcciones Mecánicas Dupra, S.L., Alicante, Spain). The screw diameter is 25 cm and its length-to-diameter ratio (L/D) is 24. Further details about the extruder can be found elsewhere [29]. During melt processing, the temperature profile was set as follows: 140 ^{o}C (hopper)–150 ^{o}C– 155 ^{o}C–160 ^{o}C (die), whereas screw rotation speed was adjusted to 20 rpm. The extruded strands were pelletized with an air-knife unit. The resultant pellets were dried at 60 ^{o}C for 72 h to remove moisture. **Table IV.1.1.1** gathers the set of compositions prepared.

Table IV.1.1.1. Summary of compositions according to the weight (wt%) of bio-based high-density polyethylene (bio-HDPE) in which naringin (NAR), gallic acid (GA), caffeic acid (CA), and quercetin (QUER) were added as parts per hundred resin (phr) of bio-HDPE.

Sample	Bio-HDPE (wt%)	NAR (phr)	GA (phr)	CA (phr)	QUER (phr)
Bio-HDPE	100	0	0	0	0
Bio-HDPE + NAR	100	0.8	0	0	0
Bio-HDPE + GA	100	0	0.8	0	0
Bio-HDPE + CA	100	0	0	0.8	0
Bio-HDPE + QUER	100	0	0	0	0.8

Bio-HDPE films were obtained by thermo-compression of the melt-compounded pellets using a 10-ton hydraulic press from Robima S.A. (Valencia, Spain) equipped with two hot aluminum plates and a temperature controller from Dupra S.A. (Castalla, Spain) [30]. The process was carried out at 130 ^{o}C, in which approximately 5 g of pellets were placed between the two hot plates and a pressure of 40 MPa was applied for 3 min. Films sizing 10 cm × 10 cm, with a mean thickness of approximately 250 μm, were attained. The films were stored at room conditions, that is, 23 ^{o}C and 50% relative humidity (HR), for at least 15 days in dark conditions before characterization.

Characterization of films

Color measurements

A colorimetric spectrophotometer Konica CM-3600d Colorflex-DIFF2, from Hunter Associates Laboratory, Inc. (Reston, VA, USA), was used to determine the color coordinates and color changes of the films. Calibration of the instrument was performed with a white standard tile. The CIE Lab color space coordinates L*, a*, b* were determined using the standard illuminant D65 and an observer angle of 10^{o}. In this system, L* represents luminance, where L* = 0 indicates dark and L* = 100 means lightness, whereas the color coordinates a* and b* represent color changes from red to green and from yellow to blue, respectively. The color difference (ΔE_{ab}*) was calculated using **Equation IV.1.1.1**:

$$\Delta E_{ab}^{*}=\sqrt{(\Delta L^{*})^{2}+(\Delta a^{*})^{2}+(\Delta b^{*})^{2}} \qquad \textbf{Equation IV.1.1.1}$$

where ΔL*, Δa*, and Δb* represent the variations in the L*, a*, and b* coordinates, respectively, between the neat bio-HDPE film and the films of bio-HDPE containing the natural antioxidants. The average values of at least 5 readings were reported. The color changes on the films were evaluated based on the ΔE_{ab}* values according to the following assessment [31]: <1 means an unnoticeable color difference, values ranging between 1–2 indicate a slight difference in color that can only be noticed by an experienced observer, values in the 2–3.5 range indicate a noticeable difference by an inexperienced observer, values in the range of 3.5–5 indicate a clear noticeable difference, and values >5 indicate that different colors are noticeable.

Microscopy

Morphologies of the fracture surfaces of the bio-HDPE films were observed by field emission scanning electron microscopy (FESEM). A ZEISS ULTRA 55 FESEM microscope (Oxfrod Instruments, Abingdon, UK) was used at an acceleration voltage of 2 kV. To this end, the film samples were cryo-fractured by immersion in liquid nitrogen and, thereafter, coated with a gold-palladium alloy (Quorun Technologies Ltd. EMITECH mod. SC7620 sputter coater, East Sussex, UK).

UV-Vis spectroscopy

A Cary Series Ultraviolet-Visible-near-IR (UV–Vis–NIR) spectrophotometer (Agilent Technologies, Inc., Santa Clara, CA, USA) was used to obtain the UV–Vis absorption spectra of the bio-HDPE films. An incident radiation wavelength between 200 and 500 nm was set. All samples were studied in their thin film form and three replicates were tested.

Infrared spectroscopy

A chemical analysis of the as received natural antioxidants and the bio-HDPE film samples was also performed by Attenuated Total Reflectance-Fourier Transform Infrared Spectroscopy (ATR-FTIR) spectroscopy. Tests were performed in a Pekin-Elmer equipment Spectrum BX FTIR (Beaconsfield, UK) coupled with an ATR MIRacle™ Pike

Technologies (Madison, WI, USA). Twenty scans were averaged in the region from 4000 to 600 cm^{-1} at a resolution of 4 cm^{-1}.

Mechanical tests

Tensile tests were carried out on rectangular bio-HDPE film samples with a total length and width of 100 mm and 10 mm, respectively. A universal test machine (Elib 50 S.A.E. Ibertest, Madrid, Spain) was used following the ISO 527-3:2018 guidelines. A load cell of 10 kN and a cross-head speed of 2 mm min^{-1} were used during the tests. Measurements were performed at room conditions and at least six films of each sample were analyzed.

Thermal tests

Differential scanning calorimetry (DSC) was performed on the bio-HDPE films using an average weight sample of 5–7 mg in a Mettler-Toledo 821 calorimeter (Mettler-Toledo, Schwerzenbach, Switzerland). The samples were placed in 40-µL aluminum-sealed crucibles and two types of DSC tests were performed. The first test was aimed to identify the onset oxidation temperature (OOT) and it was based on a dynamic heating ramp from 30 to 350 ^{o}C at a heating rate of 5 ^{o}C min^{-1} in air atmosphere.

The second test, which allowed to obtain the oxidation induction time (OIT), consisted of a heating ramp from 30 to 210 ^{o}C at a heating rate of 5 ^{o}C min^{-1} in air atmosphere followed by an isotherm at 210 ^{o}C for a period of 300 min. The melting temperature (T_m) was determined from the heating step during the first test. Additionally, the degree of crystallinity (X_C) was calculated from the first heating ramp using **Equation IV.1.1.2**:

$$X_C = \left[\frac{\Delta H_m - \Delta H_{CC}}{\Delta H_m^0 \times w}\right] \times 100\ (\%) \qquad \textbf{Equation IV.1.1.2}$$

where ΔH_m (J g^{-1}) and ΔH_{CC} (J g^{-1}) represent, respectively, the melt and cold crystallization enthalpies of bio-HDPE, while ΔH_m^0 (J g^{-1}) is the melt enthalpy of a theoretically fully crystalline bio-HDPE (293 J g^{-1}) [32] and the term w represents the weight fraction of bio-HDPE in the sample.

Thermogravimetric analysis (TGA) was also conducted for the bio-HDPE film samples using an average weight of 15–25 mg in a PT1000 from Linseis (Selb, Germany). Samples were first placed in standard 70-µL alumina crucibles and subjected to a heating program in air atmosphere from 30 to 700 ^{o}C at a heating rate of 20 ^{o}C min^{-1}. The temperature measured for a mass loss of 5% ($T_{5\%}$) was considered as the onset degradation temperature, while the temperature at the maximum degradation rate (T_{deg}) was determined from the first derivative thermogravimetry (DTG) curves. All the thermal tests were performed in triplicate.

Antioxidant measurements

The antioxidant activity of the films containing the phenolic compounds was analyzed by the inhibition assay of 2,2-diphenyl-1-picrylhydrazyl radical (DPPH), which is a stable and commercially available organic nitrogen radical that shows hydrogen acceptor ability towards antioxidants. In methanol solution, DPPH presents a strong violet color that fades as the reduction proceeds in the presence of an antioxidant substance and the progress of this reaction can be recorded by spectrophotometry [33]. The antioxidant activity of the bio-HDPE films was determined following the procedure described by Goñi *et al.* [34]. To this end, a stock solution of DPPH (Sigma Aldrich S.A) at 0.025 g L^{-1} in methanol (≥99.8%, HPLC grade, Panreac Quimica S.A., Barcelona, Spain) was prepared and placed into dark glass flasks.

Thereafter, about 100 mg of each film sample was immersed in 5 mL of the stock solution in the flasks, which corresponds to a maximum concentration of antioxidant of nearly 160 ppm. The flaks were immediately kept hermetically closed and protected from light without stirring for one week. Absorbance measurements of the different samples were taken at 1, 24, 96, and 168 h. Vials without film sample were also prepared under the same conditions as the control. After each period, the films were removed from the vials and the absorbance of the resultant solution was measured using a Cary Series UV–Vis–NIR spectrophotometer at 517 nm, where the unpaired electron of the free DPPH radical presents maximum absorbance. The percentage of DPPH inhibition of each film was determined using **Equation IV.1.1.3**, which also takes into account the absorbance of the films in methanol without DPPH as blank [35]:

$$\text{DPPH Inhibition} = \left[\frac{A_c-(A_s-A_b)}{A_c}\right]\times 100\ (\%) \qquad \textbf{Equation IV.1.1.3}$$

where A_c, A_b, and A_s correspond to the absorbance values of the DPPH solution without film, methanol with film, and the DPPH solution with film, respectively. Measurements were done in triplicate.

Statistical analysis

Results were evaluated at 95% confidence level ($p \leq 0.05$) by one-way analysis of variance (ANOVA) according to Tukey's test for the significant differences among the samples with the use of OriginPro 8 software (OriginLab Corporation, Northampton, MA, USA).

RESULTS AND DISCUSSION

Optical and morphological properties

In food packaging applications, color and transparency are important attributes of films. The visual aspect of the neat bio-HDPE film and the bio-HDPE films containing the phenolic compounds is shown in **Figure IV.1.1.2**. As it can be seen in the images, there was a clear variation in the film color after the incorporation of the different phenolic compounds. Whereas a low but still noticeable variation in color was produced in the NAR-containing bio-HDPE film, the other natural antioxidants yielded strong color changes in the films. The different colors attained in the bio-HDPE films can be ascribed to the natural and intrinsic color of each phenolic compound due to the most natural antioxidants having inherently strong colors [10]. The color of the antioxidants depends on different factors such as the number of hydroxyl (–OH) and methoxyl (–OCH_3) groups as well as their position in the molecule [36]. For instance, the color tends to be blue if the chemical structure shows a large number of –OH groups, while the presence of –OCH_3 groups favors the development of red tonalities [15]. As an example, the natural antioxidant curcumin is known to show a strong yellow color due to the chemical structure of this flavonol-type flavonoid [37]. In the case of QUER, its characteristic intense yellow color has been particularly ascribed to the conjugation of the double bond in ring C with the delocalized π electrons of ring B [38]. Furthermore, the brown color of GA can be attributable to chemical moieties and the presence of

remaining pigments from fruits [39]. For CA, the formation of chlorogenic acid has been reported to produce certain brown discoloration in food [40]. When these natural antioxidants are mixed with biopolymers, as expected, the final samples tend to be colored [15]. For instance, Kirschweng *et al.* [38] reported that QUER colored polyolefins to yellowish red at a content as low as 5 ppm, while discoloration was intense at 500 ppm. However, the induced color slightly decreased during consecutive processing steps due to consumption of the flavonoid.

Figure IV.1.1.2. Visual appearance of the thermo-compressed bio-based high-density polyethylene (bio-HDPE) films containing naringin (NAR), gallic acid (GA), caffeic acid (CA), and quercetin (QUER).

Color differences of the bio-HDPE films were quantified in **Table IV.1.1.2** by the values of L* (luminance) and the a* (green to red), and b* (blue to yellow) coordinates as well as the color change, that is, ΔE_{ab}*, after the incorporation of the different antioxidants. It can be noticed that the addition of 0.8 phr of each antioxidant caused a significant decrease in the luminance L* value, being more intense in the sample with CA, indicating that lightness was reduced in all the bio-HDPE films. One can observe

that the GA-containing film developed higher values of a* and b* of 0.19 and 13.26, respectively, corroborating the reddish yellow coloring. Higher values of a*, that is, 4.80, but lower of b*, that is, −1.32, were attained for the bio-HDPE film with CA, as an indication of the developed bluish red hue. The highest color variation was observed for the addition of QUER, having values of 0.57 and 49.00 for a* and b*, respectively, and supporting the development of a strong yellow color in the biopolymer film sample. In all cases, the ΔE_{ab}* values were higher than 5, indicating that different colors can be easily noticed by an unexperienced observer. The highest color change was produced after the addition of QUER, having a value of ΔE_{ab}* of 54.47. Similarly, Marcos *et al.* [41] showed that the incorporation of 2.82 wt% of α–tocopherol and olive leaf extract with antioxidant properties into poly(butylene adipate-*co*-terephthalate) (PBAT) yielded ΔE_{ab}* values of 9.04 and 40.40, respectively, indicating that natural antioxidants are very prone to coloring biopolymers. Furthermore, it is noteworthy to indicate that color intensities can be related to the different solubility of the natural additives in polyolefins [42]. It is also important to mention that, despite the differences in color, the contact transparency of the films was nearly unaffected.

Table IV.1.1.2. Color parameters (L*, a*, b*) and difference (ΔE_{ab}*) of the thermo-compressed bio-based high-density polyethylene (bio-HDPE) films containing naringin (NAR), gallic acid (GA), caffeic acid (CA), and quercetin (QUER).

Film	L*	a*	b*	ΔE_{ab}*
bio-HDPE	81.60 ± 0.52^{a}	−1.82 ± 0.04^{a}	−4.16 ± 0.11^{a}	-
bio-HDPE + NAR	79.24 ± 0.26^{b}	−3.53 ± 0.06^{b}	5.11 ± 0.13^{b}	9.73 ± 0.14^{a}
bio-HDPE + GA	63.16 ± 0.29^{c}	0.19 ± 0.10^{c}	13.26 ± 0.31^{c}	25.45 ± 0.41^{b}
bio-HDPE + CA	55.48 ± 0.23^{d}	4.80 ± 0.15^{d}	−1.32 ± 0.11^{d}	27.10 ± 0.22^{c}
bio-HDPE + QUER	69.95 ± 0.49^{e}	0.57 ± 0.25^{e}	49.00 ± 1.49^{e}	54.47 ± 1.54^{d}

$^{a–e}$ Different letters in the same column indicate a significant difference among the samples ($p < 0.05$).

Figure IV.1.1.3 shows the FESEM images of the cryo-fracture surfaces of the film samples, in which the left images offers a general overview of the film surfaces after fracture while the right images gives more detail about the presence of the phenolic compounds. The latter FESEM micrographs were marked by yellow arrows and circles to indicate the presence of the natural compounds. In **Figure IV.1.1.3**a,b, one can see that the surface of bio-HDPE showed some macro-cracks and the presence of several filaments that correspond to the plastic deformation of the green polyolefin during

fracture. This morphology is in agreement with previous works for HDPE [43, 44] and it is an indication of the high ductility of the film sample. **Figure IV.1.1.3**c,d shows the cryo-fracture surface of the bio-HDPE film containing NAR, in which the same morphology can be seen with some round microparticles of the polyphenol embedded in the biopolymer matrix. A very similar fracture was attained during the morphological analysis of the cryo-fracture surface of the GA-containing bio-HDPE film, shown in **Figure IV.1.1.3**e,f, where round and well dispersed microparticles of the phenolic compound were observed. Indeed, the morphology of GA is typically characterized by crystals of a small size and a regular shape, with an apparently smooth surface [45]. In the case of the bio-HDPE film containing CA, shown in **Figure IV.1.1.3**g,h, some flakes of the natural compound were also embedded in the green polyolefin matrix. According to Luzi *et al.* [46], CA presents an irregular cubic crystal structure with a length distribution ranging between 5 and 50 μm. Finally, larger particles with a mineral-like aspect corresponding to QUER can be observed in **Figure IV.1.1.3**i,j. The latter morphology is in agreement with previous studies that have reported that this flavonoid, in its powdered form, consists of irregular rod structures [47, 48]. Therefore, the FESEM analysis confirmed the effective dispersion of the natural antioxidants, though the morphology of the fracture surfaces of the bio-HDPE films was nearly unaffected by the presence of the phenolic compounds.

Chemical properties

UV–Vis spectroscopy was carried out on the compression-molded films to verify the presence of the phenolic compounds after their incorporation into the bio-HDPE matrix. **Figure IV.1.1.4** shows the UV–Vis spectra obtained for the different thin film samples. According to Anna *et al.* [49], the peak observed at approximately 203 nm in the bio-HDPE spectrum corresponds to the characteristic peak for olefin-conjugated carbonyl groups. For the UV–Vis spectra of the bio-HDPE films containing the natural antioxidants, major changes were observed in the band at approximately 205 nm, which can be related to the $\pi \rightarrow \pi^*$ transitions within the aromatic ring of the phenolic molecules. For the NAR-containing bio-HDPE sample, the flavanone glycoside also showed the characteristic contributions for ring 1 and 2 structures, which were seen as low-intense and flat peaks at 284 and 324 nm, respectively [50, 51]. In the spectrum of the bio-HDPE sample containing GA, in addition to the strong peak at 205 nm, showing oversaturation, a new peak appeared at 254 nm that is also due to the aromatic ring of the phenolic acid

[52]. For the sample of bio-HDPE with CA, the characteristic peak in the UV-vis region of aromatic rings of phenols also produced a new band at 213 nm. The band at the shorter wavelength is known as the B-band and the one at longer wavelength as the C-band [53]. Finally, in the bio-HDPE film with QUER, one can observe the presence of a low-intense peak at 274 nm. According to Dolatabadi *et al.* [54], QUER, like most flavones and flavonols, exhibits two major absorption bands in the UV–vis region, one at 372 nm (band I), representing B-ring absorption of the cinnamoyl system, and the other at 256 nm (band II), which is considered to be associated with the absorption involving the A ring benzoyl system. Therefore, the presence of these new bands in the bio-HDPE films confirms the presence of the natural phenolic compounds in the green polyolefin.

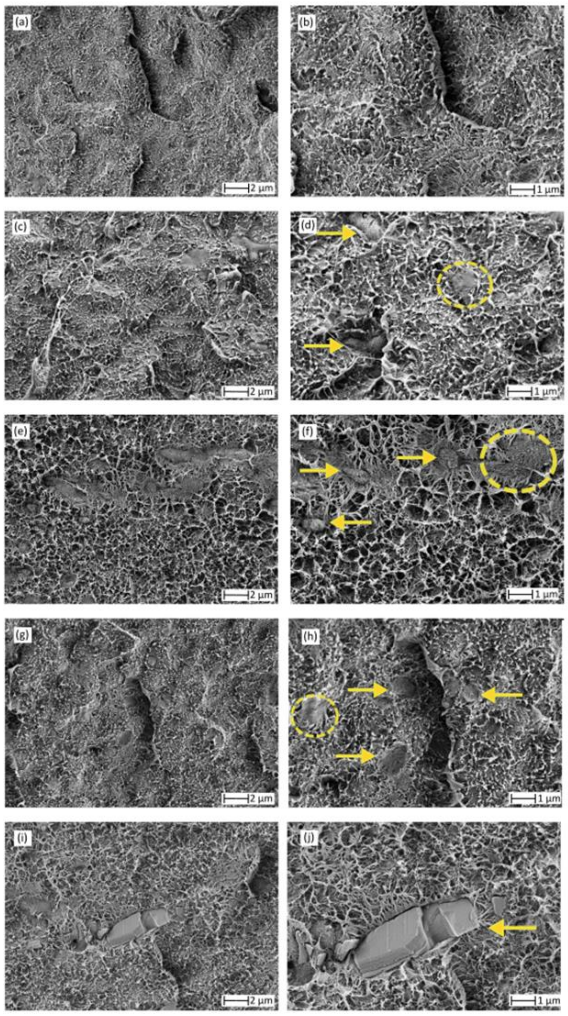

Figure IV.1.1.3. Field emission scanning electron microscopy (FESEM) micrographs of the cryo-fracture surfaces of the thermo-compressed films of: (a,b) neat bio-based high-density polyethylene (bio- HDPE); (c,d) bio-HDPE + naringin (NAR); (e,f) bio-HDPE + gallic acid (GA); (g,h) bio-HDPE + caffeic acid (CA); (i,j) bio-HDPE + quercetin (QUER). Left images were taken at 5,000× with scale of 2 µm and right images were taken at 10,000x with scale of 1 µm. Yellow arrows indicate the presence of the phenolic compounds.

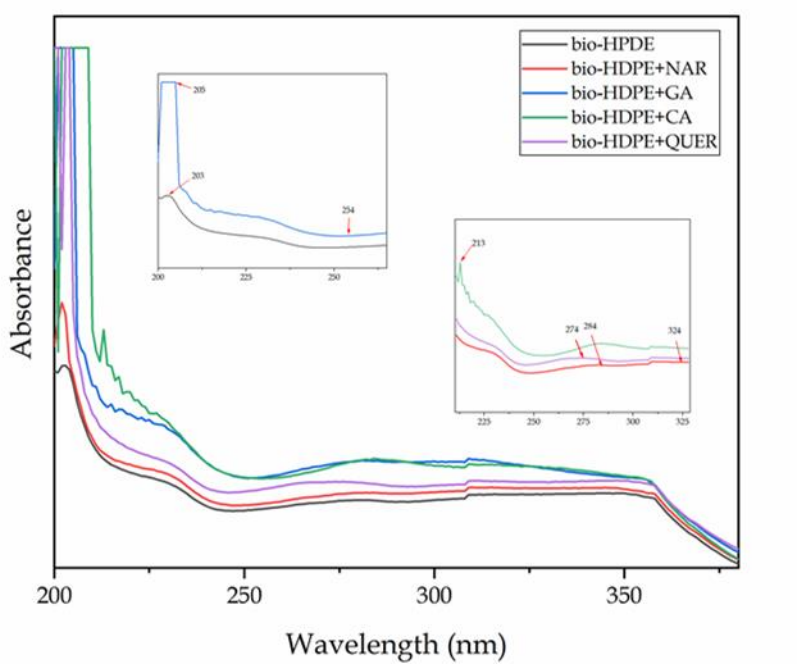

Figure IV.1.1.4. Ultraviolet–Visible (UV–Vis) spectra of the thermo-compressed bio-based high-density polyethylene (bio-HDPE) films containing naringin (NAR), gallic acid (GA), caffeic acid (CA), and quercetin (QUER).

Chemical analysis of the natural antioxidants and their interaction with the bio-HDPE matrix was also carried out by FTIR spectroscopy. **Figure IV.1.1.5** shows the ATR-FTIR spectra of the neat phenolic compounds in their power form and the bio-HDPE films after their incorporation. In **Figure IV.1.1.5**a, the spectra of the natural antioxidants are gathered, including arrows to show the main and relevant peaks. Regarding the NAR spectrum, one can observe the main characteristic peaks of –OH at 3420 cm^{-1} and for the C=O and C–O–C bonds at 1646 cm^{-1} [55]. The spectrum also showed the C–C signals that arise from the benzene ring at approximately 1578, 1518, and 1450 cm^{-1}. In the case of GA, the peaks at 3492 and 3272 cm^{-1} correspond to the stretching modes of O–H, whereas the intense bands in the region from 1382 to 1060 cm^{-1} are ascribed to stretching and bending vibrations of C–C and C–H bonds of the aromatic ring, respectively. Additionally, in the region from 1308 to 1174 cm^{-1}, different peaks related to the bending vibrations of C–H in the aromatic ring and O–H of the phenol group were observed [56]. In addition, the stretching and bending vibrations of C–O groups appeared in the region from 1021 to 628 cm^{-1}. In the FTIR spectrum of CA, this phenolic acid was mostly characterized by its hydroxyl and carbonyl functional groups. One can observe the presence of two parallel peaks that correspond to the vibration of O–H group attached to the benzene ring centered at 1274 and 1214 cm^{-1} [57]. Furthermore, in the

region from 1700 to 1600 cm^{-1}, the broad band with three intensities at 1642, 1618, and 1598 cm^{-1} was due to C=O stretching. In this regard, Gunasekaran *et al.* [58] indicated that this signal habitually generates a strong band with high intensity and a relatively interference-free region. Finally, the main peaks seen for QUER were located from 1600 to 1100 cm^{-1}, corresponding to the aromatic bending and stretching of C–C bonds and also O–H phenolic bending [59, 60]. The most intense peaks were seen at 1512, 1430, 1352, 1314, 1210, and 1162 cm^{-1}.

In order to analyze and confirm the presence of the phenolic compounds and ascertain their chemical interaction with the green polyolefin, FTIR spectroscopy was also performed on the thermo-compressed film samples. **Figure IV.1.1.5**b shows the ATR-FTIR spectra of neat bio-HDPE film and the bio-HDPE films containing the antioxidants. In the neat bio-HDPE spectrum, one can notice the presence of strong peaks centered at approximately 2916, 2848, 1462, and 720 cm^{-1}. The first two peaks have been assigned to the asymmetric and sym- metric stretching C–H of CH_2, respectively, while the two other bands are due to bending and rocking deformations [61]. Other, less intense peaks, but still noticeable, were seen at 1376 and 1304 cm^{-1}, corresponding to the CH_3 symmetric and twisting deformations, respectively. A very weak peak was also observed at 1696 cm^{-1}, which has been ascribed to carbonyl compounds formed as the oxidation products of polyethylene [62]. One can observe that the addition of the different natural antioxidants yielded small and very subtle variations in the peaks of the FTIR spectrum of bio-HDPE, indicating that their interaction with the green polyolefin was low. Some of the C–C and C–H signals, which arise from the benzene rings of the phenol groups in the 3000–2800 cm^{-1} region, altered some of CH_2-related peaks present in bio-HDPE, particularly in the case of QUER-containing film. Similarly, other slight band changes were observed at lower wavenumbers, from 1400 to 1060 cm^{-1}, which can be ascribed to stretching and bending vibrations of C–C and C–H bonds of the aromatic rings in the phenolic compounds. The band at 720 cm^{-1}, which is due to rocking deformations of C–H bonds, shifted to lower wavenumbers after the addition of the phenolic compounds, this change being more significantly in the case of CA. It is also worth noting that the C=O stretching band, seen at approximately 1642 and 1618 cm^{-1}, increased due to the presence of the natural antioxidants.

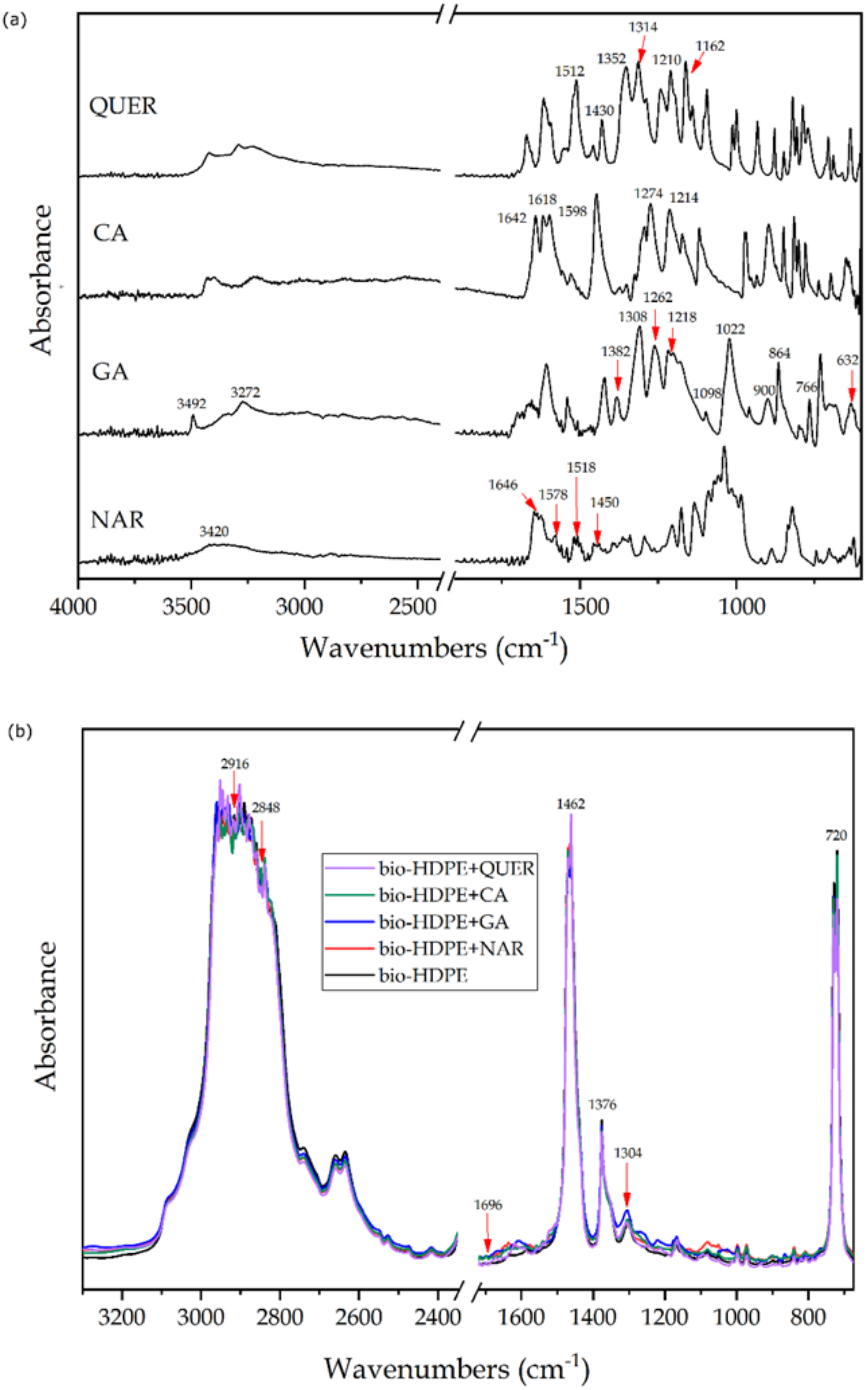

Figure IV.1.1.5. Fourier transform infrared (FTIR) spectra of: (a) natural antioxidants in powder form, from bottom to top, naringin (NAR), gallic acid (GA), caffeic acid (CA), and quercetin (QUER); (b) thermo-compressed bio-based high-density polyethylene (bio-HDPE) films containing NAR, GA, CA, and QUER.

Mechanical properties

Figure IV.1.1.6 shows bar graphs with the mechanical properties of the bio-HDPE films obtained after the tensile tests. **Figure IV.1.1.6**a–c respectively show the

values of elastic modulus, maximum tensile strength, and elongation at break. In the case of the neat bio-HDPE, the film samples showed values of 1018.96 MPa, 20.77 MPa, and 13.53%, respectively. These mechanical properties indicate that the bio-HDPE film is an elastic and ductile material, which is in agreement with the cryo-fracture surfaces shown above and also in our previous study [63]. Results indicated that the addition of 0.8 phr of the different natural antioxidants did not significantly affect the mechanical properties, which also agrees with the previous morphological analysis. Despite that, it was observed that there was a slight decrease in the mechanical performance, in particular for the elongation-at-break values.

The slight reduction in mechanical strength can be explained by the plasticizing effect caused by the addition of the phenolic compounds and also a decrease in the biopolymer's crystallinity. In terms of ductility, however, the lower values can be related to the presence of phenol particles that were not soluble or showed low interaction with the bio-HDPE matrix, which is supported both by the cryo-fracture surfaces and the FTIR analysis of the films reported above. In any case, the attained differences were not significant since the content of additive was very low.

The present results are also in agreement with previous studies reporting the mechanical properties of films containing natural antioxidants. For instance, Luzi *et al.* [64] showed that the incorporation of 5 wt% GA and umbelliferone yielded a slight decrease, but still not significant, in the overall mechanical performance of poly(ethylene-*co*-vinyl alcohol) (EVOH) films. Similarly, Sun *et al.* [65] showed that the addition of GA at 0.5 phr in chitosan films produced a slight decrease in their ductility. In the study performed by Colín-Chávez *et al.* [66], the addition of 2.9 wt% of marigold extract reduced the elongation-at-break values but increased the tensile strength of LDPE films. However, in all cases, no significant differences were observed. It is also worth mentioning the results agree with those obtained by Ramos *et al.* [67], after the incorporation of an equimolar mixture of carvacrol and thymol at 4, 6, and 8 wt% in PP films.

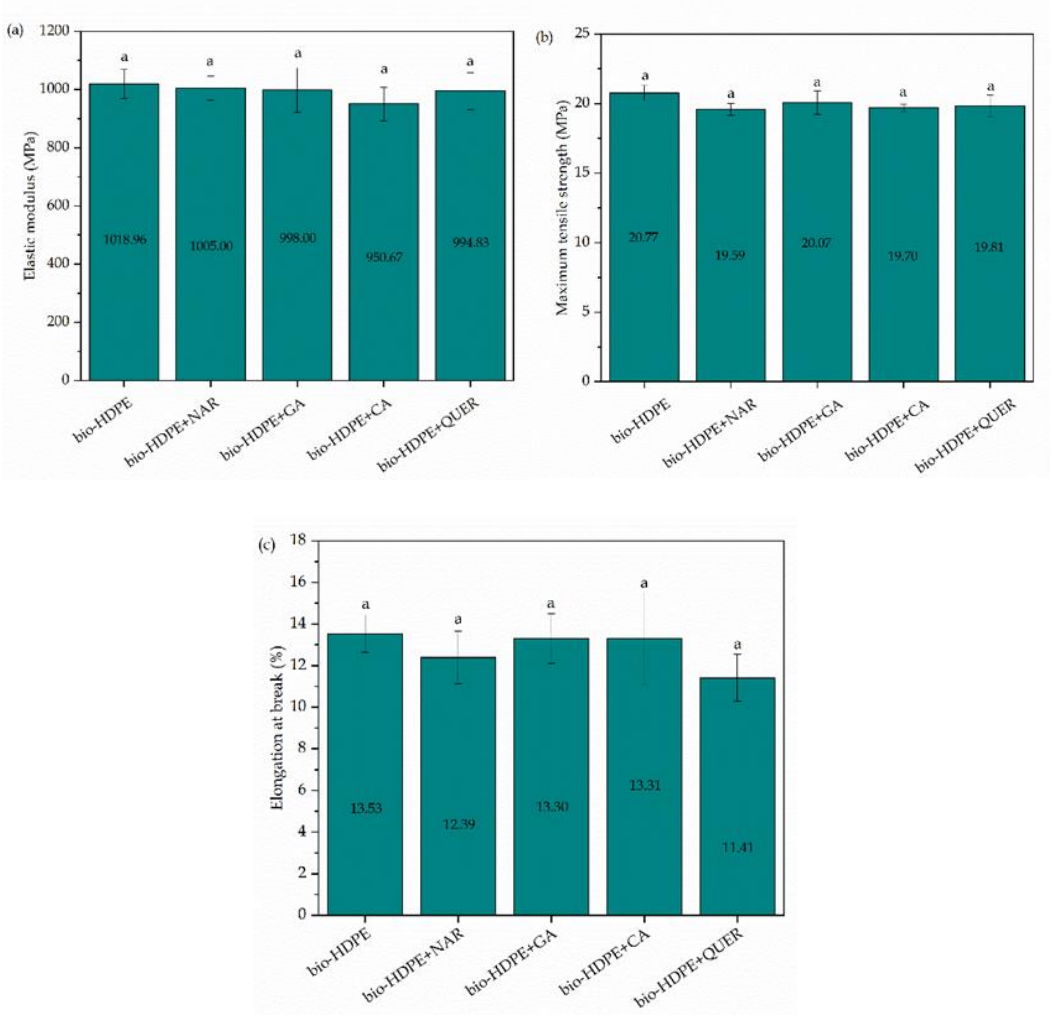

Figure IV.1.1.6. Mechanical properties of the thermo-compressed bio-based high-density polyethylene (bio-HDPE) films containing naringin (NAR), gallic acid (GA), caffeic acid (CA), and quercetin (QUER) in terms of: (a) elastic modulus; (b) maximum tensile strength; (c) elongation at break. Different letters in the same property indicate a significant difference among the samples ($p < 0.05$).

Thermal properties

The analysis of the thermal properties of the bio-HDPE films containing the different phenolic compounds was carried out by DSC and TGA. **Figure IV.1.1.7** shows the dynamical DSC curves of the films, whereas **Table IV.1.1.3** gathers the main thermal parameters obtained from the curves. One can notice that both the neat bio-HDPE film and the bio-HDPE films containing the natural antioxidant films showed a single sharp endothermic peak corresponding to the melting process of the green polyolefin crystals in the thermal range from 125 to 140 ^{o}C. In the case of the neat bio-HDPE film, this peak was centered at approximately 135 ^{o}C, which corresponds to the T_m value of bio-HDPE and is also in agreement with previous studies for this biopolymer [68]. The

incorporation of the phenolic compounds reduced the T_m values by up to 3 ºC, suggesting that the natural antioxidants restricted the development of the green polyolefin crystals. As a result, biopolymer crystals with lower lamellae thicknesses or more imperfections were developed after the incorporation of the natural antioxidants. This fact was further supported by a slight reduction of the crystallinity degree, that is, X_C, from 64.1% for the neat bio-HDPE to values in the 58.5–63.9% range. However, this reduction was only significant in the case of the bio-HDPE films with CA. It is also worth indicating that, in all cases, high degrees of crystallinity were attained since the bio-HDPE grade used to produce the films was specifically designed for injection molding to develop thin-walled parts. Therefore, its high MFI, which is related to its low M_W, could favor crystallization during film formation by thermo-compression. In this context, López-de-Dicastillo *et al.* [69] indicated that natural antioxidants, for instance ascorbic acid, ferulic acid, QUER or green tea extract, can induce a lower and more deficient crystallinity structure in EVOH. The fact that different levels of crystallinity were attained for each type of antioxidant could be related to the different morphologies and the role of the phenolic compounds as nucleating agents in bio-HDPE. In this sense, it has been reported that the presence of the antioxidant particles can produce two antagonistic effects, that is, a nucleating effect on the polyolefin, which induces the growth of a large number of crystals, but also a decrease in crystal size because of imperfections [70].

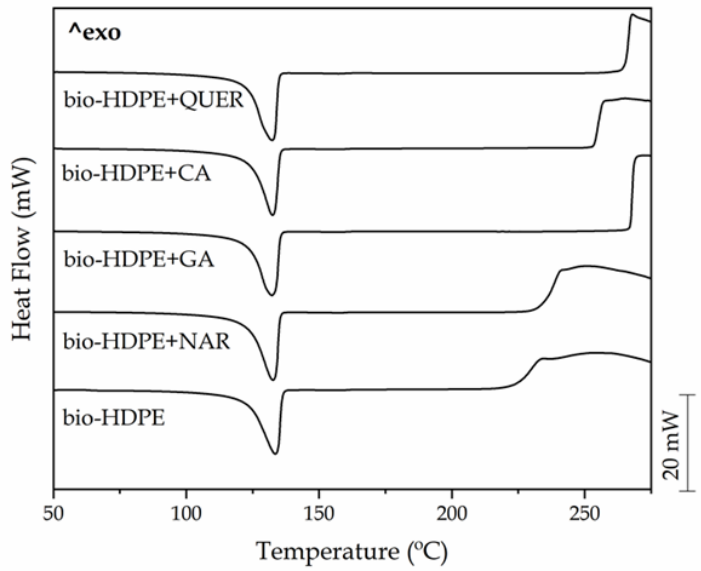

Figure IV.1.1.7. Heating curves obtained by differential scanning calorimetry (DSC) of the thermo-compressed bio-based high-density polyethylene (bio-HDPE) films containing naringin (NAR), gallic acid (GA), caffeic acid (CA), and quercetin (QUER).

Table IV.1.1.3. Main thermal parameters of the thermo-compressed bio-based high-density polyethylene (bio-HDPE) films containing naringin (NAR), gallic acid (GA), caffeic acid (CA), and quercetin (QUER) in terms of melting temperature (T_m), normalized melting enthalpy (ΔH_m), degree of crystallinity (X_C), onset oxidation temperature (OOT), and oxidation induction time (OIT).

Film	T_m (°C)	ΔH_m (J g^{-1})	X_C (%)	OOT (°C)	OIT (min)
bio-HDPE	134.9 ± 0.9^a	187.8 ± 1.6^a	64.1 ± 0.9^a	223.7 ± 1.6^a	4.5 ± 0.4^a
bio-HDPE + NAR	132.1 ± 0.8^b	186.9 ± 1.8^a	63.8 ± 0.8^a	232.2 ± 1.4^b	9.2 ± 0.5^b
bio-HDPE + GA	131.7 ± 0.7^b	186.1 ± 1.9^a	63.5 ± 1.0^a	266.7 ± 1.9^c	109.3 ± 1.6^c
bio-HDPE + CA	134.1 ± 0.8^a	171.3 ± 1.3^b	58.5 ± 0.7^b	253.6 ± 2.1^d	42.7 ± 0.9^d
bio-HDPE + QUER	131.8 ± 0.7^b	187.1 ± 2.0^a	63.9 ± 0.9^a	265.2 ± 1.9^c	137.9 ± 1.8^e

$^{a-e}$ Different letters in the same column indicate a significant difference among the samples ($p < 0.05$).

Table IV.1.1.3 also shows the T_{onset} of degradation, also called OOT, when it takes place in air or in any atmosphere rich in oxygen. This thermal oxidation can be seen in the DSC curves as the exothermic peak formed when high temperatures are reached. This parameter is considered as a common indicator used for ascertaining the polymer thermal-oxidative stability so it can be used to determine the thermal protection versus oxidation offered by added antioxidants [71]. One can observe that the neat bio-HDPE film started thermal oxidation at 223.7 °C, which is very similar to the value reported in our previous work for this green polyolefin [63]. It can also be observed that the different phenolic compounds provided different improvements in the thermal-oxidative stability of bio-HDPE. For instance, the addition of NAR resulted in an improvement in the OOT value of 8.5 °C, while CA yielded a more notable increase of 29.9 °C. The highest enhancement was observed, however, in the GA- and QUER-containing bio-HDPE films, which showed OOT values of 266.7 and 265.2 °C, respectively, providing an increase of 43 and 41.5 °C. Therefore, the incorporation of these natural phenols, particularly GA and QUER, greatly improved the thermal stability of the green polyolefin against oxidation at high processing temperatures.

In this context, phenols can prevent oxidation by neutralizing peroxide radicals. According to Kriston *et al.* [72], phenolic compounds can protect polyolefins from cross-linking reactions due to the formation of hydroperoxides by the transfer of a hydrogen atom from the phenolic fraction to the peroxy radical. Other authors such as Dopico-García *et al.* [73] also demonstrated that the use of natural extracts can successfully provide polyolefins with stabilization against degradation by thermal oxidation. Their

antioxidant activity is based on the *o*-dihydroxy structure of catechin's B ring, which confers greater stability to the radical form and participates in the delocalization of the electrons for the effective elimination of radicals. Moreover, different research groups have analyzed the effectiveness of some specific flavonoids as thermal stabilizers for polymer processing [74]. In particular, Zaharescu *et al.* [75] obtained an improvement in the thermal stability of ethylene-propylene-diene (EPDM) after the incorporation of NAR and CA. Both natural antioxidants delayed thermal oxidation significantly, especially when using large amounts of antioxidants. Similar improvements were obtained in the study performed by Samper *et al.* [11], in which 0.5 wt% of silibinin (SIL) and QUER acted as effective oxidative retardants for PP, successfully delaying T_{onset}. In particular, QUER has shown to be an efficient antioxidant in LDPE and other polymers [42]. The high antioxidant capacity of QUER is based on the particular chemical structure of this flavonol. When it reacts with a free radical, it donates a proton and becomes a radical itself, but the resulting unpaired electron is delocalized by resonance in the benzene structure, making the QUER radical too low in energy to be reactive [76]. Furthermore, the B ring *o*-dihydroxyl groups, the 4-oxo group in conjugation with the 2,3-alkene, and the 3-and 5-hydroxyl groups, can also donate electrons to the rings and, thus, increase the number of available resonance forms. In the case of GA, the higher improvement attained can also be related to an improved dispersion due to its lower M_W, generating a better contact with peroxyl radical in the biopolymer chains. For instance, contents as low as 0.3% of GA have successfully delayed the OOT value of bio-HDPE by more than 35 ^oC [63].

The stabilizing effect of the natural antioxidants was also analyzed through OIT measurements. **Figure IV.1.1.8** shows the isothermal curves of the bio-HDPE films when heated at 210 ^oC for a span time of 300 min. During the heating ramp, all the bio-HDPE samples first melted and then reached the selected temperature after 36 min. Thereafter, thermal oxidation was seen as an exothermic peak in the DSC curves and the OIT values were determined as the time taken to start thermal decomposition. This value can be very valuable to understand the degradation occurring in the green polyolefin when it is extruded or processed at high temperatures. As also shown in **Table IV.1.1.3**, one can see that neat bio-HDPE degraded in only 4.5 min after reaching 210 ^oC. Interestingly, in all cases, the addition of the different natural antioxidants successfully delayed the onset of thermal degradation. NAR, with an OIT of 9.2 min, enhanced the oxidative thermal

exposure time of bio-HDPE by more than 100% though it provided the lowest improvement, as similar to that found above for OOT. The incorporation of CA, GA, and, more importantly, QUER achieved OIT values for bio-HDPE of approximately 42.7, 109.3, and 137.9 min, respectively. The here-attained OIT values point out that these natural phenolic compounds are very promising additives to improve the oxidative thermal degradation of bio-HDPE. Similar results have been reported for α-tocopherol, which was also compared in terms of thermal protection with synthetic antioxidants such as butylated hydroxytoluene (BHT) [77]. Similarly, the work of Li *et al.* [78] showed that the incorporation of 0.1 wt% of dendritic antioxidant delayed the OIT of PP and LDPE at 200 ºC by approximately 40 and 50 min, respectively. Authors also demonstrated that the observed OIT values were higher than those obtained with commercial antioxidants Irganox® 1010 and 3114 by BASF (Ludwigshafen, Germany), which are sterically hindered phenolic antioxidants and achieved values in the range of 15–25 min. However, it is worth mentioning that, in comparison with the present study, the quantities of antioxidant added was much lower. Other studies have reported the addition of higher contents of commercial antioxidants, such as Irganox® L135 and L57 (BASF) at 0.5 wt%, a phenolic and amine antioxidants, respectively, showing OIT values of 3.58 min and 5.92 min for a lubricant base oil [79].

TGA was also performed on the green polyolefin films to study the thermal stability of the samples after the incorporation of the different natural antioxidants. **Figure IV.1.1.9** shows the TGA and DTG curves of the neat bio-HDPE film and the films of bio-HDPE with the phenolic compounds. The thermal values obtained from the TGA curves are summarized in **Table IV.1.1.4**. In **Figure IV.1.1.9**a, the evolution of mass (%) as a function of temperature is represented, while **Figure IV.1.1.9**b shows their DTG curves (mg s^{-1}). It can be observed that the neat bio-HDPE showed values of $T_{5\%}$ and T_{deg} of 355.1 and 473.7 ºC, respectively.

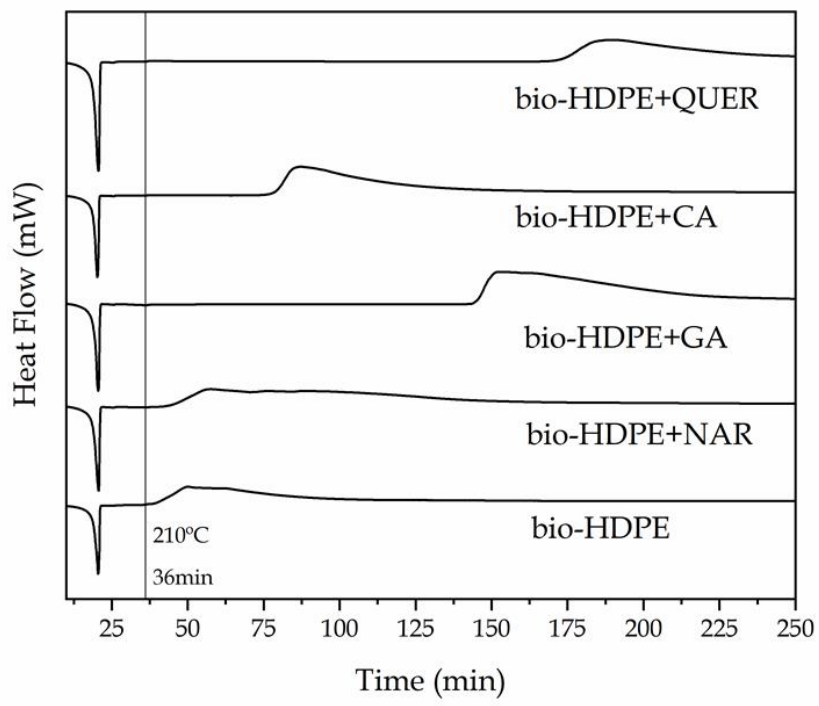

Figure IV.1.1.8. Isothermal curves obtained by differential scanning calorimetry (DSC) of the thermo-compressed bio-based high-density polyethylene (bio-HDPE) films containing naringin (NAR), gallic acid (GA), caffeic acid (CA), and quercetin (QUER).

The addition of the natural antioxidants significantly delayed the onset of thermal degradation, that is, $T_{5\%}$, by 7–21 ºC. Although a similar improvement was achieved in all cases, the highest $T_{5\%}$ value was attained for the NAR-containing bio-HDPE sample, showing a value of 376.1 ºC. In the case of T_{deg}, all the natural antioxidants yielded a slight improvement, of approximately 5–8 ºC, indicating that their major contribution takes place during the initiation of thermal degradation. It is also worth indicating that, in all samples, thermal degradation of bio-HDPE occurred in a single step, as reported earlier [68].

However, it is possible to observe a lower thermal decomposition rate of bio-HDPE up to approximately 400 ºC, which can be seen as a shoulder in the DTG curve, followed by a faster degradation rate. This phenomenon has been ascribed to two consecutive degradation steps in polyolefins, first the decomposition of the C–C covalent bonds by free radicals and then the sequential thermal degradation and breakdown of the polymer chains [80]. One can notice that this shoulder nearly vanished in the bio-HDPE films containing the phenolic compounds, suggesting that they actively participated as free radical scavengers due to the high reactivity of their hydroxyl

substituents [63]. Finally, with regard to the residual mass, one can observe that all bio-HDPE films yielded very similar values from 0.25 to 0.30% at 700 ºC.

The improvement in thermal stability reported by TGA also correlates well with the results obtained by other previous studies. For instance, Luzi *et al.* [64] showed that 5 wt% of GA led to an increase in T_{onset} and T_{deg} of approximately 44 and 20 ºC, respectively. The study performed by Samper *et al.* [11] indicated that the addition of QUER at 0.75 wt% in PP allowed to delay T_{onset} by nearly 32 ºC, while NAR yielded a thermal improvement of 10 ºC. Additionally, in the study carried out by Hernández-Hernández-Fernández *et al.* [81], an improvement of approximately 30 ºC in the T_{onset} of PP films after the addition of 0.1 wt% of CA was reported.

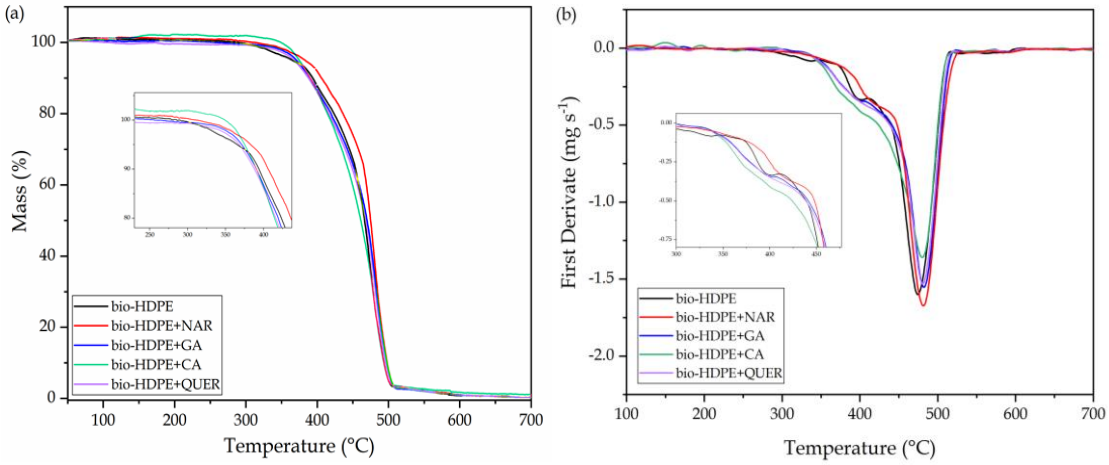

Figure IV.1.1.9. (a) Thermogravimetric analysis (TGA) and (b) first derivative (DTG) curves of the thermo-compressed bio-based high-density polyethylene (bio-HDPE) films containing naringin (NAR), gallic acid (GA), caffeic acid (CA), and quercetin (QUER).

Table IV.1.1.4. Main thermal decomposition parameters of the thermo-compressed bio-based high-density polyethylene (bio-HDPE) films containing naringin (NAR), gallic acid (GA), caffeic acid (CA), and quercetin (QUER) in terms of onset degradation temperature measured for a mass loss of 5% ($T_{5\%}$), temperature of maximum degradation (T_{deg}), and residual mass at 700 ºC.

Film	$T_{5\%}$ (ºC)	T_{deg} (ºC)	Residual Mass (%)
bio-HDPE	355.1 ± 1.2^{a}	473.7 ± 1.0^{a}	0.30 ± 0.94^{a}
bio-HDPE+NAR	376.1 ± 0.5^{b}	481.6 ± 0.8^{b}	0.27 ± 1.21^{a}
bio-HDPE+GA	366.3 ± 0.8^{c}	482.1 ± 1.1^{c}	0.29 ± 1.16^{a}
bio-HDPE+CA	371.7 ± 1.0^{c}	479.4 ± 1.2^{b}	0.25 ± 0.92^{a}
bio-HDPE+QUER	362.2 ± 0.8^{b}	481.3 ± 0.5^{c}	0.28 ± 1.63^{a}

$^{a–c}$ Different letters in the same column indicate a significant difference among the samples ($p < 0.05$).

Antioxidant activity

Although the main objective of the present study was to improve the thermal oxidation stability of bio-HDPE by the addition of the natural phenolic compounds, the antioxidant activity of the films was also determined by a release mechanism. To this end, the DPPH free radical method was carried out immersing the films in methanol. This antioxidant assay is based on an electron-transfer that produces a color change in the alcoholic solution from violet/purple of the stable radical DPPH to the yellow colored diphenyl-picrylhydrazine, which can be followed by UV-Vis spectroscopy. **Figure IV.1.1.10** shows the DDPH inhibition percentages for each sample at different times for a whole period of one week. It can be observed that all the phenolic compounds successfully provided antioxidant activity. Furthermore, the absorbances of all the DPPH solutions were nearly stabilized in 96 h, in most cases showing no significant differences, though the values slightly increased. The resultant antioxidant activity of the bio-HDPE films containing the natural compounds can be ascribed to their phenolic groups (ArOH), which could stabilize the DPPH radical (DPPH•) to its non-radical form (DPPH–H). This process has been reported to occur via two different mechanisms [82]: **Equation IV.1.1.4** a direct abstraction of phenol H-atom and **Equation IV.1.1.5** an electron transfer process from ArOH or its phenoxide anion (ArO−) to DPPH•, which can be summarized according to the proposed scheme:

$$ArOH + DPPH\bullet \rightarrow ArO\bullet + DPPH\text{-}H \qquad \textbf{Equation IV.1.1.4}$$

$$ArO\bullet + DPPH\bullet \rightarrow products \qquad \textbf{Equation IV.1.1.5}$$

The HAT mechanism **Equation IV.1.1.4** is predominant in apolar solvents, but in polar solvents, such as methanol, the ET mechanism **Equation IV.1.1.5** also becomes important due to it is capability of forming strong hydrogen bonds with the ArOH molecules [83]. One can also notice that the GA and CA antioxidants were shown to be 2–3 fold more active than NAR and QUER. In particular, whereas NAR and QUER reached a DPPH inhibition of up to 21.95% and 29.33%, respectively, GA and CA presented values of 64.42% and 82.09%. The differences attained among the bio-HDPE film samples can be mainly related to the different released amounts of each phenolic compound into the methanol medium. In the cases of GA and CA, their lower M_W values

could favor their diffusion from the bio-HDPE matrix. The highest antioxidant activity attained for CA can be related to the fact that cinnamic acid derivatives are known to be more potent free radical scavengers than benzoic acid derivatives, such as GA, which is based on their enhanced resonance stabilization that arises from the conjugation of π electrons in the ring with the π bond in the side-chain [84]. It is also interesting to note that the neat bio-HDPE film showed a slight value of DPPH inhibition (9.45%). This result may be due to some radical scavenging capacity of the bio-HDPE itself and/or the presence of antioxidant added by the manufacturer. A similar effect was previously observed for linear low-density polyethylene (LLDPE), which was ascribed to a slow diffusion of DPPH from the methanol solution into the polyolefin film, decreasing its concentration [34]. From the above, the here-developed bio-HDPE containing the natural compounds can also be of interest for active food packaging, particularly in the case of GA and CA. For instance, the resultant films can avoid or delay biochemical reactions such as oxidation of fats and sugars caused by light that generates unpleasant aromas and flavors [85].

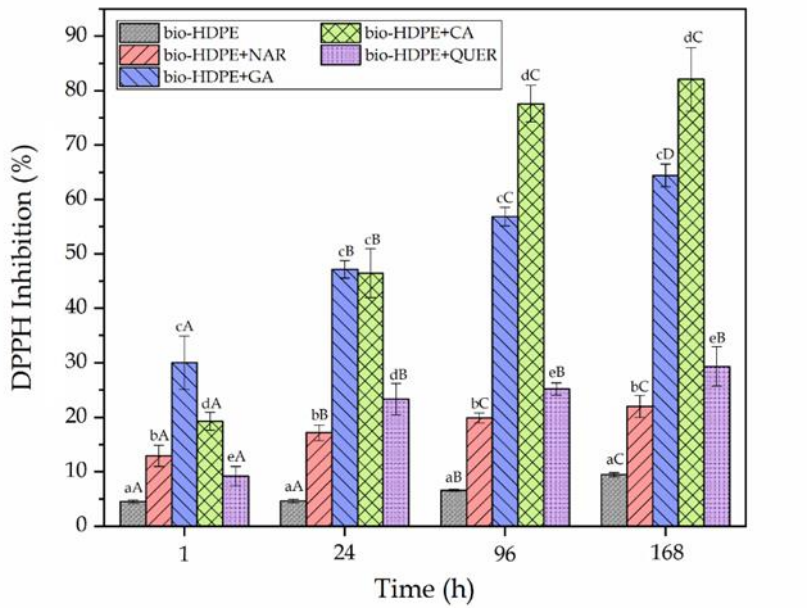

Figure IV.1.1.10. Percentage of 2,2-diphenyl-1-picrylhydrazyl radical (DPPH) inhibition of the thermo-compressed bio-based high-density polyethylene (bio-HDPE) films containing naringin (NAR), gallic acid (GA), caffeic acid (CA), and quercetin (QUER). $^{a-e}$ Different letters in the same period for different samples indicate a significant difference ($p < 0.05$). $^{A-C}$ Different letters for the same sample in different periods indicate a significant difference ($p < 0.05$).

CONCLUSIONS

The present study has evaluated the potential use of different phenolic compounds present in citrus fruits and grapes, which can be found as food processing by-products of the juice industries, as natural antioxidants in bio-HDPE films. Results showed that the incorporation of NAR, GA, CA, and QUER at 0.8 phr into bio-HDPE was successfully achieved. In terms of optical properties, the natural compounds yielded significant colors to the green polyolefin, however the films were still contact transparent. The cryo-fracture surfaces indicated that the phenolic compounds were embedded and well dispersed in the bio-HDPE matrix and the fracture behavior remained unaltered. The chemical analyses confirmed the successful inclusion of the phenolic compounds in the bio-HDPE matrix, though their interaction with the green polyolefin matrix was low. The bio-HDPE films were very ductile and, although the natural antioxidants slightly reduced the mechanical properties due to their limited solubility in the green polyolefin matrix, differences were not significant due to the low content of natural additive incorporated. Regarding the resistance to thermal oxidation, the use of the phenolic compounds yielded very promising results. All the here-tested phenolic compounds successfully increased the oxidative thermal stability of bio-HDPE, showing GA and particularly QUER the highest performance. Finally, the antioxidant activity of the phenol-containing bio-HDPE films was assessed by the DPPH free radical method in methanol solution. The results showed that the GA- and CA-containing films presented high antioxidant properties and could be potential candidates for active food packaging applications. The improved antioxidant performance of GA, CA, and, more importantly, QUER, was ascribed to the presence of multiple hydroxyl groups and aromatic heterocyclic rings that provide these molecules with the features to permit the delocalization and the scavenging of free radicals.

Therefore, one can consider that the present phenolic compounds, which are naturally present in citrus fruits and grapes, can represent a suitable alternative to synthetic antioxidants, for which safety and environmental issues have been raised over time. In particular, QUER, a major representative of the flavonol subclass, have been shown to effectively improve the thermo-oxidative degradation of green polyolefins, which can allow the enlargement of their processing and applications in the packaging sector. Alternatively, the use of GA, and particularly CA, is very promising to develop active systems in food packaging applications by a release mechanism. Future works

will explore the use of minimally processed phenolic extracts obtained from by-products of citrus and grape juices and related food industries. These phenolic compounds, which are contained mainly in the skins, albedos, and seeds of fruits and berries, can be released by hydrolysis and heat breakdown from certain esters or more complex molecules. The alternative use of the natural extracts will avoid the implementation of preparative chromatographic methods to isolate the pure phenolic compounds that, otherwise, could increase the cost and thus the viability of the valorization process. Furthermore, although these compounds are natural and show a great deal of potential for food packaging, their applications should also consider their possible migration and toxicological effects as well as negative effects on the sensory attributes, especially in terms of flavor.

FUNDING

This research work was funded by the Spanish Ministry of Science and Innovation (MICI) project number MAT2017-84909-C2-2-R.

ACKNOWLEDGMENTS

S. Rojas-Lema is a recipient of a Santiago Grisolia grant from Generalitat Valenciana (GVA) (GRISOLIAP/2019/132). S. Torres-Giner. acknowledges MICI for his Ramón y Cajal contract (RYC2019- 027784-I). Microscopy services of the Universitat Politècnica de València (UPV) are acknowledged for their help in collecting and analyzing the FESEM images.

REFERENCES

[1] S. Torres-Giner, L. Gil, L. Pascual-Ramírez, and J. Garde-Belza. *Packaging: Food waste reduction*, in *Encyclopedia of Polymer Applications*. 2018, CRC Press: Boca Raton, FL, USA, p. 1990.

[2] R.P. Babu, K. O'connor, and R. Seeram. *Current progress on bio-based polymers and their future trends.* Progress in Biomaterials, 2013, 2(1), p. 8.

[3] G. Chen, S. Li, F. Jiao, and Q. Yuan. *Catalytic dehydration of bioethanol to ethylene over TiO2/γ-Al2O3 catalysts in microchannel reactors.* Catalysis Today, 2007, 125(1-2), p. 111-119.

[4] L. Quiles-Carrillo, N. Montanes, A. Jorda-Vilaplana, R. Balart, and S. Torres-Giner. *A comparative study on the effect of different reactive compatibilizers on injection-molded pieces of bio-based high-density polyethylene/polylactide blends.* Journal of Applied Polymer Science, 2019, 136(16), p. 47396.

[5] S. Torres-Giner, A. Torres, M. Ferrándiz, V. Fombuena, and R. Balart. *Antimicrobial activity of metal cation-exchanged zeolites and their evaluation on injection-molded pieces of bio-based high-density polyethylene.* Journal of Food Safety, 2017, 37(4), p. e12348.

[6] J. Araújo, W. Waldman, and M. De Paoli. *Thermal properties of high density polyethylene composites with natural fibres: Coupling agent effect.* Polymer Degradation and Stability, 2008, 93(10), p. 1770-1775.

[7] L. Quiles-Carrillo, N. Montanes, V. Fombuena, R. Balart, and S. Torres-Giner. *Enhancement of the processing window and performance of polyamide 1010/bio-based high-density polyethylene blends by melt mixing with natural additives.* Polymer International, 2020, 69(1), p. 61-71.

[8] J. Wang, Z. Du, and T. Lian. *Extrusion–calendering process of single-polymer composites based on polyethylene.* Polymer Engineering & Science, 2018, 58(12), p. 2156-2165.

[9] D. Tátraaljai, L. Major, E. Földes, and B. Pukánszky. *Study of the effect of natural antioxidants in polyethylene: performance of β-carotene.* Polymer Degradation and Stability, 2014, 102, p. 33-40.

[10] B. Kirschweng, B. Vörös, D. Tátraaljai, M. Zsuga, E. Földes, and B. Pukánszky. *Natural antioxidants as melt stabilizers for PE: Comparison of silymarin and quercetin.* European Polymer Journal, 2017, 90, p. 456-466.

[11] M. Samper, E. Fages, O. Fenollar, T. Boronat, and R. Balart. *The potential of flavonoids as natural antioxidants and UV light stabilizers for polypropylene.* Journal of Applied Polymer Science, 2013, 129(4), p. 1707-1716.

[12] X. Gao, G. Hu, Z. Qian, Y. Ding, S. Zhang, D. Wang, and M. Yang. *Immobilization of antioxidant on nanosilica and the antioxidative behavior in low density polyethylene.* Polymer, 2007, 48(25), p. 7309-7315.

[13] W. Yu, T. Reitberger, T. Hjertberg, J. Oderkerk, F. Costa, V. Englund, and U.W. Gedde. *Chlorine dioxide resistance of different phenolic antioxidants in polyethylene.* Polymer Degradation and Stability, 2015, 111, p. 1-6.

[14] K.A. Iyer, L. Zhang, and J.M. Torkelson. *Direct use of natural antioxidant-rich agro-wastes as thermal stabilizer for polymer: Processing and recycling.* ACS Sustainable Chemistry & Engineering, 2016, 4(3), p. 881-889.

[15] A. Masek. *Flavonoids as natural stabilizers and color indicators of ageing for polymeric materials.* Polymers, 2015, 7(6), p. 1125-1144.

[16] K.W. Kong, A.R. Ismail, S.T. Tan, K.M. Nagendra Prasad, and A. Ismail. *Response surface optimisation for the extraction of phenolics and flavonoids from a pink guava puree industrial by-product.* International Journal of Food Science & Technology, 2010, 45(8), p. 1739-1745.

[17] P.d.P.M. Barbosa, A.R. Ruviaro, and G.A. Macedo. *Comparison of different Brazilian citrus by-products as source of natural antioxidants.* Food Science and Biotechnology, 2018, 27(5), p. 1301-1309.

[18] A. Bocco, M.-E. Cuvelier, H. Richard, and C. Berset. *Antioxidant activity and phenolic composition of citrus peel and seed extracts.* Journal of Agricultural and Food Chemistry, 1998, 46(6), p. 2123-2129.

[19] J.V. Madeira Jr and G.A. Macedo. *Simultaneous extraction and biotransformation process to obtain high bioactivity phenolic compounds from Brazilian citrus residues.* Biotechnology Progress, 2015, 31(5), p. 1273-1279.

[20] P. Hernández-Carranza, R. Ávila-Sosa, J. Guerrero-Beltrán, A. Navarro-Cruz, E. Corona-Jiménez, and C. Ochoa-Velasco. *Optimization of antioxidant compounds*

extraction from fruit by-products: Apple pomace, orange and banana peel. Journal of Food Processing and Preservation, 2016, 40(1), p. 103-115.

[21] K. Koyama, N. Goto-Yamamoto, and K. Hashizume. *Influence of maceration temperature in red wine vinification on extraction of phenolics from berry skins and seeds of grape (Vitis vinifera).* Bioscience, Biotechnology, and Biochemistry, 2007, 71(4), p. 958-965.

[22] M. Arabi, M. Ghaedi, and A. Ostovan. *Synthesis and application of in-situ molecularly imprinted silica monolithic in pipette-tip solid-phase microextraction for the separation and determination of gallic acid in orange juice samples.* Journal of Chromatography B, 2017, 1048, p. 102-110.

[23] C. Magnani, V.L.B. Isaac, M.A. Correa, and H.R.N. Salgado. *Caffeic acid: a review of its potential use in medications and cosmetics.* Analytical Methods, 2014, 6(10), p. 3203-3210.

[24] C.M. Spagnol, R.P. Assis, I.L. Brunetti, V.L.B. Isaac, H.R.N. Salgado, and M.A. Corrêa. *In vitro methods to determine the antioxidant activity of caffeic acid.* Spectrochimica Acta Part A: Molecular and Biomolecular Spectroscopy, 2019, 219, p. 358-366.

[25] A.V.A. David, R. Arulmoli, and S. Parasuraman. *Overviews of biological importance of quercetin: A bioactive flavonoid.* Pharmacognosy Reviews, 2016, 10(20), p. 84.

[26] A. Wach, K. Pyrzyńska, and M. Biesaga. *Quercetin content in some food and herbal samples.* Food Chemistry, 2007, 100(2), p. 699-704.

[27] Y. Numata and H. Tanaka. *Quantitative analysis of quercetin using Raman spectroscopy.* Food Chemistry, 2011, 126(2), p. 751-755.

[28] M.D. Samper-Madrigal, O. Fenollar, F. Dominici, R. Balart, and J. Kenny. *The effect of sepiolite on the compatibilization of polyethylene–thermoplastic starch blends for environmentally friendly films.* Journal of Materials Science, 2015, 50(2), p. 863-872.

[29] Á. Agüero, D. Garcia-Sanoguera, D. Lascano, S. Rojas-Lema, J. Ivorra-Martinez, O. Fenollar, and S. Torres-Giner. *Evaluation of different compatibilization strategies to improve the performance of injection-molded green composite pieces made of polylactide reinforced with short flaxseed fibers.* Polymers, 2020, 12(4), p. 821.

[30] S. Rojas-Lema, L. Quiles-Carrillo, D. Garcia-Garcia, B. Melendez-Rodriguez, R. Balart, and S. Torres-Giner. *Tailoring the properties of thermo-compressed polylactide*

films for food packaging applications by individual and combined additions of lactic acid oligomer and halloysite nanotubes. Molecules, 2020, 25(8), p. 1976.

[31] A. Agüero, M.d.C. Morcillo, L. Quiles-Carrillo, R. Balart, T. Boronat, D. Lascano, S. Torres-Giner, and O. Fenollar. *Study of the influence of the reprocessing cycles on the final properties of polylactide pieces obtained by injection molding*. Polymers, 2019, 11(12), p. 1908.

[32] D. Castro, A. Ruvolo-Filho, and E. Frollini. *Materials prepared from biopolyethylene and curaua fibers: Composites from biomass.* Polymer Testing, 2012, 31(7), p. 880-888.

[33] R.L. Prior, X. Wu, and K. Schaich. *Standardized methods for the determination of antioxidant capacity and phenolics in foods and dietary supplements.* Journal of Agricultural and Food Chemistry, 2005, 53(10), p. 4290-4302.

[34] M.L. Goñi, N.A. Gañán, M.C. Strumia, and R.E. Martini. *Eugenol-loaded LLDPE films with antioxidant activity by supercritical carbon dioxide impregnation.* The Journal of Supercritical Fluids, 2016, 111, p. 28-35.

[35] K.J. Figueroa-Lopez, A.A. Vicente, M.A. Reis, S. Torres-Giner, and J.M. Lagaron. *Antimicrobial and antioxidant performance of various essential oils and natural extracts and their incorporation into biowaste derived poly (3-hydroxybutyrate-co-3-hydroxyvalerate) layers made from electrospun ultrathin fibers.* Nanomaterials, 2019, 9(2), p. 144.

[36] A.H. Elhamirad and M.H. Zamanipoor. *Thermal stability of some flavonoids and phenolic acids in sheep tallow olein.* European Journal of Lipid Science and Technology, 2012, 114(5), p. 602-606.

[37] D. Tátraaljai, B. Kirschweng, J. Kovács, E. Földes, and B. Pukánszky. *Processing stabilisation of PE with a natural antioxidant, curcumin.* European Polymer Journal, 2013, 49(6), p. 1196-1203.

[38] B. Kirschweng, K. Bencze, M. Sárközi, B. Hégely, G. Samu, J. Hári, D. Tátraaljai, E. Földes, M. Kállay, and B. Pukánszky. *Melt stabilization of polyethylene with dihydromyricetin, a natural antioxidant.* Polymer Degradation and Stability, 2016, 133, p. 192-200.

[39] B.J. Ahn, K.K. Gaikwad, and Y.S. Lee. *Characterization and properties of LDPE film with gallic-acid-based oxygen scavenging system useful as a functional packaging material.* Journal of Applied Polymer Science, 2016, 133(43), p. 44138.

[40] J. Pokorný, N. Yanishlieva, and M. Gordon. *Antioxidants in food: practical applications*. 2001, Boca Raton, FL, USA: Elsevier, p. 1-288.

[41] B. Marcos, C. Sárraga, M. Castellari, F. Kappen, G. Schennink, and J. Arnau. *Development of biodegradable films with antioxidant properties based on polyesters containing a-tocopherol and olive leaf extract for food packaging applications.* Food Packaging and Shelf Life, 2014, 1(2), p. 140-150.

[42] D. Tátraaljai, E. Földes, and B. Pukánszky. *Efficient melt stabilization of polyethylene with quercetin, a flavonoid type natural antioxidant.* Polymer Degradation and Stability, 2014, 102, p. 41-48.

[43] J. Du, L. Zhao, Y. Zeng, L. Zhang, F. Li, P. Liu, and C. Liu. *Comparison of electrical properties between multi-walled carbon nanotube and graphene nanosheet/high density polyethylene composites with a segregated network structure.* Carbon, 2011, 49(4), p. 1094-1100.

[44] W. Tang, M.H. Santare, and S.G. Advani. *Melt processing and mechanical property characterization of multi-walled carbon nanotube/high density polyethylene (MWNT/HDPE) composite films.* Carbon, 2003, 41(14), p. 2779-2785.

[45] C. Liu, C. Chen, H. Ma, E. Yuan, and Q. Li. *Characterization and DPPH radical scavenging activity of gallic acid-lecithin complex.* Tropical Journal of Pharmaceutical Research, 2014, 13(8), p. 1333-1338.

[46] F. Luzi, L. Torre, and D. Puglia. *Antioxidant Packaging Films Based on Ethylene Vinyl Alcohol Copolymer (EVOH) and Caffeic Acid.* Molecules, 2020, 25(17), p. 3953.

[47] M. Kakran, R. Shegokar, N.G. Sahoo, S. Gohla, L. Li, and R.H. Müller. *Long-term stability of quercetin nanocrystals prepared by different methods.* Journal of Pharmacy and Pharmacology, 2012, 64(10), p. 1394-1402.

[48] J. Yan, Y.-H. Wu, D.-G. Yu, G.R. Williams, S.-M. Huang, W. Tao, and J.-Y. Sun. *Electrospun acid–base pair solid dispersions of quercetin.* RSC Advances, 2014, 4(102), p. 58265-58271.

[49] P. Anna, G. Bertalan, G. Marosi, I. Ravadits, and M. Maatoug. *Effect of interface modification on the photo-stability of pigmented polyethylene films.* Polymer Degradation and Stability, 2001, 73(3), p. 463-466.

[50] D. Mandial, P. Khullar, H. Kumar, G.K. Ahluwalia, and M.S. Bakshi. *Naringin–Chalcone Bioflavonoid-Protected Nanocolloids: Mode of Flavonoid Adsorption, a Determinant for Protein Extraction.* ACS Omega, 2018, 3(11), p. 15606-15614.

[51] Y. Sun, J. Wang, S. Gu, Z. Liu, Y. Zhang, and X. Zhang. *Simultaneous determination of flavonoids in different parts of Citrus reticulata 'Chachi'fruit by high performance liquid chromatography – photodiode array detection.* Molecules, 2010, 15(8), p. 5378-5388.

[52] J. Liu, J.-f. Lu, J. Kan, and C.-h. Jin. *Synthesis of chitosan-gallic acid conjugate: Structure characterization and in vitro anti-diabetic potential.* International Journal of Biological Macromolecules, 2013, 62, p. 321-329.

[53] M. Friedman and H.S. Jürgens. *Effect of pH on the stability of plant phenolic compounds.* Journal of Agricultural and Food Chemistry, 2000, 48(6), p. 2101-2110.

[54] J.E.N. Dolatabadi, A. Mokhtarzadeh, S.M. Ghareghoran, and G. Dehghan. *Synthesis, characterization and antioxidant property of quercetin-Tb (III) complex.* Advanced Pharmaceutical Bulletin, 2014, 4(2), p. 101.

[55] X. Ma, Z. Chen, R. Chen, X. Zheng, X. Chen, and R. Lan. *Imprinted β-cyclodextrin polymers using naringin as template.* Polymer International, 2011, 60(10), p. 1455-1460.

[56] Y.P. Neo, S. Ray, J. Jin, M. Gizdavic-Nikolaidis, M.K. Nieuwoudt, D. Liu, and S.Y. Quek. *Encapsulation of food grade antioxidant in natural biopolymer by electrospinning technique: A physicochemical study based on zein–gallic acid system.* Food Chemistry, 2013, 136(2), p. 1013-1021.

[57] A. Belay, H.K. Kim, and Y.H. Hwang. *Binding of caffeine with caffeic acid and chlorogenic acid using fluorescence quenching, UV/vis and FTIR spectroscopic techniques.* Luminescence, 2016, 31(2), p. 565-572.

[58] S. Gunasekaran, G. Sankari, and S. Ponnusamy. *Vibrational spectral investigation on xanthine and its derivatives – theophylline, caffeine and theobromine.* Spectrochimica Acta Part A: Molecular and Biomolecular Spectroscopy, 2005, 61(1-2), p. 117-127.

[59] A. Kumari, S.K. Yadav, Y.B. Pakade, B. Singh, and S.C. Yadav. *Development of biodegradable nanoparticles for delivery of quercetin.* Colloids and Surfaces B: Biointerfaces, 2010, 80(2), p. 184-192.

[60] Y. Zhang, Y. Yang, K. Tang, X. Hu, and G. Zou. *Physicochemical characterization and antioxidant activity of quercetin-loaded chitosan nanoparticles.* Journal of Applied Polymer Science, 2008, 107(2), p. 891-897.

[61] J. Gulmine, P. Janissek, H. Heise, and L. Akcelrud. *Polyethylene characterization by FTIR.* Polymer Testing, 2002, 21(5), p. 557-563.

[62] M. Sugimoto, A. Shimada, H. Kudoh, K. Tamura, and T. Seguchi. *Product analysis for polyethylene degradation by radiation and thermal ageing.* Radiation Physics and Chemistry, 2013, 82, p. 69-73.

[63] L. Quiles-Carrillo, S. Montava-Jordà, T. Boronat, C. Sammon, R. Balart, and S. Torres-Giner. *On the Use of Gallic Acid as a Potential Natural Antioxidant and Ultraviolet Light Stabilizer in Cast-Extruded Bio-Based High-Density Polyethylene Films.* Polymers, 2020, 12(1), p. 31.

[64] F. Luzi, D. Puglia, F. Dominici, E. Fortunati, G. Giovanale, G. Balestra, and L. Torre. *Effect of gallic acid and umbelliferone on thermal, mechanical, antioxidant and antimicrobial properties of poly (vinyl alcohol-co-ethylene) films.* Polymer Degradation and Stability, 2018, 152, p. 162-176.

[65] X. Sun, Z. Wang, H. Kadouh, and K. Zhou. *The antimicrobial, mechanical, physical and structural properties of chitosan–gallic acid films.* LWT-Food Science and Technology, 2014, 57(1), p. 83-89.

[66] C. Colín-Chávez, H. Soto-Valdez, E. Peralta, J. Lizardi-Mendoza, and R.R. Balandrán-Quintana. *Fabrication and properties of antioxidant polyethylene-based films containing marigold (Tagetes erecta) extract and application on soybean oil stability.* Packaging Technology and Science, 2013, 26(5), p. 267-280.

[67] M. Ramos, A. Jiménez, M. Peltzer, and M.C. Garrigós. *Characterization and antimicrobial activity studies of polypropylene films with carvacrol and thymol for active packaging.* Journal of Food Engineering, 2012, 109(3), p. 513-519.

[68] N. Montanes, D. Garcia-Sanoguera, V. Segui, O. Fenollar, and T. Boronat. *Processing and characterization of environmentally friendly composites from biobased polyethylene and natural fillers from thyme herbs.* Journal of Polymers and the Environment, 2018, 26(3), p. 1218-1230.

[69] C. López-de-Dicastillo, J. Gómez-Estaca, R. Catalá, R. Gavara, and P. Hernández-Muñoz. *Active antioxidant packaging films: development and effect on lipid stability of brined sardines.* Food Chemistry, 2012, 131(4), p. 1376-1384.

[70] T. Xu, H. Lei, and C. Xie. *The effect of nucleating agent on the crystalline morphology of polypropylene (PP).* Materials & Design, 2003, 24(3), p. 227-230.

[71] M. Xin, Y. Ma, W. Lin, K. Xu, and M. Chen. *Use of dihydromyricetin as antioxidant for polypropylene stabilization.* Journal of Thermal Analysis and Calorimetry, 2015, 120(3), p. 1741-1747.

[72] I. Kriston, Á. Orbán-Mester, G. Nagy, P. Staniek, E. Földes, and B. Pukánszky. *Melt stabilisation of Phillips type polyethylene, Part II: Correlation between additive consumption and polymer properties.* Polymer Degradation and Stability, 2009, 94(9), p. 1448-1456.

[73] M. Dopico-García, M. Castro-López, J. López-Vilariño, M. González-Rodríguez, P. Valentao, P. Andrade, S. García-Garabal, and M. Abad. *Natural extracts as potential source of antioxidants to stabilize polyolefins.* Journal of Applied Polymer Science, 2011, 119(6), p. 3553-3559.

[74] G.E. Zaikov and A. Jiménez. *Polymer and biopolymer analysis and characterization*. 2007, New York: Nova Publishers, p. 1-253.

[75] T. Zaharescu, S. Jipa, A. Mantsch, and D. Henderson. *Stabilization effects of naringenin and caffeic acid on γ-irradiatedEPDM.* Radiation Physics and Chemistry, 2013, 84, p. 35-38.

[76] C. Mariani, A. Braca, S. Vitalini, N. De Tommasi, F. Visioli, and G. Fico. *Flavonoid characterization and in vitro antioxidant activity of Aconitum anthora L.(Ranunculaceae).* Phytochemistry, 2008, 69(5), p. 1220-1226.

[77] S. Weigl, K. Bretterbauer, W. Schöfberger, and C. Paulik. *Synthesis and oxidative stability of phenolic antioxidants immobilized by cellulose nanocrystals.* Polymer Degradation and Stability, 2016, 128, p. 253-259.

[78] C. Li, J. Wang, M. Ning, and H. Zhang. *Synthesis and antioxidant activities in polyolefin of dendritic antioxidants with hindered phenolic groups and tertiary amine.* Journal of Applied Polymer Science, 2012, 124(5), p. 4127-4135.

[79] C.L. Higgins, S.V. Filip, A. Afsar, and W. Hayes. *Evaluation of thermal and oxidative stability of three generations of phenolic based novel dendritic fuel and lubricant additives.* Reactive and Functional Polymers, 2019, 142, p. 119-127.

[80] R. Jana, P. Mukunda, and G. Nando. *Thermogravimetric analysis of compatibilized blends of low density polyethylene and poly (dimethyl siloxane) rubber.* Polymer Degradation and Stability, 2003, 80(1), p. 75-82.

[81] J. Hernández-Fernández, E. Rayón, J. López, and M.P. Arrieta. *Enhancing the thermal stability of polypropylene by blending with low amounts of natural antioxidants.* Macromolecular Materials and Engineering, 2019, 304(11), p. 1900379.

[82] D. Villaño, M. Fernández-Pachón, M.L. Moyá, A. Troncoso, and M. García-Parrilla. *Radical scavenging ability of polyphenolic compounds towards DPPH free radical.* Talanta, 2007, 71(1), p. 230-235.

[83] M.C. Foti, C. Daquino, and C. Geraci. *Electron-transfer reaction of cinnamic acids and their methyl esters with the DPPH• radical in alcoholic solutions.* The Journal of Organic Chemistry, 2004, 69(7), p. 2309-2314.

[84] S. Agatonovic-Kustrin, E. Kustrin, and D. Morton. *Phenolic acids contribution to antioxidant activities and comparative assessment of phenolic content in mango pulp and peel.* South African Journal of Botany, 2018, 116, p. 158-163.

[85] M. Moghadam, M. Salami, M. Mohammadian, M. Khodadadi, and Z. Emam-Djomeh. *Development of antioxidant edible films based on mung bean protein enriched with pomegranate peel.* Food Hydrocolloids, 2020, 104, p. 105735.

Adaptado del artículo

IV.1.2. Manufacturing and characterization of high-density polyethylene composites with active fillers from persimmon peel flour with improved antioxidant activity and hydrophobicity

Sandra Rojas-Lema[1,2], Diego Lascano[1,2], Juan Ivorra-Martinez[1], Jaume Gomez-Caturla[1], Rafael Balart[1], and Daniel Garcia-Garcia[1]

[1]Technological Institute of Materials (ITM), Universitat Politècnica de València (UPV), Plaza Ferrándiz y Carbonell 1, 03801 Alcoy, Spain.

[2]Escuela Politécnica Nacional, Quito 170517, Ecuador.

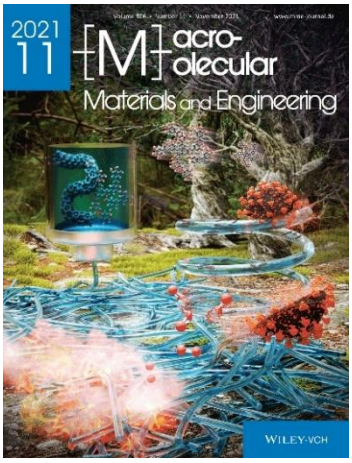

Macromolecular Materials and Engineering

2021, 306(11), p. 2100430

RESEARCH ARTICLE

Macromolecular Materials and Engineering
www.mame-journal.de

Manufacturing and Characterization of High-Density Polyethylene Composites with Active Fillers from Persimmon Peel Flour with Improved Antioxidant Activity and Hydrophobicity

Sandra Rojas-Lema, Diego Lascano, Juan Ivorra-Martinez, Jaume Gomez-Caturla, Rafael Balart, and Daniel Garcia-Garcia*

The potential of persimmon peel waste (PPF) as renewable active filler in biobased polyethylene composites, with improved antioxidant properties and resistance to water uptake is shown. To improve the interaction between the hydrophilic biofiller and the highly hydrophobic matrix, several compatibilization approaches are assessed. The first approach consists of using a polyethylene grafted copolymer with maleic anhydride (PE-g-MA). The second approach consists of modifying the PPF surface with two treatments before compounding with Bio-HDPE. The first consists on conventional silanization with (3-glycidyloxypropyl)trimethoxysilane, while the second consists on esterification with palmitoyl chloride. The results show an improvement of the matrix/biofiller interaction, as observed by field emission scanning electron microscopy (FESEM), leading to an increase in Young's modulus of 10% in composites compatibilized with PE-g-MA, and silanized PPF compared to composites without compatibilizer and no surface treatment on PPF. Interestingly, treatment with palmitoyl chloride leads to an increase in the hydrophobic behavior of composites keeping the water contact angle virtually constant at 128°. This effect is also reflected in a clear decrease in water absorption capacity of only 0.3 wt% over 9 weeks. Finally, PPF increases stabilization against oxidation, improving the oxidation induction time from 4.8 min (Bio-HDPE) to 82.5 min for composites with silanized PPF.

1. Introduction

The trend to incorporate fruits and vegetables of high nutritional value as a fundamental basis in people's daily diet has increased considerably in recent years.[1] Several studies have demonstrated that they can help in the prevention and treatment of degenerative diseases, largely due to the large number of active compounds with antioxidant properties.[2–4] This has led to a remarkable growth in consumption and production of the persimmon fruit in different countries and regions, including Europe, which is the world's second-largest producer with 8.5% market share, behind China (87.6%), between 2015 and 2019 according to the Food and Agriculture Organization of the United Nations.[5] The popularity of this fruit is due to the great benefits it brings to people's health, since it is a food with a great source of dietary fiber, tannins, vitamin C, phenolic compounds, among others, besides having a low content of saturated fats and calories.[6,7] This has triggered an increase in its consumption and industrialization, where the flesh is preferred for the preparation of juices, jams, ice cream, among others.[8–10] As a result, a large amount of waste is generated from the peel, calyx, and seeds. Several alternatives have been proposed to take advantage of these wastes since they are rich in valuable compounds. In this regard, persimmon peel has attracted attention because it can serve as a source of active compounds, due to its high carotenoids, polyphenols and proanthocyanidins content, which have a great antioxidant effect.[8] Another feasible approach for the valorization of agro-industrial and food wastes is the production of the so called wood-plastic composites (WPC), or more accurately, natural fiber reinforced plastics (NFRP) which aim obtaining environmentally friendly composites by combining a polymeric matrix (thermosetting or thermoplastic) and natural fillers (usually lignocellulosic materials) in the form of particles, fibers or fine powders to give a series of wood-like materials with balanced properties. In addition to minimizing the environmental impact of industrial wastes, the use of these lignocellulosic fillers has a positive effect on reducing the overall production costs, and can contribute to more sustainable materials.[11,12]

S. Rojas-Lema, D. Lascano, J. Ivorra-Martinez, J. Gomez-Caturla, R. Balart, D. Garcia-Garcia
Technological Institute of Materials (ITM)
Universitat Politècnica de València (UPV)
Plaza Ferrándiz y Carbonell 1, Alcoy 03801, Spain
E-mail: dielas@epsa.upv.es
S. Rojas-Lema, D. Lascano
Escuela Politécnica Nacional
Quito 17-01-2759, Ecuador
The ORCID identification number(s) for the author(s) of this article can be found under https://doi.org/10.1002/mame.202100430

DOI: 10.1002/mame.202100430

Manufacturing and characterization of high-density polyethylene composites with active fillers from persimmon peel flour with improved antioxidant activity and hydrophobicity

Abstract

The potential of persimmon peel waste (PPF) as renewable active filler in biobased polyethylene composites, with improved antioxidant properties and resistance to water uptake is shown. To improve the interaction between the hydrophilic biofiller and the highly hydrophobic matrix, several compatibilization approaches are assessed. The first approach consists of using a polyethylene grafted copolymer with maleic anhydride (PE-*g*-MA). The second approach consists of modifying the PPF surface with two treatments before compounding with Bio-HDPE. The first consists on conventional silanization with (3-glycidyloxypropyl)trimethoxysilane, while the second consists on esterification with palmitoyl chloride. The results show an improvement of the matrix/biofiller interaction, as observed by field emission scanning electron microscopy (FESEM), leading to an increase in Young's modulus of 10% in composites compatibilized with PE-*g*-MA, and silanized PPF compared to composites without compatibilizer and no surface treatment on PPF. Interestingly, treatment with palmitoyl chloride leads to an increase in the hydrophobic behavior of composites keeping the water contact angle virtually constant at 128°. This effect is also reflected in a clear decrease in water absorption capacity of only 0.3 wt% over 9 weeks. Finally, PPF increases stabilization against oxidation, improving the oxidation induction time from 4.8 min (Bio-HDPE) to 82.5 min for composites with silanized PPF.

Keywords: Biopolyethylene; compatibilization; natural fillers; persimmon peel; revalorization residues.

INTRODUCTION

The trend to incorporate fruits and vegetables of high nutritional value as a fundamental basis in people's daily diet has increased considerably in recent years [1]. Several studies have demonstrated that they can help in the prevention and treatment of degenerative diseases, largely due to the large number of active compounds with antioxidant properties [2-4]. This has led to a remarkable growth in consumption and production of the persimmon fruit in different countries and regions, including Europe, which is the world's second-largest producer with 8.5% market share, behind China (87.6%), between 2015 and 2019 according to the Food and Agriculture Organization of the United Nations [5]. The popularity of this fruit is due to the great benefits it brings to people's health, since it is a food with a great source of dietary fiber, tannins, vitamin C, phenolic compounds, among others, besides having a low content of saturated fats and calories [6, 7]. This has triggered an increase in its consumption and industrialization, where the flesh is preferred for the preparation of juices, jams, ice cream, among others [8-10]. As a result, a large amount of waste is generated from the peel, calyx, and seeds. Several alternatives have been proposed to take advantage of these wastes since they are rich in valuable compounds. In this regard, persimmon peel has attracted attention because it can serve as a source of active compounds, due to its high carotenoids, polyphenols, and proanthocyanidins content, which have a great antioxidant effect [8]. Another feasible approach for the valorization of agro-industrial and food wastes is the production of the so called wood-plastic composites (WPC), or more accurately, natural fiber reinforced plastics (NFRP) which aim obtaining environmentally friendly composites by combining a polymeric matrix (thermosetting or thermoplastic) and natural fillers (usually lignocellulosic materials) in the form of particles, fibers or fine powders to give a series of wood-like materials with balanced properties. In addition to minimizing the environmental impact of industrial wastes, the use of these lignocellulosic fillers has a positive effect on reducing the overall production costs, and can contribute to more sustainable materials [11, 12]. Currently, commodity thermoplastic materials such as polypropylene (PP) and polyethylene (PE) top the list of the most commonly used materials for WPC manufacturing due to the ease of processing by conventional methods, and good final properties such as flexibility, good chemical resistance and lightness, among others [13]. This has placed high-density polyethylene (HDPE) as the third most used material in the European market, with a

share of 12.4% [14]. This has raised concerns about the uncontrolled use of petroleum-derived materials, which has triggered the search for new biomaterials to replace the current ones [15]. To this end, recent research is being focused on developing polymers from renewable resources. Polyethylene can be obtained from renewable resources by the polymerization of ethylene monomer derived from the catalytic dehydration of bioethanol from sugarcane [16]. This biobased polyethylene has identical properties to those of its petrochemical counterpart.

One of the main drawbacks in the manufacture of wood-plastic composites or polymers filled with lignocellulosic particles, is the poor compatibility between the thermoplastic matrix and the natural fillers, due to the difference in polarity. Lignocellulosic fillers are highly hydrophilic due to the large number of hydroxyl groups present in their structure, which can also favor aggregates formation, while polymeric matrices usually are highly hydrophobic. This difference results in composites with poor mechanical properties since loads cannot be appropriately transferred between the lignocellulosic filler and the surrounding matrix [17]. To this end, many research studies have focused on assessing the usefulness of different types of strategies to improve the interaction between these two components. These techniques include the use of compatibilizers such as graft copolymers, which act as a bridge between the matrix and the biofiller, thus enhancing their interaction [18, 19]. Polyethylene grafted with maleic anhydride (PE-*g*-MA) is one of the most widely used compatibilizers in WPC with polyethylene matrices due to its dual functionality that can interact with both the polyethylene matrix (polyethylene segment chains in PE-*g*-MA), and the lignocellulosic filler (by the interaction of maleic anhydride with hydroxyl groups in lignocellulosic filler). Garcia-Garcia *et al.* [20], studied the effect of different types of maleic anhydride-based compatibilizers, namely polyethylene-*graft*-maleic anhydride (PE-*g*-MA), polypropylene-*graft*-maleic anhydride (PP-*g*-MA), and polystyrene-block-poly(ethylene-*ran*-butylene)-*block*-polystyrene-*graft*-maleic anhydride (SEBS-*g*-MA), on the compatibility of biobased polyethylene composites reinforced with peanut shell flour. Scanning electron microscopy images revealed that the use of these compatibilizers enhanced the interaction between the peanut shell flour and the surrounding matrix, leading to an improvement in its tensile properties. The dual functionality of these copolymers causes the anhydride groups to react with the hydroxyl (-OH) groups available in the biofiller to form ester groups and, on the other

hand, the polyethylene segments of these copolymers can rearrange to interact with the polyethylene matrix, thus helping to improve their interaction and dispersion.

Another strategy to improve the compatibility between the reinforcement and the matrix in WPCs or NFRP is to carry out surface treatments on the fillers with the main aim of blocking the hydroxyl groups with the subsequent decrease in hydrophilicity. Several surface treatments such as mercerization, silanization, esterification, among others, have proven to be very effective in reducing the hydrophilic nature of biofillers [13, 21-23]. The modification of the biofillers by alkoxy silanes leads to a strong interaction between the hydroxyl (-OH) groups contained in the biofillers with the hydrolyzed alkoxy groups, which give silanol groups (-Si-OH) [24]. In addition, it has been shown that esterification of the hydroxyl groups of the biofillers by treatment with fatty acids or their salts, such as palmitoyl chloride or with anhydrides such as acetic anhydride, positively contributes to increase their hydrophobic behavior, thus increasing their affinity with the highly hydrophobic matrices. Bijaisoradat *et al.* [25] improved the hydrophobic nature of wood flour (WF) in recycled polyethylene composite materials, by two different surface treatments, namely silanization with propyltrimethoxysilane and esterification with acetic anhydride. Both processes led to a remarkable improvement on filler dispersion and compatibility. Moreover, both surface treatments improved the mechanical properties and thermal stability of the obtained composite materials. Dominici *et al.* [26] investigated the effect of surface treatments, such as alkali bleaching and palmitoyl chloride esterification, on overall properties of biobased polyethylene composites and coffee silver-skin. In addition, reactive graft copolymerization with maleic anhydride was performed for the alkali treated samples to improve their compatibility with the matrix. They reported a remarkable increase in the hydrophobic nature of the coffee silverskin particles treated with palmitoyl chloride, leading to a water absorption of barely 0.2 wt% compared to 0.7 wt% of untreated coffee silverskin particles after an immersion period of one month.

The purpose of this work is to develop high environmentally friendly lignocellulosic particle-filled polymer composites with biobased high-density polyethylene (Bio-HDPE) matrix and an active biofiller from persimmon peel flour (PPF). In this study, two different strategies are proposed to improve polymer-filler interaction. The first approach considers the use of a graft copolymer compatibilizer, namely polyethylene-*graft*-maleic anhydride (PE-*g*-MA), while a second strategy con-

sists of two different surface treatments of PPF with (3-glycidyloxypropyl)trimethoxysilane or with palmitoyl chloride. The effect of these different compatibilizing strategies on mechanical properties (tensile, impact strength and hardness), dynamic-mechanical thermal behaviour (DMTA), morphology, thermal and color properties of Bio-HDPE/PPF composites with a constant PPF loading of 20 wt% was carried out. The effect of different surface treatments on the wetting properties of PPF was also evaluated by dynamic contact angle and water uptake characterization. Finally, the antioxidant effect of PPF phenolic compounds on Bio-HDPE/PPF composites was studied by (2,2- diphenyl-1-picryl-hydrazyl-hydrate) DPPH inhibition assay and oxidation induction time (OIT) at a constant temperature.

EXPERIMENTAL

Materials

A commercial biobased high-density polyethylene (Bio-HDPE) grade SHA7260 from Braskem and supplied by FKuR Kunststoff GmbH (Willich, Germany) was used as the polymer matrix. This Bio-HDPE contains at least 94% biobased content and has a melt flow rate of (20 g per 10 min), and a density of 0.955 g cm^{-3}.

The filler was obtained from persimmon peel waste of the Spanish "Rojo Brillante" persimmon fruit (Diospyros kaki). Persimmon peel was micronized following several stages. The first stage consisted of washing with water to remove unwanted impurities (paper labels, dust, and so on). Next, the drying process was carried out in an oven at a constant temperature of 65 °C for 5 days to remove moisture and flesh remains. Finally, the dried waste was ground in a Retsch Gmbh model ZM 1000 ultracentrifugal mill (Haan, Germany) with a sieve size of 250 µm and a rotation speed of 12,000 rpm. Persimmon peel flour (PPF) with particles of an average diameter of 60–125 µm was obtained, as shown in **Figure IV.1.2.1** The total fiber, soluble fiber, and insoluble fiber are 1.73, 0.82, and 0.87 g per 100 g, respectively. In addition, the minerals present in persimmon peel are potassium (266 g per 100 g), magnesium (12.7 g per 100 g), sodium (4.49 g per 100 g), manganese (0.23 g per 100 g), iron (0.27 g per 100 g), zinc (0.035 g per 100 g), copper (0.03 g per 100 g), and calcium (0.029 g per 100 g) [27].

The compatibilizer used was a polyethylene-*graft*-maleic-anhydride copolymer, (PE-*g*-MA) supplied by Sigma Aldrich (Madrid, Spain). This has an approximate amount

of 0.5 wt% maleic anhydride, a melting point T_m of 107 °C, and a viscosity of 500 cP (at 140 °C). Persimmon peel flour (PPF) was subjected to two types of surface treatments. The first was based on a functionalization treatment with (3-glycidyloxypropyl)trimethoxysilane (GLYMO) supplied by Sigma Aldrich (Madrid, Spain), with a density of 1.07 g cm^{-3} (at 25 °C). The second surface treatment consisted of hydrophobization with palmitoyl chloride in the presence of 1,2 dichloroethane and pyridine, all provided by Sigma Aldrich (Madrid, Spain). The chemical structure of the PE-*g*-MA copolymer, as well as the two surface-modification compounds is shown in **Scheme IV.1.2.1**.

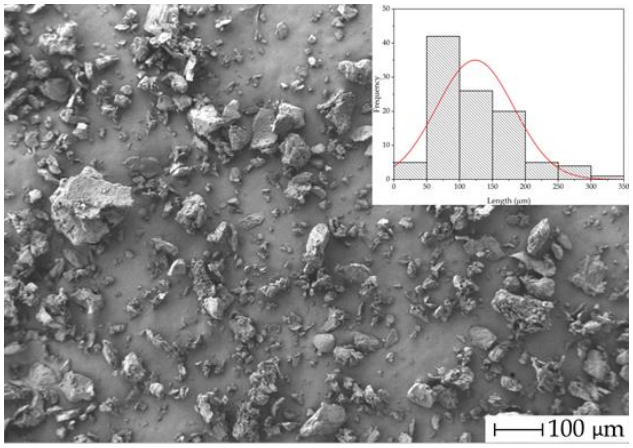

Figure IV.1.2.1. FESEM image of persimmon peel flour (PPF) particles at 50x with a marker scale of 100 µm.

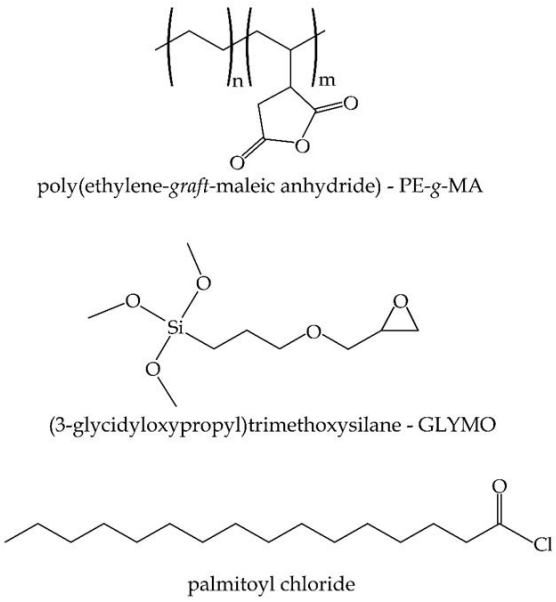

Scheme IV.1.2.1. Chemical structure of the maleic anhydride copolymer (PE-*g*-MA), and the two chemicals used to selectively modify the surface of persimmon peel flour.

Surface treatments on persimmon peel flour (PPF)

The PPF silanization process was carried out by immersing the flour particles in a solution of distilled water containing 1 wt% GLYMO relative to the total PPF loading, as suggested by Quiles-Carrillo *et al.* [28]. The solution was stirred for 2 h at room temperature using a magnetic stirrer until a homogeneous solution was obtained.

Then, the particles were removed, washed repeatedly with distilled water, and finally dried in an oven at a temperature of 80 °C for 12 h. **Scheme IV.1.2.2** shows a plot of the surface treatment of lignocellulosic particles by silanization. As it can be seen, esterification allows the silane to anchor into hydrophilic lignocellulose outer layer by a condensation reaction. In addition, the free silanols can react to form a polysiloxane layer [29].

The hydrophobization treatment of PPF was carried out according to the procedure described by García-García *et al.* [30] Prior to treatment, the PPF was dried in an oven for 12 h at a temperature of 80 °C to prevent moisture absorption. In a three-necked round-bottomed flask containing a 130 mL solution of 1,2-dichloroethane and 5 g of the flour particles were introduced, stirred with a magnetic stirrer, and heated to 70 °C. Once the temperature was reached, 7 mL of pyridine was introduced under a nitrogen atmosphere, followed by the addition of 11 mL of palmitoyl chloride. Magnetic stirring and a constant temperature of 70 °C was maintained throughout the reaction time (90 min).

The particles were then extracted and washed with 1,2-dichloroethane and distilled water. Finally, the particles were dried at 80 °C for 12 h. This reaction allows the anchoring of a highly hydrophobic layer by blocking the hydroxyl groups contained in the lignocellulosic particles by esterification reactions, as shown in **Scheme IV.1.2.3** [31].

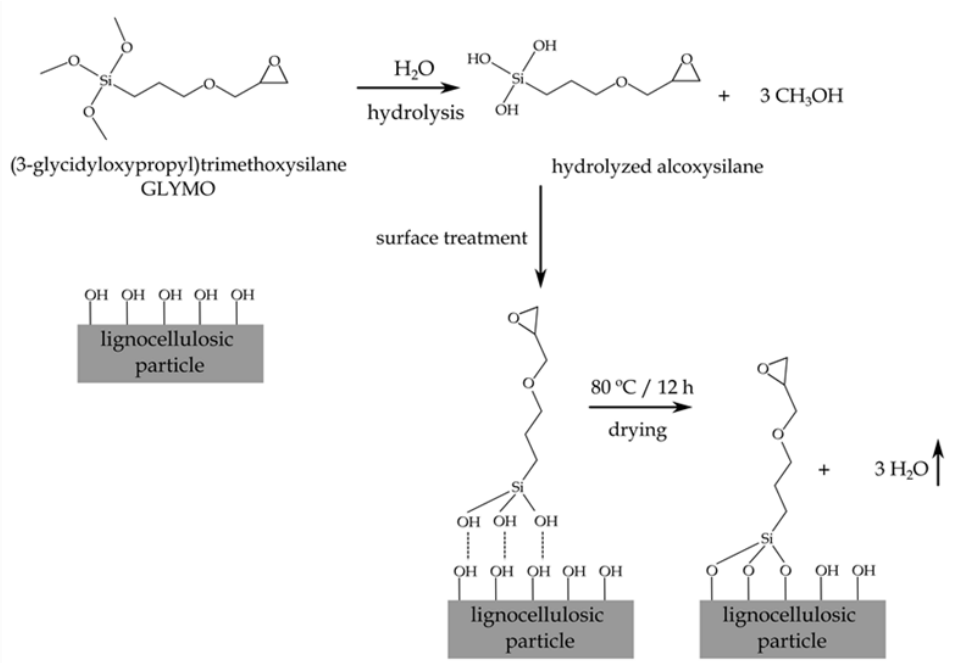

Scheme IV.1.2.2. Representation of the surface treatment of lignocellulosic particles from persimmon peel flour by silanization with GLYMO.

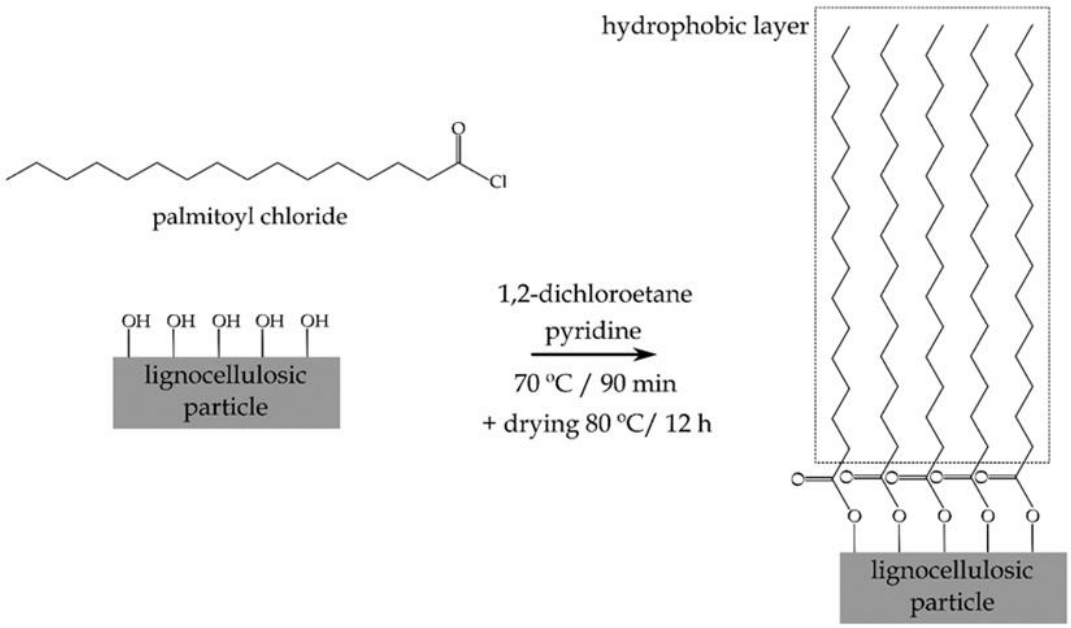

Scheme IV.1.2.3. Representation of the hydrophobic surface treatment of lignocellulosic particles from persimmon peel flour by using palmitoyl chloride.

The visual appearance of the PPF before and after the two surface treatments can be seen in **Figure IV.1.2.2.**

Figure IV.1.2.2. Photographs of a) untreated persimmon peel flour, b) persimmon peel flour after silanization with GLYMO treatment, and c) persimmon peel flour after hydrophobization treatment with palmitoyl chloride.

Manufacturing of Bio-HDPE/PPF composites

To remove the moisture content in the PPF (6 wt% at 25 °C), the PPF was subjected to a drying process in an oven at 65 °C for 12 h, prior to the manufacture of the composites. All formulations were first weighed and manually mixed in a ziplock bag prior to compounding by extrusion. All composites contained a constant PPF loading of 20 wt%. As for the PE-*g*-MA formulation, 2 wt% was used, and was directly mixed with the other components during the extrusion process. Samples were labeled with the code Bio-HDPE/PPF-XX, where XX stands for the compatibilization strategy: silanization with GLYMO (SI), compatibilization with polyethylene-*graft*-maleic (MA), and hydrophobization with palmitoyl chloride (PC).

The extrusion process was carried out in a twin-screw co-rotating extruder from Dupra S.L. (Alicante, Spain). The temperature profile was set considering the maximum melting temperature of a conventional high-density polyethylene (HDPE), starting at the feed hopper, and ending at the nozzle with 135–140–145–150 °C, and the rotation speed was set to 25 rpm. Once the filaments were collected, they were cooled down to room temperature, and pelletized in an air knife unit. To obtain standard specimens for tensile and Charpy impact tests, pellets of each formulation were molded on a Sprinter-11 Erinca S.L injection molding machine (Barcelona, Spain). The temperature profile was 140 °C in the feed hopper, 150 °C in the screw area and 160 °C in the injection nozzle. The injection and cooling times were set at 5 and 30 s, respectively.

PPF characterization

Wettability

The wettability of treated and untreated PPF was characterized by dynamic contact angle using an Easy drop FM140 goniometer supplied by Krüss Equipments (Hamburg, Germany). The characterization was carried out at room temperature with distilled water droplets of 15 µL, and the dynamic water contact angle was measured at different times up to 120 s.

Morphological analysis

Morphological analysis of PPF particles was assessed by field emission scanning electron microscopy (FESEM). A Zeiss Ultra 55 FESEM microscope provided by Oxford Instruments (Abingdon, UK) was employed. An electron accelerating voltage of 1.5 kV was set. Prior to analysis, PPF particles were sputter-coated by applying an ultra-thin layer of gold-palladium in a EM MED20 high-vacuum sputter coater provided by Leica Microsystem (Milton Keynes, UK). The particle size was obtained using Image J Launcher v 1.41.

Bio-HDPE/PPF composites characterization

Mechanical properties

The mechanical properties of neat Bio-HDPE and Bio-HDPE/PPF composites were analyzed by tensile, impact strength (Charpy) and hardness tests. Tensile tests were conducted on a ELIB 30 universal testing machine from Ibertest (Madrid, Spain); the test parameters and the dimensions of the dog-bone specimens were in accordance with ISO 527. A 5 kN load cell with a crosshead speed of 10 mm min^{-1} was used. The tensile modulus, E (MPa), tensile strength, σ_t (MPa), and elongation at break, ε_b (%) were measured by this test. At least 5 different specimens were tested and the corresponding tensile parameters were averaged.

The Charpy impact test was carried out to determine the impact strength. It was performed on a Charpy pendulum from Metrotec S.A. (San Sebastian, Spain) using a 1-J pendulum following ISO 179. The test was carried out on notched specimens ("V"

notch type, 2 mm depth), and five specimens of each formulation were tested to obtain reliable data, showing the average value.

Shore D hardness was obtained at room temperature using a durometer model 673-D of J. Bot S.A. (Barcelona, Spain), following the guidelines of ISO 868, with a stabilization time of 15 s. This process was performed at five different points and averaged for all formulations.

Morphological characterization

Morphological analysis of the fractured surfaces of Bio-HDPE/PPF composites after impact testing was performed by field emission scanning electron microscopy (FESEM). A Zeiss Ultra 55 FESEM microscope provided by Oxford Instruments (Abingdon, UK) was employed. An electron accelerating voltage of 1.5 kV was used. Prior to analysis, sample surfaces were sputter-coated by applying an ultra-thin layer of gold-palladium in a model EM MED20 high-vacuum coater provided by Leica Microsystem (Milton Keynes, UK).

Thermal properties

Thermal characterization of Bio-HDPE and Bio-HDPE/PPF composites was carried out by differential scanning calorimetry (DSC). The DSC tests were conducted in an 821 DSC calorimeter from Mettler-Toledo Inc. (Schwerzenbach, Switzerland) with samples of 5 – 8 mg. A dynamic thermal program was scheduled to obtain the main thermal transitions. This test consisted of three stages: an initial heating from 30 to 180 °C was used to remove the thermal history derived from the manufacturing processes. This step was followed by a cooling cycle to −25 °C. Finally, the samples were heated to 220 °C. The heating and cooling rate was set at 10 °C min^{-1}, under a constant nitrogen atmosphere of 66 mL min^{-1}. The crystallization temperature was obtained from the cooling cycle, while the melting enthalpy and melting peak temperature were collected from the second heating cycle. The crystallinity percentage of each sample was obtained by **Equation IV.1.2.1**.

$$X_c = \left[\frac{\Delta H_m}{\Delta H_m^0 \times w}\right] \times 100\ (\%) \qquad \textbf{Equation IV.1.2.1}$$

where ΔH_m^0 corresponds to the theoretical melting enthalpy of a fully crystalline HDPE (293 J g^{-1}) [26], ΔH_m stands for the melting enthalpy in (J g^{-1}), and w is the weight fraction of the polymer in the sample.

A second DSC test was carried out to analyze the effect of PPF on the oxidation induction time (OIT) of the Bio-HDPE matrix. This test consisted of two steps: the first one was a heating from 30 to 210 ^oC at a heating rate of 5 ^oC min^{-1}, followed by an isothermal step at a constant temperature of 210 ^oC for 200 min; the test was carried out under air atmosphere to assess the effect of PPF on polymer oxidation.

The degradation and thermal stability at high temperatures of Bio-HDPE and its composites, as well as persimmon peel flour, were studied by thermogravimetric analysis (TGA) on a Linseis TGA1000 thermobalance (Selb, Germany), in standard alumina crucibles with a capacity of 70 µL. The weight of the different samples was maintained in a range between 15 and 20 mg. The samples were heated from 30 up to 800 °C at a heating rate of 10 °C min^{-1} under nitrogen atmosphere with a flow rate of 66 mL min^{-1}. The parameters obtained from the thermogravimetric curves were the onset temperature (T_{onset}), measured at 5% weight loss, and the temperature of maximum degradation rate (T_{deg}) extracted from the first derivative curve (DTG).

Dynamic-mechanical thermal analysis (DMTA)

The dynamic-mechanical thermal behaviour of Bio-HDPE and Bio-HDPE/PPF composites was evaluated by dynamic mechanical thermal analysis (DMTA). A dynamic analyzer model DMA1 from Mettler-Toledo (Schwerzenbach, Switzerland) was used; the system operates under cantilever/simple bending conditions. Rectangular specimens (20 x 7 x 1 mm^3) were subjected to a heating cycle ranging from -150 to 125 °C with a heating rate of 2 °C min^{-1}. The frequency and maximum flexural deflection were set to 1 Hz and 0.1%, respectively. The evolution of the storage modulus (E') and the dynamic damping factor (tan δ) as a function of temperature was monitored throughout the test.

Color measurements

The effect of surface-treated PPF on the color of Bio-HDPE/PPF composites was analyzed using a KONICA CM-3600d Colorflex-DIFF2 colorimeter from Hunter

Associates Laboratory (Reston, Virginia, USA). The CIELab color scale (coordinates L*, a* and b*) was collected, where L* indicates brightness, a* shows the range between red and green colors, and b* shows the range between yellow and blue colors. The device was calibrated considering a standard white tile and a mirror unit for black. The total color difference (ΔE_{ab}*) was determined by **Equation IV.1.2.2**:

$$\Delta E_{ab}^{*} = \sqrt{(\Delta L^{*})^{2} + (\Delta a^{*})^{2} + (\Delta b^{*})^{2}} \qquad \textbf{Equation IV.1.2.2}$$

where ΔL*, Δa*, and Δb* are the differences between the color coordinates of the samples and the reference color.

Water uptake analysis

The water absorption of Bio-HDPE and Bio-HDPE/PPF composites was studied in accordance to ISO 62:2008. Rectangular samples (80 x 10 x 4 mm^3) were immersed in distilled water for a period of 9 weeks. The test was performed at room temperature. The samples were extracted from the distilled water, dried with absorbent paper and weighed on an analytical balance model AG245 from Mettler-Toledo (Schwerzenbach, Switzerland) with an accuracy of 0.001 g. The samples then were immersed again in the distilled water. This process was repeated once per week on the same day during the test period. To ensure the accuracy of the data, all measurements were repeated in triplicate. The percentage of water absorption was obtained using **Equation IV.1.2.3**.

$$\text{Water absorption} = \left[\frac{W_t - W_0}{W_0}\right] \times 100\ (\%) \qquad \textbf{Equation IV.1.2.3}$$

where W_t is the weight of the dry sample in grams at any time t and W_0 is the weight of the initial dry sample in grams.

Antioxidant measurement

The antioxidant effect of PPF phenolic compounds on Bio-HDPE/PPF composites was assessed by a 2,2-diphenyl-1-picrylhydrazyl radical (DPPH) inhibition test. DPPH is a stable nitrogenous organic radical that exhibits hydrogen acceptor capacity towards antioxidants. By means of spectrophotometry, the color change that occurs during the reduction of the violet color of DPPH in a methanol solution due to

the presence of antioxidant compounds was analyzed. A standard solution of 2,2-diphenyl-1-picrylhydrazyl supplied by Sigma Aldrich (Madrid, Spain) was prepared at 0.025 g L^{-1} in methanol (≥ 99.8%) of HPLC grade supplied by Panreac Química (Barcelona, Spain) and placed in dark glass vials. Films of each sample weighing ~100 mg were prepared and immersed in 5 mL of the standard solution, giving a maximum antioxidant concentration of ~160 ppm. The vials containing the samples and a control (no sample) were closed and kept in light-free and shaking conditions for one week. The absorbance of the samples was recorded at 1, 24, 72, and 168 h, in triplicate, using an Agilent Technologies (Barcelona, Spain) Cary series UV-Vis-NIR spectrophotometer at 517 nm, where the unpaired electron of the free DPPH radical has the highest absorbance. The percentage inhibition of DPPH was calculated according to **Equation IV.1.2.4**.

$$\text{DPPH Inhibition} = \left[\frac{A_c-(A_s-A_b)}{A_c}\right]\times 100\ (\%) \qquad \textbf{Equation IV.1.2.4}$$

where A_c, A_s correspond to the absorbance of DPPH without sample and with samples, respectively. A_b stands for the absorbance of the samples in methanol without DPPH.

RESULTS AND DISCUSSION

Effect of surface treatment on wetting properties and morphology of PPF

Wettability

To investigate the effect of surface treatments on the wetting properties of persimmon peel flour, the evolution of the dynamic water contact angle over time was studied, as shown in **Table IV.1.2.3** and **Figure IV.1.2.4.** As can be seen in **Figure IV.1.2.4**, the reference value of contact angle (t = 0) for the untreated PPF, silane-treated PPF and palmitoyl chloride-treated PPF is 112.4°, 118.5°, and 128.6°, respectively. The evolution of the contact angle for the untreated PPF, shows a clear decrease with time due to its hydrophilic nature, reaching values close to 40° after 60 s and, while after 120 s, untreated PPF is completely wet with a contact angle below 30°, thus showing a highly hydrophilic behavior, typical of most lignocellulosic fillers. As indicated by Vogler [32], surfaces with a contact angle of less than 65° have a hydrophilic character, this being a typical behavior of biofillers, due to the large number of hydroxyl groups (-OH) present

in their structure [33]. Regarding the evolution of the contact angle of PPF after silanization with GLYMO, it is worthy to note that it rapidly decreases in a similar way to untreated PPF during the first 30 s; after this time the decrease is less pronounced, reaching a constant value of 50°. These results suggest that some of the hydroxyl groups available in PPF have reacted with the hydrolyzed alkoxysilane, thus reducing the affinity of PPF to water absorption [24]. This phenomenon has been observed by several studies by using FTIR characterization. In particular, the intensity of the band corresponding to the hydroxyl groups of cellulose (3200 cm^{-1}) decreases, while a new peak located at 1200 cm^{-1} can be detected, which is attributed to Si-O-Si vibration. Moreover, the appearance of a peak at 800 cm^{-1} corresponding to Si-OH which is attributed to the reaction between the silanol groups (Si-OH), and the hydroxyl groups (-OH) of cellulose, thus confirming the condensation between them, which proves the anchoring of the hydrolized alkoxysilane into the outmost layer of the lignocellulosic particles [30, 34, 35]. The PPF treated with palmitoyl chloride exhibits practically unchanged contact angle values during the 120 s of measurement (128.6°), thus demonstrating the high efficiency of the treatment in providing a high hydrophobic behaviour to the PPF (contact angle > 65°). In fact, it can be considered a superhydrophobic behaviour since the water contact angle is even greater than 150°.

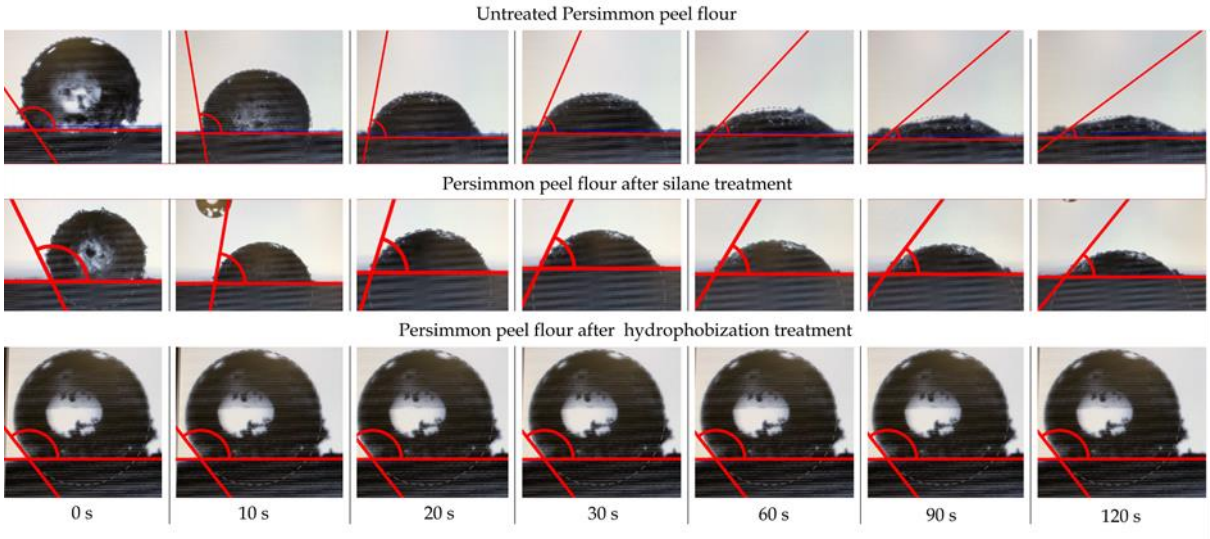

Figure IV.1.2.3. Comparative plots of the evolution of the dynamic water contact angle of untreated persimmon peel flour (upper row), persimmon peel flour after silanization with GLYMO treatment (middle row), and persimmon peel flour after hydrophobization with palmitoyl chloride (bottom row).

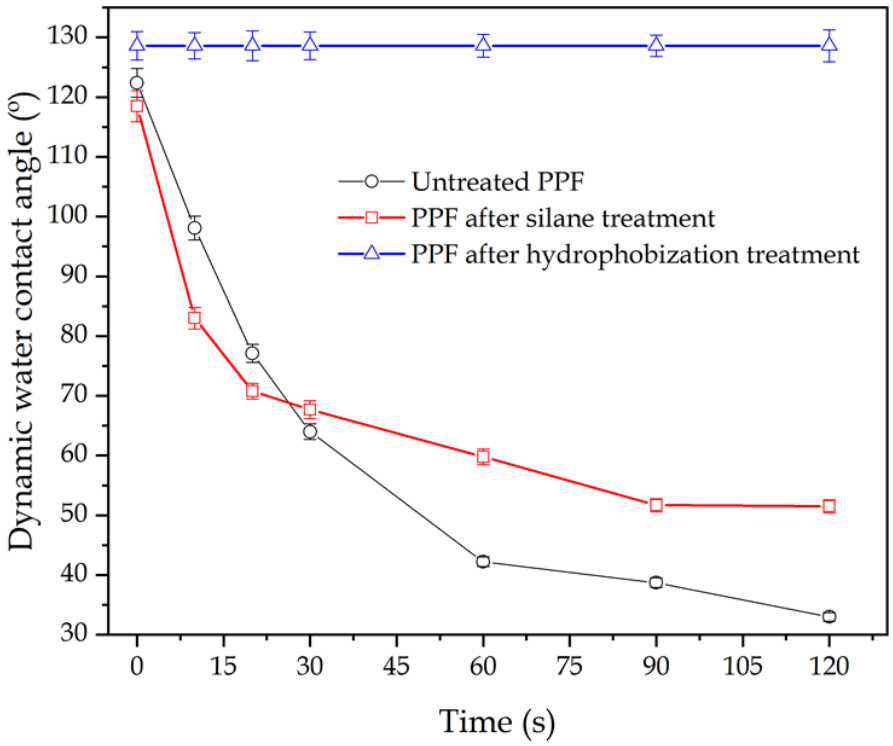

Figure IV.1.2.4. Variation of the dynamic water contact angle of persimmon peel flour as a function of time with different treatments: untreated, after silanization with GLYMO, and after hydrophobization with palmitoyl chloride.

Particle size and aggregation

To study the morphology and aggregate formation of PPF particles after both surface treatments, the washed and dried particles were observed by FESEM (**Figure IV.1.2.5**). **Figure IV.1.2.5**a shows PPF-SI powder with a particle size ranging from 70 to 90 µm. In addition, these particles present irregular shapes with a very slight roughness, due to the anchorage of the silanes on the PPF surface.

The effect of the palmitoyl chloride treatment is also evident since the PPF particles exhibit a rough surface, as shown in **Figure IV.1.2.5**b, due to the thin hydrophobic layer formed on their surface. The particle size is smaller, with an average particle size in the range of 50 – 70 µm, thus indicating a lower tendency to form particle aggregates, which has a positive effect on particle dispersion [36].

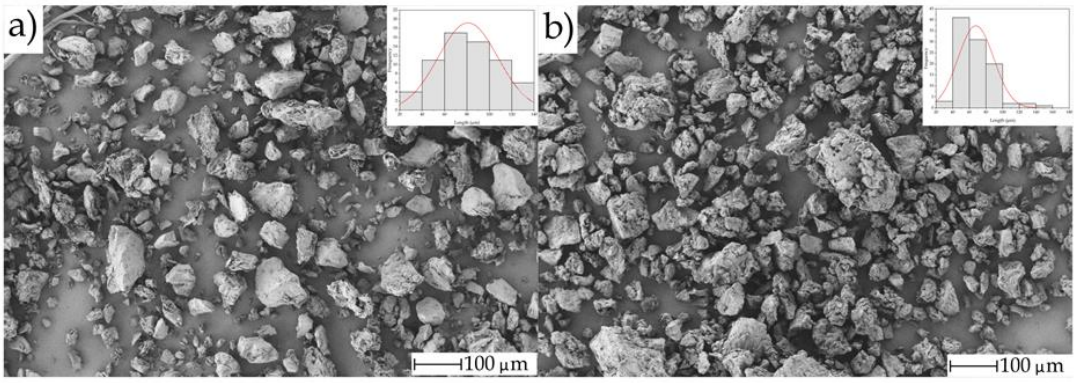

Figure IV.1.2.5. FESEM images of the persimmon peel flour after a) silanization with GLYMO, and b) hydrophobization with palmitoyl chloride. Images were taken at 100x, with a marker scale of 100 µm.

Characterization of Bio-HDPE/PPF composites

Mechanical properties of Bio-HDPE/PPF composites

The tensile mechanical properties (E, σ_t, ε_b), impact strength, and Shore D hardness of neat Bio-HDPE and Bio-HDPE/PPF composites are gathered in **Table IV.1.2.1**. Regarding the tensile tests, it can be observed that the addition of PPF leads to a significant decrease in the percentage of elongation at break (%ε_b) from 609.7% for neat Bio-HDPE to ~10% for the Bio-HDPE/PPF composites without any compatibilization strategy, as well as a slight decrease in the Young's modulus (E) and the tensile strength (σ_t), reducing the typical ductile behaviour of HDPE [37]. This effect can be attributed to the fact that, due to the highly hydrophilic nature of untreated PPF and the hydrophobic nature of the HDPE matrix, a low affinity occurs, which makes the interaction between them relatively low, leading to a reduction in their tensile properties due to the stress concentration phenomenon [20]. As for Bio-HDPE/PPF composites, it can be observed that the different compatibilization strategies have a positive effect on the mechanical performance of Bio-HDPE/PPF composites. On the one hand, it can be seen that the treatments do not significantly affect the tensile strength, which remains practically unchanged for all samples.

On the other hand, silane-treated PPF composites show a 10% and 20% increase in Young's modulus and elongation at break, respectively, compared to untreated PPF-filled composites. In addition, there is a 13% increase in the Young's modulus of the PE-*g*-MA compatibilized composite compared to the non- compatibilized sample (Bio-

HDPE/PPF). This effect may be referred to the increased interaction between the PPF and the Bio-HDPE matrix since PE-*g*-MA can interact with both the polymer matrix (polyethylene chain segments in PE-*g*-MA) and the ligno-cellulosic particle (due to the interactions between maleic anhydride and the hydroxyl groups in persimmon peel flour) [38, 39]. Improved interaction in Bio-HDPE/PPF-SI composites could be related to the reaction of the hydroxyl (-OH) groups present in PPF with the hydrolyzed silanol groups of GLYMO during silanization, as observed in other studies [24, 40]. Likewise, in the case of Bio-HDPE/PPF-MA, on one side, the reaction between maleic anhydride and the -OH groups of PPF, and on the other side, the PE segment chains in PE-*g*-MA, tend to interact with polyethylene chains of Bio-HDPE matrix, these two phenomena having a positive effect on increased interaction [41-43]. It should be noted that surface treatment with palmitoyl chloride enhances the hydrophobic nature of the PPF particles [36]. This has to two effects: firstly, it prevents aggregation of the particles, thus aiding a better particle dispersion into the Bio-HDPE polymer matrix, [44] and secondly, a thin hydrophobic layer formed around the particles increases their compatibility with the Bio-HDPE matrix (which is highly hydrophobic), [45] thus resulting in better interaction between the PPF surfaces and the Bio-HDPE matrix [46]. These results are consistent with those reported by Garcia-Garcia *et al.* [20] and Dominici *et al.* [26] in composites of biobased polyethylene and spent coffee ground wastes, where the hydrophobic nature of the coffee waste was enhanced by palmitoyl acid-based treatments.

Table IV.1.2.1. Summary of the mechanical properties (tensile properties, Shore-D hardness and impact strength) of the neat Bio-HDPE and Bio-HDPE/PPF composites.

Code	E [MPa]	σ_t [MPa]	ε_b [%]	Impact Strength [kJ m^{-2}]	Shore D hardness
Bio-HDPE	201.3 ± 6.5	21.6 ± 0.3	609.7 ± 38.1	4.8 ± 0.3	56.6 ± 0.9
Bio-HDPE/PPF	187.2 ± 9.5	15.0 ± 0.8	10.0 ± 0.7	2.0 ± 0.1	60.4 ± 0.9
Bio-HDPE/PPF-SI	224.5 ± 8.7	16.9 ± 0.4	12.0 ± 0.4	2.6 ± 0.3	57.8 ± 0.8
Bio-HDPE/PPF-MA	227.0 ± 6.5	16.2 ± 0.3	9.8 ± 0.1	2.6 ± 0.5	60.0 ± 1.4
Bio-HDPE/PPF-PC	170.0 ± 7.9	17.4 ± 0.2	15.1 ± 0.7	3.1 ± 0.2	60.6 ± 0.5

The impact strength obtained in a Charpy test can be useful to assess improved toughness. It can be observed that the impact energy absorption capacity of Bio-HDPE is drastically reduced with the addition of untreated PPF (less than the half). As mentioned, the low interaction due to the incompatibility between highly hydrophilic PPF particles and the highly hydrophobic polyethylene matrix results in small gaps between the particles and the matrix, as well as microcracks [20]. Considering the PPF-reinforced samples, it can be observed that the different compatibilization strategies lead to an increase in the impact-absorbed energy compared to composites with untreated PPF filler and no other compatibilizer. This increase in the absorbed-energy is due to the enhanced interaction between the biofiller and the surrounding polyethylene matrix, leading to a decrease in gap size, thus preventing microcrack growth. As can be seen, composites with hydrophobized PPF with palmitoyl chloride (Bio- HDPE/PPF-PC) offer the highest impact energy absorption of all composites in this study, with an impact strength of 3.1 kJ m^{-2}, which represents an increase of ~56% over composites with untreated PPF. This is due to the higher hydrophobicity of the PPF achieved with palmitoyl chloride, which results in better particle dispersion into the polyethylene matrix and better compatibility with the matrix, preventing crack formation and growth [44]. Finally, it can be observed that the addition of PPF in the Bio-HDPE matrix causes an increase in hardness, with an increase of ~7% on the shore D scale with respect to neat Bio-HDPE.

Morphology of Bio-HDPE/PPF composites

To study the effect of the different compatibilization strategies, the fractured surfaces of the impact-tested samples of neat Bio- HDPE and Bio-HDPE/PPF composites were observed by FESEM (**Figure IV.1.2.6**). **Figure IV.1.2.6**a shows the fracture corresponding to the neat Bio-HDPE sample, which presents a rough and irregular surface, marked by the presence of valleys and peaks, which is consistent with a ductile fracture typical of HDPE [37]. The addition of PPF clearly causes a disruption in the Bio-HDPE matrix, observed with the presence of large gaps between the PPF particles and the surrounding matrix, as indicated by the red arrows in **Figure IV.1.2.6**b, thus revealing a low interaction as mentioned above due to the different hydrophobic nature of both components. This makes the different deformation capacity of the filler and the matrix more noticeable, [47] causing a mixed fracture type, where a ductile-type fracture is observed for the matrix and a pull-off phenomenon for PPF particles can also be

detected. As shown in **Figure IV.1.2.6**c,d, both the use GLYMO-silanized PPF particles, and the use of PE-*g*-MA compatibilizer in composites, increase the interfacial interaction between the matrix and the filler, resulting in a noticeable decrease in the gaps between PPF particles and the surrounding matrix, as indicated by the green circles. These morphologies are responsible for improved mechanical properties, with a slight increase in tensile strength and, mainly, in impact-absorbed energy. Finally, it can be observed that the composites materials with hydrophobized PPF particles with palmitoyl chloride also offer a clear decrease in the size of the gap between the embedded PPF particles and the polyethylene matrix (**Figure IV.1.2.6**e), which is a clear evidence of improved compatibility between them due to a marked increase in the hydrophobic nature of the PPF. Moreover, this increase in hydrophobicity is also responsible for lower aggregate formation, as seen previously, thus improving their distribution in the polymer matrix, as indicated by the blue arrows.

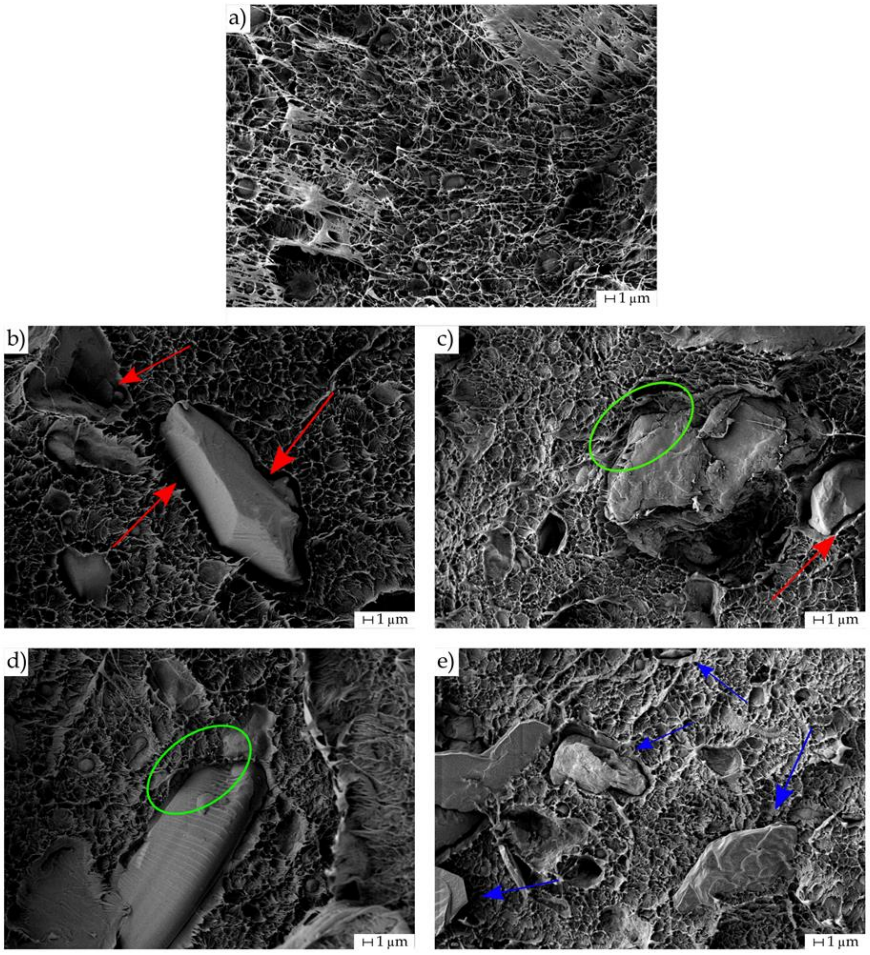

Figure IV.1.2.6. FESEM images of the fracture surfaces of a) Bio-HDPE, b) Bio-HDPE/PPF, c) Bio-HDPE/PPF-SI, d) Bio-HDPE/PPF-MA, and e) Bio-HDPE/PPF-PC. Images were taken at 2500x, with a marker scale of 1 µm.

Thermal properties of Bio-HDPE/PPF composites

Figure IV.1.2.7 displays the calorimetric curves obtained from the DSC (dynamic) runs. **Figure IV.1.2.7**a,b corresponds to the cooling step and the second heating step, respectively. These were used to calculate the crystallization peak temperature (T_c), the melting peak temperature (T_m) and the melting enthalpy (ΔH_m). As can be seen, the addition of PPF in the Bio-HDPE matrix hardly affects its crystallization and its characteristic melting peak temperature, obtaining in all reinforced samples very similar temperatures, around 116 and 130 °C, respectively, in accordance with the typical crystallization and melting of HDPE [48].

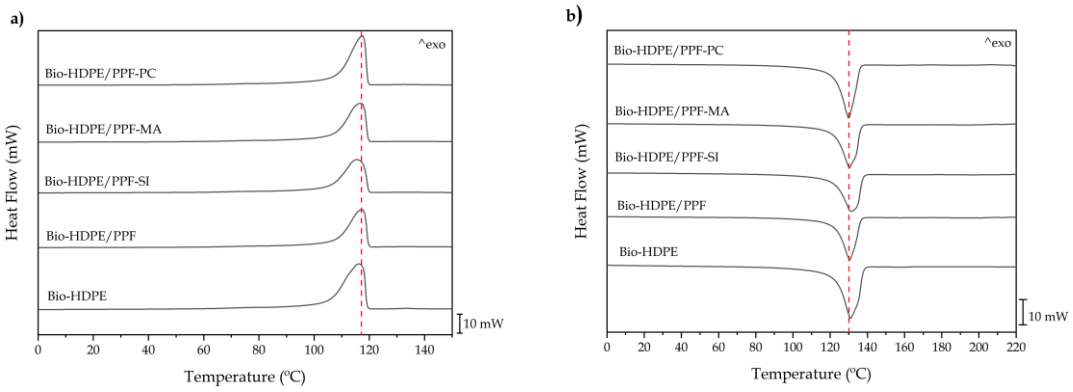

Figure IV.1.2.7. DSC curves of Bio-HDPE, and Bio-HDPE/PPF composites: a) cooling step, b) 2nd heating step.

Concerning crystallinity (**Table IV.1.2.2**), it can be seen how the addition of PPF in the Bio-HDPE matrix causes a decrease in the degree of crystallinity down to 66%, remaining practically constant in Bio-HDPE/PPF composites with silane-treated PPF and in the composites compatibilized with PE-*g*-MA (X_c ~ 66%). However, it can be observed that the addition of hydrophobized PFF with palmitoyl chloride leads to an increase in crystallinity up to 74%. This increase is due to the fact that the smaller particle size and a better dispersion can exert a nucleating effect that contributes to increase the degree of crystallinity of the Bio-HDPE matrix [49].

Table IV.1.2.2. Summary of thermal parameters obtained by DSC curves of neat Bio-HDPE and Bio-HDPE/PPF composites.

Code	T_c [°C]	T_m [°C]	ΔH_m [J g^{-1}]	X_c [%]
Bio-HDPE	116.2 ± 2.3	130.9 ± 2.4	206.8 ± 3.8	70.6 ± 1.3
Bio-HDPE/PPF	117.2 ± 2.1	130.9 ± 2.0	156.2 ± 2.7	66.6 ± 1.5
Bio-HDPE/PPF-SI	115.6 ± 2.1	131.3 ± 2.0	155.2 ± 2.3	66.2 ± 1.3
Bio-HDPE/PPF-MA	116.7 ± 2.5	130.4 ± 2.7	154.7 ± 3.3	66.0 ± 1.3
Bio-HDPE/PPF-PC	117.3 ± 2.5	129.9 ± 2.7	174.5 ± 3.7	74.4 ± 1.5

The stabilization effect of PPF biofiller on Bio-HDPE/PPF composites was assessed by isothermal DSC. **Figure IV.1.2.8** shows the DSC curves corresponding to the isothermal DSC runs at 210 °C of different Bio-HDPE/PPF composites to determine the oxidation stability over time. Bearing in mind that all the composites have undergone melting process of Bio-HDPE matrix, it can be observed that the time at which the oxidation process occurs differs for the different samples. The oxidation induction time (OIT) was determined under isothermal conditions in air atmosphere at 210 °C. At this temperature, Bio-HDPE can undergo oxidation due to processing temperatures, UV light, oxidant atmosphere, and so on [50]. The OIT can be identified by the onset of an exothermic peak, related to thermo-oxidation. As expected, degradation of unfilled Bio-HDPE occurs shortly after reaching 210 °C (OIT 4.8 min). The effect of the addition of PPF into the Bio-HDPE matrix is remarkable and positive in terms of thermal stabilization. This is directly related to the large amount of phenolic compounds (caffeic, *p*-coumaric, ferulic and gallic acids) as well as other antioxidant compounds such as proan-thocyanidins, which reduce the oxidative effect by free radical scavenging [51, 52]. The total number of hydroxyl groups could significantly affect their antioxidant activity due to their reactivity [53]. Such compounds, in the case of untreated PPF, are readily available to provide antioxidant properties to the Bio-HDPE matrix as they are in direct contact with it, causing the OIT to be delayed by ~43 min, thus achieving a noticeable stabilization effect compared to neat Bio-HDPE. However, it is worthy to high-light two different behaviours: composites containing hydrophobized PPF particles with palmitoyl chloride (Bio-HDPE/PPF-PC) and composites with silanized PPF particles with GLYMO (Bio-HDPE/PPF-SI). In the first case, it can be observed that the PPF-reinforced sample treated with palmitoyl chloride shows a premature degradation, with

an OIT of 5.7 min, only 1 min above that of neat Bio-HDPE. This is due to the fact that the thin hydrophobic layer that covers the PPF particles prevents the transfer of the antioxidant compounds from PPF to the Bio-HDPE matrix, leading to poor stabilization properties. On the other hand, composites with silanized GLYMO+PPF particles show a great improvement in OIT, bringing the degradation of the Bio-HDPE/PPF-SI composite to 82.5 min. This may be due to the strong interaction generated between the functional organic silane with the polyethylene chains and the antioxidants (phenols) of the PPF [54], producing a higher retention of these antioxidants in the HDPE matrix and, as a consequence, an improvement in OIT, as proposed by Albarino and Schonhorn [55, 56]. These results are consistent with those obtained by Quiles-Carrillo *et al.* [57], who achieved delays in OIT of 56 and 240 min in an HDPE matrix by adding natural antioxidants, namely 0.3 and 0.8 phr of gallic acid. They showed even better results than those obtained by Kabir *et al.* [58] when using a commercial antioxidant such as Irganox 1010, which delayed the OIT of LDPE from 2 to 35.9 min. These results demonstrate the high value of persimmon wastes (peels) as a source of antioxidant compounds of natural origin, which can be used in food sectors, as well as being a viable alternative to replace synthetic antioxidants used to reduce the oxidation induction time of PE and other polyolefins [59, 60].

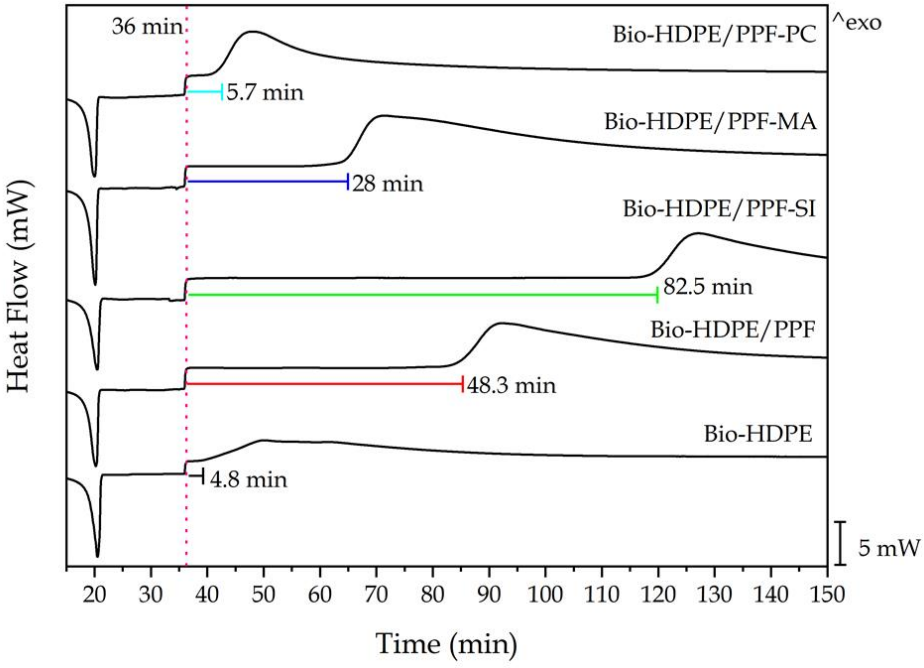

Figure IV.1.2.8. DSC isothermal curves at 210 °C of Bio-HDPE and Bio-HDPE/PPF composites.

In addition, the thermal stability at high temperatures was also studied. **Figure IV.1.2.9** gathers the thermograms obtained by TGA analysis. The main thermal degradation parameters obtained from TGA are shown in **Table IV.1.2.3**. As can be seen, neat Bio-HDPE undergoes thermal degradation in a single-step process, with a degradation onset temperature (T_{onset}) of 345.3 °C, and a maximum degradation rate temperature of 450.8 °C, which generally corresponds to the degradation of carbon atoms, according to the literature [20]. The thermal degradation of persimmon peel flour is in accordance with the typical degradation profile of a lignocellulosic filler, characterized by three main steps. The first step takes place at 110 °C with a mass loss of ~2.5–3% corresponding to the removal of residual moisture. The next stage involves a mass loss of about 60%, which generally corresponds to the depolymerization of hemicellulose and cellulose, and the degradation of pectin, in the range of 220–380 °C. The third stage corresponds to the degradation of residual lignin up to 600 °C [49]. However, it can be observed that the residual mass of the composites is relatively low and similar because both the Bio-HDPE matrix and the natural filler degrade completely at 700 °C.

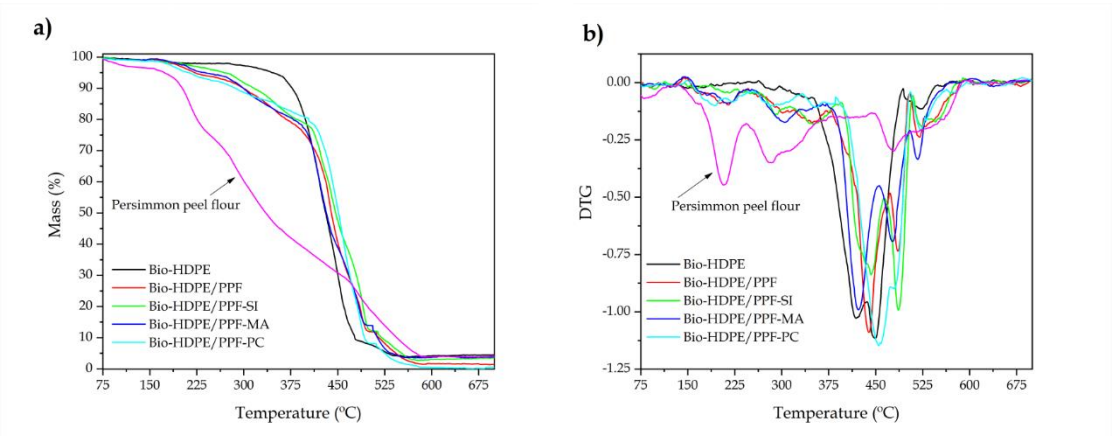

Figure IV.1.2.9. Comparative plots of a) thermogravimetric (TGA) curves and b) DGT curves of Bio-HDPE, Bio-HDPE/PPF composites, and persimmon peel flour.

As shown in **Figure IV.1.2.9**a, the addition of PPF in Bio-HDPE results in a remarkable reduction of the T_{onset} of Bio-HDPE/PPF composites, lowering the temperature largely from 345.3 °C (Bio-HDPE) to 221.3 °C (Bio-HDPE/PPF), this effect can be attributed to the poor stability of lignocellulosic fillers at low temperatures where premature degradation of organic compounds (hemicellulose) occurs [26], as shown in **Figure IV.1.2.9**b. Nevertheless, Bio-HDPE-PPF composites with some coupling agent

show a slight improvement in T_{onset}, the most noticeable being the sample containing silane-treated PPF with a temperature of 268.3 °C (47 °C higher than untreated PPF), approximately. These results are in agreement with those obtained by DSC. In addition, the maximum degradation rate temperature was delayed for all cases in Bio-HDPE/PPF composites compared to neat Bio-HDPE. This may be attributed to the presence of antioxidants from the polyphenolic compounds in PPF, suggesting that the greatest contribution of antioxidant compounds occurs at high temperatures. The delay is up to ~36 °C in the case of the silane-pretreated PPF (PPF-SI), where it is more noticeable due to the better retention of the antioxidant properties as a result of the enhanced interaction between the PPF particles and the HDPE matrix [55]. Although the use of PE-*g*-MA provides good interaction between the matrix and the filler, this is the composite with the lowest T_{deg}, about 10 °C lower than PPF-SI. As suggested by Araújo *et al.* [61], the enhanced interaction obtained by the reaction of the maleic anhydride groups of PE-*g*-MA with the (-OH) groups of PPF also enhances the interaction during the degradation process; as a result, when the HDPE degrades, it accelerates the degradation of PPF and, consequently, the resulting composite is also more sensitive to thermal degradation.

Table IV.1.2.3. Summary of thermal parameters obtained by TGA of the Bio-HDPE sample and Bio-HDPE/PPF composites.

Code	T_{onset} [°C]	T_{deg_1} [°C]	T_{deg_2} [°C]	Residual mass [%]
Bio-HDPE	345.3 ± 6.9	450.8 ± 9.0	-	4.5 ± 0.01
Bio-HDPE/PPF	221.3 ± 4.4	439.4 ± 8.8	485.4 ± 9.7	1.4 ± 0.01
Bio-HDPE/PPF-SI	268.3 ± 4.8	442.4 ± 8.9	486.4 ± 9.7	3.5 ± 0.02
Bio-HDPE/PPF-MA	237.3 ± 4.3	422.4 ± 9.3	476.3 ± 10.5	3.8 ± 0.02
Bio-HDPE/PPF-PC	212.8 ± 4.7	454.9 ± 6.8	479.4 ± 7.2	0.5 ± 0.01

Dynamic-mechanical characterization of Bio-HDPE/PPF composites

The dynamic-mechanical thermal analysis (DMTA) curves of neat Bio-HDPE and Bio-HDPE/PPF composites are shown in **Figure IV.1.2.10**. **Figure IV.1.2.10**a illustrates the effect of the addition of PPF in the Bio-HDPE matrix on the evolution of the storage modulus (E′) in the temperature range from -150 to 125 °C. In general, the storage modulus shows a marked tendency to decrease with increasing temperature. At low temperatures (-125 °C) the behavior of Bio-HDPE/PPF composites with three

compatibilization strategies is very similar to that of neat Bio-HDPE, exhibiting approximately E′ values close to 2275 MPa (**Table IV.1.2.4**). This phenomenon can be attributed to a rather good polymer-particle interaction, which causes these particles to show a pseudo-lubricating effect that makes them slide more easily between the HDPE chains, resulting in more homogeneous composites [47]. It can also be observed that Bio-HDPE/PPF (untreated PPF) composites show a higher E′ value (2592 MPa) compared to neat Bio-HDPE; this is related to the absence of compatibility between both components, as previously described in the FESEM characterization. The addition of untreated PPF causes a restriction of the mobility of the polyethylene chains due to the interference they have with the matrix, and as a consequence a higher stiffness is obtained [62]. As the temperature increases, a large decrease in E′ values are observed. This transition at about -100 °C is related to the glass to rubber transition region. This is mainly due to the softening of the HDPE matrix caused by the contribution of thermal energy to the chains, which favors their mobility [63]. At -50 °C the Bio-HDPE/PPF composites show higher storage modulus values than neat Bio-HDPE with values close to 1438 MPa. As suggested by Sewda and Maiti [47], PE and biofiller expand and contract in a different way due to their nature, resulting in an increase in the mobility restriction of the HDPE chains. By increasing the temperature above 50 °C, the storage modulus decreases markedly for all composites down to values of 500 MPa, which is related to the α-transition of low branched polyethylenes.

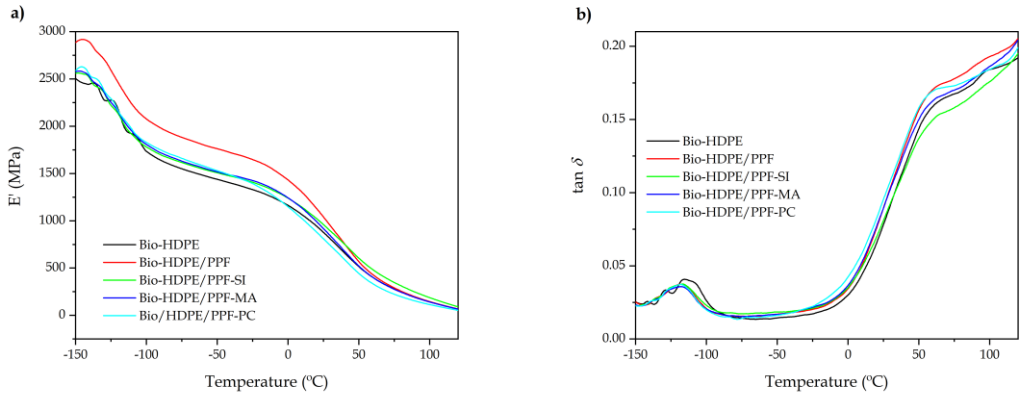

Figure IV.1.2.10. Comparative plots of the evolution of a) Storage modulus and b) damping factor (tan δ) as a function of the temperature of the Bio-HDPE sample, and Bio-HDPE/PPF composites.

Figure IV.1.2.10b depicts the curves corresponding to the dynamic damping factor (tan δ) over a temperature range from -150 to 125 °C of neat Bio-HDPE and Bio-

HDPE/PPF composites. High-density polyethylene typically exhibits two types of relaxations that are observed with temperature variation. The γ-relaxation that usually appears in the temperature range between -140 and -100 °C, which is related to the motion of a small part of the chains in the amorphous region of the polymer, and is associated with the glass transition temperature (T_g) and the second relaxation, called α-relaxation, which occurs at temperatures between 0 and 120 °C, with a peak at 40–50 °C, and is associated with the motion of the chains folds on the surface of the lamellae in the crystalline regions [47, 63]. It can be observed that Bio-HDPE presents a glass transition temperature (identified by the peak of the γ-transition) with a value of -115 °C and the α-transition at a temperature of ~50 °C, which are consistent with the results reported by Jorda-Reolid *et al.* [64]. The addition of PPF leads to a small decrease in the glass transition temperature by about 3 °C, due to the increased interaction between the PPF particles and the matrix, as above-mentioned. A decrease in the intensity of the γ-relaxation peak can be observed due to the increased internal friction caused by the PPF, which restricts the movement of the polyethylene chains [13].

Table IV.1.2.4. Dynamic-mechanical thermal properties (DMTA) of neat Bio-HDPE and Bio-HDPE/PPF composites in terms of storage modulus (E′) at different temperatures, and glass transition temperature (T_g).

Code	E′ at -125 °C [MPa]	E′ at -50 °C [MPa]	E′ at 50 °C [MPa]	T_g [°C]
Bio-HDPE	2275 ± 45	1439 ± 29	515 ± 10	-115.3 ±2.3
Bio-HDPE/PPF	2592 ± 52	1763 ± 35	570 ± 11	-118.1 ± 2.1
Bio-HDPE/PPF-SI	2221 ± 33	1509 ± 23	606 ± 12	-116.2 ± 2.1
Bio-HDPE/PPF-MA	2256 ± 34	1518 ± 23	522 ± 10	-118.1 ± 2.1
Bio-HDPE/PPF-PC	2295 ± 50	1530 ± 34	444 ± 10	-118.2 ± 2.0

Water uptake analysis

The water absorption of Bio-HDPE/PPF composites as a function of immersion time is shown in **Figure IV.1.2.11**. As can be seen, the water absorption of unfilled Bio-HDPE is practically negligible during the test period, due to its non-polar character and high hydrophobicity [65]. The addition of PPF has a clear impact on water absorption capacity, showing an increasing trend over time in all composites. This may be due to

several factors, one of which is the existence of small voids and pores in the structure due to the lack of interaction between the matrix and the filler. The existence of these voids in the internal structure of the composite materials enables water to enter, thus increasing their water absorption [66].

Another factor is the hydrophilic nature of the biofillers, due to the large number of hydroxyl groups present in PPF, belonging to phenols, proanthocyanidins, condensed tannins and fiber content (cellulose, hemicellulose, and lignin), which promote water absorption by hydrogen bonding [7, 67, 68]. This effect is evident after the first week of immersion, especially in composites containing untreated PPF. This may be related to the fact that the access to the available hydroxyl groups (-OH) is greater, thus enhancing the interaction with water. In spite of this, maximum water absorption values do not exceed 0.7% during the 9 weeks. It can be seen that composites compatibilized with PE-*g*-MA and composites with silanized PPF show a similar behavior, obtaining a remarkable decrease in water absorption, with asymptotic values of 0.45%. This is mainly due to the decrease in available hydroxyl groups (-OH), which hinders their interaction with water, causing the percentage of water saturation to decrease with respect to composites with untreated PPF. Bio-HDPE/PPF composites compatibilized with PE-*g*-MA show lower water uptake due to a higher polymer-particle interaction because of the possible reaction of maleic anhydride with some -OH groups of PPF [18].

On the other hand, during the silanization of PPF with GLYMO, the hydroxyl groups generated after the hydrolysis of the alkoxysilane can also react with some hydroxyl groups present in PPF [24]. Finally, it can be observed that composites with hydrophobized PPF with palmitoyl chloride show the lowest water absorption after 9 weeks of immersion (0.3%). This can be attributed to the esterification reaction between the hydroxyl groups present in the PPF with palmitic acid, which gives the material a hydrophobic nature, as previously described by dynamic water contact angle [30, 69]. The hydrophobic nature of the high-density polyethylene matrix remains virtually invariable during long exposure to water.

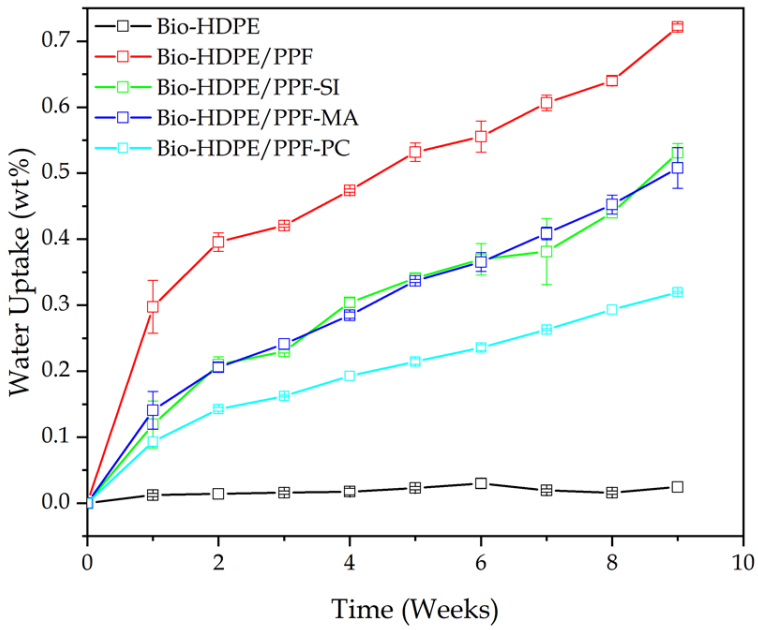

Figure IV.1.2.11. Evolution of the water uptake as a function of the immersion time of neat Bio-HDPE and Bio-HDPE/PPF composites.

Colorimetry properties

Figure IV.1.2.12 shows the visual appearance of neat Bio-HDPE and Bio-HDPE/PPF composites. It can be appreciated that the addition of PPF has a clear effect on the color change of the Bio-HDPE/PPF samples, shifting from a white tone characteristic of HDPE to a darker tone, due to the natural orange-red color of the persimmon peel flour provided by the amount of total carotenoids (*β*-cryptoxanthi, zeaxanthin, among others) and lycopene content [70, 71].

The CIELab color coordinates as well as the ΔE_{ab}* of the Bio-HDPE and Bio-HDPE/PPF composites are listed in **Table IV.1.2.5**. As previously mentioned, the color change caused by the incorporation of PPF is noticeable, resulting in a significant decrease in lightness (L* coordinate), as well as positive values for the a* and b* coordinates in all Bio-HDPE/PPF composites, compared to unfilled Bio-HDPE. It can also be observed that the different surface treatments on PPF have a slight effect on the final color of the samples. In fact, Bio-HDPE/PPF-SI composite shows a lighter brown color than the other composites, tending more to a yellowish (b*) and reddish (a*) appearance. This is probably due to the large number of antioxidant compounds in persimmon peel, which prevents the formation of quinones by interaction with oxygen, thus preventing the blackening of the compounds [72]. Interestingly, the treatment with

palmitoyl chloride in PPF causes a slight darkening of the samples, since the hydrophobic layer around the particles slightly inhibits the antioxidant action, thus resulting in darker particles. Subsequently, the corresponding composites offer a surface appearance similar to dark woods such as oak wood [73].

This feature can be particularly attractive for some industrial sectors such as furniture, as the hydrophobic layer created around the particles can serve as a protective film, reducing the interaction with external agents such as oxygen, UV light and water, thus reducing surface deterioration over long exposure periods. As Nzokou *et al.* [74], suggests that the surface finish (varnish) of woods can cause both color and roughness to remain for more than 1000 and 450 h unchanged.

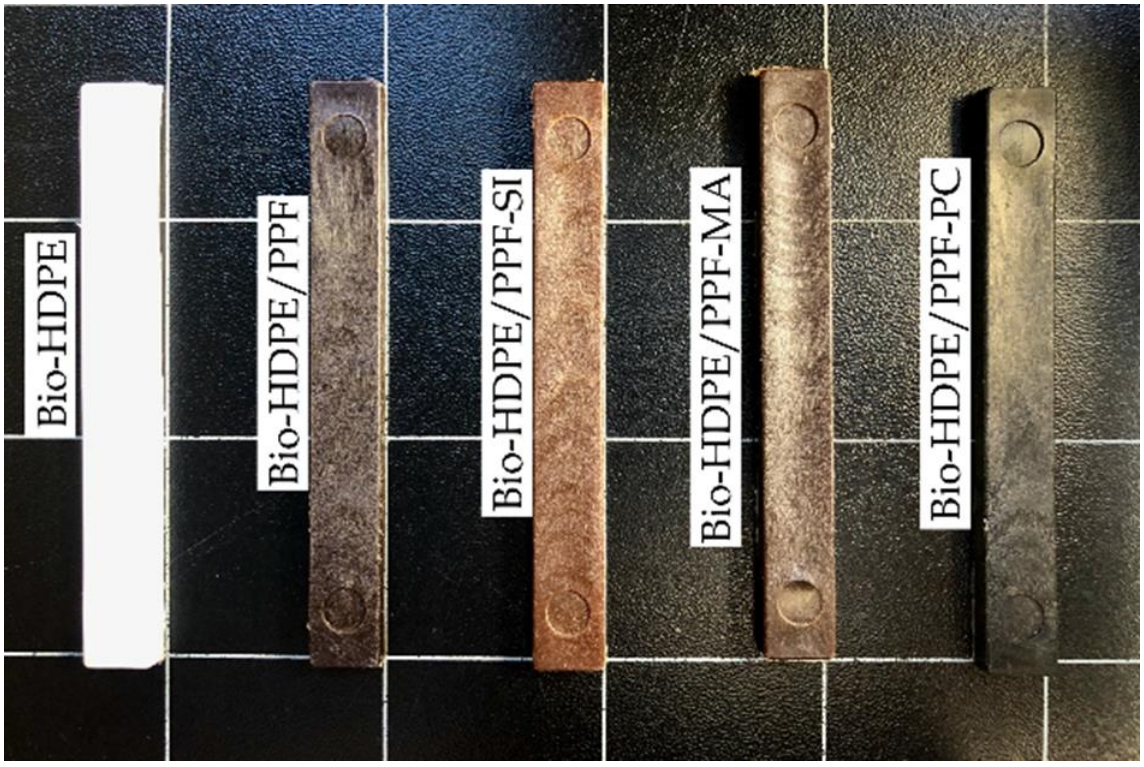

Figure IV.1.2.12. Visual appearance of the Bio-HDPE sample and the Bio-HDPE/PPF composites.

Table IV.1.2.5. Summary of the CIELAB color coordinates of the Bio-HDPE sample and the Bio-HDPE/PPF composites.

Code	L*	a*	b*	ΔE_{ab}*
Bio-HDPE	72.1 ± 1.1	-2.3 ± 0.0	-4.5 ± 0.1	-
Bio-HDPE/PPF	33.8 ± 0.6	2.1 ± 0.2	3.1 ± 0.3	39.3 ± 0.7
Bio-HDPE/PPF-SI	36.2 ± 1.1	4.3 ± 0.1	5.5 ± 0.2	37.9 ± 1.0
Bio-HDPE/PPF-MA	33.5 ± 0.7	1.6 ± 0.2	2.2 ± 0.3	39.4 ± 0.8
Bio-HDPE/PF-PC	32.1 ± 1.2	0.7 ± 0.1	1.2 ± 0.2	40.5 ± 1.2

Antioxidant capacity of Bio-HDPE/PPF composites

The antioxidant activity of persimmon peel is known to be provided by phenolic compounds, including gallic acid, ferulic acid, caffeic acid and *p*-coumaric acid, as well as carotenoids (*β*-carotene, and lycopene), and proanthocyanidins (condensed tannins) [7, 68, 75]. However, the amount of these compounds may vary due to factors such as fruit variety, climate, cultivation, harvesting and storage processes [70, 76, 77]. The study of antioxidant activity was based on the reduction of DPPH by electron transfer, which was measured by UV-Vis spectroscopy, where an increase in antioxidant activity was observed by a color change from violet to yellow [78]. **Figure IV.1.2.13** shows the DPPH radical scavenging activity of Bio-HDPE samples and Bio-HDPE/PPF composites with respect to time (1 week). As suggested by Rojas-Lema *et al.* [79] in high-density polyethylene composites, the DPPH• radical can be stabilized by the phenolic groups contained in the natural compounds to its non-radical form DPPH-H. It can be noticed that after only one day (24 h) the absorbance of the composites with MA and with silanized and hydrophobized PPF practically stabilizes, obtaining values of 89, 83 and 92%, respectively. Inferring that the hydroxyl groups available in PPF almost completely reduce DPPH radicals. Although the PPF content remains constant for all Bio-HDPE derived composites, the antioxidant activity is slightly affected by the compatibilizing strategy. This effect is particularly noticeable in the composites with PPF treated with silanes, where a retarding effect on the release of the antioxidant compounds is observed, stabilizing at 72 h with values close to 76%. This could be related to the fact that hydrolyzed silanols may rearrange the geometry of the available hydroxyl groups,

leading to electron delocalization, which can affect the antioxidant activity (slowing and/or decreasing it) [80].

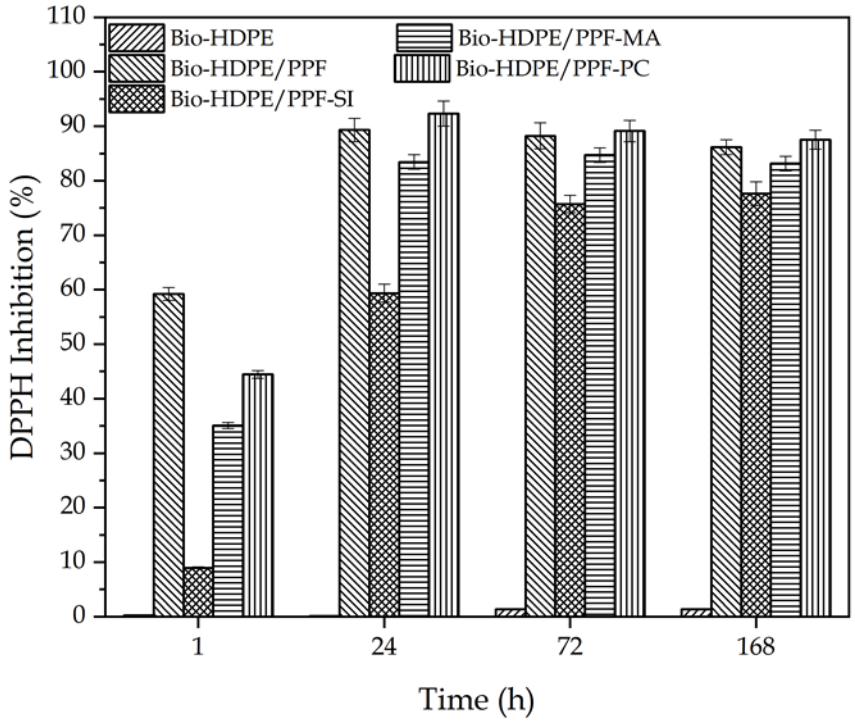

Figure IV.1.2.13. Percentage of 2,2-diphenyl-1-picrylhydrazyl radical (DPPH) inhibition of neat Bio-HDPE and Bio-HDPE/PPF composites.

CONCLUSIONS

Persimmon peel flour (PPF) waste is an interesting biofiller for Bio-HDPE-based composites, that can be processed by injection molding. The effect of different compatibilization strategies to enhance the interaction between the highly hydrophobic particles and the highly hydrophobic Bio-HDPE matrix has been assessed. Overall, it was found that the addition of PPF in the Bio-HDPE matrix resulted in a reduction of both tensile strength and elongation at break due to stress concentration phenomena. These effects were clearly diminished by using different compatibilization strategies: the use of a conventional PE-*g*-MA copolymer during compounding, and a second strategy focused on a selective surface treatment of PPF.

The efficiency of two different surface treatments on PPF were studied: one silanization process with GLYMO, and a hydrophobizing treatment with palmitoyl chloride. All three strategies contribute to reduce the gap between the PPF particles and the surrounding Bio-HDPE matrix, thus leading to more cohesion. A marked improvement

in absorbed energy after impact was observed in PPF-composites hydrophobized with palmitoyl chloride, leading to an increase in the elongation at break, due to both improved particle dispersion in the matrix and improved particle compatibility with each other. The water absorption capacity was significantly reduced compared to composites with untreated PPF particles. These results are of great value considering that one of the weaknesses of composites of natural origin is their high sensitivity to water absorption, which causes changes in their dimensions when exposed to humid environments. The benefits of using persimmon fruit wastes as a source of natural antioxidants were clearly evidenced, obtaining a high inhibition of DPPH radicals, as well as delaying the oxidation induction time of the Bio-HDPE matrix. Therefore, the use of persimmon peel waste is an interesting approach to new wood-like composite materials with improved thermal stability. On the other hand, the hydrophobic surface treatment of PPF has demonstrated a clear advantage, as water uptake is significantly reduced.

ACKNOWLEDGEMENTS

The authors want to thank the Spanish Ministry of Science and Innovation, grant number MEN PID2020-116496RB-C22 for funding this research. D.L. wants to thank UPV for the grant received though the PAID-01-18 program. S. Rojas-Lema. is a recipient of a Santiago Grisolia grant from Generalitat Valenciana (GVA) (GRISOLIAP/2019/132). J. Gomez-Caturla. wants to thank Universitat Politècnica de València for his FPI grant from (SP20200080). J. Ivorra-Martinez thanks the Spanish Ministry of Science, Innovation and Universities for his FPU grant (FPU19/01759). Microscopy services at UPV are acknowledged for their help in collecting and analyzing FESEM images.

REFERENCES

[1] M.C. López-Marcos, C. Bailina, M. Viuda-Martos, J.A. Pérez-Alvarez, and J. Fernández-López. *Properties of dietary fibers from agroindustrial coproducts as source for fiber-enriched foods.* Food and Bioprocess Technology, 2015, 8(12), p. 2400-2408.

[2] R.H. Liu. *Health benefits of fruit and vegetables are from additive and synergistic combinations of phytochemicals.* The American Journal of Clinical Nutrition, 2003, 78(3), p. 517S-520S.

[3] D.W. Wilson, P. Nash, H.S. Buttar, K. Griffiths, R. Singh, F. De Meester, R. Horiuchi, and T. Takahashi. *The role of food antioxidants, benefits of functional foods, and influence of feeding habits on the health of the older person: An overview.* Antioxidants, 2017, 6(4), p. 81.

[4] J. Boyer and R.H. Liu. *Apple phytochemicals and their health benefits.* Nutrition Journal, 2004, 3(1), p. 1-15.

[5] F.a.A.O.C.S. (FAOSTAT). *Production share of Persimmons by region*. 2021 [Cited 23/04/2021]; Available from: http://www.fao.org/faostat/en/#data/QC/visualize.

[6] R. Lucas-González, M. Viuda-Martos, J.A.P. Álvarez, and J. Fernández-López. *Changes in bioaccessibility, polyphenol profile and antioxidant potential of flours obtained from persimmon fruit (Diospyros kaki) co-products during in vitro gastrointestinal digestion.* Food Chemistry, 2018, 256, p. 252-258.

[7] J.R.V. Matheus, C.J.d. Andrade, R.F. Miyahira, and A.E.C. Fai. *Persimmon (Diospyros Kaki L.): Chemical properties, bioactive compounds and potential use in the development of new products–A review.* Food Reviews International, 2020, 38(4), p. 384-401.

[8] S. Gea-Botella, L. Agulló, N. Martí, M. Martínez-Madrid, V. Lizama, F. Martín-Bermudo, G. Berná, D. Saura, and M. Valero. *Carotenoids from persimmon juice processing.* Food Research International, 2021, 141, p. 109882.

[9] A. Sharma, A.K. Dhiman, S. Attri, and P. Ramachandran. *Studies on preparation and preservation of persimmon (Diospyros kaki L.) pulp.* Journal of Food Processing and Preservation, 2021, p. e15274.

[10] S. Karaman, Ö.S. Toker, F. Yüksel, M. Çam, A. Kayacier, and M. Dogan. *Physicochemical, bioactive, and sensory properties of persimmon-based ice cream: Technique for order preference by similarity to ideal solution to determine optimum concentration.* Journal of Dairy Science, 2014, 97(1), p. 97-110.

[11] S.W. Kariuki, J. Wachira, M. Kawira, and G.M. Leonard. *Characterization of prototype formulated particleboards from agroindustrial lignocellulose biomass bonded with chemically modified cassava peel starch.* Advances in Materials Science and Engineering, 2019, 2019, p. 1-19.

[12] L. Quiles-Carrillo, R. Balart, T. Boronat, S. Torres-Giner, D. Puglia, F. Dominici, and L. Torre. *Development of Compatibilized Polyamide 1010/Coconut Fibers Composites by Reactive Extrusion with Modified Linseed Oil and Multi-functional Petroleum Derived Compatibilizers.* Fibers and Polymers, 2021, 22, p. 728-744.

[13] F. Burgada, E. Fages, L. Quiles-Carrillo, D. Lascano, J. Ivorra-Martinez, M.P. Arrieta, and O. Fenollar. *Upgrading Recycled Polypropylene from Textile Wastes in Wood Plastic Composites with Short Hemp Fiber.* Polymers, 2021, 13(8), p. 1248.

[14] PlasticsEurope. *Plastics- the Facts 2020: An analysis of European plastics production, demand and waste data*. 2020, PlasticsEurope: Belgium, Europe, p. 1-64.

[15] R.P. Babu, K. O'connor, and R. Seeram. *Current progress on bio-based polymers and their future trends.* Progress in Biomaterials, 2013, 2(1), p. 1-16.

[16] A. Morschbacker. *Bio-ethanol based ethylene.* Journal of Macromolecular Science®, Part C: Polymer Reviews, 2009, 49(2), p. 79-84.

[17] E.M. Fernandes, J.F. Mano, and R.L. Reis. *Polyethylene composites with lignocellulosic material*, in *Polyethylene-Based Blends, Composites and Nanocomposites*. 2015, John Wiley & Sons, Inc.: Hoboken, New Jersey, p. 117-162.

[18] H. Gao, Y. Xie, R. Ou, and Q. Wang. *Grafting effects of polypropylene/polyethylene blends with maleic anhydride on the properties of the resulting wood–plastic composites.* Composites Part A: Applied Science and Manufacturing, 2012, 43(1), p. 150-157.

[19] A.A. Ramachandran, L.P. Mathew, and S. Thomas. *Effect of MA-g-PP compatibilizer on morphology and electrical properties of MWCNT based blend nanocomposites: New strategy to enhance the dispersion of MWCNTs in immiscible poly (trimethylene terephthalate)/polypropylene blends.* European Polymer Journal, 2019, 118, p. 595-605.

[20] D. Garcia-Garcia, A. Carbonell-Verdu, A. Jordá-Vilaplana, R. Balart, and D. Garcia-Sanoguera. *Development and characterization of green composites from bio-based polyethylene and peanut shell.* Journal of Applied Polymer Science, 2016, 133(37), p. 43940.

[21] B. Ferrero, V. Fombuena, O. Fenollar, T. Boronat, and R. Balart. *Development of natural fiber-reinforced plastics (NFRP) based on biobased polyethylene and waste fibers from Posidonia oceanica seaweed.* Polymer Composites, 2015, 36(8), p. 1378-1385.

[22] S. Chen, M. Yang, Y. Han, H. Liu, and H. Zou. *Hydrophobically modified sustainable bio-based polyurethane for controllable release of coated urea.* European Polymer Journal, 2021, 142, p. 110114.

[23] H. Ismail, S. Shuhelmy, and M. Edyham. *The effects of a silane coupling agent on curing characteristics and mechanical properties of bamboo fibre filled natural rubber composites.* European Polymer Journal, 2002, 38(1), p. 39-47.

[24] Á. Agüero, D. Garcia-Sanoguera, D. Lascano, S. Rojas-Lema, J. Ivorra-Martinez, O. Fenollar, and S. Torres-Giner. *Evaluation of different compatibilization strategies to improve the performance of injection-molded green composite pieces made of polylactide reinforced with short flaxseed fibers.* Polymers, 2020, 12(4), p. 821.

[25] O. Bijaisoradat, L. Yue, I. Manas-Zloczower, and H. Manuspiya. *Wood flour-high density polyethylene composites: Influence of silanization and esterification on mechanical properties.* Journal of Applied Polymer Science, 2021, 138(15), p. 50197.

[26] F. Dominici, D. García García, V. Fombuena, F. Luzi, D. Puglia, L. Torre, and R. Balart. *Bio-polyethylene-based composites reinforced with alkali and palmitoyl chloride-treated coffee silverskin.* Molecules, 2019, 24(17), p. 3113.

[27] S. Gorinstein, Z. Zachwieja, M. Folta, H. Barton, J. Piotrowicz, M. Zemser, M. Weisz, S. Trakhtenberg, and O. Màrtín-Belloso. *Comparative contents of dietary fiber, total phenolics, and minerals in persimmons and apples.* Journal of Agricultural and Food Chemistry, 2001, 49(2), p. 952-957.

[28] L. Quiles-Carrillo, T. Boronat, N. Montanes, R. Balart, and S. Torres-Giner. *Injection-molded parts of fully bio-based polyamide 1010 strengthened with waste derived slate fibers pretreated with glycidyl-and amino-silane coupling agents.* Polymer Testing, 2019, 77, p. 105875.

[29] E. Rojo, M.V. Alonso, B. Del Saz-Orozco, M. Oliet, and F. Rodriguez. *Optimization of the silane treatment of cellulosic fibers from eucalyptus wood using response surface methodology.* Journal of Applied Polymer Science, 2015, 132(26), p. 42157.

[30] D. García-García, A. Carbonell, M. Samper, D. García-Sanoguera, and R. Balart. *Green composites based on polypropylene matrix and hydrophobized spend coffee ground (SCG) powder.* Composites part B: Engineering, 2015, 78, p. 256-265.

[31] K.-H. Choi, K.S. Lee, J.H. Lee, and J.-Y. Ryu. *Hydrophobization of Cellulose Sheets by Gas Grafting of Palmitoyl Chloride by Using Hot Press.* Carbohydrate Polymers, 2020, 246, p. 116487.

[32] E.A. Vogler. *Structure and reactivity of water at biomaterial surfaces.* Advances in Colloid and Interface Science, 1998, 74(1-3), p. 69-117.

[33] R. Martínez-Las Heras, E. Landines, A. Heredia, M. Castelló, and A. Andrés. *Influence of drying process and particle size of persimmon fibre on its physicochemical, antioxidant, hydration and emulsifying properties.* Journal of Food Science and Technology, 2017, 54(9), p. 2902-2912.

[34] T. Lu, S. Liu, M. Jiang, X. Xu, Y. Wang, Z. Wang, J. Gou, D. Hui, and Z. Zhou. *Effects of modifications of bamboo cellulose fibers on the improved mechanical properties of cellulose reinforced poly (lactic acid) composites.* Composites Part B: Engineering, 2014, 62, p. 191-197.

[35] S. Qian and K. Sheng. *PLA toughened by bamboo cellulose nanowhiskers: Role of silane compatibilization on the PLA bionanocomposite properties.* Composites Science and Technology, 2017, 148, p. 59-69.

[36] J. Xu, J. Xu, Y. Cao, X. Ji, and Y. Yan. *Fabrication of non-flaking, superhydrophobic surfaces using a one-step solution-immersion process on copper foams.* Applied Surface Science, 2013, 286, p. 220-227.

[37] O. Daramola, A. Taiwo, I. Oladele, J. Olajide, S. Adeleke, B. Adewuyi, and E. Sadiku. *Mechanical properties of high density polyethylene matrix composites reinforced with chitosan particles.* Materials Today: Proceedings, 2021, 38, p. 682-687.

[38] H. Nitz, P. Reichert, H. Römling, and R. Mülhaupt. *Influence of compatibilizers on the surface hardness, water uptake and the mechanical properties of poly (propylene) wood flour composites prepared by reactive extrusion.* Macromolecular Materials and Engineering, 2000, 276(1), p. 51-58.

[39] A.C. Wibowo, S.M. Desai, A.K. Mohanty, L.T. Drzal, and M. Misra. *A solvent free graft copolymerization of maleic anhydride onto cellulose acetate butyrate bioplastic by reactive extrusion.* Macromolecular Materials and Engineering, 2006, 291(1), p. 90-95.

[40] I.C. Cabrera, S. Berlioz, A. Fahs, G. Louarn, and P. Carriere. *Chemical functionalization of nano fibrillated cellulose by glycidyl silane coupling agents: A grafted silane network characterization study.* International Journal of Biological Macromolecules, 2020, 165, p. 1773-1782.

[41] S. Sahi, H. Djidjelli, and A. Boukerrou. *Study of the properties and biodegradability of the native and plasticized corn flour-filled low density polyethylene composites for food packaging applications.* Materials Today: Proceedings, 2021, 36, p. 67-73.

[42] H. Salmah and A. Azieyanti. *Properties of recycled polyethylene/chitosan composites: The effect of polyethylene-graft-maleic anhydride.* Journal of Reinforced Plastics and Composites, 2011, 30(3), p. 195-202.

[43] H.-S. Kim, B.-H. Lee, S.-W. Choi, S. Kim, and H.-J. Kim. *The effect of types of maleic anhydride-grafted polypropylene (MAPP) on the interfacial adhesion properties of bio-flour-filled polypropylene composites.* Composites Part A: Applied Science and Manufacturing, 2007, 38(6), p. 1473-1482.

[44] Z. Qu and Q. Yu. *Synthesizing super-hydrophobic ground granulated blast furnace slag to enhance the transport property of lightweight aggregate concrete.* Construction and Building Materials, 2018, 191, p. 176-186.

[45] W. Liu, Z. Xie, X. Yang, Y. Wu, C. Jia, T. Bo, and L. Wang. *Surface modification mechanism of stearic acid to zirconia powders induced by ball milling for water-based injection molding.* Journal of the American Ceramic Society, 2011, 94(5), p. 1327-1330.

[46] Z. Cao, M. Daly, L.M. Geever, I. Major, C.L. Higginbotham, and D.M. Devine. *Synthesis and characterization of high density polyethylene/peat ash composites.* Composites Part B: Engineering, 2016, 94, p. 312-321.

[47] K. Sewda and S. Maiti. *Mechanical properties of HDPE/bark flour composites.* Journal of Applied Polymer Science, 2007, 105(5), p. 2598-2604.

[48] Q. Zhang, M.U. Khan, X. Lin, H. Cai, and H. Lei. *Temperature varied biochar as a reinforcing filler for high-density polyethylene composites.* Composites Part B: Engineering, 2019, 175, p. 107151.

[49] Á. Agüero, D. Lascano, D. Garcia-Sanoguera, O. Fenollar, and S. Torres-Giner. *Valorization of linen processing by-products for the development of injection-molded green composite pieces of polylactide with improved performance.* Sustainability, 2020, 12(2), p. 652.

[50] L. Quiles-Carrillo, N. Montanes, V. Fombuena, R. Balart, and S. Torres-Giner. *Enhancement of the processing window and performance of polyamide 1010/bio-based high-density polyethylene blends by melt mixing with natural additives.* Polymer International, 2020, 69(1), p. 61-71.

[51] I. Kriston, Á. Orbán-Mester, G. Nagy, P. Staniek, E. Földes, and B. Pukánszky. *Melt stabilisation of Phillips type polyethylene, Part II: Correlation between additive consumption and polymer properties.* Polymer Degradation and Stability, 2009, 94(9), p. 1448-1456.

[52] P.-M. Li, G.-R. Du, and F.-W. Ma. *Phenolics concentration and antioxidant capacity of different fruit tissues of astringent versus non-astringent persimmons.* Scientia Horticulturae, 2011, 129(4), p. 710-714.

[53] P.-G. Pietta. *Flavonoids as antioxidants.* Journal of Natural Products, 2000, 63(7), p. 1035-1042.

[54] Q. Pan, B. Wang, Z. Chen, and J. Zhao. *Reinforcement and antioxidation effects of antioxidant functionalized silica in styrene–butadiene rubber.* Materials & Design, 2013, 50, p. 558-565.

[55] R. Albarino and H. Schonhorn. *Retention of antioxidants in polyethylene by silane coupling agents.* Journal of Applied Polymer Science, 1973, 17(11), p. 3323-3335.

[56] R. Albarino and H. Schonhorn. *Retention of thermal antioxidants in polyethylene by silane coupling agents. II. Concentration and induction time studies.* Journal of Applied Polymer Science, 1974, 18(3), p. 635-649.

[57] L. Quiles-Carrillo, S. Montava-Jordà, T. Boronat, C. Sammon, R. Balart, and S. Torres-Giner. *On the Use of Gallic Acid as a Potential Natural Antioxidant and Ultraviolet Light Stabilizer in Cast-Extruded Bio-Based High-Density Polyethylene Films.* Polymers, 2020, 12(1), p. 31.

[58] A.S. Kabir, H. Li, H. Yuan, T. Kuboki, and C.C. Xu. *Effects of de-polymerized lignin content on thermo-oxidative and thermal stability of polyethylene.* Journal of Analytical and Applied Pyrolysis, 2019, 140, p. 413-422.

[59] A. Sanches-Silva, D. Costa, T.G. Albuquerque, G.G. Buonocore, F. Ramos, M.C. Castilho, A.V. Machado, and H.S. Costa. *Trends in the use of natural antioxidants in active food packaging: a review.* Food Additives & Contaminants: Part A, 2014, 31(3), p. 374-395.

[60] W. Yu, T. Reitberger, T. Hjertberg, J. Oderkerk, F. Costa, V. Englund, and U.W. Gedde. *Chlorine dioxide resistance of different phenolic antioxidants in polyethylene.* Polymer Degradation and Stability, 2015, 111, p. 1-6.

[61] J. Araújo, W. Waldman, and M. De Paoli. *Thermal properties of high density polyethylene composites with natural fibres: Coupling agent effect.* Polymer Degradation and Stability, 2008, 93(10), p. 1770-1775.

[62] N. Montanes, D. Garcia-Sanoguera, V. Segui, O. Fenollar, and T. Boronat. *Processing and characterization of environmentally friendly composites from biobased polyethylene and natural fillers from thyme herbs.* Journal of Polymers and the Environment, 2018, 26(3), p. 1218-1230.

[63] D. Castro, A. Ruvolo-Filho, and E. Frollini. *Materials prepared from biopolyethylene and curaua fibers: Composites from biomass.* Polymer Testing, 2012, 31(7), p. 880-888.

[64] M. Jorda-Reolid, J. Gomez-Caturla, J. Ivorra-Martinez, P.M. Stefani, S. Rojas-Lema, and L. Quiles-Carrillo. *Upgrading Argan Shell Wastes in Wood Plastic Composites with Biobased Polyethylene Matrix and Different Compatibilizers.* Polymers, 2021, 13(6), p. 922.

[65] S.K. Najafi, M. Tajvidi, and M. Chaharmahli. *Long-term water uptake behavior of lignocellulosic-high density polyethylene composites.* Journal of Applied Polymer Science, 2006, 102(4), p. 3907-3911.

[66] D. Lascano, D. Garcia-Garcia, S. Rojas-Lema, L. Quiles-Carrillo, R. Balart, and T. Boronat. *Manufacturing and characterization of green composites with partially biobased epoxy resin and flaxseed flour wastes.* Applied Sciences, 2020, 10(11), p. 3688.

[67] Y. Wen, C.-H. Tsou, C. Gao, J.-C. Chen, Z. Tang, Z. Chen, T. Yang, J. Du, Y. Yu, and M.-C. Suen. *Evaluating distillers grains as bio-fillers for high-density polyethylene.* Journal of Polymer Research, 2020, 27, p. 167.

[68] C. Conesa, N. Laguarda-Miró, P. Fito, and L. Seguí. *Evaluation of Persimmon (Diospyros kaki Thunb. cv. Rojo Brillante) industrial residue as a source for value added products.* Waste and Biomass Valorization, 2019, 11, p. 3749-3760.

[69] Y. Zhang, Y. Xue, H. Toghiani, J. Zhang, and C.U. Pittman. *Modification of wood flour surfaces by esterification with acid chlorides: Use in HDPE/wood flour composites.* Composite Interfaces, 2009, 16(7-9), p. 671-686.

[70] Y. Qi, X. Liu, Q. Zhang, H. Wu, D. Yan, Y. Liu, X. Zhu, X. Ren, and Y. Yang. *Carotenoid accumulation and gene expression in fruit skins of three differently colored persimmon cultivars during fruit growth and ripening.* Scientia Horticulturae, 2019, 248, p. 282-290.

[71] A. Salvador, L. Arnal, C. Besada, V. Larrea, A. Quiles, and I. Pérez-Munuera. *Physiological and structural changes during ripening and deastringency treatment of persimmon fruit cv.'Rojo Brillante'.* Postharvest Biology and Technology, 2007, 46(2), p. 181-188.

[72] G. Lukmandaru, T. Ashitani, and K. Takahashi. *Color and chemical characterization of partially black-streaked heart-wood in teak (Tectona grandis).* Journal of Forestry Research, 2009, 20(4), p. 377-380.

[73] H. Turgut Sahin, M. Burak Arslan, S. Korkut, and C. Sahin. *Colour changes of heat-treated woods of red-bud maple, European hophornbeam and oak.* Color Research & Application, 2011, 36(6), p. 462-466.

[74] P. Nzokou, D.P. Kamdem, and A. Temiz. *Effect of accelerated weathering on discoloration and roughness of finished ash wood surfaces in comparison with red oak and hard maple.* Progress in Organic Coatings, 2011, 71(4), p. 350-354.

[75] S. Yaqub, U. Farooq, A. Shafi, K. Akram, M.A. Murtaza, T. Kausar, and F. Siddique. *Chemistry and functionality of bioactive compounds present in persimmon.* Journal of Chemistry, 2016, 2016, p. 1-13.

[76] L. Arnal and M. Del Río. *Effect of cold storage and removal astringency on quality of persimmon fruit (Diospyros kaki, L.) cv. Rojo Brillante.* Food Science and Technology International, 2004, 10(3), p. 179-185.

[77] C. Besada, L. Arnal, and A. Salvador. *Improving storability of persimmon cv. Rojo Brillante by combined use of preharvest and postharvest treatments.* Postharvest Biology and Technology, 2008, 50(2-3), p. 169-175.

[78] J.-H. Choe, H.-Y. Kim, Y.-J. Kim, E.-J. Yeo, and C.-J. Kim. *Antioxidant activity and phenolic content of persimmon peel extracted with different levels of ethanol.* International Journal of Food Properties, 2014, 17(8), p. 1779-1790.

[79] S. Rojas-Lema, S. Torres-Giner, L. Quiles-Carrillo, J. Gomez-Caturla, D. Garcia-Garcia, and R. Balart. *On the Use of Phenolic Compounds Present in Citrus Fruits and Grapes as Natural Antioxidants for Thermo-Compressed Bio-Based High-Density Polyethylene Films.* Antioxidants, 2021, 10(1), p. 14.

[80] E. Choe and D.B. Min. *Chemistry and reactions of reactive oxygen species in foods.* Critical Reviews in Food Science and Nutrition, 2006, 46(1), p. 1-22.

Adaptado del artículo

IV.1.3. Improved performance of environmentally friendly blends of biobased polyethylene and kraft lignin compatibilized by reactive extrusion with dicumyl peroxide.

Sandra Rojas-Lema[1,2], Juan Ivorra-Martinez[1], Diego Lascano[1,2], Daniel Garcia-Garcia[1], and Rafael Balart[1]

[1]Technological Institute of Materials (ITM), Universitat Politècnica de València (UPV), Plaza Ferrándiz y Carbonell 1, 03801 Alcoy, Alicante, Spain.

[2]Escuela Politécnica Nacional, Quito 170517 Ecuador.

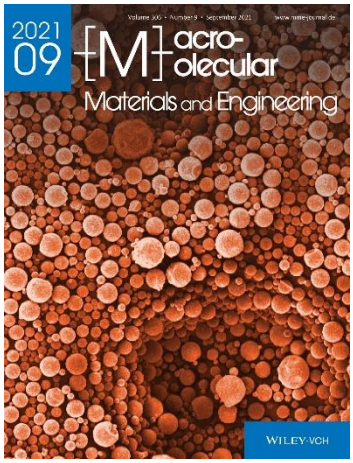

Macromolecular Materials and Engineering

2021, 306(9), p. 2100196.

RESEARCH ARTICLE

Macromolecular Materials and Engineering

www.mame-journal.de

Improved Performance of Environmentally Friendly Blends of Biobased Polyethylene and Kraft Lignin Compatibilized by Reactive Extrusion with Dicumyl Peroxide

Sandra Rojas-Lema, Juan Ivorra-Martinez, Diego Lascano, Daniel Garcia-Garcia, and Rafael Balart**

In this work, different contents (0.25, 0.50, 0.75, and 1 phr) of dicumyl peroxide (DCP) are incorporated into the bio-based high-density polyethylene (bioPE)/kraft lignin (KL) blends with a composition of 80 and 20 wt%, respectively with the aim of improving overall performance. The samples are obtained by reactive extrusion and injection-molding process, and then their overall performance is assessed by tensile tests, thermal analysis, optical and surface appearance, and wettability studies. The obtained mechanical properties confirm the successful interaction between bioPE and KL due to the addition of organic peroxide, which plays a key role in compatibilization. In particular, bioPE/KL blends with 1 phr of DCP achieve an increase in elongation at break of about 300% together with a noticeable increase in the impact strength of about 29% higher than the uncompatibilized bioPE/KL blend, while the tensile modulus decreases 42%. In addition, images obtained by field emission scanning electron microscopy show that the presence of DCP in the blends enhances better dispersion of KL into the bioPE matrix. The wettability analysis indicates that KL and DCP affect the hydrophobicity of the neat bioPE. Therefore, the resultant blends can be considered as potential sustainable polymers with balanced properties.

1. Introduction

Lignin is an aromatic copolymer considered the second most abundant component of wood after cellulose.[1] It is constituted by three phenyl-propanols, namely, guaiacyl-propanol, syringyl-propanol, and *p*-hydroxy-phenyl propanol repeating units.[2,3] Lignin contains a large variety of functional groups, such as hydroxyls groups, carboxyl groups, which can form efficient H-bounding interactions.[4] In addition, lignin is considered the main renewable source of aromatic structures.[5] Different kinds of lignins, called technical lignins, are obtained after the delignification process, such as kraft lignin (KL), soda lignin, and organosolv lignin. KL, which is obtained from the kraft pulping process in the paper industry, accounts for the highest percentage in the lignin industry with approximately 85%.[2,6] Nevertheless only 2% of the KL is currently upgraded into high-value added products. The remaining KL is normally used in energy production, especially in the alkali recovery process, which indicates that this biopolymer is not properly valorized.[7,8] This lack of use of KL provides a great opportunity to develop new studies and possible applications. Currently, there are some areas in which KL has shown some promising results such as biochemicals after chemical pyrolysis or degradation,[7] as a heavy metal adsorbent,[9] as hydrogels,[10,11] and as filler,[12] among others.

The use of lignin as a polymer reinforcement has proven to be a good alternative due to its positive effects on the thermal and mechanical properties, oxidation delay, and thermal stability of lignin-based blends.[13–15] Some of the advantages of using lignin as reinforcement are its availability, low cost, biodegradable properties, environmentally friendly nature, and, its relative homogeneous distribution when blended with other materials.[16] Lignin has been considered a good filler to be used in polymeric matrices.[17] In some cases, lignin has been used to replace inorganic fillers, due to lignin is not abrasive and has low density.[18] Some of these studies include polypropylene (PP),[19,20] and polyvinyl alcohol (PVA)[21] as polymer matrices. Despite there are some studies related to polyethylene (PE) and lignin blends, the rise of bio-based PE (bioPE) gives an interesting opportunity to give high environmentally friendly polymer blends. BioPE, also known as "green PE", comes from bioethanol obtained in the processing of food crops such as

S. Rojas-Lema, J. Ivorra-Martinez, D. Lascano, D. Garcia-Garcia, R. Balart
Technological Institute of Materials (ITM)
Universitat Politècnica de València (UPV)
Alcoy 03801, Spain
E-mail: sanrole@epsa.upv.es; rbalart@mcm.upv.es
S. Rojas-Lema, D. Lascano
Escuela Politécnica Nacional
Quito 170517 Ecuador

The ORCID identification number(s) for the author(s) of this article can be found under https://doi.org/10.1002/mame.202100196

DOI: 10.1002/mame.202100196

Improved performance of environmentally friendly blends of biobased polyethylene and kraft lignin compatibilized by reactive extrusion with dicumyl peroxide.

Abstract

In this work, different contents (0.25, 0.50, 0.75, and 1 phr) of dicumyl peroxide (DCP) are incorporated into the bio-based high-density polyethylene (bioPE)/kraft lignin (KL) blends with a composition of 80 and 20 wt%, respectively with the aim of improving overall performance. The samples are obtained by reactive extrusion and injection-molding process, and then their overall performance is assessed by tensile tests, thermal analysis, optical and surface appearance, and wettability studies. The obtained mechanical properties confirm the successful interaction between bioPE and KL due to the addition of organic peroxide, which plays a key role in compatibilization. In particular, bioPE/KL blends with 1 phr of DCP achieve an increase in elongation at break of about 300% together with a noticeable increase in the impact strength of about 29% higher than the uncompatibilized bioPE/KL blend, while the tensile modulus decreases 42%. In addition, images obtained by field emission scanning electron microscopy show that the presence of DCP in the blends enhance better dispersion of KL into the bioPE matrix. The wettability analysis indicates that KL and DCP affect the hydrophobicity of the neat bioPE. Therefore, the resultant blends can be considered as potential sustainable polymers with balanced properties.

Keywords: bio-polyethylene; blends; dicumyl peroxide; kraft lignin; reactive compatibilization.

INTRODUCTION

Lignin is an aromatic copolymer considered the second most abundant component of wood after cellulose [1]. It is constituted by three phenyl-propanols, namely, guaiacyl-propanol, syringyl-propanol, and p-hydroxy-phenyl propanol repeating units [2, 3]. Lignin contains a large variety of functional groups, such as hydroxyls groups, carboxyl groups, which can form efficient H-bounding interactions [4]. In addition, lignin is considered the main renewable source of aromatic structures [5]. Different kinds of lignins, called technical lignins, are obtained after the delignification process, such as kraft lignin (KL), soda lignin, and organosolv lignin. KL, which is obtained from the kraft pulping process in the paper industry, accounts for the highest percentage in the lignin industry with approximately 85% [2, 6]. Nevertheless only 2% of the KL is currently upgraded into high-value added products. The remaining KL is normally used in energy production, especially in the alkali recovery process, which indicates that this biopolymer is not properly valorized [7, 8]. This lack of use of KL provides a great opportunity to develop new studies and possible applications. Currently, there are some areas in which KL has shown some promising results such as biochemicals after chemical pyrolysis or degradation [7] as a heavy metal adsorbent [9], as hydrogels [10, 11], and as filler [12], among others.

The use of lignin as a polymer reinforcement has proven to be a good alternative due to its positive effects on the thermal and mechanical properties, oxidation delay and thermal stability of lignin-based blends [13-15]. Some of the advantages of using lignin as reinforcement are its availability, low cost, biodegradable properties, environmentally friendly nature, and, its relative homogeneous distribution when blended with other materials [16]. Lignin has been considered a good filler to be used in polymeric matrices [17]. In some cases, lignin has been used to replace inorganic fillers, due to lignin is not abrasive and has low density [18]. Some of these studies include polypropylene (PP) [19, 20], and polyvinyl alcohol (PVA) [21], as polymer matrices. Despite there are some studies related to polyethylene (PE) and lignin blends, the rise of bio-based PE (bioPE) gives an interesting opportunity to give high environmentally friendly polymer blends. BioPE, also known as "green PE", comes from bioethanol obtained in the processing of food crops such as sugarcane, maize, and wheat. BioPE is currently used due to its

simplest chemical structure, and its wide commercial applications, being, therefore, an interesting alternative to petroleum-based PE [22-25].

However, the incorporation of lignin in polymeric matrices cause some difficulties, due to their inherent differences in physical and chemical properties. One of the reasons is related to the polar nature of the phenolic and aliphatic -OH groups contained in the lignin structure, which causes incompatibility and low miscibility when blended with nonpolar synthetic polymers [14]. Therefore, some research works have focused on minimizing this drawback. For instance, some authors have focused their studies on a previous modification of lignin before it is blended with other nonpolar polymers [18, 26]. Besides, another possibility is the use of reactive extrusion (REX) with organic peroxides such as dicumyl peroxide (DCP) [27], benzoyl peroxide [28] or 2.5-dimethyl-2.5-di(tert-butylperoxy)hexane [29], among others, which provide free radical formation in both lignin and base polymer, thus allowing somewhat improved interaction. On the other hand, the use of copolymers with dual functionality (polar-nonpolar) such as maleic anhydride grafted LDPE and PP [30, 31], PE grafted with glycidyl methacrylate (PE-*g*-GMA) [32], represent a technical solution, but the overall properties are not remarkably improved. Reactive extrusion (REX) is a simple technique that allows reaction between polymers during the extrusion process. The reaction is related to formation of free radicals. For this reason, organic peroxides are of particular interest in REX.

DCP is widely used as a cross-linking agent, because peroxides activate the reaction between the polymer and functional chemical groups and form grafted and/or branched copolymers in the blend. According to Anbarasan *et al.* [33] DCP has shown higher efficiency in crosslinking HDPE, against other peroxides such as O,O-t-butyl O-2-ethylhexylperoxycarbonate, t-butyl peroxybenzoate, t-butyl 3,5,5-trimethylperoxyhexanoate, and t-butyl 2-ethylperoxyhexanoate. DCP must be used in low amounts so that it can contribute to the thermoplasticity of the material; otherwise, it could lead to gel formation and even more, to fully crosslinked structure [29, 34]. Compatibilization by REX with DCP has been successfully used to improve the compatibility in physical blends with low miscibility, as is the case of poly(3-hydroxybutyrate) and poly(ε-caprolactone) blends [35], ethylene-vinyl acetate copolymer (EVA-c) with virgin and recycled polyethylene (PE) blends [36], and, poly(lactide)/poly(butylene adipate-*co*-terephthalate) (PLA/PBAT) blends [37]. DCP

has also been successfully used to improve polymer-fiber interactions in high-density PE-sisal fiber composites, with a typical DCP loading of 1 phr, showing its efficiency during REX of fiber-reinforced composites [38]. In addition, REX has been developed using other compatibilizers, for instance, Mei *et al.* [4] reported that interfacial interactions between lignin and ethylene-propylene-diene monomer (EPDM) could be improved with the use of maleic anhydride grafted PE-octene elastomer (POE-MA) as a reactive compatibilizer. Moreover, they reported the use of 3-amino-1,2,4- triazole (ATA) as POE-MA modifier to enhance improved reactivity. They concluded that the addition of 20 phr POE-MA, 5 phr ATA, and 20–40 phr lignin to EPDM matrix gave the best-balanced properties. Huang *et al.* [39], recently reported formation of coordination-based energy sacrificial bonds in the interface between lignin nanoparticles (LNP) and a polyolefin elastomer (POE) as rubber matrix to obtain high-performance thermoplastic elastomers.

Nevertheless, currently, there are no research works related to the use of DCP in REX compatibilization of renewable high-density PE and KL. For this reason, the aim of this study is to obtain environmentally friendly bio-based blends/composites by using bio-PE as a matrix, KL as filler, and DCP to enhance compatibilization by REX, since these materials have become an interesting alternative to substitute petroleum-based materials. To achieve this, different contents of DCP, namely 0.25, 0.50, 0.75, 1 weight parts of DCP per one hundred weight parts of the bioPE/KL blend (phr) were used in the REX process. The obtained samples from REX were further processed by injection-molding and characterized by tensile tests, thermal and thermomechanical analysis, morphological structure, optical appearance, and wettability studies.

EXPERIMENTAL

Materials

Bio-HDPE, SHA7260 grade, with a density of 0.955 g cm^{-3} was supplied in pellet form by FKuR Kunststoff GmbH (Willich, Germany) and manufactured by Braskem (São Paulo, Brazil). KL with low sulfonate content was supplied by Sigma-Aldrich S.A. (Madrid, Spain). DCP (98% purity) with a molecular weight of 270.37 g mol^{-1} was supplied by Sigma-Aldrich S.A. (Madrid, Spain).

Manufacturing of bioPE/KL blends by reactive extrusion (REX)

BioPE and KL were pre-homogenized in a zipper bag with DCP powder in different proportions as shown in **Table IV.1.3.1**. The amount of KL was set to a constant loading of 20 wt%. Kadla and Kubo [40] reported the study of blends between KL at different loadings (25, 50, 75, 87.5, 95, and 100 wt%) and poly(ethylene oxide) (PEO).

They proved blends containing 25 wt% KL showed the highest elongation at break with a value of 19.7%, while other KL content in the blends were characterized by lower elongation at break values under 5%. On the other hand, Thakur *et al.* [41] reported a decrease in elongation at break in polybutylene succinate (PBS)-lignin blends above 30% lignin. Therefore, in this study, the KL content was set to 20 wt% and the effect of DCP loading was evaluated.

The materials were subjected to REX in a co-rotating twin-screw extruder from Construcciones Mecánicas Dupra, S.L., (Alicante, Spain). The screw diameter was 25 mm and the length-to-diameter ratio (L/D) was 24. During the melt processing, the temperature profile was set as follows: 153 °C (hopper) – 158 °C – 160 °C – 163 °C (die), whereas screw rotation speed was adjusted to 19 rpm to allow reactive compatibilization. The extruded strands were pelletized with an air-knife unit. The resultant pellets were dried at 60 °C for 72 h to remove moisture.

Table IV.1.3.1. Summary of compositions according to the weight (wt%) and phr of bioPE with KL and DCP in different contents.

Sample	bioPE [wt%]	KL [wt%]	DCP [phr]
bioPE	100	-	-
bioPE/KL	80	20	-
bioPE/KL/0.25-DCP	80	20	0.25
bioPE/KL/0.50-DCP	80	20	0.50
bioPE/KL/0.75-DCP	80	20	0.75
bioPE/KL/1-DCP	80	20	1

Caracterization

Color measurements

A colorimetric spectrophotometer Konica CM-3600d Colorflex-DIFF2, from Hunter Associates Laboratory, Inc. (Reston, VA, USA), was used to determine the color coordinates and color changes of the samples. Calibration of the instrument was performed with a white standard tile. The CIE Lab color space coordinates L*, a*, b* were determined using the standard illuminant D65 and an observer angle of 10°. Coordinate L* represents luminance, where L* = 0 indicates dark and L* = 100 stands for lightness, meanwhile color coordinates a* and b* represent color changes from red to green and from yellow to blue, respectively. The color difference (ΔE_{ab}^*) was calculated using **Equation IV.1.3.1**.

$$\Delta E_{ab}^* = \sqrt{(\Delta L^*)^2 + (\Delta a^*)^2 + (\Delta b^*)^2} \qquad \textbf{Equation IV.1.3.1}$$

where ΔL*, Δa* and Δb* represent the variations in the L*, a* and b* coordinates, respectively. The average values of at least 5 readings, were reported. The color changes on the samples were evaluated based on the ΔE_{ab}^*. Values < 1 means an unnoticeable color difference, values ranging between 1–2 indicate a slight color difference that can only be noticed by an experienced observer, values in the range of 2–3.5 indicate a noticeable difference by an inexperienced observer, values in the range of 3.5–5 indicate a noticeable difference and values above 5 indicate that different colors are noticeable.

Microscopy characterization

The morphologies of the fractured surfaces of the injection-molded pieces after impact tests, were observed by field emission scanning electron microscopy (FESEM). A ZEISS ULTRA 55 FESEM microscope (Oxford Instruments, Abingdon, UK) was used at an acceleration voltage of 2 kV. Before the analysis, the samples were coated with a gold-palladium alloy in a sputter coater EMITECH mod. SC7620 Quorum Technologies Ltd., (East Sussex, UK).

Mechanical tests

Tensile tests of the injection-molded pieces after REX were carried out at room temperature in a universal test machine Elib 50 from S.A.E. Ibertest (Madrid, Spain), following the guidelines of ISO 527-1:2012. A load cell of 5 kN and a cross-head speed of 5 mm min^{-1} were used during the tests. At least five different samples were tested for each composition and the corresponding parameters were averaged.

Impact strength was carried out in a Charpy pendulum (1-J) on notched (0.25 mm radius V-notch) rectangular samples with dimensions of 80 x 10 mm^2, using a Metrotec S.A. (San Sebastián, Spain), following the guidelines of ISO 179-1:2010. Regarding hardness, a Shore D durometer 673-D from J. Bot S.A. Instrument (Barcelona, Spain) was used, according to ISO 868:2003 standard. Five different samples values were averaged.

Thermal characterization

Samples were subjected to differential scanning calorimetry (DSC) analysis. The average weight used for each sample was comprised between 5 - 7 mg. The equipment used was a Mettler-Toledo 821 calorimeter (Schwerzenbach, Switzerland). Samples were placed in 40-µL aluminum-sealed crucibles, and the most relevant thermal parameters were obtained through a thermal cycle in three stages: initial heating from 30 °C to 160 °C, then a cooling to -50 °C, and finally a second heating to 250 °C, at a heating/cooling rate of 10 °C min^{-1} in nitrogen atmosphere (with a constant flow rate of 66 mL min^{-1}). In the cooling stage it was identified the crystallization temperature (T_c), while the melting temperature (T_m) and the melting enthalpy (ΔH_m) were collected from the second heating step. Additionally, crystallinity degree (X_c) was obtained, using **Equation IV.1.3.2**.

$$X_c = \left[\frac{\Delta H_m}{\Delta H_m^0 \times w}\right] \times 100\ (\%) \qquad \textbf{Equation IV.1.3.2}$$

where, ΔH_m (J g^{-1}) corresponds to the melting enthalpy, ΔH_m^0 (J g^{-1}) is the melting enthalpy for a theoretical 100% crystalline bioPE, with a value of 293 (J g^{-1}), [42] and w is the weight fraction of bioPE used in the sample.

The thermal stability of the different samples was analyzed by thermogravimetry (TGA) in a PT1000 from Linseis (Selb, Germany). Samples sizing 15–25 mg were first placed in standard 70-µL alumina crucibles and subjected to a heating program in a nitrogen atmosphere from 30 °C to 700 °C at a heating rate of 10 °C min^{-1}. The temperature measured for a mass loss of 5% ($T_{5\%}$) was considered as the onset degradation temperature, while the temperatures at the maximum were determined from the first derivative thermogravimetry curves (DTG). All the tests were performed by triplicate to ensure reproducibility.

Dynamic mechanical thermal characterization

The dynamic mechanical thermal analysis (DMTA) was performed in a DMA-1 model from Mettler-Toledo S.A. (Barcelona, Spain), using a single cantilever setup. The injection-molded samples were subjected to a temperature sweep program from -150 °C to 120 °C at a heating rate of 2 °C min^{-1}. The selected frequency was 1 Hz with a force of 0.02 N. The maximum flexural deformation or cantilever deflection was set to 10 µm. Tests were made in triplicate.

Wettability

The static water-contact angle (θ) of bioPE and bioPE/KL blends with different percentages of DCP used in REX was obtained following the ISO 828:2013 standard, in an optical goniometer EasyDrop-FM140 from Kruss Equipment (Hamburg, Germany), and analyzed at room temperature. The liquid used for the analysis was distilled water with a volume of approximately 5 µL. All contact angles were measured at 7 s after the droplet was poured into the surface. At least, five different measurements for each film were obtained and averaged.

Statistical analysis

The statistical analysis was carried out by evaluating the results at 95% confidence level ($p \leq 0.05$) by one-way analysis of variance (ANOVA) following Tukey's test for the significant differences among the samples, using for this OriginPro 8 software (OriginLab Corporation, Northampton, MA, USA).

RESULTS AND DISCUSSION

Optical appearance and morphological properties of bioPE-KL blends

In nature, lignin presentation is almost colorless. However, when it is converted by different processes to technical lignin such as kraft lignin, soda lignin, or organosolv lignin, its color changes to a dark one. This is due to the addition of some chromophores (quinone groups, conjugated double bonds, carbonyl groups, and free radicals) and auxochrome (phenolic hydroxyl groups, hydroxyl groups, and carboxyl groups) during the isolation processes [13, 43]. In this context, the addition of the KL to the bioPE matrix causes a significative color variation regarding the neat bioPE sample, achieving a dark brown color. In other studies, similar were observed [32]. This difference between the sample appearance is presented in **Figure IV.1.3.1**, while the surface colour values obtained are gathered in **Table IV.1.3.2**. The importance to analyze the color variation in the blends is because it allows finding possible similarity in appearance with other wood plastic composites (WPC), which raises the possibility to use them in different applications related. In particular, bioPE/KL compatibilized by REX with DCP, offer a dark brown color, it is possible to compare it with *Eucalyptus gummifera*, which is a species within the Eucalyptus family, that presents values of 37.36, 22.50, 23.35, for *L**, *a**, and *b**, respectively [44]. In this regard, bioPE/KL blends offered a similar lightness value to that of *Eucalyptus gummifera*, while values obtained for *a** and *b** show some slight variation, which indicates that the blends obtained in this study present low red and yellow appearance.

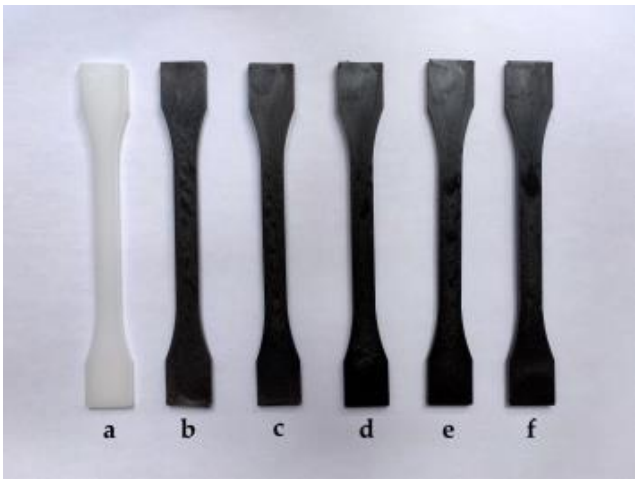

Figure IV.1.3.1. Injection-molded samples of bioPE/KL blends with different DCP amounts used in REX compatibilization: a) neat bioPE; b) bioPE/KL; c) bioPE/KL/0.25-DCP; d) bioPE/KL/0.50-DCP, e) bioPE/KL/0.75-DCP, and f) bioPE/KL/1-DCP.

Table IV.1.3.2. Color parameters (L*, a*, b*) and color difference (ΔE_{ab}*) of injection-molded samples of bioPE/KL blends with different DCP amounts used in the REX compatibilization.

Sample	L*	a*	b*	ΔE_{ab}*
bioPE	73.2 ± 0.9 [a]	-1.8 ± 0.6 [a]	-5.0 ± 0.1 [a]	-
bioPE/KL	32.3 ± 0.8 [b]	0.5 ± 0.0 [b]	1.1 ± 0.2 [b]	41.5 ± 0.8 [a]
bioPE/KL/0.25-DCP	32.3 ± 0.7 [b]	0.6 ± 0.0 [b]	1.7 ± 0.1 [c]	41.6 ± 0.7 [a]
bioPE/KL/0.50-DCP	32.1 ± 0.8 [b]	0.7 ± 0.1 [b]	2.1 ± 0.1 [d]	41.9 ± 0.7 [a]
bioPE/KL/0.75-DCP	30.7 ± 0.4 [c]	0.8 ± 0.1 [b]	2.2 ± 0.2 [d,e]	43.2 ± 0.3 [b]
bioPE/KL/1-DCP	30.3 ± 0.3 [c]	0.7 ± 0.0 [b]	1.9 ± 0.2 [c,e]	43.6 ± 0.3 [b]

[a-e] Different letters in the same column indicate a significant difference among the samples ($p < 0.05$).

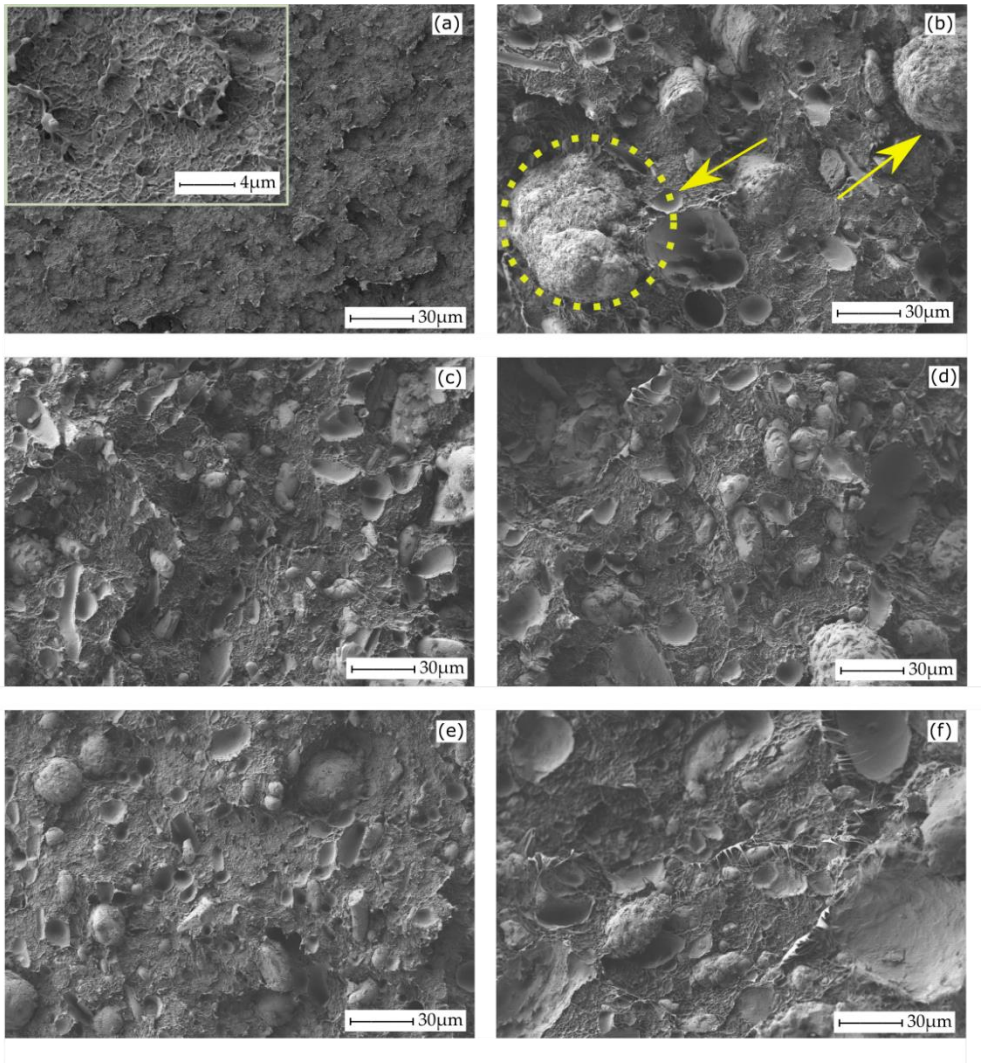

Figure IV.1.3.2. FESEM micrographs of the fractured surfaces of injection-molded samples of bioPE/KL blends with different DCP amounts used in REX compatibilization: (a) neat bioPE, (b) bioPE/KL, (c) bioPE/KL/0.25-DCP, (d) bioPE/KL/0.50-DCP, (e) bioPE/KL/0.75-DCP, (f) bioPE/KL/1-DCP. Images were taken at 500x with scale markers of 30 µm.

Figure IV.1.3.2 gathers the FESEM images of the fractured samples of neat bioPE, uncompatibilized bioPE/KL blend, and bioPE/KL blends subjected to REX with different DCP amounts. In **Figure IV.1.3.2**(a) it is possible to observe the fracture surface of neat bioPE, which shows high roughness and irregularities all over the surface. This is considered as a typical fracture surface of a ductile polymer, and it is in accordance with the work by Quiles-Carrillo *et al.* [45]. **Figure IV.1.3.2**b shows the morphology of the uncompatibilized bioPE/KL blend. KL can be identified as the embedded phase with spherical and irregular shapes of KL. Similar findings were reported by Chen *et al.* [46] In addition, it is possible to identify some KL aggregates and holes over the surface, which indicate the poor compatibility between both biopolymers, since lignin particles tend to pull-out from the fractured surfaces [22]. This behavior is in total agreement with the study reported by He *et al.* [47] where content of LNP higher than 5 wt% shows also poor compatibility in a PVA matrix. One can also observe larger KL particles or aggregates since particles tend to interact with the same particles strongly due to the action of their hydrogen bonds and non-covalent π-π interaction between phenyl rings [48], which cause coalescence and promote aggregation, especially when the amount of lignin used is high [49]. REX with DCP leads to some differences in morphology.

In general, lignin aggregates are not observed which is representative for improved lignin dispersion into the bioPE matrix [22]. as it is can be seen in **Figure IV.1.3.2**c-f with increasing DCP in the REX process. It is important to remark that the dispersion state of the fillers in a polymer matrix could affect the polymer composites' performance [46]. Hence, if there is a good dispersion, it may improve the interaction between the bioPE and the KL. Furthermore, as observed in the FESEM images of the REX-compatibilized blends, increasing the DCP content in the REX process, the aggregate disappears, thus indicating lignin domains are shorter and more homogeneous. This is best observed in the sample subjected to REX compatibilization with 1 phr DCP **Figure IV.1.3.2**f. Therefore, it can be seen that reactive extrusion (REX) with DCP is a technical solution to overcome the intrinsic immiscibility between the highly nonpolar bioPE matrix and the highly hydrophilic lignin polymer.

Mechanical properties of bioPE/KL blends

Table IV.1.3.3 gathers some of mechanical properties of the uncompatibilized and REX-compatibilized bioPE/KL blends with increasing DCP content. As expected, neat bioPE is a very ductile polymer, with a tensile modulus of 778.4 MPa, a tensile strength of 18.2 MPa and a very high elongation at break (in fact it does not break in the used equipment). Similar tensile properties were reported by Espinach *et al.* [50] for neat bioPE. This is related to its T_g, that is commonly located below -100 °C [51]. Then, with the addition of KL into the bioPE matrix, an increase in the tensile modulus of about 12% and a decrease in the tensile strength of about 13%, respectively, were observed, which could be related to the aromatic and rigid structure of the lignin, and also due to its large interfacial area [46]. On the other hand, elongation at break is dramatically decreased down to values of 21.3%. Elongation at break is directly related to material's cohesion and poor interaction between the nonpolar bioPE and the polar KL, leads to poor stress transfer which, in turn, leads to a decrease in mechanical properties related to cohesion, such as elongation at break. This phenomenon leads to a more brittle blend [45]. A similar phenomenon was reported by Abdelwahab *et al.* [52] when lignin was added to PP matrix. Sameni *et al.* [53] also reported an increase in the tensile strength and tensile modulus in high-density PE (HDPE) reinforced with different loadings of soda lignin.

Table IV.1.3.3. Mechanical properties of the injection-molded samples of neat bioPE, uncompatibilized bioPE/KL blend and bioPE/KL blend compatibilized by REX with varying DCP content: tensile modulus (E), tensile strength at yield (σ_y), elongation at break (ε_b), impact energy, and Shore D hardness.

Sample	E [MPa]	σ_y [MPa]	ε_b [%]	Impact Energy [kJ m^{-2}]	Hardness [Shore D]
bioPE	778.4 ± 36.8^{a}	18.2 ± 0.7^{a}	NB	2.4 ± 0.1^{a}	58.2 ± 0.4^{a}
bioPE/KL	874.7 ± 76. ^{b}	15.8 ± 0.3^{b}	21.3 ± 1.7^{a}	1.5 ± 0.1^{b}	60.7 ± 1.0^{b}
bioPE/KL/0.25-DCP	564.2 ± 32.4^{b,c}	15.3 ± 0.4^{b,c}	23.0 ± 2.8^{a}	1.4 ± 0.0^{b}	60.8 ± 0.4^{b}
bioPE/KL/0.50-DCP	572.0 ± 35.7^{c}	15.1 ± 0.0^{c}	35.9 ± 1.6^{b}	1.5 ± 0.1^{b}	61.0 ± 0.0^{b}
bioPE/KL/0.75-DCP	545.1 ± 4.5	15.7 ± 0.1^{b}	63.1 ± 6.6^{c}	1.6 ± 0.3^{b,c}	61.0 ± 0.0^{b}
bioPE/KL/1-DCP	503.8 ± 32.9^{d}	16.8 ± 0.3^{d}	66.6 ± 6.0^{c}	1.9 ± 0.3^{c}	61.20 ± 0.4^{b}

$^{a-d}$ Different letters in the same column indicate a significant difference among the samples ($p < 0.05$).

As can be observed in **Table IV.1.3.3**, after the REX process with increasing DCP, the tensile modulus of the compatibilized bioPE/KL blends decreases, being greater this decrement as DCP content increases in REX process. In this case, the lowest tensile modulus was obtained for the sample compatibilized by REX with 1 phr DCP, with a value of 503.8 MPa, which indicates a decrease close to 42% regarding the uncompatibilized bioPE/KL blend. Also, it can be seen REX with DCP hardly affected the tensile strength of the composites, which allowed to obtain very similar values of about 15 MPa. Only in the case of bioPE/KL blend subjected to REX with 1 phr DCP shows a slight increase in the tensile strength with a value of 16.8 MPa, which corresponds to an increase of the 6% regarding the bioPE/KL blend.

The most noticeable finding is that a remarkable improvement in the elongation at break is obtained in REX-compatibilized bioPE/KL blends with increasing DCP content. As can be observed in **Table IV.1.3.3**, with the increase of DCP during the REX compatibilization process, a higher elongation at break was obtained, being the highest values 63.1% and 66.5% which correspond to REX with 0.75 phr DCP and 1 phr DCP, respectively, which indicates an increase nearly three times with regard to the uncompatibilized bioPE/KL blend. This improvement in the elongation at break could be related to the better dispersion and less tendency of KL to form aggregates as previously observed by FESEM analysis. Similar findings were reported by Ferri *et al.* [51] in immiscible poly(lactide)-poly(ethylene) blends by REX with DCP, which allowed a noticeable improvement in elongation at break in PLA/bioPE blends. On the other hand, the work by Fei *et al.* [54] indicated that the use of DCP as a crosslinking or reactive compatibilizer agent allowed to improve mechanical properties of poly [(3-hydroxybutyrate)-*co*-(3-hydroxyvalerate)] (PHBV); in particular, the elongation at break increased from 4% to 11%. Finally, Ma *et al.* [55] also observed as the incorporation of 0.5% of DCP allowed the increase of elongation at break from 8% to 400% in PHBV/PBS blends by reactive compatibilization.

Regarding the impact-absorbed energy, it can be observed that the incorporation of KL in the polymeric matrix of bioPE promotes a noticeable decrease in toughness compared to neat bioPE. This is due to the lack of interaction between these two materials, which causes stress concentration, generating, therefore, a brittle material, together with the aggregate formation phenomenon [51]. Neat bioPE presents an impact strength of 2.4 kJ m^{-2}, whilst the uncompatibilized bioPE/KL blends shows a clear

decrease down to 1.5 kJ m^{-2}, which represents a percentage decrease of 37%. As above-mentioned, some mechanical properties are particularly sensitive to material's cohesion and the impact strength is, together with the elongation at break, one of these properties, since the lack of interface interactions leads to poor load transfer and, subsequently, both the elongation at break and the impact strength decrease. Nevertheless, the effect of increasing DCP during the REX compatibilization process, is positive since it provides slightly increased impact strength values. REX compatibilization with 0.75 phr DCP and 1 phr DCP led to impact strength values of 1.6 and 1.9 kJ m^{-2}, which represent an increase of around 7% and 29% regarding the uncompatibilized bioPE/KL blend Garcia-Garcia *et al.* [35], observed a similar tendency when using DCP as a reactive compatibilizer in binary poly (3-hydroxybutyrate) (P3HB) and poly (ε-caprolactone) (PCL) blends, obtaining a percentage increase in the impact-absorbed energy over 230% using 1 wt% of DCP during REX. Bova *et al.* [34], reported a noticeable increase in the tensile strength of about 134% in blends of acrylonitrile-butadiene rubber (NBR)/softwood kraft lignin (SKL), by using DCP at 2.5 phr during reactive mixing. According to the obtained results, it is possible to say that REX compatibilization with DCP is an interesting approach to improve the interaction between bioPE and KL, with the subsequent positive effect on material's cohesion properties, such as elongation at break and impact strength that are remarkably improved with increasing DCP content during REX.

Finally, regarding to Shore D hardness, **Table IV.1.3.3** shows an increase in the hardness after blending with KL with values from 58.2 for neat bioPE to 60.7 for the uncompatibilized bioPE/KL blend. However, REX with different DCP loadings seems to have a very slight effect on hardness, since the Shore D hardness values for all bioPE/KL blends is close to 61. Therefore, it can be concluded that REX with DCP allows some compatibilization between bioPE and KL. REX compatibilization also prevents aggregate formation and this also has a positive effect on overall mechanical behaviour of bioPE/KL blends. During REX, DCP recomposes at processing temperatures in the extruder and then, free radicals are formed in both bioPE and KL, thus allowing reaction between both polymers [56, 57].

Thermal properties of bioPE/KL blends

Figure IV.1.3.3 shows the DSC curves corresponding to the cooling step (**Figure IV.1.3.3**a) and second heating step (**Figure IV.1.3.3**b) once the thermal history has been

removed. **Figure IV.1.3.4** shows the DSC characteristic curve of neat KL, in which, the glass transition temperature (T_g) can be clearly identified by the step of the base line at about 160 °C. **Figure IV.1.3.3**a shows bioPE crystallization peak during the cooling step. The crystallization temperature (T_c) for neat bioPE is close to was to 116.8 °C. The effect of REX with different DCP amounts is almost negligible since there is not a relevant change in the peak temperature (see **Table IV.1.3.4**). A slight decrease in T_c can be detected in REX-compatibilized bioPE/KL blends with 1 phr DCP. This decrease could be related to an increase in the molecular weight, branching, or reduction in chain mobility, which did not allow a good crystallization process when during cooling, causing some imperfect and small crystals and also in less quantity [58]. A similar tendency for crystallization was observed by shown in Zattera *et al.* [36]. They revealed a decrease in T_c with increasing DCP in REX of LDPE-v/EVA. This effect was more pronounced since the amount of DCP used that was over 1 phr. The melt peak of bioPE can be clearly seen in **Figure IV.1.3.3**b, located at about 130.9 °C and typical of an HDPE. This melt peak temperature (T_m) is almost the same for the uncompatibilized bioPE/KL blend. It is also worthy to note that REX with DCP does not affect the melt peak temperature with values close to 130 °C. Regarding the melt enthalpies, neat bioPE showed a normalized value of 185.4 J g^{-1}, while the uncompatibilized blend of bioPE with 20 wt% KL is close to 150.2 J g^{-1}, which is almost 19% lower than neat bioPE, due to the dilution effect. As slight decrease in the melt peak enthalpies can be detected in REX-compatibilized bioPE/KL blends with increasing DCP content. This could be related to less perfect crystals due to branches or crosslinked segments obtained during REX which, in turn, promote a slight decrease in crystallinity. A similar behavior was observed by Zattera *et al.* [36], in LDPE-vEVA blends subjected to REX with DCP in the 1–4 phr. With regard to the degree of crystallinity, despite some tendency could be assessed by seeing the values in **Table IV.1.3.4**, it is worthy to note that the crystallinity degree of neat bioPE is slightly increased for uncompatibilized bioPE/KL blends, while a slight decrease in crystallinity is detected in REX-compatibilized bioPE/KL blends as the DCP content increases, due to hindering provided by potential branching, crosslinking after reaction between both polymers (**Table IV.1.3.4**). This slight decrease in crystallinity provided by REX, agrees with the previous mechanical results since lower crystallinity leads to lower tensile modulus. This trend was also reported by Khonakdar *et al.* [58], in which, an increase of DCP in reactive compatibilization, causes a decrease in the melt peak temperature, crystallization temperature, and the degree of

crystallinity. As above-mentioned, **Figure IV.1.3.4** shows the DSC profile of neat KL, with an amorphous phase and a glass transition temperature (T_g) of 160.5 °C. It is worthy to remark that the T_g of KL can be affected by its molecular weight, thermal history, degree of crosslinking and, polydispersity, among others [53, 59]. Similar T_g values for lignin have been reported by Huang *et al.* [59], with values of about 162 °C. The dilution effect does not allow a clear observation of the T_g in DSC thermograms collected in **Figure IV.1.3.4**b. Nevertheless, in a qualitative way, a slight step in the baseline can be seen at about 160 °C in all bioPE/KL blends.

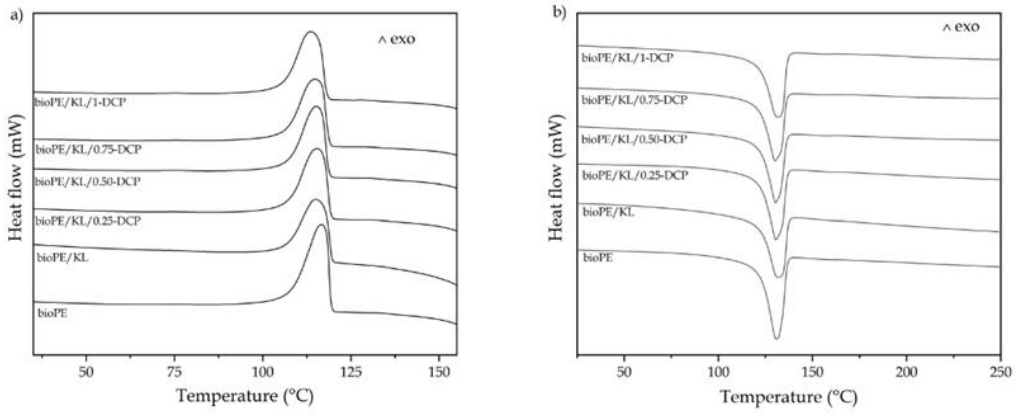

Figure IV.1.3.3. DSC thermograms of neat bioPE, uncompatibilized bioPE/KL blend and REX-compatibilized bioPE/KL blends with different DCP content, a) cooling and b) second heating cycle after the removal of the thermal history.

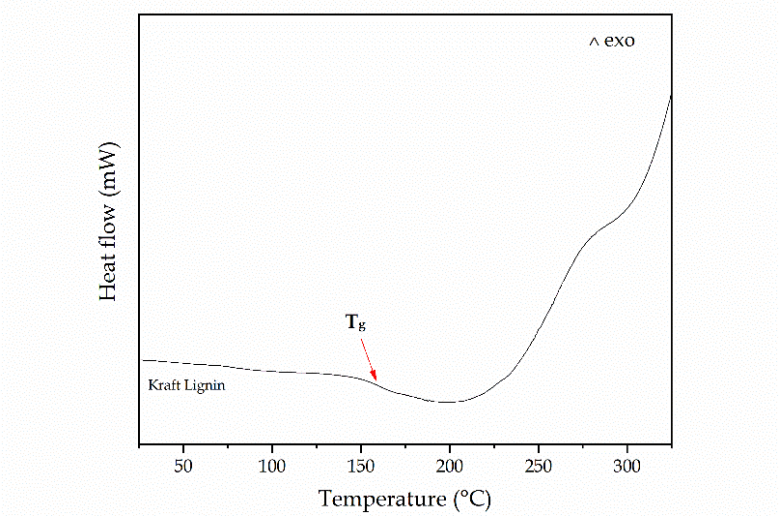

Figure IV.1.3.4. DSC thermogram of KL showing its glass transition temperature (T_g).

Table IV.1.3.4. Main thermal parameters of neat bioPE, uncompatibilized bioPE/KL blend and bioPE/KL blend compatibilized by REX with varying DCP content in terms of melting temperature (T_m), cooling temperature (T_c), normalized melting enthalpy (ΔH_m) and crystallinity degree (X_c).

Sample	T_c [°C]	T_m [°C]	ΔH_m [J g^{-1}]	X_c [%]
bioPE	116.8 ± 0.6[a]	130.9 ± 0.9[a]	185.4 ± 0.4[a]	63.3 ± 0.2[a]
bioPE/KL	115.5 ± 0.8[a]	131.2 ± 0.5[a]	150.2 ± 0.5[b]	64.1 ± 0.4[a,b]
bioPE/KL/0.25-DCP	115.4 ± 0.5[a,b]	130.6 ± 0.4[a]	147.7 ± 0.3[b,c]	63.0 ± 0.5[a,c]
bioPE/KL/0.50-DCP	115.3 ± 0.6[b]	130.4 ± 0.4[a]	146.5 ± 0.5[c,d]	62.5 ± 0.8[a]
bioPE/KL/0.75-DCP	114.9 ± 0.9[b]	130.1 ± 0.9[a]	146.9 ± 0.8[d]	62.6 ± 0.3[c]
bioPE/KL/1-DCP	113.7 ± 0.5[b]	131.2 ± 0.7[a]	146.3 ± 0.4[d]	62.4 ± 0.2[c]

[a-d] Different letters in the same column indicate a significant difference among the samples ($p < 0.05$).

Figure IV.1.3.5 shows the thermogravimetric (TGA) curves for neat bioPE, uncompatibilized bioPE/KL blend, and REX-compatibilized bioPE/KL blend with increasing DCP loading. The thermal stability values obtained through TGA are summarized in **Table IV.1.3.5** with the onset degradation temperature ($T_{5\%}$), and the maximum degradation rates obtained by the first derivative of the TGA curve (1st DTG). Two main degradation peak values can be detected as a consequence of the reaction between both polymers in the REX process. It can be seen that neat KL shows lower thermal stability than neat bioPE.

As one knows, lignin possesses a complex polymer structure that is progressively decomposed in a wide temperature range comprised between 200 °C and 500 °C. For this reason, the initial weight loss in lignin is higher than in bioPE that decomposes in a single step process. This initial weight loss in lignin could also be related to moisture due to its hydrophilicity [60]. Nevertheless, main degradation of lignin occurs between 200 °C and 500 °C, which is related to fragmentation of inter-unit linkages [61], and corresponds to about of 40% of the weight loss. REX compatibilization of bioPE/KL blends with DCP has a positive effect on thermal stabilization at high temperatures, while the effect on the onset degradation temperature is not positive.

REX with DCP increases the content of tertiary carbons which are prone to thermal decomposition. Anyway, since the difference between $T_{5\%}$ of neat bioPE (343.3 °C) and neat KL (138.1 °C) is so high, the first weight loss is attributable to lignin

decomposition and, hence, the overall thermal stability of the bioPE/KL blends is compromised [58]. Similar results were reported by, Krupa and Luyt [62]. They report the effect of DCP content on thermal properties of LLDPE/wax (80/20) blends. In fact, the onset degradation temperature for the uncompatibilized bled is 395.1 °C while the compatibilized blend by REX with 0.5 wt% DCP leads to a decrease in the onset degradation temperature down to 384.8 °C.

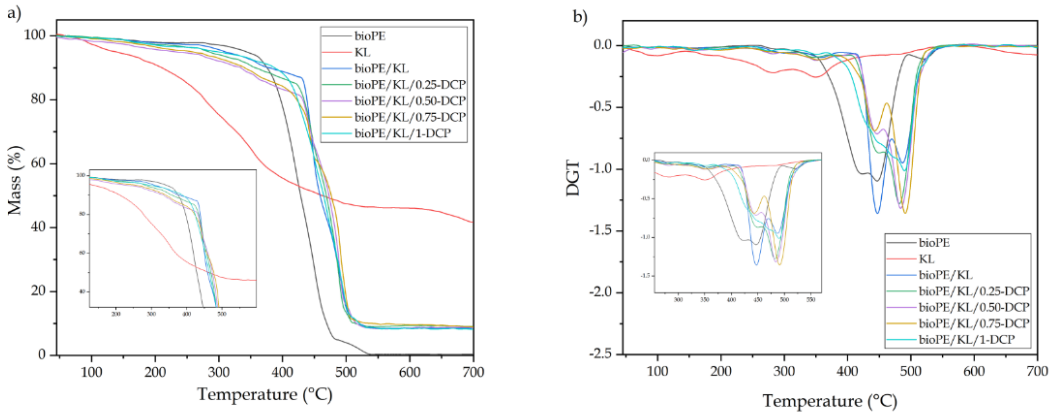

Figure IV.1.3.5. a) Thermogravimetric analysis (TGA) and b) first derivative (DTG) curves of the neat bioPE, uncompatibilized bioPE/KL blend and REX-compatibilized bioPE/KL blends with different DCP content.

However, within the samples of bioPE/KL composites, the one with 1 phr DCP showed the highest $T_{5\%}$, which was 298.6 °C, this suggests that with high values of DCP is possible to improve T_{onset} temperatures in bioPE/KL composites. Furthermore, it can be seen the neat bioPE shows a noticeable weight loss after at 361 °C, and it is evident a weight loss delay in the blends of bioPE/KL and bioPE/KL/DCP. Since, it was observed a remarkable weight loss of bioPE/KL composite that starts from 429.7 °C, while in bioPE/KL/DCP composites this weight loss begins after 400 °C in all cases, probably due to the effect of KL addition, into the composites, since KL has in its structure aromatic phenyl groups that are considered very stable due to the overlapping of p-orbitals, which allows complete delocalization of the π electrons, in addition due to the presence of hydroxyl groups that contribute with the stability of these aromatic groups, which prevents its early break, that later only occur at high temperatures [63, 64]. A similar trend is observed the study performed by Gordobil *et al.* [60], in that study blends with polylactic acid (PLA) and KL presented high thermal stability, regarding PLA sample.

Lignin degradation is a complex process that takes place in a wide temperature range. As observed in **Figure IV.1.3.5**b, KL shows two main DTG peaks. A first one located at 282.4 °C (first major degradation of lignin by pyrolysis) and a second peak at 349.7 °C related to a second major pyrolysis degradation of lignin by pyrolysis [65, 66]. Furthermore, it is evident there are two main weight loss stages for all bioPE/KL blends. The first one is observed between 442.8 °C and 447.1 °C and is related to the maximum degradation rate of neat bioPE maximum located at 447.8 °C as shown in **Figure IV.1.3.5**b. The second peak appears above 480 °C in all bioPE/KL blends, which could be related to inter-unit linkages fragmentation, release of monomeric phenols into the vapor phase [61, 67], or release of aromatics and CO_2 [65]. It is also important to bear in mind that the KL peak at 349.7 °C that corresponds to lignin is observed in all the composites with bioPE in **Figure IV.1.3.5**b. Finally, it was observed a residue at 700 °C for bioPE of 0.4%, while for KL the value was 41.6%; similar values were also reported by Gordobil *et al.* [60] and El Mansouri *et al.* [67].

Table IV.1.3.5. Main thermal decomposition parameters of neat bioPE, uncompatibilized bioPE/KL blend and bioPE/KL blend compatibilized by REX with varying DCP content in terms of onset degradation temperature ($T_{5\%}$), temperature of maximum degradation (T_{deg1}, T_{deg2}) and residual mass at 700 °C.

Sample	$T_{5\%}$ [°C]	T_{deg1} [°C]	T_{deg2} [°C]	Residual mass [%]
bioPE	343.3 ± 0.5 ^{a}	447.8 ± 1.0 ^{a}	-	0.4 ± 0.3 ^{a}
bioPE/KL	138.1 ± 0.9 ^{b}	282.4 ± 0.8 ^{b}/349.7 ± 0.6 ^{c}	481.2 ± 0.8 ^{a}	41.6 ± 0.5 ^{b}
bioPE/KL/0.25-DCP	309.7 ± 0.8 ^{c}	446.1 ± 1.2 ^{a}	481.7 ± 0.8 ^{a}	8.4 ± 0.8 ^{c}
bioPE/KL/0.50-DCP	284.3 ± 1.0 ^{d}	446.2 ± 0.6 ^{a}	483.3 ± 1.0 ^{a}	9.1 ± 1.3 ^{c}
bioPE/KL/0.75-DCP	232.3 ± 1.2 ^{e}	444.6 ± 1.1 ^{a}	484.8 ± 1.3 ^{a}	8.7 ± 0.9 ^{c}
bioPE/KL/1-DCP	258.2 ± 0.8 ^{f}	442.8 ± 1.4 ^{a}	491.4 ± 0.7 ^{a}	8.9 ± 1.1 ^{c}

$^{a-f}$ Different letters in the same column indicate a significant difference among the samples ($p < 0.05$).

Dynamic mechanical properties of bioPE/KL blends

The dynamic mechanical behavior of neat bioPE and bioPE/KL blends was studied through the variation of storage modulus (E′) and the dynamic damping factor (tan δ) as function of the temperature. In **Table IV.1.3.6** the different values can be observed. **Figure IV.1.3.6**a gathers the plots of the storage modulus (E′) with increasing

temperature. The typical dynamic mechanical thermal characterization of bioPE, revels three peaks below the meting process, labelled as γ, β, and α relaxations that correspond to the different chain mobility related to a temperature increase. The γ-relaxation usually occurs in the temperature range from -150 to -100 ^{o}C, and it has been associated with the motion of the polymer chains in the amorphous phase [68]. According to Khonakdar *et al.* [58] and Munaro and Akcelrud [69], this relaxation process is directly related to the glass transition temperature (T_g). The β-relaxation can be found at a temperature range close or under room temperature. This is mainly associated with the segmental motions of the side chains in the non-crystalline region [69], while the α-relaxation normally occurs at temperatures above room temperature, just approaching to the melting temperature. The α-relaxation is associated with the crystalline region; in particular, it is related to the motion of chain folds at the surface of the crystalline lamellae [68]. As can be seen in **Figure IV.1.3.6**a, the γ- and β-relaxation can be clearly detected. The glass transition temperature for neat bioPE, was identified by following the peak maximum of the dynamic damping factor, at a peak maximum at -114.6 ^{o}C (**Figure IV.1.3.6**b). Above the T_g, E′ values for bioPE decrease in a remarkable way since bioPE changes to an elastic-viscous behavior [70]. This happens when temperature exceeds the α-relaxation of the biopolymer [71]. In particular, the storage modulus (E′) of bioPE shows a value of 1485.6 MPa at -75 °C. Above the T_g, bioPE becomes more and more ductile (increase in the viscous component) and the corresponding E′ values are remarkably reduced down to 118.2 MPa at 100 °C (more than 200 °C above its T_g). However, with the addition of KL to the polymeric matrix, it is observed a remarkable increase in E′ at -75 °C with a value of 1823.6 MPa. It is important to remind that lignin has a T_g of about 160 °C, which makes it more elastic up to this temperature.

On the other hand, REX compatibilization with 0.50, 0.75, and 1 phr of DCP leads to an increase in the storage modulus (E′) to high values above 1900 MPa. This could be explained due to the stiffening effect that cause the addition of KL and the REX process with DCP, which reduced the viscous constituent and restrict the polymer mobility, giving rise to the elastic component [72]. This corroborates that REX with DCP provides somewhat compatibilization between bioPE and KL [73].

Figure IV.1.3.6b, shows the evolution of the dynamic damping factor (tan δ) of neat bioPE and bioPE/KL blends. The glass transition temperature (T_g) of the different samples was identified as the peak of tan δ and ranged between -108 °C to -120 °C (**Figure**

IV.1.3.6b). It is also worth noting that uncompatibilized bioPE/KL blends, and specially REX-compatibilized bioPE/KL blends with DCP offer lower tan δ values, which could indicate that these materials show a more elastic response, and therefore, they have the potential to store the applied load rather than to dissipate/loss it [71].

Table IV.1.3.6. Dynamic mechanical analysis (DMTA) parameters of neat bioPE, uncompatibilized bioPE/KL blend and REX-compatibilized bioPE/KL/DCP with increasing DCP content.

Sample	T_g [°C]	E′ at -75 °C [MPa]	E′ at 100 °C [MPa]
bioPE	-114.6 ± 0.8^{a}	1485.6 ± 7.3^{a}	118.2 ± 1.2^{a}
bioPE/KL	-118.9 ± 0.7^{a}	1823.6 ± 9.1^{b}	167.1 ± 1.4^{b}
bioPE/KL/0.25-DCP	-117.8 ± 1.0^{a}	1746.8 ± 8.6^{c}	175.5 ± 0.9^{b,c}
bioPE/KL/0.50-DCP	-117.2 ± 0.8^{a}	1956.1 ± 8.4^{d}	180.3 ± 1.1^{c}
bioPE/KL/0.75-DCP	-118.8 ± 1.3^{a}	1934.9 ± 6.9^{d,e}	168.9 ± 1.5^{c}
bioPE/KL/1-DCP	-120.2 ± 1.2^{a}	1928.4^{e}	157.1 ± 0.8^{d}

$^{a\text{-}e}$ Different letters in the same column indicate a significant difference among the samples ($p < 0.05$).

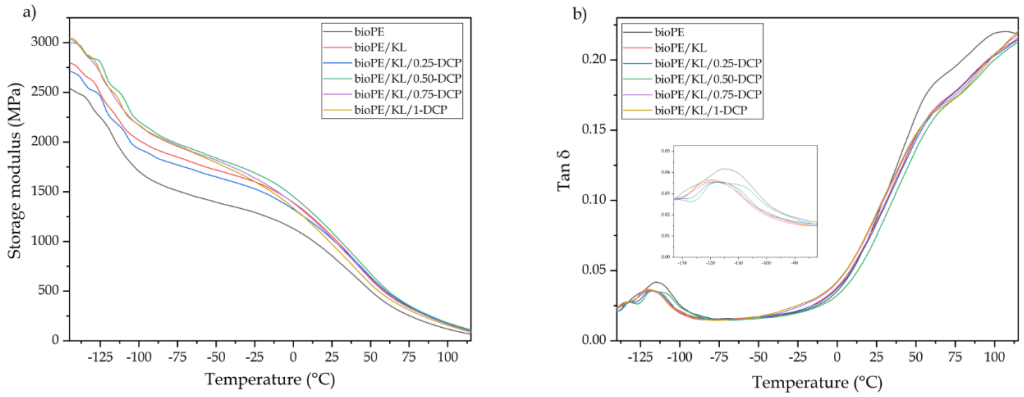

Figure IV.1.3.6. DMTA curves of the injection-molded pieces of neat bioPE, uncompatibilized bioPE/KL blend, and REX-compatibilized bioPE/KL with increasing DCP content, (a) Storage modulus (E′), and (b) Dynamic damping factor (tan δ).

Wettability of bioPE/KL blends

In general, surfaces with a water-contact angle between 0° to 30° can be considered as hydrophilic materials, on the other hand, a value above 90° indicates hydrophobic materials [74]. **Figure IV.1.3.7** clearly indicates the angles obtained by the different samples. In this regard, neat bioPE is a highly hydrophobic polymer due to its nonpolar structure, which leads to a water-contact angle (θ_w) of 95.1° [53]. The addition

of KL causes a decrease in the hydrophobicity of bioPE, as expected, due to the polar groups contained in lignin. Hence, the water-contact angle decreases to 85°, which is still high. Despite lignin has polar groups, it shows low hydrophilicity [75]. A similar behaviour was reported by Sousa Junior *et al.* [76] in which PP showed a water-contact angle of 107.22°, and then with the addition of acid or alkali kraft lignin, the water-contact angle decreased to values between 91° and 98°, depending on the lignin content. REX with increasing DCP content, leads to a decrease in the water-contact angle, reaching a value of 71.4° for the REX-compatibilized blend with 1 phr DCP.

It seems REX provides more polarity to the surface as a consequence of the reaction products obtained after the decomposition of DCP in the extruder and the subsequent free radical formation which could lead to branching, crosslinking, among others [77]. These results agree with those reported by Ararat and Murillo [78], in which the effect of DCP on surface wetting properties of a blend of LDPE and a maleinized hyperbranched polyester is studied. They concluded that the water-contact angle is lower for increasing the DCP content in the reactive compatibilization process. In fact, the initial water-contact angle of neat LDPE was 96°, and was decreased to 78°, 62°, and 54°, with reactive compatibilization using 0.5, 1.0 and 1.5 wt% DCP, respectively.

According to Bova *et al.* [34], the use of DCP remarkably improves mechanical strength of acrylonitrile-butadiene rubber with different lignins, thus showing the efficiency of DCP as reactive compatibilizer in these blends. As it has been previously shown in FESEM characterization, as the DCP loading increases, the dispersed lignin domain phase is clearly lowered which, in turn, increases the surface area of lignin. Furthermore, it is important to bear in mind that KL usually contains some salt impurities. Gordobil *et al.* [79] reported the presence of some residual carbohydrates, ashes, and sulfur in KL. These impurities, together with the finer KL domains contribute to the observed increased hydrophilicity with increasing DCP.

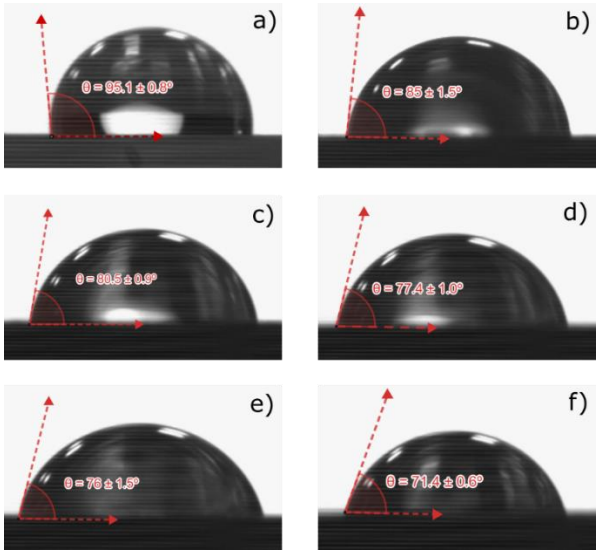

Figure IV.1.3.7. Wettability through contact angle measurements of a) neat bioPE, b) bioPE/KL, c) bioPE/KL/0.25-DCP, d) bioPE/KL/0.50-DCP, e) bioPE/KL/0.75-DCP, and f) bioPE/KL/1-DCP.

CONCLUSIONS

BioPE and KL blends were successfully compatibilized by REX with an organic peroxide, namely DCP in the 0 – 1 phr range. The tensile tests indicated a remarkable improvement in mechanical properties after the REX process with increasing DCP content. In particular, REX with 1 phr DCP led to a bioPE/KL blend with an increase in elongation at break of about 300% with regard the uncompatibilized blend. Similar tendency was observed for the impact strength, thus giving evidence that REX with DCP is a feasible, easy, and cost-effective process to provide some compatibility between bioPE and KL. FESEM revealed a phase separation (drop-like) in uncompatibilized bioPE/KL blends, with lignin aggregates. The use of REX with increasing DCP content, prevents aggregate formation and the lignin size domain is remarkably reduced, thus indicating a better particle dispersion. DSC revealed a slight decrease in the degree of crystallinity of bioPE in REX-compatibilized bioPE/KL blends due to formation of less perfect crystals resulting from the branched or crosslinked species obtained during the REX process which provide more polar properties to the surfaces, as corroborated by a decrease in the water-contact angle (θ_w) with increasing DCP content in the REX process. Despite lignin is less thermally stable than bioPE, the overall thermal stability of these blends is not compromised in terms of processing temperatures. Moreover, these blends show a dark brown color that could be interesting for use of these blends as a WPC. Therefore, the results obtained in this work offer the possibility to use a natural polymer

(KL) in bioPE matrix to obtain a material with overall balanced properties using reactive extrusion (REX) with DCP.

ACKNOWLEDGEMENTS

S. Rojas-Lema is a recipient of a Santiago Grisolía grant from Generalitat Valenciana (GVA) (GRISOLIAP/2019/132). D. Lascano wants to thank Universitat Politècnica de València (UPV) for the grant received through the PAID-01-18 program. J. Ivorra-Martinez. wants to thank the Spanish Ministry of Science, Innovation and Universities for his FPU grant (FPU19/01759). Microscopy services at UPV are acknowledged for their help in using and collecting FESEM images.

REFERENCES

[1] M.A. Abdelwahab, S. Taylor, M. Misra, and A.K. Mohanty. *Thermo-mechanical characterization of bioblends from polylactide and poly (butylene adipate-co-terephthalate) and lignin*. Macromolecular Materials and Engineering, 2015, 300(3), p. 299-311.

[2] A. Tejado, C. Pena, J. Labidi, J. Echeverria, and I. Mondragon. *Physico-chemical characterization of lignins from different sources for use in phenol–formaldehyde resin synthesis.* Bioresource Technology, 2007, 98(8), p. 1655-1663.

[3] S. Huang, N. Mahmood, M. Tymchyshyn, Z. Yuan, and C.C. Xu. *Reductive de-polymerization of kraft lignin for chemicals and fuels using formic acid as an in-situ hydrogen source.* Bioresource Technology, 2014, 171, p. 95-102.

[4] J. Mei, W. Liu, J. Huang, and X. Qiu. *Lignin-reinforced ethylene-propylene-diene copolymer elastomer via hydrogen bonding interactions.* Macromolecular Materials and Engineering, 2019, 304(4), p. 1800689.

[5] A. Duval and M. Lawoko. *A review on lignin-based polymeric, micro-and nano-structured materials.* Reactive and Functional Polymers, 2014, 85, p. 78-96.

[6] H. Li, Y. Deng, B. Liu, Y. Ren, J. Liang, Y. Qian, X. Qiu, C. Li, and D. Zheng. *Preparation of nanocapsules via the self-assembly of kraft lignin: A totally green process with renewable resources.* ACS Sustainable Chemistry & Engineering, 2016, 4(4), p. 1946-1953.

[7] Q. Tang, Y. Qian, D. Yang, X. Qiu, Y. Qin, and M. Zhou. *Lignin-based nanoparticles: A review on their preparations and applications.* Polymers, 2020, 12(11), p. 2471.

[8] N. Jamil, P. Kumar, and R. Batool. *Soil microenvironment for bioremediation and polymer production*. 2020: Wiley Online Library, p. 380.

[9] H. Chen, X. Qu, N. Liu, S. Wang, X. Chen, and S. Liu. *Study of the adsorption process of heavy metals cations on Kraft lignin.* Chemical Engineering Research and Design, 2018, 139, p. 248-258.

[10] A. Zerpa, L. Pakzad, and P. Fatehi. *Hardwood kraft lignin-based hydrogels: production and performance.* ACS Omega, 2018, 3(7), p. 8233-8242.

[11] Y. Meng, J. Lu, Y. Cheng, Q. Li, and H. Wang. *Lignin-based hydrogels: A review of preparation, properties, and application.* International Journal of Biological Macromolecules, 2019, 135, p. 1006-1019.

[12] H. Jeong, J. Park, S. Kim, J. Lee, and J.W. Cho. *Use of acetylated softwood kraft lignin as filler in synthetic polymers.* Fibers and Polymers, 2012, 13(10), p. 1310-1318.

[13] S.C. Lee, T.M.T. Tran, J.W. Choi, and K. Won. *Lignin for white natural sunscreens.* International Journal of Biological Macromolecules, 2019, 122, p. 549-554.

[14] H. Sadeghifar and D.S. Argyropoulos. *Macroscopic behavior of kraft lignin fractions: melt stability considerations for lignin–polyethylene blends.* ACS Sustainable Chemistry & Engineering, 2016, 4(10), p. 5160-5166.

[15] X. Tian, Z. Fang, R.L. Smith, Z. Wu, and M. Liu. *Properties, chemical characteristics and application of lignin and its derivatives*, in *Production of biofuels and chemicals from lignin*. 2016, Springer, p. 3-33.

[16] O.A.T. Dias, D.R. Negrão, D.F.C. Gonçalves, I. Cesarino, and A.L. Leão. *Recent approaches and future trends for lignin-based materials.* Molecular Crystals and Liquid Crystals, 2017, 655(1), p. 204-223.

[17] M. Wei, L. Fan, J. Huang, and Y. Chen. *Role of star-like hydroxylpropyl lignin in soy-protein plastics.* Macromolecular Materials and Engineering, 2006, 291(5), p. 524-530.

[18] L. Dehne, C.V. Babarro, B. Saake, and K.U. Schwarz. *Influence of lignin source and esterification on properties of lignin-polyethylene blends.* Industrial Crops and Products, 2016, 86, p. 320-328.

[19] O. Dias, D. Negrão, R. Silva, C. Funari, I. Cesarino, and A. Leao. *Studies of lignin as reinforcement for plastics composites.* Molecular Crystals and Liquid Crystals, 2016, 628(1), p. 72-78.

[20] G. Cazacu, M.C. Pascu, L. Profire, A. Kowarski, M. Mihaes, and C. Vasile. *Lignin role in a complex polyolefin blend.* Industrial Crops and Products, 2004, 20(2), p. 261-273.

[21] S. Kumar, A. Mohanty, L. Erickson, and M. Misra. *Lignin and its applications with polymers.* Journal of Biobased Materials and Bioenergy, 2009, 3(1), p. 1-24.

[22] L. Hu, T. Stevanovic, and D. Rodrigue. *Compatibilization of kraft lignin-polyethylene composites using unreactive compatibilizers.* Journal of Applied Polymer Science, 2014, 131(21), p. 41040.

[23] G.M. Farias, P. Agrawal, R.B. Hanken, J.P. de Araújo, A.D. de Oliveira, and T.J. de Mélo. *Effect of EVA copolymer containing different VA content on the thermal and rheological properties of bio-based high-density polyethylene/ethylene vinyl acetate blends.* Journal of Thermal Analysis and Calorimetry, 2021, p. 1-13.

[24] I. Tsiropoulos, A.P. Faaij, L. Lundquist, U. Schenker, J.F. Briois, and M.K. Patel. *Life cycle impact assessment of bio-based plastics from sugarcane ethanol.* Journal of Cleaner Production, 2015, 90, p. 114-127.

[25] D. Garcia-Garcia, A. Carbonell-Verdu, A. Jordá-Vilaplana, R. Balart, and D. Garcia-Sanoguera. *Development and characterization of green composites from bio-based polyethylene and peanut shell.* Journal of Applied Polymer Science, 2016, 133(37), p. 43940.

[26] A. Tribot, G. Amer, M.A. Alio, H. de Baynast, C. Delattre, A. Pons, J.-D. Mathias, J.-M. Callois, C. Vial, and P. Michaud. *Wood-lignin: Supply, extraction processes and use as bio-based material.* European Polymer Journal, 2019, 112, p. 228-240.

[27] M. Przybysz, M. Marć, M. Klein, M.R. Saeb, and K. Formela. *Structural, mechanical and thermal behavior assessments of PCL/PHB blends reactively compatibilized with organic peroxides.* Polymer Testing, 2018, 67, p. 513-521.

[28] W. Brostow, T. Datashvili, and K.P. Hackenberg. *Effect of different types of peroxides on properties of vulcanized EPDM+ PP blends.* Polymer Composites, 2010, 31(10), p. 1678-1691.

[29] R. Muthuraj, M. Misra, and A.K. Mohanty. *Biodegradable compatibilized polymer blends for packaging applications: A literature review.* Journal of Applied Polymer Science, 2018, 135(24), p. 45726.

[30] R. Sailaja and M. Deepthi. *Mechanical and thermal properties of compatibilized composites of polyethylene and esterified lignin.* Materials & Design, 2010, 31(9), p. 4369-4379.

[31] G. Toriz, F. Denes, and R. Young. *Lignin-polypropylene composites. Part 1: Composites from unmodified lignin and polypropylene.* Polymer Composites, 2002, 23(5), p. 806-813.

[32] M. Ghozali, E. Triwulandari, A. Haryono, and E. Yuanita. *Effect of lignin on morphology, biodegradability, mechanical and thermal properties of low linear density polyethylene/lignin biocomposites*. in *IOP Conference Series: Materials Science and Engineering*. 2017. IOP Publishing. p. 012022.

[33] R. Anbarasan, O. Babot, and B. Maillard. *Crosslinking of high-density polyethylene in the presence of organic peroxides.* Journal of Applied Polymer Science, 2004, 93(1), p. 75-81.

[34] T. Bova, C.D. Tran, M.Y. Balakshin, J. Chen, E.A. Capanema, and A.K. Naskar. *An approach towards tailoring interfacial structures and properties of multiphase renewable thermoplastics from lignin–nitrile rubber.* Green Chemistry, 2016, 18(20), p. 5423-5437.

[35] D. Garcia-Garcia, E. Rayón, A. Carbonell-Verdu, J. López-Martínez, and R. Balart. *Improvement of the compatibility between poly (3-hydroxybutyrate) and poly (ε-caprolactone) by reactive extrusion with dicumyl peroxide.* European Polymer Journal, 2017, 86, p. 41-57.

[36] A. Zattera, O. Bianchi, R.d. Oliveira, L. Canto, C. Ferreira, and M. Zeni. *Influence of composition and crosslinking on mechanical and thermal properties of recycled polyethylene/eva mixtures.* Progress in Rubber, Plastics and Recycling Technology, 2006, 22(2), p. 69-87.

[37] P. Ma, X. Cai, Y. Zhang, S. Wang, W. Dong, M. Chen, and P. Lemstra. *In-situ compatibilization of poly (lactic acid) and poly (butylene adipate-co-terephthalate) blends by using dicumyl peroxide as a free-radical initiator.* Polymer Degradation and Stability, 2014, 102, p. 145-151.

[38] E. Ahmad and A. Luyt. *Effects of organic peroxide and polymer chain structure on morphology and thermal properties of sisal fibre reinforced polyethylene composites.* Composites Part A: Applied Science and Manufacturing, 2012, 43(4), p. 703-710.

[39] J. Huang, W. Liu, and X. Qiu. *High performance thermoplastic elastomers with biomass lignin as plastic phase.* ACS Sustainable Chemistry & Engineering, 2019, 7(7), p. 6550-6560.

[40] J.F. Kadla and S. Kubo. *Miscibility and hydrogen bonding in blends of poly (ethylene oxide) and kraft lignin.* Macromolecules, 2003, 36(20), p. 7803-7811.

[41] V.K. Thakur, M.K. Thakur, P. Raghavan, and M.R. Kessler. *Progress in green polymer composites from lignin for multifunctional applications: a review.* ACS Sustainable Chemistry & Engineering, 2014, 2(5), p. 1072-1092.

[42] F. Dominici, D. García García, V. Fombuena, F. Luzi, D. Puglia, L. Torre, and R. Balart. *Bio-polyethylene-based composites reinforced with alkali and palmitoyl chloride-treated coffee silverskin.* Molecules, 2019, 24(17), p. 3113.

[43] X. Qiu, J. Yu, D. Yang, J. Wang, W. Mo, and Y. Qian. *Whitening sulfonated alkali lignin via H2O2/UV radiation and its application as dye dispersant.* ACS Sustainable Chemistry & Engineering, 2018, 6(1), p. 1055-1060.

[44] K. Krisdianto. *Color differences of pine and eucalypt woods measured by microflash-200®.* Indonesian Journal of Forestry Research, 2007, 4(2), p. 83-91.

[45] L. Quiles-Carrillo, N. Montanes, A. Jorda-Vilaplana, R. Balart, and S. Torres-Giner. *A comparative study on the effect of different reactive compatibilizers on injection-molded pieces of bio-based high-density polyethylene/polylactide blends.* Journal of Applied Polymer Science, 2019, 136(16), p. 47396.

[46] F. Chen, W. Liu, S.I. Seyed Shahabadi, J. Xu, and X. Lu. *Sheet-like lignin particles as multifunctional fillers in polypropylene.* ACS Sustainable Chemistry & Engineering, 2016, 4(9), p. 4997-5004.

[47] X. He, F. Luzi, X. Hao, W. Yang, L. Torre, Z. Xiao, Y. Xie, and D. Puglia. *Thermal, antioxidant and swelling behaviour of transparent polyvinyl (alcohol) films in presence of hydrophobic citric acid-modified lignin nanoparticles.* International Journal of Biological Macromolecules, 2019, 127, p. 665-676.

[48] W. Zhao, L.-P. Xiao, G. Song, R.-C. Sun, L. He, S. Singh, B.A. Simmons, and G. Cheng. *From lignin subunits to aggregates: insights into lignin solubilization.* Green Chemistry, 2017, 19(14), p. 3272-3281.

[49] B. Bozsódi, V. Romhányi, P. Pataki, D. Kun, K. Renner, and B. Pukánszky. *Modification of interactions in polypropylene/lignosulfonate blends.* Materials & Design, 2016, 103, p. 32-39.

[50] F.X. Espinach, E. Espinosa, R. Reixach, A. Rodríguez, P. Mutjé, and Q. Tarrés. *Study on the macro and micromechanics tensile strength properties of orange tree pruning fiber as sustainable reinforcement on bio-polyethylene compared to oil-derived polymers and its composites.* Polymers, 2020, 12(10), p. 2206.

[51] J.M. Ferri, D. Garcia-Garcia, E. Rayón, M.D. Samper, and R. Balart. *Compatibilization and characterization of polylactide and biopolyethylene binary blends by non-reactive and reactive compatibilization approaches.* Polymers, 2020, 12(6), p. 1344.

[52] M.A. Abdelwahab, M. Misra, and A.K. Mohanty. *Injection molded biocomposites from polypropylene and lignin: Effect of compatibilizers on interfacial adhesion and performance.* Industrial Crops and Products, 2019, 132, p. 497-510.

[53] J. Sameni, S.A. Jaffer, and M. Sain. *Thermal and mechanical properties of soda lignin/HDPE blends.* Composites Part A: Applied Science and Manufacturing, 2018, 115, p. 104-111.

[54] B. Fei, C. Chen, S. Chen, S. Peng, Y. Zhuang, Y. An, and L. Dong. *Crosslinking of poly [(3-hydroxybutyrate)-co-(3-hydroxyvalerate)] using dicumyl peroxide as initiator.* Polymer International, 2004, 53(7), p. 937-943.

[55] P. Ma, D.G. Hristova-Bogaerds, P.J. Lemstra, Y. Zhang, and S. Wang. *Toughening of PHBV/PBS and PHB/PBS Blends via In situ Compatibilization Using Dicumyl Peroxide as a Free-Radical Grafting Initiator.* Macromolecular Materials and Engineering, 2012, 297(5), p. 402-410.

[56] C. Mao, C.X. Liang, Y.Q. Mao, L. Li, X.M. Hou, and J. Shen. *Modification of polyethylene with Pluronics F127 for improvement of blood compatibility.* Colloids and Surfaces B: Biointerfaces, 2009, 74(1), p. 362-365.

[57] V. Katiyar. *Non-isothermal degradation kinetics of PLA-functionalized gum (fG) biocomposite with dicumyl peroxide (DCP).* Journal of Thermal Analysis and Calorimetry, 2019, 138(1), p. 195-210.

[58] H. Khonakdar, J. Morshedian, U. Wagenknecht, and S. Jafari. *An investigation of chemical crosslinking effect on properties of high-density polyethylene.* Polymer, 2003, 44(15), p. 4301-4309.

[59] C. Huang, J. He, R. Narron, Y. Wang, and Q. Yong. *Characterization of kraft lignin fractions obtained by sequential ultrafiltration and their potential application as a biobased component in blends with polyethylene.* ACS Sustainable Chemistry & Engineering, 2017, 5(12), p. 11770-11779.

[60] O. Gordobil, R. Delucis, I. Egüés, and J. Labidi. *Kraft lignin as filler in PLA to improve ductility and thermal properties.* Industrial Crops and Products, 2015, 72, p. 46-53.

[61] F. Bertini, M. Canetti, A. Cacciamani, G. Elegir, M. Orlandi, and L. Zoia. *Effect of ligno-derivatives on thermal properties and degradation behavior of poly (3-hydroxybutyrate)-based biocomposites.* Polymer Degradation and Stability, 2012, 97(10), p. 1979-1987.

[62] I. Krupa and A. Luyt. *Thermal properties of uncross-linked and cross-linked LLDPE/wax blends.* Polymer Degradation and Stability, 2000, 70(1), p. 111-117.

[63] A.A. Morandim-Giannetti, J.A.M. Agnelli, B.Z. Lanças, R. Magnabosco, S.A. Casarin, and S.H. Bettini. *Lignin as additive in polypropylene/coir composites: Thermal, mechanical and morphological properties.* Carbohydrate Polymers, 2012, 87(4), p. 2563-2568.

[64] L.R. Chiappero, S.S. Bartolomei, D.A. Estenoz, E.A. Moura, and V.V. Nicolau. *Lignin-based polyethylene films with enhanced thermal, opacity and biodegradability properties for agricultural mulch applications.* Journal of Polymers and the Environment, 2021, 29(2), p. 450-459.

[65] M. Zhang, F.L. Resende, A. Moutsoglou, and D.E. Raynie. *Pyrolysis of lignin extracted from prairie cordgrass, aspen, and Kraft lignin by Py-GC/MS and TGA/FTIR.* Journal of Analytical and Applied Pyrolysis, 2012, 98, p. 65-71.

[66] D. Shen, S. Gu, K. Luo, S. Wang, and M. Fang. *The pyrolytic degradation of wood-derived lignin from pulping process.* Bioresource Technology, 2010, 101(15), p. 6136-6146.

[67] N.-E. El Mansouri, Q. Yuan, and F. Huang. *Synthesis and characterization of kraft lignin-based epoxy resins.* BioResources, 2011, 6(3), p. 2492-2503.

[68] R. Sirotkin and N. Brooks. *The dynamic mechanical relaxation behaviour of polyethylene copolymers cast from solution.* Polymer, 2001, 42(24), p. 9801-9808.

[69] M. Munaro and L. Akcelrud. *Correlations between composition and crystallinity of LDPE/HDPE blends.* Journal of Polymer Research, 2008, 15(1), p. 83-88.

[70] S. Torres-Giner, N. Montanes, O. Fenollar, D. García-Sanoguera, and R. Balart. *Development and optimization of renewable vinyl plastisol/wood flour composites exposed to ultraviolet radiation.* Materials & Design, 2016, 108, p. 648-658.

[71] J. Ivorra-Martinez, L. Quiles-Carrillo, T. Boronat, S. Torres-Giner, and J. A Covas. *Assessment of the mechanical and thermal properties of injection-molded poly (3-hydroxybutyrate-co-3-hydroxyhexanoate)/hydroxyapatite nanoparticles parts for use in bone tissue engineering.* Polymers, 2020, 12(6), p. 1389.

[72] H. Kargarzadeh, A. Galeski, and A. Pawlak. *PBAT green composites: Effects of kraft lignin particles on the morphological, thermal, crystalline, macro and micromechanical properties.* Polymer, 2020, 203, p. 122748.

[73] Á. Agüero, D. Garcia-Sanoguera, D. Lascano, S. Rojas-Lema, J. Ivorra-Martinez, O. Fenollar, and S. Torres-Giner. *Evaluation of different compatibilization strategies to improve the performance of injection-molded green composite pieces made of polylactide reinforced with short flaxseed fibers.* Polymers, 2020, 12(4), p. 821.

[74] A. Jordá-Vilaplana, V. Fombuena, D. García-García, M. Samper, and L. Sánchez-Nácher. *Surface modification of polylactic acid (PLA) by air atmospheric plasma treatment.* European Polymer Journal, 2014, 58, p. 23-33.

[75] K. Kaewtatip and J. Thongmee. *Effect of kraft lignin and esterified lignin on the properties of thermoplastic starch.* Materials & Design, 2013, 49, p. 701-704.

[76] R.R.d. Sousa Junior, J.R. Gouveia, A.M. Nacas, L.B. Tavares, N.M. Ito, E.N.d. Moura, F.A. Gaia, R.F. Pereira, and D.J.d. Santos. *Improvement of polypropylene adhesion by kraft lignin incorporation.* Materials Research, 2019, 22(2), p. e20180123.

[77] C.B. Luna, D.D. Siqueira, E.M. Araújo, R.M. Wellen, and T. Jeferson Alves de Mélo. *Approaches on the acrylonitrile-butadiene-styrene functionalization through maleic anhydride and dicumyl peroxide.* Journal of Vinyl and Additive Technology, 2020, 27(2), p. 308–318.

[78] C. Ararat and E. Murillo. *Evaluation of the structural, thermal, rheological and morphological properties of polyethylene functionalized with a maleinized hyperbranched polyester*. in *Journal of Physics: Conference Series*. 2019. San José de Cúcuta, Colombia: IOP Publishing. p. 012069.

[79] O. Gordobil, R. Moriana, L. Zhang, J. Labidi, and O. Sevastyanova. *Assesment of technical lignins for uses in biofuels and biomaterials: Structure-related properties, proximate analysis and chemical modification.* Industrial Crops and Products, 2016, 83, p. 155-165.

BLOCK 2

IV.2. Biopolymeric materials from poly(ester) matrices combined with natural additives, fillers, and nanofillers.

Adaptado del artículo

IV.2.1. Tailoring the properties of thermo-compressed polylactide films for food packaging applications by individual and combined additions of lactic acid oligomer and halloysite nanotubes

Sandra Rojas-Lema[1], Luis Quiles-Carrillo[1], Daniel Garcia-Garcia[1], Beatriz Melendez-Rodriguez[2], Rafael Balart[1], and Sergio Torres-Giner[2].

[1] Technological Institute of Materials (ITM), Universitat Politècnica de València (UPV), Plaza Ferrándiz y Carbonell 1, 03801 Alcoy, Spain.

[2] Novel Materials and Nanotechnology Group, Institute of Agrochemistry and Food Technology (IATA), Spanish National Research Council (CSIC), Calle Catedrático Agustín Escardino Benlloch 7, 46980 Paterna, Spain.

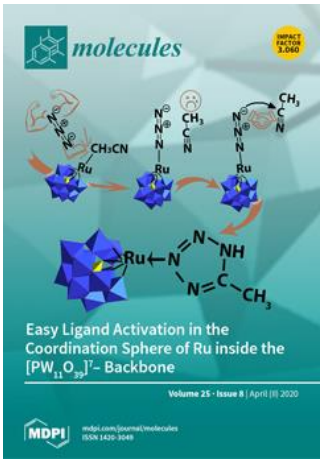

Molecules

2020, 25(8), p. 1976.

molecules

MDPI

Article

Tailoring the Properties of Thermo-Compressed Polylactide Films for Food Packaging Applications by Individual and Combined Additions of Lactic Acid Oligomer and Halloysite Nanotubes

Sandra Rojas-Lema [1], Luis Quiles-Carrillo [1], Daniel Garcia-Garcia [1], Beatriz Melendez-Rodriguez [2], Rafael Balart [1] and Sergio Torres-Giner [2,*]

[1] Technological Institute of Materials (ITM), Universitat Politècnica de València (UPV), Plaza Ferrándiz y Carbonell 1, 03801 Alcoy, Spain; sanrole@epsa.upv.es (S.R.-L.); luiquic1@epsa.upv.es (L.Q.-C.); dagarga4@alumni.upv.es (D.G.-G.); rbalart@mcm.upv.es (R.B.)

[2] Novel Materials and Nanotechnology Group, Institute of Agrochemistry and Food Technology (IATA), Spanish National Research Council (CSIC), Calle Catedrático Agustín Escardino Benlloch 7, 46980 Paterna, Spain; beatriz.melendez@iata.csic.es

* Correspondence: storresginer@iata.csic.es; Tel.: +34-963-900-022

Academic Editors: Alfonso Jimenez and María del Carmen Garrigós
Received: 14 April 2020; Accepted: 22 April 2020; Published: 23 April 2020

check for updates

Abstract: In this work, films of polylactide (PLA) prepared by extrusion and thermo-compression were plasticized with oligomer of lactic acid (OLA) at contents of 5, 10, and 20 wt%. The PLA sample containing 20 wt% of OLA was also reinforced with 3, 6, and 9 parts per hundred resin (*phr*) of halloysite nanotubes (HNTs) to increase the mechanical strength and thermal stability of the films. Prior to melt mixing, ultrasound-assisted dispersion of the nanoclays in OLA was carried out at 100 °C to promote the HNTs dispersion in PLA and the resultant films were characterized with the aim to ascertain their potential in food packaging. It was observed that either the individual addition of OLA or combined with 3 *phr* of HNTs did not significantly affect the optical properties of the PLA films, whereas higher nanoclay contents reduced lightness and induced certain green and blue tonalities. The addition of 20 wt% of OLA increased ductility of the PLA film by nearly 75% and also decreased the glass transition temperature (T_g) by over 18 °C. The incorporation of 3 *phr* of HNTs into the OLA-containing PLA films delayed thermal degradation by 7 °C and additionally reduced the permeabilities to water and limonene vapors by approximately 8% and 47%, respectively. Interestingly, the highest barrier performance was attained for the unfilled PLA film plasticized with 10 wt% of OLA, which was attributed to a crystallinity increase and an effect of "antiplasticization". However, loadings of 6 and 9 *phr* of HNTs resulted in the formation of small aggregates that impaired the performance of the blend films. The here-attained results demonstrates that the properties of ternary systems of PLA/OLA/HNTs can be tuned when the plasticizer and nanofiller contents are carefully chosen and the resultant nanocomposite films can be proposed as a bio-sourced alternative for compostable packaging applications.

Keywords: PLA; OLA; HNTs; ultrasound-assisted dispersion; nanocomposites; food packaging

Academic Editors: Alfonso Jimenez and María del Carmen Garrigós

1. Introduction

Most commercial plastic packaging is currently made of non-biodegradable polymers derived from petroleum that is currently causing disposal problems and leakage into the oceans [1]. To solve these environmental issues, recent studies have been directed towards the development osf food

Tailoring the properties of thermo-compressed polylactide films for food packaging applications by individual and combined additions of lactic acid oligomer and halloysite nanotubes

Abstract

In this work, films of polylactide (PLA) prepared by extrusion and thermo-compression were plasticized with oligomer of lactic acid (OLA) at contents of 5, 10, and 20 wt%. The PLA sample containing 20 wt% of OLA was also reinforced with 3, 6, and 9 parts per hundred resin (phr) of halloysite nanotubes (HNTs) to increase the mechanical strength and thermal stability of the films. Prior to melt mixing, ultrasound-assisted dispersion of the nanoclays in OLA was carried out at 100 ºC to promote the HNTs dispersion in PLA and the resultant films were characterized with the aim to ascertain their potential in food packaging. It was observed that either the individual addition of OLA or combined with 3 phr of HNTs did not significantly affect the optical properties of the PLA films, whereas higher nanoclay contents reduced lightness and induced certain green and blue tonalities. The addition of 20 wt% of OLA increased ductility of the PLA film by nearly 75% and also decreased the glass transition temperature (T_g) by over 18 ºC. The incorporation of 3 phr of HNTs into the OLA-containing PLA films delayed thermal degradation by 7 ºC and additionally reduced the permeabilities to water and limonene vapors by approximately 8% and 47%, respectively. Interestingly, the highest barrier performance was attained for the unfilled PLA film plasticized with 10 wt% of OLA, which was attributed to a crystallinity increase and an effect of "antiplasticization". However, loadings of 6 and 9 phr of HNTs resulted in the formation of small aggregates that impaired the performance of the blend films. The here-attained results demonstrate that the properties of ternary systems of PLA/OLA/HNTs can be tuned when the plasticizer and nanofiller contents are carefully chosen and the resultant nanocomposite films can be proposed as a bio-sourced alternative for compostable packaging applications.

Keywords: PLA; OLA; HNTs; ultrasound-assisted dispersion; nanocomposites; food packaging.

INTRODUCTION

Most commercial plastic packaging is currently made of non-biodegradable polymers derived from petroleum that is currently causing disposal problems and leakage into the oceans [1]. To solve these environmental issues, recent studies have been directed towards the development of food packaging materials based on biopolymers that have the two-fold environmental advantage of being biobased, that is, obtained from renewable resources, and biodegradable, that is, disintegrable in controlled compost soil due to their potentially hydrolysable ester bonds [2]. Among them, polylactide (PLA) is nowadays considered the front-runner in the emerging bioplastics market, showing an annual consumption of 140,000 tons within a bioplastics market that is growing by 20–30% each year [3]. Moreover, PLA as well as other thermoplastic biopolymers such polyhydroxyalkanoates (PHAs) and thermoplastic starch (TPS) present good thermal and mechanical properties and they can be melt processed by film and sheet extrusion, injection molding, thermoforming, foaming, fiber spinning, etc. [4, 5]. In particular, the physical properties of PLA are fairly similar to those of petrochemical-based polymers with high strength and low toughness, such as polystyrene (PS) and polyethylene terephthalate (PET) [6]. Current applications of PLA in the food packaging industry include food trays, disposable glasses for cold drinks, lids, and straws, among others [7].

However, in general terms, biopolymers can be either strongly plasticized by sorption of moisture or show, for instance, low-to-medium barrier properties to gases and aroma [8]. In particular, the main performance drawbacks of PLA are mainly associated to its low thermal resistance, excessive brittleness, and insufficient barrier to oxygen and water compared to other benchmark packaging polymers like PET [9]. It is, thus, of great industrial interest to increase the overall performance of biopolymers in order to generate 'added value' arguments to counteract their current pricing and enable the substitution for more established petrochemical polymers. In this context, the use of novel plasticizers and nanoclays has a significant potential to enhance the physical performance of PLA materials. In this context, lactic acid oligomer (OLA) has been proposed as an alternative to common plasticizers for producing flexible films of PLA by taking advantage of their similar chemical structure and renewable origin [10]. Thus, amounts from 10 to 30 wt% of OLA are required to provide a substantial reduction of

the PLA's glass transition temperature (T_g) as well as to obtain adequate mechanical properties for films manufacturing [11, 12]. For instance, it was reported that 20 wt% of OLA improves substantially ductility with a significant decrease in T_g [13].

In the large field of nanotechnology, polymer matrix based nanocomposites have become a prominent area of current research and development [14]. There are several types of nanoclays that can be utilized to prepare PLA nanocomposites such as montmorillonite (MMT), sepiolite, cellulose nanowhiskers (CNWs), graphene nanoplatelets (GNPs), carbon nanotubes (CNTs) or halloysite nanotubes (HNTs), among others [15]. Nanofillers can promote higher improvements at lower contents (≤5 wt%) over classical fillers due to their high aspect ratio since at least one filler dimension is below 100 nm. This morphology renders a high surface area by which their reinforcement efficiency can match that of microcomposites with 40–50 wt% of loadings. Although HNTs have been less studied than layered silicates, this nanoclay offers unique properties for food packaging applications such as natural origin, abundant availability, low density, non-toxic characteristics, low cost (~0.45 USD g^{-1}), and high rigidity [16]. More interestingly, HNT offers easy dispersability due to the low density of hydroxyl (–OH) groups on the surface [17]. This nanoclay consists on natural aluminosilicate ($Al_2Si_2O_5(OH)_4 \cdot 2H_2O$) crystallites in which the hollow tubular morphology is formed by layer rolling. In particular, HNT displays a high aspect ratio with nanotube length up to 15 μm with internal and external diameters in the ranges of 10–100 nm and 20–200 nm, respectively [18, 19]. Moreover, halloysite is chemically similar to kaolinite and exhibits a predominantly hollow tubular structure with multiple siloxane (Si–O) groups located at the external surface [20]. Compared to MMT, there are only weak secondary interactions between adjacent tubes via hydrogen bonds and Van der Waals forces and, therefore, no organomodification is habitually needed to achieve a homogeneous dispersion of HNTs in condensation polymers [21]. Besides, HNT exhibits high-cation exchange capability, thus it has high possibility to form hydrogen bonds by combination of their oxygen atoms with the hydrogen atoms from PLA [22].

Polymer nanocomposites containing HNTs have been prepared either via water solution mixing or melt blending due to they can be easily separated in polymer molten by shear based on their excellent hydrophilicity [23]. There are a few studies in the scientific literature reporting the incorporation of HNTs into PLA by different melt routes. For instance, Murariu *et al.* [24] reported a reinforcing phenomenon on PLA by

using HNTs surface-treated by silanization with 3-(trimethoxysilyl) propyl methacrylate (TMSPM) and noticeable improvements in tensile strength were observed. Later, Liu *et al.* [25] prepared PLA/HNTs composites by melt compounding and injection molding. Hydrogen bonding interaction between PLA and HNTs was reported, showing a significant increase in tensile, flexural, and impact properties by nanocomposites prepared by melt compounding. PLA/HNTs composite foams were prepared by Wu *et al.* [26] by means of batch processing method using supercritical carbon dioxide (Sc-CO_2) as physical blowing agent. The addition of 5 wt% HNTs increased the cell density and reduced the mean cell size. In another study, Prashantha *et al.* [27] incorporated quaternary ammonium salt with benzoalkonium chloride treated HNTs into PLA in a high shear twin-screw extruder using masterbatch dilution process, showing improvements in the mechanical properties due to the better interfacial compatibility induced by the modification of the nanotube surface. Stoclet *et al.* [28] compared the thermomechanical and flame retardant properties of PLA/HNTs nanocomposites prepared using a water-assisted extrusion process and conventional extrusion process. It was found that the injection of water into the polymer melt induced a better dispersion of the HNTs into the PLA matrix and also prevented polymer degradation during the extrusion due to a barrier effect of the water molecules that preferentially locate at the HNT–PLA interface.

However, the improvement in the properties is not only related to the nanofiller content but also to the dispersion of HNTs in the PLA and the interaction between HNTs and PLA. De Silva *et al.* [29] prepared PLA/HNTs films by solution casting method to ascertain their properties for packaging applications. It was observed that the films reinforced with 5 wt% of HNTs yielded the optimum results due to a better interfacial adhesion between HNTs and PLA, while at higher loadings the nanotubes highly aggregated and the mechanical properties were slightly inferior. Similarly, Othman *et al.* [30] analyzed the effect of incorporating different concentrations (0–5 wt%) of HNTs and glycerol on the mechanical and thermal properties of the nanocomposites. It was found that the addition of 3 wt% HNTs yielded the optimum mechanical properties due to the uniform distribution and dispersion of the nanoclays, while the addition of glycerol plasticized the nanocomposites to improve their processability. More recently, Risyon *et al.* [31] studied the effect of varying the nanoclays content on the properties of PLA films aimed to food packaging applications. The optimum concentration of HNTs was also

3 wt% and the resultant nanocomposites films demonstrated potential to extend the shelf life of packaged cherry tomatoes.

Being focused on the particular case of food packaging applications, this study reports whether the performance of PLA formulations can be tailored by the single and dual addition of OLA and HNTs. To this end, the HNTs were previously ultrasonicated in OLA liquid at mild temperature to improve their dispersion and the films were prepared by thermo-compression. The optical, morphological, thermal, mechanical, and barrier properties of the resultant binary and ternary systems of PLA/OLA and PLA/OLA/HNTs films were analyzed and related to their compositions.

RESULTS AND DISCUSSION

Optical properties of the PLA/OLA/HNTs films

The appearance of the PLA films obtained by thermo-compression after the individual addition of OLA and combined addition of OLA with HNTs are gathered in **Figure IV.2.1.1**. A simple naked eye observation of these images reveals that the transparency and color characteristics of the PLA film were not affected by the addition of OLA. However, when HNTs were incorporated, the films became a little more opaque and slightly yellow, although they were still contact transparent.

Table IV.2.1.1 gathers the L*, a*, b* coordinate values and the color difference (ΔE_{ab}*) between the neat PLA film and the PLA/OLA blend films and PLA/OLA/HNTs composite films. In the case of the PLA/OLA films, all samples yielded very similar color parameters than the neat PLA film, showing slightly higher values for the color coordinate b* (blue to yellow). In particular, b* increased from −0.48, for the neat PLA film, up to –0.22, for the PLA blend film with 20 wt% of OLA, whereas the L* (luminance) and a* (green to red) were 30.24 and −0.3, respectively, thus showing no significant difference ($p < 0.05$). Thus, the PLA/OLA films were slightly yellowish but color variation remained unnoticeable (ΔE_{ab}* < 1), which is in agreement with previous optical studies about plasticized PLA materials by OLA [11].

Figure IV.2.1.1. Visual aspect of the polylactide (PLA)/oligomer of lactic acid (OLA)/halloysite nanotubes (HNTs) films.

However, the incorporation of HNTs progressively reduced lightness and slightly induced certain green and blue tonalities to the PLA films. In particular, for the PLA/OLA composite filled with 9 parts per hundred resin (phr) of HNTs, L* increased to 38.19 whereas a* and b*, respectively decreased to −1.27 and −2.31. In the case of the

PLA/OLA composite film with the lowest nanofiller content, that is 3 phr of HNTs, ΔE_{ab}* was 1.65, so that only an experienced observer could notice the color difference (ΔE_{ab}* ≥ 1 and <2). In general, the color differences increased for the PLA/OLA films with loadings of 6 phr and 9 phr of HNTs. In particular, the ΔE_{ab}* values were 5.15 (noticeable color difference, ΔE_{ab}* ≥ 3.5 and < 5), and 7.68 (different colors, ΔE_{ab}* ≥ 5), respectively. The significant color change induced in the PLA/OLA films can be ascribed to the titanoferrous impurities naturally present in HNT [32]. In any case, the contact transparency was preserved and the resultant nanocomposite films can be of interest for food packaging applications [33, 34].

Table IV.2.1.1. Color parameters (L*, a*, b*) and color difference (ΔE_{ab}*) of the polylactide (PLA)/oligomer of lactic acid (OLA)/halloysite nanotubes (HNTs) films.

Film	L*	a*	b*	$\Delta E_{a,b}$*
PLA	30.79 ± 0.31^{a}	−0.32 ± 0.06^{a}	−0.48 ± 0.03^{a}	-
PLA + 5% OLA	30.67 ± 0.27^{a}	−0.38 ± 0.04^{a}	−0.30 ± 0.09^{b}	0.36 ± 0.03^{a}
PLA + 10% OLA	30.36 ± 0.15^{a}	−0.25 ± 0.05^{a}	−0.15 ± 0.08^{c}	0.64 ± 0.09^{b}
PLA + 20% OLA	30.24 ± 0.03^{a}	−0.30 ± 0.06^{a}	−0.22 ± 0.08^{bc}	0.66 ± 0.08^{b}
PLA + 20% OLA + 3% HNTs	32.35 ± 0.06^{b}	−0.61 ± 0.04^{b}	−0.89 ± 0.05^{d}	1.65 ± 0.25^{c}
PLA + 20% OLA + 6% HNTs	35.72 ± 0.27^{c}	−1.01 ± 0.02^{c}	−1.76 ± 0.11^{e}	5.15 ± 0.48^{d}
PLA + 20% OLA + 9% HNTs	38.19 ± 0.64^{d}	−1.27 ± 0.13^{d}	−2.31 ± 0.15^{f}	7.68 ± 0.39^{e}

$^{a–f}$ Different letters in the same column indicate a significant difference among the samples (p < 0.05).

Morphology of the PLA/OLA/HNTs films

Figure IV.2.1.2 shows the transmission electron microscopy (TEM) micrographs of the HNTs after ultrasonication. **Figure IV.2.1.2**a shows the morphology of one isolated HNT in which it is possible to distinguish the tubular structure of the nanoclay. Measurements taken on this TEM micrograph revealed that a single HNT presents a wall of 17.3 nm that is formed by rolled aluminosilicate layers (see inset with zoomed-in TEM image within **Figure IV.2.1.2**a) with a tubular shape sizing 23.4 nm in diameter due to the differential specific volume between both sides of the layer and the lumen. The particular shape of HNTs can also be clearly seen in **Figure IV.2.1.2**b, showing that lumen diameters were comprised between 19.5–26.9 nm. As also observed in this TEM image, even after ultrasonic treatment in acetone using a low viscosity medium, HNTs still tended to form aggregates due to presence of –OH groups [18, 19]. However, Rong

et al. [35] reported that ultrasonication is effective for breaking HNT bundles, although the nanotube's length can also be reduced at high power and long times. Therefore, HNTs can be easily dispersed in low viscosity polar solvents, but their dispersion in hydrophobic polymers with high melt viscosity is not straightforward.

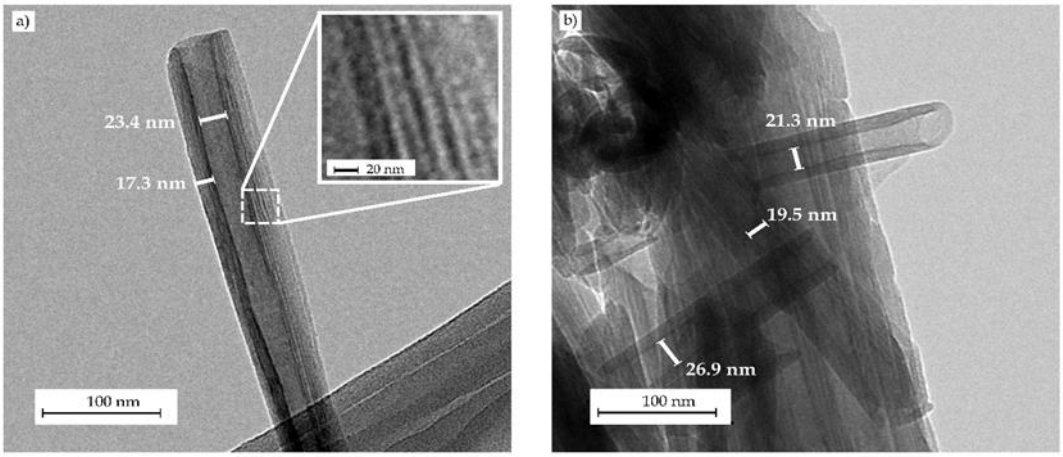

Figure IV.2.1.2. Transmission electron microscopy (TEM) images corresponding to (a) individual isolated halloysite nanotube (HNT) and (b) aggregate of HNTs. Images were taken at 52,000x showing scale markers of 100 nm.

Figure IV.2.1.3 gathers the field emission scanning electron microscopy (FESEM) images taken at 2,000x of the cryo-fractured surfaces of the PLA films containing different OLA loadings. **Figure IV.2.1.3**a shows the morphology attained for the neat PLA film in which a smooth and homogeneous surface with some microcracks and large filaments can be observed. This type of fracture suggests that the film was brittle, although certain plastic deformation also occurred. One can observe in **Figure IV.2.1.3**b that the addition of 5 wt% of OLA did not modify the type of fracture, nevertheless, the presence of microcracks was lower and some plastic flow lines can be observed, which suggests increased ductile properties. However, contents of 10 wt% and 20 wt% of OLA, respectively shown in **Figure IV.2.1.3**c,d, yielded to a rough surface with multiple macrocracks and thin plastic filaments. As also observed in our previous study [36], the presence of OLA successfully inhibited microcrack formation and the cracks grew to a greater extent, thus suggesting that the film absorbed more energy and deformed more intensively during fracture. It should be noted that no sign of phase separation could be detected since PLA and OLA have the same chemical structure. In particular, PLA and OLA show very similar solubility parameters, that is, 19.5 $(J\ cm^3)^{1/2}$ and 17.7 $(J\ cm^3)^{1/2}$ for the biopolymer and its oligomer, respectively, indicating that they are miscible at

high ratios [10]. Furthermore, no evaporation of the OLA plasticizer or vapor release from the blends was observed during film formation at high temperatures and pressures, indicating that their thermal stability was enough for melt processing.

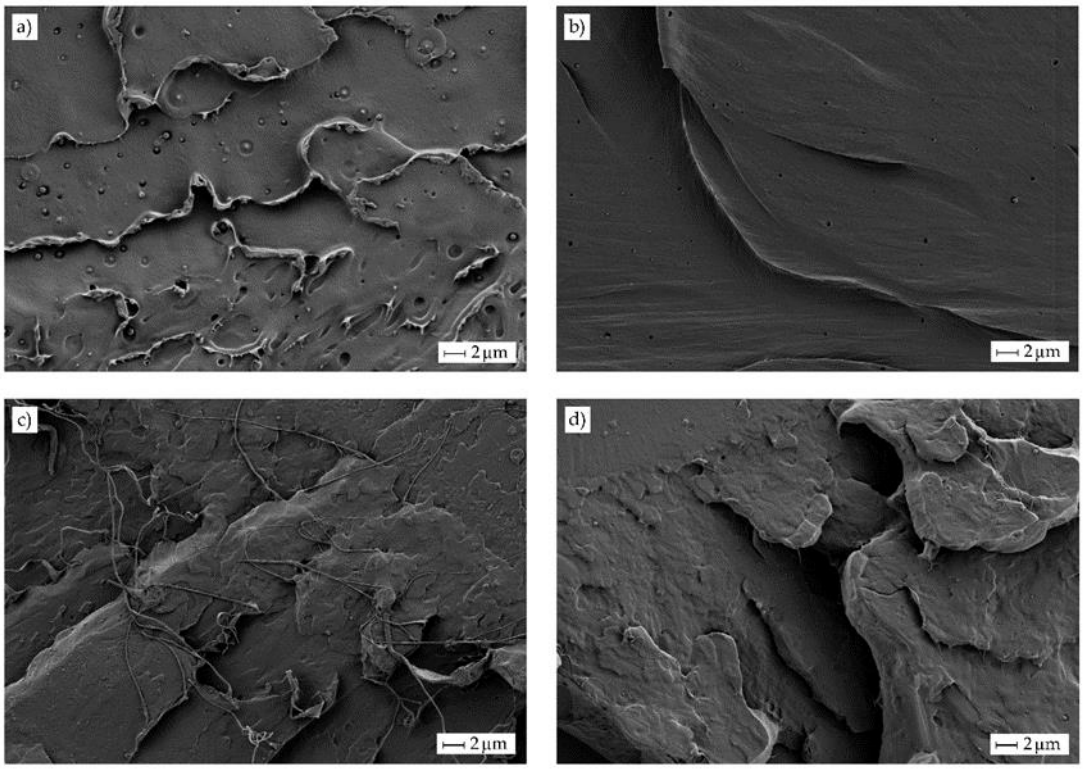

Figure IV.2.1.3. Field emission scanning electron microscopy (FESEM) images of the fracture surfaces of the polylactide (PLA) films with different weight contents (wt%) of oligomer of lactic acid (OLA): (a) PLA; PLA + 5 wt% OLA; (c) PLA + 10 wt% OLA; (d) PLA + 20 wt% OLA. Images were taken at 2,000× showing scale markers of 2 µm.

Particle dispersion is a key factor when using nanoparticles. This problem is much more pronounced for highly hydrophilic nanoparticles such as HNTs, which tend to form aggregates by conventional melt blending. **Figure IV.2.1.4** shows a comparative study performed by FESEM on the fracture surfaces of the PLA/OLA films filled with 20 wt% of OLA and 6 phr of HNTs with two dispersion procedures prior to melt compounding. The images corresponding to the nanocomposite films prepared using HNTs dispersed by conventional magnetic stirring in OLA are shown in **Figure IV.2.1.4**a,b. The second process consisted on ultrasonication in OLA heated at 100 ^{o}C, to reduce its viscosity, and the fracture surfaces of the resultant nanocomposite films are included in **Figure IV.2.1.4**c,d. As one can see, the conventional process with magnetic stirring did not allow good dispersion and micro-aggregates sizing approximately 18 µm x 7 µm were enclosed in the PLA/OLA matrix. Furthermore, a poor interaction

between the aggregate and the surrounding PLA/OLA matrix can be observed due to the large particle size. As opposite, good nanoparticle dispersion was attained in the surface fractures of the nanocomposite films obtained with HNTs previously ultrasonicated.

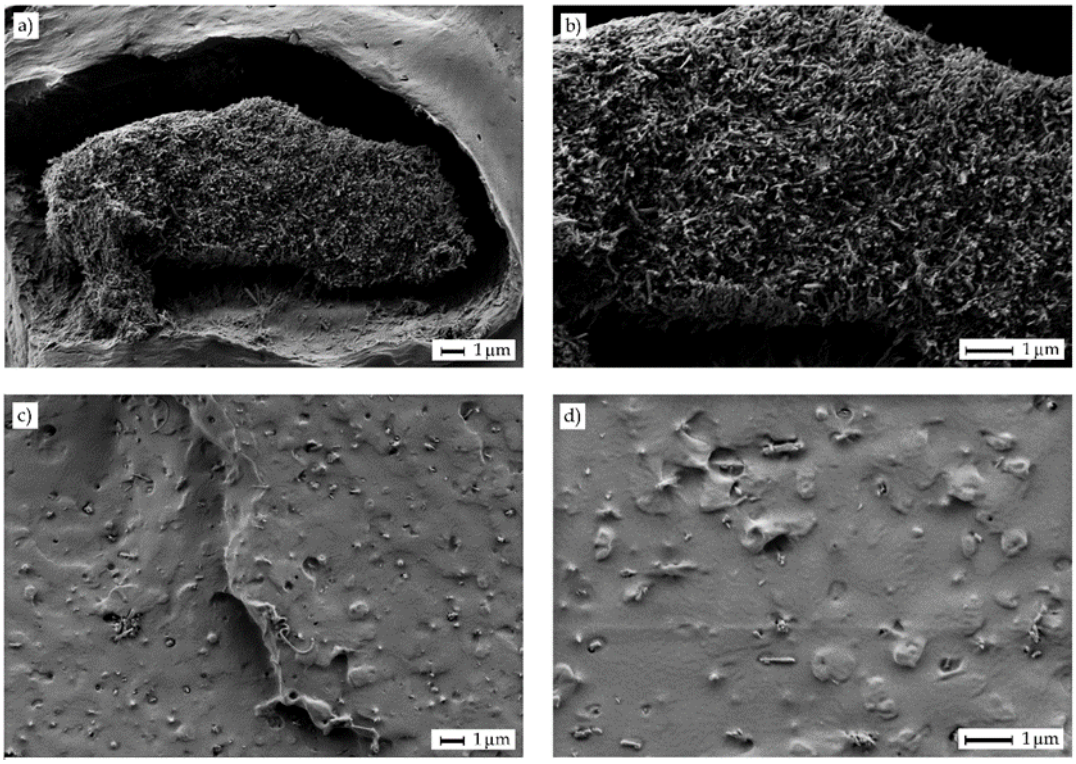

Figure IV.2.1.4. Field emission scanning electron microscopy (FESEM) images of the fracture surfaces of the polylactide (PLA) films containing 20 wt% of oligomer of lactic acid (OLA) and 6 parts per hundred resin (phr) of halloysite nanotubes (HNTs): (a,b) HNTs were dispersed in OLA by magnetic stirring; (c,d) HNTs were ultrasonicated in OLA at 100 ºC. Images on the left were taken at 5,000x, while images on the right at 10,000x. Scale markers at both magnifications represent 1 µm.

The usefulness of ultrasonication in OLA medium for the HNTs dispersion in PLA was further assessed as a function of the nanoclay content. **Figure IV.2.1.5** gathers the FESEM images taken at 5,000x of the surface fractures of the PLA films containing 20 wt% of OLA and different HNTs loadings. The type of fracture surface observed in the PLA film, shown in **Figure IV.2.1.5**a, was kept for all the ternary system films combining OLA and HNTs. Efficient dispersion of HNTs can be seen in **Figure IV.2.1.5**b when 3 phr of HNTs was incorporated into the PLA/OLA matrix (see white arrows). The homogeneous dispersion of HNTs can be related to their good affinity with both PLA and OLA. High interactions between the biopolymer and nanoclay are known to take place by the formation of hydrogen bonds between the terminal –OH groups of

PLA and the Si–OH groups of HNTs [21] and also between the oxygen atoms of the carboxyl (–COOH) group of PLA and the hydrogen atoms of the –OH groups present in HNTs [25]. Furthermore, the negative charges of the oxygen atoms on the HNTs surface can attract the positive charges of the hydrogen atoms on the PLA/OLA matrix [28], thus potentially forming new hydrogen bonds.

Figure IV.2.1.5c, corresponding to composite film filled with 6 phr of HNTs, a combination of domains with well-dispersed HNTs (white arrows) and some small HNTs aggregates (white ellipses) in the 0.5–1.0 μm range can be observed. It is worthy to note that, even though some aggregates were formed, the original aggregate size of HNTs, sizing 18 μm in length and 7 μm in width, was remarkably reduced after the ultrasound-assisted dispersion process. Finally, a greater number of large aggregates were noticed in the FESEM micrograph for the fracture surface of the PLA/OLA film filled with 9 phr of HNTs, which is included in **Figure IV.2.1.5**d. The dispersion of this nanocomposite film was also observed using a focused ion beam scanning electron microscopy (FIB-SEM) equipped with tridimensional (3D) tomography. The resultant Video S1 (see Supplementary information) taken by electron microscopy tomography (EMT) also demonstrated that, in this nanocomposite sample, nanotubes were highly dispersed within the PLA/OLA matrix but large aggregates or bundles of several microns were also formed. Moreover, many little cavities or micro-voids can be observed in the FESEM image, which led to a porous-like surface and suggests that the dispersed HNTs did not break but pulled out of the matrix during cryo-fracture. This finding has already been described by De Silva *et al.* [37], who correlated nanotubes pullout to their poor interfacial adhesion with the PLA matrix. This observation was also clearly detectable when the nanofiller contents were above 5 wt%, regardless of the processing method and it also intensified for high HNTs loadings [29].

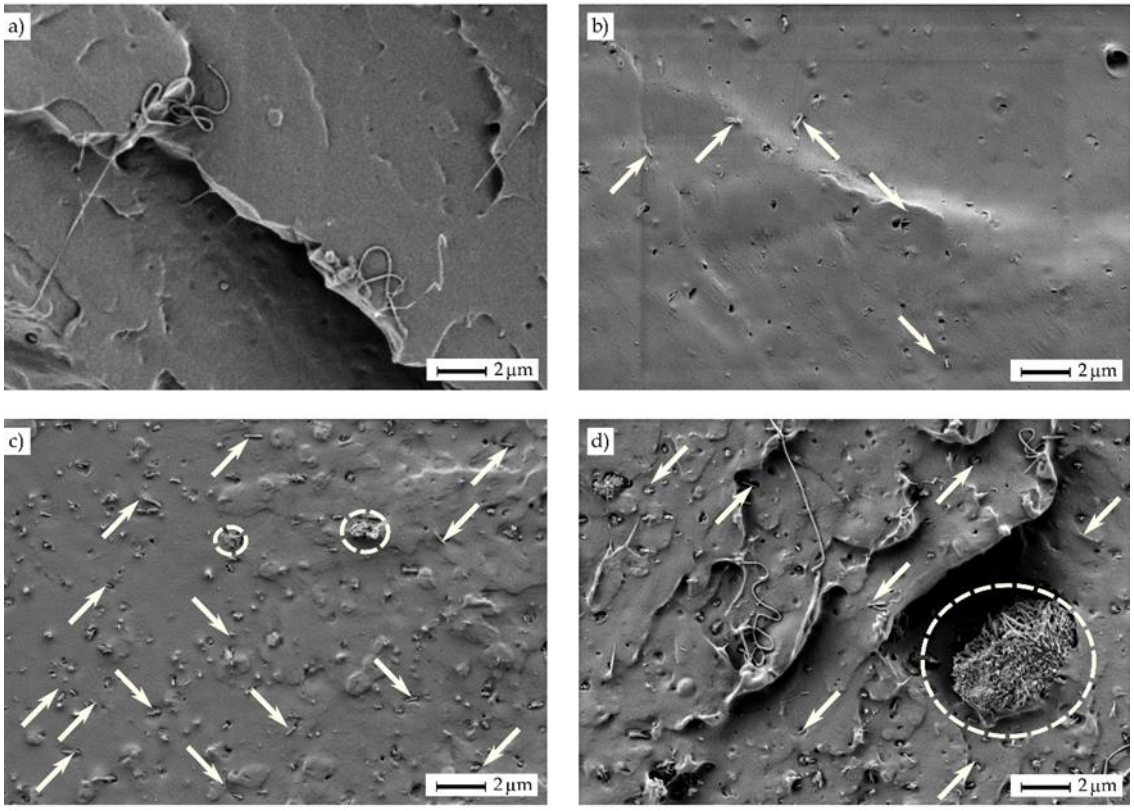

Figure IV.2.1.5. Field emission scanning electron microscopy (FESEM) images of the fracture surfaces of the polylactide (PLA) films containing 20 wt% of oligomer of lactic acid (OLA) and different parts per hundred resin (phr) of halloysite nanotubes (HNTs): (a) PLA; (b) PLA + 20 wt% OLA + 3 phr HNTs; PLA + 20 wt% OLA + 6 phr HNTs; (d) PLA + 20 wt% OLA + 9 phr HNTs. Images were taken at 5,000x with scale markers of 2 µm.

Mechanical properties of the PLA/OLA/HNTs films

Table IV.2.1.2 gathers the results of the tensile tests of the thermo-compressed films of neat PLA, PLA/OLA, and PLA/OLA/HNTs composites. In relation to the neat PLA, one can observe that the film showed mechanical properties of a hard but brittle material with values of tensile elastic modulus (E_t) of 2846.3 MPa, tensile strength at yield (σ_y) of 54.3 MPa, and elongation at break (ε_b) of 3.52%. As one expected, the addition of OLA resulted in a plasticization of the PLA film, yielding a significant increment in the flexibility and a decrease in tensile strength. In particular, the ε_b values gradually increased to 3.99%, 5.69%, and 6.14%, for OLA contents of 5, 10, and 20 wt%, respectively, while σ_y was reduced to 53.5, 49.1, and 42.3 MPa. In the case of the PLA film containing 10 and 20 wt% of OLA, this represents an increase in ductility of nearly 62% and 75%, respectively. One can also observe that the E_t values also decreased, which can be directly related to the combined decrease in rigidity and the increase in ductility, since the tensile modulus represents the stress (σ) to strain (ε) ratio in the linear (elastic)

region. A similar effect was reported by Armentano *et al.* [11], for PLA blends with poly(3-hydroxybutyrate) (PHB) incorporating different amounts of OLA. At plasticizer contents of 20 and 30 wt%, ε_b increased approximately by 57% and 164%, respectively. In another study, Burgos *et al.* [10] also showed that PLA/OLA blends at 20–25 wt% of plasticizer yielded up to 75-fold increases in ductility compared to neat PLA, thus suggesting that the type of OLA has high influence on the final ductile properties. The behavior observed was explained by the reduction of the macromolecular chains cohesion when the OLA plasticizer lubricates the PLA matrix. In this regard, Martin and Avérous [13] found that 20 wt% of OLA reduced E_t by 63% whereas ε_b increased up to 200%. However, our recent study reported that the use of impact-modifier type of OLA unexpectedly reduced the ductility of injection-molded pieces of PLA due to it rather acted as rubber-like filler in the PLA matrix [36]. Therefore, the different values attained can be mainly related to the OLA type since the here-used grade is mainly aimed to plasticize biopolyesters and it will be discussed later.

Table IV.2.1.2. Mechanical properties of the polylactide (PLA)/oligomer of lactic acid (OLA)/halloysite nanotubes (HNTs) films in terms of elastic modulus (E_t), strength at yield (σ_y), and elongation at break (ε_b).

Film	E_t (MPa)	σ_y (MPa)	ε_b (%)
PLA	2846.3 ± 137^{a}	54.3 ± 0.9^{a}	3.52 ± 0.2^{a}
PLA + 5% OLA	2745.6 ± 146^{a}	53.5 ± 1.0^{a}	3.99 ± 0.5^{a}
PLA + 10% OLA	2532.8 ± 103^{b}	49.1 ± 0.7^{b}	5.69 ± 0.3^{b}
PLA + 20% OLA	2469.4 ± 112^{b}	42.3 ± 0.9^{c}	6.14 ± 0.3^{b}
PLA + 20% OLA + 3% HNTs	2854.1 ± 103^{a}	57.8 ± 1.0^{d}	4.23 ± 0.2^{c}
PLA + 20% OLA + 6% HNTs	2927.6 ± 105^{a}	47.8 ± 1.1^{b}	3.74 ± 0.4^{a}
PLA + 20% OLA + 9% HNTs	2651.3 ± 102^{ab}	39.1 ± 1.3^{e}	3.16 ± 0.6^{d}

$^{a–e}$ Different letters in the same column indicate a significant difference among the samples ($p < 0.05$).

With regards to the PLA/OLA/HNTs composite films, one can observe that the incorporation of 3 and 6 phr of HNTs progressively increased the E_t and σ_y values whereas ε_b significantly decreased. At the highest nanofiller content, that is, 9 phr of HNTs, all the mechanical parameters drastically decreased. Therefore, the highest mechanical performance was attained for the PLA/OLA film containing 3 phr of HNTs, reaching E_t, σ_y, and ε_b values of 2854.1 MPa, 57.8 MPa, and 4.23%, respectively, and thus outperforming the neat PLA film. These findings point out that the mechanical

properties of the PLA/OLA/HNTs nanocomposite films were affected by the nanofiller content, which can be related to the dispersion of the HNTs in the PLA/OLA matrix observed above during the morphological analysis. Similar findings were reported, for instance, by De Silva *et al.* [29], who found that σ_y of solution-casted PLA films increased by 40% with increasing HNTs up to 5 wt% whereas contents of 10 wt% decreased the strength of the composites. In another studies, Othman *et al.* [30, 38] showed that 3 wt% of HNTs resulted in the optimal mechanical properties due to the uniform distribution or dispersion of the nanoclay, whereas contents above 5 wt% led to agglomeration. Risyon *et al.* [31] also found that the optimum concentration of HNTs in PLA films was 3 wt% since it led to higher numbers of hydrogen bonds between PLA and HNTs compared to the films loaded with higher concentrations of HNTs, which provided higher mechanical resistance and rigidity but also restricted the mobility of the PLA chains and thus reduced ductility of the PLA films. Therefore, the properties attained herein are in agreement with previous studies, showing that the optimum loading content of HNT in PLA is 3 phr. However, it is also worth noting that the mechanical properties were also enhanced for a content of 6 phr of HNTs, which suggests that the presence of OLA could potentially favor the dispersion of slightly higher amount of nanofiller by plasticizing the PLA matrix.

Thermal properties of the PLA/OLA/HNTs films

Figure IV.2.1.6 shows the differential scanning calorimetry (DSC) thermograms collected during the second heating of the thermo-compressed PLA films. **Table IV.2.1.3** gathers the average values of the main thermal transitions obtained from the DSC curves. The enthalpies associated with the cold crystallization and the melting processes are also reported in the table. In the 60–70 ^{o}C range, one can observe a step change in the base lines, which corresponds to the T_g of PLA. This second-order thermal transition was located at 62.5 ^{o}C for neat PLA. The exothermic peaks located between 100 ^{o}C and 125 ^{o}C correspond to the cold crystallization temperature (T_{cc}) of PLA. In the case of the neat PLA film, this peak showed a low intensity and it was located at 121.2 ^{o}C. Finally, in the thermal range of 140–160 ^{o}C, the crystalline PLA domains melted. One can observe in the thermogram of the neat PLA that the melting process occurred in a single endothermic peak, centered at 150.8 ^{o}C. In addition to the characteristic values of T_g, T_{cc}, and, T_m, the enthalpies corresponding to the cold crystallization (ΔH_{cc}) and melting (ΔH_m) were collected from the DSC curves. The latter parameter was determined to

ascertain the maximum degree of crystallinity ($X_{c\ max}$), resulting in a value of approximately 18% for the neat PLA film. This parameter gives more information about the effect of the additives on PLA since it does not consider the crystals formed during cold crystallization.

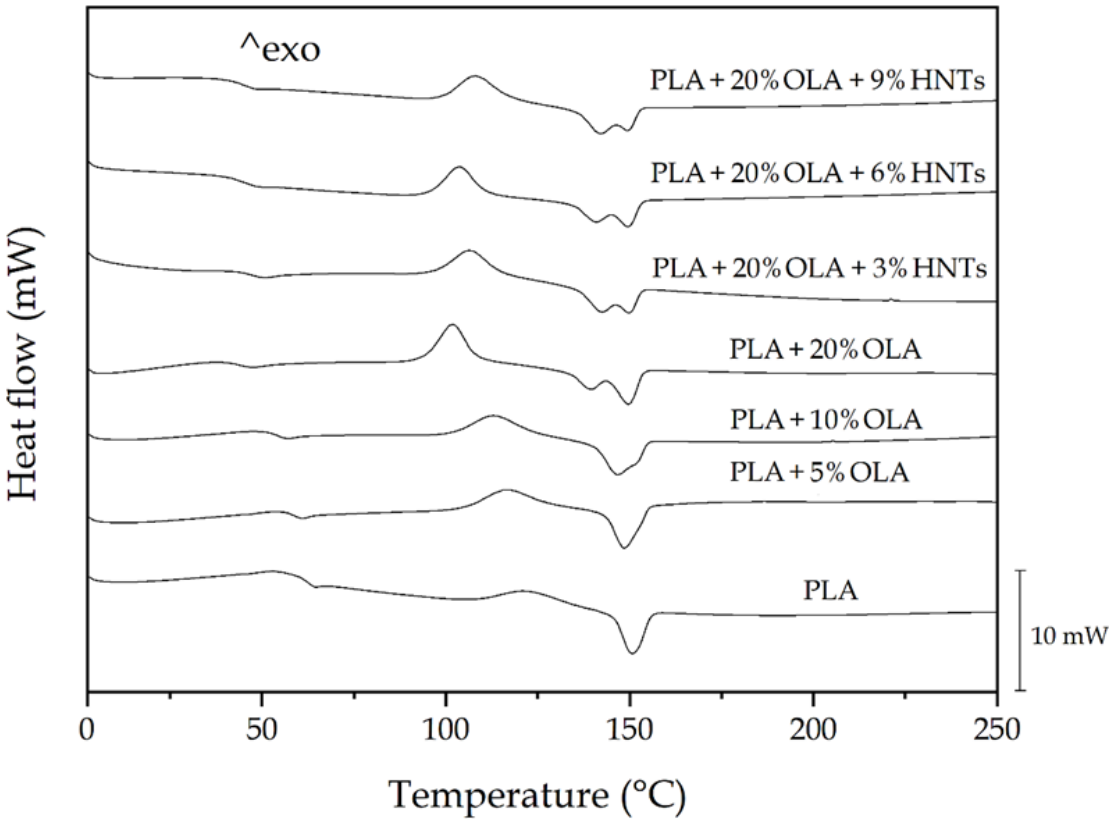

Figure IV.2.1.6. Differential scanning calorimetry (DSC) thermograms taken during second heating of the polylactide (PLA)/oligomer of lactic acid (OLA)/halloysite nanotubes (HNTs) films.

The addition of OLA produced a gradual and significant reduction of all the thermal values observed by DSC, that is, T_g, T_{cc}, and T_m. The more intense reduction was attained for T_g, due to the plasticizing effect of OLA, showing values of 58.7, 54.3, and 43.9 °C for the films containing 5, 10, and 20 wt%, respectively. Similar reductions have been reported in previous studies [12, 13], indicating that the addition of 10–20 wt% of OLA to PLA induced a decreased in T_g in the 20–40 °C range. Furthermore, the presence of a single T_g, located between that of PLA and OLA, being the latter reported in the 10–30 °C range [39], suggests that the biopolymer and its oligomer were fully miscible at all the given composition studied here.

Table IV.2.1.3. Thermal properties of the polylactide (PLA)/oligomer of lactic acid (OLA)/halloysite nanotubes (HNTs) films in terms of glass transition temperature (T_g), cold crystallization temperature (T_{cc}), melting temperature (T_m), cold crystallization enthalpy (ΔH_{cc}), melting enthalpy (ΔH_m), and degree of crystallinity ($X_{c\ max}$).

Film	T_g (°C)	T_{cc} (°C)	T_m (°C)	ΔH_{cc} (J g^{-1})	ΔH_m (J g^{-1})	$X_{c\ max}$ (%)
PLA	62.5 ± 0.6[a]	121.2 ± 0.8[a]	150.8 ± 0.5[a]	6.98 ± 0.8[a]	16.80 ± 0.5[a]	18.06 ± 0.51[a]
PLA + 5% OLA	58.7 ± 0.5[b]	116.1 ± 0.4[b]	148.7 ± 0.3[b]	15.92 ± 0.4[b]	20.68 ± 0.3[b]	23.41 ± 0.32[b]
PLA + 10% OLA	54.3 ± 0.6[c]	112.8 ± 0.7[c]	146.9 ± 0.4[c]	17.03 ± 0.4[c]	21.63 ± 0.4[c]	25.84 ± 0.54[c]
PLA + 20% OLA	43.9 ± 0.8[d]	101.9 ± 0.6[d]	138.8 ± 0.6[d] / 150.0 ± 0.5[a]	25.63 ± 0.6[d]	26.20 ± 0.6[d]	35.21 ± 0.45[d]
PLA + 20% OLA + 3% HNTs	46.9 ± 1.0[e]	106.5 ± 0.4[e]	142.1 ± 0.4[e] / 150.2 ± 0.8[a]	19.13 ± 0.9[e]	22.98 ± 0.7[e]	31.82 ± 0.84[e]
PLA + 20% OLA + 6% HNTs	46.8 ± 0.8[e]	103.6 ± 0.7[de]	141.7 ± 0.8[e] / 149.7 ± 0.3[a]	20.75 ± 0.6[e]	22.26 ± 0.8[e]	31.71 ± 0.62[e]
PLA + 20% OLA + 9% HNTs	47.3 ± 0.9[e]	108.1 ± 0.8[e]	141.1 ± 0.7[e] / 149.4 ± 0.6[a]	20.50 ± 0.5[e]	21.55 ± 0.5[e]	31.57 ± 0.73[e]

[a–e] Different letters in the same column indicate a significant difference among the samples ($p < 0.05$).

The fact that PLA cold crystallized at lower temperature can also be related to the plasticization phenomenon of PLA provided by OLA since it is known to promote the motion of the PLA chains [36]. Other authors have ascribed this effect to a heterogeneous nucleation of the short length OLA molecules by which the cold crystallization process of PLA is favored [40]. In the thermogram of the PLA samples containing 20 wt% of OLA, one can observe the presence of two overlapped peaks. The first one appeared at nearly 139 °C and the second one at 150 °C. This double-peak phenomenon has been ascribed to the coexistence of two different crystal size populations [41] or, more frequently, to crystal reorganization upon melting in biopolyesters [42].

During this process, imperfect crystals melt at lower temperatures and the amorphous regions order into packed spherulites with thicker lamellar thicknesses that, thereafter, melt at higher temperatures. Moreover, broader melting peaks were observed, pointing out to the formation of more heterogeneous crystallites. However, it should be noticed that the T_m value that corresponds to the higher melting peak was

significantly not different than that attained in the neat PLA sample and the other OLA-containing PLA films, suggesting that similar crystallites were formed in all the materials. Furthermore, the $X_{c\ max}$ values increased with the OLA content, which has been previously related to the inherent plasticizing effect of OLA [12, 36]. Therefore, the presence of OLA in the PLA matrix hindered crystallization to some extent by impairing proper chain packing. However, higher amount of biopolyester was able to crystallize due to the enhanced mobility of the PLA chains by the lubricating effect of the oligomer. This result confirms both the high miscibility and interaction between the biopolyester and its oligomer and it opens up the possibility to develop highly crystalline PLA materials.

As opposite to OLA, one can observe that the addition of HNTs shifted the T_g of the PLA/OLA blend to slightly higher values, in the 46–48 ^{o}C range. Moreover, the thermal parameters showed no significant differences ($p > 0.05$) for all the nanocomposites. This result is in agreement with the studies performed by Liu *et al.* [25] and Wu *et al.* [26], who indicated that the filler hinders the movement of the PLA chains. It further supports the delay observed in cold crystallization, which was reduced from nearly 102 ^{o}C, for the unfilled blend, to up to approximately 108 ^{o}C for the nanocomposite film containing 9 phr of HNTs.

Moreover, whereas the melting profile of the blend nearly remained constant irrespective of the amount of nanoclay, showing T_m values in the 140–150 ^{o}C range, the $X_{c\ max}$ values decreased from over 35% to values in the range of 31–32%. While most studies have reported that HNTs act as nucleating agents for PLA [27, 28, 31], the present results indicate that the presence of OLA in the PLA matrix could prevent the crystal growth from the nanoclays surface. This finding also suggests that OLA could be preferentially located in the nanofiller-to-matrix interface due to its higher miscibility with PLA, which can potentially favor HNTs dispersion but also suppresses their nucleation.

Thermogravimetric analysis (TGA) was carried out to study the thermal stability of the PLA/OLA/HNTs blends. **Figure IV.2.1.7** shows the TGA curves of the PLA/OLA/HNTs films, in which **Figure IV.2.1.7**a includes the evolution of the mass with temperature, while **Figure IV.2.1.7**b shows their respective first derivate thermogravimetric (DTG) curves. The thermal stability values extracted from the TGA

curves are summarized in **Table IV.2.1.4**, gathering the temperature required for a loss of weight of 5% ($T_{5\%}$), which is representative for the onset of degradation, the maximum degradation rate temperature (T_{deg}), and the amount of residual mass at 600 ºC.

(**a**)

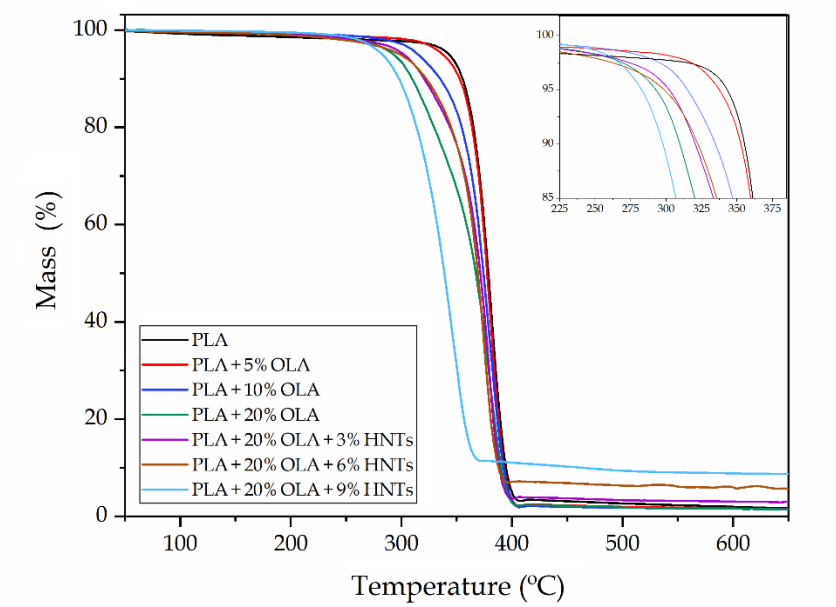

(**b**)

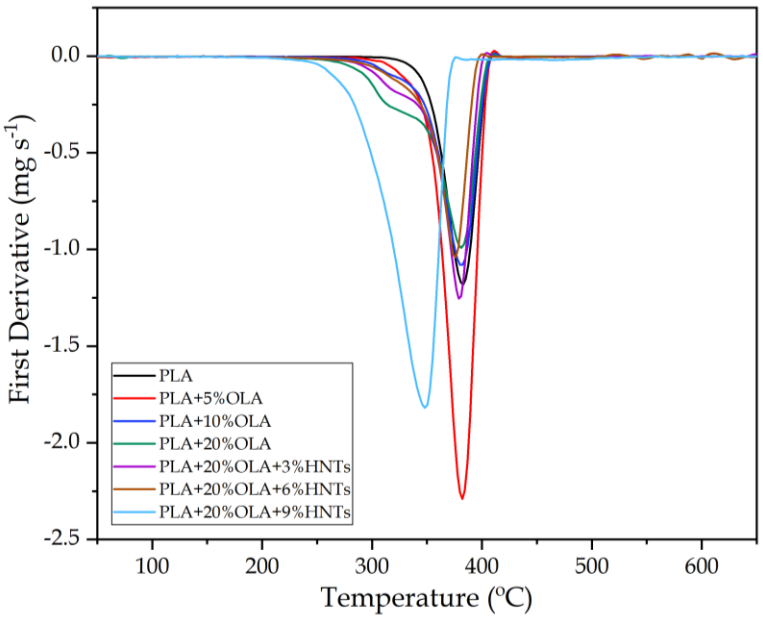

Figure IV.2.1.7. (a) Thermogravimetric analysis (TGA) and (b) first derivate thermogravimetric (DTG) curves of the polylactide (PLA)/oligomer of lactic acid (OLA)/halloysite nanotubes (HNTs) films.

Table IV.2.1.4. Main thermal degradation parameters of the polylactide (PLA)/oligomer of lactic acid (OLA)/halloysite nanotubes (HNTs) films in terms of onset temperature of degradation ($T_{5\%}$), degradation temperature (T_{deg}), and residual mass at 600 °C.

Film	$T_{5\%}$ (°C)	T_{deg} (°C)	Residual mass (%)
PLA	342.2 ± 1.2^{a}	383.0 ± 1.3^{a}	1.9 ± 0.8^{a}
PLA + 5% OLA	335.3 ± 1.0^{b}	382.5 ± 1.0^{a}	1.6 ± 0.6^{b,c}
PLA + 10% OLA	313.3 ± 0.9^{c}	382.4 ± 0.8^{a}	1.6 ± 1.1^{a}
PLA + 20% OLA	292.5 ± 1.2^{d}	381.8 ± 0.9^{a}	1.6 ± 0.9^{c}
PLA + 20% OLA + 3% HNTs	299.5 ± 1.4^{e}	381.0 ± 1.1^{a}	3.1 ± 1.0^{b}
PLA + 20% OLA + 6% HNTs	296.5 ± 0.9^{f}	376.7 ± 0.8^{b}	5.7 ± 0.7^{d}
PLA + 20% OLA + 9% HNTs	282.4 ± 1.1^{g}	348.7 ± 0.7^{c}	8.8 ± 1.2^{e}

$^{a-g}$ Different letters in the same column indicate a significant difference among the samples ($p < 0.05$).

One can observe that neat PLA thermally degraded in a single step in the range from approximately 330 to 400 °C as previously reported by Agüero *et al.* [43]. In particular, the neat PLA film showed respective $T_{5\%}$ and T_{deg} values of 342.2 and 383 °C. The inset image within **Figure IV.2.1.7**a shows that the addition of OLA gradually reduced the thermal stability of PLA, being more intensely for the onset of degradation since the $T_{5\%}$ values gradually reduced to 335.3, 313.3, and 292.5 °C for additions of 10, 20, and 30 wt%, respectively. This is in agreement with previous studies reporting about the thermal stability of PLA/OLA blends [12, 36, 44], which related the lower stability of the blends to the lower T_g and the inherently poor thermal stability of OLA. Finally, all the PLA/OLA blends showed residual mass values below 2 wt%.

On one hand, the addition of 3 and 6 phr of HNTs, particularly the lowest content, induced a positive increase in the onset degradation, showing $T_{5\%}$ values of 299.5 and 296.5 °C, respectively. On the other hand, HNTs contents of 9 phr reduced the thermal stability of the PLA/OLA film, whereby both $T_{5\%}$ and T_{deg} decreased by approximately 10 °C and 33 °C, respectively. These results indicate that the addition of low HNTs amounts successfully improved the thermal stability of PLA/OLA film due to the good dispersion of HNTs in the PLA matrix.

This finding is in agreement with the study recently performed by Risyon *et al.* [31], who found that $T_{5\%}$, T_{deg}, and residual mass improved since well-dispersed HNTs formed tortuous paths that provided physical thermal barriers to the PLA film. In this

regard, nanoclays can be responsible for delaying the sample weight loss by the formation of tortuous paths that hinders the diffusion of volatile degradation products out of the material and, for the particular case of HNTs, certain sorption during degradation could additionally occur due to their hollow structure and high porosity [45].

The fact that thermal stability was lower at the highest HNTs content further confirms that the nanofillers agglomerated and, hence, reduced the heat barrier effect and catalyzed thermal degradation. The catalytic action of halloysite on the pyrolysis of PLA has been ascribed to the presence of Brönsted acid sites, such as hydrophilic Si–OH and aluminum hydroxide (Al–OH) groups, on the external surface of the clay [28]. One can also observe that the residual mass progressively increased with the HNT content since the nanoclay is thermally stable at high temperatures and it can also act as a heat barrier, which could enhance the formation of char after thermal decomposition.

Thermomechanical properties of the PLA/OLA/HNTs films

Dynamic mechanical thermal analysis (DMTA) was carried out to determine the thermomechanical properties of the PLA/OLA/HNTs films. In **Figure IV.2.1.8** the storage modulus (E′) and dynamic damping factor (tan δ) were recorded as a function of temperature. **Figure IV.2.1.8**a gathers the evolution of E′ with temperature in which one can observe that all the PLA-based films presented a similar profile. In particular, the samples showed high E′ values, that is, high stiffness, at temperatures below 40 ºC and then E′ sharply decreased from 50 to 80 ºC. This thermomechanical change indicates that the alpha (α)-relaxation of the biopolymer, which is related to its T_g, was exceeded. Finally, E′ increased in the 85–100 ºC range due to the occurrence of cold crystallization. These results correlated well with the DSC analysis described above.

Table IV.2.1.5 shows the E′ values of the storage modulus measured at 30, 75, and 110 ºC, being these temperatures representative of the stored elastic energy of PLA in its three states, that is, amorphous glassy, amorphous rubber, and semicrystalline. The addition of OLA shifted the E′ curves to significantly lower temperatures, confirming the plasticizing effect of the oligomer, which is in agreement with both the DSC analysis and our previous study [36]. It is worthy to note, however, that the E′ values increased, especially at the 10 wt% loading. This observation suggests that the OLA-containing

PLA films developed higher crystallinity, which was also observed during the DSC analysis. This increment in rigidity was more noticeable at 110 ºC, once PLA finished its cold crystallization. In particular, the E' values increased from 30.1 MPa, for the neat PLA film, up to 93.2 MPa, for the PLA film containing 10 wt% of OLA. One can also observe that lower values were attained at 20 wt% of OLA, which can be related to the formation of a highly plasticized PLA structure. As determined above during the mechanical properties, the addition of HNTs in the glassy state yielded an increase in E'. Similar results were reported by Prashantha *et al.* [27], who observed a general increase of E, with increasing the nanofiller content. However, at high temperatures, the nanocomposite films showed lower E' values than the unfilled PLA/OLA films, which can also be ascribed to the potential of the latter sample to develop higher crystallinity. One can also notice that the PLA/OLA films with the lowest HNTs contents, that is, 3 phr and 6 phr, showed significantly higher values than that containing 9 phr due to the higher dispersion attained in these nanocomposite films.

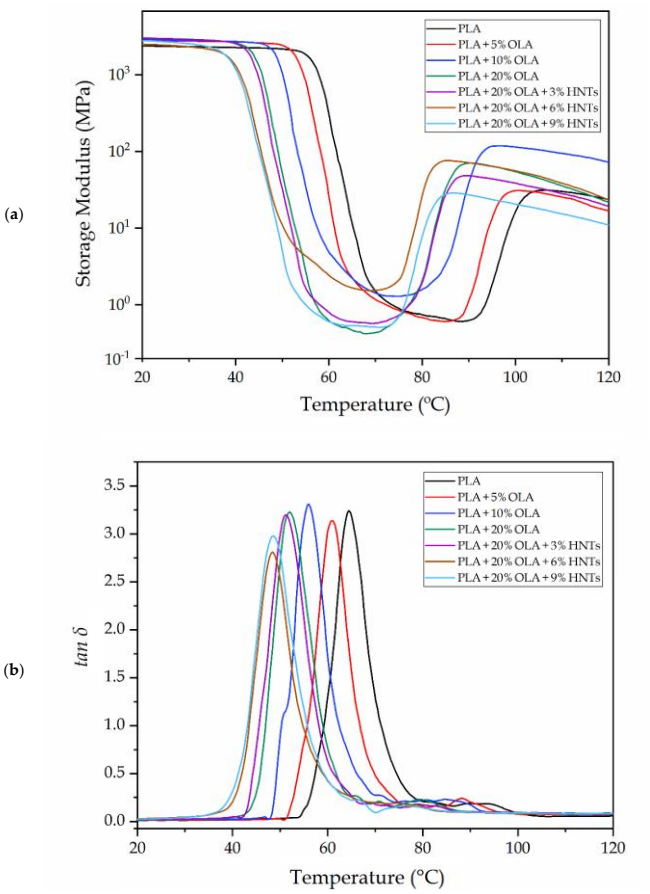

Figure IV.2.1.8. Evolution as a function of temperature of the (a) storage modulus and (b) dynamic damping factor (tan δ) of the polylactide (PLA)/oligomer of lactic acid (OLA)/halloysite nanotubes (HNTs) films.

Figure IV.2.1.8b shows the evolution of tan δ versus temperature. The tan δ peaks represent the change in the thermomechanical behavior of PLA when the α-relaxation of the biopolymer is reached, which relates to the T_g of the biopolyester. As also shown in **Table IV.2.1.5**, the α-relaxation peak for the neat PLA film was located at 64.1 ºC, which is slightly lower than the T_g value obtained by DSC analysis. One can observe that the peak values gradually decreased with the OLA content, down to 52 ºC for the PLA film containing 20 wt%, being ascribed to the plasticization of the PLA matrix as also stated by DSC. The tan δ peaks of PLA/HNTs nanocomposite films slightly broaden and shifted to lower temperatures compared to that of neat PLA for contents of 6 phr and 9 phr of HNTs. Broadening of tan δ and eventual shift to lower temperatures for nanocomposites indicate an increase in the segmental motions of the polymer blend [46]. This result observed for the nanocomposite films with high nanoclay loadings differs with the above-shown DSC results and also previous DMTA studies of PLA/HNTs composites [27]. The here-attained thermomechanical change suggests a hydrolytic effect of the nanoclay during extrusion on the PLA/OLA blend by which the biopolymer's molecular weight (M_W) is reduced and the molecular motion is favored due the chains are shorter.

Table IV.2.1.5. Thermomechanical properties of the polylactide (PLA)/oligomer of lactic acid (OLA)/halloysite nanotubes (HNTs) films in terms of glass transition temperature (T_g) and storage modulus (E′) measured at 30, 75, and 110 ºC, and glass transition temperature (T_g).

Film	T_g (°C)	E′ (MPa)		
		30 °C	75 °C	110 °C
PLA	64.1 ± 0.9[a]	2321.8 ± 122.1[a]	0.9 ± 0.1[a]	30.1 ± 2.8[a]
PLA + 5% OLA	60.7 ± 0.6[b]	2732.2 ± 139.2[b]	0.8 ± 0.2[a]	25.0 ± 1.6[b]
PLA + 10% OLA	56.0 ± 1.0[c]	2785.5 ± 120.2[b]	1.3 ± 0.2[b]	93.2 ± 2.9[c]
PLA + 20% OLA	52.0 ± 1.1[d]	2892.7 ± 107.4[c]	0.6 ± 0.1[a]	36.1 ± 1.9[d]
PLA + 20% OLA + 3% HNTs	51.2 ± 0.7[d]	2883.6 ± 119.3[c]	0.7 ± 0.1[a]	27.8 ± 3.0[b]
PLA + 20% OLA + 6% HNTs	48.4 ± 0.7[e]	2318.2 ± 101.5[a]	2.0 ± 0.2[c]	37.9 ± 2.7[e]
PLA + 20% OLA + 9% HNTs	48.3 ± 0.8[e]	2536.9 ± 102.1[f]	0.7 ± 0.1[a]	15.0 ± 2.1[f]

[a–f] Different letters in the same column indicate a significant difference among the samples ($p < 0.05$).

Barrier properties of the PLA/OLA/HNTs films

The water vapor permeability (WVP) and limonene permeability (LP) of the PLA films containing OLA and HNTs are shown in **Table IV.2.1.6**. Biodegradable films for packaging applications habitually show low water barrier resistance, which strongly limits their application for food packaging purposes due to physical and chemical deterioration of foodstuff. It can be observed that the neat PLA film presented a WVP value of 1.22×10^{-14} kg m m^{-2} Pa^{-1} s^{-1}, which indicates that PLA is a medium-to-low barrier material to water vapor, being similar to that reported in our previous study [9]. Unexpectedly, the addition of OLA reduced the permeability to water vapor of the PLA film. Particularly, the blend containing 10 wt% of OLA showed the highest barrier properties with a WVP value of 0.65×10^{-14} kg m m^{-2} Pa^{-1} s^{-1}. This barrier enhancement can be attributed to the densification of PLA produced by the increase in crystallinity after the OLA addition [47], which was also previously corroborated by DSC and DMTA. Similar results were reported by Ambrosio-Martín *et al.* [44], who associated the reduction of the vapor permeability with an effect of "antiplasticization". In this regard, several works have demonstrated reductions in gas permeability associated with a fractional free volume reduction phenomenon in polymers by the incorporation of low amounts of low-M_W additives [48, 49]. Since water is a condensable molecule and hence permeability is based on a solubility phenomenon rather than diffusion one, the reduced concentration of sorbed water vapor due to the occupancy of free volume of the amorphous regions PLA by the OLA molecules could explain the higher barrier properties. The higher value observed for the PLA blend with 20 wt% of OLA further confirms the highly plasticization attained in this PLA film, which seems to predominate over "antiplasticization" at high contents. In any case, all the OLA-containing PLA films showed significantly higher barrier performance than the neat PLA film. Similar results were obtained during the analysis of the limonene transport properties, which are usually carried out as a standard system to test aroma barrier. The LP value was reduced from 3.33×10^{-15} kg m m^{-2} Pa^{-1} s^{-1}, for the neat PLA film, to 0.94×10^{-15} kg m m^{-2} Pa^{-1} s^{-1} and 1.72×10^{-15} kg m m^{-2} Pa^{-1} s^{-1} for the PLA films containing 10 and 20 wt% of OLA, respectively. Therefore, the here-studied type of OLA performed as an "antiplasticizer" at contents of 10 wt% in the PLA, whereas higher concentrations trigger plasticization possibly through the formation of clusters of additive molecules. These results confirm

that the addition of low-to-medium contents of OLA is very promising for the development of medium barrier films of PLA.

Table IV.2.1.6. Water vapor permeability (WVP) and limonene permeability (LP) of the polylactide (PLA)/oligomer of lactic acid (OLA)/halloysite nanotubes (HNTs) films.

Film	WVP x 10^{14} (kg m m^{-2} Pa^{-1} s^{-1})	LP x 10^{15} (kg m m^{-2} Pa^{-1} s^{-1})
PLA	1.22 ± 0.03[a]	3.33 ± 0.08[a]
PLA + 5% OLA	0.85 ± 0.05[b]	3.31 ± 0.07[a]
PLA + 10% OLA	0.65 ± 0.03[c]	0.94 ± 0.01[b]
PLA + 20% OLA	0.87 ± 0.02[b]	1.72 ± 0.10[c]
PLA + 20% OLA + 3% HNTs	0.80 ± 0.02[d]	0.91 ± 0.03[b]
PLA + 20% OLA + 6% HNTs	0.88 ± 0.03[b]	1.30 ± 0.09[d]
PLA + 20% OLA + 9% HNTs	0.88 ± 0.02[b]	1.42 ± 0.15[d]

[a–d] Different letters in the same column indicate a significant difference among the samples ($p < 0.05$).

Interestingly, the incorporation of low amounts of HNTs induced a further significant reduction of both water and limonene vapors. In particular, the PLA/OLA nanocomposite film containing 3 phr of HNTs showed WPV and LP values of 0.80 × 10^{-14} kg m m^{-2} Pa^{-1} $s^{-1}$and 0.91 × 10^{-15} kg m m^{-2} Pa^{-1} s^{-1}, respectively, which represents reductions of approximately 8% and 47% compared with the unfilled PLA/OLA film. This barrier enhancement can be ascribed to the efficient dispersion of HNTs in the PLA/OLA matrix, which results in the formation of tortuous paths that reduced the diffusion of the vapor molecules through the PLA film [50]. The lower reduction attained for water vapor in comparison with limonene vapor can related to the hydrophilic nature of HNTs since they exhibit permanent negative charges on their surface by which water molecules entrapment can be increased [51]. As similar to other properties, when higher contents of HNTs were incorporated, that is, 6 and 9 phr, the WVP and LP values increased, which can also be due to agglomeration of nanoclays by which no tortuous path was formed. Similar results were reported by Risyon *et al.* [31], who showed water and oxygen barrier improvements of approximately 21% and 33%, respectively, when 3 phr of HNTs was incorporated into PLA films whereas higher contents led to higher permeability.

MATERIALS AND METHODS

Materials

PLA Ingeo™ Biopolymer 2003D was supplied in pellets form by NatureWorks LLC (Minnetonka, MN, USA). This PLA grade has a melt flow rate (MFR) of 6 g (10 min)$^{-1}$ measured at 210 ^{o}C and 2.16 kg and a true density of 1.24 g cm^{-3}. It has been specifically designed for extrusion for use in fresh food packaging and food serviceware applications. OLA was provided by Condensia Química S.A. (Barcelona, Spain) as Glyplast® OLA 8 in liquid form. It has a density of 1.11 g cm^{-3}, a viscosity of 22.5 mPa s at 100 ^{o}C, an ester content >99%, a maximum acid index of 2.5 mg KOH g^{-1}, and a maximum water content of 0.1 wt%. According to the manufacturer, this OLA grade is obtained from renewable raw materials and is biodegradable (UN 20200:2006), being specifically designed as PLA plasticizer to obtain stretch films. HNTs were purchased at Sigma-Aldrich S.A. (Madrid, Spain) with reference 685445 in powder form. HNTs are characterized by a M_W of 294.19 g mol^{-1} and a true density of 2.53 g cm^{-3}. According to the manufacturer, the nanotubes are 1–3 μm long with a diameter in the 30–70 nm range, resulting in a surface area of 64 m^2 g^{-1}, a pore volume of 1.26–1.34 mL g^{-1}, and a cation exchange capacity of 8.0 meq g^{-1}. Acetone and $_D$-limonene, with 98% purity, were also obtained from Sigma-Aldrich S.A.

Films preparation

The as-received PLA pellets were dried overnight in a dehumidifier MDEO from Industrial Marsé (Barcelona, Spain) at 60 ^{o}C to eliminate residual moisture since the biopolyester has a high sensitivity to hydrolysis. The OLA content was tested in concentrations of 5, 10, and 20 wt% with respect to PLA. Thereafter, for a fixed a content of 20 wt% of OLA, HNTs were incorporated at 3, 6, and 9 phr of PLA/OLA blend. The selected content of OLA was chosen since it yielded the highest stability and performance for PLA according to Burgos *et al.* [10]. The corresponding HNTs loadings were previously dispersed in OLA by the ultrasound-assisted technique in an ultrasonicator model Sonoplus HD 2200 from Bandelin Electronic GmbH & Co. kg (Berlin, Germany) for 5 min using an amplitude of 80% to attain homogenous mixtures. As the OLA additive is a rather viscous liquid at room temperature, it was first heated up to 60 ^{o}C. During the ultrasound assisted dispersion the temperature increased up to

100 ºC due to internal friction. Conventional magnetic stirring for 5 min was also performed for each HNTs-containing OLA dispersion min for comparison. **Table IV.2.1.7** gathers the code and composition of the prepared samples.

Table IV.2.1.7. Code and composition of each sample according to the weight content (wt%) of polylactide (PLA) and oligomer of lactic acid (OLA) in which the halloysite nanotubes (HNTs) were added as parts per hundred resin (phr) of blend.

Code	PLA (wt%)	OLA (wt%)	HNTs (phr)
PLA	100	0	0
PLA + 5% OLA	95	5	0
PLA + 10% OLA	90	10	0
PLA + 20% OLA	80	20	0
PLA + 20% OLA + 3% HNTs	80	20	3
PLA + 20% OLA + 6% HNTs	80	20	6
PLA + 20% OLA + 9% HNTs	80	20	9

The mixtures were melt-compounded in a twin-screw extruder from Construcciones Mecánicas Dupra, S.L. (Alicante, Spain) equipped with a screw diameter of 25 mm and a length-to-diameter (L/D) ratio of 24. Further details of the equipment can be found elsewhere [52]. The rotating speed was set to 25 rpm and the temperature profile was: 165 ºC (feeding hopper)–170 ºC–175 ºC–180 ºC (extrusion die).

The strands were cooled in air, granulated in pellets in an air-knife unit, and dried at 60 ºC for 72 h to remove moisture. Thereafter, the pellets were thermo-compressed using a 10-Tn hydraulic press from Robima S.A. (Valencia, Spain) equipped with two hot aluminum plates and a temperature controller from Dupra S.A. (Castalla, Spain) [53]. For this, about 5 g of each composition was thermo-compressed at 180 ºC with a pressure of 40 MPa tons for 3 min in a square frame of 10 cm x 10 cm by two hot plates and air cooled at room conditions. Films with a mean thickness of approximately 250 μm were attained and stored at 23 ºC y 50% relative humidity (HR) for, at least, 15 days prior to characterization.

Films characterization

Color measurements

Changes in color were measured in a colorimetric spectrophotometer Konica CM-3600d Colorflex-DIFF2, from Hunter Associates Laboratory, Inc. (Reston, VA, USA). The Commission Internationale de l'Eclairage (CIE) standard illuminant D65 was used to measure the CIE Lab color space coordinates L*, a, and *b* using an observer angle of 10^{o}. In the selected L*, a*, and b* color space, L* stands for the luminance, where L* = 0 represents dark and L* = 100 indicates clarity or lightness, and the a*b* pair represents the chromaticity coordinate, where a* > 0 is red, a* < 0 is green, b* > 0 is yellow, and b* < 0 is blue. The L*, a*, and b* coordinate values were obtained on five different film samples and the color change, that is, ΔE_{ab}^{*}, was calculated using **Equation IV.2.1.1**

$$\Delta E_{ab}^{*}=\sqrt{(\Delta L^{*})^{2}+(\Delta a^{*})^{2}+(\Delta b^{*})^{2}} \qquad \textbf{Equation IV.2.1.1}$$

where ΔL*, Δa*, and Δb* correspond to the differences between the color parameters of the tested films and the values of the neat PLA film. Color change evaluation was performed using the following assessment [54]: unnoticeable ($\Delta E_{ab}^{*} < 1$), only an experienced observer can notice the difference ($\Delta E_{ab}^{*} \geq 1$ and < 2), an inexperienced observer notices the difference ($\Delta E_{a}^{*} \geq 2$ and < 3.5), the samples show clear noticeable difference ($\Delta E_{ab}^{*} \geq 3.5$ and < 5), and the observer notices different colors ($\Delta E_{ab}^{*} \geq 5$).

Microscopy

The morphology of HNTs was studied by TEM using a Philips CM10 (Eindhoven, the Netherlands) with an acceleration voltage of 100 kV. Prior to TEM observation, a small amount of HNTs was dispersed in acetone and subjected to ultrasound dispersion in an ultrasound bath Sonicador SONOPULS from Bandelin Electronic GmbH & Co. kg for 5 min at room temperature. Then, a drop of this dispersion was poured onto a carbon grid and subjected to solvent evaporation at room temperature.

The films were cryo-fractured by immersion in liquid nitrogen and their fracture surfaces were observed by FESEM in a ZEISS ULTRA 55 FESEM microscope from Oxfrod Instruments (Abingdon, UK). The microscope worked at an acceleration voltage

of 2 kV. The fracture surfaces were previously coated with a gold-palladium alloy in a Quorun Technologies Ltd. EMITECH mod. SC7620 sputter coater (East Sussex, UK).

Mechanical tests

The mechanical properties of the films were determined by tensile tests in a universal test machine ELIB 30 from S.A.E. Ibertest (Madrid, Spain) following the guidelines of ISO 527-3:2018 with rectangular samples sizing 100 mm x 10 mm. The selected load cell was 10 kN whereas the cross-head speed was set to 2 mm min^{-1}. At least six different specimens per formulation were tested in room conditions.

Thermal Tests

DSC was carried out to study the thermal transitions of samples in a Mettler-Toledo 821 calorimeter (Schwerzenbach, Switzerland). An average weight of 5–7 mg of each sample was placed in 40-µL aluminum-sealed crucible and subjected to a three-step program in inert atmosphere of nitrogen with a constant flow of 30 mL min^{-1}. The samples were heated from 30 to 200 ^{o}C, cooled down to 0 ^{o}C, and heated up again to 250 ^{o}C. All heating/cooling rates were set at 10 ^{o}C min^{-1} and $X_{c\ max}$ was calculated using **Equation IV.2.1.2** [36]:

$$X_{c\ max} = \left[\frac{\Delta H_m}{\Delta H_m^0 \times w}\right] \times 100\ (\%) \qquad \textbf{Equation IV.2.1.2}$$

where ΔH_m (J g^{-1}) corresponds to the melting enthalpy of PLA, ΔH_m^0 (J g^{-1}) is the theoretical value of a fully crystalline PLA, that is, 93.0 J g^{-1} [55], and w indicates the weight fraction of PLA in the sample.

TGA was performed to determine the thermal stability of films using a TGA/SDTA 851 thermobalance from Mettler-Toledo Inc. (Schwerzenbach, Switzerland). Samples with an average weight between 5 and 7 mg were placed in standard alumina crucibles (70 µL) and subjected to a single-step thermal program from 30 to 650 ^{o}C at a heating rate of 20 ^{o}C min^{-1} in an air atmosphere. All the thermal tests were performed by triplicate.

Thermomechanical tests

DMTA was conducted in a DMA-1 model from Mettler-Toledo S.A. (Barcelona, Spain), working in tension mode. Rectangular film samples sizing 10 mm x 5 mm were subjected to a temperature sweep program from −50 ◦C to 120 ºC at a heating rate of 2 ºC min^{-1}. The offset strength was set at 1 N, the offset deformation at 150%, and the control deformation at 6 μm. The DMTA tests were run in triplicate to obtain reliable data.

Permeability measurements

WVP was determined for the PLA-based films according to the ASTM E96-95 gravimetric method. For this, 5 ml of distilled water were poured into a Payne permeability cup (Ø = 3.5 cm) from Elcometer Sprl (Hermallesous-Argenteau, Belgium). The films were placed in the cups so that on one side they were exposed to 100% RH, avoiding direct film contact with water. The cups containing the films were then secured with silicon rings and stored in a desiccator at 25 ºC and 0% RH. Identical cups with aluminum foils were used as control samples to estimate water loss through the sealing. The cups were weighed periodically using an analytical balance with ± 0.0001 g accuracy. Water vapor permeation rate (WVPR), also called water permeance when corrected for permeant partial pressure, was determined from the steady-state permeation slope obtained from the regression analysis of weight loss data per unit area versus time, in which the weight loss was calculated as the total cell loss minus the loss through the sealing. WVP was obtained, in triplicate, by correcting the permeance by the average film thicknesses.

LP was also determined according to ASTM E96-95 gravimetric method. Similarly, 5 mL of D-limonene was placed inside the Payne permeability cups and the cups containing the films were stored under controlled conditions, that is, 25 ºC and 40% RH. Limonene permeation rate (LPR) was obtained from the steady-state permeation slopes. The weight loss was calculated as the total cell loss minus the loss through the sealing plus the water sorption gained from the environment measured in samples with no permeant. LP was calculated taking into account the average sheet thickness in each case, measuring three replicates per sample.

Statistical analysis

The values of the film properties were evaluated by analysis of variance (ANOVA) with 95% confidence interval level ($p \leq 0.05$). For this purpose, a multiple comparison test (Tukey) was followed using the software OriginPro8 (OriginLab Corporation, Northampton, MA, USA).

CONCLUSIONS

Due to their renewable origin and high ductility, OLA-containing PLA films have recently received considerable attention for a use in compostable flexible packaging. The addition of the here-tested OLA plasticizer did not only contribute to the improvement of the ductility and reduction of PLA's T_g but also, up to contents of 10 wt%, it performed as an "antiplasticizer", making the films more crystalline and attractive for medium barrier applications. However, despite these advantages, the resultant blend films also showed some limitations, such as lower mechanical strength and reduced thermal stability. To optimize the properties of the PLA/OLA blend films, different amounts of HNTs were co-added with OLA by means of ultrasonication at mild temperature to facilitate their subsequent dispersion in the PLA matrix. According to optical, mechanical, thermal, and barrier characterizations, the performance of the plasticized PLA films was significantly improved by reinforcement of the nanofillers. It was observed that either the individual addition of OLA or the combined addition with low HNTs loadings did not significantly alter the transparency and color properties of the PLA films. The morphological analysis revealed that the use of ultrasound-assisted HNTs dispersion significantly avoided formation of aggregates in the PLA/OLA matrix, particularly for films with the lowest HNTs contents, that is, 3 phr. Nevertheless, higher HNTs loadings resulted in the formation of small aggregates that led to the drop of the mechanical and thermal properties of the blend and also reduced lightness and induced color changes to the PLA films.

From the above, the present research study demonstrates that the mechanical and thermal properties of PLA films can be tuned by carefully selecting the contents added of OLA plasticizer and HNTs, while improving other valuable properties such as the thermomechanical resistance and barrier against water and aroma vapors. One can, therefore, conclude that PLA films with low-to-medium contents of OLA and low

loadings of HNTs are technically viable for use in applications in the food packaging industry.

FUNDING

This research work was funded by the Spanish Ministry of Science and Innovation (MICI) project numbers RTI2018-097249-B-C21 and MAT2017-84909-C2-2-R.

ACKNOWLEDGMENTS

S. Rojas-Lema is a recipient of a Santiago Grisolia grant from Generalitat Valenciana (GVA) (GRISOLIAP/2019/132). L. Quiles-Carrillo. wants to thank GVA for his FPI grant (ACIF/2016/182) and the Spanish Ministry of Education, Culture, and Sports (MECD) for his FPU grant (FPU15/03812), while D. Garcia-Garcia also acknowledges GVA for his postdoctoral contract (APOSTD/2019/201). B. Melendez-Rodriguez and S. Torres-Giner acknowledge MICIU for her FPI grant (BES-2016-077972) and his Juan de la Cierva–Incorporation contract (IJCI-2016-29675), respectively. Microscopy services of the Universitat Politècnica de València (UPV) are acknowledged for their help in collecting and analyzing the FESEM images. The authors also thank Enrique Navarro from the microscopy services at Universitat de València (UPV) and Sebastian Schädler from the Carl Zeiss Microscopy Customer Center Europe for collecting the FIB-SEM images and recording the video. Authors also thank Condensia Química S.A. for kindly supplying Glyoplast® OLA 8.

REFERENCES

[1] S. Torres-Giner, L. Gil, L. Pascual-Ramírez, and J.A. Garde-Belza. *Packaging: Food Waste Reduction*, in *Encyclopedia of Polymer Applications*. 2018, CRC Press: Boca Raton, FL, USA, p. 1990.

[2] S. RameshKumar, P. Shaiju, K.E. O'Connor, and R.B. P. *Bio-based and biodegradable polymers - State-of-the-art, challenges and emerging trends.* Current Opinion in Green and Sustainable Chemistry, 2020, 21, p. 75-81.

[3] K. Madhavan Nampoothiri, N.R. Nair, and R.P. John. *An overview of the recent developments in polylactide (PLA) research.* Bioresource Technology, 2010, 101(22), p. 8493-8501.

[4] K. Petersen, P.V. Nielsen, and M.B. Olsen. *Physical and mechanical properties of biobased materials - Starch, polylactate and polyhydroxybutyrate.* Starch/Staerke, 2001, 53(8), p. 356-361.

[5] C.J. Weber, V. Haugaard, R. Festersen, and G. Bertelsen. *Production and applications of biobased packaging materials for the food industry.* Food Additives and Contaminants, 2002, 19(sup1), p. 172-177.

[6] R. Auras, B. Harte, and S. Selke. *An Overview of Polylactides as Packaging Materials.* Macromolecular Bioscience, 2004, 4(9), p. 835-864.

[7] L.T. Lim, R. Auras, and M. Rubino. *Processing technologies for poly(lactic acid).* Progress in Polymer Science, 2008, 33(8), p. 820-852.

[8] D. Cava, E. Giménez, R. Gavara, and J.M. Lagaron. *Comparative performance and barrier properties of biodegradable thermoplastics and nanobiocomposites versus PET for food packaging applications.* Journal of Plastic Film and Sheeting, 2006, 22(4), p. 265-274.

[9] L. Quiles-Carrillo, N. Montanes, J. Lagaron, R. Balart, and S. Torres-Giner. *In situ compatibilization of biopolymer ternary blends by reactive extrusion with low-functionality epoxy-based styrene–acrylic oligomer.* Journal of Polymers and the Environment, 2019, 27(1), p. 84-96.

[10] N. Burgos, V.P. Martino, and A. Jiménez. *Characterization and ageing study of poly(lactic acid) films plasticized with oligomeric lactic acid.* Polymer Degradation and Stability, 2013, 98(2), p. 651-658.

[11] I. Armentano, E. Fortunati, N. Burgos, F. Dominici, F. Luzi, S. Fiori, A. Jiménez, K. Yoon, J. Ahn, and S. Kang. *Processing and characterization of plasticized PLA/PHB blends for biodegradable multiphase systems.* eXPRESS Polymer Letters, 2015, 9(7), p. 583-596.

[12] N. Burgos, D. Tolaguera, S. Fiori, and A. Jiménez. *Synthesis and Characterization of Lactic Acid Oligomers: Evaluation of Performance as Poly(Lactic Acid) Plasticizers.* Journal of Polymers and the Environment, 2014, 22(2), p. 227-235.

[13] O. Martin and L. Avérous. *Poly(lactic acid): plasticization and properties of biodegradable multiphase systems.* Polymer, 2001, 42(14), p. 6209-6219.

[14] D.R. Paul and L.M. Robeson. *Polymer nanotechnology: Nanocomposites.* Polymer, 2008, 49(15), p. 3187-3204.

[15] S. Sinha Ray and M. Bousmina. *Biodegradable polymers and their layered silicate nanocomposites: In greening the 21st century materials world.* Progress in Materials Science, 2005, 50(8), p. 962-1079.

[16] D. Rawtani and Y.K. Agrawal. *Multifarious applications of halloysite nanotubes: A review.* Reviews on Advanced Materials Science, 2012, 30(3), p. 282-295.

[17] M. Liu, B. Guo, Q. Zou, M. Du, and D. Jia. *Interactions between halloysite nanotubes and 2,5-bis(2-benzoxazolyl) thiophene and their effects on reinforcement of polypropylene/halloysite nanocomposites.* Nanotechnology, 2008, 19(20), p. 205709.

[18] P. Pasbakhsh, G.J. Churchman, and J.L. Keeling. *Characterisation of properties of various halloysites relevant to their use as nanotubes and microfibre fillers.* Applied Clay Science, 2013, 74, p. 47-57.

[19] M. Du, B. Guo, and D. Jia. *Newly emerging applications of halloysite nanotubes: a review.* Polymer International, 2010, 59(5), p. 574-582.

[20] B. Singh. *Why does halloysite roll? – A new model.* Clays and Clay Minerals, 1996, 44(2), p. 191-196.

[21] B. Lecouvet, J.G. Gutierrez, M. Sclavons, and C. Bailly. *Structure–property relationships in polyamide 12/halloysite nanotube nanocomposites.* Polymer Degradation and Stability, 2011, 96(2), p. 226-235.

[22] R. Kamble, M. Ghag, S. Gaikawad, and B.K. Panda. *Halloysite nanotubes and applications: A review.* Journal of Advanced Scientific Research, 2012, 3(2), p. 25-29.

[23] M. Liu, B. Guo, M. Du, and D. Jia. *Drying induced aggregation of halloysite nanotubes in polyvinyl alcohol/halloysite nanotubes solution and its effect on properties of composite film.* Applied Physics A, 2007, 88(2), p. 391-395.

[24] M. Murariu, A.-L. Dechief, Y. Paint, S. Peeterbroeck, L. Bonnaud, and P. Dubois. *Polylactide (PLA)—halloysite nanocomposites: Production, morphology and key-properties.* Journal of Polymers and the Environment, 2012, 20(4), p. 932-943.

[25] M. Liu, Y. Zhang, and C. Zhou. *Nanocomposites of halloysite and polylactide.* Applied Clay Science, 2013, 75-76, p. 52-59.

[26] W. Wu, X. Cao, Y. Zhang, and G. He. *Polylactide/halloysite nanotube nanocomposites: Thermal, mechanical properties, and foam processing.* Journal of Applied Polymer Science, 2013, 130(1), p. 443-452.

[27] K. Prashantha, B. Lecouvet, M. Sclavons, M.F. Lacrampe, and P. Krawczak. *Poly(lactic acid)/halloysite nanotubes nanocomposites: Structure, thermal, and mechanical properties as a function of halloysite treatment.* Journal of Applied Polymer Science, 2013, 128(3), p. 1895-1903.

[28] G. Stoclet, M. Sclavons, B. Lecouvet, J. Devaux, P. Van Velthem, A. Boborodea, S. Bourbigot, and N. Sallem-Idrissi. *Elaboration of poly(lactic acid)/halloysite nanocomposites by means of water assisted extrusion: structure, mechanical properties and fire performance.* RSC Advances, 2014, 4(101), p. 57553-57563.

[29] R.T. De Silva, P. Pasbakhsh, K.L. Goh, S.-P. Chai, and J. Chen. *Synthesis and characterisation of poly (lactic acid)/halloysite bionanocomposite films.* Journal of Composite Materials, 2014, 48(30), p. 3705-3717.

[30] S.H. Othman, N. Hassan, A. Talib Rosnita, R. Kadir Basha, and P. Risyon Nazratul. *Mechanical and thermal properties of PLA/halloysite bio-nanocomposite films: effect of halloysite nanoclay concentration and addition of glycerol.* Journal of Polymer Engineering, 2017, 37(4), p. 381–389.

[31] N.P. Risyon, S.H. Othman, R.K. Basha, and R.A. Talib. *Characterization of polylactic acid/halloysite nanotubes bionanocomposite films for food packaging.* Food Packaging and Shelf Life, 2020, 23, p. 100450.

[32] B. Szczepanik, P. Słomkiewicz, M. Garnuszek, P. Rogala, D. Banaś, A. Kubala-Kukuś, and I. Stabrawa. *Effect of temperature on halloysite acid treatment for efficient*

chloroaniline removal from aqueous solutions. Clays and Clay Minerals, 2017, 65(3), p. 155-167.

[33] L. Introzzi, J.M. Fuentes-Alventosa, C.A. Cozzolino, S. Trabattoni, S. Tavazzi, C.L. Bianchi, A. Schiraldi, L. Piergiovanni, and S. Farris. *"Wetting enhancer" pullulan coating for antifog packaging applications.* ACS Applied Materials & Interfaces, 2012, 4(7), p. 3692-3700.

[34] M.P. Arrieta, J. López, S. Ferrándiz, and M.A. Peltzer. *Characterization of PLA-limonene blends for food packaging applications.* Polymer Testing, 2013, 32(4), p. 760-768.

[35] R. Rong, X. Xu, S. Zhu, B. Li, X. Wang, and K. Tang. *Facile preparation of homogeneous and length controllable halloysite nanotubes by ultrasonic scission and uniform viscosity centrifugation.* Chemical Engineering Journal, 2016, 291, p. 20-29.

[36] D. Lascano, G. Moraga, J. Ivorra-Martinez, S. Rojas-Lema, S. Torres-Giner, R. Balart, T. Boronat, and L. Quiles-Carrillo. *Development of injection-molded polylactide pieces with high toughness by the addition of lactic acid oligomer and characterization of their shape memory behavior.* Polymers, 2019, 11(12), p. 2099.

[37] R.T. De Silva, M. Soheilmoghaddam, K.L. Goh, M.U. Wahit, S.A.H. Bee, S.-P. Chai, and P. Pasbakhsh. *Influence of the processing methods on the properties of poly(lactic acid)/halloysite nanocomposites.* Polymer Composites, 2016, 37(3), p. 861-869.

[38] S.H. Othman, H.N. Ling, R.A. Talib, M.N. Naim, N.P. Risyon, and M. Saifullah. *PLA/MMT and PLA/Halloysite bio-nanocomposite films: Mechanical, barrier, and transparency.* Journal of Nano Research, 2019, 59, p. 77-93.

[39] G. Schliecker, C. Schmidt, S. Fuchs, R. Wombacher, and T. Kissel. *Hydrolytic degradation of poly(lactide-co-glycolide) films: effect of oligomers on degradation rate and crystallinity.* International Journal of Pharmaceutics, 2003, 266(1), p. 39-49.

[40] Q. Xing, X. Zhang, X. Dong, G. Liu, and D. Wang. *Low-molecular weight aliphatic amides as nucleating agents for poly (L-lactic acid): Conformation variation induced crystallization enhancement.* Polymer, 2012, 53(11), p. 2306-2314.

[41] J. Zhang, K. Tashiro, H. Tsuji, and A.J. Domb. *Disorder-to-Order Phase Transition and Multiple Melting Behavior of Poly(l-lactide) Investigated by Simultaneous Measurements of WAXD and DSC.* Macromolecules, 2008, 41(4), p. 1352-1357.

[42] M. Yasuniwa, S. Tsubakihara, Y. Sugimoto, and C. Nakafuku. *Thermal analysis of the double-melting behavior of poly(L-lactic acid).* Journal of Polymer Science Part B: Polymer Physics, 2004, 42(1), p. 25-32.

[43] A. Agüero, M.C. Morcillo, L. Quiles-Carrillo, R. Balart, T. Boronat, D. Lascano, S. Torres-Giner, and O. Fenollar. *Study of the influence of the reprocessing cycles on the final properties of polylactide pieces obtained by injection molding.* Polymers, 2019, 11(12), p. 1908.

[44] J. Ambrosio-Martín, M.J. Fabra, A. Lopez-Rubio, and J.M. Lagaron. *An effect of lactic acid oligomers on the barrier properties of polylactide.* Journal of Materials Science, 2014, 49(8), p. 2975-2986.

[45] S. Torres-Giner, N. Montanes, T. Boronat, L. Quiles-Carrillo, and R. Balart. *Melt grafting of sepiolite nanoclay onto poly(3-hydroxybutyrate-co-4-hydroxybutyrate) by reactive extrusion with multi-functional epoxy-based styrene-acrylic oligomer.* European Polymer Journal, 2016, 84, p. 693-707.

[46] S. Torres-Giner, N. Montanes, O. Fenollar, D. García-Sanoguera, and R. Balart. *Development and optimization of renewable vinyl plastisol/wood flour composites exposed to ultraviolet radiation.* Materials & Design, 2016, 108, p. 648-658.

[47] G. Miquelard, A. Guinault, C. Sollogoub, and M. Gervais. *Combined compatibilization and plasticization effect of low molecular weight poly (lactic acid) in poly (lactic acid)/poly (3-hydroxybutyrate-co-3-hydroxyvalerate) blends.* eXPRESS Polymer Letters, 2018, 12(2), p. 114-125.

[48] N.M. Larocca and L.A. Pessan. *Effect of antiplasticisation on the volumetric, gas sorption and transport properties of polyetherimide.* Journal of Membrane Science, 2003, 218(1), p. 69-92.

[49] Y. Maeda and D.R. Paul. *Effect of antiplasticization on gas sorption and transport. III. Free volume interpretation.* Journal of Polymer Science Part B: Polymer Physics, 1987, 25(5), p. 1005-1016.

[50] D.S. Aldana, E.D. Villa, M. De Dios Hernández, G.G. Sánchez, Q.R. Cruz, S.F. Gallardo, H.P. Castillo, and L.B. Casarrubias. *Barrier properties of polylactic acid in cellulose based packages using montmorillonite as filler.* Polymers, 2014, 6(9), p. 2386-2403.

[51] M.J. Saif and H.M. Asif. *Escalating applications of halloysite nanotubes.* Journal of the Chilean Chemical Society, 2015, 60, p. 2949-2953.

[52] Á. Agüero, D. Garcia-Sanoguera, D. Lascano, S. Rojas-Lema, J. Ivorra-Martinez, O. Fenollar, and S. Torres-Giner. *Evaluation of different compatibilization strategies to improve the performance of injection-molded green composite pieces made of polylactide reinforced with short flaxseed fibers.* Polymers, 2020, 12(4), p. 821.

[53] S. Torres-Giner, N. Montanes, V. Fombuena, T. Boronat, and L. Sanchez-Nacher. *Preparation and characterization of compression-molded green composite sheets made of poly(3-hydroxybutyrate) reinforced with long pita fibers.* Advances in Polymer Technology, 2018, 37(5), p. 1305-1315.

[54] K.J. Figueroa-Lopez, S. Torres-Giner, D. Enescu, L. Cabedo, M.A. Cerqueira, L.M. Pastrana, and J.M. Lagaron. *Electrospun active biopapers of food Waste derived poly(3-hydroxybutyrate-co-3-hydroxyvalerate) with short-term and long-term antimicrobial performance.* Nanomaterials, 2020, 10(3), p. 506.

[55] S. Torres-Giner, J.V. Gimeno-Alcañiz, M.J. Ocio, and J.M. Lagaron. *Optimization of electrospun polylactide-based ultrathin fibers for osteoconductive bone scaffolds.* Journal of Applied Polymer Science, 2011, 122(2), p. 914-925.

Artículo adaptado de

IV.2.2. Peroxide-induced synthesis of maleic anhydride-grafted poly(butylene succinate) and its compatibilizing effect on poly(butylene succinate)/pistachio shell flour composites.

Sandra Rojas-Lema[1], Jordi Arevalo[1], Jaume Gomez-Caturla[1], Daniel Garcia-Garcia[1], and Sergio Torres-Giner[2].

[1]Technological Institute of Materials (ITM), Universitat Politècnica de València (UPV), Plaza Ferrándiz y Carbonell 1, 03801 Alcoy, Spain.

[2]Research Institute of Food Engineering for Development (IIAD), Universitat Politècnica de València (UPV), Camino de Vera s/n, 46022 Valencia, Spain.

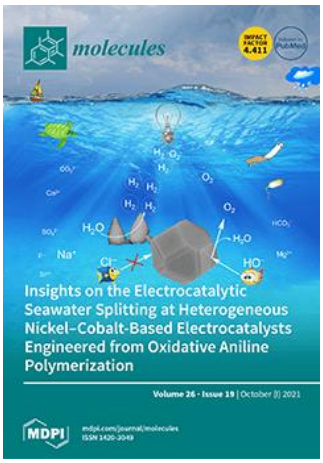

Molecules

2021, 26(19), p. 5927.

molecules

MDPI

Article

Peroxide-Induced Synthesis of Maleic Anhydride-Grafted Poly(butylene succinate) and Its Compatibilizing Effect on Poly(butylene succinate)/Pistachio Shell Flour Composites

Sandra Rojas-Lema [1,*], Jordi Arevalo [1], Jaume Gomez-Caturla [1], Daniel Garcia-Garcia [1] and Sergio Torres-Giner [2,*]

[1] Technological Institute of Materials (ITM), Universitat Politècnica de València (UPV), Plaza Ferrándiz y Carbonell 1, 03801 Alcoy, Spain; jorarag1@epsa.upv.es (J.A.); jaugoca@epsa.upv.es (J.G.-C.); dagarga4@epsa.upv.es (D.G.-G.)

[2] Research Institute of Food Engineering for Development (IIAD), Universitat Politècnica de València (UPV), Camino de Vera s/n, 46022 Valencia, Spain

* Correspondence: sanrole@epsa.upv.es (S.R.-L.); storresginer@upv.es (S.T.-G.)

Abstract: Framing the Circular Bioeconomy, the use of reactive compatibilizers was applied in order to increase the interfacial adhesion and, hence, the physical properties and applications of green composites based on biopolymers and food waste derived lignocellulosic fillers. In this study, poly(butylene succinate) grafted with maleic anhydride (PBS-*g*-MAH) was successfully synthetized by a reactive melt-mixing process using poly(butylene succinate) (PBS) and maleic anhydride (MAH) that was induced with dicumyl peroxide (DCP) as a radical initiator and based on the formation of macroradicals derived from the hydrogen abstraction of the biopolymer backbone. Then, PBS-*g*-MAH was used as reactive compatibilizer for PBS filled with different contents of pistachio shell flour (PSF) during melt extrusion. As confirmed by Fourier transform infrared (FTIR), PBS-*g*-MAH acted as a bridge between the two composite phases since it was readily soluble in PBS and could successfully form new esters by reaction of its multiple MAH groups with the hydroxyl (–OH) groups present in cellulose or lignin of PSF and the end ones in PBS. The resultant compatibilized green composites were, thereafter, shaped by injection molding into 4-mm thick pieces with a wood-like color. Results showed significant increases in the mechanical and thermomechanical rigidity and hardness, meanwhile variations on the thermal stability were negligible. The enhancement observed was related to the good dispersion and the improved filler-matrix interfacial interactions achieved by PBS-*g*-MAH and also to the PSF nucleating effect that increased the PBS's crystallinity. Furthermore, water uptake of the pieces progressively increased as a function of the filler content, whereas the disintegration in controlled compost soil was limited due to their large thickness.

Keywords: biopolymers; green composites; reactive compatibilization; food waste valorization; Circular Bioeconomy

Citation: Rojas-Lema, S.; Arevalo, J.; Gomez-Caturla, J.; Garcia-Garcia, D.; Torres-Giner, S. Peroxide-Induced Synthesis of Maleic Anhydride-Grafted Poly(butylene succinate) and Its Compatibilizing Effect on Poly(butylene succinate)/Pistachio Shell Flour Composites. *Molecules* **2021**, *26*, 5927. https://doi.org/10.3390/molecules26195927

Academic Editor: Andrea Maio

Received: 2 August 2021
Accepted: 24 September 2021
Published: 30 September 2021

1. Introduction

The rising concern toward environmental issues has stimulated research efforts in the perspective of reducing plastic waste given the fact that, in recent decades, the disposal and non-biodegradability of petroleum derived plastics have caused serious water and land pollution issues. In this context, fully or partially bio-based and biodegradable polymers currently represent the most promising options to replace petrochemical polymers. Some of the biopolymer matrices commonly used are biopolyesters, which mainly include polyhydroxyalkanoates (PHAs) and polylactides (PLAs) as well as aliphatic polyesters that are fully or partially obtained from petroleum but are biodegradable, such as poly(ε-caprolactone) (PCL), poly(butylene succinate) (PBS), poly(butylene succinate-*co*-butylene adipate) (PBSA), polybutylene(adipate-*co*-terephthalate) (PBAT), etc. [1]. Among them, PBS

Peroxide-induced synthesis of maleic anhydride-grafted poly(butylene succinate) and its compatibilizing effect on poly(butylene succinate)/pistachio shell flour composites.

Abstract

Framing the Circular Bioeconomy, the use of reactive compatibilizers was applied in order to increase the interfacial adhesion and, hence, the physical properties and applications of green composites based on biopolymers and food waste derived lignocellulosic fillers. In this study, poly(butylene succinate) grafted with maleic anhydride (PBS-*g*-MAH) was successfully synthetized by a reactive melt-mixing process using poly(butylene succinate) (PBS) and maleic anhydride (MAH) that was induced with dicumyl peroxide (DCP) as a radical initiator and based on the formation of macroradicals derived from the hydrogen abstraction of the biopolymer backbone. Then, PBS-*g*-MAH was used as reactive compatibilizer for PBS filled with different contents of pistachio shell flour (PSF) during melt extrusion. As confirmed by Fourier transform infrared (FTIR), PBS-*g*-MAH acted as a bridge between the two composite phases since it was readily soluble in PBS and could successfully form new esters by reaction of its multiple MAH groups with the hydroxyl (–OH) groups present in cellulose or lignin of PSF and the end ones in PBS. The resultant compatibilized green composites were, thereafter, shaped by injection molding into 4-mm thick pieces with a wood-like color. Results showed significant increases in the mechanical and thermomechanical rigidity and hardness, meanwhile variations on the thermal stability were negligible. The enhancement observed was related to the good dispersion and the improved filler-matrix interfacial interactions achieved by PBS-*g*-MAH and also to the PSF nucleating effect that increased the PBS's crystallinity. Furthermore, water uptake of the pieces progressively increased as a function of the filler content, whereas the disintegration in controlled compost soil was limited due to their large thickness.

Keywords: biopolymers; green composites; reactive compatibilization; food waste valorization; circular bioeconomy.

INTRODUCTION

The rising concern toward environmental issues has stimulated research efforts in the perspective of reducing plastic waste given the fact that, in recent decades, the disposal and non-biodegradability of petroleum derived plastics have caused serious water and land pollution issues. In this context, fully or partially bio-based and biodegradable polymers currently represent the most promising options to replace petrochemical polymers. Some of the biopolymer matrices commonly used are biopolyesters, which mainly include polyhydroxyalkanoates (PHAs) and polylactides (PLAs) as well as aliphatic polyesters that are fully or partially obtained from petroleum but are biodegradable, such as poly(ε-caprolactone) (PCL), poly(butylene succinate) (PBS), poly(butylene succinate-*co*-butylene adipate) (PBSA), polybutylene(adipate-*co*-terephthalate) (PBAT), etc. [1]. Among them, PBS is a semicrystalline polyester that can naturally degrade in industrial composting facilities and, under certain conditions, in natural environmental conditions due to the action of some bacteria and fungi [2]. PBS is currently produced at the industrial level by condensa- tion polymerization, that is, polycondensation of petroleum derived 1,4-butanediol and succinic acid. However, both the diacid and diol monomers are underdevelopment to be obtained by the bacterial fermentation route from renewable resources [3]. In general terms, PBS presents good processability and balanced mechanical and thermal properties, closely comparable to some polyolefins [4, 5]. In particular, it shows tensile and impact strengths similar to those of polypropylene (PP), whereas its glass transition temperature (T_g) and melting temperature (T_m) are approximately −32 and 115 ^oC, respectively, resulting in a thermal profile similar than low-density polyethylene (LDPE) [6]. Furthermore, this biopolyester has a wide melt-processing window, which makes it suitable for extrusion, film blowing, injection molding, fiber spinning, or thermoforming, finding potential ap- plications as packaging films, office supplies, clothing, bags for compost, vegetation nets, mulching films [7, 8] and also in biomedical applications [9, 10]. Nevertheless, PBS is still currently considered an expensive biopolymer, with prices in the 3–6 USD kg^{-1} range, which is considered to be the main limitation for applications of products fully based on this biopolyester [11].

In this regard, the use cost-effective lignocellulosic fillers could facilitate the market penetration of PBS into the plastics industry in the form of green composites. Thus, the most interesting options are related to the valorization of food or agricultural

residues since these raw materials are virtually free and can further improve biodegradability, contributing to the development of the so-called Circular Bioeconomy [12]. As a result, a wide range of agricultural and food waste derived fillers have been recently incorporated into biopolymers in the form of particles or fibers, for example, almond shell [13], coconut fibers [13], orange peel [14], hazelnut shell [15], or coffee husk [16]. In the frame of the Circular Bioeconomy, significant efforts have been particularly dedicated to promote nutshells as lignocellulosic fillers for green composites [17]. In this context, "pistachio" (*Pistacia vera L.*), a genus that belongs to the *Anacardiaceae*, is a nut cultivated and available mostly in The United States, Middle East, and some Mediterranean countries [18, 19]. In recent years, the annual production of pistachio has increased, especially in Turkey and Iran, reaching a global production of 638,000 t [20]. The pistachio fruit can be classified as a semidry drupe and it is characterized by a high nutritional value, unique flavor, and a bright green color under a purplish skin [21]. However, the seed (kernel) is encased by a thin soft and clear brown coat (testa) enclosed by a creamy lignified shell (endocarp) that is surrounded by a green to yellow-red colored fleshy hull (mesocarp and epicarp), which are not edible and constitute approximately 50 wt.% of the pistachio nut [22]. Both the hulls and hard shells are currently considered waste from the pistachio industry and, therefore, become a great source of residue or by-product of low economic value. Besides, in the nut trade, it must be considered that pistachio has the advantage that is unique because of shell splitting naturally before harvesting, offering an economical and sustainable advantage compared to almonds or walnuts where their kernels require to be separated from their shells by mechanical cracking [23].

The current major applications of pistachio shell are related to animal feeding and general uses as biomass [24, 25], being more recently explored as a source energy [26]. However, interestingly, pistachio shell particles present high hardness since it is mainly composed by cellulose (~31 wt.%), hemicellulose (~42 wt.%), lignin (~21 wt.%), crude protein (~1 wt.%), and ashes (~1 wt.%) [27], so these can be ground to produce the so-called pistachio shell flour (PSF) that can be used to prepare polymer composites with higher mechanical strength and hardness. For instance, Gürü *et al.* [28] investigated the possibility of using PSF particles with urea-formaldehyde in composites of particleboard with improved hardness and fire retardant properties.

In other study, powder of pistachio shell was mixed with a polyester resin (Polipol 3401-TAB) in order to obtain a polymer composite [29], showing that low filler content of 5 and 10 wt.% allows to achieve a better dispersion of the particles and higher mechanical properties. Later, in the research performed by Najafabadi et al. [30], high-density polyethylene (HDPE) was filled with PSF and nanoclays (Cloisite 20A) to improve the mechanical resistance of the polyolefin. More recently, Karaağaç [31] reported the addition of pistachio shell powder as filler in a rubber matrix composed of natural rubber (SIR 20) and styrene-butadiene (CAROM 1502), improving the abrasion resistance, thermal stability, and tensile and aging properties. Nevertheless, this residue has been barely used as raw material in combination with biopolymers to yield green composites.

Unfortunately, the incorporation of lignocellulosic fillers into polymers habitually leads to several issues due to the polar hydroxyl (−OH) groups present on the surface of cellulose having difficulty in forming a well-bonded interface with the non-polar polymer/biopolymer matrix since the hydrogen bonds tend to prevent the wetting of the filler surfaces. This low compatibility between both composite components then affects the filler-matrix interfacial adhesion, which can result in poor filler dispersion and large particle agglomeration, both being detrimental for the mechanical performance of the polymer composites. Furthermore, the presence of the hydrophilic fillers frequently promotes undesirable water uptake phenomena that can cause dimensional changes and ageing in the polymer composites [32]. As a result, different strategies have been used to enhance interfacial adhesion in polymer composites, improving their final properties [33]. Among them, filler surface modification with silane coupling agents [34-36], chemical treatments such as alkenyl succinic anhydride (ASA) or sodium hydroxide (alkaline treatment) [37, 38], and plasma treatment [39], have been explored. Furthermore, promising results have been recently achieved by means of the addition of reactive compatibilizers during the extrusion or compounding process, the so-called reactive extrusion [40, 41], which is also more cost-effective and easier to scale up. Among the different compatibilizers, the use of graft copolymers containing reactive groups, such as maleic anhydride (MAH) or glycidyl methacrylate (GMA), represents an effective way to improve the interfacial interaction between the polymer and filler and immiscible biopolymer blends [42]. For instance, based on these

reactive compatibilizers, a feasible and robust strategy has been recently developed to prepare stable co-continuous blends of PBAT and PLA [43, 44].

The use of the same polymer or a highly soluble one as the MAH-grafted matrix makes these agents very compatible with the polymer matrix, whereas the reactive groups can interact with the –OH groups present on the lignocellulosic filler surface, forming covalent bonds during manufacturing by melt mixing at high temperature. Using this approach, Tserki *et al.* [45] prepared and, thereafter, incorporated poly(butylene succinate-*co*-butylene adipate) grafted with maleic anhydride (PBSA-*g*-MAH) at 5 wt.% into green composites of PBSA with spruce and olive husk flours at 30 wt.%. Results demonstrated that an increase in the mechanical strength in the green composite ~33% to 56% was observed. More specifically, for spruce flour composites, the tensile strength increased from 18.5 to 26.5 MPa, reaching values in the range of unfilled PBSA. In another study, Kennouche *et al.* [46] showed that a high compatibilization was achieved in composites of PHBV/PBS/halloysite nanotubes (HNTs) by poly(3-hydroxybutyrate-*co*-3-hydroxyvalerate) grafted with maleic anhydride (PHBV-*g*-MAH). Authors reported an improved dispersion of PBS nodules in the immiscible biopolymer blend with a preferential location of HNTs, owing to the diffusion and emulsifying effect of the PHBV-*g*-MAH chains. More recently, Muthuraj *et al.* [47] described composites of PBS/PBAT with miscanthus fibers at 50 wt.% successfully compatibilized by previously prepared MAH-grafted blends of PBS/PBAT. In particular, tensile strength was increased by approximately 69% when compared to the uncompatibilized composite.

In the present study, green composites of PBS/PSF at different weight ratios, that is, 5, 10, 20, and 30 wt.% of filler, were prepared for the first time. In order to enhance the compatibility between PBS and PSF, poly(butylene succinate) grafted with maleic anhydride (PBS-*g*-MAH) was previously synthesized by a melt-grafting process induced by the presence of an organic peroxide as a radical initiator and, thereafter, added as reactive compatibilizer during melt extrusion at a constant 1/6 (*wt*/*wt*) ratio in relation to the filler content in the green composite. The resultant compounded pellets were finally shaped into pieces by injection molding and characterized to evaluate the performance of the newly developed green composites.

RESULTS

Morphology of PSF

Particle morphology, that is, shape, size, and aspect ratio, plays an important role in the reinforcement of polymer composites. **Figure IV.2.2.1** shows the morphology of the PSF particles observed by FESEM and their respective length and diameter histograms. One can observe in **Figure IV.2.2.1**a that the lignocellulosic particles displayed a rod-like morphology, although some platelets and ellipsoidal-like particles were also formed. A similar sheet-like structure was also observed by Muthuraj *et al.* [47]. The particles also showed a rough surface, which can be attributed to the grinding process performed on hard shells due to their high lignin composition. The particle surfaces also displayed high porosity, as it can be inferred from **Figure IV.2.2.1**b, showing a FESEM micrograph of the lignocellulosic particles taken at higher magnification. This morphology could be beneficial to interactions with the biopolymer matrix by acting as anchoring points. In this regard, da Silva *et al.* [48] reported a similar microstructure for the pistachio shell, indicating that both their surface and cross-section show a dense surface with few cracks. This observation is also in agreement with Yang and Lua [49], who showed that the surface of pistachio shell was quite dense without any pores except for some occasional cracks. Regarding the dimensions of the micronized particles, **Figure IV.2.2.1**c,d gather the histograms in terms of their length and diameter values, respectively. The particles presented an average value of length of 85.8 ± 47.2 μm, whereas the average diameter was 16.1 ± 8.8 μm, resulting in aspect ratio or length/diameter (L/D) of approximately 5. In both cases, the particle dimensions were defined by a classical monomodal distribution with a long tale for the fraction of larger particles. Therefore, this particle morphology is based on a relatively low size, which can offer a positive effect on the overall properties of the polymer composite. In this regard, Kadhim *et al.* [50] proposed that small lignocellulosic particles, of approximately 53 μm, promoted higher mechanical performance in comparison with particles larger than 100 μm in poly(methyl methacrylate) (PMMA) composites.

Optical properies of PBS/PSF composites

Figure IV.2.2.2 shows the resultant injection-molded pieces of the PBS and PBS/PSF com- posites at different filler loadings. This visual appearance is essential in

the role that an end product plays in consumers and applications. One can observe that the unfilled PBS sample showed a "cream" color with no transparency. Then, the pieces developed a light brown color when the micronized powder of PSF was added to PBS, which was progressively intensified as a function of the filler content. This color variation can be mainly ascribed to the intrinsic yellow-to-brown color of PSF. However, the strong color variations, particularly at the highest filler contents, can also be influenced by the local high temperature increases that could occur during melt mixing of these formulations due to their higher specific mechanical energy.

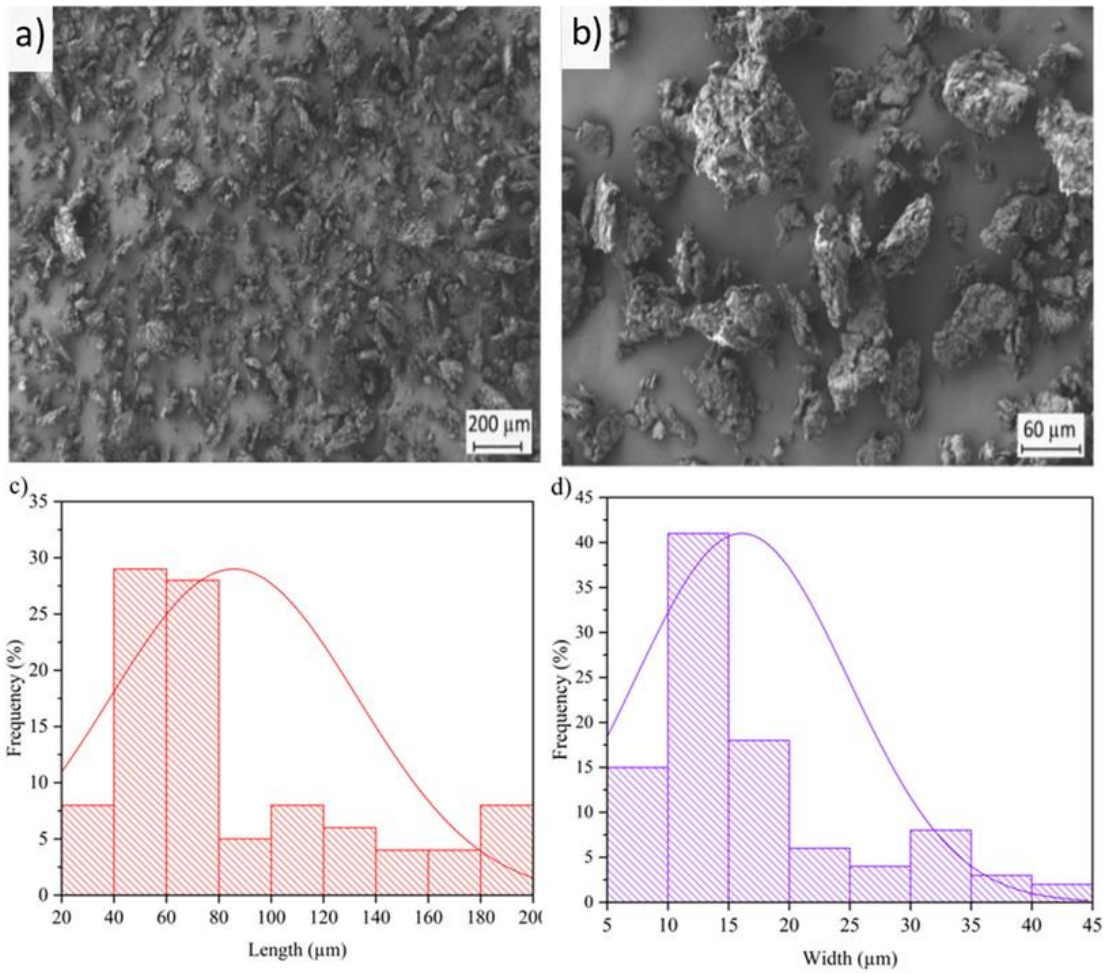

Figure IV.2.2.1. (a) Field emission scanning electron microscopy (FESEM) images of micronized pistachio shell flour (PSF) taken with a magnification of 50x and a scale marker of 200 µm; (b) FESEM image of PSF taken with a magnification of 200x and a scale marker of 60 µm; (c) histogram of the PSF particle length; (d) histogram of the PSF particle width.

Figure IV.2.2.2. Visual appearance of the injection-molded pieces of poly(butylene succinate) (PBS)/pistachio shell flour (PSF) compatibilized with poly(butylene succinate) grafted with maleic anhydride (PBS-*g*-MAH).

Table IV.2.2.1 shows the results of the colorimetric measurements in terms of the L*a*b* color coordinates and the color difference, that is, ΔE_{ab}*, between the PBS piece and the green composite pieces. One can observe that PBS exhibited a white-to-yellow tonality with values of L* = 83.8 and values of a* and b* of 1.8 (green) and 1.1 (yellow), respectively. The incorporation of 5 wt.% PSF resulted in a significant color change with a lower luminosity (L* = 71.8), which represented a percentage difference of 14.3%, and a brownish tonality with values of a* and b* of 1.1 (red) and 15.8 (yellow), respectively. The highest addition of PSF both significantly reduced L*, down to 57.8, and increased a* and b* up to values of 6.8 and 25.1, respectively.

Therefore, the total color variation between PBS and the different green composite samples increased significantly with the filler content, and it was higher than 19 in all cases. According to the proposed visual evaluation [51], a color variation of ΔE_{ab}* > 5 implied that an observer can easily notice different colors. Furthermore, the green composite pieces showed a similar color tonality than some natural woods, a characteristic key property of wood plastic composites (WPCs). For instance, oak without treatment shows color coordinates of L* = 64.46, a* = 6.77, and b* = 20.17, while pine treated at 160 ^{o}C presents coordinates of L* = 64.98, a* = 9.34, and b* = 27.14 [52].

Table IV.2.2.1. Luminance (L*), color coordinates (a*,b*), and color difference (ΔE_{ab}*) of the injection- molded pieces of poly(butylene succinate) (PBS)/pistachio shell flour (PSF) compatibilized with poly(butylene succinate) grafted with maleic anhydride (PBS-*g*-MAH).

Piece	L*	a*	b*	ΔE_{ab}*
PBS	83.8 ± 0.1^{a}	−1.8 ± 0.1^{a}	1.1 ± 0.2^{a}	-
PBS-5PSF	71.8 ± 0.2^{b}	1.1 ± 0.1^{b}	15.8 ± 0.2^{b}	19.0 ± 0.5^{a}
PBS-10PSF	67.6 ± 0.1^{c}	2.8 ± 0.2^{c}	20.1 ± 0.1^{c}	25.0 ± 0.5^{b}
PBS-20PSF	61.8 ± 0.1^{d}	5.1 ± 0.2^{d}	23.0 ± 0.1^{d}	31.2 ± 0.7^{c}
PBS-30PSF	57.8 ± 0.2^{e}	6.8 ± 0.2^{e}	25.1 ± 0.1^{e}	35.7 ± 0.6^{d}

$^{a–e}$ Different letters in the same column indicate a significant difference among the samples ($p < 0.05$).

Mechanical properties of PBS/PSF composites

Table IV.2.2.2 shows the mechanical properties of the PBS/PSF composite pieces obtained from the tensile tests. These results are usually of great interest to evaluate the effect of the lignocellulosic filler on the biopolymer and the performance of the composite pieces for different applications. The tensile test results were expressed in terms of tensile modulus (E), maximum tensile strength (σ_{max}), and elongation at break (ε_b).

Table IV.2.2.2. Mechanical properties of the injection-molded pieces of poly(butylene succinate) (PBS)/pistachio shell flour (PSF) compatibilized with poly(butylene succinate) grafted with maleic anhydride (PBS-*g*-MAH) in terms of tensile modulus (E), maximum tensile strength (σ_{max}), elongation at break (ε_b), Shore D hardness, and impact strength.

Piece	E (MPa)	σ_{max} (MPa)	ε_b (%)	Shore D Hardness	Impact Strength (kJ m^{-2})
PBS	598.8 ± 13.4^{a}	27.8 ± 0.5^{a}	225.5 ± 15.2^{a}	62.9 ± 0.7^{a}	11.4 ± 0.8^{a}
PBS-5PSF	605.6 ± 15.2^{b}	23.1 ± 1.3^{b}	42.9 ± 3.5^{b}	63.6 ± 0.6^{a}	6.8 ± 0.4^{b}
PBS-10PSF	655.5 ± 18.7^{c}	20.1 ± 0.8^{c}	27.7 ± 1.7^{c}	67.8 ± 0.4^{b}	5.6 ± 0.2^{c}
PBS-20PSF	852.2 ± 28.7^{d}	17.0 ± 0.5^{d}	15.9 ± 0.7^{d}	68.8 ± 0.4^{b}	3.3 ± 0.3^{d}
PBS-30PSF	1039.6 ± 32.5^{e}	16.0 ± 1.0^{d}	9.7 ± 1.1^{e}	69.5 ± 0.5^{c}	2.9 ± 0.3^{e}

$^{a–e}$ Different letters in the same column indicate a significant difference among the samples ($p < 0.05$).

As a reference point, the properties of the unfilled PBS pieces were analyzed, showing a ductile behavior with E and σ_{max} values of 598.8 and 27.8 MPa, respectively, being the εb value 225.5%. These values are similar to those reported earlier for injection-molded PBS pieces [53], whereas the differences can be ascribed to the molecular weight

(M_W) and crystallinity of the PBS sample. In this regard, Jin *et al.* [54] showed values of E, tensile strength at yield (σ_y), and εb in the ranges of 280–400 MPa, 24–35 MPa, and 250–640%, respectively, with significant variations depending on the biopolymer's M_W. In particular, the mechanical properties increased with the number-average-molecular weight (Mn) of PBS up to 4.1 × 104 g mol^{-1}, which is similar to the grade used herein, and then decreased with further increasing of Mn. Authors concluded indicating that the best mechanical performance is neither attained for the sample with the highest crystallinity nor for the sample with the highest M_W. One can further observe that the incorporation of PSF increased the E value of the PBS pieces; however, it also resulted in a material with a lower deformation capacity so that the ductile properties of the injection-molded pieces were reduced. In this way, E values of 655.5 and 1039.6 MPa were obtained for the 10PSF and 30PSF pieces, which represents percentage improvements of approximately 9.5% and 79.6%, respectively, compared to the unfilled PBS piece. However, the effect of PSF on the tensile strength also followed a decreasing trend as a function of the amount of lignocellulosic filler. This variation resulted in σ_{max} values of 17.0 MPa for the 20PSF piece and 16.0 MPa for the 30PSF piece, which means percentage reductions of approximately 38.8% and 42.2%, respectively. In this regard, it can be considered that the presence of lignocellulosic particles inside the biopolymer matrix acted as a stress concentration and resulted in a lower tensile strength [50, 55]. Furthermore, the ductility of the pieces was significantly reduced with the PSF content. In the case of the PBS-5PSF, the ε_b value decreased to 42.9%, being approximately 5 times lower than the neat PBS piece. The incorporation of higher amounts of filler further reduced the ductility of the material, but the percentage differences were smaller. For instance, the εb value for the PBS-30PSF piece, with 30 wt.% PSF, reached a value of 9.7%. This embrittlement phenomenon is commonly observed in polymer composites due to the reduction of the movement capacity of the polymer chains by the filler presence and it is particularly critical in the plastic deformation zone, which is drastically reduced [56, 57]. The mechanical results reported herein agrees with previous works based on polymer composites filled with pistachio shells. For instance, the work of Kadhim *et al.* [50] reported that powder of pistachio shell could successfully reinforce PMMA, increasing E from nearly 1 GPa to up to 1.35 GPa, whereas σ_y and ε_b decreased from 66 MPa and 5% to approximately 46 MPa and 1.8%.

Table IV.2.2.2 also shows the results of the Shore D hardness tests. In the case of the unfilled PBS pieces, it showed a hardness value of 62.9. Similar to the E values, the incorporation of PSF to PBS yielded a progressive increase in the hardness of the pieces, which is related to the reduction of the movement of the biopolymer chains [58]. In particular, hardness increased from 63.6, for the PBS-5PSF piece, to 69.5, for that of PBS-30PSF. This Shore D hardness value is relatively close to, for instance, that of PLA, that is, ~79, which is considered to be a hard biopolymer material [51]. Finally, results of the Charpy impact test showed a significant reduction in the energy absorption capacity when the micronized lignocellulosic particles were introduced. For instance, whereas the neat PBS piece yielded an impact energy absorption of 11.4 kJ m^{-2}, the addition of 5 wt.% PSF resulted in a value of 6.8 kJ m^{-2} while the use of 30 wt.% PSF resulted in a value of 2.9 kJ m^{-2}, which respectively represents percentage reductions of approximately 40.4% and 74.6%. Impact strength is highly related to the deformation capacity of the material, and those materials with a higher deformation ability show a higher energy absorption in Charpy impact test. In comparison with a previous work in which PBS was filled with 30 wt.% of almond shell flour (ASF), the incorporation of the lignocellulosic particles also decreased impact strength from 16.5 to 1.8 kJ m^{-2}; however, the use of maleinized linseed oil (MLO) as compatibilizer increased toughness in the green composite to 3.8 kJ m^{-2} [53].

Morphology of PBS/PSF composites

In **Figure IV.2.2.3**, field emission scanning electron microscopy (FESEM) micrographs with the surface fractures of the green composite pieces after the Charpy impact tests can be observed. It can be seen that the morphology of the surface fracture changed from a rough surface, as seen in **Figure IV.2.2.3**a in the case of the unfilled PBS piece, to a smoother fracture surface with the presence of microcracks in the green composite pieces shown in **Figure IV.2.2.3**b–e. The latter morphology, with a lower roughness, can be ascribed to the embrittlement of the PBS matrix due to the presence of the lignocellulosic fillers [59]. It should also be underlined the absence of gap surrounding the PSF surface in contact with PBS since the lignocellulosic fillers were completely embedded in the biopolymer matrix, suggesting that PBS-*g*-MAH successfully compatibilized the two components of the green composite. Similar morphological observations have been previously reported for PBS/ASF compatibilized by MLO, who indicated that a good compatibilization is achieved when the size

of these gaps are reduced or even removed [60]. Similar findings were also reported by Phua *et al.* [61], who similarly proposed PBS-*g*-MAH for improving the interaction of PBS in nanocomposites prepared with organically modified montmorillonite (OMMT).

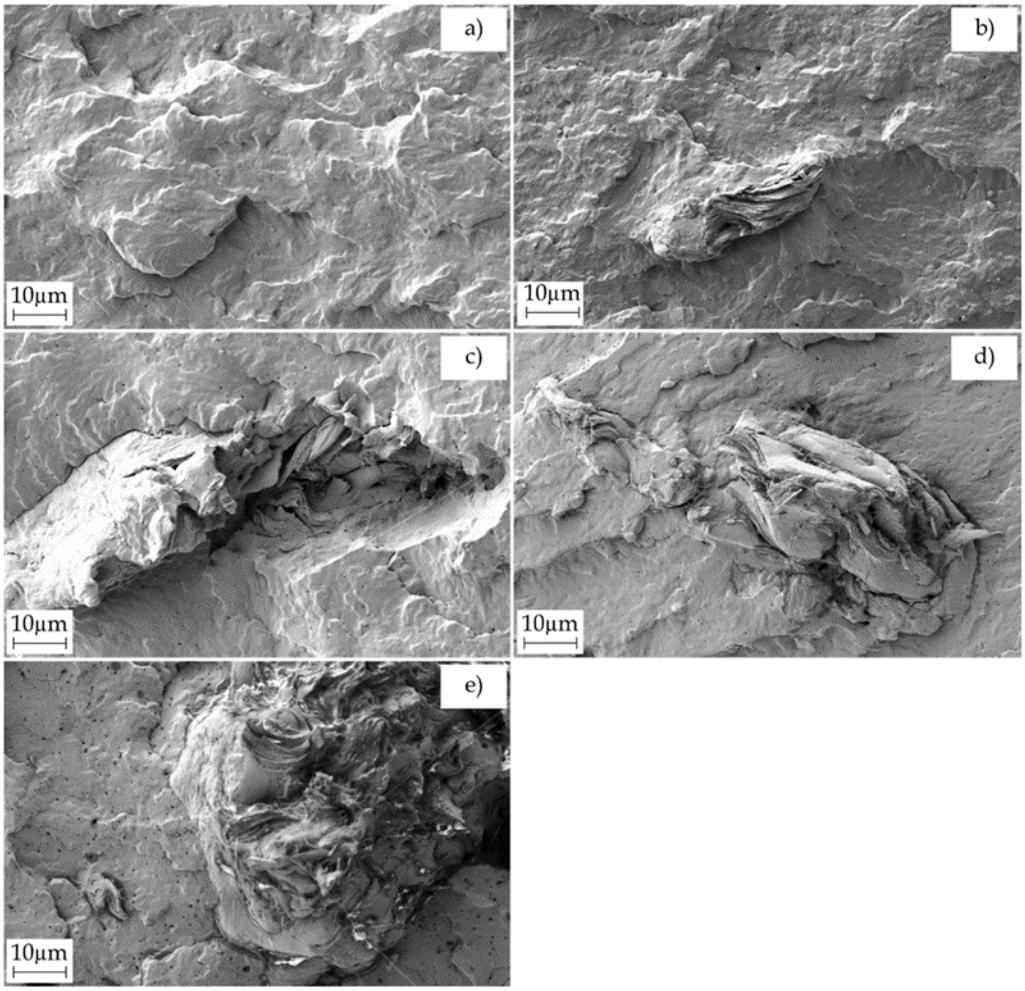

Figure IV.2.2.3. Field emission scanning electron microscopy (FESEM) images of the fracture surfaces of the injection-molded pieces of poly(butylene succinate) (PBS)/pistachio shell flour (PSF) compatibilized with poly(butylene succinate) grafted with maleic anhydride (PBS-*g*-MAH): (a) PBS, (b) PBS-5PSF, (c) PBS-10PSF, (d) PBS-20PSF, and (e) PBS-30PSF. Images were taken at 1,000x with scale markers of 10 µm.

Spectroscopic properties of PBS/PSF composites

Figure IV.2.2.4 shows the attenuated total reflection-Fourier transform infrared (ATR-FTIR) spectra of the PSF powder, the PBS-*g*-MAH dough, and the injection-molded pieces of neat PBS and its green composites with PSF and PBS-*g*-MAH. It can be seen in **Figure IV.2.2.4**a that the FTIR spectrum of PSF was mainly characterized by the presence of three strong peaks. It can be observed the first broad and intense band at ~1,035 cm^{-1} wavelength, which can be correlated with C–O stretching vibrations in

alcohols and phenols of lignocellulose, and it belongs to the polyglykosidic moieties (polyol) [48]. Then, the second strong peak arose at 2910 cm^{-1}, and it corresponds to (C–H) vibrations in methyl (–CH_3) and methylene (–CH_2–) groups of cellulose and lignin [62]. This band has been indicated to be contrary to the δ(C–H) vibrational bands for –CH_3 and –CH_2– groups due to the skeletal C–C vibrations in aromatic rings, which were also found for pistachio nut shells and located herein at around 1263 and 1412 cm^{-1} [49]. The latter bands overlapped with those attributed to C–O–H in-plane bending and C–O stretching for carboxyl (–COOH) groups in lignin [48].

Finally, the third and also broad peak seen in the region of 3000–3600 cm^{-1} is indicative of the large presence of hydroxyl (–OH) groups in pistachio shell [63]. Other minor peaks were seen at 1664 cm^{-1}, which occurs due to C=C vibrations in aromatic rings and olefinic ν(C–C) absorptions present in lignin, and at 1735 cm^{-1} due to the C=O stretching of the carbonyl (C=O) group, which is mainly associated with hemicellulose [48]. Therefore, from the FTIR spectrum of PSF, it was confirmed the lignocellulosic nature of the food waste derived filler as well as the presence of several oxygen groups on its chemical structure such as carbonyl groups, ethers, esters, alcohols, and phenol groups.

The characteristic peaks for PBS, in both the unfilled piece and the green composite pieces, were seen as a strong and sharp band at ~1714 cm^{-1} wavelength, ascribed to the C=O stretching of the ester groups in biopolyester, in addition to multiple peaks in the 1100–1200 cm^{-1} region mainly corresponding to the C–O stretching vibration in the ester groups, and the broad and low-intense peaks at 1330 and 2960 cm^{-1} due the symmetric and asymmetric stretching vibrations of –CH_2– groups [54]. In relation to the strongest peak, it was reported that the PBS biopolymer can show three absorption bands at 1736, 1720, and 1714 cm^{-1} wavelengths that are stemmed from C=O stretching modes in the mobile amorphous fraction (MAF), rigid amorphous fraction (RAF) (or intermediate phase), and crystalline phase, respectively [64]. Since the crystal lattices should have the strongest confinement effect on C=O groups in the lamellar structure of the PBS crystal, including physical and hydrogen bonding, it was suggested that it is more reasonable to assign the 1714 cm^{-1} band to the C=O in crystal lattices. Therefore, this further confirms the high crystallinity achieved in the PBS samples during injection molding.

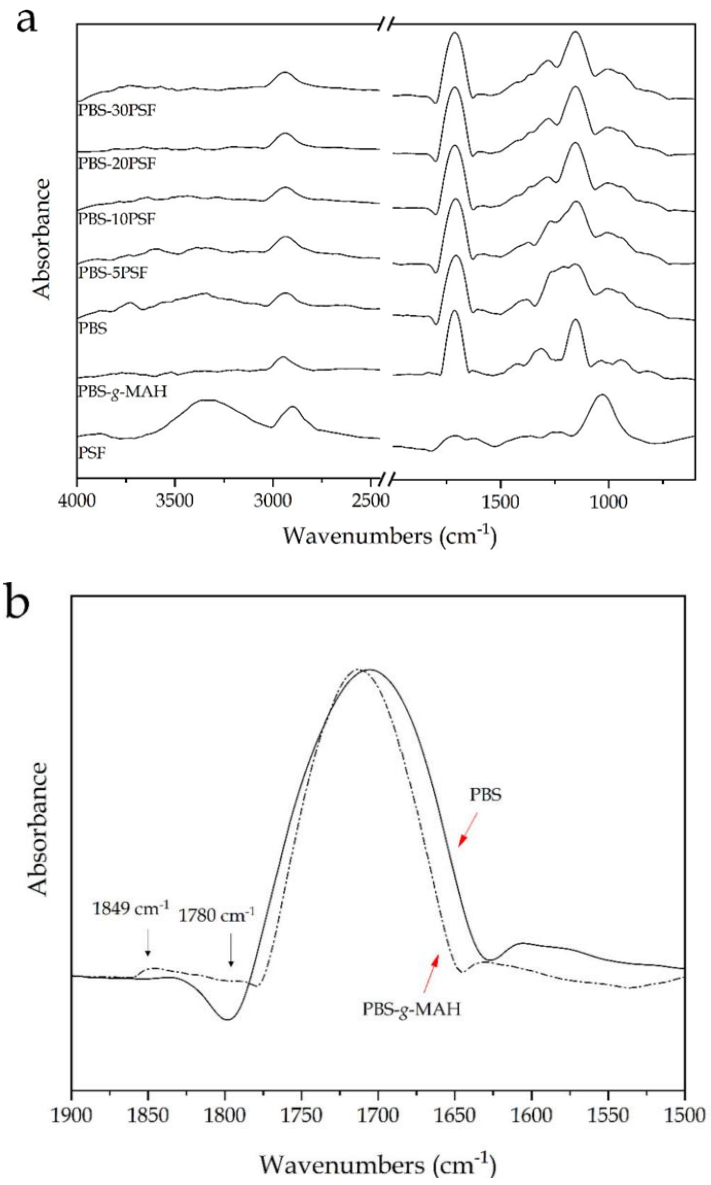

Figure IV.2.2.4. (a) Fourier transform infrared (FTIR) spectra, from bottom to top, of pistachio shell flour (PSF); poly(butylene succinate) grafted with maleic anhydride (PBS-*g*-MAH), poly(butylene succinate) (PBS), and PBS-5PSF, PBS-10PSF, PBS-20PSF, and PBS-30PSF green composites; (b) Detail of the PBS-*g*-MAH and PBS spectra in the 1900–1500 cm^{-1} region to show the MAH grafting onto PBS.

The outcome of the MAH grafting onto PBS was also investigated by FTIR. The strongest absorption signal was the one attributed to the C=O stretching vibrations of ester groups in PBS, which slightly shifted to ~1720 cm^{-1} and also narrowed due to crystalline phase disruption and potential loss. By comparison of the PBS-*g*-MAH and PBS spectra in the 1900–1500 cm^{-1} region, one can observe in **Figure IV.2.2.4**b that there was a new signal absorption band at 1849 cm^{-1}, which is characteristic for succinic

anhydride groups and has been formerly attributed to the symmetric C=O stretching bonds of MAH [65]. Furthermore, this was accompanied by a signal level increase at nearly 1780 cm^{-1}, corresponding to their symmetric stretching. Moreover, the peak related to (C–H) vibration of PBS was shifted in the PBS-*g*-MAH spectrum from approximately 2965 cm^{-1} to 2980 cm^{-1} as a result of the grafting process since it could be affected by the $=CH_2$ vibration of the cyclic MAH that was reported to arise at 3058 cm^{-1}. Although the band changes in the PBS-*g*-MAH were subtle, these have already served to demonstrate the reactive grafting process of MAH at the diol unit of PBS [45, 61]. All these newly formed bands and band distortions are, thus, representative of the functional groups available in the grafted biopolymer [66-69]. In addition to this, these new peaks did not appear in either the neat PBS spectrum or green composite spectra, suggesting that these groups were removed or consumed during melt grafting.

Finally, it can be observed that all the green composites showed very similar FTIR spectra than neat PBS, with the most noticeable change in the intensity increase of the peak centered at ~1163 cm^{-1}. This band change can be ascribed to the presence of PSF in PBS, with a strong contribution of the C–O stretching vibration signals, which was seen at a lower wavelength in the spectrum of the biopolyester. Furthermore, the subsequent broadening of signals in the region of 1300–1400 cm^{-1}, from which multiple peaks with low intensity arise, could be attributed to esters (e.g., R–CO–O–R'), ethers (e.g., R–O–R'), or phenol groups newly formed due to the grafting reaction of –OH groups of cellulose and lignin with the MAH groups present in PBS-*g*-MAH. Moreover, the intensity of the peaks observed in the 1150–1300 cm^{-1} decreased, which has been ascribed to −C–O–C− groups in the ester linkages of PBS [61], suggesting that the proportional contribution of the original groups in the biopolyester was reduced and also observed at higher wavenumbers due to the potential formation of new ones. Therefore, these peaks variations point to an esterification reaction achieved by the functional MAH groups present in PBS-*g*-MAH with the −OH groups of PSF. The scheme of this process is proposed in **Figure IV.2.2.5**, which illustrates the grafting mechanism of PSF onto PBS by PBS-*g*-MAH. Although PBS-*g*-MAH is readily soluble in PBS, part of their multiple MAH can also react with the −OH end groups of the biopolyester, both present in acids or alcohols, following the scheme shown in **Figure IV.2.2.5**a. Moreover, according to the final scheme proposed in **Figure IV.2.2.5**b, other MAH groups can connect with –OH

groups present in the cellulose or lignin of PSF by esterification [70]. Therefore, the here-developed PBS-*g*-MAH acted as a bridge between the PSF filler and the PBS matrix.

Thermal properties of PBS/PSF composites

Figure IV.2.2.6 shows the differential scanning calorimetry (DSC) curves for the injection- molded pieces of PBS and its green composites with PSF in the thermal range from 140 ºC to 20 ºC during cooling (**Figure IV.2.2.6**a) and from 40 ºC to 175 ºC in the second heating (**Figure IV.2.2.6**b). In **Table IV.2.2.3**, the main thermal parameters obtained from the cooling and heating thermograms are summarized, that is, the crystallization temperature (T_C), cold crystallization temperature (T_{CC}), melting temperature (T_m), and the amount of crystallinity (X_C) determined from the melting enthalpy (ΔH_m) of the samples. One can observe that the neat PBS sample first crystallized from the melt at 69.7 ºC and, thereafter, further cold crystallized at 96.6 ºC prior to melting at 113.4 ºC. This melting peak value is in the range established for the semi-crystalline PBS homopolymer, showing values from 112 to 116 ºC [7] and also in agreement with those obtained by Kim *et al.* [71] and Chen *et al.* [72] who reported values of 112.2 ºC and 114.2 ºC, respectively. The formation of PBS crystals during both cooling and also, to a lesser extent, heating, the so-called cold crystallization, has been reported elsewhere, showing T_C, T_{CC}, and T_m values of 80.5, 102.5, and 114.6 ºC, respectively [73]. In particular, cold crystallization is a phenomenon mainly associated with high-M_W PBS due to the lower number of chain ends involved and, subsequently, reduction in the free volume [74, 75].

The incorporation of PSF promoted crystallization from the melt but also slightly delayed cold crystallization, particularly at low filler contents, reaching the highest T_C and T_{CC} values at 77.7 and 102 ºC, respectively, for the PBS-5PSF sample. This observation suggests that the presence of the lignocellulosic fillers favored crystallization of the PBS molecules. However, the values of T_m were significantly unaltered whereas the percentage of crystallinity, measured as X_C, increased from 51.8%, for the neat PBS, up to nearly 63% for the green composites containing 20 and 30 wt.% PSF. This result indicates that the lignocellulosic fillers acted as heterogeneous nuclei during the formation of crystals and a greater number of molecules could crystallize from the melt. The nucleating effect on PBS of other fillers, such as calcium carbonate and distiller grains, has been previously reported by Chen *et al.* [72] and other authors

[76, 77]. Similar results were also observed by Liminana *et al.* [78], who reported an increase in the PBS crystallinity after the incorporation of ASF in different contents from 10 to 50 wt.%. Furthermore, the filler effect on crystal growth could also be maximized by the use of the PBS-*g*-MAH compatibilizer that, as shown above during the morphological analysis, successfully enhanced the interactions between the PBS matrix and the lignocellulosic particles [79]. In this regard, Phua *et al.* [61] suggested that the improved interaction between PBS and fillers by PBS-*g*-MAH contributed to the crystallization increase of the biopolyester.

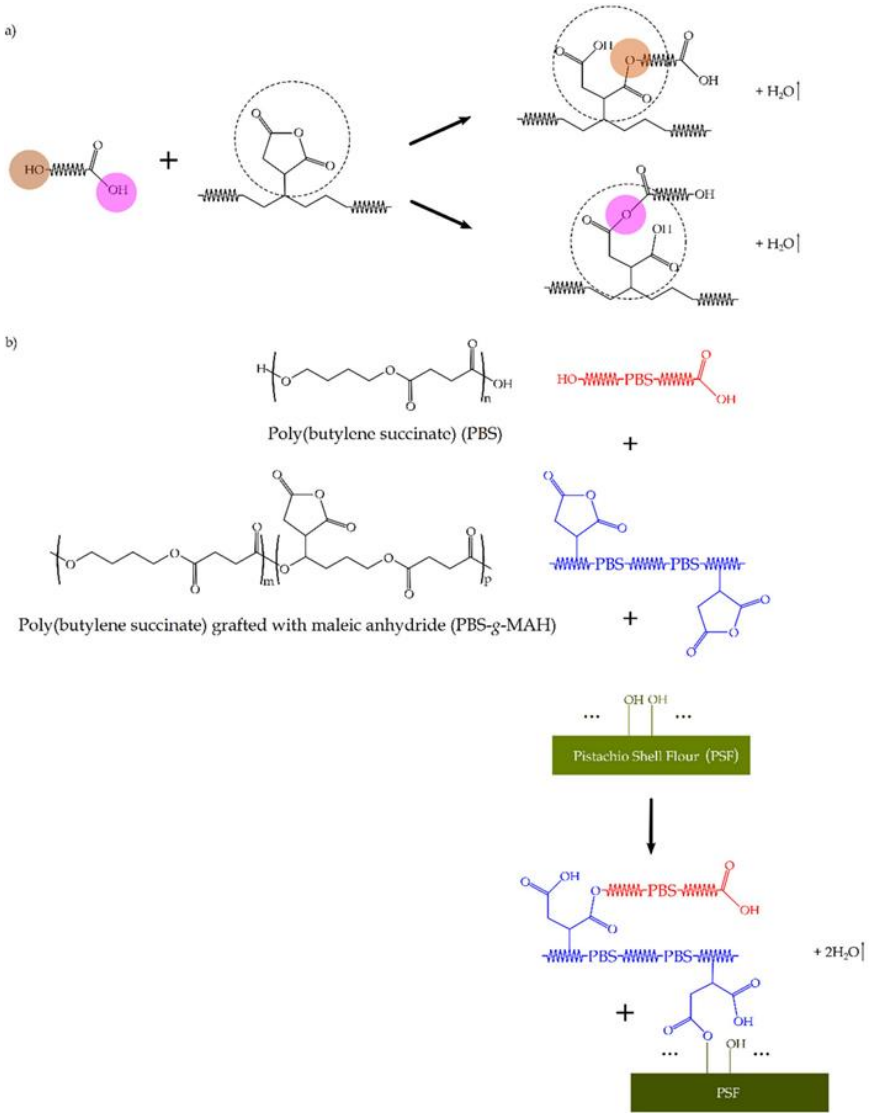

Figure IV.2.2.5. (a) Chemical reaction between the hydroxyl (−OH) end groups of poly(butylene succinate) (PBS) with maleic anhydride (MAH) groups; (b) Melt-grafting process of cellulose or lignin of pistachio shell flour (PSF) onto PBS by esterification reaction of their −OH groups with poly(butylene succinate) grafted with maleic anhydride (PBS-*g*-MAH).

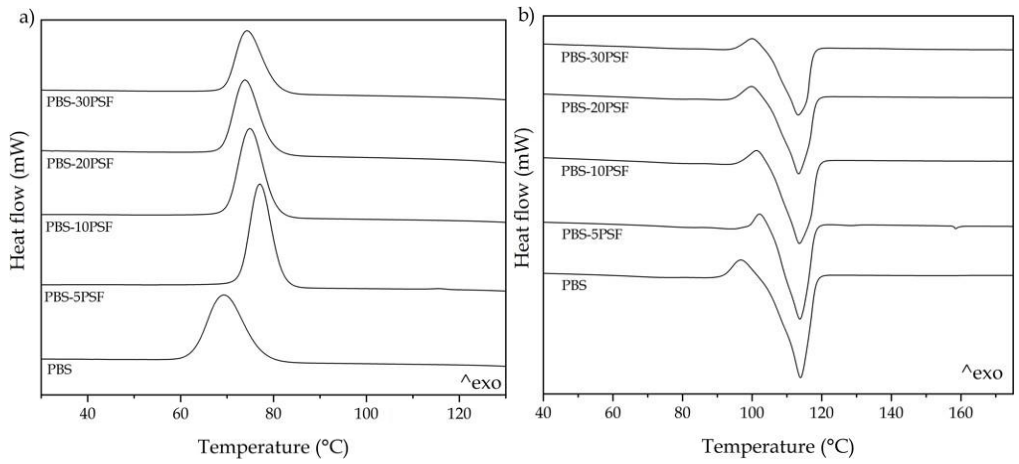

Figure IV.2.2.6. Differential scanning calorimetry (DSC) thermograms taken during cooling (a) and second heating (b) of the injection-molded pieces of poly(butylene succinate) (PBS)/pistachio shell flour (PSF) compatibilized with poly(butylene succinate) grafted with maleic anhydride (PBS-*g*-MAH).

Table IV.2.2.3. Main thermal parameters of the injection-molded pieces of poly(butylene succinate) (PBS)/pistachio shell flour (PSF) compatibilized with poly(butylene succinate) grafted with maleic anhydride (PBS-*g*-MAH) in terms of crystallization temperature (T_c), crystallization enthalpy (ΔH_c), cold crystallization temperature (T_{cc}), cold crystallization enthalpy (ΔH_{cc}), melting temperature (T_m), melting enthalpy (ΔH_m), and crystallinity degree (X_c).

Piece	T_c (°C)	ΔH_c (J g^{-1})	T_{cc} (°C)	ΔH_{cc} (J g^{-1})	T_m (°C)	ΔH_m (J g^{-1})	X_c (%)
PBS	69.7 ± 0.9^a	63.8 ± 0.8^a	96.6 ± 0.4^a	5.3 ± 0.8^a	113.4 ± 0.8^a	62.5 ± 0.9^a	51.8 ± 1.2^a
PBS-5PSF	77.7 ± 1.1^b	65.9 ± 0.5^a	102.0 ± 0.7^b	3.0 ± 0.4^b	113.3 ± 0.5^a	57.3 ± 0.7^b	52.2 ± 0.9^a
PBS-10PSF	75.5 ± 0.7^c	64.2 ± 1.0^a	101.4 ± 0.6^b	3.5 ± 0.6^c	113.0 ± 0.7^a	56.9 ± 1.1^b	54.9 ± 1.0^b
PBS-20PSF	74.3 ± 0.6^d	53.8 ± 1.2^b	99.7 ± 0.4^c	3.5 ± 0.8^c	112.8 ± 1.0^a	56.6 ± 0.8^b	62.8 ± 1.2^c
PBS-30PSF	74.7 ± 1.1^d	48.2 ± 0.5^c	99.8 ± 0.9^c	2.5 ± 0.5^d	112.9 ± 0.6^a	47.5 ± 1.2^c	62.7 ± 0.7^c

$^{a–d}$ Different letters in the same column indicate a significant difference among the samples ($p < 0.05$).

Figure IV.2.2.7 shows the thermogravimetric analysis (TGA) and first derivative thermogravimetry (DTG) curves, respectively gathered in **Figure IV.2.2.7**a,b, for the PBS pieces and their green composite pieces with different contents of PSF.

Table IV.2.2.4 presents the main thermal parameters obtained from the thermogravimetric curves, that is, the onset degradation temperature that was considered for the temperature with a loss of 5% ($T_{5\%}$), temperature of maximum degradation (T_{deg}), corresponding to the maximum degradation rate and identified in the corresponding DTG curves, and residual mass at 700 ºC. In the case of PSF, like other biomass, three different mass losses were seen during the degradation process, which have been ascribed to drying, devolatilization, and charring [80].

The first mass loss, at ~100 ºC, is related to the removal of moisture present in the lignocellulosic material. The second one, in the thermal range from 200 to 400 ºC, represents the thermal decomposition of holocellulose, that is, the degradation of hemicellulose (210–325 ºC) and cellulose (310–400 ºC) [81]. This zone is known as the "active pyrolysis zone" due to its high rate of devolatilization, where occurs the majority of the pyrolysis with a mass loss of ~55% [40].

Finally, the third zone of degradation started at approximately 310 ºC, and it corresponds to the thermal decomposition of the rest of cellulose and lignin, which occurs from 400 ºC. This stage is termed "passive pyrolysis" since the mass loss rate is lower compared with the previous stage, and it can be seen as a tailing section in the DGT curve [81].

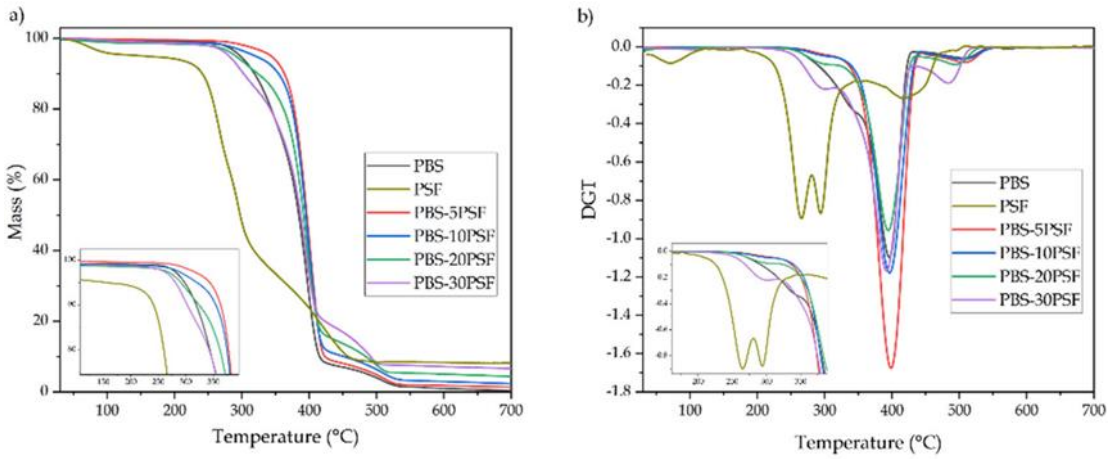

Figure IV.2.2.7. Thermogravimetric analysis (TGA) curves (a) and first derivate thermogravimetric (DTG) curves (b) of the injection-molded pieces of poly(butylene succinate) (PBS)/pistachio shell flour (PSF) compatibilized with poly(butylene succinate) grafted with maleic anhydride (PBS-*g*-MAH).

Table IV.2.2.4. Main decomposition parameters of the injection-molded pieces of poly(butylene succinate) (PBS)/pistachio shell flour (PSF) compatibilized with poly(butylene succinate) grafted with maleic anhydride (PBS-*g*-MAH) in terms of onset degradation temperature at a mass loss of 5% ($T_{5\%}$), temperature of maximum degradation (T_{deg}), and residual mass at 700 °C.

Piece	$T_{5\%}$ (°C)	T_{max} (°C)	Residual Mass (%)
PSF	224.8 ± 0.9[a]	264.8 ± 0.8[a]/293.7 ± 1.1[b]	8.2 ± 0.9[a]
PBS	296.6 ± 1.0[b]	398.3 ± 0.7[c]	0.4 ± 0.2[b]
PBS-5PSF	341.9 ± 0.8[c]	401.6 ± 1.5[c]	1.4 ± 0.5[c]
PBS-10PSF	318.3 ± 0.7[d]	399.0 ± 0.7[c]	2.3 ± 0.7[d]
PBS-20PSF	290.9 ± 1.2[e]	397.4 ± 0.8[c]	4.4 ± 0.5[e]
PBS-30PSF	279.6 ± 1.0[f]	394.9 ± 1.0[c]	6.6 ± 0.8[f]

[a–f] Different letters in the same column indicate a significant difference among the samples ($p < 0.05$).

One can observe that PBS was thermally stable up to ~297 °C and, opposite to other reports [61, 82], thermal degradation was seen to occur in two steps. Nevertheless, a two-step thermal decomposition behavior has been widely observed in biopolyesters [83, 84]. It can be seen that the main and fast mass loss took place from nearly 300 to 405 °C, and it corresponds to the main degradation of the biopolymer backbone, yielding the formation of char with a mass loss of over 90%. The second decomposition step was observed in the 405–525 °C range, and it is related to the thermo-oxidative degradation of the char produced during the first degradation step, associated with a loss of nearly the totality of the remaining biopolyester. This degradation profile has been reported to occur in thermostable polyesters subjected to air atmosphere [85]. Furthermore, the thermal stability of the green composites, interestingly, revealed that the samples with low filler loadings, that is, filled with 5 and 10 wt.% PSF, significantly delayed $T_{5\%}$. In particular, the PBS-5PSF and PBS-10PSF green composite pieces yielded values of 341.9 °C and 318.3 °C. Meanwhile, the PBS samples filled with 20 and 30 wt.% PSF, that is, PBS-20PSF and PBS-30PSF, achieved slightly, but still significant, lower onset values of degradation than the neat PBS sample (290.9 °C and 279.6 °C, respectively). This result suggests that, at low filler contents, the good filler-to-matrix interaction achieved by PBS-*g*-MAH induced a positive effect on thermal degradation due to grafting of the PBS molecules onto the lignocellulosic particles. However, the highest content of fillers slightly impaired the thermal degradation of PBS, which is an effect reported and ascribed to the inherently lower thermal stability of lignocellulose [86]. It is also worth mentioning that, in all cases, due to the presence of the lignocellulosic fillers, the char

mass produced during the second degradation step increased. Therefore, in terms of the residual mass, measured at 700 ºC, it increased as a function of the PSF loading incorporated in the samples, from 0.4 wt.% for neat PBS, up to a value of 6.6 wt.% in the PBS-30PSF piece. This residual mass corresponds to inorganic residues, such as silica, contained in PSF [72].

Thermomechanical properties of PBS/PSF composites

Figure IV.2.2.8 shows the dynamical mechanical thermal analysis (DMTA) curves for the neat PBS pieces and the PBS/PSF composite pieces. **Table IV.2.2.5** gathers the most relevant thermomechanical parameters, namely the storage modulus measured at −45, 25, and 70 ºC, which correspond to temperatures below and above each transition region, and also the dynamic damping factor (tan δ). In **Figure IV.2.2.8**a, which shows the evolution of the loss modulus as function of temperature, it can be observed that the PBS piece presented at −45 ºC the highest value, that is, 1973.3 MPa. This high value of storage modulus is due to the amorphous region of the biopolyester at this temperature being in its vitreous state.

At higher temperatures, the PBS and its green composites showed two relaxation regions at approximately −40 ºC and 30 ºC, and these low- and high-temperature transitions are respectively related to its β-and α-relaxations. In particular, the low-temperature transition has been ascribed to the β-relaxation of the amorphous fractions of PBS, and it is also considered the glass transition of the biopolyester, for which a T_g value of −30 ºC has been reported elsewhere [87]. Therefore, in the temperature range from −40 to 25 ºC, the storage modulus suffered the most pronounced drop, reaching a value of 440 MPa. Thereafter, from nearly 35 ºC, a low-intense reduction in the storage modulus was observed, which is indicative of the α-relaxation process related to the PBS polymer crystalline fractions [47]. Thus, the storage modulus of the PBS pieces dropped to a value of 214.3 MPa at 70 ºC, which is close to the initiation of cold crystallization reported above during DSC analysis.

One can further see that the incorporation of PSF reinforced the PBS matrix, and this effect can be easily noticed by the increase in the storage modulus along the whole thermal range tested. Thus, the highest value was attained for the PBS with 30 wt.% of PSF, showing a value of 2161.1 MPa at −45 ºC. This observation agrees with the previous

mechanical results, indicating that the lignocellulosic fillers reinforced the PBS matrix and restricted the movement of the biopolymer chains [78]. This result also points out that the use of the PBS-*g*-MAH as compatibilizer facilitates the interaction of PSF with PBS.

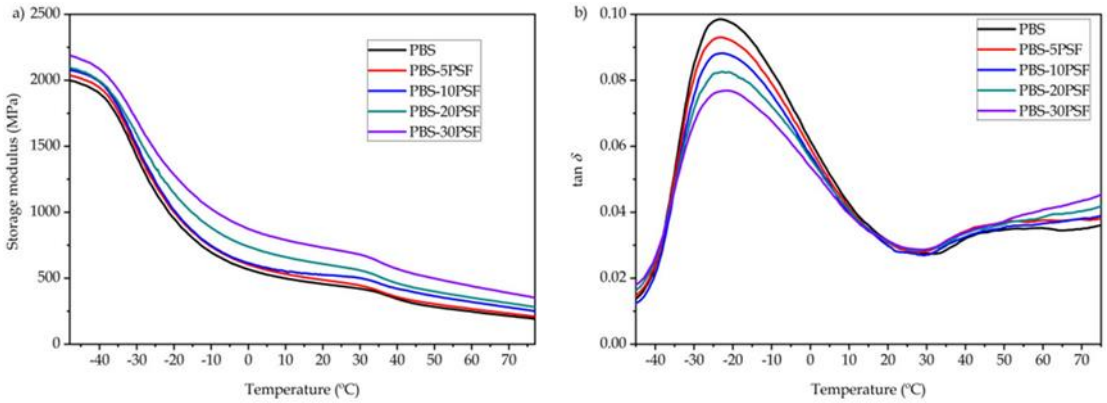

Figure IV.2.2.8. Evolution as function of the temperature of the storage modulus (a) and dynamic damping factor (tan δ) (b) of the injection-molded pieces of poly(butylene succinate) (PBS)/pistachio shell flour (PSF) compatibilized with poly(butylene succinate) grafted with maleic anhydride (PBS-*g*-MAH).

Table IV.2.2.5. Thermomechanical properties of the injection-molded pieces of poly(butylene succinate) (PBS)/pistachio shell flour (PSF) compatibilized with poly(butylene succinate) grafted with maleic anhydride (PBS-*g*-MAH) in terms of storage modulus measured at −45, 25, and 70 °C and dynamic damping factor (tan δ) peak.

Piece	Storage Modulus (MPa)			Tan δ Peak (°C)
	−45 °C	25 °C	70 °C	
PBS	1973.3 ± 30^{a}	440 ± 10^{a}	214.3 ± 12^{a}	−23.3 ± 0.2^{a}
PBS-5PSF	2016.1 ± 35^{a,b}	468 ± 21^{a}	233.1 ± 20^{a,b}	−23.0 ± 0.1^{b}
PBS-10PSF	2056.5 ± 37^{a,b}	516 ± 14^{b}	279.9 ± 22^{b,c}	−22.7 ± 0.3^{c}
PBS-20PSF	2072.2 ± 38^{a,b}	585 ± 12^{c}	310.3 ± 17^{c}	−22.3 ± 0.4^{d}
PBS-30PSF	2161.1 ± 34^{b}	705 ± 15^{d}	387.0 ± 21^{d}	−21.8 ± 0.2^{e}

$^{a–e}$ Different letters in the same column indicate a significant difference among the samples ($p < 0.05$).

Figure IV.2.2.8b provides the evolution with temperature of tan δ, also called damping factor, which allows to identify the main relaxations of PBS. As it can also be observed in the **Table IV.2.2.5**, the neat PBS showed a tan δ peak of −23.3 °C, which is related to its T_g and ascribed to the β-relaxation, whereas it was followed by a low-intense second peak at nearly 45 °C due to the α-relaxation. It can also be observed that the position of the damping factor peaks slightly increased to higher temperatures with

the incorporation of PSF, which may indicate that these fillers caused some inhibition of the PBS chain motion [88]. As suggested above, this effect can also be ascribed to the higher interaction achieved due to the reactive grafting with PBS-*g*-MAH. A similar behavior was reported by Liminana *et al.* [60] with an increase of T_g in samples of PBS reinforced with ASF and compatibilized with MLO. Furthermore, it is worth mentioning that all the green composite samples presented lower values of tan δ peak than the unfilled PBS sample, decreasing progressively with the PSF content. This reduction is characteristic to materials with lower energy dissipation and reduced toughness, which can be explained by the fact that the biopolymer with amorphous regions was partially replaced with hard lignocellulosic fillers [89].

Water uptake of PBS/PSF composites

Figure IV.2.2.9 shows the evolution of water uptake with time in a 14-week immersion period for the PBS pieces and the PBS/PSF composite pieces. In the case of the neat PBS piece, it reached an absorption value of ~0.73 wt.% after 14 weeks of immersion in water. A similar value was reported previously by Frollini *et al.* [90], confirming the high hydrophobicity of this biopolyester. Furthermore, it can be observed in the graph that the introduction of the lignocellulosic fillers notably increased the amount of water absorbed in the material during the immersion period. In general, a direct relationship can be observed between the amount of this type of waste derived filler, based on lignocellulose and the total water absorbed in the polymer composite sample [91]. This fact is ascribed to the hydrophilic nature of lignocellulose due to the large amount of free –OH groups on the filler surface [92]. For instance, water uptake increased up to 2.23 wt.% for the green composite pieces filled with 10 wt.% PSF, that is, PBS-10PSF, whereas it reached a value of 6.14 wt.% for a 30 wt.% filler loading, that is, PBS-30PSF. In this regard, Gairola *et al.* [93] also reported that PSF shows a great tendency to entrap water, showing a value of water absorption of 2.75 wt.% after 7 days for a thermosetting epoxy composite with 10 wt.% PSF. Nevertheless, it is worth remarking that all these tests were carried out using injection-molded pieces that were laterally uncoated when fully immersed in water, which may represent more aggressive conditions than those typically found for end-use applications of WPCs.

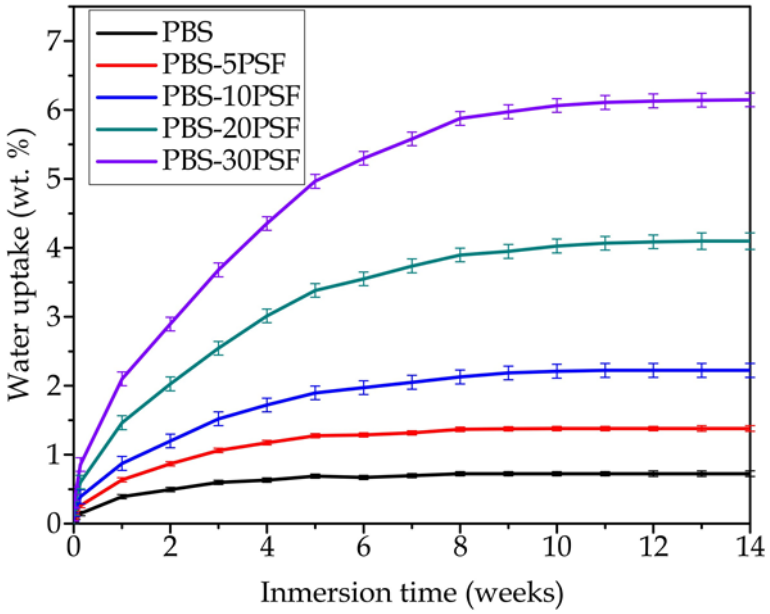

Figure IV.2.2.9. Evolution of the water uptake during a 14-week immersion period of the injection-molded pieces of poly(butylene succinate) (PBS)/pistachio shell flour (PSF) compatibilized with poly(butylene succinate) grafted with maleic anhydride (PBS-*g*-MAH).

One can also observe that, at the end of the immersion period analyzed, that is, 14 weeks, all samples saturated their water absorption capability. However, the largest mass increases occurred in the first weeks of immersion and, interestingly, this was seen to occur more rapidly in the unfilled PBS sample and the green composites with lower filler loadings. For example, the green composite pieces containing 5 wt.% PSF saturated after approximately 5 weeks, whereas water uptake was stabilized after 9 weeks of immersion in the green composite pieces filled with 20 and 30 wt.% of lignocellulosic fillers. In general terms, the use of reactive compatibilizers that show the capacity of anchoring the lignocellulosic fillers to the polymer matrix, which is the case of PBS-*g*-MAH, can slightly reduce water uptake due to the reduction in the number of freely available –OH groups [94]. However, better results in terms of hydrophobicity have been achieved by chemical pre-treatments on the filler surface [95]. For instance, it has been reported that lignocellulosic waste flour pre-treated with acetylation or propionylation led to a significant reduction in the percentage of water uptake in PBS green composites, of nearly 50%, whereas the use of compatibilizers yielded lower reductions. This fact was attributed to the substitution of hydrophilic –OH groups of the lignocellulosic material with acetyl and propionyl groups, rendering the lignocellulosic flour surface more hydrophobic [96]. In the case of the compatibilizer addition, the water absorption reduction can be mainly attributed to the formation of covalent bonds between the MAH

groups and the –OH groups at flour surface [97], which are therefore less effective than chemically modified lignocelluloses.

Disintegration in controlled compost soil of PBS/PSF composites

The disintegration behavior of the PBS and PBS/PSF pieces under controlled compost- ing conditions was analyzed for a period of 112 days, that is, 16 weeks. This timeframe goes beyond the "reasonably short period of time" described in international standards of compostability. In particular, the EN 13432 or ASTM D6400 standards require the plastic articles certified as compostable to disintegrate after 12 weeks or 84 days, and completely biodegrade after 180 days, which means that at least 90% of the bioplastic material will have been converted to carbon dioxide (CO_2), water, and biomass. **Figure IV.2.2.10** shows results of the disintegration tests in terms of the evolution of the percentage of weight loss (**Figure IV.2.2.10**a) and the visual aspect of the pieces at each tested time during composting (**Figure IV.2.2.10**b). It can be observed that, during the first 4 weeks of composting, the mass loss was very subtle, and the visual aspect of the pieces remained nearly unaltered. Then, higher rates of disintegration were observed after nearly 35 days of composting, from which all the PBS samples started to loss mass relatively fast whereas the piece surfaces were seen to be eroded. From the week 6 up to approximately 3 months, the pieces showed a linear and very steep degradation progression. At this time, however, the degradation rate was noticeably reduced, and the mass loss reached a value of approximately 20 wt.% at the end of the test. In this regard, it is worth noting that the test was conducted at 58 ^{o}C and 55% RH, which are certainly favorable conditions in terms of high temperature and humidity for the hydrolytic degradation of PBS. On the base of the here-attained uncompleted disintegration process, other authors [98, 99] also found a similar degradation profile for PBS, identifying three phases with different degradation speeds, namely the lag phase with a low rate (<5 days), biodegradation phase where the rate was accelerated (6–66 days), and *plateau* phase in which disintegration leveled off (>67 days). Authors also concluded that the shape and format of the PBS articles played a major role during disintegration in controlled compost. In particular, whereas PBS powder with an average particle size of 42 μm and the resultant 40 μm thermo-compressed film sizing 1 cm x 1 cm showed biodegradation percentages after 90 days of 71.9 and 60.7 wt.%, respectively, the as-received granules of ~3 mm only disintegrated up to 14.1 wt.%. It

was then confirmed that biodegradability of PBS under composting conditions is mainly controlled by the sample's specific surface area.

In another study, it was observed that PBS sheet samples of 30 mm 30 mm 1 mm were discolored after one month and their surface was completely damaged by the microorganisms of biodegradation after 3 months, but the sheets did not fully disintegrate in 5 months [45] Therefore, the previous finding supports and agrees with the percentages of degradation achieved herein for the injection-molded pieces of PBS with a thickness of 4 mm, which was approximately 13.4 wt.% for 91 days and 18.3 wt.% at the end of the test, that is, after 112 days.

One can also observe that the incorporation of PSF together with PBS-*g*-MAH increased the disintegration rate during the second biodegradation phase, that is, from days 35 to 70. Then, disintegration progressively increased with the filler content, and this effect may be ascribed to the higher tendency of the fillers to entrap water, as described above during the water uptake analysis, which could then transfer water into the composite by means of the capillary effect favoring the biopolymer hydrolysis of the ester groups [100]. Nevertheless, around day 60, it can be observed that this tendency changed, and the disintegration rate of PBS increased faster than in the case of the green composites. These mass loss changes were correlated with the visual images of the pieces at different times of disintegration, where it can be seen that the unfilled PBS fragmented to a higher extend at the end of the assay, although the development of color dark-to-black changes occurred earlier in the case of the green composites. A similar trend was observed by Quiles-Carrillo *et al.* [14] during the biodegradation process of green composites of PLA with orange peel flour (OPF) compatibilized by MLO, also showing a slightly slower degradation profile in the final weeks for the green composites in comparison to the unfilled biopolyester. The slower degradation rate in the green composites can be mainly ascribed to a latter increase in water diffusion resistance through the composite due to a tortuosity effect of the fillers on the biopolymer matrix during the *plateau* phase [101]. Furthermore, the use of PBS-*g*-MAH could reduce the –OH concentration and, thus, reduce the water activity.

Other authors further suggested that the presence of remaining DCP amounts, which was used herein as radical initiator for the synthesis of PBS-*g*-MAH, could also interfere with the biopolymer chain scission, delaying the biodegradability process [102].

Additionally, it has also been indicated that the presence of diverse mineral fillers, such as talk and chalk, which can be present in minor quantities in pistachio shell, together with silica, can also influence the disintegration behavior of PBS [98, 99]. In any case, one should conclude that the large thickness of the pieces certainly limited the appropriate disintegration evaluation of PBS under industrial composting conditions so that the actual effect of the lignocellulosic fillers on compostability was difficult to elucidate.

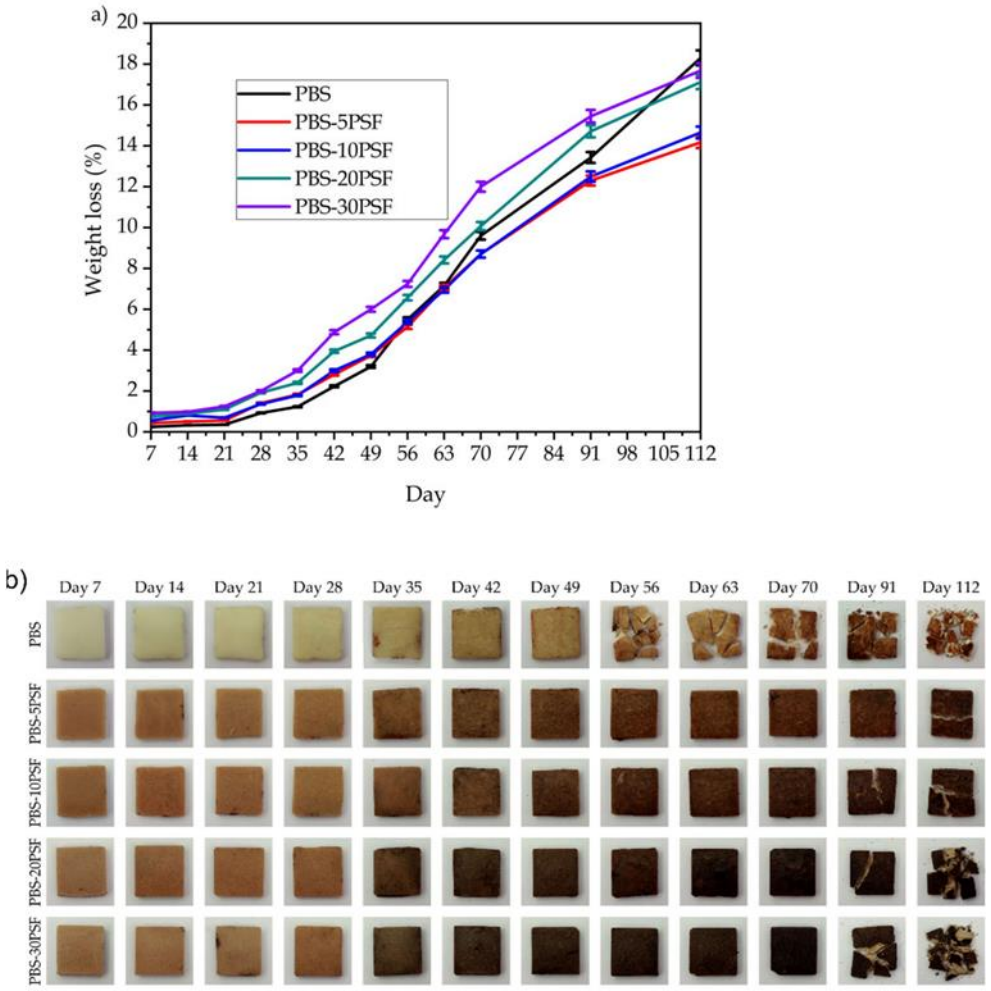

Figure IV.2.2.10. Weight loss as a function of elapsed time during disintegration test in controlled compost soil (a) and visual aspect (b) of the injection-molded pieces of poly(butylene succinate) (PBS)/pistachio shell flour (PSF) compatibilized with poly(butylene succinate) grafted with maleic anhydride (PBS-*g*-MAH).

DISCUSSION

The present study demonstrates the high potential of pistachio shells, a residue of the agricultural and food industries, to be manufactured in the form of flour for serving as a reinforcing filler in combination with biodegradable polymers to yield green

composites in the frame of the circular bioeconomy. The incorporation into PBS by melt mixing of low and moderate contents of PSF, below 20 wt.%, and subsequent shaping using injection molding successfully led to the development of material pieces with a wood-like appearance, higher rigidity and hardness, improved crystallinity, and high thermal stability. To improve the inherently low compatibility between this waste derived lignocellulosic, PBS-*g*-MAH was synthetized using DCP as an initiator in a previous step. The grafting methodology achieved herein offers the possibility to produce tailor-made compatibilizers for different green composites since these can be produced with the same biopolymer as the base resin, so that it is fully miscible with the composite matrix, whereas it contains multiple reactive MAH groups that can chemically interact with the –OH groups in the cellulose or lignin present on the filler surface by esterification or with those of the biopolyester. As a result of this melt-grafting process, the interfacial filler-matrix adhesion is improved, and the properties of the green composites are enhanced and/or higher filler contents can be loaded. Future works will be dealing with the development of new green composites based on this approach, including the valorization of other agricultural, food, or marine wastes, and also a deeper understanding of their degradation mechanisms in different environments.

MATERIALS AND METHODS

Materials

PBS Bionolle 1020MD was supplied by Showa Denko Europe (Munich, Germany) which is a liner aliphatic biopolyester characterized by a density of 1.26 g cm^{-3} and a melt flow rate (MFR) of 25 g per 10 min (190 ^{o}C and 2.16 kg). It shows a M_n of 3.7 × 104 g mol^{-1} and a dispersity ($Đ = M_W/M_n$) of 1.65 [103]. This PBS grade is mainly designed for injection molding and it is certified as compostable according to the EN-13432 standard. MAH and DCP, with purity of 98%, were both purchased at Sigma-Aldrich S.A. (Madrid, Spain) in the form of fine powder.

PSF was obtained from Micronizados Vegetales S.L. (Córdoba, Spain) as a waste of the food industry. The pistachio shells were cleaned and ground into powder form using a jaw crusher. The collected powder was then sieved to obtain a flour composed of particles with a mean size of less than 75 μm. The raw pistachio shells and the resultant flour in powder form are shown in **Figure IV.2.2.11**.

Figure IV.2.2.11. (a) Pistachio shells; (b) Resultant pistachio shell flour (PSF) after milling and sieving.

Grafting procedure

The grafting reaction was carried out an internal mini-mixer (HAAKETM PolyLabTM QC, Thermo Fisher Scientific, Karlsruhe, Germany) under the conditions established by Phua *et al.* [61] in the presence of an organic peroxide initiator. Initially, the PBS pellets were physically premixed with the MAH and DCP powders at contents of 10 and 1 parts per hundred resin (phr) of PBS, respectively. Then, the resultant mixture was fed into the melt-mixing device and processed at 135 ^{o}C for 7 min. Thereafter, the resultant dough was purified by refluxing in chloroform (Panreac S.A., Barcelona, Spain) for 4 h, and the hot solution was filtered and precipitated into cold methanol (Sigma-Aldrich S.A.). Finally, in order to remove any unreacted reagents, it was washed with methanol several times, followed by drying at 60 ^{o}C for 24 h in an air-circulating oven CARBOLITE Eurotherm 2416 CG (Hope Valley, UK).

The degree of grafting (G_d) for PBS-*g*-MAH was determined through titration also following the determination proposed by Phua *et al.* [61]. Briefly, 1 g of purified PBS-*g*- MAH was refluxed for 1 h in 100 mL of chloroform. Then, 10 mL of distilled water were added and titrated immediately with 0.025 M potassium hydroxide (KOH, Sigma-Aldrich S.A.) using phenolphthalein (Fisher Scientific SL, Madrid, Spain) as indicator. G_d was calculated using **Equation IV.2.2.1**.

$$G_d(\%)=\left[\frac{N \times (V_1 - V_0) \times 98.06}{1000 \times W \times 2}\right] \times 100 \qquad \textbf{Equation IV.2.2.1}$$

where N is the KOH concentration [M], V_0 and V_1 represent the KOH volume [mL] for blank solution and for titration of PBS-*g*-MAH, respectively, and W is the sample weight [g]. A grafting efficiency or G_d value of 3.84 ± 0.27% was attained.

Figure IV.2.2.12 shows the reaction mechanism to obtain the grafted material, that is, PBS-*g*-MAH. The reaction starts with the peroxide decomposition to form the primary DCP free radicals (I) that abstract the hydrogen atom from PBS backbone to yield PBS macroradicals during the initiation step (II). These biopolymer macroradicals are formed mainly from chain transfer reactions by free radicals that are generated from thermal decomposition of organic initiators [104]. The resultant macroradicals propagated and set off the grafting of MAH onto PBS (III). The reaction continued until the resultant PBS-MAH macroradicals might undergo hydrogen transfer from another biopolymer chains, MAH, or the initiator and formed the so-called PBS-*g*-MAH (IV). Alternatively, the PBS-MAH macroradicals can react with other radicals in the system, such as MAH, PBS, or primary radicals to form a different structure of PBS-*g*-MAH (V). The formation of side groups and side chains is mainly due to addition of PBS macroradicals to the double bond of MAH molecules and also the combination of PBS macroradicals with those of PBS-MAH. In this regard, it should be considered that other unwanted reaction pathways could occur, for example, the homopolymerization of MAH, that is, PBS-(MAH-)$_n$, resulting in a product with higher grafting degree but lesser compatibilization efficiency.

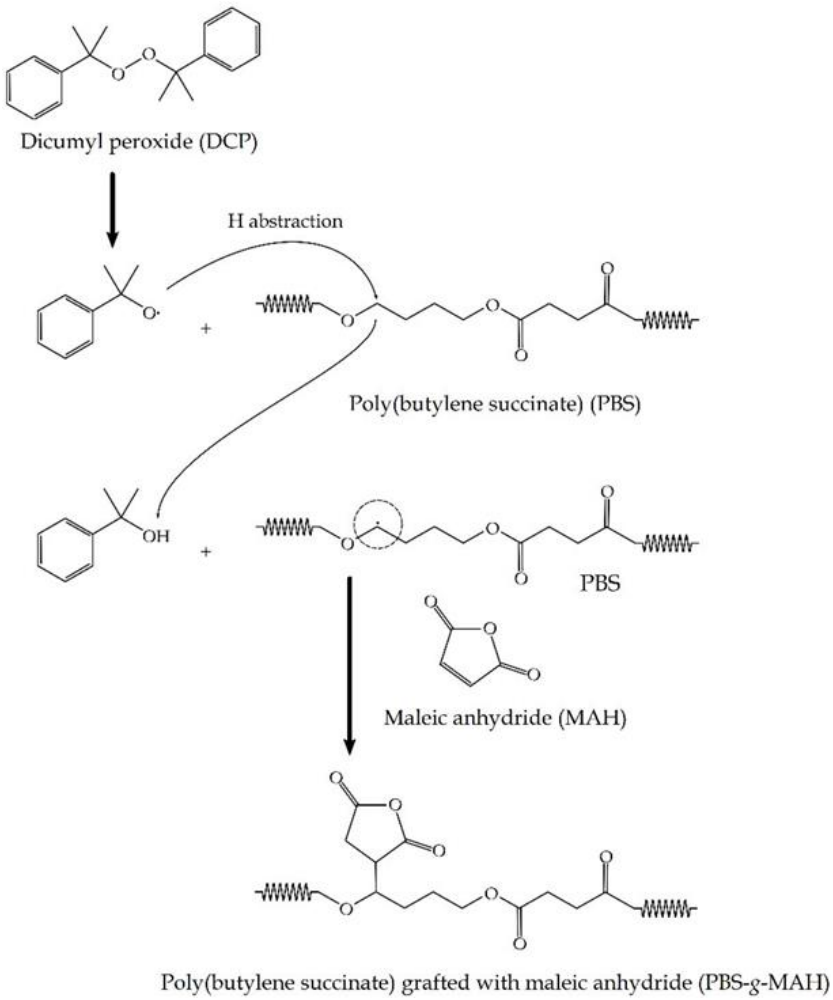

Figure IV.2.2.12. Reaction mechanism to obtain poly(butylene succinate) grafted with maleic anhydride (PBS-*g*-MAH) from poly(butylene succinate) (PBS) and maleic anhydride (MAH) induced by the presence of dicumyl peroxide (DCP).

Preparation of PBS/PSF composites

PBS, PBS-*g*-MAH, and PSF were first dried at 50 ºC for 24 h in an air-circulating oven CARBOLITE Eurotherm 2416 CG to avoid hydrolysis by moisture during the extrusion process. **Table IV.2.2.6** shows the compositions used for the compounding process, where PBS-*g*-MAH was added at a constant 1/6 (*wt*/*wt*) ratio in relation to the PSF content. The mixtures were weighed and pre-mixed manually in a zip bag that were fed into a co-rotating extruder of Mecánicas Dupra S.L. (Castalla, Spain). This extruder has a diameter of 25 mm and a L/D ratio of 24. Compounding was carried out at 25 rpm and temperatures of 115–120–125–130 ºC (from the hopper to the die), resulting in a residence time of approximately 1 min.

Table IV.2.2.6. Summary of compositions according to the weight content (wt.%) of poly(butylene succinate) (PBS), pistachio shell flour (PSF), and poly(butylene succinate) grafted with maleic anhydride (PBS-*g*-MAH).

Composition	PBS (wt.%)	PSF (wt.%)	PBS-*g*-MAH (wt.%)
PBS	100.00	0.00	0.00
PBS-5PSF	94.20	5.00	0.83
PBS-10PSF	88.30	10.00	1.67
PBS-20PSF	76.60	20.00	3.30
PBS-30PSF	65.00	30.00	5.00

Test specimens were thereafter obtained by injection molding using a Meteor 270/75 from Mateu & Solé (Barcelona, Spain) machine. The processing conditions consisted of a temperature profile of 120–125–130–135 ^{o}C (from the hopper to the injection nozzle), cavity filling and cooling times of 1 and 10 s, respectively, and a clamping force of 75 t. Standard samples with an average thickness of 4 mm were produced.

Characterization of PBS/PSF composite pieces

Morphological characterization

The morphology of the PSF particles and the fractured samples obtained from the Charpy tests were studied by field emission scanning electron microscopy (FESEM) in a ZEISS ULTRA 55 microscope from Oxford Instruments (Abingdon, UK) using an acceleration voltage of 2 kV. Prior to observation, the samples were sputtered with a gold-palladium alloy in an EMITECH sputter coating SC7620 model from Quorum Technologies, Ltd. (East Sussex, UK). The FESEM measurements were carried out using an acceleration voltage of 2 kV. Size values were obtained using the ImageJ program in 1.8 version from the National Institutes of Health (Bethesda, MD, USA) using, at least, 20 FESEM images in their original magnification.

Color characterization

Color changes were measured with a Konica CM-3600d Colorflex-DIFF2, from Hunter Associates Laboratory, Inc. (Reston, VA, USA). The CIELAB color space (L*, a*,

b*) was determined in which L* refers to lightness of the sample while the coordinates a* stands for the green (a* < 0) to red (a* > 0) and b* for the blue (b* < 0) to yellow (b* > 0). **Equation IV.2.2.2** shows the expression used to obtain the color differences compared with the neat PBS piece.

$$\Delta E_{ab}{}^{*}=\sqrt{(\Delta L^{*})^{2}+(\Delta a^{*})^{2}+(\Delta b^{*})^{2}} \qquad \textbf{Equation IV.2.2.2}$$

Evaluation of color change was assessed following previous criteria [51]: unnoticeable ($\Delta E_{ab}{}^{*} < 1$), only an experienced observer can notice the difference ($\Delta E_{ab}{}^{*} \geq 1$ and < 2), an unexperienced observer notices the difference ($\Delta E_{ab}{}^{*} \geq 2$ and < 3.5), clear noticeable difference ($\Delta E_{ab}{}^{*} \geq 3.5$ and < 5), and the observer notices different colors ($\Delta E_{ab}{}^{*} \geq 5$).

Mechanical characterization

The tensile properties of the PBS/PSF pieces with dimensions of 150 mm x 10 mm x 4 mm were obtained using the ELIB 50 universal test machine from Ibertest (Madrid, Spain) according to ISO 527-1:2012 with a 5 kN load cell and a testing speed of 5 mm min^{-1}.

Hardness was measured according to ISO 868:2003 with a Shore-D scale using a 676-D hardness tester from J. Bot Instruments (Barcelona, Spain) on rectangular samples sizing 80 mm x 10 mm x 4 mm. Finally, impact strength was measured according to ISO 179-1:2010 with a 1-J pendulum from Metrotec S.A. (San Sebastian, Spain), using V-notched samples with a radius of 0.25 mm and sizes of 80 mm x 10 mm x 4 mm. All measurements were carried out at room temperature and, for each of the test, at least 6 measurements were performed.

Infrared spectroscopy

Chemical analysis of the PSF powder, PBS-*g*-MAH, and the pieces of PBS and PBS/PSF composites was performed by ATR-FTIR spectroscopy. For the test, a Bruker S.A Vector 22 (Madrid, Spain) was used, coupled to a PIKE MIRacleTM single reflection diamond ATR accessory (Madison, WI, USA). Spectra were collected as the average of 10 scans between 4000 and 500 cm^{-1} with a resolution of 2 cm^{-1}.

Thermal analysis

DSC was carried out in a Mettler-Toledo 821 calorimeter (Schwerzenbach, Switzerland). All the tests were performed with samples with an average weight of 6–7 mg, and the thermal program was divided into three stages: a first heating from 25 to 130 ^{o}C, followed by a cooling to 0 ^{o}C, and a second heating to 250 ^{o}C, all with all heating/cooling rates at 10 ^{o}C min^{-1}. Tests were run in nitrogen atmosphere with a flow-rate of 66 mL min^{-1} using standard sealed aluminum crucibles with a capacity of 40 µL. The degree of crystallinity (X_C) was measured following **Equation IV.2.2.3**:

$$X_c = \left[\frac{\Delta H_m - \Delta H_{cc}}{\Delta H_m^0 \times w}\right] \times 100\ (\%) \qquad \textbf{Equation IV.2.2.3}$$

where ΔH_m (J g^{-1}) is the melting enthalpy, ΔH_m^0 (J g^{-1}) represents the theoretical enthalpy of a fully crystalline sample of PBS with a value of 110.3 J g^{-1} [53, 105], and the term w is the weight fraction of PBS.

Thermal degradation of the green composite pieces was assessed by TGA in a LINSEIS TGA 1000 (Selb, Germany). All samples, with a weight of 15–17 mg, were placed in 70 µL alumina crucibles, a dynamic heating program from 40 to 700 ^{o}C at a heating rate of 10 ^{o}C min^{-1} in air atmosphere. All thermal tests were performed in triplicate to obtain averaged results.

Thermomechanical characterization

Dynamical mechanical thermal analysis (DMTA) was carried out in a DMA1 dynamic analyzer from Mettler-Toledo (Schwerzenbach, Switzerland), working in single cantilever flexural mode. Rectangular samples sizing 20 mm x 6 mm x 2.7 mm were subjected to a dynamic temperature sweep from −45 to 75 ^{o}C and a heating rate of 2 ^{o}C min^{-1}. The selected frequency was set at 1 Hz, and the maximum deformation was 10 µm.

Water absorption test

Injection-molded samples of 4 mm x 10 mm x 80 mm were immersed in distilled water at room temperature. Samples were first weighted in a balance and then immersed in distilled water. All of them were wrapped within a metal grid to ensure the correct

immersion. Thereafter, the weight of all the sample pieces was measured in intervals of different time intervals for up to 14 weeks. For each measurement, prior to annotate weight, the surface moisture of the samples was removed with tissue paper. The amount of absorbed water during the process was calculated following **Equation IV.2.2.4**:

$$\text{Water absorption} = \left[\frac{W_t - W_0}{W_0}\right] \times 100\ (\%) \qquad \textbf{Equation IV.2.2.4}$$

where W_0 and W_t represent the initial weight before the immersion and the weight of the sample after each immersion time.

Disintegration test

Disintegration of the PBS/PSF composite pieces was evaluated under composting conditions at 58 ºC and 55% RH following the recommendations of ISO 20200. Injection-molded pieces sizing 20 mm x 20 mm x 4 mm were placed in a carrier bag and buried in a controlled soil compost made of sawdust (40 wt.%), rabbit-feed (30 wt.%), ripe compost (10 wt.%), corn starch (10 wt.%), saccharose (5 wt.%), corn seed oil (4 wt.%), and urea (1 wt.%). Once a week, each sample was unburied from the composting facility, washed with distilled water, dried, and weighed in an analytical balance. The weight loss during disintegration was calculated using **Equation IV.2.2.5**:

$$\text{Weight loss} = \left[\frac{W_0 - W_{te}}{W_0}\right] \times 100\ (\%) \qquad \textbf{Equation IV.2.2.5}$$

where W_0 is weight of the sample before the immersion and W_{te} is the weight of the sample in each measure. All tests were carried out by triplicate to obtain an average.

FUNDING

This research was funded by the Ministry of Science and Innovation (MICI) project number MAT2017-84909-C2-2-R.

ACKNOWLEDGMENTS

S. Rojas-Lema is grateful to Generalitat Valenciana (GVA) for her Grisolia GRISOLIAP/2019/132. S. Torres-Giner acknowledges MICI for his Ramón y Cajal contract (RYC2019-027784-I).

REFERENCES

[1] S. Torres-Giner, K.J. Figueroa-Lopez, B. Melendez-Rodriguez, C. Prieto, M. Pardo-Figuerez, and J.M. Lagaron. *Emerging trends in biopolymers for food packaging*, in *Sustainable Food Packaging Technology*. 2021: Weinheim, Germany, p. 1-33.

[2] P. Bajpai. *Biobased polymers: properties and applications in packaging*. 2019, Amsterdam, Nehtherlands: Elsevier, p. 250.

[3] R.P. Babu, K. O'Connor, and R. Seeram. *Current progress on bio-based polymers and their future trends.* Progress in Biomaterials, 2013, 2(1), p. 8.

[4] F. Signori, M. Pelagaggi, S. Bronco, and M.C. Righetti. *Amorphous/crystal and polymer/filler interphases in biocomposites from poly (butylene succinate).* Thermochimica acta, 2012, 543, p. 74-81.

[5] A. Bhatia, R.K. Gupta, S.N. Bhattacharya, and H. Choi. *Compatibility of biodegradable poly (lactic acid)(PLA) and poly (butylene succinate)(PBS) blends for packaging application.* Korea-Australia rheology journal, 2007, 19(3), p. 125-131.

[6] N. Jacquel, F. Freyermouth, F. Fenouillot, A. Rousseau, J.P. Pascault, P. Fuertes, and R. Saint-Loup. *Synthesis and properties of poly(butylene succinate): Efficiency of different transesterification catalysts.* Journal of Polymer Science Part A: Polymer Chemistry, 2011, 49(24), p. 5301-5312.

[7] J. Xu and B.-H. Guo. *Microbial succinic acid, its polymer poly (butylene succinate), and applications*, in *Plastics from bacteria*. 2010, Springer: Heidelberg, Germany, p. 347-388.

[8] V. Siracusa, N. Lotti, A. Munari, and M. Dalla Rosa. *Poly (butylene succinate) and poly (butylene succinate-co-adipate) for food packaging applications: Gas barrier properties after stressed treatments.* Polymer Degradation and Stability, 2015, 119, p. 35-45.

[9] H.H. Cheng, J. Xiong, Z.N. Xie, Y.T. Zhu, Y.M. Liu, Z.Y. Wu, J. Yu, and Z.X. Guo. *Thrombin-loaded poly(butylene succinate)-based electrospun membranes for rapid hemostatic application.* Macromolecular Materials and Engineering, 2018, 303(2), p. 1700395.

[10] M. Gigli, M. Fabbri, N. Lotti, R. Gamberini, B. Rimini, and A. Munari. *Poly (butylene succinate)-based polyesters for biomedical applications: A review.* European Polymer Journal, 2016, 75, p. 431-460.

[11] A. Nazrin, S. Sapuan, M. Zuhri, R. Ilyas, R. Syafiq, and S. Sherwani. *Nanocellulose reinforced thermoplastic starch (TPS), polylactic acid (PLA), and polybutylene succinate (PBS) for food packaging applications.* Frontiers in chemistry, 2020, 8, p. 213.

[12] R. Liu, Y. Peng, J. Cao, Y.J.C.S. Chen, and Technology. *Comparison on properties of lignocellulosic flour/polymer composites by using wood, cellulose, and lignin flours as fillers.* Composites Science and Technology, 2014, 103, p. 1-7.

[13] L. Quiles-Carrillo, N. Montanes, C. Sammon, R. Balart, and S. Torres-Giner. *Compatibilization of highly sustainable polylactide/almond shell flour composites by reactive extrusion with maleinized linseed oil.* Industrial Crops and Products, 2018, 111, p. 878-888.

[14] L. Quiles-Carrillo, N. Montanes, J.M. Lagaron, R. Balart, and S. Torres-Giner. *On the use of acrylated epoxidized soybean oil as a reactive compatibilizer in injection-molded compostable pieces consisting of polylactide filled with orange peel flour.* Polymer International, 2018, 67(10), p. 1341-1351.

[15] S. Montava-Jordà, L. Quiles-Carrillo, N. Richart, S. Torres-Giner, and N. Montanes. *Enhanced interfacial adhesion of polylactide/poly(ε-caprolactone)/walnut shell flour composites by reactive extrusion with maleinized linseed oil.* Polymers, 2019, 11(5), p. 758.

[16] D.L. Ortiz-Barajas, J.A. Arévalo-Prada, O. Fenollar, Y.J. Rueda-Ordóñez, and S. Torres-Giner. *Torrefaction of coffee husk flour for the development of injection-molded green composite pieces of polylactide with high sustainability.* Applied Sciences, 2020, 10(18), p. 6468.

[17] N. Sutivisedsak, H.N. Cheng, C.S. Burks, J.A. Johnson, J.P. Siegel, E.L. Civerolo, and A. Biswas. *Use of nutshells as fillers in polymer composites.* Journal of Polymers and the Environment, 2012, 20(2), p. 305-314.

[18] Y. Tonbul. *Pyrolysis of pistachio shell as a biomass.* Journal of Thermal Analysis and Calorimetry, 2008, 91(2), p. 641-647.

[19] N. Kasiri and M. Fathi. *Production of cellulose nanocrystals from pistachio shells and their application for stabilizing Pickering emulsions.* International journal of biological macromolecules, 2018, 106, p. 1023-1031.

[20] A. Taghizadeh-Alisaraei, H.A. Assar, B. Ghobadian, and A. Motevali. *Potential of biofuel production from pistachio waste in Iran.* Renewable and Sustainable Energy Reviews, 2017, 72, p. 510-522.

[21] B. Ling, B. Zhang, R. Li, and S. Wang. *Nutritional quality, functional properties, bioactivity, and microstructure of defatted pistachio kernel flour.* Journal of the American Oil Chemists' Society, 2016, 93(5), p. 689-699.

[22] N. Cardullo, M. Leanza, V. Muccilli, and C. Tringali. *Valorization of agri-food waste from pistachio hard Shells: extraction of polyphenols as natural antioxidants.* Resources, 2021, 10(5), p. 45.

[23] M. Kashaninejad and L. Tabil. *Pistachio (Pistacia vera L.)*, in *Postharvest biology and technology of tropical and subtropical fruits*. 2011, Elsevier: Cambridge, England, p. 218-247e.

[24] E. Apaydin-Varol, E. Pütün, and A.E. Pütün. *Slow pyrolysis of pistachio shell.* Fuel, 2007, 86(12-13), p. 1892-1899.

[25] C. Okutucu, G. Duman, S. Ucar, I. Yasa, and J. Yanik. *Production of fungicidal oil and activated carbon from pistachio shell.* Journal of analytical and applied pyrolysis, 2011, 91(1), p. 140-146.

[26] K. Açıkalın, F. Karaca, and E. Bolat. *Pyrolysis of pistachio shell: Effects of pyrolysis conditions and analysis of products.* Fuel, 2012, 95, p. 169-177.

[27] F. Hesam, B.G. Tarzi, M. Honarvar, and M. Jahadi. *Pistachio (Pistacia vera) shell as a new candidate for enzymatic production of xylooligosaccharides.* Journal of Food Measurement and Characterization, 2021, 15(1), p. 33-45.

[28] M. Gürü, M. Şahin, S. Tekeli, and H. Tokgöz. *Production of polymer matrix composite particleboard from pistachio shells and improvement of its fire resistance by fly ash.* High Temperature Materials and Processes, 2009, 28(3), p. 191-195.

[29] M. Alsaadi, A. Erkliğ, and K. Albu-khaleefah. *Effect of pistachio shell particle content on the mechanical properties of polymer composite.* Arabian Journal for Science and Engineering, 2018, 43(9), p. 4689-4696.

[30] M.A. Najafabadi, S.N. Khorasani, and J.M. Esfahani. *High density polyethylene/pistachio shell flour/nanoclay composites-effect of accelerated weathering conditions on mechanical properties, relative brightness and total colour change.* Polymers and Polymer Composites, 2017, 25(4), p. 299-308.

[31] B. Karaağaç. *Use of ground pistachio shell as alternative filler in natural rubber/styrene–butadiene rubber-based rubber compounds.* Polymer composites, 2014, 35(2), p. 245-252.

[32] D. Lascano, R. Guillen-Pineda, L. Quiles-Carrillo, J. Ivorra-Martínez, R. Balart, N. Montanes, and T. Boronat. *Manufacturing and characterization of highly environmentally friendly sandwich composites from polylactide cores and flax-polylactide faces.* Polymers, 2021, 13(3), p. 342.

[33] Á. Agüero, D. Garcia-Sanoguera, D. Lascano, S. Rojas-Lema, J. Ivorra-Martinez, O. Fenollar, and S. Torres-Giner. *Evaluation of different compatibilization strategies to improve the performance of injection-molded green composite pieces made of polylactide reinforced with short flaxseed fibers.* Polymers, 2020, 12(4), p. 821.

[34] A. Carbonell-Verdú, D. García-García, A. Jordá, M. Samper, and R. Balart. *Development of slate fiber reinforced high density polyethylene composites for injection molding.* Composites Part B: Engineering, 2015, 69, p. 460-466.

[35] L. Quiles-Carrillo, T. Boronat, N. Montanes, R. Balart, and S. Torres-Giner. *Injection-molded parts of fully bio-based polyamide 1010 strengthened with waste derived slate fibers pretreated with glycidyl- and amino-silane coupling agents.* Polymer Testing, 2019, 77, p. 105875.

[36] A. Gharbi, R.B. Hassen, and S. Boufi. *Composite materials from unsaturated polyester resin and olive nuts residue: The effect of silane treatment.* Industrial Crops and Products, 2014, 62, p. 491-498.

[37] B.A. Acha, M.I. Aranguren, N.E. Marcovich, and M.M. Reboredo. *Composites from PMMA modified thermosets and chemically treated woodflour.* Polymer Engineering & Science, 2003, 43(5), p. 999-1010.

[38] M.H. Mohammed and B. Dauda. *Unsaturated polyester resin reinforced with chemically modified natural fibre.* IOSR Journal of Polymer and Textile Engineering, 2014, 1(4), p. 31-38.

[39] X. Yuan, K. Jayaraman, and D. Bhattacharyya. *Effects of plasma treatment in enhancing the performance of woodfibre-polypropylene composites.* Composites Part A: Applied Science and Manufacturing, 2004, 35(12), p. 1363-1374.

[40] B. Melendez-Rodriguez, S. Torres-Giner, A. Aldureid, L. Cabedo, and J.M. Lagaron. *Reactive melt mixing of poly(3-hydroxybutyrate)/rice husk flour composites with purified biosustainably produced poly(3-hydroxybutyrate-co-3-hydroxyvalerate).* Materials, 2019, 12(13), p. 2152.

[41] S. Torres-Giner, N. Montanes, T. Boronat, L. Quiles-Carrillo, and R. Balart. *Melt grafting of sepiolite nanoclay onto poly(3-hydroxybutyrate-co-4-hydroxybutyrate) by reactive extrusion with multi-functional epoxy-based styrene-acrylic oligomer.* European Polymer Journal, 2016, 84, p. 693-707.

[42] R. Muthuraj, M. Misra, and A.K. Mohanty. *Biodegradable compatibilized polymer blends for packaging applications: A literature review.* Journal of Applied Polymer Science, 2018, 135(24), p. 45726.

[43] J. Chen, C. Rong, T. Lin, Y. Chen, J. Wu, J. You, H. Wang, and Y. Li. *Stable co-continuous PLA/PBAT blends compatibilized by interfacial stereocomplex crystallites: toward full biodegradable polymer blends with simultaneously enhanced mechanical properties and crystallization rates.* Macromolecules, 2021, 54(6), p. 2852-2861.

[44] H. Wang, B. Wei, X. Gu, T. Lin, and Y. Li. *Determining the optimal molecular architecture for reactive splicing compatibilization: Toward a better understanding of reactive polymer processing.* Polymer, 2020, 208, p. 122948.

[45] V. Tserki, P. Matzinos, and C. Panayiotou. *Novel biodegradable composites based on treated lignocellulosic waste flour as filler. Part II. Development of biodegradable composites using treated and compatibilized waste flour.* Composites Part A: Applied Science and Manufacturing, 2006, 37(9), p. 1231-1238.

[46] S. Kennouche, N. Le Moigne, M. Kaci, J.-C. Quantin, A.-S. Caro-Bretelle, C. Delaite, and J.-M. Lopez-Cuesta. *Morphological characterization and thermal properties of compatibilized poly (3-hydroxybutyrate-co-3-hydroxyvalerate)(PHBV)/poly (butylene succinate)(PBS)/halloysite ternary nanocomposites.* European Polymer Journal, 2016, 75, p. 142-162.

[47] R. Muthuraj, M. Misra, and A.K. Mohanty. *Biocomposite consisting of miscanthus fiber and biodegradable binary blend matrix: compatibilization and performance evaluation.* RSC advances, 2017, 7(44), p. 27538-27548.

[48] J.C.G. da Silva, J.L.F. Alves, W.V.d.A. Galdino, R.d.F.P.M. Moreira, H.J. José, R.F. de Sena, and S.L.F. Andersen. *Combustion of pistachio shell: physicochemical characterization and evaluation of kinetic parameters.* Environmental Science and Pollution Research, 2018, 25(22), p. 21420-21429.

[49] T. Yang and A.C. Lua. *Characteristics of activated carbons prepared from pistachio-nut shells by physical activation.* Journal of Colloid and Interface Science, 2003, 267(2), p. 408-417.

[50] N.N. Kadhim, Q.A. Hamad, and J.K. Oleiwi. *Tensile and morphological properties of PMMA composite reinforced by Pistachio Shell powder used in denture applications*. in *2nd International Conference on Materials Engineering and Science, IConMEAS 2019*. 2020. American Institute of Physics Inc.

[51] A. Agüero, M.C. Morcillo, L. Quiles-Carrillo, R. Balart, T. Boronat, D. Lascano, S. Torres-Giner, and O. Fenollar. *Study of the influence of the reprocessing cycles on the final properties of polylactide pieces obtained by injection molding.* Polymers, 2019, 11(12), p. 1908.

[52] Š. Barcík, M. Gašparík, and E.Y. Razumov. *Effect of temperature on the color changes of wood during thermal modification.* Cellulose Chemistry and Technology, 2015, 49(9-10), p. 789-798.

[53] P. Liminana, D. Garcia-Sanoguera, L. Quiles-Carrillo, R. Balart, and N. Montanes. *Development and characterization of environmentally friendly composites from poly (butylene succinate)(PBS) and almond shell flour with different compatibilizers.* Composites Part B: Engineering, 2018, 144, p. 153-162.

[54] T.-x. Jin, M. Zhou, S.-d. Hu, F. Chen, Q. Fu, and Y. Fu. *Effect of molecular weight on the properties of poly(butylene succinate).* Chinese Journal of Polymer Science, 2014, 32(7), p. 953-960.

[55] H.-X. Huang and J.-J. Zhang. *Effects of filler–filler and polymer–filler interactions on rheological and mechanical properties of HDPE–wood composites.* Journal of Applied Polymer Science, 2009, 111(6), p. 2806-2812.

[56] K.S. Chun, S. Husseinsyah, and H. Osman. *Mechanical and thermal properties of coconut shell powder filled polylactic acid biocomposites: Effects of the filler content and silane coupling agent.* Journal of Polymer Research, 2012, 19(5), p. 9859.

[57] J. Kajaks, K. Kalnins, and R. Naburgs. *Wood plastic composites (WPC) based on high-density polyethylene and birch wood plywood production residues.* International Wood Products Journal, 2018, 9(1), p. 15-21.

[58] J. Ivorra-Martinez, J. Manuel-Mañogil, T. Boronat, L. Sanchez-Nacher, R. Balart, and L. Quiles-Carrillo. *Development and characterization of sustainable composites from bacterial polyester poly(3-hydroxybutyrate-co-3-hydroxyhexanoate) and almond shell flour by reactive extrusion with oligomers of lactic acid.* Polymers, 2020, 12(5), p. 1097.

[59] J.M. Ferri, D. Garcia-Garcia, N. Montanes, O. Fenollar, and R. Balart. *The effect of maleinized linseed oil as biobased plasticizer in poly(lactic acid)-based formulations.* Polymer International, 2017, 66(6), p. 882-891.

[60] P. Liminana, L. Quiles-Carrillo, T. Boronat, R. Balart, and N. Montanes. *The effect of varying almond shell flour (ASF) loading in composites with poly(butylene succinate (PBS) matrix compatibilized with maleinized linseed oil (MLO).* Materials, 2018, 11(11), p. 2179.

[61] Y.J. Phua, W.S. Chow, and Z.A. Mohd Ishak. *Reactive processing of maleic anhydride-grafted poly(butylene succinate) and the compatibilizing effect on poly(butylene succinate) nanocomposites.* Express Polymer Letters, 2013, 7(4), p. 340-354.

[62] T. El-Nabarawy, N.S. Petro, and S. Abdel-Aziz. *Adsorption characteristics of coal-based activated carbons. II. adsorption of water vapour, pyridine and benzene.* Adsorption Science & Technology, 1997, 15(1), p. 47-57.

[63] Y.H. Çelik, R. Yalcin, T. Topkaya, E. Başaran, and E. Kilickap. *Characterization of hazelnut, pistachio, and apricot kernel shell particles and analysis of their composite properties.* Journal of Natural Fibers, 2021, 18(7), p. 1054-1068.

[64] S.-F. Yao, X.-T. Chen, and H.-M. Ye. *Investigation of structure and crystallization behavior of poly(butylene succinate) by fourier transform infrared spectroscopy.* The Journal of Physical Chemistry B, 2017, 121(40), p. 9476-9485.

[65] J. John, J. Tang, Z. Yang, and M. Bhattacharya. *Synthesis and characterization of anhydride-functional polycaprolactone.* Journal of Polymer Science Part A: Polymer Chemistry, 1997, 35(6), p. 1139-1148.

[66] R. Chandra and R. Rustgi. *Biodegradation of maleated linear low-density polyethylene and starch blends.* Polymer Degradation and Stability, 1997, 56(2), p. 185-202.

[67] Y. Wang, D. Ji, C. Yang, H. Zhang, C. Qin, and B. Huang. *Structure and properties of maleated high-density polyethylene.* Journal of Applied Polymer Science, 1994, 52(10), p. 1411-1417.

[68] C.S. Wu, H.T. Liao, and S.M. Lai. *Study on the graft reaction of maleic anhydride onto metallocene-based polyethylene-octene elastomer.* Polymer - Plastics Technology and Engineering, 2002, 41(4), p. 645-661.

[69] Z.Z. Yu, Y.C. Ou, Z.N. Qi, and G.H. Hu. *Toughening of nylon 6 with a maleated core-shell impact modifier.* Journal of Polymer Science, Part B: Polymer Physics, 1998, 36(11), p. 1987-1994.

[70] A.K. Bledzki, S. Reihmane, and J. Gassan. *Properties and modification methods for vegetable fibers for natural fiber composites.* Journal of Applied Polymer Science, 1996, 59(8), p. 1329-1336.

[71] H.-S. Kim, H.-J. Kim, J.-W. Lee, and I.-G. Choi. *Biodegradability of bio-flour filled biodegradable poly (butylene succinate) bio-composites in natural and compost soil.* Polymer Degradation and Stability, 2006, 91(5), p. 1117-1127.

[72] R.-y. Chen, W. Zou, H.-c. Zhang, G.-z. Zhang, Z.-t. Yang, G. Jin, and J.-p. Qu. *Thermal behavior, dynamic mechanical properties and rheological properties of poly (butylene succinate) composites filled with nanometer calcium carbonate.* Polymer Testing, 2015, 42, p. 160-167.

[73] R. Chen, W. Zou, H. Zhang, G. Zhang, and J. Qu. *Crystallization behavior and thermal stability of poly (butylene succinate)/poly (propylene carbonate) blends prepared by novel vane extruder*. in *AIP Conference Proceedings*. 2016. AIP Publishing LLC. p. 050002.

[74] D.K. Song and Y.K. Sung. *Synthesis and characterization of biodegradable poly(1,4-butanediol succinate).* Journal of Applied Polymer Science, 1995, 56(11), p. 1381-1395.

[75] M.S. Nikolic and J. Djonlagic. *Synthesis and characterization of biodegradable poly(butylene succinate-co-butylene adipate)s.* Polymer Degradation and Stability, 2001, 74(2), p. 263-270.

[76] X. Luo, J. Li, J. Feng, T. Yang, and X. Lin. *Mechanical and thermal performance of distillers grains filled poly (butylene succinate) composites.* Materials & Design, 2014, 57, p. 195-200.

[77] J. Balart, D. García-Sanoguera, R. Balart, T. Boronat, and L. Sánchez-Nacher. *Manufacturing and properties of biobased thermoplastic composites from poly (lactid acid) and hazelnut shell wastes.* Polymer composites, 2018, 39(3), p. 848-857.

[78] P. Liminana, D. Garcia-Sanoguera, L. Quiles-Carrillo, R. Balart, and N. Montanes. *Optimization of maleinized linseed oil loading as a biobased compatibilizer in poly (butylene succinate) composites with almond shell flour.* Materials, 2019, 12(5), p. 685.

[79] A. Bendahou, H. Kaddami, H. Sautereau, M. Raihane, F. Erchiqui, and A. Dufresne. *Short palm tree fibers polyolefin composites: effect of filler content and coupling agent on physical properties.* Macromolecular Materials and Engineering, 2008, 293(2), p. 140-148.

[80] S. Gupta, G.K. Gupta, and M.K. Mondal. *Thermal degradation characteristics, kinetics, thermodynamic, and reaction mechanism analysis of pistachio shell pyrolysis for its bioenergy potential.* Biomass Conversion and Biorefinery, 2020, p. 1-15.

[81] K. Açıkalın. *Pyrolytic characteristics and kinetics of pistachio shell by thermogravimetric analysis.* Journal of Thermal Analysis and Calorimetry, 2012, 109(1), p. 227-235.

[82] S.-H. Lee and S. Wang. *Biodegradable polymers/bamboo fiber biocomposite with bio-based coupling agent.* Composites Part A: Applied Science and Manufacturing, 2006, 37(1), p. 80-91.

[83] H.-S. Kim, B.-H. Lee, S.-W. Choi, S. Kim, and H.-J. Kim. *The effect of types of maleic anhydride-grafted polypropylene (MAPP) on the interfacial adhesion properties of bio-flour-filled polypropylene composites.* Composites Part A: Applied Science and Manufacturing, 2007, 38(6), p. 1473-1482.

[84] S. Montava-Jorda, D. Lascano, L. Quiles-Carrillo, N. Montanes, T. Boronat, A.V. Martinez-Sanz, S. Ferrandiz-Bou, and S. Torres-Giner. *Mechanical Recycling of*

Partially Bio-Based and Recycled Polyethylene Terephthalate Blends by Reactive Extrusion with Poly(styrene-co-glycidyl methacrylate). Polymers, 2020, 12(1), p. 174.

[85] Y. Bautista, A. Gozalbo, S. Mestre, and V. Sanz. *Thermal degradation mechanism of a thermostable polyester stabilized with an open-cage oligomeric silsesquioxane.* Materials, 2017, 11(1), p. 22.

[86] D. Shen, S. Gu, K. Luo, S. Wang, and M. Fang. *The pyrolytic degradation of wood-derived lignin from pulping process.* Bioresource technology, 2010, 101(15), p. 6136-6146.

[87] B. Hexig, H. Alata, N. Asakawa, and Y. Inoue. *Novel biodegradable poly(butylene succinate)/poly(ethylene oxide) blend film with compositional and spherulite-size gradients.* Journal of Polymer Science Part B: Polymer Physics, 2005, 43(4), p. 368-377.

[88] N. Lin, D. Fan, P.R. Chang, J. Yu, X. Cheng, and J. Huang. *Structure and properties of poly (butylene succinate) filled with lignin: A case of lignosulfonate.* Journal of Applied Polymer Science, 2011, 121(3), p. 1717-1724.

[89] S. Torres-Giner, N. Montanes, O. Fenollar, D. García-Sanoguera, and R. Balart. *Development and optimization of renewable vinyl plastisol/wood flour composites exposed to ultraviolet radiation.* Materials & Design, 2016, 108, p. 648-658.

[90] E. Frollini, N. Bartolucci, L. Sisti, and A. Celli. *Poly(butylene succinate) reinforced with different lignocellulosic fibers.* Industrial Crops and Products, 2013, 45, p. 160-169.

[91] H. Kiani, A. Ashori, and S.A. Mozaffari. *Water resistance and thermal stability of hybrid lignocellulosic filler-PVC composites.* Polymer Bulletin, 2011, 66(6), p. 797-802.

[92] F. Burgada, E. Fages, L. Quiles-Carrillo, D. Lascano, J. Ivorra-Martinez, M.P. Arrieta, and O. Fenollar. *Upgrading recycled polypropylene from textile wastes in wood plastic composites with short hemp fiber.* Polymers, 2021, 13(8), p. 1248.

[93] S. Gairola, S. Gairola, H. Sharma, and P.K. Rakesh. *Impact behavior of pine needle fiber/pistachio shell filler based epoxy composite*. in *2nd International Conference on New Frontiers in Engineering, Science and Technology, NFEST 2019*. 2019. Institute of Physics Publishing.

[94] L. Quiles-Carrillo, N. Montanes, D. Garcia-Garcia, A. Carbonell-Verdu, R. Balart, and S. Torres-Giner. *Effect of different compatibilizers on injection-molded green composite pieces based on polylactide filled with almond shell flour.* Composites Part B: Engineering, 2018, 147, p. 76-85.

[95] V.A. Alvarez and A. Vázquez. *Influence of fiber chemical modification procedure on the mechanical properties and water absorption of MaterBi-Y/sisal fiber composites.* Composites Part A: Applied Science and Manufacturing, 2006, 37(10), p. 1672-1680.

[96] V. Tserki, P. Matzinos, S. Kokkou, and C. Panayiotou. *Novel biodegradable composites based on treated lignocellulosic waste flour as filler. Part I. Surface chemical modification and characterization of waste flour.* Composites Part A: Applied Science and Manufacturing, 2005, 36(7), p. 965-974.

[97] J. Gassan and A.K. Bledzki. *The influence of fiber-surface treatment on the mechanical properties of jute-polypropylene composites.* Composites Part A: Applied Science and Manufacturing, 1997, 28(12), p. 1001-1005.

[98] S. Tolga, S. Kabasci, and M. Duhme. *Progress of disintegration of polylactide (PLA)/poly(butylene succinate) (PBS) blends containing talc and chalk inorganic fillers under industrial composting conditions.* Polymers, 2021, 23(1), p. 1-19.

[99] J.H. Zhao, X.Q. Wang, J. Zeng, G. Yang, F.H. Shi, and Q. Yan. *Biodegradation of poly(butylene succinate) in compost.* Journal of Applied Polymer Science, 2005, 97(6), p. 2273-2278.

[100] L.Y. Mwaikambo, E. Martuscelli, and M. Avella. *Kapok/cotton fabric-polypropylene composites.* Polymer Testing, 2000, 19(8), p. 905-918.

[101] A.P. Mathew, K. Oksman, and M. Sain. *Mechanical properties of biodegradable composites from poly lactic acid (PLA) and microcrystalline cellulose (MCC).* Journal of Applied Polymer Science, 2005, 97(5), p. 2014-2025.

[102] R. Kumar, M.K. Yakubu, and R.D. Anandjiwala. *Biodegradation of flax fiber reinforced poly lactic acid.* Express Polymer Letters, 2010, 4(7), p. 423–430.

[103] M. Puchalski, G. Szparaga, T. Biela, A. Gutowska, S. Sztajnowski, and I. Krucińska. *Molecular and supramolecular changes in polybutylene succinate (PBS) and polybutylene succinate adipate (PBSA) copolymer during degradation in various environmental conditions.* Polymers, 2018, 10(3), p. 251.

[104] W. Gabara and S. Porejko. *Grafting of maleic anhydride on polyethylene. I. Mechanism of grafting in a heterogeneous medium in the presence of radical initiators.* Journal of Polymer Science Part A-1: Polymer Chemistry, 1967, 5(7), p. 1547-1562.

[105] R. Muthuraj, M. Misra, and A.K. Mohanty. *Injection molded sustainable biocomposites from poly (butylene succinate) bioplastic and perennial grass.* ACS Sustainable Chemistry & Engineering, 2015, 3(11), p. 2767-2776.

BLOCK 3

IV.3. Extraction of different biopolymers from agro-industrial residues and their combinations to obtain films.

Adaptado del artículo

IV.3.1. Faba bean protein films reinforced with cellulose nanocrystals as edible food packaging material

Sandra Rojas-Lema[1], Klara Nilsson[2], Jon Trifol[3], Maud Langton[2], Jaume Gomez-Caturla[1], Rafael Balart[1], Daniel Garcia-Garcia[1], Rosana Moriana[2,3,4]

[1]Technological Institute of Materials (ITM), Universitat Politècnica de València (UPV), Plaza Ferrándiz y Carbonell 1, 03801 Alcoy, Spain.

[2] Department of Molecular Sciences, Swedish University of Agricultural Sciences (SLU), Box 7051, SE-750 07, Uppsala, Sweden.

[3]Department of Fibre and Polymer Technology, School of Engineering Sciences in Chemistry, Biotechnology and Health, Royal Institute of Technology (KTH), SE-100 44, Stockholm, Sweden.

[4] RISE Bioeconomy and Health. Research Institute of Sweden (RISE), Drottning Kristinas väg 61, SE-114 28, Stockholm, Sweden.

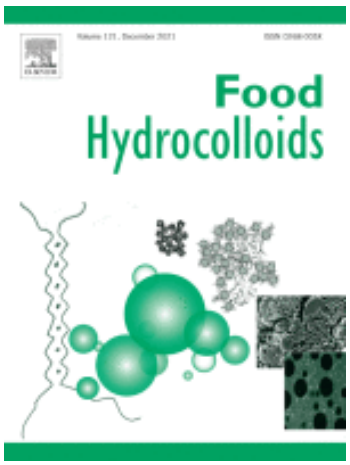

Food Hydrocolloids

2021, 121, p. 107019.

Food Hydrocolloids 121 (2021) 107019

Contents lists available at ScienceDirect

Food Hydrocolloids

journal homepage: www.elsevier.com/locate/foodhyd

"Faba bean protein films reinforced with cellulose nanocrystals as edible food packaging material"

Sandra Rojas-Lema [a], Klara Nilsson [b], Jon Trifol [c], Maud Langton [b], Jaume Gomez-Caturla [a], Rafael Balart [a], Daniel Garcia-Garcia [a,*], Rosana Moriana [b,c,d]

[a] Instituto de Tecnología de Materiales (ITM), Universitat Politècnica de València (UPV), Plaza Ferrándiz y Carbonell 1, 03801, Alcoy, Alicante, Spain
[b] Department of Molecular Sciences, Swedish University of Agricultural Sciences (SLU), Box 7051, SE-750 07, Uppsala, Sweden
[c] Department of Fibre and Polymer Technology, School of Engineering Sciences in Chemistry, Biotechnology and Health. Royal Institute of Technology (KTH), SE-100 44, Stockholm, Sweden
[d] RISE Bioeconomy and Health, Research Institute of Sweden (RISE), Drottning Kristinas Väg 61, SE-114 28, Stockholm, Sweden

ARTICLE INFO

Keywords:
Faba beans
Proteins films
Cellulose nanocrystals (CNCs)
Food packaging
Pine cone

ABSTRACT

In the present work, transparent films were obtained by the solution casting method from faba bean protein isolate (FBP), reinforced with different cellulose nanocrystals (CNCs) content (1, 3, 5 and 7 wt%), obtained by acid hydrolysis of pine cone, and using glycerol as plasticizer. The influence of different CNCs loadings on the mechanical, thermal, barrier, optical, and morphological properties was discussed. Microstructurally, the FTIR and FESEM results corroborated the formation of intramolecular interactions between the CNCs and proteins that lead to more compact and homogeneous films. These interactions had a positive influence on the mechanical strength properties, which is reflected in higher tensile strength and Young's modulus in reinforced films with respect to the control film, resulting in stiffer films as the CNCs content increases. Thermal stability of the FBP films was also improved with the presence of CNCs, by increasing the characteristic onset degradation temperature. In addition, the linkages formed between the CNCs, and proteins reduced the water affinity of the reinforced films, leading to a reduction in their moisture content and water solubility, and an increase in their water contact angle, obtaining more hydrophobic films as the CNCs content in the matrix increased. The addition of CNCs in the FBP film also considerably improved its barrier properties, reducing its water vapour transmission rate (WVTR) and oxygen transmission rate (OTR). The present work shows the possibility of obtaining biobased and biodegradable films of CNC-reinforced FBP with improved mechanical, thermal and barrier properties, and low water susceptibility, which can be of great interest in the food packaging sector as edible food packaging material.

1. Introduction

In recent years, the worldwide consumption of plastics has increased in a remarkable way, mainly due to its high versatility and low price. Only in Europe there was a total production of 57.9 million tonnes in 2019, with the packaging industry being the main consumer with a 39.6% of the total (Plastics Europe, 2020). The high consumption of plastics generates a large amount of waste that causes serious environmental problems, especially when used as single-use packaging materials. This has led to an increase in environmental concern in society which, together with petroleum depletion, has led to a considerable increase in the research and development of new, more environmentally friendly materials capable of replacing traditional synthetic plastics (Liminana, Garcia-Sanoguera, Quiles-Carrillo, Balart, & Montanes, 2018). Among the sustainable materials that have received the most attention, biodegradable polymeric films from renewable sources that are abundant in nature such as proteins, lipids and polysaccharides, have positioned as an actual alternative to synthetic polymer films, and are characterized by their biodegradability, wide availability, and low cost (Zhang et al., 2016). Protein films are characterized by their non-toxicity, biodegradability and good barrier properties to oxygen, lipids and flavourings (Reddy, Jiang, & Yang, 2012). However, they have a number of drawbacks compared to synthetic polymers that limit their massive use in sectors such as packaging. Among these

* Corresponding author.
E-mail address: dagarga4@epsa.upv.es (D. Garcia-Garcia).

https://doi.org/10.1016/j.foodhyd.2021.107019
Received 4 February 2021; Received in revised form 5 July 2021; Accepted 6 July 2021
Available online 10 July 2021

Faba bean protein films reinforced with cellulose nanocrystals as edible food packaging material

Abstract

In the present work, transparent films were obtained by the solution casting method from faba bean protein isolate (FBP), reinforced with different cellulose nanocrystals (CNCs) content (1, 3, 5 and 7 wt%), obtained by acid hydrolysis of pine cone, and using glycerol as plasticizer. The influence of different CNCs loadings on the mechanical, thermal, barrier, optical, and morphological properties was discussed. Microstructurally, the FTIR and FESEM results corroborated the formation of intramolecular interactions between the CNCs and proteins that lead to more compact and homogeneous films. These interactions had a positive influence on the mechanical strength properties, which is reflected in higher tensile strength and Young's modulus in reinforced films with respect to the control film, resulting in stiffer films as the CNCs content increases. Thermal stability of the FBP films was also improved with the presence of CNCs, by increasing the characteristic onset degradation tem- perature. In addition, the linkages formed between the CNCs, and proteins reduced the water affinity of the reinforced films, leading to a reduction in their moisture content and water solubility, and an increase in their water contact angle, obtaining more hydrophobic films as the CNCs content in the matrix increased. The addition of CNCs in the FBP film also considerably improved its barrier properties, reducing its water vapour transmission rate (WVTR) and oxygen transmission rate (OTR). The present work shows the possibility of obtaining biobased and biodegradable films of CNC-reinforced FBP with improved mechanical, thermal and barrier properties, and low water susceptibility, which can be of great interest in the food packaging sector as edible food packaging material.

Keywords: Faba beans; proteins films; cellulose nanocrystals (CNCs); food packaging; pine cone.

INTRODUCTION

In recent years, the worldwide consumption of plastics has increased in a remarkable way, mainly due to its high versatility and low price. Only in Europe there was a total production of 57.9 million tonnes in 2019, with the packaging industry being the main consumer with a 39.6% of the total [1]. The high consumption of plastics generates a large amount of waste that causes serious environ- mental problems, especially when used as single-use packaging materials. This has led to an increase in environmental concern in society which, together with petroleum depletion, has led to a considerable increase in the research and development of new, more environmentally friendly materials capable of replacing traditional synthetic plastics [2]. Among the sustainable materials that have received the most attention, biodegradable polymeric films from renewable sources that are abundant in nature such as proteins, lipids and polysaccharides, have positioned as an actual alternative to synthetic polymer films, and are characterized by their biodegradability, wide availability, and low cost [3]. Protein films are characterized by their non-toxicity, biodegradability and good barrier properties to oxygen, lipids and flavourings [4]. However, they have a number of drawbacks compared to synthetic polymers that limit their massive use in sectors such as packaging. Among these disadvantages, it is worthy to note their low mechanical strength, poor water vapour barrier properties and high water sensitivity due to the highly hydrophilic nature of the proteins [5]. Although these properties highly depend on the protein structure and the method of film preparation [6].

Legume seeds are a cheap source of protein with high nutritional value, which makes them an interesting raw material for use in the manufacture of bio-based materials for the packaging sector due to their sustainability [7]. One of the most consumed legumes worldwide is faba bean (*Vicia Faba* L.), which is characterized by its low cost and high quality protein content, which can contain up to 27.34% protein (dry weight), depending on the cultivation conditions and the variety [8]. Faba bean has long been a basic food staple in Middle Eastern and Southeast Asian countries, however, its main use has been as a livestock feed, although it has also been used as a cover crop to restore nitrogen content and prevent soil erosion [9, 10]. This makes it an excellent raw material for protein extraction for use as films in the food packaging industry. However, currently, the use of faba bean proteins to produce biodegradable films is still very

limited. Some works such as those carried out by Saremnezhad *et al.* [11] Montalvo-Paquini *et al.* [12] analyzed the effect of different pH values, and plasticizer content of film forming solution on the physical and chemical properties of faba bean protein films. On the other hand, Hopkins *et al.* [13] observed that faba bean protein films with 50% glycerol content, had better tensile strength and opacity and lower water permeability than protein films obtained from other legumes such as peas, lupins, lentils, and soybeans.

On the other hand, the formulation of protein films requires the use of plasticizers to reduce their brittleness and increase their functionality. The plasticizer molecules interact by hydrogen bonding with aminoacid groups in protein chains, thus reducing the intermolecular forces between them, resulting in an increase in their mobility, which translates into an increase in the flexibility, toughness and tear strength of the films [14, 15]. Some of the most commonly used plasticizers for the manufacture of protein films are sorbitol, polyethylene glycol and glycerol, being glycerol one of the most effective for the production of stable, flexible and less brittle films [16, 17]. Glycerol is one of the most important by-products of biodiesel production, which is generated in large amounts due to the remarkable increase in biodiesel production, becoming a waste product with an associated economic and environmental cost [18, 19]. Glycerol represents approximately 10 wt% of total biodiesel production [20]. Therefore, the use of glycerol as plasticizers in protein films, in addition to increasing the ductile mechanical properties of the films, can be an effective alternative to convert a by-product of the biodiesel industry into a high value-added product [21].

One of the approaches to overcome the above-mentioned drawbacks of protein films is the use of nanoparticles. The use of small amounts of nanoparticles has shown good potential to improve the mechanical and barrier properties of protein films [22]. Inorganic nanoparticles such as montmorillonite [23-26], TiO_2 [27-29], halloysite nanotubes [30, 31], or carbon nanotubes [32] have been successfully employed to reduce the drawbacks of protein films. However, the use of renewable and biodegradable nano-particles has gained relevance in recent years due to their greater environmentally friendliness. In this way, cellulose nanocrystals (CNCs) obtained from agroforestry residues are considered one of the most promising reinforcing agents due to their biodegradability, abundance, variety, chemical modification capacity and price [33]. Cellulose nanocrystals consist of highly crystalline rod-like particles, obtained from

biomass, usually by acid hydrolysis, with dimensions of around 10–20 nm in width and several hundred nanometers in length, giving rise to high aspect ratios [34]. CNCs are characterized by high strength, high elastic modulus and low density [35], despite their physico-chemical properties depend on the cellulose source, and on synthesis process conditions [36, 37]. CNCs are also characterized by good compatibility with hydrophilic polymers [38]. The effect of CNC incorporation has been previously studied in soy [3, 38-40], whey [41], amaranth [42], or canola [43] protein films, showing that the presence of nanoparticles in the protein matrix leads to intramolecular interactions between both phases, resulting in more compact films with better mechanical properties and better barrier properties.

The main objective of the present work is to evaluate the effect of the incorporation of different CNC content extracted from pine cone (1, 3, 5 and 7 wt%) on the mechanical properties, thermal stability, barrier properties, optical properties, water susceptibility (moisture content, contact angle and water solubility) and the microstructure on glycerol-plasticized faba bean protein-based biodegradable films.

EXPERIMENTAL

Materials

Faba beans used in this work (*Gloria* variety) were supplied by RISE (Research Institutes of Sweden). Pine cones (*Pinus Pinea*) were collected from a local pine forest in Alicante (Spain). Sodium hydroxide (NaOH, 99.0% purity) and hydrochloric acid (HCl, 36% purity) were supplied by VWR (Darmstadt, Germany). Glycerol was purchased from POCH S.A. (Gliwice, Poland).

Faba bean protein isolation

The faba bean protein (FBP) isolation was done following the method described by Langton *et al.* [44] with some modifications. First, the faba beans were dehulled with a dehuller, and the beans were milled in a rotary mill from Brabender (Duisburg, Germany) with a 1.5 mm mesh screen. Subsequently, faba bean flour was mixed in distilled water at a ratio 1:10 (w/v) and the pH of the obtained solution was adjusted to 9.0 using 2 M NaOH to increase solubility of the protein. The suspension was stirred at room temperature for 1 h, and then was centrifuged in a Sorvall Lynx 6000 centrifuge

from Thermo Scientific (Langenselbold, Germany) at 3700 G for 30 min and 18 ºC. The pH of supernatant was adjusted to 4.0 using 1 M HCl to precipitate the protein, stirred at room temperature for 1.5 h and centrifuged at 3700 G for 30 min and 18 ºC. The precipitates were collected and re-dispersed in distilled water at a ratio 1:10 (w/v). The suspension was adjusted to pH 4 and centrifuged again with the same described conditions. Finally, the precipitate protein was frozen and lyophilized to obtain FBP.

Preparation of pine cone nanocrystals

Pine cone nanocrystals were obtained by acid hydrolysis according to our previous work [45]. Briefly, grinded pine cone particles were first subjected to an alkaline treatment in a 4.5% NaOH solution for 2 h at 80 ºC followed by bleaching process using a solution made up of 1.7 wt% aqueous sodium hypochlorite, acetate buffer (0.2 M, pH 4.8) and water (1:1:1) for 4 h at 80 ºC, in order to remove extractives, hemicellulose and lignin of the raw material. Subsequently, the bleached fibres were hydrolysed with sulfuric acid (65 wt%) for 45 min at 45 ºC. The excess acid was then removed from the solution by washing with Milli-Q water by repetitive centrifugation and finally by dialysis. The resulting suspension was sonicated to promote CNCs dispersion and then centrifuged to remove the remaining unhydrolyzed fibres. The collected suspension was then stored in a refrigerator for further use.

Preparation of reinforced protein films

Preparation of FBP films was done by solution casting process. Control protein films were prepared dissolving FBP (5% w/v), glycerol (50% w/w based on the dry weight of FBP) and distilled water. The pH of the solution was adjusted to 10.5 using a 1M NaOH solution and was mechanically stirred for 1 h. After this, the solution was denatured by heating at 85 ºC for 30 min in a water bath and cooled down at room temperature. For the CNCs-reinforced films, the same procedure was followed as for the control film, however in this case the appropriate amounts of CNCs were incorporated (1, 3, 5 and 7 wt% on the dry weight of FBP) after the denaturation process, keeping the solution in a stirrer for 30 min. The resulting solutions were casted into a polystyrene Petri dish and dried at 40 ºC for 24 h. Then, the dried films were peeled off and conditioned at 52% relative humidity (RH) and 25 ºC for 48 h prior to testing. All films

were prepared in triplicate. **Table IV.3.1.1** summarizes the composition of all the developed films.

Table IV.3.1.1. Composition and codes for faba beans proteins (FBP) films with different pine cone cellulose nanocrystals content.

Samples	Content			
	Proteins (g)	Glycerol (g)	Water (g)	CNC (wt% on dry proteins)
FBP	5	2.5	100	0
FBP_CNC-1	5	2.5	100	1
FBP_CNC-3	5	2.5	100	3
FBP_CNC-5	5	2.5	100	5
FBP_CNC-7	5	2.5	100	7

Characterization techniques

Films thickness

The thickness of the FBP films was determined at ten random points around each film sample using a manual micrometer Mitutoyo No. 2109S-10 (Tokyo, Japan) with 0.001 mm sensitivity. The average value of each film was determined and used in calculations for mechanical properties, oxygen transmission rate, water vapour transmission rate and transparency.

Mechanical properties

The mechanical tensile properties, namely the tensile strength (TS), the Young's modulus (E) and the elongation at break (ε) of FBP films were determined following the standard method ASTM D882-02, using a Linkam TST-350 tensile stage (Linkam Scientific Instruments, Ltd., U.K.) with a 20 N load cell. Preconditioned FBP films were cut into rectangular strips (30 x 4 mm^2) and placed between the tensile grips. The initial grip distance was set at 15 mm and the crosshead speed at 5 mm min^{-1}. At least five specimens from each film were tested at room temperature and the average results were obtained.

Thermogravimetric analysis (TGA)

Thermal behaviour of different FBP films obtained was analyzed by thermogravimetric analysis using a Mettler-Toledo TGA/DSC 1 thermobalance (Schwerzenbach, Switzerland). Samples with a total weight between 8 and 10 mg were placed in an alumina crucible (70 µL) and heated from 30 to 800 ^{o}C at a constant heating rate of 10 ^{o}C min^{-1} under nitrogen atmosphere (flow rate 50 mL min^{-1}). All samples were analyzed in triplicate to ensure reproducibility.

Moisture content

Moisture content of FBP films samples was determined gravimetrically by measuring the weight loss of films, with a size of 1 x 1 cm^2, before and after drying in an oven at 105 ^{o}C for 24 h, to attain a constant weight. The moisture content of each film was calculated according to the following **Equation IV.3.1.1**.

$$\text{Moisture content} = \left[\frac{W_i - W_f}{W_i}\right] \times 100\ (\%) \qquad \textbf{Equation IV.3.1.1}$$

where W_i and W_f are the initial and dried weight of the samples respectively. Three replications of each film were used for calculating the moisture content average.

Solubility

The solubility of FBP films in water was determined according to the method proposed by Masamba *et al.* [46] with minor modifications. Rectangular pieces of films (10 x 10 mm^2) were dried in an oven at 105 ^{o}C for 24 h, until constant weight. The weight of the dried films was measured, and then the films were placed into a test tube with 10 mL of distilled water. The tubes were slowly and periodically stirred for 24 h at 25 ^{o}C. After that period, the non-solubilized fraction was dried in the oven at 105 ^{o}C for 24 h in order to determine the weight of dry matter not dissolved in water. The % solubility of each film was determined using the following **Equation IV.3.1.2**:

$$\text{Solubility} = \left[\frac{W_i - W_f}{W_i}\right] \times 100\ (\%) \qquad \textbf{Equation IV.3.1.2}$$

where W_i is the initial weight of the sample and W_f is the sample weight after drying. The measurements were made in triplicate.

Static contact angle measurements

The static contact angle (θ) of each preconditioned FBP films was measured by an optical goniometer model FM140 (110/220 V, 50/60 Hz) from KRÜSS GmbH (Hamburg, Germany) at room temperature. This goniometer is equipped with a video capture kit and analysis software (Drop Shape Analysis SW21; DSA1). Five different water droplets, using distilled water as contact liquid, were deposited onto the film surface with a micro syringe and ten measurements were obtained for each drop and averaged. The contact angle was measured 30 s after depositing the drop to obtain stabilized values.

Transparency

FBP films transparency was determined using a UV–Vis spectrophotometer Perkin Elmer model Lambda 2 (Massachusetts, EEUU) according to ASTM D1746. Preconditioned film specimens were cut into rectangle shape and directly placed in the spectrophotometer cell. The percent transmittance of light at 600 nm in each film was measured by triplicate, and the transparency value was calculated by the following **Equation IV.3.1.3**:

$$\text{Transparency} = \left[\frac{\text{Log}T_{600}}{x}\right] \qquad \textbf{Equation IV.3.1.3}$$

where T_{600} is the transmittance at 600 nm of each film and x is the film thickness (mm).

Colour of films

The effect of CNCs in the colour properties of FBP films was studied in a colorimeter model KONICA CM-3600d COLORFLEX-DIFF2 from Hunter Associates Laboratory (Virginia, EEUU) calibrated using a white standard. The CIELAB colour space was used to measure the degree of L* (lightness), a* (red-green) and b* (yellow-blue) of each film. Five measurements were made at random positions over each film surface and average values were calculated. Total colour difference (ΔE_{ab}*) was calculated using the following **Equation IV.3.1.4**:

$$\Delta E_{ab}{}^{*}=\sqrt{(\Delta L^{*})^{2}+(\Delta a^{*})^{2}+(\Delta b^{*})^{2}} \qquad \textbf{Equation IV.3.1.4}$$

where ΔL*, Δa* and Δb* are the differences between the corresponding colour parameters of the samples and the colour parameter values of the control film (L* = 66.6, a* = 5.5, b* = 37.0).

Oxygen transmission rate (OTR)

The oxygen transmission rate (OTR) of the FBP films was obtained using an OTR Permeation Analyzer Mocon OX-TRAN model 2/20 from Modern Controls Inc. (Minneapolis, USA) equipped with a coulometric oxygen sensor in accordance with ASTM D3985-95. The area of measurement of the samples was 5 cm^2 and the OTR measurements were performed at 23 ^oC and 50% RH. Before the analysis, the samples were conditioned for 2 days at 23 ^oC and 50% RH. At least two samples of each film were tested.

Water vapour transmission rate (WVTR)

The WVTR test was conducted gravimetrically in triplicate following ASTM E96-95. Conditioned circular films were sealed on permeability cups TQC Sheen B.V. model VF2200 (Capelle aan den IJssel, Netherlands) containing 2 g of $CaCl_2$ (0% RH) with an exposed area of 10 cm^2. Later, the cups were placed in a desiccator at 25 ± 1 ^oC containing a saturated $Mg(NO_3)\cdot 6H_2O$ solution to reach a relative humidity of 54% ± 3%. The cups were weighed each hour for a total period of 8 h using an analytical balance. The changes in cup weight were plotted as a function of time and the slope was calculated by linear regression. Finally, the WVTR (normalized) was calculated according to the following **Equation IV.3.1.5** [47]:

$$WVTR=\left[\frac{n\times l}{A}\right] \qquad \textbf{Equation IV.3.1.5}$$

where n is the slope of the straight line, l is the thickness of the film (normalized) and A is the exposed area of the film.

Field emission scanning electron microscopy (FESEM)

The morphology of the cross section of nitrogen cryofractured films was studied in a field emission scanning electron microscope (FESEM) ZEISS model ULTRA55 (Eindhoven, The Netherlands) with an operating voltage of 1 kV. Prior to the morphological characterization, the cryofracture surface of films were coated with a thin layer of platinum in a high vacuum sputter coater EM MED20 from Leica Microsystems (Mil-ton Keynes, United Kingdom).

Attenuated total reflection-Fourier transform infrared (ATR-FTIR) spectroscopy

The FBP films spectra were recorded by attenuated total reflection method (ATR) in an infrared spectrometer Perkin-Elmer Spectrum BX (Perkin-Elmer Spain S.L., Madrid, Spain). Each sample was subjected to 20 scans between 4000 and 600 cm^{-1} with a resolution of 4 cm^{-1}. After attenuation of total reflectance and baseline correction, spectra were normalized with a limit ordinate of 1.5 absorbance units.

RESULTS AND DISCUSSION

Mechanical properties

The mechanical properties of the control film (FBP) and films reinforced with different CNCs content are shown in **Figure IV.3.1.1**. As can be seen, the incorporation of low CNCs content (1 and 3 wt%) to the FBP film hardly affects the strength and tensile modulus, obtaining values very similar to those of the unreinforced FBP film. However, it is observed that the addition of higher CNCs amounts (5 and 7 wt%) results in a considerable increase in tensile strength, with values of 5.3 MPa and 6.5 MPa for the films reinforced with 5 and 7 wt% of CNCs respectively, which represents a percentage increase of 22.3% and 50.5% respectively, with respect to the unreinforced film (4.3 MPa). The tensile strength values obtained with the film reinforced with 7 wt% CNCs are higher than those obtained with other protein films reinforced with similar or higher amounts of CNCs [39, 43, 48].

This tendency is also observed in Young's modulus, where it can be seen that the addition of 5 and 7 wt% of CNCs into the FBP film resulted in an increase of 43.7% and 76.1% respectively with respect to the unreinforced protein film (67.1 MPa). Therefore, the incorporation of CNCs into the FBP film resulted in an increase in its stiffness, which

increases with the amount of reinforcement in the matrix. This is due to the increased hydrogen bonds formed between the protein matrix and the reinforcement as CNCs loading increases, thus increasing the cohesion of the films and reducing their flexibility [39, 48]. This same trend with respect to mechanical strength properties was observed by Sukyai *et al.* [48] who studied the effect of different content of cellulose nanocrystals from sugarcane bagasse (0, 2, 5 and 8 wt%) in whey protein films. In this case, the authors observed that the addition of 8 wt% CNCs to the whey protein film resulted in an increase in tensile strength from 2.30 MPa to 4.93 MPa and Young's modulus from 57.56 MPa to 187.42 MPa with respect to the unreinforced whey protein film.

With respect to the elongation at break, **Figure IV.3.1.1** shows how the addition of CNCs results in a decrease of ductile mechanical properties of the FBP film. In this case, it is observed that the control film shows an elongation at break of about 105%. This elongation at break is significantly higher than the elongation at break obtained in other protein films with similar plasticizer content, such as soy protein films [49] or whey protein films [50]. The addition of 1 wt% of CNCs considerably reduces the elongation at break of the control film, changing from 104.4% in FBP film to 63.9%. For higher amounts of CNCs (3 and 5 wt%) the elongation at break decreases to around 54%, while for films reinforced with 7 wt% CNCs the elongation decreases to 48.9%, which represents a decrease of around 53.1% with respect to the elongation at break of the control film. This decrease in elongation at break is typical of protein films reinforced with cellulose nanocrystals, since the interactions of the CNCs with the proteins lead to a reduction in the polymer chains' mobility, thus reducing their ductility [51].

Comparing the mechanical properties of unreinforced FBP films and films reinforced with different CNCs content with those of synthetic films used in the food packaging sector, it can be observed that the elongation at break obtained in the control film is higher than that of widely used materials such as PET (70%) or HDPE (20–50%). However, these materials have higher tensile strength values than FBP films. On the other hand, it is observed that the tensile strength achieved by the FBP film reinforced with 7 wt% CNCs has a tensile strength value similar to that of LDPE (7–25 MPa) and EVA (6–19 MPa) [52].

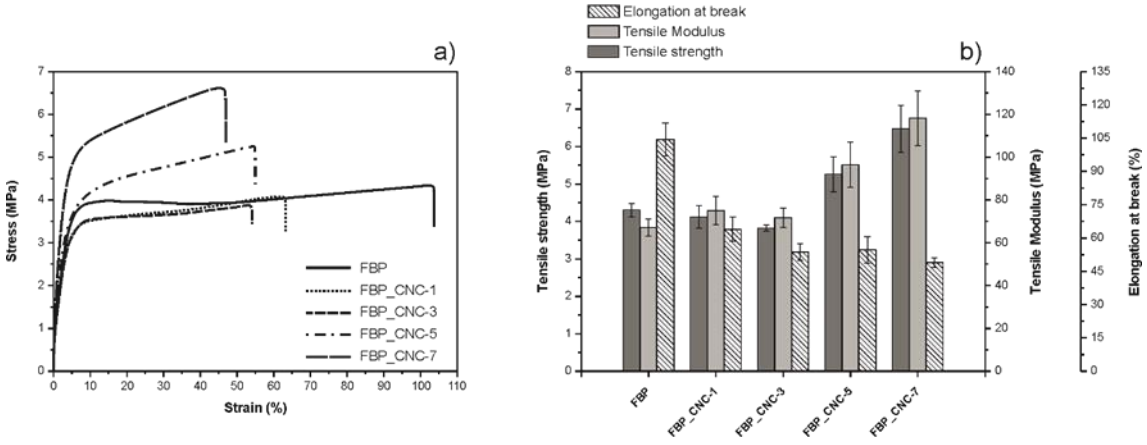

Figure IV.3.1.1. Tensile properties of unreinforced (control) FBP film and FBP film reinforced with different CNCs content: a) stress-strain curves and b) tensile properties.

Thermal properties

The thermal stability of unreinforced FBP film and films reinforced with different CNCs content was studied by thermogravimetric analysis. **Figure IV.3.1.2** shows the mass loss curves of the FBP films with respect to temperature and their corresponding first derivative curves (DTG). Additionally, **Table IV.3.1.2** gathers the most relevant thermal degradation properties, namely the onset degradation temperature of each film and the maximum degradation temperatures in each of the different degradation stages, as well as the percentage of mass loss obtained in each of them. As can be seen in all the curves, three main stages can be identified. The weight loss that occurs at low temperatures (30–125 ^{o}C) is related to the moisture loss absorbed by the films. The second degradation stage (125–280 ^{o}C) is attributed to the loss of low molecular weight protein fractions and glycerol evaporation. Finally, the third stage (280-500 ^{o}C), is related to the protein and CNCs degradation [43]. As shown in **Table IV.3.1.2**, the control film (FBP) has a higher moisture content than the CNCs-reinforced films. This is a clear evidence of the increased hydrophobicity of the film due to the presence of the CNCs, as their interaction with the proteins reduces the number of active sites capable of reacting with the water molecules, thus reducing the moisture content of the film. It can also be observed that the FBP film onset degradation temperature increases with the presence of CNCs, with higher values as the CNCs content increases. In this case, the highest onset degradation temperature is obtained for the film reinforced with 7 wt% CNCs, with an increase of about 15 ^{o}C with respect to the control film. On the other hand, if the third degradation stage is observed, related to the degradation of the proteins and CNCs, it

can be seen that the reinforced films present higher thermal stability with increasing CNCs content. This increase in degradation temperature in reinforced films may be due to the higher thermal stability of CNCs compared to proteins, as well as the formation of strong intermolecular bonds between CNCs and the matrix phase resulting in improved thermal stability compared to the control film [43, 53]. In this case, the highest degradation temperature (T_{max3}) was obtained in the film reinforced with 7 wt% of CNCs, with a value of 318.9 ºC. This is due to the higher number of interactions established between the proteins and CNCs, resulting in an increase in their thermal stability.

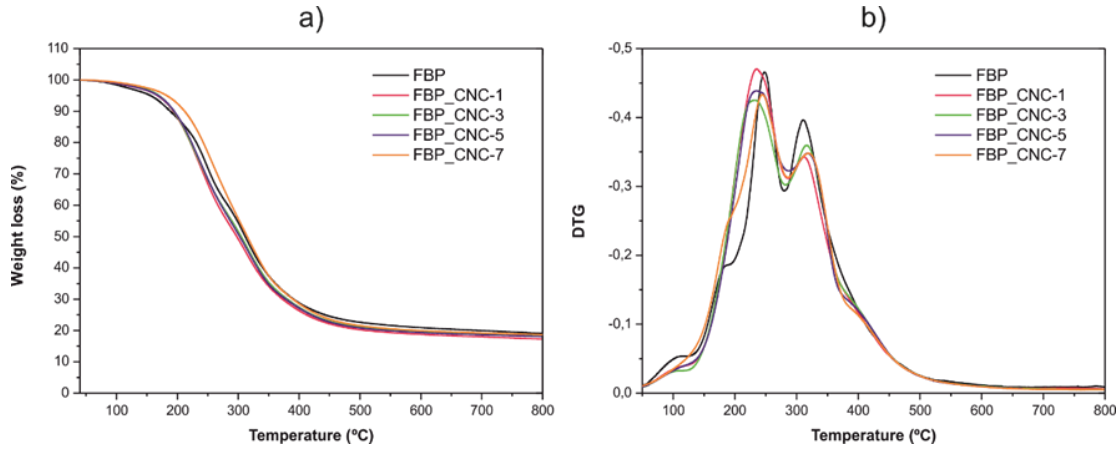

Figure IV.3.1.2. a) TGA curves and b) DTG curves of unreinforced (control) FBP film and FBP film reinforced with different CNCs content.

Table IV.3.1.2. Thermal parameters of unreinforced (control) FBP film and FBP film reinforced with different CNCs content.

Samples	T_0[a] (ºC)	Stage 1 30 - 125 ºC	Stage 2 125-280 ºC		Stage 3 280-500 ºC		Residue Mass (%)
		Mass loss (%)	Mass loss (%)	T_{max2} (ºC)	Mass loss (%)	T_{max3} (ºC)	
FBP	155.9 ± 0.1	2.8 ± 0.2	34.2 ± 2.9	245.9 ± 1.2	44.1 ± 3.3	311.9 ± 1.5	18.9 ± 0.3
FBP_CNC-1	165.4 ± 1.9	2.1 ± 0.0	45.6 ± 1.6	237.9 ± 1.7	35.3 ± 1.3	311.7 ± 0.7	17.1 ± 0.3
FBP_CNC-3	166.7 ± 1.4	2.0 ± 0.1	39.6 ± 1.6	235.0 ± 2.7	40.0 ± 1.2	316.4 ± 0.4	18.4 ± 0.3
FBP_CNC-5	167.1 ± 1.0	2.1 ± 0.0	43.7 ± 1.2	232.8 ± 1.9	36.3 ± 0.9	318.5 ± 0.5	17.9 ± 0.3
FBP_CNC-7	170.8 ± 2.1	1.9 ± 0.2	43.2 ± 3.4	243.7 ± 3.7	36.3 ± 3.0	318.9 ± 0.6	18.6 ± 0.1

[a] T_0 is calculated at 5% weight loss.

Water susceptibility

Moisture content, water solubility and contact angle values of different FBP films are shown in **Table IV.3.1.3**. As can be seen, the addition of CNCs to the protein film results in a slight reduction in the moisture content of the films, being this reduction greater for higher CNCs contents (5 and 7 wt%). This decrease in the moisture content of the reinforced films may be due to the interactions formed between the hydroxyl groups of the CNCs and the free functional groups of the proteins, which reduce the number of available active sites capable of interacting with the water molecules, resulting in an increase in the hydrophobicity [41]. This reduction of hydrophilic groups in the protein film due to interactions with CNCs also leads to an increase in the surface hydrophobicity. As can be seen in **Table IV.3.1.3**, the contact angle of the control film (56.7º) increases after the addition of CNCs, being higher as the CNCs concentration in the film increases. In this case, the maximum contact angle is obtained for the FBP film reinforced with 7 wt% CNCs, with a contact angle of 66.7º, which represents an increase of 21.4% with respect to the control film [42]. This increase in FBP film hydrophobicity after CNCs incorporation is of great interest for food packaging applications. However, the contact angle is still lower than that of materials used as food packaging such as LDPE (100.2º), HDPE (92.4º) or PP (90º), which is evidence of their hydrophilic nature [54, 55].

Table IV.3.1.3 shows the water solubility values of the different films. Water solubility is an important property to be considered in food packaging applications where the film has to be in contact with food that contains a large amount of water. In this case it is observed that the unreinforced FBP film shows a low water solubility compared to other protein films, such as soy protein films [39, 49], whey protein [48] or amaranth protein films [42]. This low solubility of the films was evidenced by the good structural integrity obtained after 24 h of immersion in water, which showed that only small amounts of low molecular weight peptides and plasticizer were dissolved in the water during the test [56]. In this case, it is observed that the incorporation of CNCs in the FBP film decreases its water solubility, obtaining a reduction in solubility of around 10% for films with CNCs contents of 3, 5 and 7 wt% compared to the control film. This reduction in solubility is due to the strong hydrogen bonding interactions established between the hydroxyl groups of CNCs and the carboxyl and amino groups of proteins, which improve their cohesion and reduce their susceptibility to water molecules [51, 57].

Some authors have reported that this reduction in water solubility may also be influenced by the high crystallinity of the CNCs [58].

Table IV.3.1.3. Moisture content, water solubility and contact angle for unreinforced (control) FBP film and FBP film reinforced with different CNCs content.

Samples	Sample				
	FBP	**FBP_CNC-1**	**FBP_CNC-3**	**FBP_CNC-5**	**FBP_CNC-7**
Moisture content (%)	15.9 ± 0.5	15.4 ± 0.6	15.3 ± 0.7	14.2 ± 0.3	14.3 ± 0.9
Water solubility (%)	34.6 ± 0.5	33.6 ± 0.2	31.7 ± 0.5	31.1 ± 1.1	31.5 ± 0.8
Contact angle (º)	56.7 ± 1.3	57.4 ± 2.1	61.6 ± 1.4	64.6 ± 3.1	66.7 ± 1.0

Chemical structural properties

The chemical interactions between CNCs and the proteins during film production were assessed by ATR-FTIR. **Figure IV.3.1.3** shows the FTIR spectra of the unreinforced FBP film and the films reinforced with different CNCs content. As can be seen, the control film spectra (FBP) shows the main absorption bands of the peptide linkage which are the peak at 1630 cm^{-1} corresponding to the amide I band (C=O stretching), the peak at 1538 cm^{-1} attributed to the amide II band (N–H bending and C–N stretching) and the peak at 1238 cm^{-1} corresponding to the amide III band (N–H bending and C–N stretching) [12]. Other characteristic peaks appearing in the spectra are the peak at 3272 cm^{-1} related to the N–H and O–H groups of the proteins, and the peak at 1038 cm^{-1} associated with C–C and C–O stretching vibrations.

On the other hand, the peaks located in the range between 800 and 1150 cm^{-1} are attributed to the glycerol used as a film plasticizer [48, 51, 59]. After the incorporation of CNCs, no significant changes in the spectra were observed. However, it is observed that in the reinforced films a new peak appears at 1158 cm^{-1} related to the saccharide structures of CNCs [40], as well as a change in the intensity of the bands associated to the amide I, II, and III compared to the control film. These differences are most evident in the case of the film reinforced with 7 wt% CNCs. This suggests the formation of interactions between the main polypeptide chains of proteins and the CNCs, consisting

mainly of hydrogen bonds between the amino and carboxyl groups of the proteins and the hydroxyl groups of the CNCs [51, 60].

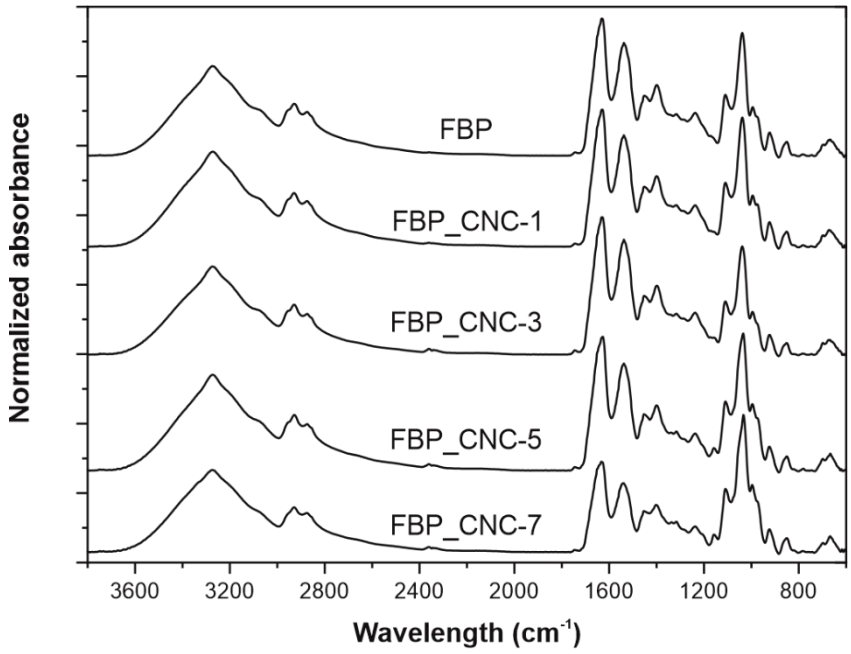

Figure IV.3.1.3. FTIR spectra of unreinforced (control) FBP film and FBP film reinforced with different CNCs content.

Morphological properties

The FESEM images of the cryofractured cross section of the different films are gathered in **Figure IV.3.1.4**. As can be seen, the control film has a smooth and homogeneous surface, with the presence of small microcracks and numerous surface pores. After the CNCs incorporation, a modification of the fracture surface is observed. In this case, CNCs-reinforced films have a higher cross-section roughness, which increases as the CNCs content in the film increases. Furthermore, it is observed that the CNCs incorpo- ration in the film leads to a reduction in the size and pore number on the surface, resulting in a more homogeneous and uniform surface. This is most noticeable in samples reinforced with small CNCs content (1% and 3%). This reduction in the size and number of pores on the surface evidences the good interaction between the functional groups of the proteins, the glycerol and the CNCs, which results in more compact and resistant films, but with a lower molecular mobility, which is reflected in the mechanical properties with an increase in the tensile strength and a decrease in the elongation at break [40, 43, 61].

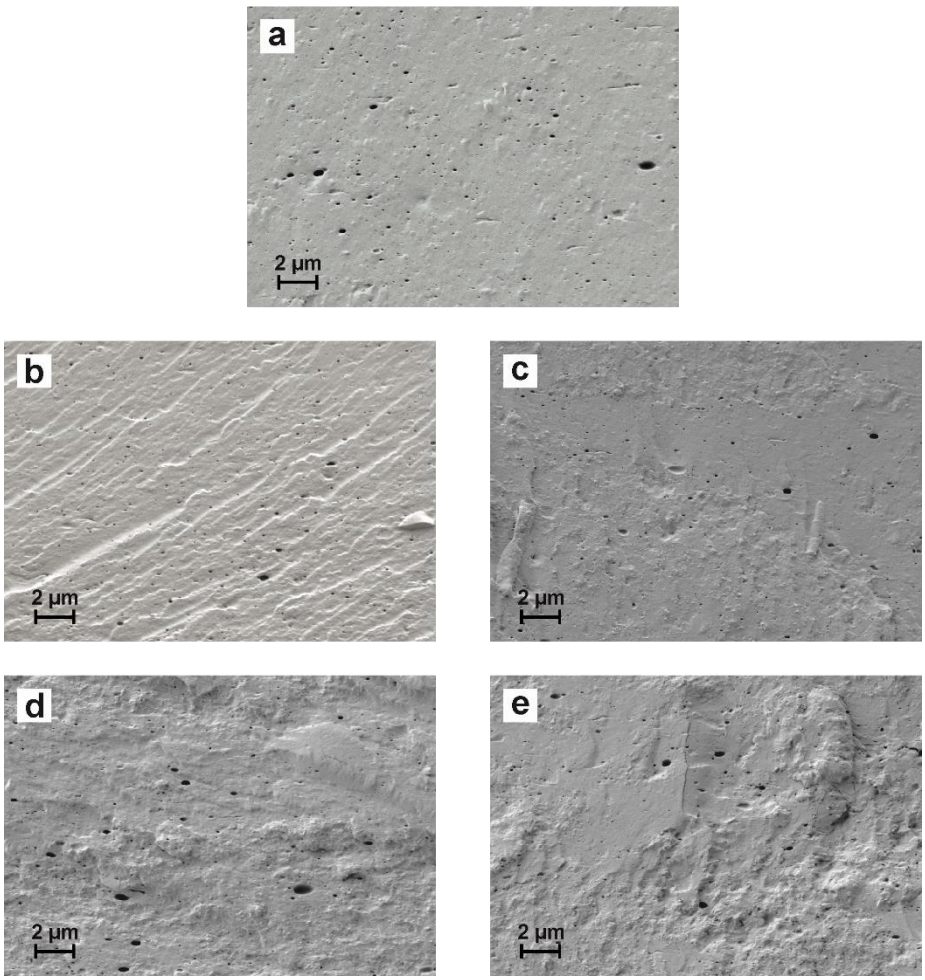

Figure IV.3.1.4. Field emission scanning electron microscopy (FESEM) images at 5,000x of cryofractured cross section of FBP-based films: (a) FBP (control); (b) FBP_CNC-1; (c) FBP_CNC-3; (d) FBP_CNC-5 and (e) FBP_CNC-7.

Barrier properties

Figure IV.3.1.5 shows the OTR and WVTR values of unreinforced FBP film (control), and films reinforced with different CNCs content. As can be seen in **Figure IV.3.1.5**a, the CNCs addition to the control FBP film results in a reduction of the OTR values, being this reduction greater as the CNCs content in the film increases. In this case, the lowest OTR value was obtained in the film with a CNCs content of 7 wt% (3.67 x 10^3 mL µm m^{-2} day^{-1}), obtaining an OTR value 36.2% lower than the control film (5.75 × 10^3 mL µm m^{-2} day^{-1}). This OTR decrease is due to the formation of a dense network structure by the interaction between proteins and CNCs which results in an increase in the tortuosity of the diffusion pathway of the oxygen molecules, hindering their transfer through the film and thus increasing its oxygen barrier property [62]. This reduction of

oxygen permeability is of great importance in the food packaging sector, as it allows to increase the product's shelf life.

In the same way, it can be seen in **Figure IV.3.1.5**b that the WVTR is also reduced by the presence of CNCs, improving the water barrier property of the FBP films. In this case, the addition of 1 wt% CNCs hardly affects the water vapour permeability. However, higher CNCs content results in a decrease in WVTR with respect to the control film, leading to a greater decrease as the CNC content in the film increases. The WVTR of the control film was 2.93 × 10^4 g µm m^{-2} day^{-1}, reducing to 2.27 × 10^4 g µm m^{-2} day^{-1} after incorporating 7 wt% CNCs, a decrease of about 22.7%. This improvement of the water vapour barrier property of the reinforced films can be influenced by several aspects, such as the decrease of the films' hydrophilicity due to the presence of CNCs, or the increase of the tortuosity of the diffusion path of water molecules due to the presence of highly crystalline CNCs. In addition, the restricted polymer chain mobility and the higher matrix structure density obtained due to the strong interactions of the functional groups of proteins and CNCs also contribute to the reduction of the water vapour permeability of CNC-reinforced films [63, 64].

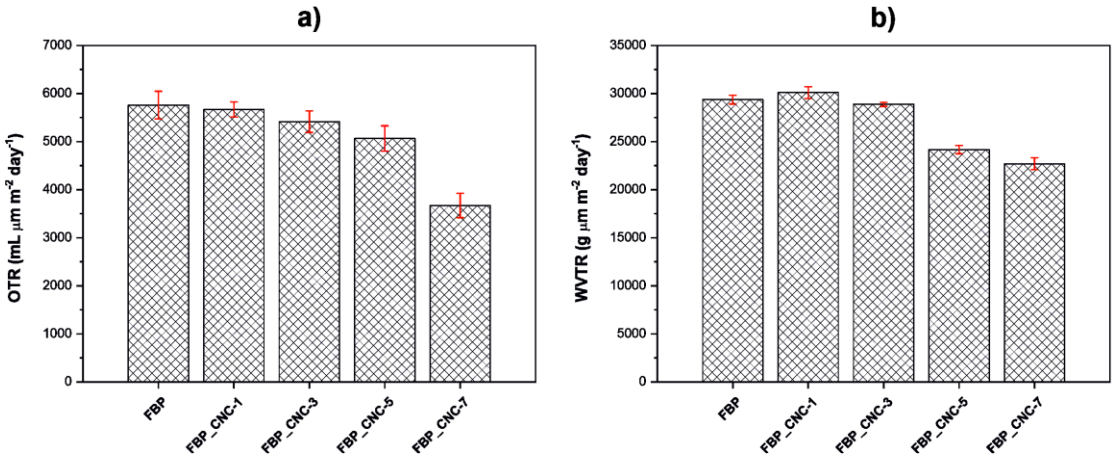

Figure IV.3.1.5. a) OTR and b) WVTR of unreinforcing (control) FBP film and FBP film reinforcing with different CNCs content.

Colour and transparency properties

Figure IV.3.1.6 shows the light transmission in the UV and visible ranges and the transparency of unreinforced FBP film and films reinforced with different CNCs content. As can be seen, all films show a good ability to absorb UV light at wavelengths between 250 and 300 nm, while for wavelengths between 300 and 400 nm, the CNCs addition to

the FBP film reduces the UV light absorption, which is of interest in the food preservation packaging sector. In the visible range region (400–700 nm), the FBP film shows a high transmittance percentage, which is reduced after the CNCs incorporation. As can be seen in **Figure IV.3.1.6**a, the transmittance decreases as the CNC content of the film increases.

The films' transparency is one of the most important properties to be considered for their use in the food packaging industry. **Figure IV.3.1.6**b shows that the control film has a high transparency, however, after CNCs addition, this transparency is slightly reduced, obtaining a higher opacity as the CNCs content in the film increases. The decrease in transparency of the reinforced films may be related to light scattering caused by the dispersed CNCs in the matrix which leads to a reduction of light passing through the film. The increased opacity of reinforced films may also be due to the formation of CNCs aggregates during film fabrication, which cause a slight darkening and make it difficult for light to pass through the matrix [41, 51]. This loss of transparency in CNCs-reinforced protein films has also been observed by several authors such a Sukyai *et al.* [48], Han *et al.* [38] or Huang *et al.* [65]. In this case, FBP films are less transparent than other CNCs-reinforced films, such as CNCs-reinforced whey protein films from sugar cane bagasse [48]. However, it is worth noting that the control film and the FBP film reinforced with 1 wt% of CNCs show higher transparency than the commercial LDPE film used for food packaging, 4.26 A mm^{-1}, being this very similar to that obtained in the FBP films reinforced with 3, 5 and 7 wt% of CNCs [66].

Table IV.3.1.4 shows the surface colour values of unreinforced film and films reinforced with different CNCs content. As can be seen, the incorporation of CNCs into the FBP films results in a slight increase in L* and a decrease in the a* and b* coordinate values, which is representative for a slight increase of the brown colour in the samples, probably due to the formation of CNC aggregates in the film. However, the ΔE_{ab}* values of the CNC-reinforced films show that the reinforcement addition into the FBP film hardly alters its colour properties.

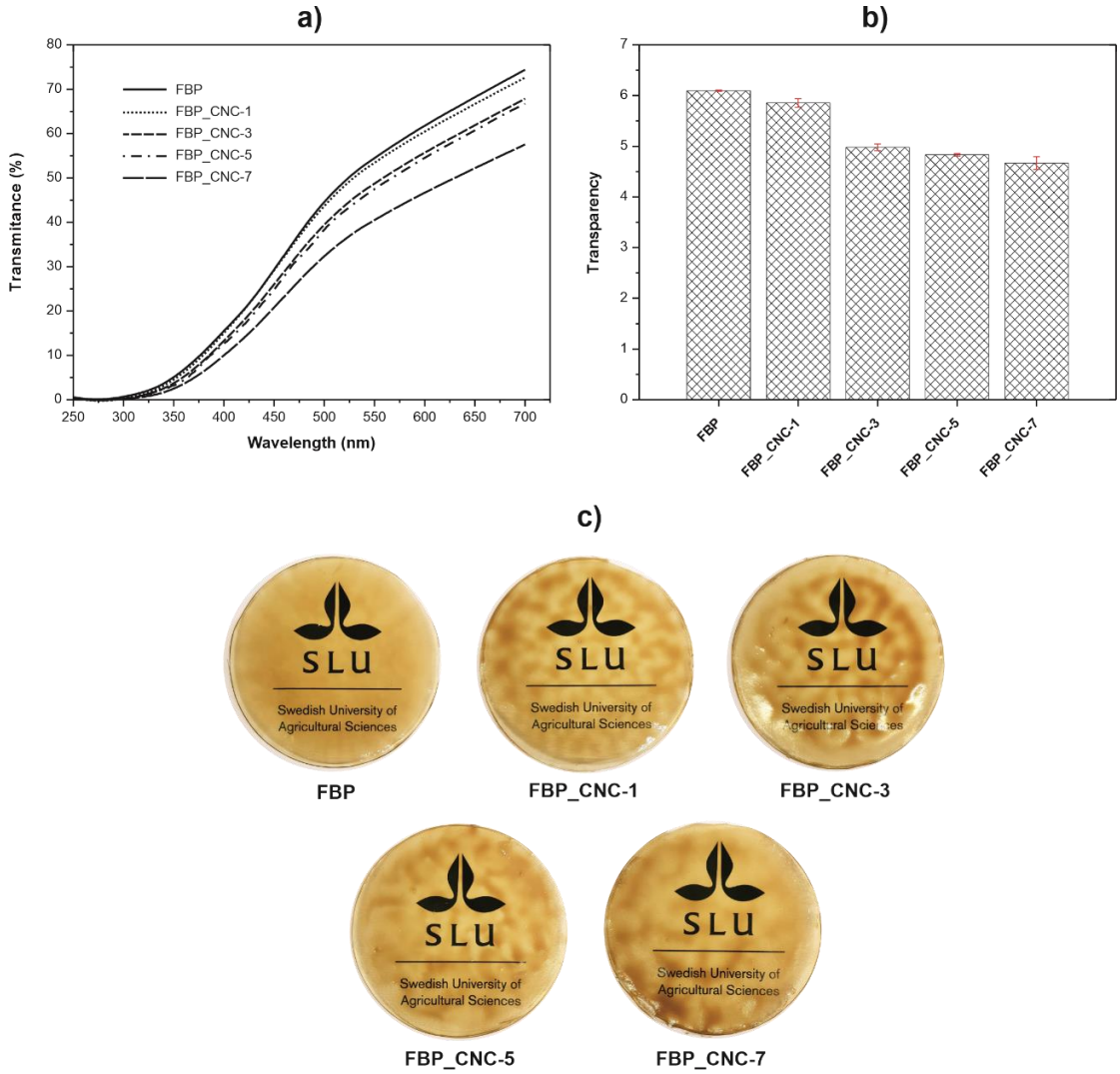

Figure IV.3.1.6. a) transmittance, b) transparency and c) macroscopic aspect of unreinforced (control) FBP film and FBP film reinforced with different CNCs content.

Table IV.3.1.4. Colour parameters from CIELab space of unreinforced (control) FBP films and FBP film reinforced with different CNCs content.

Parameter	FBP	FBP_CNC-1	FBP_CNC-3	FBP_CNC-5	FBP_CNC-7
L*	66.6 ± 0.4	68.0 ± 0.7	69.8 ± 1.3	68.6 ± 1.6	69.4 ± 1.4
a*	5.5 ± 0.3	4.3 ± 0.3	3.9 ± 0.6	5.1 ± 0.7	4.0 ± 0.5
b*	37.0 ± 0.5	34.5 ± 0.8	35.6 ± 1.2	35.1 ± 1.3	34.2 ± 1.2
ΔE_{ab}* (Control)[a]	-	3.1	3.8	2.7	4.2

[a] ΔE_{ab}* is calculated from the colour difference between FBP film and each FBP/CNC film.

CONCLUSIONS

In the present work, the effect of the incorporation of different CNCs content (1, 3, 5, and 7 wt%) synthesized from pine cone on the mechanical, thermal, barrier, water susceptibility, optical and morphological properties of faba bean protein (FBP) films has been evaluated. The CNCs addition to the FBP film resulted in the formation of intra-molecular interactions between the hydroxyl groups of the CNCs and the amino and carboxyl groups of the proteins, mainly through hydrogen bonds. This chemical affinity resulted in more compact films with lower chain mobility, which was reflected in the mechanical properties of the reinforced films through an increase in tensile strength and Young's modulus and a decrease in the elongation at break compared to the unreinforced FBP film. In this case, the incorporation of 7 wt% CNC in the FBP film resulted in an increase in tensile strength and Young's modulus of 50.5 and 76.1% respectively with respect to the control film, as well as a decrease in elongation at break of about 53.1%. The thermal stability of the FBP film was also affected by the presence of CNCs, increasing the onset degradation temperature as the CNC content in the film increases. In this case, an increase of 15 ^{o}C was obtained in the onset degradation temperature of the film reinforced with 7 wt% of CNCs compared to the control film. A slight increase in the maximum degradation temperature was also observed in the reinforced films with respect to the FBP film. The interactions formed between the CNCs and the proteins also reduced the amount of active sites able to react with the water molecules in the proteins, which resulted in an increase in the hydrophobicity of the CNC-reinforced films, as evidenced by a reduction in moisture content and water solubility and an increase in their contact angles. The CNCs addition to the FBP film also significantly improved its barrier properties, reducing its WVTR and OTR as the CNC content in the matrix increased. In this case, the film reinforced with 7 wt% CNC obtained 36.2 and 22.7% lower OTR and WVTR values, respectively, compared to the unreinforced FBP film. Finally, it was observed that the presence of CNCs in the FBP film led to an increase in its opacity as the CNCs content increases. This work has shown that CNCs obtained from pine cone are of great interest to improve some physical and mechanical properties of FBP films, obtaining biobased and biodegradable materials that could present attracting potential for use in the food packaging sector as edible food packaging material. These films could be a potential solution to reduce the amount of non-degradable food packaging waste of petrochemical origin.

ACKNOWLEDGEMENTS

This research was supported by the Ministry of Science and Innovation (MICI) [MAT2017-84909-C2-2-R]. S. Rojas-Lema thanks the Generalitat Valenciana (GVA) for the financial support through a Santiago Grisolia grant (GRISOLIAP/2019/132). D. Garcia Garcia wants to thank the Ministry of Science, Innovation and Universities for their financial support through the "Jose Castillejo" mobility grant (CAS19/00332).

REFERENCES

[1] Plastics Europe. *An analysis of European plastics production, demand and waste data*. 2020. [Consulted July 5]; Available from https://www.plasticseurope.org/en/resources/market-data.

[2] P. Liminana, D. Garcia-Sanoguera, L. Quiles-Carrillo, R. Balart, and N. Montanes. *Development and characterization of environmentally friendly composites from poly (butylene succinate)(PBS) and almond shell flour with different compatibilizers.* Composites Part B: Engineering, 2018, 144, p. 153-162.

[3] S. Zhang, C. Xia, Y. Dong, Y. Yan, J. Li, S.Q. Shi, and L. Cai. *Soy protein isolate-based films reinforced by surface modified cellulose nanocrystal.* Industrial Crops and Products, 2016, 80, p. 207-213.

[4] N. Reddy, Q. Jiang, and Y. Yang. *Preparation and properties of peanut protein films crosslinked with citric acid.* Industrial Crops and Products, 2012, 39, p. 26-30.

[5] T. Bourtoom. *Edible protein films: properties enhancement.* International Food Research Journal, 2009, 16(1), p. 1-9.

[6] P.R. Salgado, S.E.M. Ortiz, S. Petruccelli, and A.N. Mauri. *Biodegradable sunflower protein films naturally activated with antioxidant compounds.* Food Hydrocolloids, 2010, 24(5), p. 525-533.

[7] E. Makri, E. Papalamprou, and G. Doxastakis. *Study of functional properties of seed storage proteins from indigenous European legume crops (lupin, pea, broad bean) in admixture with polysaccharides.* Food Hydrocolloids, 2005, 19(3), p. 583-594.

[8] S.P. Samaei, M. Ghorbani, D. Tagliazucchi, S. Martini, R. Gotti, T. Themelis, F. Tesini, A. Gianotti, T.G. Toschi, and E. Babini. *Functional, nutritional, antioxidant, sensory properties and comparative peptidomic profile of faba bean (Vicia faba, L.) seed protein hydrolysates and fortified apple juice.* Food Chemistry, 2020, 330, p. 127120.

[9] O. Nivala, E. Nordlund, K. Kruus, and D. Ercili-Cura. *The effect of heat and transglutaminase treatment on emulsifying and gelling properties of faba bean protein isolate.* LWT - Food Science and Technology, 2020, p. 110517.

[10] J. Vioque, M. Alaiz, and J. Girón-Calle. *Nutritional and functional properties of Vicia faba protein isolates and related fractions.* Food Chemistry, 2012, 132(1), p. 67-72.

[11] S. Saremnezhad, M. Azizi, M. Barzegar, S. Abbasi, and E. Ahmadi. *Properties of a new edible film made of faba bean protein isolate.* Journal of Agricultural Science and Technology, 2011, 13(2), p. 181-192.

[12] C. Montalvo-Paquini, M. Rangel-Marrón, E. Palou, and A. López-Malo. *Physical and chemical properties of edible films from faba bean protein.* Cellulose, 2014, 8, p. 125-131.

[13] E.J. Hopkins, A.K. Stone, J. Wang, D.R. Korber, and M.T. Nickerson. *Effect of glycerol on the physicochemical properties of films based on legume protein concentrates: A comparative study.* Journal of Texture Studies, 2019, 50(6), p. 539-546.

[14] A. Aguirre, R. Borneo, and A.E. León. *Properties of triticale protein films and their relation to plasticizing–antiplasticizing effects of glycerol and sorbitol.* Industrial Crops and Products, 2013, 50, p. 297-303.

[15] H. Tian, G. Guo, A. Xiang, and W.-H. Zhong. *Intermolecular interactions and microstructure of glycerol-plasticized soy protein materials at molecular and nanometer levels.* Polymer Testing, 2018, 67, p. 197-204.

[16] L.M. Pérez, G.N. Piccirilli, N.J. Delorenzi, and R.A. Verdini. *Effect of different combinations of glycerol and/or trehalose on physical and structural properties of whey protein concentrate-based edible films.* Food Hydrocolloids, 2016, 56, p. 352-359.

[17] Ó.L. Ramos, I. Reinas, S.I. Silva, J.C. Fernandes, M.A. Cerqueira, R.N. Pereira, A.A. Vicente, M.F. Pocas, M.E. Pintado, and F.X. Malcata. *Effect of whey protein purity and glycerol content upon physical properties of edible films manufactured therefrom.* Food Hydrocolloids, 2013, 30(1), p. 110-122.

[18] D. Rosa, M. Bardi, L. Machado, D. Dias, L. Silva, and Y. Kodama. *Starch plasticized with glycerol from biodiesel and polypropylene blends: mechanical and thermal properties.* Journal of Thermal Analysis Calorimetry, 2010, 102(1), p. 181-186.

[19] X. Tong, X. Luo, and Y. Li. *Development of blend films from soy meal protein and crude glycerol-based waterborne polyurethane.* Industrial Crops and Products, 2015, 67, p. 11-17.

[20] F. Yang, M.A. Hanna, and R. Sun. *Value-added uses for crude glycerol--a byproduct of biodiesel production.* Biotechnology for biofuels, 2012, 5(1), p. 1-10.

[21] Z. Ye, S. Xiu, A. Shahbazi, and S. Zhu. *Co-liquefaction of swine manure and crude glycerol to bio-oil: Model compound studies and reaction pathways.* Bioresource Technology, 2012, 104, p. 783-787.

[22] S.J. Calva-Estrada, M. Jiménez-Fernández, and E. Lugo-Cervantes. *Protein-based films: Advances in the development of biomaterials applicable to food packaging.* Food Engineering Reviews, 2019, 11(2), p. 78-92.

[23] V.M. Azevedo, M.V. Dias, H.H. de Siqueira Elias, K.L. Fukushima, E.K. Silva, J.d.D.S. Carneiro, N.d.F.F. Soares, and S.V. Borges. *Effect of whey protein isolate films incorporated with montmorillonite and citric acid on the preservation of fresh-cut apples.* Food Research International, 2018, 107, p. 306-313.

[24] V.M. Azevedo, E.K. Silva, C.F.G. Pereira, J.M.G. da Costa, and S.V. Borges. *Whey protein isolate biodegradable films: Influence of the citric acid and montmorillonite clay nanoparticles on the physical properties.* Food Hydrocolloids, 2015, 43, p. 252-258.

[25] P. Kumar, K. Sandeep, S. Alavi, V. Truong, and R. Gorga. *Preparation and characterization of bio-nanocomposite films based on soy protein isolate and montmorillonite using melt extrusion.* Journal of Food Engineering, 2010, 100(3), p. 480-489.

[26] R.C. Pereira, J.d.D.S. Carneiro, O.B. Assis, and S.V. Borges. *Mechanical and structural characterization of whey protein concentrate/montmorillonite/lycopene films.* Journal of the Science of Food and Agriculture, 2017, 97(14), p. 4978-4986.

[27] N. Fathi, H. Almasi, and M.K. Pirouzifard. *Sesame protein isolate based bionanocomposite films incorporated with TiO2 nanoparticles: Study on morphological, physical and photocatalytic properties.* Polymer Testing, 2019, 77, p. 105919.

[28] Y. Li, Y. Jiang, F. Liu, F. Ren, G. Zhao, and X. Leng. *Fabrication and characterization of TiO2/whey protein isolate nanocomposite film.* Food Hydrocolloids, 2011, 25(5), p. 1098-1104.

[29] Y. Liu, L. Xu, R. Li, H. Zhang, W. Cao, T. Li, and Y. Zhang. *Preparation and characterization of soy protein isolate films incorporating modified nano-TiO2.* International Journal of Food Engineering, 2019, 15(7).

[30] H. Kang, X. Liu, S. Zhang, and J. Li. *Functionalization of halloysite nanotubes (HNTs) via mussel-inspired surface modification and silane grafting for HNTs/soy protein isolate nanocomposite film preparation.* RSC Advances, 2017, 7(39), p. 24140-24148.

[31] X. Liu, H. Kang, Z. Wang, W. Zhang, J. Li, and S. Zhang. *Simultaneously toughening and strengthening soy protein isolate-based composites via carboxymethylated chitosan and halloysite nanotube hybridization*. Materials, 2017, 10(6), p. 653.

[32] A. Xiang, G. Guo, and H. Tian. *Fabrication and properties of acid treated carbon nanotubes reinforced soy protein nanocomposites.* Journal of Polymers and the Environment, 2017, 25(3), p. 519-525.

[33] D. Garcia-Garcia, J. Lopez-Martinez, R. Balart, E. Strömberg, and R. Moriana. *Reinforcing capability of cellulose nanocrystals obtained from pine cones in a biodegradable poly (3-hydroxybutyrate)/poly (ε-caprolactone)(PHB/PCL) thermoplastic blend.* European Polymer Journal, 2018, 104, p. 10-18.

[34] X. Xu, F. Liu, L. Jiang, J. Zhu, D. Haagenson, D.P. Wiesenborn, and interfaces. *Cellulose nanocrystals vs. cellulose nanofibrils: a comparative study on their microstructures and effects as polymer reinforcing agents.* ACS Applied Materials, 2013, 5(8), p. 2999-3009.

[35] R. Moriana, F. Vilaplana, and M. Ek. *Cellulose nanocrystals from forest residues as reinforcing agents for composites: A study from macro-to nano-dimensions.* Carbohydrate Polymers, 2016, 139, p. 139-149.

[36] H.A. Silvério, W.P.F. Neto, N.O. Dantas, and D. Pasquini. *Extraction and characterization of cellulose nanocrystals from corncob for application as reinforcing agent in nanocomposites.* Industrial Crops and Products, 2013, 44, p. 427-436.

[37] A.M. Slavutsky and M.A. Bertuzzi. *Water barrier properties of starch films reinforced with cellulose nanocrystals obtained from sugarcane bagasse.* Carbohydrate Polymers, 2014, 110, p. 53-61.

[38] Y. Han, M. Yu, and L. Wang. *Soy protein isolate nanocomposites reinforced with nanocellulose isolated from licorice residue: Water sensitivity and mechanical strength.* Industrial Crops and Products, 2018, 117, p. 252-259.

[39] A. González and C.I.A. Igarzabal. *Nanocrystal-reinforced soy protein films and their application as active packaging*. Food Hydrocolloids, 2015, 43, p. 777-784.

[40] Z. Yu, L. Sun, W. Wang, W. Zeng, A. Mustapha, and M. Lin. *Soy protein-based films incorporated with cellulose nanocrystals and pine needle extract for active packaging*. Industrial Crops and Products, 2018, 112, p. 412-419.

[41] Z. Qazanfarzadeh and M. Kadivar. *Properties of whey protein isolate nanocomposite films reinforced with nanocellulose isolated from oat husk.* International Journal of Biological Macromolecules, 2016, 91, p. 1134-1140.

[42] M.C. Condés, M.C. Añón, A.N. Mauri, and A. Dufresne. *Amaranth protein films reinforced with maize starch nanocrystals.* Food Hydrocolloids, 2015, 47, p. 146-157.

[43] A. Osorio-Ruiz, R.J. Avena-Bustillos, B.-S. Chiou, F. Rodríguez-González, and A.-L. Martinez-Ayala. *Mechanical and thermal behavior of canola protein isolate films as improved by cellulose nanocrystals.* ACS Omega, 2019, 4(21), p. 19172-19176.

[44] M. Langton, S. Ehsanzamir, S. Karkehabadi, X. Feng, M. Johansson, and D.P. Johansson. *Gelation of faba bean proteins-Effect of extraction method, pH and NaCl.* Food Hydrocolloids, 2020, 103, p. 105622.

[45] D. García-García, R. Balart, J. Lopez-Martinez, M. Ek, and R. Moriana. *Optimizing the yield and physico-chemical properties of pine cone cellulose nanocrystals by different hydrolysis time.* Cellulose, 2018, 25(5), p. 2925-2938.

[46] K. Masamba, Y. Li, J. Hategekimana, F. Liu, J. Ma, and F. Zhong. *Effect of Gallic acid on mechanical and water barrier properties of zein-oleic acid composite films.* Journal of Food Science and Technology, 2016, 53(5), p. 2227-2235.

[47] J. Trifol, D. Plackett, C. Sillard, P. Szabo, J. Bras, and A.E. Daugaard. *Hybrid poly (lactic acid)/nanocellulose/nanoclay composites with synergistically enhanced barrier properties and improved thermomechanical resistance.* Polymer International, 2016, 65(8), p. 988-995.

[48] P. Sukyai, P. Anongjanya, N. Bunyahwuthakul, K. Kongsin, N. Harnkarnsujarit, U. Sukatta, R. Sothornvit, and R. Chollakup. *Effect of cellulose nanocrystals from sugarcane bagasse on whey protein isolate-based films.* Food Research International, 2018, 107, p. 528-535.

[49] A. González, G. Gastelú, G.N. Barrera, P.D. Ribotta, and C.I.Á. Igarzabal. *Preparation and characterization of soy protein films reinforced with cellulose nanofibers obtained from soybean by-products.* Food Hydrocolloids, 2019, 89, p. 758-764.

[50] S. Galus and J. Kadzińska. *Whey protein edible films modified with almond and walnut oils.* Food Hydrocolloids, 2016, 52, p. 78-86.

[51] B. Shabanpour, M. Kazemi, S.M. Ojagh, and P. Pourashouri. *Bacterial cellulose nanofibers as reinforce in edible fish myofibrillar protein nanocomposite films.* International Journal of Biological Macromolecules, 2018, 117, p. 742-751.

[52] L. Bastarrachea, S. Dhawan, and S.S. Sablani. *Engineering properties of polymeric-based antimicrobial films for food packaging: a review.* Food Engineering Reviews, 2011, 3(2), p. 79-93.

[53] P.R. Chang, R. Jian, P. Zheng, J. Yu, and X. Ma. *Preparation and properties of glycerol plasticized-starch (GPS)/cellulose nanoparticle (CN) composites.* Carbohydrate Polymers, 2010, 79(2), p. 301-305.

[54] S. Fávaro, A. Rubira, E. Muniz, and E. Radovanovic. *Surface modification of HDPE, PP, and PET films with KMnO4/HCl solutions.* Polymer Degradation and Stability, 2007, 92(7), p. 1219-1226.

[55] T. Karbowiak, F. Debeaufort, D. Champion, and A. Voilley. *Wetting properties at the surface of iota-carrageenan-based edible films.* Journal of Colloid Interface Science, 2006, 294(2), p. 400-410.

[56] X. Wang, N. Ullah, X. Sun, Y. Guo, L. Chen, Z. Li, and X. Feng. *Development and characterization of bacterial cellulose reinforced biocomposite films based on protein from buckwheat distiller's dried grains.* International Journal of Biological Macromolecules, 2017, 96, p. 353-360.

[57] M. Abdollahi, M. Alboofetileh, R. Behrooz, M. Rezaei, and R. Miraki. *Reducing water sensitivity of alginate bio-nanocomposite film using cellulose nanoparticles.* International Journal of Biological Macromolecules, 2013, 54, p. 166-173.

[58] B. Deepa, E. Abraham, L.A. Pothan, N. Cordeiro, M. Faria, and S. Thomas. *Biodegradable nanocomposite films based on sodium alginate and cellulose nanofibrils.* Materials, 2016, 9(1), p. 50.

[59] E. Sogut. *Active whey protein isolate films including bergamot oil emulsion stabilized by nanocellulose.* Food Packaging and Shelf Life, 2020, 23, p. 100430.

[60] M. Martelli-Tosi, M.M. Masson, N.C. Silva, B.S. Esposto, T.T. Barros, O.B. Assis, and D.R. Tapia-Blácido. *Soybean straw nanocellulose produced by enzymatic or acid treatment as a reinforcing filler in soy protein isolate films.* Carbohydrate Polymers, 2018, 198, p. 61-68.

[61] S.F. Mirpoor, C.V.L. Giosafatto, P. Di Pierro, R. Di Girolamo, C. Regalado-González, and R. Porta. *Valorisation of posidonia oceanica sea balls (Egagropili) as a potential source of reinforcement agents in protein-based biocomposites.* Polymers, 2020, 12(12), p. 2788.

[62] Y. Xie, X. Niu, J. Yang, R. Fan, J. Shi, N. Ullah, X. Feng, and L. Chen. *Active biodegradable films based on the whole potato peel incorporated with bacterial cellulose and curcumin.* International Journal of Biological Macromolecules, 2020, 150, p. 480-491.

[63] V.M. Azevedo, A.C.S. de Oliveira, S.V. Borges, J.C. Raguzzoni, M.V. Dias, and A.L.R. Costa. *Pea protein isolate nanocomposite films for packaging applications: Effect of starch nanocrystals on the structural, morphological, thermal, mechanical and barrier properties.* Emirates Journal of Food and Agriculture, 2020, 32(7), p. 495-504.

[64] F. Rafieian, M. Shahedi, J. Keramat, and J. Simonsen. *Mechanical, thermal and barrier properties of nano-biocomposite based on gluten and carboxylated cellulose nanocrystals.* Industrial Crops and Products, 2014, 53, p. 282-288.

[65] S. Huang, R. Tao, A. Ismail, and Y. Wang. *Cellulose anocrystals derived from textile waste through acid hydrolysis and oxidation as reinforcing agent of soy protein film.* Polymers, 2020, 12(4), p. 958.

[66] P. Guerrero, Z.N. Hanani, J. Kerry, and K. De La Caba. *Characterization of soy protein-based films prepared with acids and oils by compression.* Journal of Food Engineering, 2011, 107(1), p. 41-49.

Adaptado del artículo

IV.3.2. The effect of pine cone lignin on mechanical, thermal and barrier properties of faba bean protein films for packaging applications

Sandra Rojas-Lema[1], Klara Nilsson[2], Maud Langton[2], Jon Trifol[3,4,5], Jaume Gomez-Caturla[1], Rafael Balart[1], Daniel Garcia-Garcia[1], Rosana Moriana[2,3,6].

[1] Technological Institute of Materials (ITM), Universitat Politècnica de València (UPV), Plaza Ferrándiz y Carbonell 1, 03801 Alcoy, Spain.

[2] Department of Molecular Sciences, Swedish University of Agricultural Sciences (SLU), Box 7051, SE-750 07, Uppsala, Sweden.

[3] Department of Fibre and Polymer Technology, School of Engineering Sciences in Chemistry, Biotechnology and Health, Royal Institute of Technology (KTH), SE-100 44, Stockholm, Sweden.

[4] Gaiker Technology Center, Basque Research and Technology Alliance (BRTA), Parque Tecnológico de Bizkaia, Edificio 202, 48170, Zamudio, Spain.

[5] Department of Chemical and Metallurgical Engineering, School of Chemical Engineering, Aalto University, P.O. Box 16300, FIN-00076 Aalto, Espoo, Finland.

[6] RISE Bioeconomy and Health, Research Institute of Sweden (RISE), Drottning Kristinas Va¨g 61, SE-114 28, Stockholm, Sweden.

Journal of Food Engineering, 2022, p. 111282.

Journal of Food Engineering 339 (2023) 111282

Contents lists available at ScienceDirect

Journal of Food Engineering

journal homepage: www.elsevier.com/locate/jfoodeng

The effect of pine cone lignin on mechanical, thermal and barrier properties of faba bean protein films for packaging applications

Sandra Rojas-Lema [a], Klara Nilsson [b], Maud Langton [b], Jon Trifol [c,d,e], Jaume Gomez-Caturla [a], Rafael Balart [a], Daniel Garcia-Garcia [a,*], Rosana Moriana [b,c,f]

[a] Instituto de Tecnología de Materiales (ITM), Universitat Politècnica de València (UPV), Plaza Ferrándiz y Carbonell 1, 03801, Alcoy, Alicante, Spain
[b] Department of Molecular Sciences, Swedish University of Agricultural Sciences (SLU), Box 7051, SE-750 07, Uppsala, Sweden
[c] Department of Fibre and Polymer Technology, School of Engineering Sciences in Chemistry, Biotechnology and Health, Royal Institute of Technology (KTH), SE-100 44, Stockholm, Sweden
[d] Gaiker Technology Center, Basque Research and Technology Alliance (BRTA), Parque Tecnológico de Bizkaia, Edificio 202, 48170, Zamudio, Spain
[e] Department of Chemical and Metallurgical Engineering, School of Chemical Engineering, Aalto University, P.O. Box 16300, FIN-00076 Aalto, Espoo, Finland
[f] RISE Bioeconomy and Health, Research Institute of Sweden (RISE), Drottning Kristinas Väg 61, SE-114 28, Stockholm, Sweden

ARTICLE INFO

Keywords:
Proteins films
Faba beans
Pine cone
Lignin
Packaging

ABSTRACT

In the present work, faba bean protein (FBP) films plasticized with glycerol and reinforced with different amounts (2.5, 5.0, 7.5 and 10% by weight of FBP) of lignin extracted from pine cones (PL) have been obtained by solution casting. The results obtained showed an elongation at break of 111.7% with the addition of 5% PL to the FBP film, which represents an increase of 107% compared to the FBP control film. On the other hand, it was observed by thermogravimetric analysis (TGA) that the incorporation of lignin improved the thermal stability of the FBP film, leading to an increase in the protein degradation temperature, being this increase higher in the sample film reinforced with 10% PL. The barrier properties of the FBP films were also affected by the presence of lignin, leading to a decrease in water vapor permeability (WVP) in comparison to the unreinforced film. The results show that the sample reinforced with 2.5% PL had the lowest WVP value, with a reduction of 25% compared to the control film. Chemical analysis by Fourier transform infrared spectroscopy (FTIR) confirmed the formation of intramolecular interactions between lignin and proteins which, together with the inherent hydrophobicity of lignin, resulted in a decrease of the moisture content in the films reinforced with PL. This research work has allowed the development of biobased and biodegradable films with attractive properties that could be of potential use in sectors such as packaging.

1. Introduction

Currently, due to growing environmental and economic problems, lignocellulosic biomass, which is a renewable resource, constitutes a promising alternative to non-renewable petroleum resources. For instance, biopolymers obtained from natural sources offer a great opportunity since they have interesting properties, such as renewability and biodegradability (Sadasivuni et al., 2020; Yadav et al., 2018) and, in some cases, they can offer even biocompatibility (Gnanasekaran, 2019; Nagarajan et al., 2019). Therefore, they can be considered as environmentally friendly materials (Bourtoom, 2009).

An interesting application of biopolymers includes packaging that could replace single-use synthetic plastics that cause a great amount of waste (Denavi et al., 2009; Dey et al., 2021; Walker et al., 2021). That is one of the reasons why different sectors such as the food industry have focused on finding materials with biodegradable properties in order to find new packaging to protect and extend food shelf life (Montalvo-Paquini et al., 2014). A wide range of biopolymers can be found in nature, among them lipid-based polymers, proteins and polysaccharides including cellulose and starch, among others (Shankar et al., 2015), that represent promising options to be used as biobased and biodegradable materials. With regard to polysaccharides, they can provide different properties, including thickening, crosslinking, and adsorption (Xia et al., 2020). In the case of cellulose, it could provide high crystallinity to these biobased materials (Khalil et al., 2017). Starch offers excellent biocompatibility and exceptional film-forming properties (Agarwal,

* Corresponding author.
E-mail addresses: sanrole@epsa.upv.es (S. Rojas-Lema), dagarga4@epsa.upv.es (D. Garcia-Garcia).

https://doi.org/10.1016/j.jfoodeng.2022.111282
Received 7 May 2022; Received in revised form 25 July 2022; Accepted 7 September 2022
Available online 10 September 2022

The effect of pine cone lignin on mechanical, thermal and barrier properties of faba bean protein films for packaging applications.

Abstract

In the present work, faba bean protein (FBP) films plasticized with glycerol and reinforced with different amounts (2.5, 5.0, 7.5 and 10% by weight of FBP) of lignin extracted from pine cones (PL) have been obtained by solution casting. The results obtained showed an elongation at break of 111.7% with the addition of 5% PL to the FBP film, which represents an increase of 107% compared to the FBP control film. On the other hand, it was observed by thermogravimetric analysis (TGA) that the incorporation of lignin improved the thermal stability of the FBP film, leading to an increase in the protein degradation temperature, being this increase higher in the sample film reinforced with 10% PL. The barrier properties of the FBP films were also affected by the presence of lignin, leading to a decrease in water vapor permeability (WVP) in comparison to the unreinforced film. The results show that the sample reinforced with 2.5% PL had the lowest WVP value, with a reduction of 25% compared to the control film. Chemical analysis by Fourier transform infrared spectroscopy (FTIR) confirmed the formation of intramolecular interactions between lignin and proteins which, together with the inherent hydrophobicity of lignin, resulted in a decrease of the moisture content in the films reinforced with PL. This research work has allowed the development of biobased and biodegradable films with attractive properties that could be of potential use in sectors such as packaging.

Keywords: Proteins films; faba beans; pine cone; lignin; packaging.

INTRODUCTION

Currently, due to growing environmental and economic problems, lignocellulosic biomass, which is a renewable resource, constitutes a promising alternative to non-renewable petroleum resources. For instance, biopolymers obtained from natural sources offer a great opportunity since they have interesting properties, such as renewability and biodegradability [1, 2], and, in some cases, they can offer even biocompatibility [3, 4]. Therefore, they can be considered as environmentally friendly materials [5].

An interesting application of biopolymers includes packaging that could replace single-use synthetic plastics that cause a great amount of waste [6-8]. That is one of the reasons why different sectors such as the food industry have focused on finding materials with biodegradable properties in order to find new packaging to protect and extend food shelf life [9]. A wide range of biopolymers can be found in nature, among them lipid-based polymers, proteins and polysaccharides including cellulose and starch, among others [10] that represent promising options to be used as biobased and biodegradable materials. With regard to polysaccharides, they can provide different properties, including thickening, crosslinking, and adsorption [11]. In the case of cellulose, it could provide high crystallinity to these biobased materials [12]. Starch offers excellent biocompatibility and exceptional film-forming properties [13].

In the case of proteins, they have been used as films for packaging, especially because of their apparent good oxygen barrier properties, and unique structure that allow having good mechanical properties. This is caused by the existence of a high amount of polar groups in its structure, leading to high intermolecular binding [14]. However, this property is still low compared with synthetic polymers [5]. Another drawback of protein films is their poor water vapor barrier due to their inherent hydrophilicity [9, 15]. To overcome some of the limitations presented by proteins, different strategies have been investigated, including mixing with hydrophobic additives, *e.g.* fatty acids [16, 17], lipids [18, 19], waxes [17, 20], or simply changing the drying conditions [6]. Another of the studied methods include the use of cross-linkers such as formaldehyde [21], glutaraldehyde [22], and glyoxal [23], among others. All these strategies try to enhance the cohesion properties of the protein polymeric matrix with the main objective of improving the barrier and mechanical properties [24].

Nevertheless, some of them give somewhat cytotoxicity and are not suitable for use in food packaging [15]. One of the most widely used alternatives to enhance the flexibility, extensibility and processability of proteins involves the use of plasticizers [25, 26], being glycerol the most commonly used because it is biodegradable, non-toxic and recyclable properties [27, 28]. Currently, the use of proteins combined with some other natural mate- rials as biopolymers is being studied. Surprisingly, despite that lignin is the second most abundant natural polymer on the earth after cellulose, its use as additive in protein-based polymers has barely been investigated [29, 30]. Lignin is an amorphous polymer that contains three phenylpropanolic monomers linked by carbon-carbon and ether bonds [30]. It has many reactive hydroxyls groups that are capable of forming strong hydrogen bonds with polymers, which could allow improving physical properties such as adhesion, adsorption, among others [31, 32].

In addition, lignin is a low-cost raw material and it has been normally used as low-value fuel [30]. Therefore, it could be used to obtain lignin-based materials with higher added value. Lignin can be considered as a good reinforcement for proteins due to its intrinsic hydrophobicity that could contribute to improve moisture resistance to protein-based films [33]. In addition, the hydrogen in the phenolic group of lignin can readily interact with some functional group in protein to give a cross-linked structure. This may contribute to the increase in tensile strength, thermal stability, and Young's modulus [33, 34]. There are some studies that report the use of lignin and its positive effects on protein-based films. Arancibia *et al.* [35], obtained bilayer films with isolated soy protein isolated, lignin, and formaldehyde. The use of lignin provided a noticeable improvement in protection against UV-VIS light, which might happen due to the strong light absorption of lignin and its capacity for autoxidation. Gomide *et al.* [36], reported the improvement in the thermal and mechanical properties in protein-based films of whey protein isolate with different amounts of lignin microparticles. Moreover, the films containing the highest amount of lignin microparticles of 0.75% (w/w) showed antioxidant properties. Zadeh *et al.* [37] reported interesting properties of isolate soy protein films for packaging applications. They reported the use of lignin-based additives, namely lignosulfonate and alkali lignin. With regard to lignosulfonate, this allowed to improve mechanical properties and water absorption, meanwhile, films with alkali lignin offered high light absorption in the UV region.

Faba bean (*Vicia faba* L.), are considered to be one of the oldest grain-legume crops, and still has an important world production [38, 39]. They are a rich source of carbohydrates (51–68%, dry matter) and proteins (20–41%, dry matter). The growing conditions and the type of grain influence the proportion of protein and carbohydrate [39]. Faba bean has been traditionally used in Mediterranean countries, as well as other countries as Pakistan, India, China among others. It has been also used as animal feed and to prevent soil erosion as a cover crop [40], so the idea to use this high-protein content bean in other high added-value applications could be promising. Faba bean has been proposed as biobased polymer for films with potential uses in the food industry [41, 42].

The purpose of the present study is to analyze how the addition of different lignin contents derived from pine cone (2.5, 5.0, 7.5, and 10 wt%) influences the thermal, mechanical, morphological, barrier and op- tical properties of FBP films. Furthermore, the effect of lignin on the water susceptibility of the FBP film, as well as on its structural modifi- cations, has also been studied. The authors expect lignin and faba bean protein to interact through hydrogen bonding, as both components possess hydroxyl functionalities that could react with each other and help to improve the linkage between them in the film.

EXPERIMENTAL

Materials

Faba beans of the *gloria variety* used were provided by the Research Institutes of Sweden (RISE). The lignin was obtained from pine cones of the *Pinus Pinea* species, collected in pine forests in the mountains of Alicante (Spain). Glycerol ($C_3H_8O_3$, purity ≥99.0%) was supplied from Sigma Aldrich (Madrid, Spain). Hydrochloric acid (HCl, purity of 36%) and sodium hydroxide (NaOH, purity >97.0%) were provided by VWR (Darmstadt, Germany).

Isolation of faba bean protein (FBP)

The isolation of bean protein (FBP) was performed according to the methodology reported by Rojas-Lema *et al.* [43], and is widely used in protein isolation. For this, faba bean were dehulled, and then milled in order to obtain a powdered flour. The milling

process was carried out in a rotary mill from Brabender (Duisburg, Germany). Subsequently, faba bean flour was added to distilled water at a ratio 1:10 (w/v) and the pH of the obtained solution was adjusted to 9.0 using a 2 M NaOH solution to improve the protein solubility. The final solution was stirred at room temperature for 1 h, then it was centrifuged in a Sorvall Lynx 6000 centrifuge from Thermo Scientific (Langenselbold, Germany) at 3700 G for 30 min and 18 ºC. The pH of supernatant was adjusted to 4.0 using a 1M HCl solution to precipitate the protein. It was stirred at room temperature for 1.5 h and centrifuged at 3700 G for 30 min and 18 ºC. The precipitates were collected and redispersed in distilled water with a ratio 1:10 (w/v). The pH of the suspension was changed to 4.0 and then, centrifuged in the same conditions as above. Finally, the precipitated protein obtained was frozen and freeze-dried.

Isolation of pine cone lignin (PL)

The lignin was extracted from a side stream of a pine cone biorefinery process as described by Trifol *et al.* [44], with minor modifications. Briefly, pine cone particles were treated with two consecutive alkali treatments, firstly at 1.5 M NaOH at 110 ºC for 1 h and thereafter at 1M NaOH and 155 ºC for 3 h. The mixture was separated by filtration and the liquor fraction obtained from the second alkali treatment was subjected to an acid precipitation in order to obtain the lignin. For this, the liquor was heated to 60 ºC under magnetic stirring, and sulfuric acid (64 wt%) was added dropwise until reaching pH 2. The solution was kept for 30 min under magnetic stirring and cooled in an ice bath. Subsequently, the solution was centrifuged at 3000 rpm for 5 min to recover the sediment fraction. Finally, the sediment was frozen and freeze-dried to obtain the pine cone lignin (PL) used.

The obtained fraction showed a lignin content of 73%, the rest was 16% of hemicelluloses (mainly xylose and arabinose), 4% of cellulose and 6% of ashes. The average molecular weight (M_w) of lignin fraction was 11,740 g mol^{-1} with a polydispersity index (PDI; M_w/M_n) of 2.92 [44].

Preparation of FBP/PL films

Faba bean protein films were prepared by a solution casting method. Control film was prepared dissolving 3% (w/v) of FBP in distilled water and then, adding 30% (w/w) of glycerol with respect to the dry weight of FBP. The resultant solution was adjusted to

pH of 10.5 using a 2 N NaOH solution and kept under mechanical stirring for 1 h. Then, the resultant solution was heated in a water bath to 80 ºC during 30 min, and then cooled down to room temperature in order to promote protein denaturation. FBP/PL films were prepared using the same process as for the control film but with the addition of different amounts of PL (2.5, 5, 7.5, and 10 wt% based on the dry weight of FBP) after 1 h of stirring. After lignin addition, the solution was adjusted to pH 10.5 and stirred by 2 h, and then denatured as indicated before. The different solutions prepared were placed into Petri dishes and dried for 24 h at 50 ºC to remove water. The films were then conditioned in a desiccator at 25 ºC and 50% relative humidity (RH) for 48 h before testing. All films were developed in triplicate. The film compositions can be observed in **Table IV.3.2.1**.

Table IV.3.2.1. Composition and coding FBP films with different amounts of PL.

Code	Content			
	Proteins (g)	**Glycerol (g)**	**Water (g)**	**PL (wt% on dry FBP)**
FBP	3	0.9	96.1	0
FBP/PL-2.5%	3	0.9	96.1	2.5
FBP/PL-5.0%	3	0.9	96.1	5.0
FBP/PL-7.5%	3	0.9	96.1	7.5
FBP/PL-10%	3	0.9	96.1	10.0

Characterization techniques

Film thickness

A micrometer from Kalkum Ezquerra (La Rioja, Spain) with a sensitivity of ±0.001 mm was used to measure the thickness of the films. All films were measured on at least ten random points in different parts of the film, and the average value was determined.

Thermal properties

The thermal stability of the FBP/PL films was examined in triplicate by thermogravimetry (TGA) on a thermogravimetric balance Linseis model PT1000 (Selb,

Germany). The samples, weighing about 13–15 mg, were placed in 70-µL standard alumina crucibles and subjected to a heating program from 30 ºC to 700 ºC at a heating rate of 10 ºC min^{-1} in nitrogen atmosphere (with a constant flow rate of 66 mL min^{-1}).

Mechanical properties

Tensile tests of the films were carried out in a universal test machine Elib 50 from S.A.E. Ibertest (Madrid, Spain), following the standard method ISO 527-3:2018. Tests were performed using a load cell of 100 N and a cross-head speed of 5 mm min^{-1} at room temperature. Rectangular samples (6 × 80 mm^2) of each film were placed between the clamps with an initial gap of 50 mm. Five samples of each composition were tested and the corresponding tensile strength, Young's modulus and elongation at break were averaged.

Moisture content

The moisture content (MC) of FBP control film and FBP/PL films was determined gravimetrically through the weight loss measurement of the films, following the procedure described by [45]. For this end, preconditioned samples (1 × 1 cm^2) were weighed. Then they were dried for 24 h in an oven at 105 ºC and weighed again. The MC of each film was obtained in triplicate following **Equation IV.3.2.1**:

$$\text{Moisture content} = \left[\frac{W_i - W_f}{W_i}\right] \times 100\ (\%) \qquad \textbf{Equation IV.3.2.1}$$

where W_i and W_f are the initial and dried weight of the samples, respectively.

Water solubility

The water solubility (WS) of FBP control film and its composites with PL was obtained triplicate following the method described by [46], with few modifications. For this, the different films were cut into square pieces (1 × 1 cm^2), dried for 24 h in an oven at 105 ºC and subsequently weighed. The films were then deposited into a tube with 10 mL of distilled water during 24 h at room temperature. The undissolved films were then dried in an oven at 105 ºC for 24 h and finally weighed. The water solubility of films was determined by following **Equation IV.3.2.2**:

$$\text{Solubility} = \left[\frac{W_i - W_f}{W_i}\right] \times 100\ (\%) \qquad \textbf{Equation IV.3.2.2}$$

where W_i is the initial weight of the sample and the W_f is the sample weight after drying.

Static contact angle

The film surface wettability was studied through the water contact angle (θ) measurement using an optical goniometer EasyDrop-FM140 from Kruss Equipment (Hamburg, Germany) following the ISO 828:2013. In this case, a drop of distilled water (5 µL) was deposited on the film surface exposed to air during the drying process and the angle between the droplet and the film surface was determined using an image analyzer software. All the contact angles measurements were carried out at 15 s after the droplet was deposited on the film surface. For each film, ten measurements of the water contact angle were collected and averaged.

Color parameters

Color of the FBP control film and its composites with PL was determined with a KONICA CM-3600d COLORFLEX-DIFF2 colorimeter, from Hunter Associates Laboratory (Virginia, USA). The colorimeter was calibrated using a standard white tile and the measurements were obtained using standard illuminant D65 and an observer angle of 10^o. L*, a*, and b* color coordinates were measured on each film. Five different measurements were taken and the corresponding color coordinates were averaged. The total color difference (ΔE) was determined by **Equation IV.3.2.3**:

$$\Delta E_{ab}^{*} = \sqrt{(\Delta L^{*})^2 + (\Delta a^{*})^2 + (\Delta b^{*})^2} \qquad \textbf{Equation IV.3.2.3}$$

where ΔL*, Δa* and Δb* are the color parameters differences between samples and the control film (L* = 40.9, a* = 1.7, b* = 11.7).

Water vapor permeability (WVP)

The WVTR test was performed gravimetrically in triplicate following the ISO 53097:2002 standard and ASTM E96-95. For this end, circular films (10 cm^2) were placed and sealed on permeability cups from TQC Sheen B.V. model VF2200 (Capelle aan den IJssel, Netherlands). Two grams of dried silica gel (0% RH) was placed in each cup and

subsequently sealed with the films and placed in a desiccator with a saturated KNO_3 solution at a RH of approximately 80% and at 25 ± 1 ^oC. Finally, each cup was weighed hourly for a total of 6 h. The variation of cup weight was plotted as a function of time and the slope was obtained by linear regression, to calculate the water vapor transmission rate (WVTR) by the following **Equation IV.3.2.4**:

$$WVTR = \left[\frac{\Delta m}{t \times A}\right] \qquad \textbf{Equation IV.3.2.4}$$

where Δm is the weight gain of the cup (kg) at time t (s) and A is the exposed area of the film (m^2).

On the other hand, the water vapor permeability (WVP) was calculated according to the following **Equation IV.3.2.5**:

$$WVP = \left[\frac{WVTR}{S \times (RH_1 - RH_2)}\right] \times e \qquad \textbf{Equation IV.3.2.5}$$

where S is saturation pressure of water vapor at test temperature (Pa), RH_1 is the relative humidity inside of the desiccator (%) and RH_2 is the relative humidity inside the cup (%) and e is the average thickness of sample (mm).

Field emission scanning electron microscopy (FESEM)

A FESEM model ZEISS ULTRA55 Oxford Instruments (Abingdon, UK) was used to analyze the morphology of the cryofractured surfaces of the different films. Prior to observation, the samples were metallized with a gold-palladium alloy in a sputter coater EMITECH mod. SC7620 Quorum Technologies Ltd., (East Sussex, UK). Samples were analyzed at an accelerating voltage of 2 kV.

Attenuated total reflection-Fourier transform infrared spectroscopy (ATR-FTIR)

The FTIR curves for the FBP films were obtained using an infrared spectrometer with an attenuated total reflection accessory (ATR) from PerkinElmer (Massachusetts, USA). Each sample was subjected to a total of 16 scans in 4000 and 500 cm^{-1} range using a resolution of 4 cm^{-1}. The obtained spectra were baseline corrected and normalized to a limiting ordinate of 1 absorbance unit.

Statistical analysis

Statistical analysis was performed to establish the effect of lignin content on the mechanical, optical and water susceptibility properties of the different obtained films. Analysis of variance (ANOVA) was performed on the experimental data and mean values were compared at a 95% confidence level ($p < 0.05$) according to Tukey's test using OriginPro2018 software.

RESULTS AND DISCUSSION

Thermal properties

The effect of PL content on the thermal stability of the FBP films was studied by thermogravimetric analysis (TGA). **Figure IV.3.2.1** shows the TGA and the first derivative curves (DTG) plots of lignin, FBP film and FBP/PL films. The main degradation temperatures of the films are summarized in **Table IV.3.2.2**. It can be seen that FBP film and its composites with PL show three degradation stages [43]. The first degradation stage is related to the evaporation of moisture contained in the films. In this first stage, the addition of lignin in the FBP film hardly has an effect on the moisture evaporation temperature, except for the sample reinforced with 10% lignin, where there is a significant increase in the degradation temperature, changing from 105.8 ^{o}C for the unreinforced FBP film up to 121.4 ^{o}C for the film reinforced with 10% PL. This increase in temperature in the first stage of the film reinforced with 10% PL may be due to the good dispersion of the lignin particles in the protein matrix, which act as a barrier effect hindering the water vapor evaporation [47].

The second degradation stage involves the degradation of the glycerol used as plasticizer. In this case, it can be observed that the addition of lignin in the FBP film leads to a slight increase in the degradation temperature, obtaining a degradation temperature of around 242 ^{o}C for all the reinforced FBP films regardless the PL content. The higher degradation temperature may also be the result of the barrier effect caused by the good dispersion of the lignin particles in the film, which delays the degradation of the glycerol [36]. Finally, the third degradation process is associated with the protein degradation, which takes place at around 295.5 ^{o}C. After the addition of different amounts of PL to the FBP films, the final degradation temperature increases as the lignin amount in the FBP matrix rises, reaching the highest degradation temperature in the sample with 10%

PL, 309.3 ºC. This increase in protein degradation temperature can be due to the higher thermal stability of lignin with respect to proteins, and also to the interactions between proteins and lignin, that lead to an improvement in the overall thermal stability compared to the control FBP film [37]. As it has been reported by Oliviero *et al.* [48], hydrogen bonding interactions between amino acid groups in zein protein and lignin functional groups have a positive effect on thermal stability. As they confirmed in zein-lignin nano-composites, these interactions are more intense at low lignin concentrations. The strong hydrogen bonding is responsible for destructuring secondary structures of the zein protein which allowed an extensive protein conformational change with a positive effect on overall properties, including mechanical and thermal behaviour.

With regard to lignin, as can be seen, its degradation occurs slowly over a wide temperature range. Several authors have shown that its degradation extends to temperatures higher than 900 ºC [49, 50]. This wide range of lignin degradation is due to the structural complexity of this molecule, which is formed by a multitude of aromatic rings with high branching. The higher thermal stability of lignin, together with fixed carbon and mineral matter formed during its pyrolysis is the reason why the residue observed at 700 ºC in the films increases as the lignin content in FBP films increases [51].

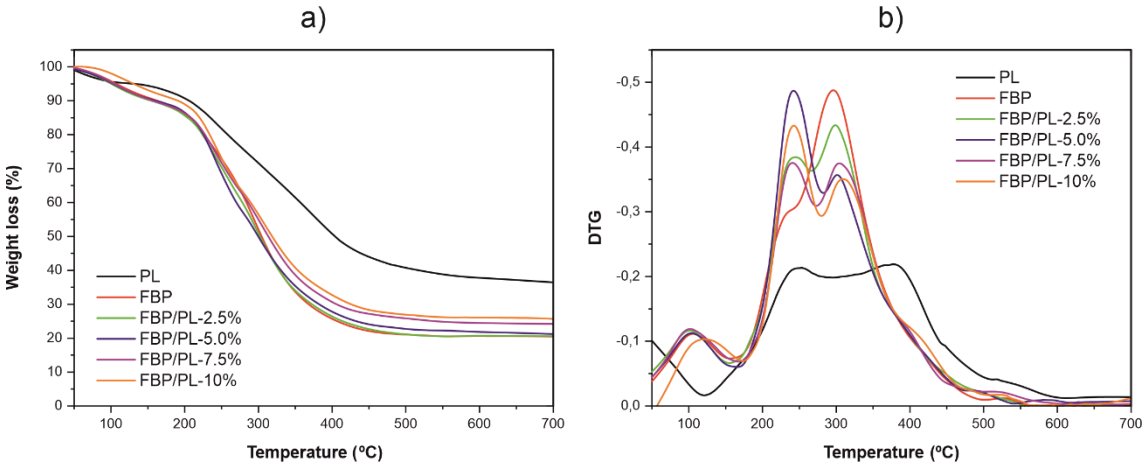

Figure IV.3.2.1. Thermogravimetric (a) and first TG derivative (b) plots of lignin and FBP films reinforced with different amounts of PL.

Table IV.3.2.2. Thermal degradation temperatures and residue mass of pine cone lignin (PL) and FBP films reinforced with different amounts of PL obtained by thermogravimetry (TGA).

Sample	T_0[a] (°C)	T_{max} Stage 1 (°C)	T_{max} Stage 2 (°C)	T_{max} Stage 3 (°C)	Residue Mass (%)
PL	48.9 ± 0.9^{a}	-	253.4 ± 2.3^{a}	377.9 ± 2.1^{a}	36.4 ± 1.1^{a}
FBP	61.9 ± 1.5^{b}	105.8 ± 2.5^{a}	236.3 ± 2.0^{b}	295.5 ± 1.9^{b}	20.5 ± 0.2^{b}
FBP/PL-2.5%	56.4 ± 2.3^{c}	101.1 ± 2.0^{a}	244.4 ± 1.2^{b}	298.4 ± 1.4^{b}	20.6 ± 0.4^{b}
FBP/PL-5.0%	55.5 ± 1.6^{c}	103.1 ± 3.1^{a}	241.5 ± 0.5^{b}	301.3 ± 2.1^{b}	21.2 ± 0.3^{b}
FBP/PL-7.5%	65.8 ± 1.5^{d}	101.3 ± 1.8^{a}	240.8 ± 1.3^{b}	304.7 ± 1.2^{b}	24.2 ± 0.3^{c}
FBP/PL-10%	88.4 ± 4.9^{e}	121.4 ± 3.7^{b}	242.4 ± 2.1^{b}	309.3 ± 1.7^{b}	25.6 ± 0.5^{d}

[a]T_0 was calculated with a weight loss of 1%. $^{a-e}$ Different letters in the same column indicate a significant difference ($p < 0.05$).

Mechanical properties

The thickness and tensile mechanical properties of FBP film and FBP/PL films are shown in **Table IV.3.2.3**. Results show that, the control film (FBP) has a tensile strength around 4.9 MPa, a Young's modulus close to 182 MPa and an elongation at break of 54%. The addition of PL to the FBP film results in higher tensile strength, with the tensile strength increasing as the PL content in the film rises. As can be seen, the FBP film reinforced with 10% PL has the highest tensile strength, with a value of 9.3 MPa, which represents an increase of around 90% with respect to the values obtained for the unreinforced FBP film. This increase in tensile strength may be due to the good compatibility between proteins, glycerol and lignin, since the hydroxyl groups (–OH) contained in FBP and glycerol are able to bind to the hydrophilic groups present in PL, creating strong linkages between the matrix and the reinforcement [36]. On the other hand, it can be observed that the Young's modulus also increases as the PL content in the FBP films increases, except in the film with a 5% of PL content, where a decrease is observed with respect to the film reinforced with 2.5% PL. In this case, the film with the highest stiffness is the FBP film containing 10% PL, with a Young's modulus value of 378.2 MPa, representing a 108% increase over the control film. As with tensile strength, the increase in Young's modulus in PL-reinforced films may be due to strong intra-molecular and intermolecular interactions between proteins and lignin that restrict segment rotation and molecular mobility, thus increasing the resistant mechanical properties [34].

Table IV.3.2.3. Thickness and tensile properties of FBP films reinforced with different amounts of PL.

Sample	Thickness (µm)	Tensile Strength (MPa)	Young's Modulus (MPa)	Elongation at break (%)
FBP	292.5 ± 12.5[a]	4.9 ± 0.2[a]	182.4 ± 17.2[a]	54.0 ± 3.5[a]
FBP/PL-2.5%	258.7 ± 11.8[b]	4.8 ± 0.5[a]	239.4 ± 12.5[b]	60.5 ± 5.9[b]
FBP/PL-5.0%	351.2 ± 33.7[c]	5.3 ± 0.8[b]	196.2 ± 8.6[c]	111.7 ± 7.7[c]
FBP/PL-7.5%	297.5 ± 17.1[d]	5.5 ± 0.4[c]	243.5 ± 9.2[d]	99.9 ± 1.9[d]
FBP/PL-10%	372.5 ± 23.3[e]	9.3 ± 0.3[d]	378.2 ± 5.2[e]	56.4 ± 4.9[e]

[a-e] Different letters in each property indicate statistically significant differences between samples ($p < 0.05$).

As shown in **Table IV.3.2.3**, the incorporation of PL to the FBP film leads to an increase in the elongation at break for all samples, except for the film reinforced with 10% PL, which has an elongation at break similar to the control film. As can be seen, the sample reinforced with 5% PL has the highest elongation at break with a value of 111.7%, which represents an increase of around 107% compared to the control film. For PL contents higher than 5%, a decrease in elongation at break is observed. This increase in the elongation at break of reinforced samples with a lignin content lower than 10% may be due to the molecular weight variation of lignin, since the low molecular weight fraction can lead to a plasticizing effect, while the high molecular weight fraction leads to brittle materials, as demonstrated by [52]. Similar behavior was observed by [34] after addition of different amounts of alkaline lignin (AL) in soy protein isolate films. They reported that the incorporation of 10% AL in the soy protein film led to a simultaneous increase in tensile strength and elongation at break, whereas higher AL content led to a decrease in the elongation at break. Duval *et al.* [53] also observed an increase in Young's modulus and a slight increase in elongation at break after addition of 15% kraft lignin in wheat gluten films. These unexpected properties in the films demonstrate the complexity of the interactions between proteins and lignin.

Water susceptibility

One of the main drawbacks of protein-based films is their high susceptibility to water due to their hydrophilic nature. **Table IV.3.2.4** shows the water solubility, moisture content and contact angle values of FBP film and FBP/PL films. The results show that, the incorporation of PL to the FBP film leads to a decrease in moisture content.

However, changes in moisture content are not statistically significant with increasing pine cone lignin content. Similar behaviour has been reported by Oliviero *et al.* [48] in zein protein and different lignin content. They reported the control zein film had a water uptake of about 12% while the addition of lignin (lignosulfonate) in the 1–10 wt% range, did not provide a significant decrease in the water uptake due to the hydrophilic nature of the sulfonic acid groups. Anyway, they observed a slight decrease in water uptake of zein-lignin (lignosulfonate) nano-composites up to 3 wt% lignin content. In contrast, they observed that the addition of alkaline lignin (AL) did provide a clear decrease in water uptake due to the hydrophobic nature of AL, specifically for a lignin content of 1 wt%.

Thus, they confirmed that depending on the type of lignin, it can tailor the moisture absorption properties. In this work, the decrease in moisture content is not statistically significant which agrees with the results reported on zein-lignosulfonate nanocomposites. In this case, the slight reduction in moisture content in films reinforced with PL could also be due to the low availability of hydrophilic groups in the protein by the formation of intermolecular interactions via hydrogen bonds between this and lignin, resulting in a reduction of the number of active sites capable of interacting with water molecules [47, 54].

With regard to the water solubility of the FBP films, **Table IV.3.2.4** shows that the addition of PL into the FBP films hardly affects it, obtaining for all the PL-reinforced FBP films similar water solubility values to that of the control FBP film, around 30%. The surface hydrophilicity of the FBP films was also confirmed by measuring the water contact angle on the film side exposed to air during films drying. As shown in **Table IV.3.2.4**, the water contact angle of the control FBP film is 57.3º. After the addition of PL into it, the water contact angle decreases with increasing PL content. It can be seen that the lowest contact angle was obtained in the film with the highest lignin content (10%), in which a water contact angle of 40.9º was obtained, representing a decrease of about 29% with respect to the control FBP film. Although this result can be contradictory, this behavior is due to the increase in surface roughness caused by the presence of lignin in the film, which favors wetting and could mask the hydrophobic effect of lignin observed in the moisture content [55].

Table IV.3.2.4. Water solubility, moisture content and contact angle of FBP films reinforced with different amounts of PL.

Samples	Water solubility (%)	Moisture content (%)	Water contact angle (°)
FBP	31.1 ± 0.6[a]	15.5 ± 1.1[a]	57.3 ± 0.3[a]
FBP/PL-2.5%	30.2 ± 0.5[a]	15.3 ± 0.6[a]	56.5 ± 0.7[a]
FBP/PL-5.0%	30.0 ± 1.2[a]	14.9 ± 0.2[a]	45.9 ± 1.2[b]
FBP/PL-7.5%	30.4 ± 0.5[a]	13.7 ± 0.1[a]	43.6 ± 1.4[c]
FBP/PL-10%	29.9 ± 0.9[a]	13.7 ± 0.4[a]	40.9 ± 0.7[d]

[a-d] Different letters in each property indicate statistically significant differences between samples ($p < 0.05$).

Structural chemical properties

Figure IV.3.2.2 shows FTIR-ATR spectra of the control FBP film and the FBP films reinforced with PL in the wavenumber range comprised between 4000 and 500 cm^{-1}. First, the control film exhibits characteristic bands between 500 and 750 cm^{-1}, which correspond to the glycerol plasticizer [36]. These bands can be observed in all the spectra shown in **Figure IV.3.2.2**. Other main peaks are observed at 900 and 1150 cm^{-1}, ascribed to the N–H bond and C–H stretching vibration (type III amide). The bands between 1400 and 1550 cm^{-1} are related to the type II amide N–H stretching, while peaks between 1600 and 1700 cm^{-1} are related to the C–O and C–N stretching vibration of the type I amide [56]. It can be observed a decrease in these last peaks with an increase in lignin concentration. This effect is especially noticeable in the FBP/PL-7.5% film. A similar phenomenon was registered by Gomide *et al.* [36], who related this decrease in the intensity of the peaks to the presence of secondary proteins that lose their conformation during the heating of the solutions that would form the film, provoking different interactions between the elements in the solution that, as a result, decrease the intensity of the main bands of the control FBP film. Another reason for this observation could be the dilution effect of faba bean proteins, as they are partially substituted by lignin. The peaks at 2850 and 2980 cm^{-1} are ascribed to the stretching of the C–H group, and the peak at 3272 cm^{-1} is associated with the O–H and N–H groups contained in the faba bean protein [26]. The addition of lignin to FBP did not provoke significant changes in the FTIR spectra, but only the protein dilution effect aforementioned and some changes in the intensity of the type III amide characteristic peaks, which could be an indicator of certain interaction between polypeptide chains in the proteins and lignin.

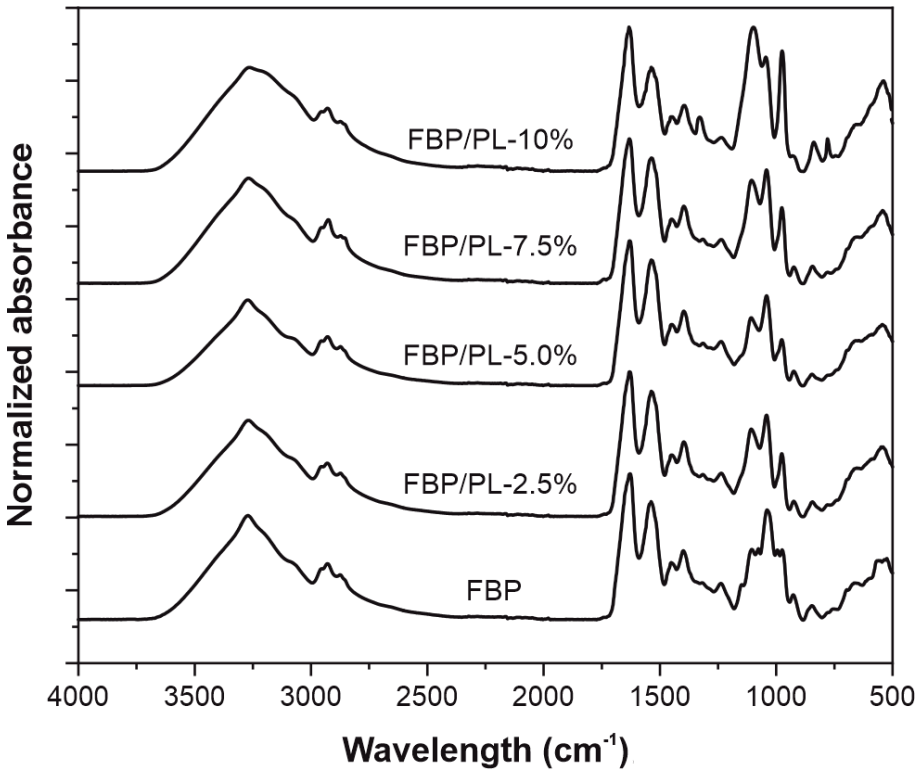

Figure IV.3.2.2. FTIR spectra of FBP films reinforced with different amounts PL.

Morphological properties

Figure IV.3.2.3 shows the cryofractured cross-sections of the different films obtained by FESEM. First, FBP control film (**Figure IV.3.2.3**a) is seen to have a homogeneous and smooth surface with some porosity in it. This morphology matches the results observed in a previous study [43]. The addition of PL changes the microstructure of the FBP films, making more pores and microcracks to appear all over the surface. The concentration and size of the pores seems to increase with the lignin content. A similar surface modification was observed by Yang *et al.* [47] in wheat gluten films containing lignin nano-particles. This is especially noticeable in the 7.5 and 10% PL samples (**Figure IV.3.2.3**d and e), which could be related to an excessive amount of lignin particles in the films, resulting in the formation of agglomerates. This increase in the number and size of pores as the lignin content increases can negatively affect the mechanical and barrier properties of the films. It has been observed that lignin reinforced FBP films with contents higher than 5% PL led to a decrease in ductile mechanical properties, lower elongation at break, and higher water permeability.

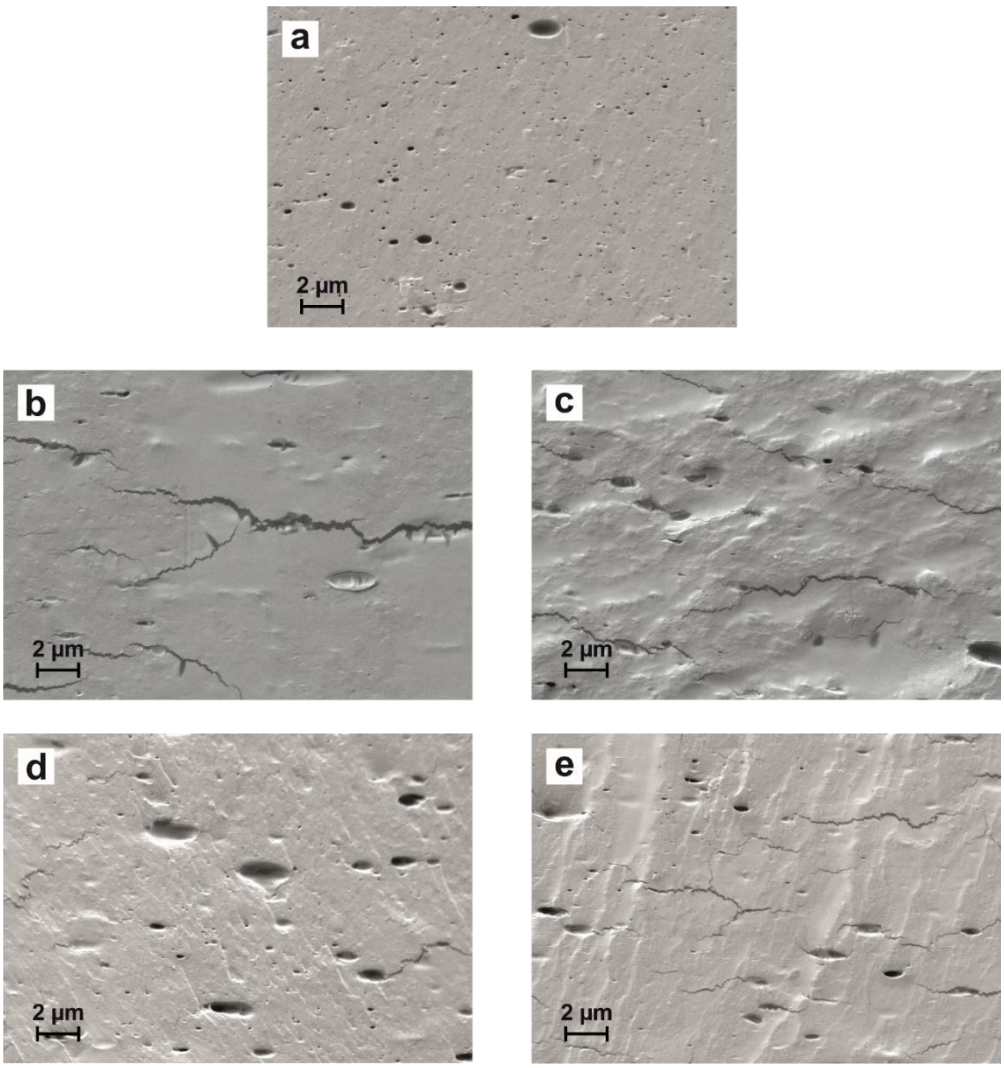

Figure IV.3.2.3. Images at 5,000x of cryofractured cross-section obtained by FESEM of the samples of (a) FBP; (b) FBP/PL-2.5%; (c) FBP/PL-5.0%; (d) FBP/PL-7.5%, and (e) FBP/PL-10%.

Water vapor barrier properties

To evaluate the barrier properties of the films, the water vapor permeability (WVP) was studied, as they are a limitation for protein films, which are highly hydrophilic. **Figure IV.3.2.4** gathers the WVP results for the FBP control film and the FBP films with PL. As can be seen, the FBP film showed a WVP of approximately 3.02 x 10^{-15} kg m m^{-2} s^{-1} Pa^{-1}. The addition of 2.5% of lignin positively affected WVP, reducing it down to 2.27 x 10^{-15} kg m m^{-2} s^{-1} Pa^{-1}, respectively, which is a reduction of permeability 24.7% to the control film. This means that barrier properties against water vapor improved in the films thanks to the incorporation of PL. This reduction could be ascribed to a good dispersion of lignin in the FBP polymeric matrix, obstructing water vapor diffusion and increasing the length of the flow path through the films [57]. Moreover,

the hydrophobicity of lignin may have supported this effect by reducing the affinity of the film towards water molecules [53]. On the other hand, the addition of moderate lignin contents in the FBP film, 5% and 7.5% PL, did not have a substantial influence on the WVP, with very similar values to those recorded in the control film. In the sample reinforced with 10% PL, it is noted that the WVP increases compared to the unreinforced film, obtaining a value of 3.39 x 10^{-15} kg m m^{-2} s^{-1} Pa^{-1}, which represents an increase of about 13%. This fact could be related to an excess of lignin particles in the film, which may have formed agglomerates that provoked the formation of less cohesive film, making water vapor diffusion easier. A similar behavior was observed by Gomide *et al.* [36]. These results agree with the findings observed in FESEM images, where sample with 10% of PL showed higher concentration of holes and pores in the microstructure, which would clearly increase water vapor permeability and decrease barrier properties.

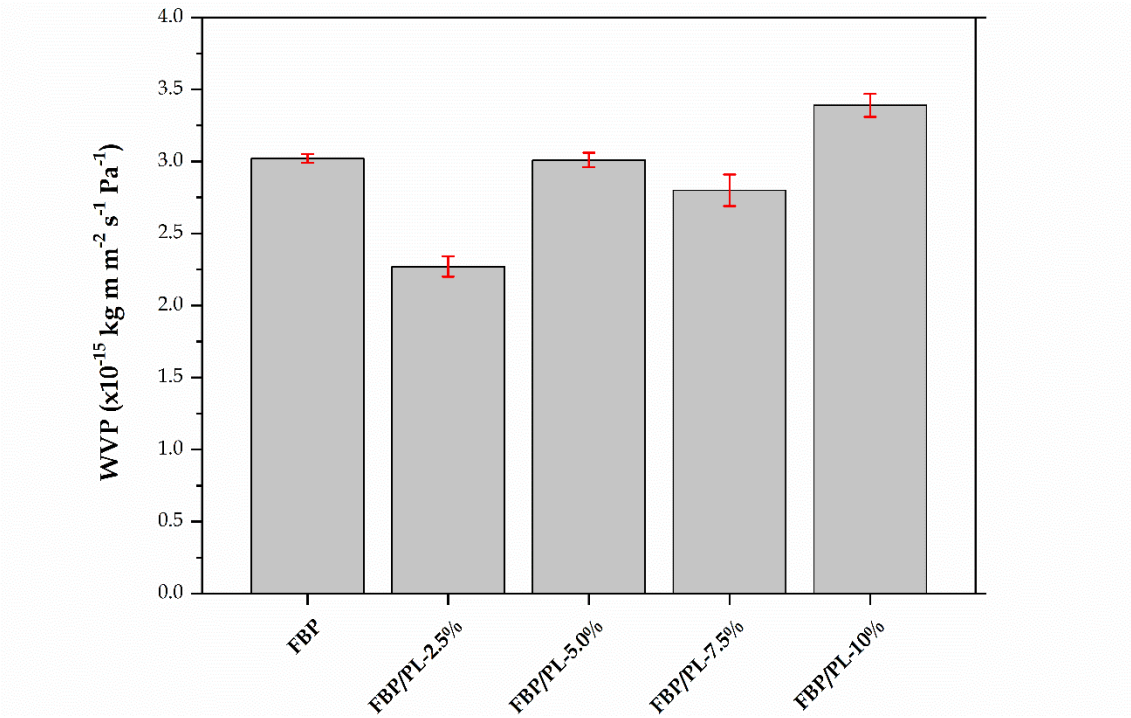

Figure IV.3.2.4. Water vapor permeability (WVP) of FBP films reinforced with different amounts of PL.

Optical properties

Visual appearance of the films is an essential aspect regarding their use in the food packaging industry, as this may affect how the customer perceive the product. At first glance, the control film is the only one that offers some transparency, while the rest of the films exhibit a strong dark color, as a result of the incorporation of lignin. The

visual appearance of the control film is very similar to the one shown in previous studies [43].

Table IV.3.2.5 gathers the main color parameters of the developed films in terms of the color coordinates of the chromatic space CIELab. L* is representative for the lightness. As expected, the control FBP film with the most translucent appearance were measured to be the lightest (L* 40.9). Incorporation of PL to the films reduced the measured L* to approximately 25 indicating that the films became darker [58]. It should be noted that all the parameters of the FBP/PL films are very similar between them, as their color is almost the same. Color coordinate a* stands for green (negative) and red (positive), so all the films have positive values due to presenting brown tonalities. Additionally, a* appears to decrease as the PL content increases, this is probably attributed to an increase in the darkness of the color with the PL content. Similarly, color coordinate b*, which represents the change from blue (negative) to yellow (positive), exhibits positive values, which was also expected due to the films having certain yellowness, especially the control FBP film. Furthermore, b* also decreases when PL is incorporated into the films, due to approaching to darker colors. Finally, as a consequence of the very similar color between all the FBP/PL films, the ΔE_{ab}* parameter is practically invariable, as it indicates the difference in color compared to the FBP control film.

Table IV.3.2.5. Optical parameters of FBP films reinforced with different amounts of PL.

Code	L*	a*	b*	ΔE_{ab}* (Control)[a]
FBP	41.0 ± 0.3^{a}	1.7 ± 0.2^{a}	11.7 ± 0.2^{a}	-
FBP/PL-2.5%	25.7 ± 0.1^{b}	0.9 ± 0.3^{b}	0.9 ± 0.1^{b}	18.7 ± 0.0^{a}
FBP/PL-5.0%	25.1 ± 0.0^{b}	0.6 ± 0.1^{c}	0.3 ± 0.1^{c}	19.5 ± 0.1^{a}
FBP/PL-7.5%	25.0 ± 0.1^{b}	0.5 ± 0.1^{d}	0.6 ± 0.1^{d}	19.4 ± 0.1^{a}
FBP/PL-10%	25.0 ± 0.2^{b}	0.2 ± 0.1^{e}	0.6 ± 0.3^{d}	19.5 ± 0.1^{a}

[a] ΔE_{ab}* is obtained from the color difference between the FBP film and every FBP/PL film. $^{a\text{-}e}$ Different letters in each property indicate statistically significant differences between samples ($p < 0.05$).

CONCLUSIONS

The present work studies the effect of the incorporation of different amounts of lignin extracted from pine cone (2.5, 5.0, 7.5, and 10 wt%) on the thermal, mechanical, morphological, water susceptibility, chemical, barrier and optical properties of glycerol-plasticized faba bean protein films. The addition of lignin in the protein film increased its ductile mechanical properties due to the plasticization effect of the low molecular weight fraction present in the lignin. In this case, an increase in the elongation at break of the lignin-reinforced films was observed, being the film reinforced with 5% the one with the highest elongation at break, 111.7%, representing an increase of 107% compared to the control film. Higher lignin contents (7.5 and 10%) led to a decrease in the elongation at break due to the formation of aggregates that promote the formation of pores and microcracks in its internal structure as could be observed in the FESEM images. Regarding the mechanical strength properties, it was observed that the addition of lignin led to an increase in tensile strength, resulting in a higher increase as the lignin content increases.

The thermal stability of the FBP film was also affected by the presence of lignin. In this case, the incorporation of lignin resulted in an increase in the thermal stability of the FBP film, increasing the characteristic degradation temperatures of glycerol and proteins. This increase in thermal stability was more evident in the 10% PL reinforced film and this was attributed to several factors such as the good dispersion of lignin in the FBP polymeric matrix which hinders the degradation of other components, the higher thermal stability of lignin and the formation of intramolecular interactions between lignin and proteins, which have been analyzed by FTIR. On the other hand, as it was stated in the hypotheses of the work, the linkages formed between the lignin and the protein, mainly through hydrogen bonds, led to a reduction in the number of active sites in the protein that are able to interact with water molecules. This phenomenon, together with the inherent hydrophobicity of lignin, led to an increase in the hydrophobicity of the lignin-reinforced FBP films, which was manifested by a decrease in moisture content. In this case, it was observed that films with a higher lignin content of 7.5 and 10% PL, showed the greatest reduction in moisture content, decreasing it by about 12% compared to the control FBP film. The addition of lignin to the FBP film also resulted in an improvement of the barrier properties, with a noticeable reduction in WVP

compared to the control FBP film. As can be seen, the film with 2.5% PL is the film with the lowest WVP value, which means a reduction of around 25% with respect to the control FBP film. In addition, it was possible to observe how the addition of lignin had a remarkable influence on the colour and opacity of the films, obtaining completely opaque and dark films. This study has demonstrated how lignin derived from pine cone could be an interesting functional additive to improve the thermal, barrier, mechanical and water susceptibility properties of faba bean protein films, allowing to obtain bio-based films that offer a high potential to be considered for their use in the packaging applications.

ACKNOWLEDGEMENTS

This research is a part of the grant PID2020-116496RB-C22 funded by MCIN/AEI/10.13039/501100011033, and the projects AICO/2021/ 025 and CIGE/2021/094 funded by Generalitat Valenciana-GVA. Funding for open access charge: Universitat Politècnica de València. S. Rojas-Lema thanks the Generalitat Valenciana-GVA for the financial support through a Santiago Grisolia grant (GRISOLIAP/2019/132). J. Gomez-Caturla wants to thank Generalitat Valenciana-GVA, for his FPI grant (ACIF/2021/185) and grant FPU20/01732 funded by MCIN/AEI/ 10.13039/501100011033 and by ESF Investing in your future. D. Garcia-Garcia wants to thank the Ministry of Science, Innovation and Universities for their financial support through the "José Castillejo" mobility grant (CAS19/00332). Microscopy services at UPV are acknowledged for their help in using and collecting FESEM images. J. Trifol also acknowledges the financial support of Academy of Finland's Flagship Programme under Projects No. 318890 and 318891 (Competence Center for Materials Bioeconomy, FinnCERES).

REFERENCES

[1] K.K. Sadasivuni, P. Saha, J. Adhikari, K. Deshmukh, M.B. Ahamed, and J.J. Cabibihan. *Recent advances in mechanical properties of biopolymer composites: A review*. Polymer Composites, 2020, 41(1), p. 32-59.

[2] A. Yadav, S. Mangaraj, R. Singh, N. Kumar, and S. Arora. *Biopolymers as packaging material in food and allied industry.* International Journal of Conservation Science, 2018, 6(2), p. 2411-2418.

[3] D. Gnanasekaran. *Green Biopolymers and Their Nanocomposites*. 2019, Gateway East, Singapore: Springer, 1-437.

[4] S. Nagarajan, S. Radhakrishnan, S.N. Kalkura, S. Balme, P. Miele, and M. Bechelany. *Overview of protein-based biopolymers for biomedical application*. Macromolecular Chemistry and Physics, 2019, 220(14), p. 1900126.

[5] T. Bourtoom. *Edible protein films: properties enhancement.* International Food Research Journal, 2009, 16(1), p. 1-9.

[6] G. Denavi, D. Tapia-Blácido, M. Añón, P. Sobral, A. Mauri, and F. Menegalli. *Effects of drying conditions on some physical properties of soy protein films.* Journal of Food Engineering, 2009, 90(3), p. 341-349.

[7] A. Dey, C.V. Dhumal, P. Sengupta, A. Kumar, N.K. Pramanik, and T. Alam. *Challenges and possible solutions to mitigate the problems of single-use plastics used for packaging food items: A review.* Journal of Food Science and Technology, 2021, 58(9), p. 3251-3269.

[8] T.R. Walker, E. McGuinty, S. Charlebois, and J. Music. *Single-use plastic packaging in the Canadian food industry: Consumer behavior and perceptions.* Humanities and Social Sciences Communications, 2021, 8(1), p. 1-11.

[9] C. Montalvo-Paquini, M. Rangel-Marrón, E. Palou, and A. López-Malo. *Physical and chemical properties of edible films from faba bean protein.* Cellulose, 2014, 8, p. 125-131.

[10] S. Shankar, J.P. Reddy, and J.-W. Rhim. *Effect of lignin on water vapor barrier, mechanical, and structural properties of agar/lignin composite films.* International Journal of Biological Macromolecules., 2015, 81, p. 267-273.

[11] S. Xia, L. Zhang, A. Davletshin, Z. Li, J. You, and S. Tan. *Application of polysaccharide biopolymer in petroleum recovery.* Polymers, 2020, 12(9), p. 1860.

[12] H. Khalil, Y. Tye, C. Saurabh, C. Leh, T. Lai, E. Chong, M. Fazita, J.M. Hafiidz, A. Banerjee, and M. Syakir. *Biodegradable polymer films from seaweed polysaccharides: A review on cellulose as a reinforcement material.* Express Polymer Letters, 2017, 11(4).

[13] S. Agarwal. *Major factors affecting the characteristics of starch based biopolymer films.* European Polymer Journal, 2021, 160, p. 110788.

[14] M. Anker, M. Stading, and A.-M. Hermansson. *Relationship between the microstructure and the mechanical and barrier properties of whey protein films.* Journal of Agricultural and Food Chemistry, 2000, 48(9), p. 3806-3816.

[15] A. González, M.C. Strumia, and C.I.A. Igarzabal. *Cross-linked soy protein as material for biodegradable films: Synthesis, characterization and biodegradation.* Journal of Food Engineering, 2011, 106(4), p. 331-338.

[16] A. Jongjareonrak, S. Benjakul, W. Visessanguan, and M. Tanaka. *Fatty acids and their sucrose esters affect the properties of fish skin gelatin-based film.* European Food Research and Technology, 2006, 222(5), p. 650-657.

[17] K. Niegelhell, M. Sußenbacher, J.r. Sattelkow, H. Plank, Y. Wang, K. Zhang, and S. Spirk. *How bound and free fatty acids in cellulose films impact nonspecific protein adsorption.* Biomacromolecules, 2017, 18(12), p. 4224-4231.

[18] M.A. Garcia, M.N. Martino, and N.E. Zaritzky. *Lipid addition to improve barrier properties of edible starch-based films and coatings.* Journal of Food Science., 2000, 65(6), p. 941-944.

[19] J.-W. Rhim. *Increase in water vapor barrier property of biopolymer-based edible films and coatings by compositing with lipid materials.* Food Science and Biotechnology, 2004, 13(4), p. 528-535.

[20] K.M. Kim, K.T. Hwang, C.L. Weller, and M.A. Hanna. *Preparation and characterization of soy protein isolate films modified with sorghum wax.* Journal of the American Oil Chemists' Society, 2002, 79(6), p. 615-619.

[21] J.W. Rhim, A. Gennadios, A. Handa, C.L. Weller, and M.A. Hanna. *Solubility, tensile, and color properties of modified soy protein isolate films.* Journal of Agricultural and Food Chemistry, 2000, 48(10), p. 4937-4941.

[22] C. Marquié. *Chemical reactions in cottonseed protein cross-linking by formaldehyde, glutaraldehyde, and glyoxal for the formation of protein films with enhanced mechanical properties.* Journal of Agricultural and Food Chemistry, 2001, 49(10), p. 4676-4681.

[23] G. Makishi, R. Lacerda, A. Bittante, H. Chambi, P. Costa, C. Gomide, R. Carvalho, and P. Sobral. *Films based on castor bean (Ricinus communis L.) proteins crosslinked with glutaraldehyde and glyoxal.* Industrial Crops and Products, 2013, 50, p. 375-382.

[24] R. De Carvalho and C. Grosso. *Characterization of gelatin based films modified with transglutaminase, glyoxal and formaldehyde.* Food hydrocolloids, 2004, 18(5), p. 717-726.

[25] S. Kokoszka, F. Debeaufort, A. Hambleton, A. Lenart, and A. Voilley. *Protein and glycerol contents affect physico-chemical properties of soy protein isolate-based edible films.* Innovative Food Science & Emerging Technologies, 2010, 11(3), p. 503-510.

[26] Ó.L. Ramos, I. Reinas, S.I. Silva, J.C. Fernandes, M.A. Cerqueira, R.N. Pereira, A.A. Vicente, M.F. Poças, M.E. Pintado, and F.X. Malcata. *Effect of whey protein purity and glycerol content upon physical properties of edible films manufactured therefrom.* Food Hydrocolloids., 2013, 30(1), p. 110-122.

[27] M. Pagliaro, R. Ciriminna, H. Kimura, M. Rossi, and C. Della Pina. *From glycerol to value-added products.* Angewandte Chemie International Edition, 2007, 46(24), p. 4434-4440.

[28] A. Wolfson, C. Dlugy, and Y. Shotland. *Glycerol as a green solvent for high product yields and selectivities.* Environmental Chemistry Letters, 2007, 5(2), p. 67-71.

[29] A.T. Austin and C.L. Ballaré. *Dual role of lignin in plant litter decomposition in terrestrial ecosystems.* Proceedings of the National Academy of Sciences, 2010, 107(10), p. 4618-4622.

[30] B.M. Upton and A.M. Kasko. *Strategies for the conversion of lignin to high-value polymeric materials: review and perspective.* Chemical Reviews., 2016, 116(4), p. 2275-2306.

[31] C. Ciobanu, M. Ungureanu, L. Ignat, D. Ungureanu, and V. Popa. *Properties of lignin–polyurethane films prepared by casting method.* Industrial Crops and Products, 2004, 20(2), p. 231-241.

[32] C. Liu, C. Xiao, and H. Liang. *Properties and structure of PVP–lignin "blend films"*. Journal of Applied Polymer Science, 2005, 95(6), p. 1405-1411.

[33] R.V. Gadhave, S. Srivastava, P.A. Mahanwar, and P.T. Gadekar. *Lignin: renewable raw material for adhesive*. Open Journal of Polymer Chemistry, 2019, 9(2), p. 27-38.

[34] J. Huang, L. Zhang, and P. Chen. *Effects of lignin as a filler on properties of soy protein plastics. II. Alkaline lignin.* Journal of Applied Polymer Science, 2003, 88(14), p. 3291-3297.

[35] M.Y. Arancibia, M.E. López-Caballero, M.C. Gómez-Guillén, and P. Montero. *Release of volatile compounds and biodegradability of active soy protein lignin blend films with added citronella essential oil.* Food Control, 2014, 44, p. 7-15.

[36] R.A.C. Gomide, A.C.S. de Oliveira, L.B. Luvizaro, M.I. Yoshida, C.R. de Oliveira, and S.V. Borges. *Biopolymeric films based on whey protein isolate/lignin microparticles for waste recovery.* Journal of Food Process Engineering, 2021, 44(1), p. e13596.

[37] E.M. Zadeh, S.F. O'Keefe, and Y.-T. Kim. *Utilization of lignin in biopolymeric packaging films.* ACS Omega., 2018, 3(7), p. 7388-7398.

[38] N.H. Alharbi and K.N. Adhikari. *Factors of yield determination in faba bean (Vicia faba).* Crop and Pasture Science, 2020, 71(4), p. 305-321.

[39] M. Hendawey and A. Younes. *Biochemical evaluation of some faba bean cultivars under rainfed conditions at El-Sheikh Zuwayid.* Annals of Agricultural Sciences, 2013, 58(2), p. 183-193.

[40] J. Vioque, M. Alaiz, and J. Girón-Calle. *Nutritional and functional properties of Vicia faba protein isolates and related fractions.* Food Chemistry., 2012, 132(1), p. 67-72.

[41] C. Montalvo-Paquini, M. Rangel-Marron, E. Palou, and A. Lopez-Malo. *Effect of pH on physical properties of edible films from faba bean protein.* Recent Advances in Chemical Engineering, Biochemistry and Computational Chemistry, 2013, p. 29-34.

[42] S. Saremnezhad, M. Azizi, M. Barzegar, S. Abbasi, and E. Ahmadi. *Properties of a new edible film made of faba bean protein isolate.* Journal of Agricultural Science and Technology, 2011, 13(2), p. 181-192.

[43] S. Rojas-Lema, K. Nilsson, J. Trifol, M. Langton, J. Gomez-Caturla, R. Balart, D. Garcia-Garcia, and R. Moriana. *Faba bean protein films reinforced with cellulose*

nanocrystals as edible food packaging material. Food Hydrocolloids., 2021, 121, p. 107019.

[44] J. Trifol, D.C. Marin Quintero, R.J.A.S.C. Moriana, and Engineering. *Pine cone biorefinery: integral valorization of residual biomass into lignocellulose nanofibrils (LCNF)-reinforced composites for packaging.* ACS Sustainable Chemistry & Engineering, 2021, 9(5), p. 2180-2190.

[45] A. González, G. Gastelú, G.N. Barrera, P.D. Ribotta, and C.I.Á. Igarzabal. *Preparation and characterization of soy protein films reinforced with cellulose nanofibers obtained from soybean by-products.* Food Hydrocolloids., 2019, 89, p. 758-764.

[46] K. Masamba, Y. Li, J. Hategekimana, F. Liu, J. Ma, and F. Zhong. *Effect of Gallic acid on mechanical and water barrier properties of zein-oleic acid composite films.* Journal of Food Science and Technology, 2016, 53(5), p. 2227-2235.

[47] W. Yang, J.M. Kenny, D.J.I.C. Puglia, and Products. *Structure and properties of biodegradable wheat gluten bionanocomposites containing lignin nanoparticles.* Industrial Crops and Products, 2015, 74, p. 348-356.

[48] M. Oliviero, L. Verdolotti, E. Di Maio, M. Aurilia, and S. Iannace. *Effect of supramolecular structures on thermoplastic Zein–Lignin bionanocomposites.* Journal of Agricultural and Food Chemistry, 2011, 59(18), p. 10062-10070.

[49] H. Haykiri-Acma, S. Yaman, and S. Kucukbayrak. *Comparison of the thermal reactivities of isolated lignin and holocellulose during pyrolysis.* Fuel Processing Technology, 2010, 91(7), p. 759-764.

[50] J. Sameni, S. Krigstin, D. dos Santos Rosa, A. Leao, and M. Sain. *Thermal characteristics of lignin residue from industrial processes.* BioResources, 2014, 9(1), p. 725-737.

[51] M. Wądrzyk, R. Janus, M. Lewandowski, and A. Magdziarz. *On mechanism of lignin decomposition–Investigation using microscale techniques: Py-GC-MS, Py-FT-IR and TGA.* Renewable Energy, 2021, 177, p. 942-952.

[52] S. Baumberger, C. Lapierre, and B. Monties. *Utilization of pine kraft lignin in starch composites: impact of structural heterogeneity.* Journal of Agricultural and Food Chemistry, 1998, 46(6), p. 2234-2240.

[53] A. Duval, S. Molina-Boisseau, and C. Chirat. *Comparison of Kraft lignin and lignosulfonates addition to wheat gluten-based materials: Mechanical and thermal properties.* Industrial Crops and Products, 2013, 49, p. 66-74.

[54] Y. Sakunkittiyut, T. Kunanopparat, P. Menut, and S. Siriwattanayotin. *Effect of kraft lignin on protein aggregation, functional, and rheological properties of fish protein-based material.* Journal of Applied Polymer Science, 2013, 127(3), p. 1703-1710.

[55] K. Crouvisier-Urion, P.R. Bodart, P. Winckler, J. Raya, R.D. Gougeon, P. Cayot, S. Domenek, F. Debeaufort, and T. Karbowiak. *Biobased composite films from chitosan and lignin: antioxidant activity related to structure and moisture.* ACS Sustainable Chemistry & Engineering, 2016, 4(12), p. 6371-6381.

[56] R.A. Carvalho, A.C.S. de Oliveira, T.A. Santos, M.V. Dias, M.I. Yoshida, and S.V. Borges. *WPI and cellulose nanofibres bio-nanocomposites: effect of thyme essential oil on the morphological, mechanical, barrier and optical properties.* Journal of Polymers and the Environment, 2020, 28(1), p. 231-241.

[57] M.V. Dias, V.M. Azevedo, T.A. Santos, C.C. Pola, B.R.B. Lara, S.V. Borges, N.F.F. Soares, É.A.A. Medeiros, and C. Sarantópoulous. *Effect of active films incorporated with montmorillonite clay and a-tocopherol: Potential of nanoparticle migration and reduction of lipid oxidation in salmon.* Packaging Technology and Science, 2019, 32(1), p. 39-47.

[58] I.L. Weatherall and B.D. Coombs. *Skin color measurements in terms of CIELAB color space values.* Journal of Investigative Dermatology., 1992, 99(4), p. 468-473.

V. CONCLUSIONS

V.1. PARTIAL CONCLUSIONS

Once the results obtained throughout this work have been described and analyzed, and considering the partial objectives set forth, the following conclusions are presented according to the established study blocks.

V.1.1. High-density bio-poly(ethylene) materials with improved properties by incorporating natural compounds and fillers.

The addition of phenolic active principles improved the thermo-oxidative stability of bio-HDPE. In the particular case of gallic acid and quercetin, a greater increase in the oxidation onset temperature (OOT) was evidenced. With the analysis carried out under isothermal conditions at 210 ^{o}C to determine the oxidation induction time (OIT), the increase in OIT in all samples with antioxidants was verified. These OIT values were more significant in bio-HDPE formulations containing gallic acid and quercetin with 109 min and 138 min, respectively, compared to the bio-HDPE without any additive with an OIT of 4.5 min. All of this confirms the exceptional antioxidant behavior presented by the samples.

Additionally, the results indicated that the mechanical properties did not suffer considerable variations with the incorporation of the active principles into the polymeric matrix. Therefore, the results show the possibility of using the developed films in the packaging sector, including potential use as active packaging.

The addition of natural fillers, in particular, persimmon peel flour (PPF), to the polymeric matrix caused a reduction in mechanical properties in terms of Young's modulus, tensile strength, and impact strength. The decrease in elongation at break was also evident due to the nature of the polymeric matrix and the natural filler, which does not allow for good interaction between the two phases. The results indicated that the samples treated with the different compatibilization methods did not show a significant change in tensile strength but only a slight decrease, while for the rest of the properties, there was an increase in their values with regard to the untreated sample (bio-HDPE/PPF), which translates into an increase in the interaction between the two phases.

The impact strength of bio-HDPE composites containing palmitoyl chloride-treated fillers increased by more than 50% with respect to the samples with untreated fillers; this was a consequence of a better dispersion of the fillers and, subsequently, improved polymer-filler interaction was achieved, which in turn prevented bio-HDPE composites from microcrack formation and growth.

The wettability analysis showed that the silanization treatment with (3-gliciloxipropil)trimetoxisilano (GLYMO) and the hydrophobizing treatment with palmitoyl chloride to the fillers counteracted the hydrophilic nature of bio-HDPE composites with untreated persimmon peel flour (Bio-HDPE/PPF). However, only bio-HDPE composites containing palmitoyl chloride-treated PPF maintained this hydrophobic behavior over time.

The addition of the natural fillers from persimmon peel flour (PPF) also provided antioxidant properties to the developed materials, which was reflected in the increased thermal stability in terms of oxidation induction time (OIT). This effect was enhanced in those containing PPF subjected to silanization with GLYMO, since it allowed an increase in the (OIT) of up to 82 min, while bio-HDPE/PPF composites with untreated persimmon peel flour (bio-HDPE/PPF) presented an (OIT) of 5 min.

The addition of Kraft lignin into the bio-HDPE matrix caused a noticeable decrease in mechanical properties. This behavior was confirmed by morphology analysis, which showed the presence of aggregate particles and holes along the polymeric matrix. Reactive extrusion (REX) with dicumyl peroxide (DCP) improved the interaction between bio-HDPE and Kraft lignin particles; this was reflected by a clear improvement of mechanical properties. It was observed that this interaction was optimum for a DCP content (1 phr), which allowed an increase in the elongation at break and in the impact resistance compared to composites obtained by conventional (non-reactive) extrusion.

The incorporation of the Kraft Lignin in the matrix evidenced a slight decrease in the thermal properties. However, it was observed that the maximum degradation temperature of the bio-HDPE composites obtained by REX with DCP was very similar to the one of neat bio-HDPE. So there was no effect on these properties after REX with DCP. The wettability analysis showed that the interaction between the polymer matrix

and the filler only caused a slight decrease in the inherent hydrophobicity of the polymer. Therefore, using Kraft lignin as a filler is viable since it reduces the amount of polymeric matrix necessary for developing a new material with interesting active properties.

V.1.2. Biopolymeric materials from poly(ester) matrices combined with natural additives, fillers, and nanofillers.

The addition of oligomers of lactic acid (OLA) into the poly(lactide) PLA matrix had a noticeable effect on on the mechanical properties since as the OLA content increased, the ductility of the PLA matrix also did, reaching an improvement of up to 75% with the highest OLA content. It was also observed a decrease in Young's modulus and tensile strength. Incorporating different amounts of halloysite nanotubes (HNTs) (3, 6, 9 phr) in the PLA matrix with 20 wt% OLA led to noticeable changes in these properties, achieving the highest mechanical performance for a HNT content of 3 phr.

The addition of OLA gradually reduced the thermal stability of PLA since a decrease in degradation onset temperature with increasing OLA content was observed. With the addition of HNTs in low contents, it was observed an increase in degradation onset temperature; this suggests that better-dispersed HNTs may provide a more homogeneous thermal barrier.

Water vapor permeability (WVP) and limonene permeability (LP) tests indicated that PLA/OLA blends with the lowest HNTs content offered a decrease in permeability of about 8% and 47%, respectively, with respect to PLA/OLA blends, which is a point to highlight, since one of the features sought in films for packaging applications is the good barrier properties.

The addition of poly(butylene succinate-grafted-maleic anhydride) copolymer (PBS-g-MAH) as compatibilizer positively affected the interaction of pistachio shell flour (PSF) as a natural filler in a poly(butylene succinate) (PBS) matrix for the formation of a composite material. This fact could be evidenced by FESEM analysis in which it was observed how the lignocellulosic PSF particles were embedded by the surrounding polymeric matrix without detectable gaps between the two phases. This effect, in turn, had a positive effect on mechanical properties since the addition of the filler reinforced

the matrix, evidencing an increase in Young's modulus as the filler content increased. As a result, the stiffness of the composite material increased. In addition, it was confirmed an increase in hardness, largely due to the increase in crystallinity quantified by thermal analysis. It was also observed that the addition of low percentages of PSF particles (5 – 10 wt%), led to an increase in the onset temperature of degradation.

The addition of PSF fillers into the polymeric matrix caused an increase in the water absorption of the composite material with time; this is due to the inherent hydrophilic characteristic of natural fillers.

V.1.3. Extraction of different biopolymers from agro-industrial residues and their combinations to obtain films.

The extraction of proteins from faba beans (FBP) and the cellulose nanocrystals (CNC) from pine cones was achieved. The proteins were used to make films and the CNCs, in different proportions, were added as reinforcements.

The addition of CNCs into the protein films increased tensile strength and Young's modulus while elongation at break was decreased. This variation in properties was more noticeable as the CNC content increased, resulting in films with higher stiffness. This CNC reinforcement also affected thermal properties, as it allowed an increase in the onset degradation temperature.

The addition of CNC into the protein films, also provided a reduction in the water affinity of the films, which resulted in a decrease in the moisture content and water solubility of the films, as well as an increase in the hydrophobicity of the sample. In addition, the CNC reinforcement improved the barrier properties since the water vapor transmission rate (WVTR) and oxygen transmission rate (OTR) were reduced.

Faba bean protein films (FBP) reinforced with lignin (PL) extracted from pine cones in different amounts were obtained. The incorporation of pine cone lignin into the films affected their mechanical properties. In particular, with the lower contents of lignin (2.5 wt%and 5 wt% FBP), an increase in the elongation at break of the material was achieved, thus leading to a decrease in Young's modulus. In contrast, the changes in

tensile strength were almost negligible. It was also evidenced an increase in the onset degradation temperature of the samples with higher lignin content.

Both moisture content and water solubility showed a slight decrease as the lignin content in the films increased. Additionally, sample films containing less than 7.5 wt% lignin showed a decrease in water vapor permeability (WVP).

V.2. GENERAL CONCLUSION

As a general conclusion of this doctoral thesis, it can be assessed that the use of biopolymers, together with the incorporation of different natural additives and agro-industrial wastes, has allowed the development of new formulations that are more respectful with the environment. Natural resources and wastes can be used as functional or active fillers in the biopolymeric matrices, and also, they constitute an important source of different components, such as active principles that can still be used for the improvement of some particular properties. In addition, the extraction and use of biopolymers from agro-industrial wastes represent a promising possibility since it once again refers to the revalorization of materials. In this way, it has been possible to obtain new biopolymeric materials with low environmental impact and good barrier properties that make them good candidates to be used in the packaging industry.